Geological Heterogeneity in Landslides: Characterization and Flow Modelling

THÈSE N^{O} 4156 (2008)

PRÉSENTÉE LE 26 AOÛT 2008

À LA FACULTE ENVIRONNEMENT NATUREL, ARCHITECTURAL ET CONSTRUIT
LABORATOIRE DE GÉOLOGIE DE L'INGÉNIEUR ET DE L'ENVIRONNEMENT
PROGRAMME DOCTORAL EN ENVIRONNEMENT

ÉCOLE POLYTECHNIQUE FÉDÉRALE DE LAUSANNE

POUR L'OBTENTION DU GRADE DE DOCTEUR ÈS SCIENCES

PAR

Boris MATTI

géologue diplômé de l'université de Lausanne
de nationalité suisse et originaire de Saanen (BE)

acceptée sur proposition du jury:

Prof. M. Schuler, président du jury
Prof. A. Parriaux, Dr L. Tacher, directeurs de thèse
Dr R. Bernasconi, rapporteur
Prof. D. Or, rapporteur
Prof. V. Simeone, rapporteur

ÉCOLE POLYTECHNIQUE
FÉDÉRALE DE LAUSANNE
Suisse
2008

A Isabella

Acknowledgements

I would like to thank my supervisors, Prof. Aurèle Parriaux and Dr Laurent Tacher from the Laboratory of Geology (GEOLEP) of the Swiss Federal Institute of Technology, who gave me the opportunity to carry out this research project and let me the freedom to go my own research direction;

Dr Pascal Turberg, who introduced me to some concepts of geophysics, and for his support and advice;

Thanks are also due to Stéphane Commend from GEOMOD for its assistance in the geomechanical modelling;

Many thanks also to the people from the GEOLEP, with whom I spent the last three years:

In particular to Mike Bensimon with whom I shared the “micro-wave” during lunch and Alina Tomaniak who provided important “secretarial” assistance;

My personal thanks go to Isabella, my family and my friends for supporting me during this part of my life;

Also many thanks to:

Andrea Mason who improved the language of some parts of this work, and filled my numerous linguistic gaps;

Finally, I would like to thank the different persons who accepted to be part of the examining board:

Prof. V. Simeone, Prof. D. Or, Dr R. Bernasconi

Abstract

Significant progress has been made these last decades in the development of hydrogeological numerical flow modelling for describing the hydrodynamic behaviour of landslides. However, these new sophisticated methods are still very seldom used in the problems of slope instability in particular because of the hydrogeological complexity which characterizes them; thin aquifers, discontinuous media, succession of saturated and unsaturated zones, low permeabilities, high hydraulic gradients, lithological heterogeneity, strong contrasts of permeabilities and heterogeneous infiltration.

Predictive models of flow in the subsurface, which are often based on homogeneous porous media types of representation, are badly adapted to natural systems that are characterized by highly heterogeneous media such as landslides. These models are good and reliable on a landslide scale (regional scale), but their quality may be affected on a local scale by strong geological heterogeneities. Geological heterogeneities of the subsurface take part in determining the hydrodynamical and geomechanical behaviour of landslides. However, their spatial distribution is partially unknown.

Thus, the principal objectives of this PhD thesis are: (i) To carry out an integrated multidisciplinary characterization study on the internal structure of landslides in flysch and Quaternary environments, in order to clarify the organisation of the geological heterogeneities and to identify the hydrodynamic implications. (ii) To propose a conceptual model representing the geological architecture and the hydrogeological functioning. (iii) To examine the effects of heterogeneity and anisotropy on flow systems. (iv) To better understand the influence of geological heterogeneities on the mechanical behaviour of large landslides by performing numerical sensitivity analyses, by means of different heterogeneity scenarios on the field parameters. (v) Finally, to test the incidences on slope stabilization techniques; evaluation of the efficiency of a drainage gallery work. The main test site of *la Frasse landslide* (VD, Switzerland) was chosen, and completed with additional landslide cases.

The main results are the following:

In most of the case studies, the landslide mass is composed of an old prehistoric stabilized mass, pinched between the active sliding mass and the bedrock, and playing an important hydrologic role. The stabilized mass and the bedrock form the substratum of the landslide.

Landslides occurring in these types of media are defined by an organized heterogeneous environment with “fracture” flows and discontinuity porosity. The overall hydraulic conductivity is low, and locally high permeable zones exist. Regional groundwater circulations are limited and form local interconnected aquicludes organised in thin aquifers, and presenting saturated and unsaturated zones.
The hydrogeological analyses showed that the system presents a bimodal permeability; (i) Low hydraulic conductivities characterizing the global matrix and defining the *capacitive fraction*, and (ii) high permeable features, with high hydraulic conductivities defining the *conductive fraction*, and favouring strong channelling effects. Besides, the observation shows that the aquifer system is generally very reactive with important magnitudes. Often, there is a straight correlation between water level variation and climatic conditions (rainy events).
Landslides are characterized by two important inflows namely effective infiltration from the surface and lateral inflows from the neighbouring units. Water transfer between the stabilized mass and the active mass may be important and thus have to be considered. The existence of water transfer between the bedrock and the landslide mass (stabilized and active) is not well established. The bedrock and the landslide mass present a hydrological behavioural independence.

Theoretical two- and three-dimensional flow models are used to investigate the effects of the spatial variability of the hydraulic conductivity on the underground flows. The role of the connectivity in generating flow channelling is examined thanks to the observation of close relations between the permeability and the hydraulic pressures. The sensitivity analysis shows clearly that the relation between local permeability and hydraulic pressures is not straight, and that the organization of the flows depends on the heterogeneity of the

hydraulic properties and their spatial correlation. Strong channelling effects are observed in highly heterogeneous porous media. The development of flow channelling as a function of the variance of the natural log permeability values and the correlation lengths is demonstrated.

The integrated multi-disciplinary geological characterization at the *La Frasse* test site combined with the hydrogeological and lithological data of several additional case studies led to the proposal of a global conceptual model. The following assumptions are considered to enable a subsequent quantification of flow components:

- The flow occurs under confined to leaky conditions, with leakage varying in space;
- The flow framework is controlled by a complex multi-layer system, isolated lenses or perched aquifer;
- The aquifer system is divided into interconnected hydrological zones presenting various degrees of saturation;
- Each hydrological zone may function individually from the others;
- Horizontally and vertically, the flow direction in the porous matrix is affected by prevailing structural patterns generating channeling effects;
- The flow is multidirectional, free and channelized, and is affected by temporal and spatial changes;
- The aquifer is under an unsteady flow regime due to seasonal variation of natural gradients;

A conceptual model based on a simple reservoir approach is proposed. It allows the representation of most of the field observations and the main characteristics, namely the *organized heterogeneity* and the *duality of the aquifers*. The system is represented by various reservoirs more or less connected and saturated. Complex storage capacities and plug-flow effects may record past events and reactive sliding processes several months after the last important rainy event. The analysis shows that function of the capacity and the degree of saturation of the system, an important hydrological event is not necessarily associated to a reactivation. And, according to the degree of complexity of the system (saturation, connectivity...) a localized geological modification (variation of permeability, reservoir burst...) may produce a chain reaction, and generate failures in unexpected places.
The conductive fraction favours the drainage of the system, whereas the capacitive fraction controls the distribution of the hydraulic heads. The role of the phreatic nappe, through the conductive fraction, is to drain and control the hydrologic equilibrium of the system. Therefore landslide remediation with the help of a deep drainage gallery is obviously the most valuable method for this type of landslide. It supports and enhances the natural effects of the conductive fraction in draining the system.

Finally, in this context the efficiency of civil engineering works was evaluated according to the heterogeneity of the medium. This study describes transient hydrogeological and geomechanical models realized jointly in 2006 by the EPFL and GeoMod SA within the framework of the stabilization work of the *La Frasse* landslide. These models evaluate the impact of a deep drainage gallery with subvertical pipes towards the surface in terms of reduction of the deformation velocities and increase of the factor of safety of the landslide. Three variants consisting of different inter pipe spacings are tested. Considering the local heterogeneities, the results show that a mean spacing between the pipes of the order of 10 m is able to control the temporal head fluctuations between the wells within a range of some meters. Moreover, this solution induces a strong diminution of the predicted displacements during a specific crisis, from 101cm for the model without drainage to around 14 cm for the drained model, and a significant gain of security (from 1.05 to 1.30).

Keywords: Landslides, geological heterogeneity, characterization, numerical models, remediation work

Version abrégée

Des progrès significatifs ont été réalisés ces dernières décennies dans le développement des méthodes de simulations numériques hydrogéologiques. Toutefois, ces nouvelles méthodes sont encore très peu utilisées dans la problématique des versants, notamment en raison de la complexité hydrogéologique qui les caractérise (aquifères minces, milieux discontinus, succession de zones saturées et non saturées, faibles perméabilités, gradients hydrauliques élevés, hétérogénéité lithologique, forts contrastes de perméabilités, infiltration hétérogène etc.).

La modélisation numérique des écoulements souterrains, souvent basée sur une représentation homogène du milieu poreux, est inadaptée aux systèmes naturels caractérisés par une forte hétérogénéité géologique, comme les glissements de terrain. Ces modèles sont fiables à l'échelle du glissement, mais à l'échelle locale, leur qualité est affectée par ces fortes hétérogénéités. Ces hétérogénéités ont de fortes répercussions en thermes hydrauliques sur les glissements, et conditionnent leur comportement hydrogéologique et géomécanique. En outre, leur détail et leur distribution est partiellement inconnu.

Les objectifs principaux de ce travail de doctorat sont: (i) Caractériser par une approche multidisciplinaire la structure géologique interne des glissements de terrain de type flysch et Quaternaire, dans le but de clarifier l'organisation des hétérogénéités et leurs implications hydrodynamiques. (ii) Proposer un modèle conceptuel du fonctionnement hydrodynamique de ces systèmes. (iii) Caractériser l'effet des hétérogénéités sur les champs de pression. (iv) Comprendre les effets de ces hétérogénéités sur le comportement des glissements de terrain au moyen de modélisations par éléments finis selon divers scénarios. (v) Et finalement, tester leurs effets sur l'efficacité de mesures d'assainissement, notamment le cas d'une galerie de drainage. Le principal site d'étude est le cas du glissement de la Frasse (VD, Suisse), complété par divers autres cas.

Les principaux résultats sont:

Dans la majorité des cas étudiés, la masse en glissement repose sur une ancienne masse stabilisée, comprise entre la masse active et le rocher en place. Elle tient un rôle important dans le fonctionnement hydraulique du système. La masse stabilisée et le rocher en place forme le substratum du glissement.

Les glissements de terrain qui surviennent dans ce type de milieu peuvent être définis par: une hétérogénéité organisée, et des écoulements de type « fracture » et de porosité discontinue. La conductivité hydraulique globale est très faible, cependant, des zones très perméables existent. Les écoulements régionaux sont limités spatialement, et forment des aquicludes plus ou moins connexes, organisés en fins aquifères, et présentant des zones saturées et non saturées. L'analyse hydrogéologique montre que ces systèmes présentent une perméabilité bimodale; (i) une faible perméabilité représentant la *fraction capacitive* du système, et (ii) une forte perméabilité définissant la *fraction conductive*, favorisant la formation de « chenaux » d'écoulement. De plus, les observations montrent que ces systèmes sont d'un point de vue hydrodynamique très nerveux avec de fortes amplitudes. Souvent, une corrélation directe entre les variations piézométriques et les conditions climatiques (fortes précipitations) peut être établie.
Concernant leur alimentation, les glissements sont caractérisés par deux types d'apports; les infiltrations de surface et les flux latéraux, provenant des terrains adjacents. Les transferts entre la masse stabilisée et la masse active doivent être pris en compte car pouvant être très importants. L'existence de transferts entre le rocher en place et le glissement de terrain n'est pas vérifiée. Les études montrent que ces deux entités présenteraient plutôt une forte indépendance comportementale.

L'effet des variabilités spatiales des perméabilités a été étudié grâce à des modélisations numériques par éléments finis en deux et trois dimensions. Le passage de l'hétérogénéité du milieu à l'hétérogénéité des écoulements n'est pas trivial. L'organisation des écoulements dépend de la variabilité des propriétés hydrauliques et de leur corrélation spatiale, c'est à dire de la connectivité spatiale des zones de propriétés hydrauliques similaires. Des études numériques et expérimentales ont mis en évidence le fait que les écoulements dans les milieux hétérogènes ont tendance à s'organiser en chenaux plus ou moins indépendants.

Ce phénomène de « chenalisation » est souvent évoqué comme une des raisons principales de l'incapacité des modèles classiques à reproduire les observations.

La caractérisation géologique effectuée grâce a une approche multidisciplinaire sur le cas de la Frasse, complétée par diverses observations hydrogéologique et lithologique de cas additionnels, a permis de proposer un modèle conceptuel global. Les hypothèses suivantes ont été définies et considérée :

- Les écoulements sont majoritairement confinés et semi-perméables;
- Les écoulements se produisent dans un système complexe d'aquifères multicouches, de lentilles perméables isolées ou/et de nappes perchées;
- Ces aquifères sont subdivisés en zones interconnectées, présentant divers degrés de saturation;
- Chaque zone de l'aquifère fonctionne indépendamment des autres;
- Horizontalement et verticalement les écoulements sont influencés par des structures géologiques favorisant la chenalisation;
- Les écoulement sont multidirectionnels, diffus et/ou chenalisés, et sont affectés par de forts changements temporel et spatial du milieu;
- Le régime des écoulements est transitoire, étant donné les variations hydrogéologiques saisonnières du système et des gradients hydrauliques ;

Un modèle conceptuel du fonctionnement hydraulique basé sur une approche simple du modèle de réservoir est proposé. Il permet de tenir compte des observations; à savoir de l'hétérogénéité structurée et de la dualité des écoulements. Le système est représenté par plusieurs réservoirs plus ou moins connectés et saturés. De complexes relations d' « emmagasinements hydriques» et d'effets piston, enregistrent et accumulent divers évènements climatiques (forte précipitations, fonte des neige) sont enregistrés, et peuvent réactiver le glissement plusieurs mois après. Les analyses ont montré que en fonction du degré de saturation de ces réservoirs, et de leur capacité hydrique, un événement hydrologique important n'occasionne pas obligatoirement une activation du glissement. Et de plus, en fonction du degré de complexité géologique et des connectivités hydrauliques internes du système, des ruptures (éclatement de poches d'eau, déchirures,…) au sein du glissement peuvent se produire à des endroits inattendus.
La fraction conductive favorise ainsi le drainage du système, alors que la fraction capacitive contrôle la distribution des charges hydrauliques en maintenant un flux de base. Le rôle de la nappe phréatique à travers la fraction conductive est de drainer le système et de contrôler l'équilibre hydrologique du système. C'est pourquoi, dans ce type de milieu, les méthodes d'assainissement les plus efficace sont les systèmes de puits ou galeries drainants. Ces systèmes participent au drainage naturel et l'améliore.

Finalement, dans ce contexte, des modèles hydrogéologiques et géomécaniques réalisés conjointement en 2006 par l'EPFL et GEOMOD S.A. dans le cadre du projet d'ouvrage d'assainissement du glissement de la Frasse ont permis d'évaluer l'efficacité d'une galerie de drainage équipée de drains. Ces modèles ne peuvent pas définir à priori l'emplacement exact des drains, mais ils permettent d'en établir l'espacement moyen, qui devra être ajusté selon les conditions locales rencontrées durant l'exécution. Les résultats montrent qu'un espacement moyen entre les drains de l'ordre de 15 m est capable d'abaisser le potentiel hydraulique d'environ 36 m le long de l'ouvrage à hauteur de la surface de glissement, et d'intercepter environ 45 % du flux hydraulique de la masse glissée. Des variantes portant cet espacement à 30 m, puis à 60 m, indiquent des abaissements de potentiel hydraulique de 34 et 30 m respectivement. Ces différences relativement faibles du point de vue hydraulique ont en revanche des implications beaucoup plus manifestes en termes de facteurs de sécurité. Au niveau des déformations (calcul couplé hydro-géomécanique), la présence de la galerie de drainage induit une forte diminution des déplacements prédits (de 101 cm dans la variante non drainée, à environ 15-20 cm pour les variantes). L'influence de l'espacement des drains sur le déplacement horizontal maximal prédit est peu marquée. Par contre, seul un espacement de l'ordre de 15 m permet un gain significatif de sécurité, indiquant un FS = 1.30, contre FS = 1.15 pour les autres variantes. Pour mémoire, la variante non assainie possède une sécurité de 1.05.

Mots clés : Hétérogénéité géologique, glissements de terrain, modélisation numérique, mesures d'assainissement

Table of content

"Be approximately right rather than exactly wrong."

John W. Tukey

1. Introduction

1.1 Scope of the thesis

Significant progress has been made these last decades in the development of hydrogeological numerical flow modelling for describing the hydrodynamic behaviour of landslides. However, these new sophisticated methods are still very seldom used in the problems of slope instability (Bonomi and Cavallin 1999; Parriaux and al. 2001a), in particular because of the hydrogeological complexity which characterizes them; thin aquifers, discontinuous media, succession of saturated and unsaturated zones, low permeabilities, high hydraulic gradients, lithological heterogeneity, strong contrasts of permeabilities and heterogeneous infiltration.

The numerical simulation of such problems is particularly convenient for clarifying the complex mechanisms that govern the movements and stability conditions of the slope, checking the coherence of the conceptual model, and for the simulation and prevision of movements in response to hydraulic pressure variations. These simulations usually aim to provide a tool for extrapolating, in time and/or space, some characteristics of the underground flows (i.e. hydraulic heads and hydraulic pressures), which can only be measured at a few points. Such models often provide a new understanding of the systems, beyond what can be observed directly in the field. In addition, complex aspects can be considered, such as the development of shear zone (Dounias et al. 1988; Troncone 2002), viscoelastoplasticity (Desai et al. 1995; Vuillet 2000) or weathering processes (Eberhardt et al. 2005).

However, few studies have been dedicated to the behaviour of very large landslides (i.e. volume greater than 1 million cubic metres and extending over several square kilometres). Such a combination of hydrogeological and hydromechanical finite element approaches has rarely been performed in studies of instability phenomena on such a scale and in three dimensions. The major difficulties in modelling such large phenomena are related to the huge area of instability, the geological heterogeneity, the unsaturated/saturated conditions of the slope and the difficulties linked to the assessment of the boundary conditions. These different points require a very accurate study of the phenomena to reproduce the real physical behaviour as closely as possible; namely, to assess critical hydrogeological conditions through an accurate phenomenological conceptualization.

Therefore, numerical flow modelling implies the use of a conceptual model (figure1.1-b) which can be defined as an image of reality. It is a theoretical construct that represents the studied system, with a set of variables (e.g. physical parameters of the underground) and a set of logical and quantitative relationships between them. It represents an abstraction which allows the complexity to be reduced according to specific objectives. Any complex field reality must be represented through a conceptual model in order to be understood and controlled.

Before the construction of this model, it is advisable to carry out some kind of inventory of these data, a synthesis laying out the current extent of knowledge. If the physical characteristics and processes of the reality are not correctly identified, the created numerical models will be marked by strong uncertainties. On the other hand, making reasonable simplifications of the true system at the time of its conceptualization means its behaviour can be better determined. Therefore, the accuracy of the numerical model is governed by the basic knowledge of the input parameters (e.g. hydraulic conductivities) and the boundary conditions.

These parameters will condition the hydraulic behaviour of the system.

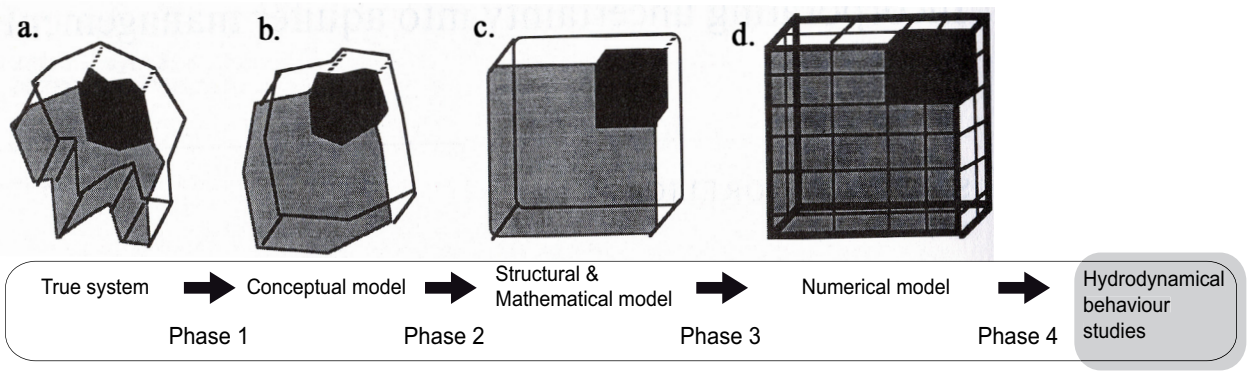

Figure 1.1: Procedure for model development showing heterogeneity and its representation, modified after Dagan and Neuman (1997). a. True system; b. Conceptual model; c. Structural & Mathematical model; d. Numerical model. The four phases of model conceptualization to simulation are summarized. Phase 1: corresponds to the development of the conceptual model and the associated field characterization. Phase 2: allows choosing the physical and mathematical framework of the problem. Phase 3: The structural & mathematical is discretized in finite element models. Phase 4: permits to validate the conceptual model thanks to numerical simulations, and to test various scenarios. Note that, this PhD thesis concentrates on phase 1, 3 and 4.

Depending on the scale of the study, the use of multiple data sets is required to constrain the interpretations of geological heterogeneity at a site (figure 1.2). Several direct or indirect field investigation methods are thus applied in order to define the main characteristics of the problem. It includes; geophysics, bore hole surveys, hydrochemical analyses, hydraulic well and infiltration tests, displacement measures, geotechnical laboratory testing. These methods allow the heterogeneity to be described, qualitatively and quantitatively. Some may delineate large-scale features, such as permeable channels, others may detect finer-scale facies transition (table 1.1).

One of the principal consequences of geological heterogeneity is that it can lead to significant variations of the fluid velocities over short distances and create preferential pathways. The existence of spatial variability of the hydraulic conductivities involves a spatial variability of the field velocities, and also a heterogeneous distribution of the resulting hydraulic pressure fields. The link between the underground geological heterogeneity of the medium, the heterogeneity of the underground flow and the hydraulic head distribution is not evident. In flow modelling, this link thus needs to be properly studied and understood in order to correctly interpret the output data (i.e. hydraulic pressures and heads). Some numerical and experimental studies have highlighted the fact that flows in heterogeneous mediums tend to be organized in more or less independent channels (Moreno and Tsang, 1994, Tsang and Neretnieks, 1998, Bruderer-Weng and al., 2004, Tiedeman and Hsieh, 2004). This channelling phenomenon is very little understood and is often evoked as one of the principal reasons for the incapacity of the traditional models to reproduce the observations.

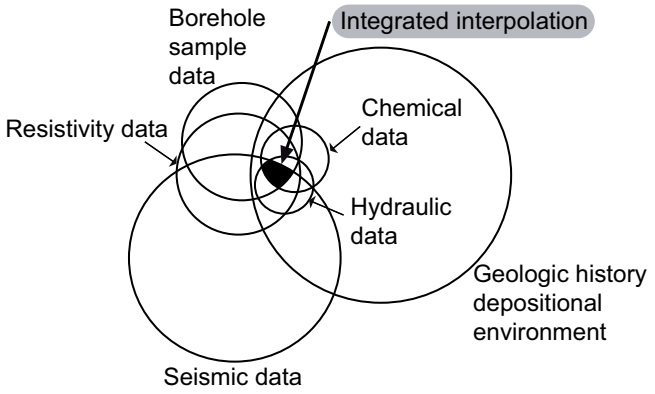

Figure 1.2: Use of multiple data sets to constrain interpretations of geological heterogeneity at a site (from Dagan and Neuman 1997).

Scale name:	Basin	Depositional environments	Channels	Stratigraphical features	Flow regime features	Pores
Approximate length scale	3 km– > 100 km	80 m–3 km	5 m–80 m	0.1 m–5 m	2 mm–0.1 m	< 2 mm
Geologic features	Basin geometry, strata geometries, structural features, lithofacies, regional facies trends	Multiple facies, facies relations, morphologic features	Channel geometry, bedding type and extent, lithology, fossil content	Abundance of sedimentary structures, stratification type, upward fining/ or coarsening	Primary sedimentary structures: ripples, cross-bedding, parting lineation, lamination, soft sediment deformation	Grain size, shape, sorting, packing, orientation, composition, cements, interstitial clays
Heterogeneity affected by	Faults (sealing) folding, External controls (tectonic, sea level, climatic history), thickness trends, unconformities	Fractures (open or tight), intrabasinal controls (on fluid dynamics and depositional mechanism)	Frequency of shale beds, sand and shale body geometries, sediment load composition	Bed boundaries, minor channels, bars, dunes	Uneven diagenetic processes, sediment transport mechanisms, bioturbation	Provenance, diagenesis, sediment transport mechanisms
Observations/ measurement techniques	Maps, seismic profiles, cross-sections	Maps, cross-sections, lithologic and geophysical logs, seismic profiles	Outcrop, cross-well tomography, lithologic and geophysical logs	Outcrop, lithologic and geophysical logs	Core plug, hand sample, outcrop	Thin section, hand lens, individual clast, aggregate analysis
Support volume of hydraulic measurements	Shallow crustal properties	Regional (long term pumping or tracer tests)	Local (short term pumping or tracer tests)	Near-well (non-pumping tests-height of screened interval)	Core plug analysis (permeameter)	Several pores (mini-permeameter)

Table 1.1: Classification of scales of sedimentary heterogeneity (from Koltermann and Gorelick 1996)

Landslides are a serious geologic hazard common to almost every country in the world, causing billions of dollars in damage and thousands of deaths and injuries globally each year. Very large landslides, most of them resulting from glacier retreat, and which may cover several square kilometres, are quite numerous in Switzerland (figure 1.3), for instance the *Cerentino* landslide located in Ticino (Southern Switzerland) with a volume of about 60 million cubic meters over an area of 0.85 km2. Most of these landslides occur in the Alps and the Prealps, although some have also occurred on the molassic Plateau or in the Jura range.
Areas that are generally prone to landslide hazards include existing old landslides and the bases of steep slopes. Areas that are typically considered safe from landslides include areas that have not moved in the past; relatively flat-lying areas away from sudden changes in slope (exception down for la *Vraconne* landslide).
A part from all types of loose quaternary sediments and fractured crystalline rocks, lithologies prone to landslide hazard include flysch sequences. In Switzerland, flysch sequences are widespread; covering about 6% of the national territory, they constitute thirty percent of the recorded instabilities in Switzerland.
Numerous studies have been carried out on these types of terrains in the last few decades to improve the understanding of the physical phenomena governing the hydrogeological conditions and the movements, including complete geological site investigations and advanced hydrogeological and geomechanical numerical modelling. Indeed, over the course of the last decade, the Laboratory of Engineering and Environmental Geology (GEOLEP) attached to the Swiss Federal Institute of Technology in Lausanne (EPFL) has taken part in important landslide remediation studies in collaboration with other offices and laboratories, performing complete three-dimensional hydrogeological models. Studies included the *la Frasse* landslide (Tacher et al. 2005 and Commend et al. 2004), the *Triesenberg* landslide (François et al. 2007), Steinernase (Locher et Tacher 2008) and the *Hohberg* landslide (Tullen 2002 and Tullen et al. 2006).
These studies allowed the following observations, which constitute the starting point of this thesis:

1. Predictive models of flow in the subsurface, which are often based on homogeneous porous media types of representation, are badly adapted to natural systems that are characterized by highly heterogeneous media such as landslides, in which the organisation of the heterogeneity is an important aspect of hydrodynamic behaviour.
2. These models which are very sensitive to environment geometry are good and reliable on a landslide scale (regional scale), but their quality may be affected on a local scale by these strong geological heterogeneities.

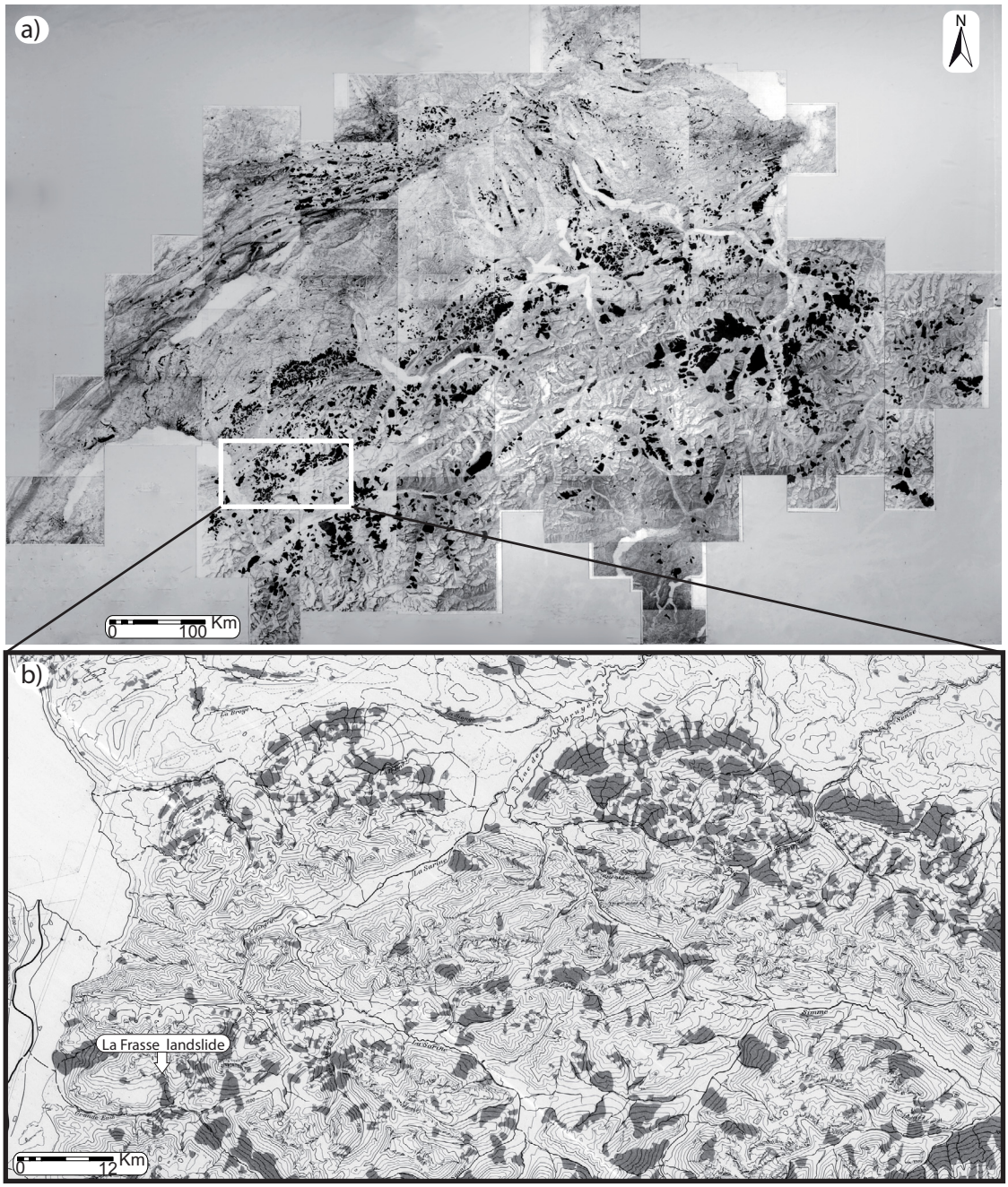

Figure 1.3: Cartographical inventory of landslides and rock falls in Switzerland (from Noverraz 1990); a) general situation, b) zoom on the "Les Préalpes vaudoises" region, with the geographical position of the la Frasse landslide.

3. The ability to predict the hydraulic response is strongly related to the input parameters. Thus, numerical flow models are reliable if the main aspects of the structure of the flow domain are captured and represented.

4. The geological heterogeneities of the subsurface take part in determining the hydrodynamical and geomechanical behaviour of landslides. However, their spatial distribution is partially unknown.

In addition:

5. In many environmental studies, the characterization of the lithological heterogeneity and spatial organisation is crucial, particularly when carrying out flow modelling.

6. Different methods of geological characterization may be used according to the scale of the study (regional, local, REV).

1.2 OBJECTIVES OF THE THESIS

To tackle the afore-mentioned problem, the principal objectives of this PhD thesis are:

(i) To carry out an integrated multidisciplinary characterization study on the internal structure of landslide in flysch and Quaternary environments, in order to clarify the organisation of the geological heterogeneities and to identify the hydrodynamic implications
(ii) To propose a conceptual model representing the geological architecture and the hydrogeological functioning
(iii) To examine the effects of heterogeneity and anisotropy on flow systems
(iv) To better understand the influence of geological heterogeneities on the mechanical behaviour of large landslides by performing numerical sensitivity analyses, by means of different heterogeneity scenarios on the field parameters
(v) Finally, to test the incidences on slope stabilization techniques; evaluation of the efficiency of a drainage gallery work

This doctoral study helps to answer the following questions:

Q1: Do these types of landslides share a common geological structure? Or should each case be considered individually?
Q2: What is the influence of a heterogeneous medium on the hydraulic pressure distributions? Is it possible to deduce a general behaviour from the geological context?
Q3: According to the geological context and the heterogeneity degree, how efficient will a given stabilization method be)?
Q4: Which stabilization method would be the most appropriate to each case study: limited works (boreholes precisely located) or, in reason of the underground structure complexity, more expensive general works (e.g. gallery with multiple drains).

Finally, as well as being applicable to engineering problems such as the role of the water in the instabilities, this PhD thesis also provides a developed and methodological scientific approach. For instance, it may also be of interest for applied sedimentological research because of the methods used for heterogeneity characterization purposes, including among others, the sophisticated Markov chain and the Hattori Entropy calculation for the characterisation of lithofacies.

1.3 SELECTED CASE STUDIES

The core of this study is based on the *la Frasse* landslide (Canton of Vaud). The choice of this reference landslide is initially justified by the regional geological context and by the quantity and quality of available data. Indeed, *la Frasse* landslide constitutes a reference case for deep-seated landslides in flysch environment at the national scale. Additional case studies have been consulted (i.e. *Triesenberg, Hohberg, Ballaigue, Travers, Creux de l'Enfer and La Lécherette*) for statistical studies on physical parameters, and for comparison purposes. The data contained in these case studies also allowed the establishment of a general conceptual model. Flow modelling was performed on the basis of theoretical models as well as on the three-dimensional model of the *la Frasse* landslide.
Table 1.2 provides a summary of the case studies examined and the methods used. Note that the data analysed in this study were either acquired in-situ in the framework of this PhD thesis, or might correspond to

data sets from former studies (in italic in table 1.2).

Methods	Analyses	Case Studies	Interpretation
Drill-cores logging	Facies distribution Markov analyses Entropy analyses	La Frasse	Vertical heterogeneity characterisation (1D) Horizontal (2D) Hydrogeological facies interpretation
Radiomagnetotelluric surveys (RMT)	Statistical studies on apparent resistivity data sets. Variography (spatial analyses)	La Frasse, Hohberg Triesenberg, Creux de l'Enfer Lécherette,Ballaigue, Travers	Heterogeneity characterisation and facies interpretation Structural considerations
Hydrochemistry	Cations/Anions, O^{18} analyses	La Frasse	Chemical variability, water sources and flow characterization and boundary conditions
Well test at horizontal drainage LFH1-2	Goodman and Jacob-Lohman (1952) analyses	La Frasse	Physical parameters determination of (K, T and Ss) and hydrogeological system analyses.
Seismic reflection surveys	*Tomography*	*La Frasse*	*Geological structures and substratum location*
Geomechanical data	*Descriptive statistic and regression analyses*	*La Frasse*	*Vertical geomechanical heterogeneity (1D)*
Infiltration tests	*Porchet analyses*	*La Frasse*	*Hydraulic permeability distribution*
Piezometric level analysis	*Annual fluctuation analyses*	*La Frasse*	*Hydrodynamic conditions*
Flow rates analysis at the borehole platform	*Annual fluctuation analyses*	*La Frasse*	*Flow variability*
Well test analysis at the borehole platform	*Porchet analyses*	*La Frasse*	*Hydraulic permeability*
Tracing test	*Tracer (Uranine) analyses*	*La Frasse*	*Groundwater origins and pathways*

Case studies location

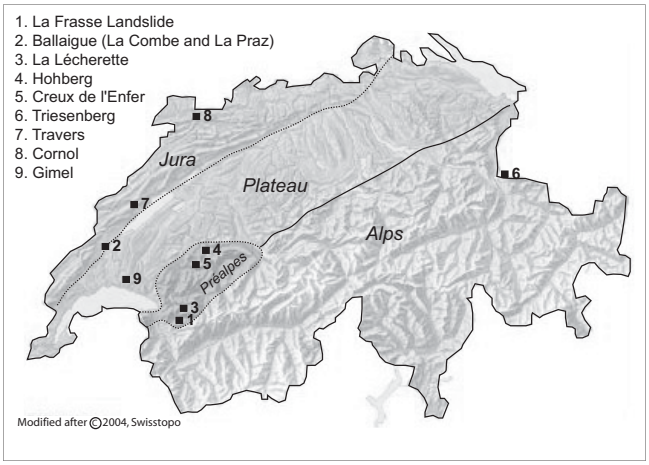

Table 1.2: Site investigation for the characterization of the geological heterogeneity: Case studies, methods, interpretations and geographical position. In italic, correspond the existing data re-interpreted in terms of geological/ hydrogeological heterogeneity and internal structures characterization in the framework of this PhD thesis

1.4 CONTENT OF THE THESIS

This PhD thesis is divided into 11 chapters:

The present chapter (**Chapter 1**) concerns the scope of the thesis and its main objectives. Short definitions of frequently used terms are provided at the end of the chapter.

Chapter 2 gives a short historical review of research on landslides. It states the basic principles of landslide studies and presents a few relevant cases.

Chapter 3 presents the general methodology and work flow. It introduces each method and the software used. Theoretical elements are given in the appendix I.

Chapter 4 "How to characterize the heterogeneity", concerns the "multidisciplinary" geological characte-

rization of the *la Frasse* landslide (Section 4.3). Numerous characterization methods are tested and a global conceptual model is proposed. In its introduction, the chapter presents the basic principles of "qualitative and quantitative" observation of the heterogeneity. A statistical study (Section 4.2) of apparent resistivity data sets from several landslides in flysch and quaternary deposits is performed. This allows primary conclusions to be drawn about the degree and the organisation of geological heterogeneity on a regional scale. A new approach for drainage design is discussed.

Chapter 5 concerns flow modelling. The information from the conceptual model of the *la Frasse* case is used for stochastic field parameter generation. The identified field data are traduced in statistical terms, allowing the generation of accurate heterogeneous media. These data are then used as input physical parameters for numerical model purposes. Next, the effects of the heterogeneity on the underground flows (i.e. hydraulic heads, pressure and velocity) are studied in detail. First, the relationship between the hydraulic permeability and the hydraulic pressure is explored through 2D and 3D theoretical models. Then, thanks to the *la Frasse* landslide FE model, a direct application on the importance of the integration of the geological heterogeneity for flow simulation is discussed. Various scenarios representing heterogeneous spatial distribution of the hydraulic conductivities are analysed.

Chapter 6 concerns the various incidences on slope stabilization techniques. The effects of hydraulic pressure on the mechanical behaviour of the slope and stabilization concepts are discussed. A practical application realized jointly in 2006 by the EPFL and GEOMOD SA in the framework of the stabilization work of the la Frasse landslide is presented. This is followed by an evaluation of the efficiency of a drainage gallery work with respect to hydrogeological and geomechanical parameter heterogeneity. Coupled hydrodynamic and geomechanical models allow the link to be shown between hydrodynamic displacements and safety factors. This last study was submitted to Landslides Journal in 2008.

Chapter 7 gives a global synthesis of the research; relations between geological heterogeneity and hydrogeology. It presents finally a conceptual model of the hydrodynamical functioning.

Chapter 8 concludes the thesis and presents the perspectives.

Chapter 9 gives all cited references

1.5 DEFINITION OF TERMS

The scope of this thesis "Geological heterogeneity in landslides: Characterization and flow modelling" refers to qualitative and quantitative descriptions of the geological underground structures. This incorporates the concepts of spatial distribution and organization and relates to some terms that may be ambiguous. The following terms are defined hereunder from the most general to the most specific one:

Variability. The term «variability», «the state or characteristic of being variable», may be applied to many different subjects: Human variability, genetic variability, heart rate variability. It may be a synonym to heterogeneity. However, it is used in this thesis in the frame of geostatistics studies; statistical variability and spatial variability. In statistics, statistical dispersion (also called statistical variability) is variability or spread in a variable or a probability distribution. Common examples of measures of statistical dispersion are the variance, standard deviation and interquartile range (e.g. in boxplot representation). Spatial variability is characterized by different values for an observed attribute or property that are measured at different geographic locations in an area. The attribute's spatial variability is assessed using spatial descriptive statistics such as the range, mean, standard deviation and coefficient of variability or regression or geostatistics.

Heterogeneity/homogeneneity. A homogeneous unit is one that has the same properties at all locations. In heterogeneous unit, hydraulic properties change spatially.

Anisotropy/isotropy. Anisotropy is the property of being directionally dependent, as opposed to isotropy, which means homogeneity in all directions. It can be defined as a difference in a physical property (hydraulic conductivity, refractive index, density, etc.) for some material when measured along different axes. Geological formations with distinct layers of sedimentary material can exhibit physical anisotropy in one direction (e.g. parallel to a layer). Most common geological environments are anisotropic due to inherited stratification or tectonic deformation (e.g. schistosity).

Scales. Dagan (1989) proposes the following classification for flow scales. 1) The REV scale (representative elementary volume) or core scale or laboratory scale, characterizes the dimensions of laboratory experiments. It is comprised between 10-1 meters and 100 meters. 2) The local scale, or site scale, is generally the order of depth of the aquifers, i.e. comprised between 101 meters and 102 meters, in the vertical and horizontal direction. This is the scale of well or tracing tests, this one for the underground flow and transport studies. On this scale the study is mainly three-dimensional. 3) The regional scale, or massif scale, of an order of 104 meters and 105 meters on the horizontal plan, corresponds to aquifers which extend further laterally than vertically. The physical variables are defined as average values in depth and the flows as bi-dimensional.

Low permeable porous environments. The term of "low permeable porous environments (LPPE)" has been defined to describe all landslides occurring in environments of loose sediments. It includes all landslides in flysch zones (*Gurnigel, la Simme and Niesen*) and those taking place in quaternary deposits (morainic terrains and fluvio-glacial drifts). They are different in terms of geological settings and inheritance, but hydrogeologically (i.e. physical parameter distribution, flow behaviour) they are very similar. Mainly composed of a very impermeable matrix, flows occur locally in connected to disconnected high permeable features.

Low permeable mass (LPM). The term of "low permeable mass (LPM)" has been defined to characterize the geological mass forming the landslides, occurring in low permeable porous environments (LPPE); such as flysch and quaternary deposit units (glacial drifts). This material is characterized by a low hydraulic conductivity, varying between 1E-6 and 1E-9 m/s, with locally high permeable zones (>1E-4 m/s), represented by intercalated fine to coarse grained sandstone beds. Regional groundwater circulations are rather limited, and form local interconnected aquicludes. This impermeable mass in general fulfils the role of the capacitive function of the aquifer system, and the intercalated permeable beds the conductive function.

High permeable features (HPF). This expression has been defined in this dissertation to characterize the high permeable zones present in the low permeable mass (LPM) of the slides. In fact, inside the low permeable mass (LPM), intense fracturing and over-trusting of the flysch mass enable rapid groundwater flow through open fracture networks. The structure and organisation of these secondary high permeability zones are not well defined. As they can extend over hundreds of meters, they can also form small disconnected lenses. The origin and shape of these high permeable features is not well defined either. As they can include sandy to gravely lenses, it also can be a matter of fractures. Therefore in this thesis the aforementioned definition includes channels, conduits, network fractures or apertures. Hydrogeologically, they equally represent the heart of the preferential channelized flow paths.

Capacitive/conductive function (CapF/CF). Terms applied to an aquifer whose behaviour is characterized by a heterogeneity and a partitioning of the reservoir which result in two principal types of functions: A conductive function, which gives place to fast flows in the inter-connected high permeable features (HPF) and which, in landslide problems, may explain the great variations of the hydraulic pressures. A capacitive function provided mainly by the low permeable mass (LPM) which is the seat of very slower rates of flow and authorizes a variable storage capacity and hydrochemical reactions. Note that these terms are actually used in karst hydrogeology, but their application to landslide problems to explain the observed phenomena

is adequate.

Channels. The term channel is commonly used in fractured media hydrogeology. Long and Billaux (1987) make a clear distinction between two important processes: fracture channels and channelized transport (or flow). A fracture channel is defined as a long narrow region of enlarged aperture formed at the intersection of two fractures or by processes such as shearing or high tectonic deformation. Channelized flow results from the non-uniform velocity in a variable-aperture fracture. The terms channel and channelling are used in both cases. In this thesis the aforementioned definitions won't be used directly. The terms channels and channelized flow, will be used to define preferential flow or rapid paths through more permeable regions.

Discontinuities. A discontinuity is a collective term referring to all structural breaks in rocks. Discontinuities comprise joints, bedding, shears, contacts, veins, and faults. Geological discontinuities represent a rupture of spatial continuity, and often have important repercussions on flow distributions.

Spatial continuity, correlation lengths and connectivity. These three terms are often linked, and used as synonyms. They are used to describe the organization of the geological structures of the media.

Connectivity. It defines the ability that a hydrogeological system may have to link different aquifers together by the means of high permeable features (HPF). The more developed the connectivity (high spatial connectivity), the more the system will be hydrodynamically controlled by its conductive component.

2. STATE OF THE ART

2.1 LANDSLIDE GENERALITIES

2.1.1 THE ROLE OF WATER IN LANDSLIDES

Several statistical analyses, carried out in particular in France, on the causes of the release of slope instabilities confirm the hydraulic origin of these phenomena. For instance, Desvarreux (1988) observed that for 250 slides, the causes were in 52% of the cases attributed to a hydraulic origin, confirmed by Lacube & Durville (1989), with a percentage of 61%. Gervreau (1991) validates these results with a statistical analysis on about fifty examples, indicating that half of them (49%) were to be associated with hydraulic phenomena, whereas 31% were related to the human activity, and the remaining 20% generally allotted to seismic phenomena. In addition, surface flows can induce external erosion which might modify the geometry of the slope and consequently weaken the conditions of stability.

The water recharge of an unstable slope is explained by various mechanisms, the main ones being the following:

1) Direct recharge: The infiltration velocity in a medium with interstitial porosity is controlled by the water content and the permeability of the ground. However, the unstable slopes are often characterized by one or more discontinuity networks (geological medium structures, fractures extension, etc) which significantly influence the infiltration of water. The following sources of infiltration are: rain (direct contributions), snow (delayed direct contributions, i.e. snow melt), hydrological network (rivers, lakes), glaciers (water infiltration due to glacier melt) and anthropic activity.
2) External recharge: Water infiltration coming from a catchment area different from the watershed of the studied site via complex underground networks.

This alimentation has three principal effects on the unstable slope:

1) Effects on the underground properties (increase of the degree of saturation):
- *An increase in the specific weight of the ground:* The factor of safety decreases when the specific weight increases.
- *Reduction in the forces of capillarity:* The stability of a slope decreases with the reduction of the forces of capillarity.

2) Hydrostatic effect:
- *A rise in the water table:* When the infiltration front reaches the water table, the piezometric level rises. This causes an increase in the hydrostatic pressure, a reduction in the total constraint and consequently increases the risk of rupture of the slope.

3) Hydrodynamic effects:
- *Seepage forces:* The solid-liquid system is subject, other than the force of gravity, to a field of forces consisting physically in viscous frictions related to the flow, which are transmitted to the grains of the solid phase of the ground. The flow is slowed down by the porous environment and transmits to the system mechanical efforts. These forces may also induce a suspension of the sediments, thus increasing the intrinsic permeabilities and the hydraulic flow and, thus, a reduction in the mechanical resistances (Reid, 1997).
- *Soil clogging:* Contrary to the percolation forces, the clogging results from the deposit of the fine particles contained in the liquid phase in the interstices of the porous environment. This phenomenon causes a

reduction in the intrinsic permeability and may change the hydraulic conditions and the pore water pressure (Frenette, 1964; Reid, 1997)

- *Decrease of the viscosity:* The presence of water increases the soils moisture and consequently decrease the viscosity

- *Modification of the elasto-plastic components of the movements:* The variation of the pressure acts on the consistence degree of the rock fabric. The water pressure reduces the available shear resistance on the discontinuities and determines active forces which tend to induce sliding. The increased pore pressure reduces the normal stress and thus the frictional strength.

2.1.2 GROUNDWATER FLOW IN LANDSLIDES

The problem of water flow through rock mass can be analysed as seepage through a porous media problem in some particular conditions of homogeneous or of equivalent homogeneous media. In this case, the seepage problem can be of a confined or unconfined type. The formulation of the flow is based on the Darcy law which states that the flow velocity is proportional to the hydraulic gradient in the flow direction. The constant proportionality is termed as the permeability coefficient. The Darcy equation is valid for linear flow with very small Reynold number values. Stability analysis can be carried out by coupling the mechanical and the flow problem even in the porous medium case. Numerical models are used to compute the variation with time of displacements, pore pressures, effective stresses and flow velocities in the discretized domain.

The choice of the flow model is of fundamental importance as far as the problem of water flowing through a rock mass is concerned. Louis (1976) divided the rock masses according to their defects and fabric into the groups which are here reported with specific references to slope stability problems (figure 2.1):

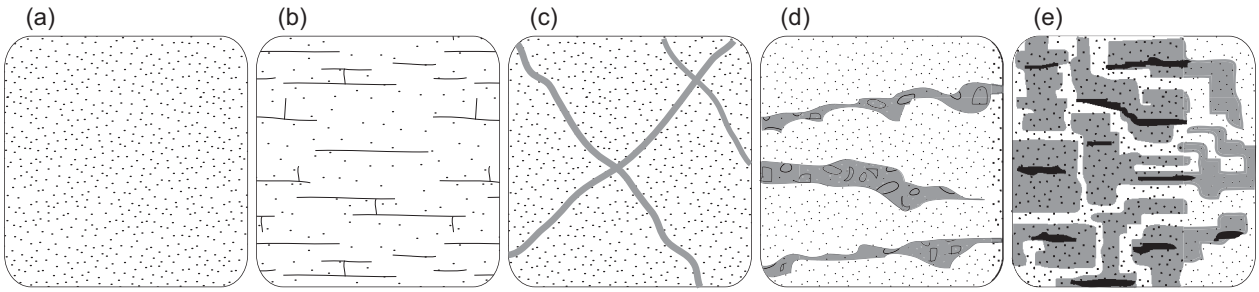

Figure 2.1: Types of media occurring in rock mass: a) Porous medium; b) Porous jointed medium; c) Porous medium with impervious barriers; d) Porous medium containing channels; e) Karstic medium.

a. Porous media, mainly homogeneous, containing only small pores

b. Porous jointed media in which fissures determine the hydraulic behaviour of the rock mass

c. Porous media containing impermeable barriers in which discontinuities are filled with an impermeable material and where rock bridges provide hydraulic connections.

d. Porous media with small channels in which water can flow and in function of the connectivity may determine the hydraulic behaviour of the rock mass.

e. Karstic media containing wide passages and caverns of various geometrical forms, created by the solution and the removal of the rock by underground water.

The rock masses are thus divided into these groups according to common types of flow passages. However, the choice of modelling a rock mass as a continuous or discontinuous medium still depends on the relative scale of slope problem.

2.1.3 HETEROGENEITY OF LANDSLIDES

Although heterogeneity relates to many physical parameters of the geological mediums, we are interested here, more particularly, in the heterogeneity of hydraulic conductivity. Hydraulic conductivity is commonly the parameter which interests hydrogeologists the most given its high heterogeneity in the majority of natural systems, and its fundamental importance in the control of flow velocities and the distribution of hydraulic pressures. Landslides are characterized by an extremely heterogeneous media, both vertically and horizontally. To the geological heterogeneity corresponds hydrogeological, mechanical and hydrochemical heterogeneity. In general a second heterogeneity due to the intense fracturing and over-trusting of the instable mass adds to the initial heterogeneity of the geological formation. The detail of this heterogeneity is unknown elsewhere than at the drilling of boreholes (very local scale), so that its representation on the scale of the slide (regional scale) is generally illusory. These contrasted permeabilities often pose in an accurate way the problem of the representativeness of the field measures. The spacing between the measured or sampled boreholes must thus be based on a prior knowledge of the extension and the dimension of the geological heterogeneities.

2.1.4 STRUCTURAL CHARACTERIZATION

The purpose of structural characterization is to describe in detail the geological medium in which the instability occurs. It comprises direct and indirect methods, and allows partial observation of the organization of the geological heterogeneities. For instance, borehole surveys (direct method) obtain precise and local information on the vertical of a given point. Geophysical surveys allow evaluating the geometry or the volume of the sliding mass in an indirect way. The physical parameters, such as hydraulic conductivity, can thus be given help to several investigation techniques, by direct or indirect observations, but the representativeness of the measure remains the principal problem. It is consequently important to recognize that each method of measurement is characteristic of a scale of observation (Gelhar 1993).

2.1.5 ANALYSIS METHODS

The classical approach to study slope instability problems, based on the establishment of the relation between hydroclimatological parameters and displacements, is interested exclusively in the causes and the effects. It does not develop the processes induced by these causes and responsible for the effects. This "black box" relation is in certain cases satisfactory, but in others, the analysis of the induced hydrogeological processes becomes essential to understand the functioning of the instability phenomenon and to predict the movements. Moreover, the analysis of landslides is most of the time based on analytical methods or numerical methods of deformation modelling. These approaches, mainly based on mechanical aspects, allow the integration of hydraulic parameters in certain cases.

2.1.5.1 ***Analytical methods***

Analytical methods are known under the term of Limit Equilibrium Methods (LEM). This approach consists in subdividing the two-dimensional field into a succession of sections of identical width to allow calculation of a factor of safety (Lambe & Whitman 1969). These static methods of calculating allow a simulation of the field conditions with fixed parameters (deterministic method) or variables (probabilistic method). They make it possible to integrate hydraulic parameters which are simplified by hydrostatic conditions, represented by one or more piezometric levels (Crosta, 2001, Fabre and al. 2000, Grivas& Chowdhury 1988 and Prina 2000). These methods are well adapted for simple cases, without significant three-dimensional

effects. On the other hand, simplifications of the hydraulic conditions mean that these models are not very representative of the complex hydrogeological processes because one varies the water levels arbitrarily to test their influence on the stability of a model. Consequently they are not adapted for hydrogeological analyses of an unstable slope, and this, more particularly in a transient mode. These methods do not allow the integration of three-dimensional effects, which may play a predominant role.

2.1.5.2 Numerical methods

The numerical methods of deformation modelling are more developed than the analytical methods and allow consideration of hydrodynamical parameters for saturated or unsaturated mediums, in steady or transient flow. However, these tools were developed with an aim of solving geotechnical problems such as the realization of an excavation, a tunnel or an earth-filled dam and are, consequently, not well adapted to simulate the realistic hydrogeological behaviour of an unstable slope. Geological media, which often include thin and pinched structures are difficult to discretize. Finally, considering transient boundary condition variations is sometimes problematic.

2.1.5.3 Hydrogeological flow modelling

To fill these gaps, the Laboratory of Engineering and Environmental Geology (GEOLEP) attached to the Swiss Federal Institute of Technology in Lausanne (EPFL), has specialized for a decade in the hydrodynamic flow modelling of these unstable slopes. In collaboration with several geological offices, and in particular with the Laboratory of Soil mechanics (LMS) of the EPFL, the landslide of the *la Frasse* (Vaud), *Hohberg* (Fribourg), *Triesenberg* (Liechtenstein), and more recently *Steinernase* (Aarau) have been the subject of very detailed three-dimensional numerical studies (Parriaux et al. 2001a, Tullen 2002, Commend et al. 2004, NCG+EPFL 2004, Tacher et al. 2005, François et al. 2007). These hydrogeological numerical models combined with hydromechanical models proved to be essential and complementary tools in the forecasting of unstable slope behaviour during climatic crisis. In the PhD thesis of Tullen (2002), three landslides were analyzed and modelled, demonstrating likewise their utility in the validation of conceptual models. This study could also show the current limits of this method. The experience gained in these various studies shows that the models are sensitive to the detail of the value and the spatial distribution of the hydrogeological parameters (e.g. permeability, storativity, porosity, effective infiltration, unsaturated parameters).

Dimensionality of the models. Two-dimensional modelling (2D) of a three-dimensional natural system (3D) constitutes an advantageous simplification (e.g. preparation of input data and iteration velocities), but accuracy of the results may be unacceptable. The vertical 2D model supposes the constancy of the hydrogeological parameters until infinite, in the perpendicular horizontal direction. In the case of a well, the imposition of a head boundary constitutes a horizontal infinite drain. Besides, the surface recharge conditions and the eventual relation to the bedrock may not be differenced laterally, and an eventual alimentation from the lateral boundaries of the slide is rather difficult to represent. This accumulation of assumptions produces a model whose hydraulic flows do not have a lateral component. On the contrary, the horizontal 2D model supposes the homogeneity of the hydrogeological parameters on the whole thickness of the slide. The calculated flows thus do not have a vertical component, which is particularly penalizing if a sliding surface exists with hydrogeological parameters differing from those of the moving mass. These models do not allow representation of a recharge from the surface (i.e. effective infiltration) and possible drainage by the substratum at the same time. Similarly, the imposition of a head potential representing a local source constitutes a complete well in the model. Moreover, if geomechanical modelling is coupled, the calculation

won't have any utility since the geomechanical model, by principle, differentiates the different constraints and the movements according to the depth. Therefore, in landslide problems, these reductions are unacceptable as the problems are fully three-dimensional. However, note that in particular cases if there is a sliding surface in the concerned problem, calculation may be performed on two-dimension only on this surface.

Flow characteristics. In soil mechanics the geomechanical mechanisms describing the landslide behaviour require temporal variations of the hydraulic pressure fields, since the elastoplastic deformations are generated by these variations of pressure. Consequently, the hydrodynamic responses of the hydrogeological modelling, then coupled to geomechanical models, are valuable only on the basis of transient simulations. Transient simulations in saturated medium require the assessment of the storage compressibility coefficient (Ss) which governs the amplitude and velocity of the response of the model on the variations of infiltrations. This coefficient takes appreciably different values according to whether the aquifer is free (for example. Ss = 0.1 [-] = effective porosity) or confined (for example Ss = 1E-4 [-]). The smaller the value; the stronger the variations of the hydraulic head in response to infiltration events are. However, underground flow in landslides may be represented, due to the strong heterogeneity and the discontinuity of the medium, as an entanglement of small, more or less connected, free and confined aquifers. Under these conditions, prudence calls for initially choosing confined Ss values, even if the nervousness of the system is slightly over-estimated.

Thus, generally, slope stability analyses are typically carried out for saturated conditions, however, recent theoretical and experimental works point to the occurrence of shallow landslides in the absence of widespread areas of positive pore-water pressure. The strong influence of the unsaturated zone, notably in transfer processes (recharge-discharge) should be taken into account. The aquifers in landslides always present an unsaturated zone of variable thickness. Taking this zone into account is very expensive in computing times, and requires the introduction of physical parameters, in general insufficiently known (i.e. permeability according to saturation, suction according to saturation. etc). Meanwhile, the problem is slightly different for deep-seated landslides, where the assumption of a general saturated medium is applied, justified and accepted (Tacher et al. 2005). In many cases, the movements are concentrated according to a sliding surface. The assumption that the overlying volume of rocks moves without internal movements can be made, so that hydrogeological modelling will be focused on a precise calculation of the hydraulic heads on the sliding surface. If this surface is located in the saturated zone (i.e. *La Frasse* landslide), a saturated model constitutes an acceptable approximation. If, on the contrary, the sliding surface is not very deep (shallow aquifers), partially or temporarily desaturated (i.e. *Triesenberg* landslide), it is essential to take into account the variable saturation. In fact, the forces of suction (negative pressures) in the unsaturated zone strongly differ according to the mode of calculation, in particular for low permeability media. Finally, if the movements are distributed over the whole thickness of the slide (i.e. *Villarbeney* or *Falli-Hölli* landslides), it is also necessary, in case of geomechanical modelling, to systematically take into account the saturation state of the ground since the suction influences the cohesion of the material.

Therefore, the choice of the modelled problem (saturated or unsaturated) depends on the natural environment, and in particular on the size of the unstable mass, the problems to be solved, the capacity and the speed of the computers, and financial aspects. In this study mainly concerning the la Frasse landslide, the problem is treated thanks to transient saturated models.

2.2 METHODOLOGICAL APPROACH

Tullen (2002) proposed a methodology allowing a better understanding of the hydrogeological processes caused by particular hydroclimatologic conditions. It aims to determine the relation between hydroclimatologic phenomena and a critical hydrogeological state, which can lead a phenomenon of instability to reactivation or to a state of rupture. And while this relation may not be approached in the same way for all instabilities throughout the world, Tullen (2002) presents a hydrogeological typology of unstable slopes in order to establish this relation individually.

Accordingly, he proposes a methodology comprising a succession of stages that are useful for the understanding of the hydrogeological processes. This approach aims at establishing a hydrogeological assessment on the scale of the slope or, if necessary, on a regional scale, in order to determine groundwater infiltration zones, trajectory and velocity of groundwater run-off as well as outlet areas. Thus he proposes a complete methodological approach to improve the understanding of the groundwater run-off systems for the unstable slopes:

- A characterization of the geological domain based on geophysical measurements in addition to the borehole data. This approach, original in the specific context of unstable slopes, makes it possible to obtain a three-dimensional representation of the heterogeneity which composes the subsurface grounds in a fast, efficient and economic way.
- A spatialization of the climatologic observations in order to take into account the distribution of the precipitations while considering the various states (rain and/or snow) that constitute the water contribution to a slope in relation to altitude.
- A hydrogeochemical characterization of the outlets, which makes it possible to assess the general groundwater circulation system within the slope, and to come to a decision about one or several possible trajectories of groundwater run-off.
- An isotopic characterization of the outlets, which allows an estimation of the altitude of infiltration of the groundwater. This characterization can also give some information on the infiltration zones. These methods also make it possible to characterize the general groundwater run-off system. In some cases, it is also possible to come to a conclusion, quantitatively speaking, concerning the mixing between several reservoirs and to estimate the time of residence of the water in the aquifer system.
- A qualitative validation of the assumptions on the basis of artificial tracing tests which will attest the existence of hydrogeological connections between a catchment area and an outlet. This approach will also provide information about the time of residence of water.
- A validation of the conceptual model on the basis of a bi- or three-dimensional numerical simulation of the groundwater run-off in order to validate the hydrological and hydrogeological relations. The calibration of these numerical models is based on a set of hydrogeological data, in particular the outlet discharge, the isotopic composition of water and/or their hydrochemical composition. These strictly hydrogeological numerical simulations can then be translated into a mechanical state to evaluate the stability of the slope.

Not all of the points suggested by this methodological approach are always essential to determine the hydrogeological processes that govern each slope. According to the characteristics of each study site and the means at disposal, some could be treated only partly, or not at all, depending on the established objectives. A hydrogeological typology of the unstable slopes should permit to propose a standard methodological approach and specific tools for analysis in direct relationship to the hydrogeological context which charac-

terizes each slope. The methodological approach suggested in Tullen (2002) was tested and validated on three representative sites through Switzerland and the alpine arc that present quite distinct characteristics of hydrogeological functioning; *Hohberg* (Fribourg), *Triesenberg* (Principality of Liechtenstein) and *Peney* (Geneva).

2.3 RELEVANT CASE STUDIES

2.3.1 LA FRASSE LANDSLIDE

The *la Frasse* landslide is situated in the "Préalpes Vaudoises" between Aigle and Les Diablerets. A complete description of this slide is given in Chapter 4.3. Thanks to a sophisticated transient hydrogeological modelling allowing the determination of the pore pressure fields in *la Frasse* landslide mass during a crisis, it has been possible to model the mechanical behaviour of the slide and obtain results that prove to be similar to the monitored data, in terms of peak velocity, distribution of velocity with time and space and total displacements (Tacher el al. 2005). Such results are reached only when appropriate constitutive modelling laws are used, and when geotechnical tests supply all the required parameters. The main results concern the potential effect of a drainage system during a crisis, like the one experienced in 1994. It can include vertical boreholes equipped with pumps or drains drilled from a gallery. The draining system reduces horizontal displacements down to 5% of the values modelled during the crisis. This effect, which appears to extend over a large width, will be even more significant if the boreholes discharge the drained water into the gallery, due to its extension in the presently stabilised landslide mass below the active zone. The modelling tools developed for *la Frasse* landslide thus provide all the necessary information to optimise the drainage scheme.

2.3.2 TRIESENBERG LANDSLIDE

The *Triesenberg* landslide (coordinated 760'000/221'000) is situated in Liechtenstein between Balzers and Vaduz. It is a very old slide at least 8'500 years (dating 14C) and represents a total volume of approximately 400 mio mP3. It covers a surface of approximately 5 kmP2 and its altitude varies between 460 and 1350 ms.m. The depth of the active zone is approximately 10 to 15 meters, locally up to 20 meters. It affects the villages of Triesenberg (situated inside the sliding area) and Triesen (located at the toe of the slide). Since the end of the seventies, periodic observations (geodesy and inclinometry) have been performed. A stabilization project on a large scale, elaborated in 1991, envisaged a drainage system around 8 km length to collect the sub-surface waters.

The hydrogeological analysis and modelling were carried out by the GEOLEP and Bernasconi Consultant (Sargans, CH), with the aim of understanding the hydrogeological behaviour, assessing the effects of climate change and supplying the geomechanical models with groundwater pressures as daily boundary conditions (François 2007 and Bernasconi-GEOLEP-LMS_final report 2006). The main results are (i) the link between the movements and the variation of the water pressure, as the major causes. (ii) The active zones are very limited in space and may be mitigated by drainage. And (iii) the increase in water pressure variation to simulate an extreme unfavourable case does not cause a general instability. It shows that the risk of a sudden collapse of the slope is very low, even in the perspective of critical climate changes.

2.3.3 HOHBERG LANDSLIDE

Three methods were combined to determine the groundwater recharge and transfer processes of a landslide prone area (Tullen et al. 2006). First, the radiomagnetotelluric method was used to investigate the distribution of electrical resistivity (ρ) of the subsurface and build a three-dimensional model of permeability (k),

through an experimental relation between ρ and k. Second, this structural model of permeability and additional climatologic data were used to fix boundary and recharge conditions to perform a three-dimensional and transient numerical simulation of the groundwater flow. Finally 18-Oxygen time series observed at the main springs were used to calibrate the model. This association of methods led to an improved characterization of the groundwater flow system on the local scale and a better understanding of the role of this system on the landslide phenomenon. This structured approach is thought to be useful in the design of specific remediation strategies to drain the unstable mass.

2.3.4 STEINERNASE LANDSLIDE

This last case is currently a PhD research in progress at the GEOLEP, and was presented at the European Geosciences Union General Assembly 2008 in Vienna (Locher and Tacher 2007). The *Steinernase* case is an evapo-transpiration controlled landslide in Switzerland between Zürich and Basel. The whole slope is creeping with faster sliding parts attending velocities up to 6 cm per year respectively 4 cm per month during crises. The slope is located in the forest, dipping 25° northwards and lies between 510 and 280 ms.m. The biggest sliding area in this slope covers about 130’000 m2 of which 30’000 m2 are sliding faster. It is a translational slide with a sliding surface at a depth of 3 (top of the slide) to 20 meters (on the base of the slide). Because of several slope stability problems during the building of the roads and the railroad, the slide has been studied since 1911. Some special relationships were discovered through analysis of the different data: From the inclinometer data it is obvious that acceleration phases occur mainly in winter. The piezometric heads clearly have seasonal variations, with a drop in summer and a rise of the water table in winter. Further on, only rainy winters lead to an important acceleration of the sliding mass, which leads to the assumption of a threshold effect. But in contrast to the movements, the precipitations are spread over the whole year and the area doesn’t have important snowfall or soil freezing to explain seasonality. The explanation proposed is evapo-transpiration; the whole area is covered by foiled trees especially beeches which consume a large amount of water during the vegetation period and nearly nothing during winter. Apart from the trees, the soil is completely uncovered and the rain can infiltrate directly during wintertime. The runoff is estimated to be very small due to the rough topography. The evapo-transpiration is calculated with a water balance model called WBS3 which was developed by Matzarakis et al.(2001) at the meteorological institute of the University of Freiburg (Germany). With the hydrogeological model (Feflow 5.2) and the calculated infiltration, the slope hydrology can be simulated and the piezometric heads are then used as input for the geomechanical model to simulate the movements.

3. METHODOLOGY OF THE THESIS

This dissertation consists of three distinct steps; geological-hydrogeological characterization, theoretical flow modelling and a practical application of 3D flow modelling on the *la Frasse* landslide to test heterogeneity and to evaluate the efficiency of a drainage gallery work. The description of the used methods and the theoretical development is exposed in the appendix I, as well as the different used software. See work flow in figure 3.1.

The first step of this PhD thesis (how to characterize geological heterogeneity) presents a multidisciplinary characterization. First, a general study on several landslides occurring in low permeable units (flysch and quaternary deposits type) is performed thanks to geophysical data sets. It allows a general concept on the geophysical variability of such instabilities to be put forward. The elaboration of new approach for the design of drainage system is discussed. Secondly, numerous investigation methods are applied to the la Frasse landslide to better understand the distribution of the underground heterogeneities and their mean implication on the hydrodynamical behaviour. It comprises radiomagnetotelluric surveys, hydrochemical analyses, lithofacies analysis, seismic reflection surveys, infiltration and well tests, flow rates analyses and tracing analyses. For each method several tools for analysis are used to qualify and quantify the degree of heterogeneity. This includes, for instance, vertical facies analysis, embedded Markov chain analyses and entropy estimations applied on the borehole logging data. Descriptive statistics and spatial exploratory analyses (i.e. variogram studies) are used, for instance on geophysical data (radiomagnetotelluric investigation), to define the variability of the studied systems and their spatial continuity. Hydrogeological data are handled thanks to Lefranc analyses, and flow rate measurements interpreted with the formulations of Goodman (1965) and Jacob and Lohman (1952). This study enables a discussion of the underground architecture (geological structures) of the medium, the hydrogeological functioning (i.e. conceptual model) and general considerations about the field application of the different methods. The detailed and integrated multi-disciplinary approach of this study allows first building a general concept (section 4.3.11) and then a global model of the hydrogeological functioning of this type of landslides (chapter 7).
Note that, concerning the section 4.3 “Heterogeneity characterisation test on the *la Frasse* case” short conclusions are formulated under the subsection “Hydrodynamical implications”. An overall synthesis on the *la Frasse* landslide is made in sections 4.3.11 and 4.4.
The second step (how to use the geological heterogeneity) studies the effects of heterogeneities on steady and unsteady state flows in porous medium. To better understand the influence of various parameters describing the geological heterogeneity, sensitivity analyses are performed on 2D and 3D groundwater numerical models. Numerical models are used to investigate the effects of spatial variability of hydrogeological parameters (hydraulic conductivity) on the hydraulic pressures and velocity distributions. The following quantities are investigated for these parameters: mean, variance (heterogeneity), correlation lengths (anisotropy) and the “channel” connectivity (spatial continuity). The types of models are 2D/3D, steady/unsteady, saturated/unsaturated flows, and concern both schematic and real studies (i.e. *La Frasse* landslide). By performing numerical sensitivity analyses on the *la Frasse* finite element model, the influence of geological heterogeneities on the behaviour of this large landslide is examined. The uncertainty on numerical models can be tested by means of different heterogeneity scenarios on the field parameters.
The third step evaluates the efficiency of civil engineering works according to the heterogeneity of the medium. In the framework of the stabilization work of the *la Frasse* landslide transient hydrogeological and geomechanical models were realized jointly in 2006 by EPFL and GEOMOD SA. The aims are the evaluation of the efficiency of the drainage gallery below the sliding mass during a crisis in terms of reduction of

the deformation velocities. In addition, the increase of the factor of safety of the landslide is evaluated.

Finally, in chapter 7, thanks to the integrated multidisciplinary study performed in chapter 4, 5 and 6, a synthesis on the global functioning model of the studied landslide types is proposed.

This series of investigation made it possible:
1. To propose a geological-hydrogeological conceptual model for landslides occurring in low permeable porous environments (incl. flysch and glacial quaternary deposits) based on several case studies and on the *la Frasse* landslide.
2. To identify the main effects of the underground heterogeneities on flow systems; particularities, organization and the implications on the stability.
3. To carry out a complete numerical investigation on the efficiency of a drainage gallery work in a large landslide, with respect to hydrogeological and geomechanical parameter heterogeneity.
4. To formulate constructive recommendations in the framework of site characterization and numerical flow modelling, and to propose a new approach concerning the design of drainage systems.

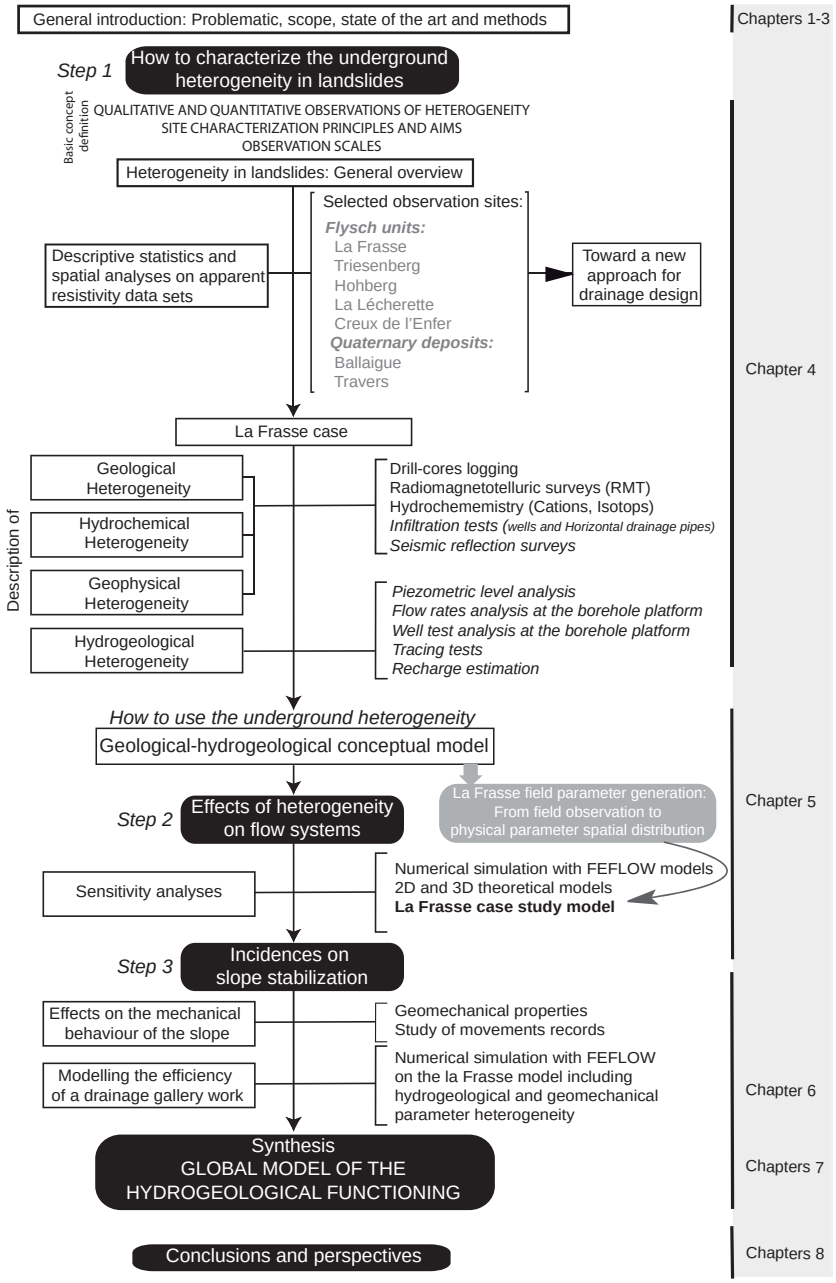

Figure 3.1: Work flow of this PhD thesis: Methodology and structure

4. How to characterize geological heterogeneity in landslides

4.1 Quantitative and qualitative observations of heterogeneity

4.1.1 Site characterization principles and aims

In a first step, the characterization of an instable site involves gathering and analyzing data to describe the morphological, geological, geomechanical, hydrogeological and hydrological properties that may be responsible of its instability. It provides the understanding of the present state based on past behaviour, and permits to predict the main future evolutions. The geological characterization realized thanks to borehole sampling and field observation describes the medium in which the instability occurs, and secondary in which the groundwater flows are taking place. It is essential to define the degree of heterogeneity and the global organization; material distribution and the spatial connectivity of the system. It encompasses the characterization of the instability itself as well as that of the surrounding units and the underlying bedrock, assessing the boundary conditions such as the principal zones of infiltration (recharge conditions). The hydrogeological characterization realized thanks to well tests, tracing tests and water level observations, defines the main organization of the aquifers and their main physical parameters; the hydraulic conductivity, the porosity, the storativity coefficient and transmissivity. It may also precise the spatial connectivity and the particularities of the various flow pathways.
Groundwaters are often the most significant factor of instability and the least characterized. For this purpose the hydrochemical analyses, besides the other methods, allows to differentiate the sampled waters function of their composition (cation ratios and isotopes) and their origin. Flow pathway and network may thus be drawn. The hydrological characterization allows principally defining the recharge of the system (boundary conditions) through past and present rain evens, and links surface and underground flows (inlets and outlets). Therefore, a multidisciplinary approach in site characterization permits quantitative and qualitative observations of the degree of heterogeneity of the system. And thus, it allows specifying the uncertainty on hazard assessment and, for instance, on the efficiency of a projected stabilization work.
In a second step, as the knowledge of the site becomes more detailed, the collected data are synthesized thanks an integrated conceptual model in two or three dimension. Finally, in a third step, this structure is described in detail into parametrical and geostatistical terms and may take the form of either a numerical or analytical models.
In the meantime, the different results have to be handled with precaution while the used method is scale dependent and has to be interpreted as such. The high heterogeneity of the hydrogeological parameters and the complexity of the structures suggest that the geological heterogeneity have to be considered through different scales depending on the studied problem (figure 4.1). Each method permits to characterize the heterogeneity at a specific scale in a satisfactory manner.

The objectives purchased in site characterizations for instability problems include the following: (1) Hazard assessment; (2) General understanding of the phenomena (how influences the water the instability?); (3) Stabilization studies (for this situation which remediation method would be the most efficient?); (4) Mechanical behaviour modelling of the slide thanks to advanced hydrogeological and geomechanical modelling and (5) Establishment of the impacts of certain facilities, practices, or natural phenomena on the stability (what would be the impact of various remedial actions?). Whatever the objectives are, site characterization has three major components: assessment of the geological and geomechanical characteristics of a site, definition of the groundwater flow system and the associated hydrological conditions.

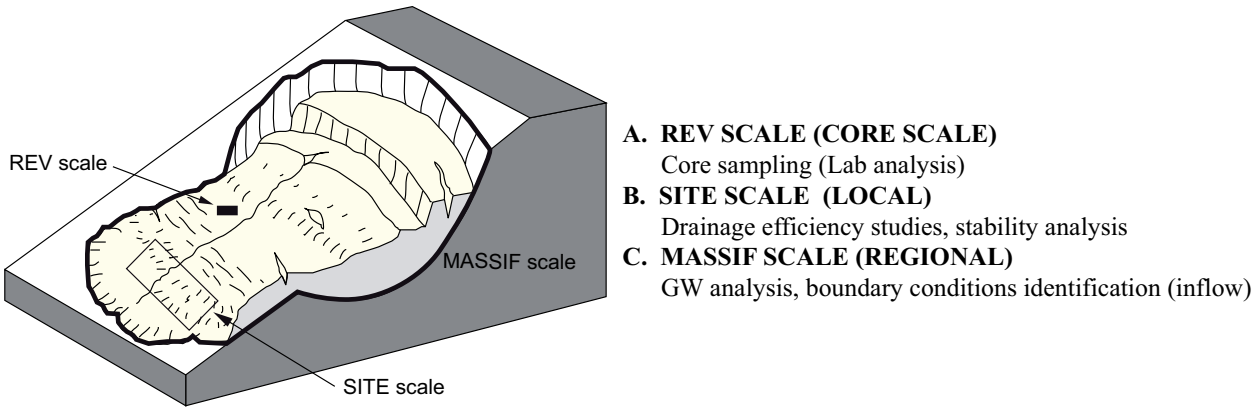

Figure 4.1: The three main study scales considered in this study. According to the investigation method, the acquired data will be scale dependent and the interpreted results will have a specific meaning at this definite scale. The extrapolation to a greater or smaller scale has therefore to be approach with great precaution. The REV scale (or core scale), corresponds to a millimetric to centimetric investigation. The site scale (or local scale), corresponds to metric to decametric investigations. The massif scale (Regional scale), corresponds to kilometric investigations.

4.1.2 OBSERVATION SCALES

Overview. Three scales have to been considered when studying a landslide (figure 4.1). According to the investigation method, the acquired data will be scale dependent and the interpreted results will have a specific meaning at this definite scale. The extrapolation to a greater or smaller scale has therefore to be approach with great precaution. The REV scale (or core scale), corresponds to a millimetric to centimetric investigation. It can be observed at the laboratory, where the heterogeneities can be analysed on the scale of the pore. These heterogeneities can take various forms: internal porosity of aggregates, fractures or microstratifications, with variable hydraulic conductivity characteristics according to sedimentary origin. Many experiments, on site or in laboratory, showed that yet at this scale, this heterogeneity can influence the water flows, as much as kilometric structures do. This scale is mainly used for geomechanical tests purpose. In laboratory, series of geotechnical investigations on drill cores may be performed; e.g. plastic compressibility, dilatance angle, cohesion, friction angle, Poisson ratio, Young's modulus, permeability, voids ratio and unit weight. The site scale (or local scale), corresponds to metric to decametric investigations; geological outcrops or aerial photo studies (faults and tectonic incidents recognitions). When the heterogeneity is studied directly on the field, for instance along a road, the strong heterogeneity of the lithology according to the mineralogical composition and spatial distribution is obvious. In the problematic of instabilities, this scale is used for detailed investigations; e.g. dimensioning of stabilization methods, well tests interpretations and local remediation works. The variations of hydraulic permeability and porosity are often irregular spatially and may concern very long distances; for instance along a section of 100 meters, hydraulic conductivities may vary from four order of magnitude and porosities; varying from 1 to 20% (Bakr et al. 1978, Sudicky 1986). The massif scale (Regional scale), corresponds to kilometric investigations, and in instability studies, it allows to consider the landslide in its totality; three dimensionally (vertical and horizontal extensions, shape and geometry). It represents the reference scale for global hydrodynamic studies; hydrodynamic behaviours, global water balances, surface recharge, lateral infiltration and hydraulic relations with the bedrock. In flow modelling, the definition of the boundary conditions will be handled at this regional scale in order to consider all the possible hydrological contribution entering into the water budget evaluation.

Scale of the models for numerical modelling. In practice, the dimension of large landslides is of a kilometric scale while the underground heterogeneities are of metric to decametric scale, with unknown geometrical and geographical characteristics (dimension, extension, orientation and location). Beside that, the representation of these heterogeneities into the models requires a very fine grid discretization, slowing considerably the computing. Hypothesis and assumptions have therefore to be made according to the studied problem and the purchased results. The three before-mentioned scales are thus commonly used.
At a regional scale, the assigned physical parameters of the model generally constitute a simplification of the true medium and, most of the time, corresponds to an equivalent homogeneous medium. These simplifications added to approximated boundary conditions (simplified head conditions, estimation of infiltration) produce a result whose interpretation at a larger scale (local) must be considered with precautions.
This scale is generally ideal to handle the problem globally, and enables to reproduce in a satisfactory manner the observed hydrodynamical behaviour. More realistic field parameter distributions taking into account the observed heterogeneity and connectivity of the system can be performed by considering the problem more locally. In figure 4.2, three models (3D) at different scales of the *la Frasse* landslide are presented; a regional scale and two models at a local scale. The third model (C) represents a specific three-dimensional portion from the local model (B), or likewise from the regional model (A). These models are different respect to their boundary conditions, the size of the mesh and the details of the distribution of their physical parameters, but, are calibrated in order to reproduce the observed hydrodynamical behaviour. The observed global water balances (inflows/outflows) are respected. According to the scale of the model, either first kind boundary conditions (Dirichtlet type) or second kind boundary conditions (Neumann type) are used. The boundary conditions from the local model are generally imported from the regional model. Increasing the scale of the model enables considerable mesh refinement and permits the representation of the smallest details of the geological heterogeneity without losing iteration speed; for instance from a size mesh of 22 meters (regional model) to 1 meter (refined local model).
The geological heterogeneity in the third model (C) does not either represent the reality of the parameter fields, but produce a plausible realization, enabling to test the effect of heterogeneities on the system (see chapter 6). In chapter 5, a method of stochastic generation of heterogeneous media is presented and applied to the la Frasse case study. The input parameters issued from the performed site characterization in section 4.3 will be used.

4.2 Heterogeneity in landslides: general overview

4.2.1 Main characteristics of instability problems

Landslides areas are geologically, hydrogeologically and structurally very particular and extremely complex. Compared to hydrogeological system of other environments, in particular alluvial aquifers, unstable slopes present some characteristics: *The table 4.1 presents the main characteristics and the hydrodynamic implications.*

a. Horizontal and vertical extension. The surface varies highly from case to case; between some dozen of square meters to several square kilometres. The thickness is generally relatively low, around 30 meters (mean value) but may reach 500 meters for the deepest. It varies spatially according several geological and morphological parameters; the slope, the morphology of the bedrock, the geological nature of the sliding mass (thin layers or massive rocks) and the local tectonic feature (faults, overlapping ...).
b. High slope angle – steep terrains. The slope is mainly around 15° but may reach locally 40°.

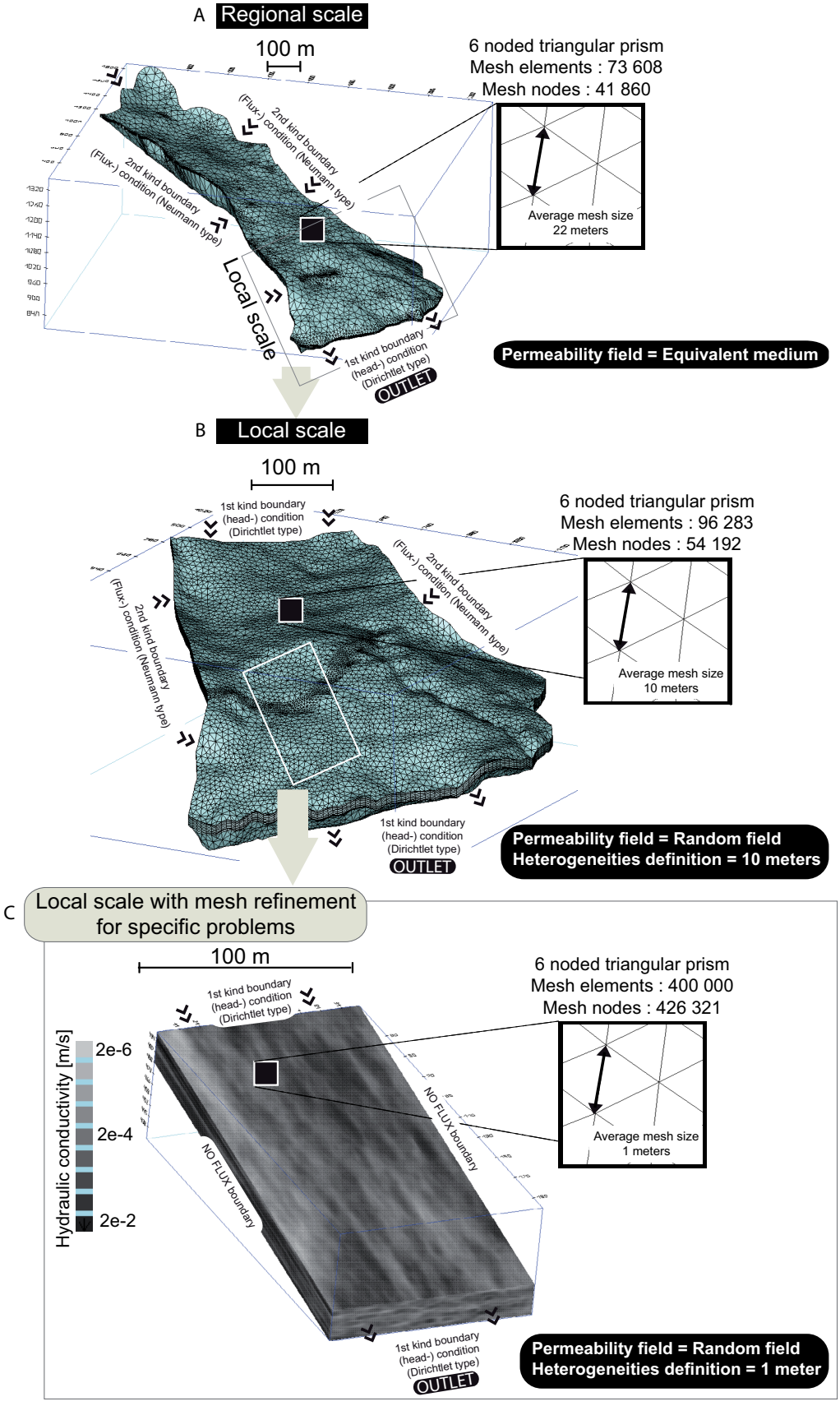

Figure 4.2: Three-dimensional models (3D) at different scales of the la Frasse landslide. (A) Regional model, (B) Local model and (C) Specific portion from the local model. These models are different respect to their boundary conditions, the size of the mesh and the details of the distribution of their physical parameters.

c. Complex geometry. The shape is generally complex and spatially limited. Laterally, the characteristic "saltbox" shape traduces the transition between the ablation and accumulation zones. In depth, the landslide is limited by the underlying bedrocks, which are strongly interacting with the sliding mass itself.
d. Deformation. Continual deformation processes cause variations of the physical parameters (permeability and porosity) and the geomechanical properties of the underground. On the surface, these deformations are represented by tension cracks in the zone of traction and scarps, while in the compression zone debris piles will appears. Note that these transformations do not only contain the cinematic components, but also consider alteration, chemical interactions and segregation phenomena during the movement. The material is thus strongly reworked, but may be more or less spatially organized.
e. Geological heterogeneity. In addition, these deformations, due to the displacements acting on the material from its original state to its state as landslide, are generally added to the initial geological heterogeneity of the material. Landslides taking place in low permeable porous environments for instance (i.e. flysch landslides) are mainly composed of clayey to silty weathered debris including variable volumes of gravels, stones and blocks and often prone to a secondary permeability induced by the phenomena of fracturing before-mentioned and sometimes karstification.
f. Discontinuous media. The structure and organisation of these structures are not well defined. Often, the structure is organized through small variable connected/disconnected lenses presenting a spatial extension less than 20 meters. However, the orientation of these secondary structures is still a controversial problem. Some observations may show that the discontinuities are rather parallel to sliding direction, while others seems to indicate that, especially close to the sliding surface, the structure could be aligned perpendicular to the displacements direction.
g. Aquifer characteristics. According to these geological and structural heterogeneities, the hydrodynamic system is generally very complex with saturated and unsaturated zones. Local aquifers can be either unconfined with free surface or confined, and locally may correspond to perched aquifers. Even the extension is often limited to several meters; they act like hydraulic plugs during recharge processes of the aquifer. Their presence complicates the drilling tests in their instrumentation and interpretation.

(Geo-)morphology	*Main characteristics*	*Hydrodynamic consequences*
Dimension/geometry	Relatively thin and a high surface area/depth ratio	Strong horizontal flow components
High slope angle	Steep terrains - consequent denivelation	High hydraulic gradients
Complex "*Bowl-shaped*" geometry	Particular boundary conditions	High lateral infiltration and yearly variable
Deformation	Anisotropic media with spatial and time variations	Preferential flow pathways
Contrasted geological material	Mostly clayey material with permeable features	Heterogeneous permeability distribution
Discontinuous media	Fast spatial connection	Transient hydraulic responses
Aquifer characteristics	Saturated to unsaturated media, with local confined aquifers	Complex pore-pressure distribution

Table 4.1: Structural and hydrogeological characteristics of landslides

4.2.2 LANDSLIDES IN FLYSCH UNITS AND QUATERNARY DEPOSITS

The term of flysch is used to indicate a terrigeneous detritic formation, composed of submarine deposits (turbidites) and imbricated in different structural and geomorphological units. The vertical facies distribution of these turbiditic sequences can be variable from one flysch to another and generates very different geotechnical and hydrogeological properties. Three types of standard sequences of flysch can be defined (Lateltin et al. 1997):

Pebbly-sandstone flysch. It consists in coarse turbiditic deposits with a prevalence of sandstone bank or cemented conglomerates forming massive and steep relief (e.g. flysch of Niesen, Frutigen, Niesenkulm, Seron and Chesselbach). These rocks disaggregate during the dissolution of the calcitic cement which binds

the flysch by the meteoritic groundwaters circulating in the relatively permeable fraction. Complex karstic networks could be identified in the Niesen flysch, with permeabilities around 1E-5 m/s (Basabe 1993). It displays predominance of rock falls and landslides in very steep cliffs. In Lateltin et al. 1997, a statistical study of the repartition of hard and weak material (sand versus clay material) of the flysch series of the Niesen has shown that the ratio is varying strongly from one place to another; from 10:1 at the bottom to 1:4 at the top of the series.

Marly-sandstone flysch. It consists in a prevalence of a marly-silty facies (up to 70% of the turbiditic sequences) with metric to decametric sandy or conglomeratic banks. They form soft relieves, with altitudes seldom exceeding 1600 meters in Switzerland ((e.g. flysch of Gurnigel; *Creux de l'Enfer, La Lécherette and Falli Hölli* landslides, and flysch of la Simme). The marly-silty facies generates soft anticlinal valley or slopes, constituting strong landslide prone areas. These soft rocks allow strong erosion, overdeepening, and deteriorate very fast in flysch soils with low permeabilities (K: 1E-7 m/s). Thus, active landslides with variable sliding surface depths may develop very rapidly. It gives rise to debris-flow events and deep translational slides.

Argillaceous flysch. They primarily consist in clayey-silty facies (more than 70% of the turbiditic sequence) with lenticular elements in a clayey-silty matrix (e.g. Wildflysch series) and very impermeable. Landslide-prone areas commonly show some rotational slides of limited extension and rather small and shallow, or debris-flow events in gullies.

Quaternary sediments in the Alpine foreland are clayey sediments to coarse gravel deposits which may form terrace complexes. In most cases they are deposited during glacial advance periods. The principal origins are the following: torrent deposits, fluvioglacial, interglacial lake sediments, colluviums, flysch-alteration soil, lodgment till, colluviums, marly screes, lateral moraine, rhodanian lodgment till, infra-morainic deposits, rhodanian sandy–gravely lodgment till, gravel pit, clay deposits from würmian retreat, clays from molassic sliding plane or lacustrine clays. Therefore, these sediments are extremely heterogeneous and according to the permeability and lithofacies may be compared to landslides in flysch environment. In CSD (1980) lithological facies percentages are given for the following formations:

- *Rhodanian moraine: (clay: 16.8%, silt 20%, sand 17.8% and gravel 40.4%);*
- *Jurassian moraine: (clay: 32.1%, silt 32.5%, sand 15.8% and gravel 17.1%);*
- *Interglacial lake sediments: (clay: 46.8%, silt 36.8%, sand 11.9% and gravel 4.5%);*

These values highlight the strong impermeable character of the interglacial lake sediments and the jurassian moraine of the quaternary deposits. On the contrary, the rhodanian moraine is showing a relatively good permeability.

Note that, the cases studied in this thesis (e.g. section 4.2.3) are mostly belonging to the "marly-sandstone flysch" type. However, the *la Frasse* landslide due to its particular heterogeneous character may be classified either in "pebbly-sandstone flysch" or in "marly-sandstone flysch" types; whereas, the *Triesenberg* landslide either in "marly-sandstone flysch" or "argillaceous flysch" types, due to its overall low impermeable character. The *Hohberg* landslide is a typical example of a landslide in a contact zone between the Wildflysch (i.e. "argillaceous flysch" type; exotic conglomeratic blocs) and the flysch of Gurnigel (i.e. "Marly-sandstone flysch" type). The landslides issuing from quaternary environments (i.e. *Ballaigues La Praz, Ballaigues Grande Combe and Travers* landslides) may be classified according to their geology in a "marly-sandstone flysch" type category.

4.2.3 Heterogeneity characterization in landslides from apparent resistivity data

4.2.3.1 Introduction

The term, apparent resistivity (Ohm.m), usually first appeared in geophysics studies that dealed with the DC electrical method. The concept of apparent resistivity (or conductivity) is simple, yet, many studies often misunderstand it with the resistivity. The differences between this too entities is that, resistivity is an intrinsic property of a microscopic volume of material, such as density. Apparent resistivity is a volume average of a heterogeneous half-space, except that the averaging is not arithmetic but dependent on each method and how it is used. The resistivity (or conductivity) measured by a method "A" will be different from that measured by a method "B". Thus the apparent resistivity of a given ground is different for every method (i.e. instrument) and for every measurement configuration. By the way, the same idea applies to other parameters, such as apparent density or apparent susceptibility that attempt to represent a real-world heterogeneous earth by an imaginary homogeneous half-space. The thing to remember, though, is that the resulting homogeneous half-space is not a simple average of the original heterogeneous earth. For these purposes the following study handles with apparent resistivities collected thanks to the same geophysical method. Note that the analytical method applied in this study may be used on other geophysical parameters.

The apparent resistivity analysed in this study were thus gathered thanks to the radiomagnetotelluric (RMT) method. The potential application areas of RMT in different hydrogeological applications has been since long time demonstrated, while RMT is useful to study spatial changes in lithology (Turberg 1994, Turberg and Müller 1997), in landfill studies (Tezkan et al. 1996 and 2000) or to map the depth of bedrock (Beylich et al. 2003 and 2004). In addition to borehole investigations it makes possible to obtain a three-dimensional representation of subsurface geophysical ground properties in a fast, efficient and economic way. In the problematic of unstable terrain, RMT method constitutes an innovative approach. Indeed, in the recent years, its application to the detection of hydrogeological structures have been carried out in complex landslide prone areas (Müller 1993, Bossy 1999, Bernasconi et al 2001, Tullen 2002, Tullen et al 2006, Turrian 2003, Krähenbühl 2007). In particular it addresses the problem of characterizing the heterogeneity of the geological material. And in many cases, it allowed measuring the subsurface distribution of electrical resistivity and evaluating the geological permeability of the subsurface terrains. In addition it permits in some cases to delineate preferential infiltration zones. Moreover, this method revealed to be likewise efficient to build three dimensional model of permeability, thanks to experimental relations between electrical resistivity ρ and the intrinsic permeability k (Tullen et al. 2006). Or, applied on very shallow landslides (< 20 meters), it might allow identifying the geometry of the mass and to locate the sliding surface (Bossy 1999).
Finally, all these studies have in common the indirect exploration of landslide areas in order to identify and to detect geological specificities and characteristics. But few of them concentrated on the structure of the acquired rough data sets. In order to fill this gap, it was decided in the framework of this PhD to investigate these data, and to define if new information about the organisation of the geological heterogeneity could be obtained. For this purposes, a complete geostatistical study on rough apparent electrical resistivity sets from several landslides is performed. The geological framework of these cases corresponds rather to low permeable porous environments. The studied statistical properties are; the spatial variability (homogeneity/heterogeneity) and the spatial continuity of the geological structures (isotropy/anisotropy).
Finally, a "multicriterion" plot permits to classify and to compare the case studies. Some conclusions and practical implications in the framework of instability remediation are drawn. The limitation of this method is finally discussed.

4.2.3.2 *Case studies and geological settings*

Nine case studies (see table 4.2 and figure 4.3 for location) are selected; seven landslide case studies and two additional sites, representing stable reference sites. The landslides are geologically characteristic of the most important instability prone areas in Switzerland (Alps, Plateau and Jura); i.e. flysch units and quaternary deposits (moraines, glacial and fluvial-glacial deposits). Landslides in flysch units are represented by five case studies (*La Frasse, Hohberg, Triesenberg, Creux de l'Enfer and la Lécherette*). *Hohberg* and the *la Frasse* landslides comprise two additional RMT surveys (surveys -S2- and -S3-). The zone -S2- of *la Frasse* is situated outside the landslide area on the left boarder in the stable flysch. Zone -S3- is situated in the so-called Lobe du Sépey (zone "GGS") representing the stabilized landslide. Zones -S2- and -S3- of the *Hohberg* landslide are considered as being potentially unstable. In addition, two landslides are occurring in quaternary deposits; *the Ballaigue "La Praz" and Travers*. *The Ballaigue "Grande Combe"* case study is considered to be more or less stable.

Case studies	Geological Unit	Geology	Activity	Area (km2)	Depth (m)	Study area (km^2)	References
Cornol	Quaternary deposits	Molassic and marly deposits	Stable	-	-	3.86	Turberg et al. (1994)
Gimel	Quaternary deposits	fluvial-glacial sediments	Stable	-	-	1.50	Kopp (2003)
La Frasse -S1-	Simme Flysch, Préalpes Supérieures	Flysch and glacial deposits	Unstable	1	30-40	0.06	Matti (2008)
La Frasse -S2-	Simme Flysch, Préalpes Supérieures	Flysch	Stable		30-41	0.06	Matti (2008)
La Frasse -S3-	Simme Flysch, Préalpes Supérieures	Flysch and glacial deposits	Stabilized		30-42	0.06	Matti (2008)
Triesenberg	Bundtsandstein and Muschelkalk units	Flysch and glacial deposits	Unstable	5.5	10-20	1.92	Tullen 2002
Hohberg -S1-	Gurnigel Flysch, Préalpes Supérieures	Flysch moraines and slope debris	Unstable		17-30	0.54	Tullen 2002
Hohberg -S2-	Gurnigel Flysch, Préalpes Supérieures	Flysch moraines and slope debris	Potentially unstable	1.6	-	0.72	Tullen 2002
Hohberg -S3-	Gurnigel Flysch, Préalpes Supérieures	Flysch moraines and slope debris	Potentially unstable		-	0.48	Tullen 2002
Creux de l'Enfer	Gurnigel Flysch, Préalpes Supérieures	Flysch moraines and slope debris	Unstable	0.4	20	0.01	Bossy 1999
La Lécherette	Submédianes units	Flysch and glacial deposits	Unstable	0.4	30	0.17	PNR31, Müller 1993
Ballaigues - Grande Combe	Quaternary deposits	Moraines and glacial deposits	Unstable	0.4	5-14	0.06	Turrian 2003
Ballaigues -La Praz	Quaternary deposits	Moraines and glacial deposits	Unstable		5-14	0.24	Turrian 2003
Travers	Quaternary deposits	Moraines and glacial deposits	Unstable	0.3	<10	0.26	Krähenbühl 2007

Table 4.2: Properties of the case studies; geology, area and references

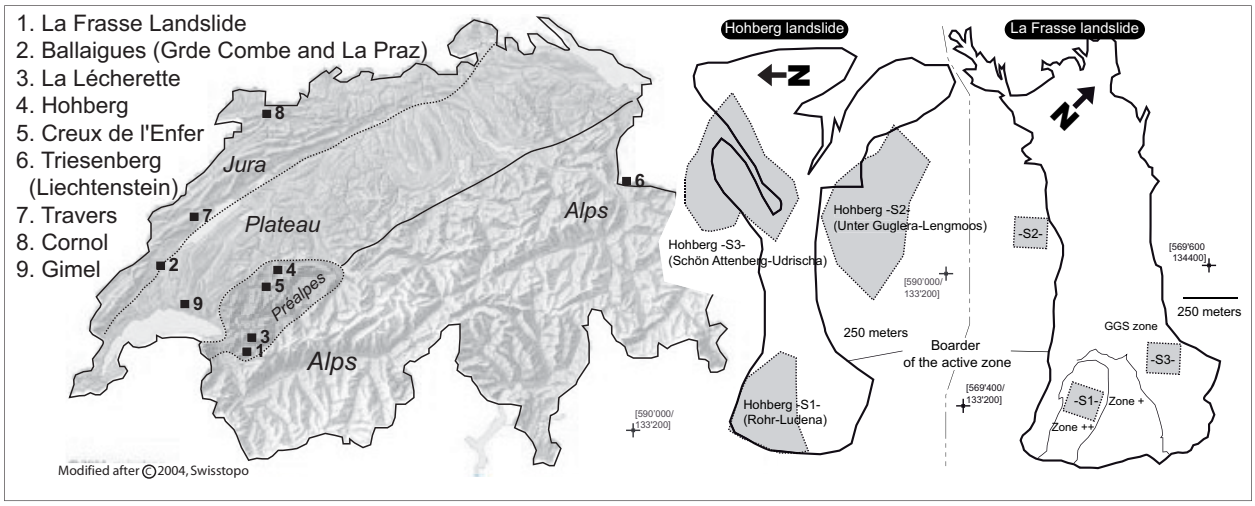

Figure 4.3: Geographical location of the studied case studies and of the three studied sites (S1, S2 and S3) of the Hohberg and la Frasse landslides.

Globally, these landslides present a surface inferior to 5 km2, with a maximal depth of 40 meters. *The Triesenberg, Creux de l'Enfer and Ballaigue "La Praz"* landslides are the thinnest one (< 20 meters). The contact between the sliding mass and the bedrock is generally well marked, since mostly constituted by limestone more or less fractured, except for the *Creux de l'Enfer* (flysch on flysch).

Additionally, two stable and homogeneous reference sites are chosen for the purpose of comparisons. The *Gimel* case study, about 1.5 km2, located on the western boarder of the Plateau molassique, is principally composed of moraines and fluvial glacial deposits from the last glaciation (i.e. Würm). The material is generally coarse and relatively homogeneous (gravels and sand) with a high permeability, and is economically

interesting for the exploitation of gravel material. The *Cornol* case study is located on the northern part of Switzerland in the Jura Mountains. It is made of tertiary molassic and marly deposits. The quaternary sediments are considered particularly rich in silt and clay particles, thus forming low permeable hydrogeological units. The surface of the studied zone is around 4 km2.

4.2.3.3 ***Data acquisition***

RMT is an electromagnetic geophysical method. It uses the properties of low to very low electromagnetic waves frequencies F (12-240 kHz) from different radio guiding transmitters and other telecommunication means. It allows measuring the apparent underground resistivities (ρa) and underlining their variations. Its principal characteristic is to proceed in vertical sounding along several parallel profiles allowing covering the zone of interest. Varying the wave's frequencies F (12-240 kHz) permits to sound the underground at different depth (figure 4.4). It permits, thanks to resistivity contrasts (table 4.3), to distinguish permeable zones (sand and gravel) to more impervious areas (clay and silt).

Material	Resistivity (Ohm.m)	Log resistivity
Gravel non-saturated	300 – 3000	2.5 – 3.5
Gravel saturated	150 – 300	2.2 – 2.5
Sand non-saturated	150 – 500	2.2 – 2.7
Sand saturated	80 – 150	1.9 – 2.2
Silt non-saturated	25 – 100	1.4 – 2.0
Silt saturated	10 - 25	1.0 – 1.4
Limestone	100 - 5000	2.0 – 3.7
Crystalline rocks	1000 - 10000	3.0 – 4.0

Table 4.3: Electrical resistivity of various geological materials.

This method may thus differentiate the conductive sub-domains (low resistivity, i.e. 10 to 100 Ohm.m) of the aquifer system from the capacitive one (resistive sub-domains (50 to 1000 Ohm.m)). The studied areas are homogeneous grid; maximum distance between the points is 20 meters. Each profile is made of 20 to 30 measurements, and each case study has between 5 and 10 profiles.
An excellent theoretical introduction to radiomagnetotelluric investigation may be found in Parasnis (1997), Turberg et al (1994), Bernasconi (2001) and Schlumberger investigation in Mari et al (1999).

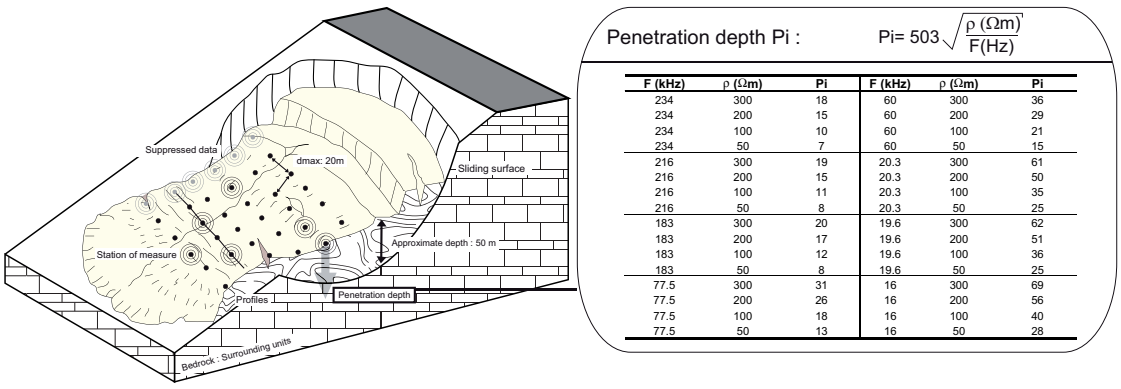

F (kHz)	ρ (Ωm)	Pi	F (kHz)	ρ (Ωm)	Pi
234	300	18	60	300	36
234	200	15	60	200	29
234	100	10	60	100	21
234	50	7	60	50	15
216	300	19	20.3	300	61
216	200	15	20.3	200	50
216	100	11	20.3	100	35
216	50	8	20.3	50	25
183	300	20	19.6	300	62
183	200	17	19.6	200	51
183	100	12	19.6	100	36
183	50	8	19.6	50	25
77.5	300	31	16	300	69
77.5	200	26	16	200	56
77.5	100	18	16	100	40
77.5	50	13	16	50	28

Figure 4.4: Relations between penetration depth (m), frequency (kHz) and electrical resistivity (Ohm.m) in radiomagnetotelluric surveys. The penetration depth of the method is function of the chosen investigation frequency and of the electrical resistivity of the material

4.2.3.4 ***Data processing***

Several studies have recognized that geophysical methods can be used to estimate the spatial correlation structures of hydraulic or geological properties (Tercier et al. 2000). Geophysical surveys may collect with a great density of points the geological underground properties (i.e. electrical resistivity, gamma ray attenuation, acoustic velocity, magnetic susceptibility), and their correlation structures may be useful for characterizing subsurface spatial heterogeneity.

In this study the analysis of RMT data sets is done directly on the rough data set; the measured apparent electrical resistivities, following a precise analysis process (figure 4.5). The statistical structure analysis describes central tendency and variability. Mean values, variance and coefficients of variation are calculated for each frequency and presented in a box-plot representation. The exploratory spatial analysis permits the identification of structures in the data sets. It is performed thanks to (semi)-variograms models, characterizing the spatial continuity (i.e. correlation lengths) or roughness of the data set. The analysis of the geostatistical structure follows the common procedure; generation of an experimental variogram, the fitting and finally the interpretation of the modelled variograms. The exploration is made perpendicular and parallel to the sliding direction.

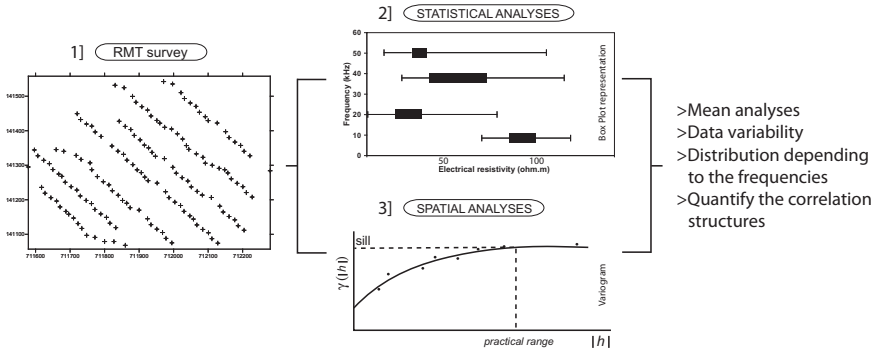

Figure 4.5: Analytical approach. After the data acquisition during the radiomagnetotelluric survey (1), the data are analyzed thanks to: (2) Statistical and (3) Spatial analyses.

The modelled variograms may exhibits several behaviours as illustrated in figure 4.6; isotropic, anisotropic or fractal properties. In a given direction -a1- or -a2-, the variogram may become stable beyond some distance |h|=a, called the range, or not at all. The range a gives a precise meaning to the intuitive concept of the zone of influence of a data set and therefore about the spatial continuity (for exponential models the correlation length = range a/3). However, there is no reason for the range to be the same in all directions of the space. In scheme B of the figure 4.6 for instance, the anisotropy is developed according to the direction -a2-. Scheme C presents a typical fractal behaviour corresponding to highly perturb geological medium.

It is important to note that the description of the variability (mean, variance, minima, maxima etc) is a quantitative characterization, whereas spatial analysis is qualitative. The assessment of variogram models consists yet, in a sense, in a personal interpretation.

4.2.3.5 ***Hypothesis***

The accurate interpretation and validation of the RMT method requires some work hypothesis; one-dimensional, no boundary effects and saturated medium, which are hardly applicable on landslides case studies. The explored medium should be considered has being essentially one-dimensional; meaning that it does not induce significant electromagnetic polarization effects (Fischer et al. 1981 and Turberg 1993). In a geological point of view, it should be essentially homogeneous and constituted by a unique unit. In which

the geophysical anisotropy, produced for instance by the fracturation of a rock massif or by the contact of two different lithological units are insignificant. In a hydrogeological point of view it should be considered as being saturated, such as the measured apparent electrical resistivity is only function of the lithology and not of the saturation ratio.

But, in landslide areas these conditions are often not filled. In fact, their specific geological contexts implicate complex structural contacts and flow field heterogeneity. Due to the geological heterogeneity, landslides are made of saturated and unsaturated zones, composed of a multitude of inter-connected aquifers. The data acquired in these contexts are thus influenced by strong resistivity contrasts and variations of the saturation ratios. Nevertheless, these characteristics may be used to investigate interesting features. The measured variability of the rough data set may inform about lithological as well as hydrogeological heterogeneity. In order to limit these inferences, the lateral extension of the studied data sets concern uniquely the unstable mass. It means that the data measured directly on the limits of the slides, showing too strong boundary effects (i.e. structural contact with limestone bedrocks: resistivity > 1000 Ohm.m), are suppressed (see figure 4.4, grey points).
Finally, the penetration depth is function of the electrical resistivity of the medium and the used frequency as indicated by the formula in figure 4.5. In the case of landslide occurring in these low permeable porous environments, the maximum penetration depth may be around 20 meters.

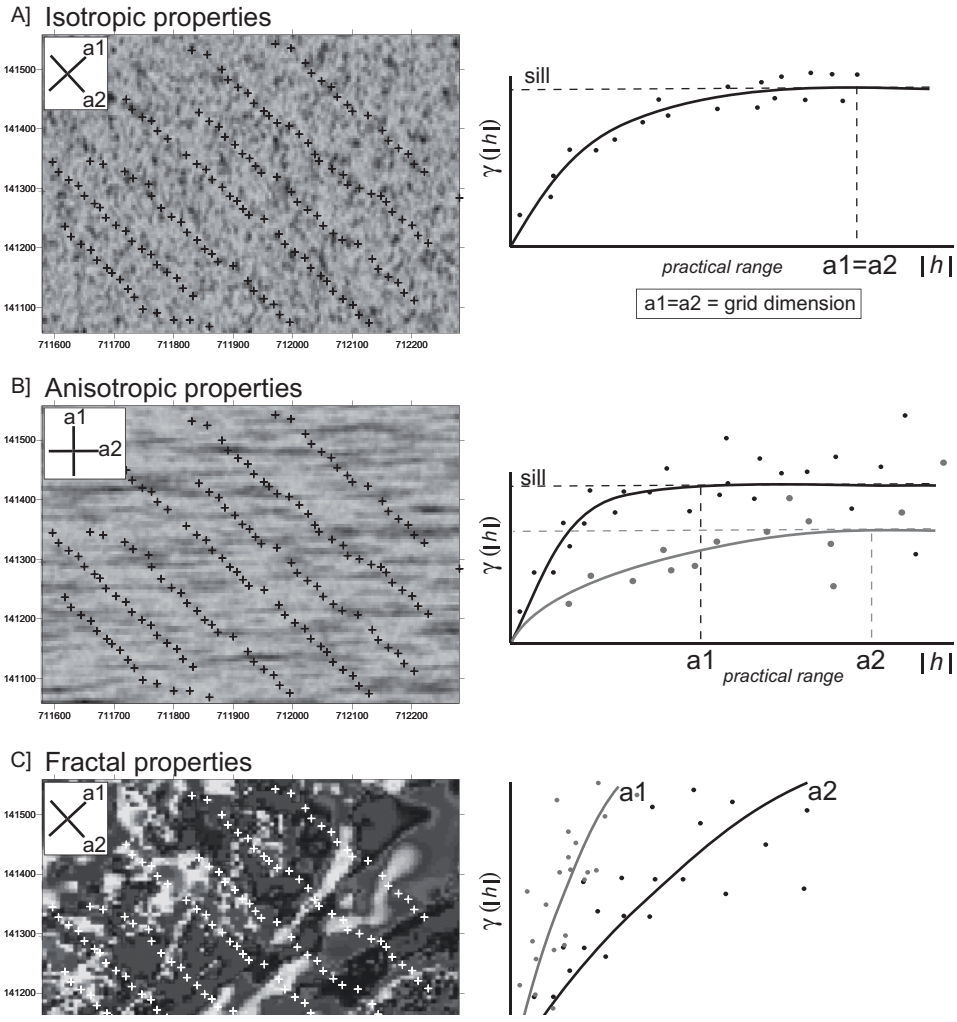

Figure 4.6: Properties and behaviours of the experimental and modelled variograms, according to the distribution of the electrical resistivities of the material (i.e. geological heterogeneity).

4.2.3.6 ***Results***

Stable environment with uniform material

The two investigated sites, *Cornol* and *Gimel*, are representative of a homogeneous geological environment. The *Cornol* site is characterized by a slightly permeable fine material (marly deposits, rich in silty clay particles). The *Gimel* site is constituted of permeable coarse material (gravel deposits). The mean resistivity for *Gimel* site is around 315 Ohm.m (frequency 183 kHz) for subsurface terrains and around 178 Ohm.m (f= 19.6 kHz) in depth. The coefficient of variation (CV) varies from 31% to 49% (table 4.4, summary in table 4.6).The CV is a normalized measure of dispersion of a probability distribution. It is defined as the ratio of the standard deviation σ to the mean μ.

The mean resistivity and variance are slightly decreasing with depth. *Cornol* site is characterized by low resistivity varying from 27 to 39 Ohm.m, typical values for low permeable medium. The coefficient of variation is slightly increasing with depth (46% to 52%) while the mean resistivity is slightly decreasing. Some spread values are recorded for the two cases (figure 4.7), but a general grouped tendency is observable.

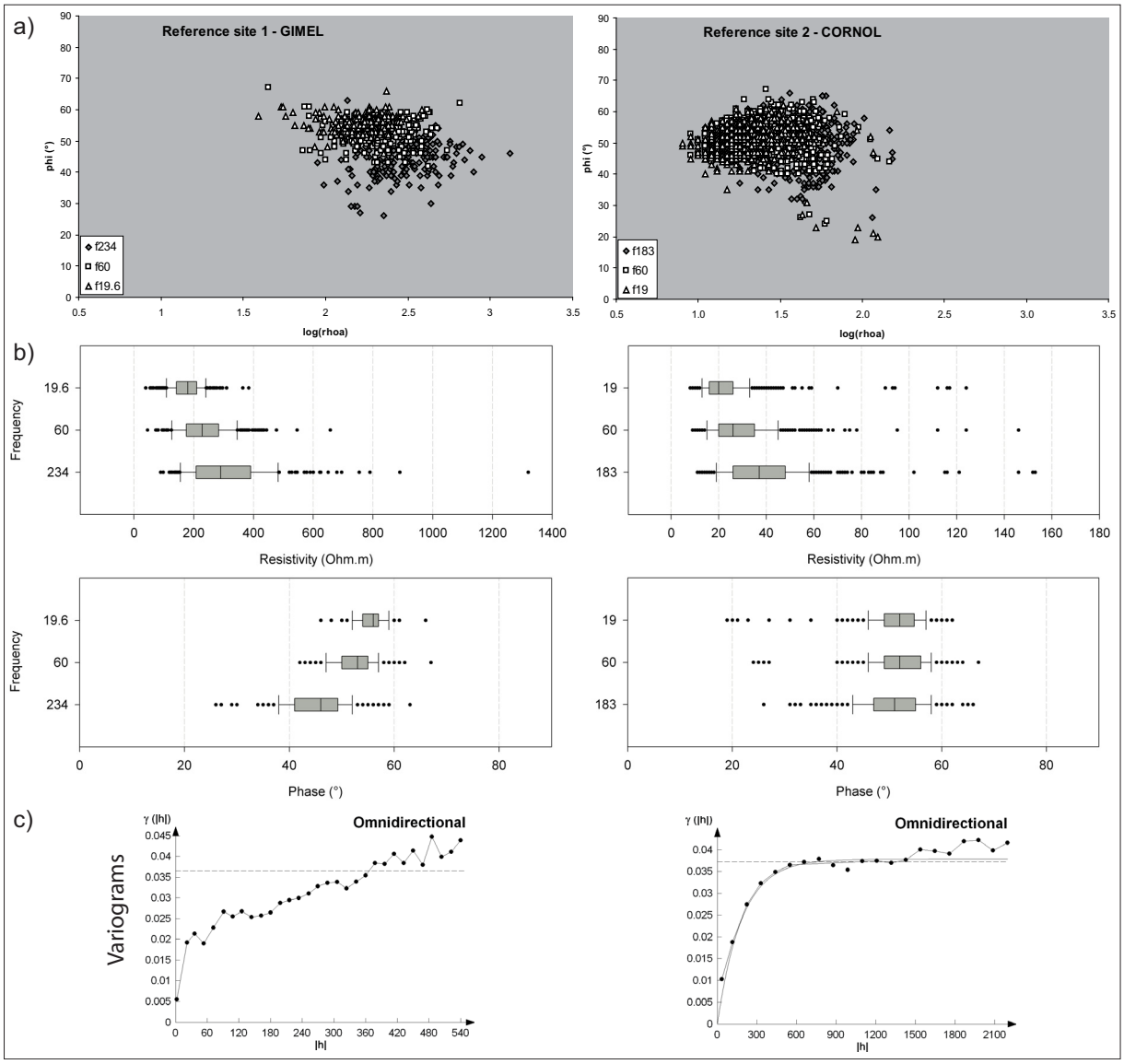

Figure 4.7: Statistical results of the two "homogeneous" reference sites; Cornol and Gimel: a) Plots of the pair data phase/electrical resistivity, b) Variability plotted thanks to a box-plot representation and c) The modelled variograms.

Concerning the spatial analysis, the variogram surfaces don't indicate any anisotropy. In absence of structured features, the correlations lengths are thus spatially uniforms. The variograms are fitted thanks to an exponential function and without nugget effects. The variograms do not exhibit fractal nature since a uniform steady increase and a level off at the sill is observed. The sill represents the limit of the variogram tending to infinity lag distances. The distance in which the difference of the variogram from the sill gets neglectable is expressed by the range. In case of exponential functions, the range represents three times the correlation lengths (λx,λy). If fractal nature were observed, the pattern of semi-variance would be repeated at different scales and the semi-variance would grow indefinitely. There are no significative statistical differences between the frequencies; the medium is thus vertically uniform. Coarse material terrains are defined by a mean resistivity of 250 Ohm.m and fine material terrains by a resistivity of 30 Ohm.m.

Unstable environment and heterogeneous material

Two types of porous environment are discussed; flysch and quaternary deposits. These terrains are strongly reworked and thus may show anisotropic and heterogeneous characteristics. The measures indicated an overall low resistivity. Being statistically not significantly different, both environments are treated together.
In table 4.4 (summary in table 4.6), one may note that globally the apparent resistivities are low and varying from 20 to 200 Ohm.m. Two groups are observable according to the degree of variability; low variability and high variability. These two groups are defined arbitrary to allow a primary classification. Low variability is defined for coefficient of variability (CV) inferior to 50%, and is characteristic of electrical resistivity around 50 and 60 Ohm.m and rarely exceeding 200. Whereas, in case studies presenting a high variability, values often exceeding 200 Ohm.m and even 1000 Ohm.m. The average resistivity remains still low; around 70 Ohm.m, except for the *la Frasse* -S2- case with a mean value around 250 Ohm.m. The distribution of the case studies in these two groups is equal (50/50%). Note that, for instance, *Hohberg* -S2- and Travers, present various degree of variability according to the frequency. At high frequency, *Travers* case shows a much higher variability than at low frequency. Thus, the degree of variability (generally around 30%) is globally relatively constant for subsurface measures and may strongly increase at lower frequencies (deep structures). Strong dispersions towards high values, indicating strong interferences of high resistive geological bodies, and especially for low frequencies (figure 4.8) are identified. Thus, despite the homogeneous character of the degree of variability, a high vertical heterogeneity is recorded.

Finally, the plots in figure 4.9 of the apparent resistivity on the phase, indicate that two landslides are standing apart from the others; the *Triesenberg* and the *Hohberg* -S1- and -S2-. A strong variability is illustrated both for the phases and the electrical resistivities. Plots concerning each case are in appendices II-1 and 2.

Spatial analysis. Variograms are modelled for each case study at each frequency in two direction; parallel and perpendicular to sliding direction. The calculated semi-variograms are presented in appendices II-3 to 10. The calculated semi-variance values are presented in table 4.5. A total of 86 variograms are calculated. Globally for high and low frequencies, the variograms increase rapidly and levelled off at the sill with some perturbation for long distances. Two direction of investigation are considered; parallel and perpendicular to the sliding direction. If the spatial correlations (i.e. spatial range divided by three in the case of an exponential adjustments) in both directions are identical the medium may be considered as isotropic (otherwise anisotropic). If the variogram is strongly perturbed, a fractal property is assessed. The spatial behaviours change greatly from a case to case and according to the studied frequency. A general tendency is that in the direction of the sliding direction, correlation lengths are (λx) are slightly longer (some dozen of meters) than in the perpendicular direction (λy). It means that the structures are rather aligned according to the

slope. The correlation lengths λx and λy are small; rather exceeding 20 meters for λy and up to 40 meters for λx.

Statistics of apparent electrical resistivity measures

	La Frasse -S1-			*La Frasse -S2-*			*La Frasse -S3-*		
	f 183	f 77.5	f 18.3	f 183	f 60	f 22.3	f 183	f 60	f 22.3
Number of values	118	118	118	94	94	94	76	76	76
Minimum	24.00	15.00	18.40	76.00	51.00	46.00	17.90	16.70	11.20
Maximum	180.00	205.00	153.00	665.00	750.00	1608.00	145.00	103.00	118.00
Range	156.00	190.00	134.60	589.00	699.00	1562.00	127.10	86.30	106.80
Mean	77.18	75.82	65.30	210.90	239.60	274.88	57.01	54.44	63.69
Variance	664	827	764	11150	17340	38594	639	282	458
Coef. of variation	33%	38%	42%	50%	55%	71%	44%	31%	34%
ESTIMATION	MEDIUM	MEDIUM	MEDIUM	HIGH	HIGH	HIGH	MEDIUM	MEDIUM	MEDIUM

	Hohberg -S1-		*Hohberg -S2-*				*Hohberg -S3-*				
	f 60	f 19.6	f 183	f 77.5	f 60	f 19.6	f 183	f 77.5	f 60	f 19.6	f 16
Number of values	187	187	324	323	214	538	181	124	241	67	242
Minimum	17.00	10.00	5.00	15.00	16.00	5.00	25.00	5.00	21.00	22	14
Maximum	129.00	104.00	475.00	450.00	166.00	450.00	764.00	1235.00	310.00	282	1140
Range	112.00	94.00	470.00	435.00	150.00	445.00	739.00	1230.00	289.00	260	1126
Mean	42.25	38.91	77.68	77.84	48.26	64.74	64.94	72.07	66.21	79.84	73.91
Variance	268	229	4097	4478	374	3425	4297	17434	1892	4062	7366
Coef. of variation	39%	39%	82%	86%	40%	90%	101%	183%	66%	80%	116%
ESTIMATION	MEDIUM	MEDIUM	VERY HIGH	VERY HIGH	LOW	VERY HIGH	VERY HIGH	VERY HIGH	HIGH	VERY HIGH	VERY HIGH

	Triesenberg			La Lécherette			Creux de l'Enfer			
	f 183	f 77.5	f 23.5	f 183	f 77.5	f 19	f 234	f 183	f 60	f 19.6
Number of values	86	86	84	104	104	104	226	226	226	538
Minimum	80.00	26.00	10.00	36.00	40.00	33.00	21.00	21.00	20.00	5.00
Maximum	7910.00	7320.00	16000.00	140.00	131.00	161.00	95.00	96.00	177.00	450.00
Range	7830.00	7294.00	15990.00	104.00	91.00	128.00	74.00	75.00	157.00	445.00
Mean	1816.40	1894.80	1957.30	62.97	67.04	70.91	38.50	38.20	43.16	64.74
Variance	1966400	2614000	4714500	488	398	570	122	130	428	3425
Coef. of variation	77%	85%	111%	35%	30%	34%	29%	30%	48%	90%
ESTIMATION	VERY HIGH	VERY HIGH	VERY HIGH	MEDIUM	MEDIUM	MEDIUM	MEDIUM	MEDIUM	MEDIUM	VERY HIGH

	Travers			*Ballaigues - Grande Combe*				Balaigues - La Praz		
	f 183	f 77.5	f 23.5	f 216	f 162	f 60	f 16	f 216	f 60	f 16
Number of values	141	141	141	43	39	82	82	41	41	41
Minimum	11.60	13.60	14.00	20.00	13.00	20.00	20.00	21.00	6.00	18.00
Maximum	150.00	124.00	106.00	1920.00	224.00	630.00	742.00	250.00	260.00	335.00
Range	138.40	110.40	92.00	1900.00	211.00	610.00	722.00	229.00	254.00	317.00
Mean	46.47	40.40	36.43	177.00	69.03	114.40	92.20	79.98	88.59	102.20
Variance	561	271	176	120400	4279	19280	12900	3977	4850	7310
Coef. of variation	51%	41%	36%	196%	95%	121%	123%	79%	79%	84%
ESTIMATION	HIGH	MEDIUM	MEDIUM	VERY HIGH	VERY HIGH	VERY HIGH	VERY HIGH	VERY HIGH	VERY HIGH	VERY HIGH

	Reference site 1 - Gimel -			Reference site 2 - Cornol -		
	f 234	f 60	f 19.6	f 183	f 60	f 19
Number of values	213	213	213	727	727	727
Minimum	89.00	45.00	39.00	11.00	9.00	8.00
Maximum	1320.00	657.00	384.00	153.00	146.00	124.00
Range	1231.00	612.00	345.00	142.00	137.00	116.00
Mean	315.70	234.60	178.00	38.87	28.77	22.74
Variance	23480	8231	2970	317	188	141
Coef. of variation	49%	39%	31%	46%	48%	52%
ESTIMATION	MEDIUM	MEDIUM	MEDIUM	MEDIUM	MEDIUM	HIGH

Table 4.4: Statistical characteristics of the measured apparent resistivities.

For low and medium frequencies (i.e. great penetration depth), a fractal nature may be often observed (i.e. *Triesenberg, Creux-de-l'Enfer and Ballaigue "La Praz" and "Combe"* landslides) with some strong nugget effects. These perturbations indicate the presence of strong electrical contrasts. Besides this, the degree of variability given by the calculate semi-variance values in table 4.5 is also systematically increasing with depths (i.e. *Triesenberg* landslides: 0.13 to 0.46) contrary to what is observed for the stable reference sites (steady or slightly decreasing with depth).

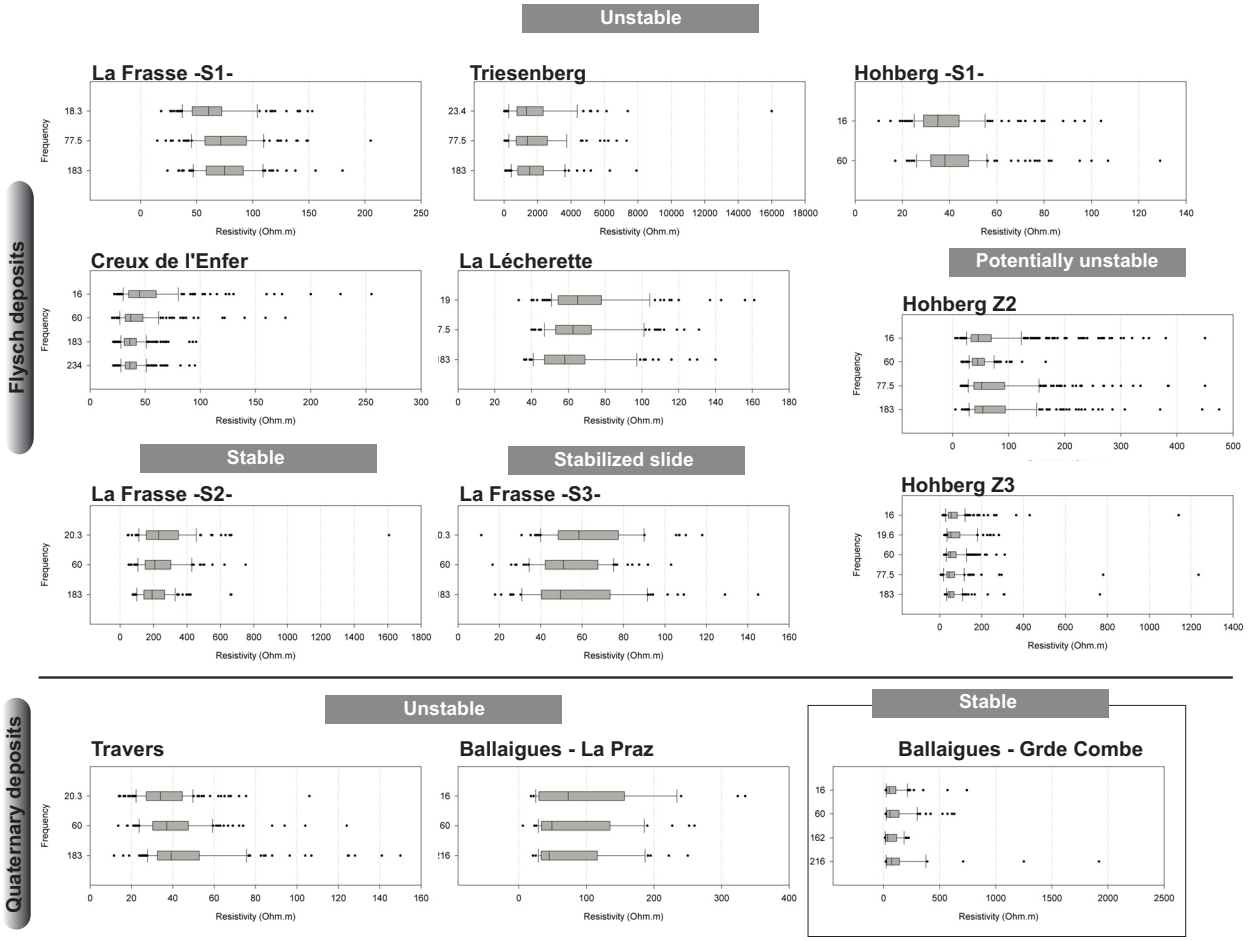

Figure 4.8: Representation of the variability thanks to box-plot representations. On the abscissa (x or horizontal scale) of the graph are represented the electrical resistivities (Ohm.m) and in ordinate (y or vertical scale) the used frequencies (kHz) for the investigation.

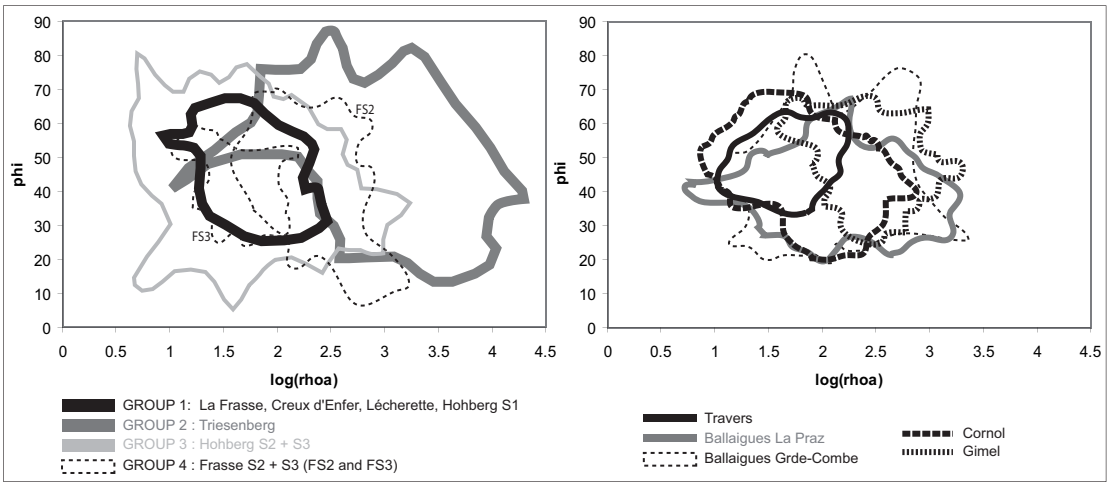

Figure 4.9: Plots of the pair data phase/electrical resistivity. This way of representation allows identifying four groups representing various degrees of heterogeneity. Homogeneous data sets present a low dispersion.

Flysch type

Case study	frequency	semi-variance //	semi-variance perp.
La Frasse -S1-	183	0.030	0.022
	77.5	0.030	0.030
	18.3	0.029	0.030
La Frasse -S2-	183	0.040	0.040
	60	0.054	0.054
	20.3	0.062	0.062
La Frasse -S3-	183	0.034	0.034
	60	0.022	0.022
	20.3	0.026	0.026
Triesenberg	183	0.130	0.130
	77.5	0.220	0.220
	23.5	0.460	0.460
Hohberg -S1-	60	0.022	0.020
	16	0.023	0.023
Hohberg -S2-	183	0.060	0.060
	77.5	0.075	0.075
	60	0.075	0.075
	16	0.610	0.610
Hohberg -S3-	183	0.048	0.048
	77.5	0.090	0.090
	60	0.810	0.810
	19.6	0.500	0.500
	16	0.540	0.540
Creux d'Enfer	234	0.011	0.011
	183	0.011	0.011
	60	0.022	0.022
	16	0.036	0.036
Lécherette	183	0.019	0.019
	77.5	0.014	0.014
	19	0.016	0.016

Quaternary deposits

Case study	frequency	semi-variance //	semi-variance perp.
Ballaigues			
La Praz	216	0.200	0.200
	60	0.180	0.180
	16	0.180	0.180
Grande Combe	216	0.170	0.170
	162	0.220	0.220
	60	0.130	0.130
	16	0.130	0.130
Travers	183	0.460	0.460
	77.5	0.150	0.150
	23.5	0.220	0.220

Reference sites

Gimel	234	0.036
	60	0.035
	19.6	0.023
Cornol	183	0.038
	77.5	0.034
	19	0.026

Table 4.5: Calculated semi-variance.

	Frasse S1	Frasse S2	Frasse S3
Number of values	118	94	76
Minimum	16	24	12
Maximum	46	142	38
Range	30	118	27
Mean	**29**	**56**	**28**
Coefficient of variation	20%	31%	17%
	Hohberg S1	**Hohberg S2**	**Hohberg S3**
Number of values	187	538	309
Minimum	13	9	0
Maximum	41	84	134
Range	28	75	134
Mean	**24**	**30**	**25**
Coefficient of variation	18%	38%	67%
	CDE	**Triesenberg**	**La Lécherette**
Number of values	228	86	104
Minimum	0	0	21
Maximum	64	416	46
Range	64	416	25
Mean	**28**	**127**	**30**
Coefficient of variation	27%	53%	16%
	Travers	**Ballaigue Praz**	**Ballaigue Grde Combe**
Number of values	141	92	82
Minimum	13	17	18
Maximum	36	163	108
Range	23	147	91
Mean	**21**	**54**	**34**
Coefficient of variation	17%	52%	50%
	Gimel	**Cornol**	
Number of values	213	764	
Minimum	0	10	
Maximum	23	89	
Range	23	79	
Mean	**16**	**19**	
Coefficient of variation	39%	43%	

Table 4.6: Summary of the global statistical results for all frequencies.

4.2.3.7 *Classification and discussions*

The first conclusion that may be drawn after this statistical analysis is that, compared to the reference site, landslide areas are non-homogeneous media, and have a more or less structured heterogeneity. And that no clear similitudes are identified between the different case studies, even if belonging to similar geological settings. In order to proceed in a more accurate interpretation, a classification is proposed. A "multicriterion" approach allows integrating and comparing the used frequency, the variability and the spatial structure (figure 4.10).

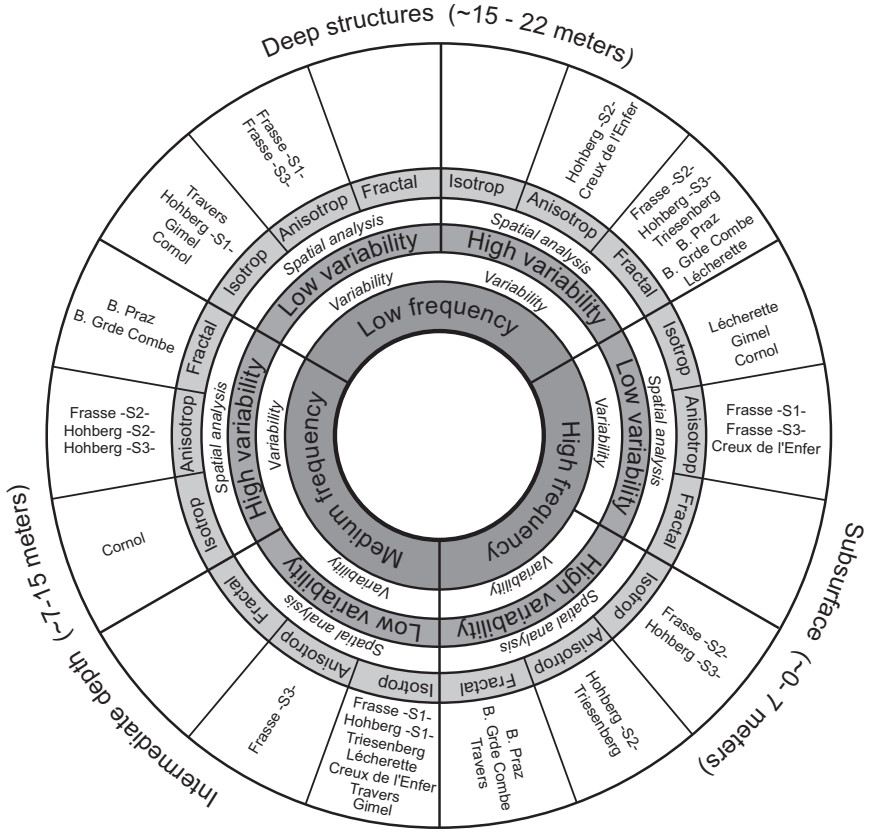

Figure 4.10: Classification of the observed behaviour. A "multicriterion" approach allows integrating and comparing the used frequency, the variability and the spatial structure.

The following observation may thus be done:

At subsurface, one may observe that all tendencies may be observed in equal proportion. The subsurface may be composed of relatively homogeneous isotropic or anisotropic media. The terrains may be structured as well as totally randomly distributed (i.e. fractal).
At intermediate depth, the media presents mostly a low variability and isotropic characteristics. Nevertheless, some cases present some perturbed behaviours.
Deep structures are mostly anisotropic and strongly disordered. However isotropic behaviours are also observable, but may concern cases that yet presented isotropic characteristics at other frequencies.

The fractal behaviour. When fractal behaviour occurs, it may concern all frequencies. Fractal behaviour means: that the medium is highly heterogeneous with physical parameters changing strongly from point to point. Geologically, it means that rocks with different geotechnical and lithological parameters are randomly

distributed and thus hardly detectable. Hydrogeologically, it means that the medium may be composed of various aquiferous zones, with inter-connected saturated and unsaturated zones. Thus, the performed statistical analyses on these rough data sets may identify either the hydrogeological or the lithological heterogeneity. In any case, whatever this heterogeneity is, it may represent an aggravating factor for slope stability.

Fractal behaviour and high variability at low frequency. The integration in the study of additional information, proper to each case study, allows giving some key elements for the understanding of the observed behaviours. According to the results of statistical analyses, the following characteristic are discussed: thickness of the sliding mass, geology of the bedrock and the slope of the area.

- Concerning the *Ballaigue "La Praz" and Ballaigue "Grande Combe", the Hohberg -S3-* and *the Triesenberg* case studies, these strong statistical disturbances may be explained by the thickness of the slide (between 5 and 20 meters) and the strong geological contrast between the mass and the bedrock.

- Concerning the *la Frasse* -S2- case study, these strong statistical disturbances may be explained by the regional geological setting. In fact, the *la Frasse* -S2- site is located outside the sliding area. Locally, this zone is represented by ten meters of quaternary and flysch deposits, overlaying the la Simme Nappe. This unit is composed by a flysch series with a north-east south-west stratification of limestones, sandstones and marls.

These observations may indicate that the penetration depth is exceeding the limit of the slide. The measures may be strongly influenced by the strong contrasts of resistivity existing between the bedrock and the sliding mass (figure 4.11). *It is important to note for the validity of the study, that the two following cases are not identified: 1) Low variability/fractal and 2) High variability/isotropic. The contrary would have brought several problems of interpretation.*

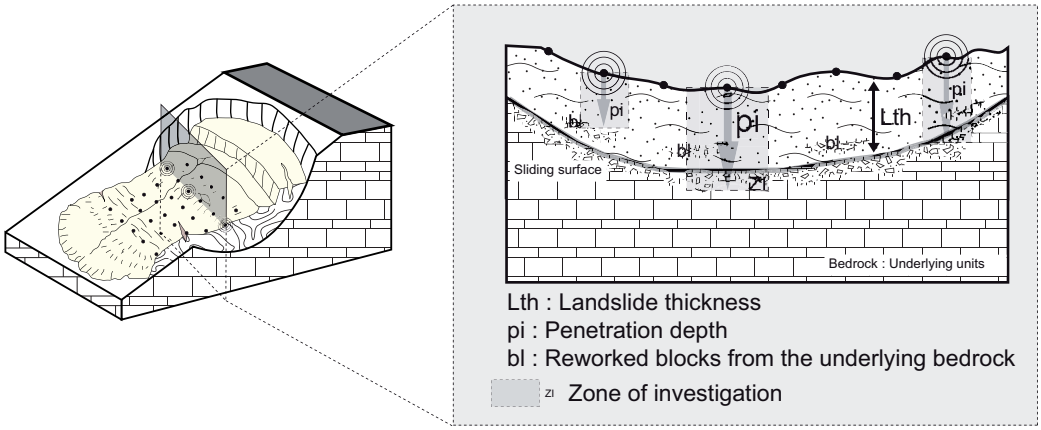

Figure 4.11: Zone of investigation and possible interactions with boundary limits. Function of the used frequency and the lithological properties of the sliding mass, the penetration depth may exceed the boundary limits. The measured apparent resistivities may be influenced by the underlying bedrock.

4.2.3.8 A new tool for drainage design ? Examples

This analytical method may constitute a new approach for drainage design in instability contexts. Indeed, the studied parameter, the apparent resistivity, informs principally about the lithological and the hydrogeological properties of the investigated sites. This statistical characterization allows defining quantitatively the heterogeneity, and qualitatively the spatial structure. The representation of the results in a "multicriterion" plot permits to identify the most important structural characteristics of the investigated site, and this at three different depths. This vertical discretization may thus allow, in the framework of a remediation evaluation, to point precisely which method has to be considered primarily, and where (subsurface, intermediate and deeply).
For instance, the identification of a strong anisotropy at subsurface, and low variability with isotropic properties in depth, would suggest in a first step to consider a rather well developed surface drainage, than an expensive underground pumping work. In the same order, the recognition of strong anisotropic and heterogeneous conditions in depths (low frequency) would claim for considering well pump drainage system.
These results may also be useful for evaluating the spacing between drainage pipes. In fact, the role of these pipes is to reduce the hydraulic pressures, and for this purpose have to be designed in order to drain out all permeable features. If an anisotropic nature is identified, the system should be oriented perpendicularly to this. Whereas, in a fractal distribution where the medium is highly chaotic, and depending on the global connectivity, the spacing of the pipes would have to be the more tightly possible in order to reach all permeable lenses. In these media, the permeability may change drastically from point to point. In the meantime, the spacing of the pipes in an isotropic medium, may be at first large designed, and then after a period of observation, if necessary, additional pipes may be added.

Case studies examples:

1. For the *Travers* case, remediation should favors surface or shallow trench drains than deep drainage wells. Indeed, the statistical analysis points out a strong variability and disordered structures at subsurface, while the underground shows a rather low variability and isotropic characteristics.
2. For the *la Frasse* cases, a coupling between surface drainage and deep draining gallery by pipes has to be considered, since heterogeneity is concerning all frequencies. The spacing and orientation of these pipes should take into account the magnitude of anisotropy.
3. For the *Triesenberg* case, the strong heterogeneous properties at each depth implicate very complex flow systems. In that case several integrated stabilization methods must be considered, since simple drainage systems may not be enough. For instance, pumped or self draining vertical wells with shallow and deep trench drains associated to retaining structures (i.e. gravity-retaining walls or reinforced earth-retaining structures)

4.2.3.9 Conclusions

These case studies are characterized by a low electrical resistivity and a heterogeneity varying strongly vertically. The structures present low spatial continuity mainly oriented parallel to the sliding direction. In the meantime, the exact position and the spatial extension of these discontinuities cannot be exactly defined. At low frequencies and especially in landslide cases with a low thickness (< 20 meters) a strong increase of the electrical resistivity variability (84% to 111%) is recorded. The modelled variograms present strong perturbed behaviours (i.e. fractal properties), probably influenced by local strong hydraulic saturation variations or by the presence of very resistive bodies (i.e. limestones units, reworked blocks or saturated

fractured zones). In any case the low resistivity of these terrains will be very sensitive to every conductive structures or body.

A "multicriterion" approach permits to classify the cases according to the investigated frequency, the heterogeneity and the spatial structure. Integrated into global remediation studies, it may represent a new tool for designing drainage systems.

The radiomagnetotelluric method enables to define the mean properties of the apparent resistivities in different landslide contexts. In the meantime, due to the scale of investigation (regional), the precision of the method, and the properties of the underground that may interfere with the measures (saturation and structural boundary conditions), these results have to be considered as being representative of a global statistical description, In the meantime this method has given interesting results. The method does not allow the location of the contact surface. The RMT method provides information to perform hydrogeological interpretations at a REGIONAL scale.

4.2.4 INFLUENCE OF STRUCTURAL SETTING AND LITHOLOGY ON LANDSLIDES

4.2.4.1 Introduction

In addition to the radiomagnetotelluric surveys presented in section 4.2.3, a comprehensive investigation of the geological patterns of these landslides (i.e. see table 4.2), occurring in low permeable environments, is completed. The geological observations are effectuated on the basis of boreholes data, from which, some geotechnical data are available. Each case study includes around five boreholes. The complete geological records may be consulted in the referenced studies in table 4.2. Certainly, this study provides a very local one-dimensional observation, but the role of some geological patterns in instability could be identified. Despite the considerable geological, hydrogeological and geotechnical heterogeneity, similarities between landslide types are observed across this geological characterization.

Globally. An overall high heterogeneity was recognized consisting in a succession of clayey to sandy beds with a main thickness around 2 meters. The heterogeneity is defined by random sequences of well to badly stratified and graded deposits. These deposits are composed of soft and weak sediments (marl, sandy shale and clay) orderly interbedded with a variable percentage of hard sediments (coarse and fine sandstone, conglomerate, greywacke and calcarenite). The proportions and successions of each material vary strongly from case to case. In the *la Frasse* landslide ("pebbly-sandstone flysch" or "marly-sandstone flysch" types, see section 4.2.2) the observed permeable/impermeable facies ratios vary from 1:4 in the most active zone "++" to 1:3 (locally 1:2) in the stabilized area (zone "+" and "GGS"), see section for the detailed lithological 4.3.4.4. Observation in l*a Lécherette* and *Creux de l'Enfer* landslides ("marly-sandstone flysch" type) shows ratios ranging respectively from 1:3 to 1:9 and from 1:1 to 1:4. Observation done in landslides taking place in Quaternary terrains (i.e. *Ballaigues Praz, Grande Combe* and *Travers* landslides) indicates also a low overall permeability; with ratios varying from 1:9 (e.g. *Ballaigues La Praz*) up to 1:2. The average ratio is in the meantime slightly lower (around 1:7; 15% of permeable material) than for the landslides in flysch terrains (around 1:5; 20% of permeable material). Globally, the impermeable character is predominant, whether if the ratios may locally strongly vary.
These deposits are structurally complex, and may crop out as: a) ordered sequences of more or less fissured and jointed layers of rock and clay or shale, b) disarranged layers of rock and highly fissured and jointed to sheared clay and shale, and c) chaotic mixture of disarranged rock elements in a clay or shale matrix.

Therefore, due to the lithological heterogeneity and geotechnical complexity, global mechanical and hydrogeological properties are very difficult to ascertain.
The overall organisation (geological architecture) is controlled by intense horizontal movements as yet observed and described in section 4.3.10 for the *la Frasse* case. Spatial and temporal heterogeneous sliding processes produce imbricated slices, separated by single or multiple surfaces. Thus, in addition to the main sliding surface, additional surfaces are recognized into the mass at various depths. For instance, in the *la Lécherette* landslide, in the borehole L1.2 two sliding surfaces are identified; a main contact at 33 meters and a secondary at 5 meters depth. Instability conditions that lead to such numerous failures can be attributed to the poor geomechanical behaviour of the sheared rock mass cut by numerous, closely spaced discontinuities and to the peculiar hydrogeological setting due to tectonic superposition of soft and hard sediments.

4.2.4.2 Relations between underground properties

The geomechanical and lithological properties are strongly linked. Geotechnical properties values of the weakest sediments (clay, shale, silt and marl) exhibit large scatters that can be ascribed to the local geological history, mineralogical composition and to the degree of internal deformation. Where weathered or tectonically sheared, their geotechnical properties are very poor (see *la Frasse* landslide), and thus strongly prone to instability. Some analysis of rock showed that the average friction angle ranges between 17° and 23° with a maximum of 30° (e.g. *Triesenberg* landslide). Higher values are obtained where abundant thick sandstone is present and for rock slumps. An increase in shear resistance is possibly related to the compaction of sediments, or in rocks where a higher percentage of calcium carbonate is observed (Elmi et al. 1993). Thus, the relative abundance of hard and competent layers (hard sediments) controls the mechanical performance of the mass and the morphological evolution of the landscape. For instance, detailed geomorphological investigations in the Marnoso-Arenacea Formation in the Umbria-Marche region in Italia (Cardinali et al. 1994) revealed that the percentage of landslide area varies between 9 and 25 percents, depending on the relative abundance of the different lithological components (hard versus soft sediments) and the structural setting.

The hydrogeological behaviour and lithological properties are strongly linked. In most of the cases, very permeable levels of sandy to conglomeratic nature are always associated to water inflows. Hard sediments have large secondary permeability related to fractures and joints. Soft sediments represent impermeable layers within the stratigraphic sequences. Primary or secondary high hydraulic conductivity fractions concentrate groundwater at the boundary of the underlying impermeable fraction. The build-up of a perched aquifer in these formations on the top of the impervious layers is a known condition of instability in various lithological environments (e.g. *Hohberg* landslide in Tullen 2002). Permeable sandstone layers within less permeable clay and silt promote the formation of confined aquifers. Depending on the structural conditions, these layers favour the build-up of pore pressures detrimental to the stability conditions (e.g. *Creux de l'Enfer, la Frasse* and *Hohberg* landslides). The aquifers are thus complex, heterogeneous and multi-layered. The pattern of groundwater circulation largely depends on the local geological setting of these materials and may be quite intricate and characteristic to each case. Finally, it is mainly observed that around shear surfaces the attitude of groundwater equipotential lines exhibits a characteristic knee-shaped form suggesting the presence of confined aquifers. The fact that slope movements are driven by the hydrological setting, i.e., the presence of confined water pressures is confirmed by measurements of artesian groundwater levels at the toe of some large landslides (e.g. *Creux de l'Enfer* and *la Frasse* landslides).
Influence of structural setting and lithological properties on failures. The outcrop of weak impermea-

ble layers (clay and silt), orderly imbedded within hard and rather more permeable sediments, constitutes the ideal anisotropic setting prone to failure. In these contexts, failures initiate as translational movements (rock block slides) and turn into disrupted rock slides or earthflows, depending on the local lithological characteristics and tectonic history. Prevalence of soft or weak rock allows the formation of larger earthflows; whereas hard rocks are related to the formation of disrupted block slides and rock slide (Guzzetti et al. 1996). In the studied cases, this differentiation is rarely possible; since the abundance of hard versus soft rocks may locally, strongly change. The observed processes are rather constituting a combination of these two processes; large earthflows with local formation of disrupted block slides and rock slide.
The tectonic units in which occur the studied cases are structurally very complex, since constituted by several thrust sheets. Thus, inside a flysch series, the dip and orientation of the layers may show strong spatial variations. If the dip is parallel to the slope, the slope is conform (dip slopes). When the dip is opposite to the slope, the slope is reverse (reverse slope). Failures may thus occur both along dip slopes and, less commonly, along reverse slopes. For instance, in the region of Adelboden (Bollinger&Noverraz 1996) the dip slopes exposed NW in the Niesen flysch series, present until 80% of the deep-seated landslides. The reverse slopes exposed SE show a modest development of landslides (20 % of the territory) and rather superficial.
In reverse slopes, landslide pattern and types of failures are controlled by topographic gradient. Failures that involve the bedrock are rotational or compound slumps where the rock is homogeneous and ductile. Where sandstone, limestone or conglomerate outcrop, the failures are represented by disrupted rock slides, falls and rock avalanches. For instance, in the instabilities of the "marly-sandstone flysch" type, the presence of thick sandstone layers controls the geometry of the rupture surface (e.g. *Falli Höli, Hohberg* or *la Lécherette* landslide).
In dip slopes, shear surface are planar, compound or complex, and develop along bedding planes, joint or cleavage systems (e.g. *la Frasse, Creux de l'Enfer* and *Triesenberg* landslide). The largest slides occur where bedding is nearly parallel to the slope or less steep than the slope.

Superficial activity. On the surface of large landslides, regardless of the structural setting, a variety of superficial movements involving the cover are present. Soil slides, minor slumps and mudflow take place after strong rainfall events, particularly in cultivated areas where infiltration to shallow depths is high. Earthflow and complex movements occur as reactivation of the main slides, particularly in the crown area where the topographic gradient is high. At the landslide toe the stream reactivations produce a hummocky topography that locally conceals the geomorphic appearance of the landslides. And according to the degree of some strong precipitation events, superficial debris flows may form.

4.2.4.3 Conclusions - Toward a conceptual model

Despite the considerable geological and geotechnical heterogeneity, similarities between landslides are observed.

a) Random successions of permeable and impermeable material
The studied landslides are characteristic by random successions of weak and hard sediments. The geometrical setting of these successions may play a major role in instability. This setting is particular to each case study, and even, may change locally inside the sliding mass.

b) Presence of sedimentary or tectonic discontinuities inside the sliding mass
Regardless to the lithological type, discontinuities provide to the slopes a strong mechanical and hydrogeo-

logical anisotropy that controls the geometry and development of failures. The sliding masses are mostly composed by numerous failures surfaces of various importance and incidence on the general dynamic. Discontinuities degrade the mechanical behaviour of the mass, constitute weak zones that provide to the slope a second order anisotropy, and facilitate the movements. At surface, these discontinuities may provide preferential infiltration zones. The water may penetrate the mass deeply, and thus contributing in the build-up and sustainment of high water pressures that favour the instability of the slope.

c) Predominant role of these lithological successions in instability

The geometrical setting of these successions promote the formation of perched aquifers and the build-up of high water pressures, even locally artesian (*Creux de l'Enfer* and *Lécherette* landslide), that can initiate and drive large deep-seated landslides. The role of the permeable facies is demonstrated since very local high flows are observed (*Creux de l'Enfer* and *la Frasse* landslides) and may generate strong internal erosion phenomena as discussed in Bossy (1999). On the one hand, if connected spatially, these high permeable pathways may drop the hydraulic pressures. On the other hand, if spatially disrupted and confined by impermeable material, overpressure zones may be generate. The formation of shear surfaces along the weakest beds of the stratigraphic sequence is also observed.

d) Hydrodynamic processes controlled by the distribution of these successions

Hard sediments (sandstone, conglomerate or loose consolidated gravelly and sandy fractions) are by far more permeable than soft sediments (clay, shale and marl), by both primary and secondary effective porosity. Hard sediments promote the formation of perched aquifers at the interface with clay, concentrating water toward joints, fractures or other higher permeability zones within largely impermeable fractions. Such hydrogeological contrasts in permeability present the ability to form local aquifer, and control and drive the movements of the slope (e.g. discussed in Tullen 2002 for the *Hohberg* landslide). Any drop in permeability produces decreases in water percolation and the build-up of a perched aquifer. This will degrade the mechanical properties and generates hazardous pore pressures that favour slope instabilities.

e) Type of failures

Landslide failures are found to be controlled by the relative position of the sedimentary and tectonic discontinuities, by the relative abundance of hard versus weak or soft rocks, and by the attitude of permeable and impermeable layers. The kinematics of these landslides is controlled by the local lithological and structural settings with a general agreement between the direction of sliding and the structural setting. In addition, abundance of clay allows for the formation of earth flow and mudflow; whereas prevalence of hard rock allows the initiation of disrupted failure, rock slide, disrupted rock slide, complex or compound slide. The contrast in competence between the lithology and the hydrogeological setting, i.e. the presence of perched aquifers within the sandstone, are thus playing a major role.

Information of landslide obtained at various scales and from multidisciplinary methods, allows the identification of landslide occurrences defined on the basis of simple geological and geomorphological considerations. Landslide-prone settings can be regarded as intermediate steps of a geomorphological continuum defined by the relative abundance of hard versus weak and soft sediments, and by the attitude and frequency of discontinuities. For instance, hard sediments capping ductile sediments and multilayers (dip or reverse) slopes are intermediate, largely unstable, conditions within two extremes represented by mostly stable mass and clay slopes (Guzzetti et al. 1996).

Thus, in order to proposed a coherent conceptual model of the hydrogeological functioning of these masses,

a detail multidisciplinary approach involving geological, geotechnical, geophysical and hydrogeological methods must be performed. This study is undertaken in the following section (4.3) on the la Frasse landslide. Thanks to a complete geological characterisation, close relations between the various underground properties are studied and compared.

And finally, thanks to the global identification performed in the present chapter, the global behaviour proper to the la Frasse landslide may be extend to the general context of landslide occurring in low permeable environment.

4.3 Heterogeneity characterisation test on the la Frasse case

4.3.1 Introduction

This general characterization, integrating data from numerous sources, aims to define the degree of geological heterogeneity and to point out the complexity of the underground flows in the *la Frasse* landslide. The final objective is to propose, first, a conceptual model for this slide, and thanks to the observations done in other landslides case studies occurring in the same geological formation (Tullen 2002), extend it to a general conceptualization.

The numerous analyses and observations presented in this chapter were performed, on the one hand, after data measured in-situ during this thesis, on the other hand, on the basis of historical hydrogeological data issued from several technical reports since 1917; Lugeon (1917-1922), Bersier (1967-1969), DUTI Détection et Utilisation de Terrains Instables (1986), NCG (1992) and NCG+EPFL (2002-2003) and 2006.

The new acquired data concern the following chapters: Hydrochemical heterogeneity, Lithofacies heterogeneity, Geophysical properties heterogeneity.

The existing data issued from the before-mentioned studies are rather concerning hydrogeological data (well tests, borehole platform flow rates...), and were compiled and analysed in the special optic to highlight the hydrogeological heterogeneity of the system. The several analyses of the hydraulic response concerning the inflow rates, for instance at the horizontal drainage systems (§4.3.8.5) were integrally performed in the framework of this thesis.

The methodology as well as the applied analytical tools are, in the special context of landslide studies, original and innovative, and mainly based on statistical basis and hydraulic response analysis methods.

- Hydrochemical heterogeneity

First a complete presentation of the hydrochemical characteristics of the surrounding aquifers is done in order to fix the studied framework. The measured physicochemical and hydrochemical parameters are briefly exposed and their heterogeneity discussed. A water classification is proposed and thanks to ^{18}O isotope analyses the probable origin discussed. Finally an estimation of the inflows through the landslide boundaries is discussed and an hydrochemical conceptual model proposed.

- Lithofacies heterogeneity

After a brief description of the explored boreholes (location and sampling methods), a vertical facies analysis is proposed. Spatial relations are discussed thanks to stratigraphic correlations essays. The facies vertical organisation and distribution is handled thanks to sophisticated embedded Markov chains and entropy calculation. Finally this facies architecture allows arguing about the geological inheritance as well as hydrogeological implications.

- Geophysical properties heterogeneity

For this purpose the radiomagnetotelluric method, yet exposed in section 4.2.3, is used. First, a short presentation of anterior geophysical studies is done. The data acquisition and processing of this method are presented and the apparent electrical resistivity and phase discussed. The true electrical resistivity are analyzed and hydrogeological implications are drawn.

- Geomechanical properties heterogeneity

Beside these investigations, and notably linked to the boreholes analysis, a short geomechanical study performed in 1986 by DUTI is presented. It handles about the vertical heterogeneity of main geomechanical properties issued from well FR2. Linear regression analyses are performed and allow understanding in a more accurate manner, the vertical properties of the geological heterogeneity of this sliding mass. These

observations are correlated with the lithofacies distribution recorded in well LF406.

- HYDROGEOLOGICAL PROPERTIES HETEROGENEITY

Several hydraulic tests undertaken at different location allow defining the physical parameters and providing accurate input parameters for numerical modelling (chapter 6):

- Infiltration tests at the borehole platform
- Infiltration tests at the wells FR1, LF1, LF2 and LF3
- Infiltration tests at the wells I301 and P302

These infiltration tests are completed with two additional studies presented in the following section (section 4.3.8): Observation of the water inflows in LFH1/LFH2 and a well test performed at the borehole platform that allowed estimating the storativity coefficient.

- FLOW HETEROGENEITY AND HYDRAULIC RESPONSE BEHAVIOUR

The general hydrodynamical behaviour (spatial and temporal) is largely discussed thanks to the observation of the evolution of the water level before 1994 (corresponding to the main crisis and the commissioning of the borehole platform see section 4.3.2.9) and after 1994. In addition, the temporal evolution of water inflow rates into two horizontal galleries is presented. The hydraulic response and behaviour of the drained zone is analyzed thanks to sophisticated methods; steady state analytical calculations of Goodman (1965) and the transient formulation of Jacob and Lohman (1952). In chapter 5, the conceptual model of the horizontal system LFH1 is used for numerical modelling in order to validate the hydrological model and the geological heterogeneity scenarios.

- HYDROGEOLOGICAL BOUNDARY CONDITIONS

A tracing test was effectuated to define the relation between the underlying stable unit and the mass itself. It aims to define the extension of the la Frasse watershed and the complex hydraulic relations between the slide and the surrounding units. For hydrogeological modelling purposes (Tacher et al. 2005), the estimation of the recharge of the slide was effectuated in order to assess the boundary conditions. The formulation and the hypothesis are largely commented.

- DISPLACEMENT RATES DISTRIBUTION HETEROGENEITY

The displacements since 1917 to 2003 are discussed. The heterogeneous spatial distribution of the displacement fields onto the landslide is done; it permits to propose a model of displacement.

4.3.2 LA FRASSE GENERAL PRESENTATION

4.3.2.1 ***Basic characteristics***

The *la Frasse* landslide is situated in the Swiss prealps (i.e. Préalpes Vaudoises) on the right shore of the la Grande Eau river (figure 4.12) in the la Vallée des Ormonts. It extends over a length of 2000 meters oriented NW to SE with a width varying between 500 and 800 meters (appendix III-1). The total surface is about 1 km^2 with a mean slope of 13°. Its maximum depth is 110 meters in the central part, but the presently active slide extends down to depths of 40 and 80 meters. The volume of the active mass represents 42 million m^3 and the total landslide volume, including the stabilised zone below the active mass, reaches 73 million m^3. Numerous studies agree to divide the slide in two principal entities being different by their volume and velocities (figure 4.13). The ¾ uphill, called "*Grand glissement supérieur*" is characteristic by a great thickness (80 meters maximum) and low velocities (5 to 20 cm/year). The ¼ downhill, the "Petit glissement rapide inférieur" is relatively thin (20 meters) and is moving sometimes very quickly (up to 20 m/year in 1966 and 1982). The accumulation zones are mainly in the "Grand glissement supérieur" zone, while the scarps concentrate principally in the *"Petit glissement rapide inférieur" zone*. The slide has a particular activity essentially in its lower part.

In addition, five main zones may be subdivided, the zone "++", zone "+", the central part ("GGS" zone), the lobe Aigle and the lobe Le Sépey. The average velocities recorded during a main crisis are, respectively, 40-60 cm/year, 15-30 cm/year, 10-15 cm/year, 5-10 cm/year and 5-10 cm/year. In depth, the numerous inclinometer readings confirm that most of the movements are concentrated on the main slip surface (NCG+EPFL 2004). Most of the time the landslide moves at these, more or less, constant velocities. Some periods of fast and brutal movement acceleration occurred like those of 1840, 1877, 1913-19, 1966, 1978, 1981-82, 1993-94 and 1999, reaching several meter in a few day (figure 4.13). These different crises had required the accomplishment of several remediation works (§4.3.2.8 and §4.3.2.9).

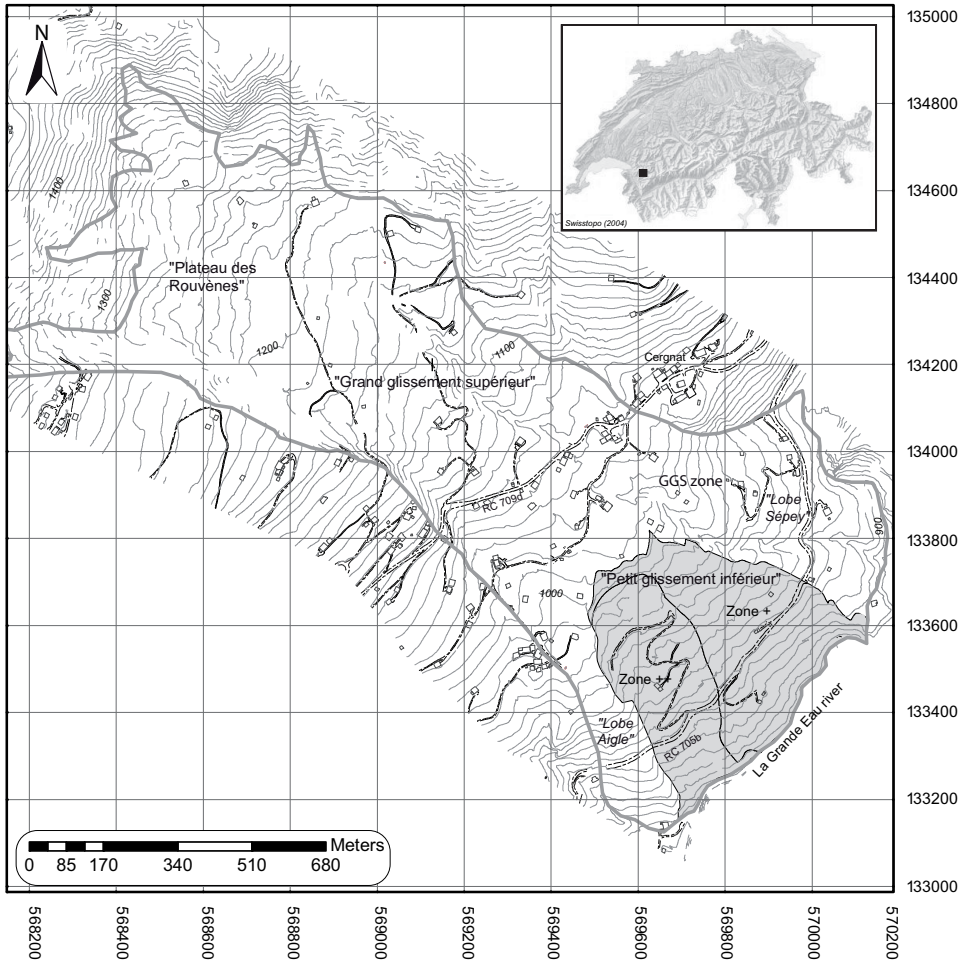

Figure 4.12: Geographical position of the la Frasse landslide.

4.3.2.2 ***Geological context***

The Swiss prealps unit is a composite unit constituted of several formations; Ultrahelvetic Nappes, Niesen Nappes, Médianes Plastiques et Rigides Nappes, Brèche Nappe and the Nappes Supérieures (Gurnigel, Simme and Gets). The slide is mainly made up by the tertiary flysch à Helminthoïdes of the Simme Nappe in the Nappes Supérieures s.l. (Lugeon et al.1922). The flysch forming the main part of the landslide is made of sandstones and clay schists with sandy blocs included in the mass. In addition, the slide has reworked a large amount of cretaceous siltstones and surface moraine fragments, thus forming a particular high heterogeneous mass. This landslide is thus well known for its extreme complex structures, inherited from long time deformations and from the geological context in which they occur. Tectonically, in its area, the major geological structure is the lying synclinal affecting the Préalpes Médianes Rigide Nappe and the la Simme Nappe (appendices III-2-3). Concerning the Préalpes Médianes Rigide, they are constituted by

Triassic and Jurassic carbonates, and by the Cretaceous sup. Couches Rouges. The Nappe of la Simme is superimposed, constituting thus the heart of the synclinal structure. It is represented by Cretaceous sup. argilo-sandy flysch, which are mainly constituting the geological mass of the landslide. This synclinal continues between le Sépey and Leysin on the right shore of the la Grande Eau River, to which its axis is parallel. Except in the landslide area, the stability of the slope is good; the reversed side of this synclinal is forming a sufficiently prominent abutment to contain the flysch mass. At the level of the landslide, this barrier was more eroded by glacial process, permitting since last glaciations (10000 years) the slip of the flysch over a width of approximately 500 meters. A tectonic weakness is equally to be noticed, since at this place, the carbonates present a thinning and several WNW-ESE faults. Thus the surrounding units are structurally complex, and mainly formed by Triassic-cretaceous carbonates. Some karstic features are developed in the Triassic limestones. In (appendix III-2) the surrounding units are schematized. It can be observed the presence of the flysch unit only in the upper part of the slide from an altitude of 1100 meters. The karstified limestones of the Cretaceous Sup unit are present above the upper limit, and through a thin band at level of Cergnat village. The lower part is embanked into the Malm limestones. The Triassic rocks are present on surface only at the toe of the slide.

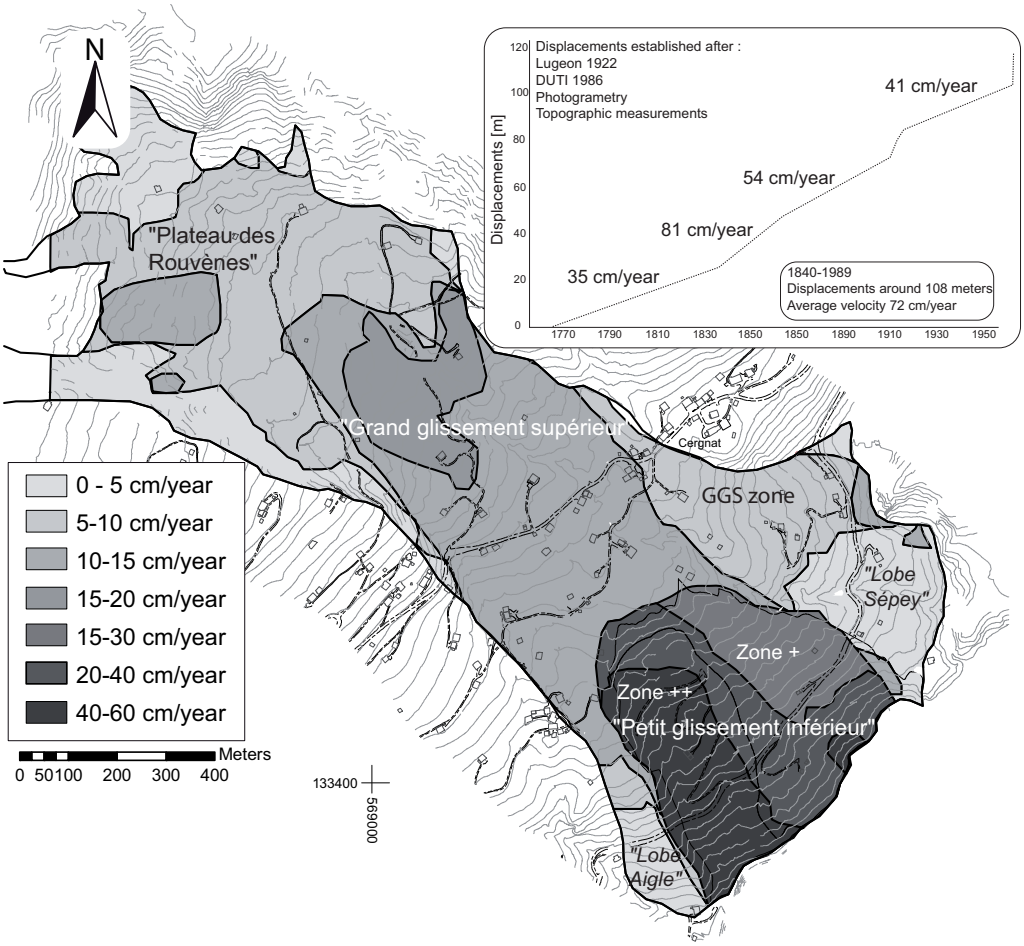

Figure 4.13: Distribution of the displacements on the la Frasse landslide and displacements rates from 1770.

4.3.2.3 ***Origin of the instability***

The origin of the instability has to be found in the disappearance of the so-called *"butée de pied de Lugeon (1922)"* which coincided in a massive structure formed by the Malm unit (figure 4.14), eroded during the last glacial erosion (-10'000 years). The glacier coming from the *"Massif des Diablerets"* formed

in that region a 45° bend in its trajectory thus intensifying the erosion processes of the Malm structures. The hypothesis of the glacial retreat has been since long time admitted, the triggering of the instability phenomena probably date from the last prehistoric glacial retreat (Lugeon 1917).

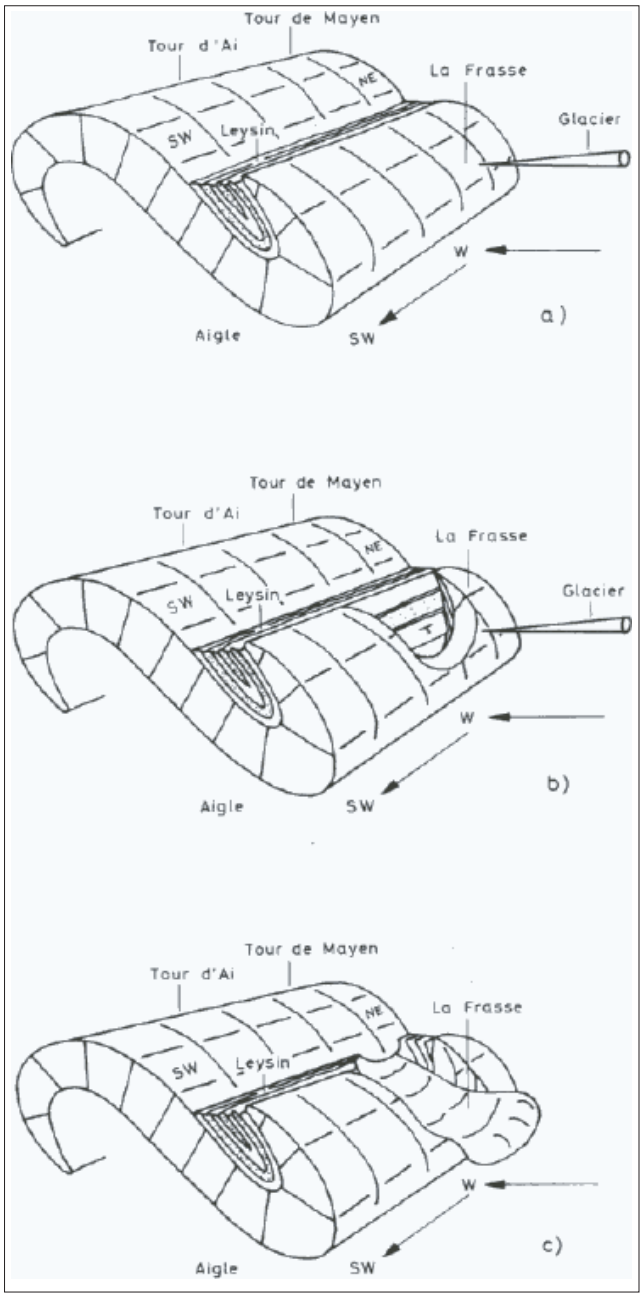

Figure 4.14: Origin of the instability of the la Frasse landslide. During the last glacial erosion (-10'000 years), the so-called "butée de pied de Lugeon (1922)" which coincided in a massive structure formed by the Malm unit was eroded (c).

The figure 4.15 (Ambrosi and Thüring 2004) shows the dynamic and evolution of the instability. The glacial retreat (sketch 1) causes decompression and elastic rebound, leaving the landslide mass in a plastic state. Then in sketch 2, the slope failure initiates at the toe of the slope and progrades uphill. In 3, due to the completion of the rupture surface, the landslide (4) enters in the kinematic phase of potentially unstable equilibrium, moving slowly downhill.

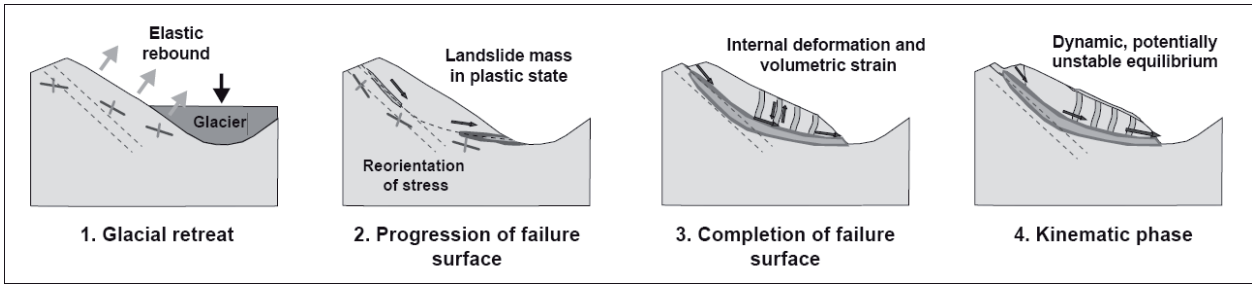

Figure 4.15: Dynamic and evolution of the instability (after Ambrosi and Thüring 2004). The glacial retreat (sketch 1) causes decompression and elastic rebound, leaving the landslide mass in a plastic state. Then the slope failure initiates at the toe of the slope and progrades uphill (sketch 2). In 3, due to the completion of the rupture surface, the landslide (4) enters in the kinematic phase of potentially unstable equilibrium, moving slowly downhill.

4.3.2.4 ***Hydrogeological context***

Due to the high heterogeneity of the materials, the hydrogeology of the zone is very complex. Underground water flows correspond to an aquifer environment of inter-granular and fracture flow, with discontinuity porosity. Because of the abundant intercalated shale and fine-grained siltstone beds, regional groundwater circulations are limited and are forming local interconnected aquicludes. Meanwhile, at the scale of the slide, the entire mass can be considered as a unique aquifer (Tacher et al. 2005). Inside the slide, intense fracturing and over-trusting of the flysch mass enable rapid groundwater flow through open fracture networks. Because its encased topography, the boundary limits of the la Frasse landslide play a major role in the recharge process. Thus, in addition to direct surface infiltration, water enters the system from the lateral boundary limits and probably locally also from the underlying Mesozoic units. In the surrounding Triassic rocks (appendix III-2), identified karstified structures allow rapid flows, and in some parts, interact with the aquifers of the slide (vertical flows). As shown in some boreholes, artesian inflows were met inside the mass, indicating that there is certainly local tendencies to recharge from the bedrock and showing that local excess of hydraulic pressures are not only present at the main slip surface but also inside the sliding mass. Indeed the hydraulic relations with the substratum are still not well defined, as there is no clear information about water inflows. Generally, the observations are rather indicating that the underlying karstified substratum of Trias and Malm is draining the water out of the slide. Due to the complexity of the general hydrogeology of this landslide, simplifications are usually adopted in the conceptual models (Tacher et al. 2005): lateral and surface infiltrations are considered, while infiltrations from the underlying units are omitted.

Concerning the hydraulic permeabilities, geological data issued from well core investigations (Norbert and de Cérenville 1999) show a high variability between boreholes spaced some 10 meters apart, indicating that 10 meters is the maximum width of the permeable structures. The permeability values calculated from Lefranc tests (NCG+EPFL, 2004) indicate an overall low shale matrix permeability of ca E-7 m/s, with locally intercalated high permeability structures (> E-3 m/s).

4.3.2.5 ***Hydrological catchment area characteristics***

The hydrological catchment of the la Frasse landslide can be sum up as follow:

- Surface: 58.8 km^2
- Perimeter: 37.2 km^2
- Average altitude: 1312 m (balanced in function of the surface)

- Maximum altitude: 2350 m
- Average slope: 20.1°

Distribution of the surface:

- Surface proportion of impermeable grounds: 1.5 %
- Surface proportion of soil: 94.9 %
- Surface proportion of forest: 43.1 %
- Average soil water retention capacity: 33.1 mm

4.3.2.6 Land Occupancy

The *La Frasse* landslide is located within an alpine zone, where rural life style predominates and where, any tourist operations have not been predicted to date. Even so, individual houses exist and the vulnerability is not low. The area is mostly made up by farms and family houses, made of wood and stones. Around 60 houses are listed and mostly dating from the XVII century. Around 20 houses are permanently habited, the others are secondary residences. Otherwise, most surfaces occupied by the slide are dedicated to extensive agriculture and by forest, particularly in the highest part of the slide. Several rivers and torrents cross the slide in the humid zones, especially in the lowest zone.
Besides the human occupation, the landslide is crossed by two principal cantonal roads:

- The cantonal road of the "*Col des Mosses*" (RC 705b) in the inferior zone (i.e. the more active).
- The cantonal road of "*Sépey-Leysin*" (RC 709d) in the upper zone (i.e. less active), parallel to the RC705b, which crosses the village of *Cergnat*.
- Several communal ways, linking the different farms and isolated houses dispatched on the whole area.

In spite the density of population, the landslide has not brought on great damages with exception perhaps of the crisis of 1966, in which 20 private properties were affected. Nevertheless, some houses are presenting evident signs of fractures due to movements and differential displacements. The electrical lines have undergone several movements, needing annual readjustment.

4.3.2.7 Historical crisis

Three main crisis have to be reported; winter/spring 1966, winter 1981-1982 and 1994. Each time very bad meteorological conditions are reported, with huge amount of precipitation on relatively short time, and a strong increase of the water table. For instance in November and December 1965, a sum of 518 mm is recorded, 235% superior than the monthly average precipitations, and respectively 163 and 147mm in February and Mars (1966). The *la Grande Eau* river presenting an important flow rate of 39 m^3/s, height times superior than the annual average. And in 1994, movements up to three meters at the RC 705 were recorded. In the meantime, numerous similar critical hydrological periods have been recorded this last century, but without generating a crisis or particular re-activation (e.g. 1968, 1970, 1979-80). For instance in 1968, 660 mm of dropped water was recorded from July to September.

4.3.2.8 Historical studies

The objective of this chapter is to present briefly the main studies that have been done this last century. In the following chapters references to these studies will be often made. The following presentation does not detail the specificity of each realized work, being yet presented in the following concerned chapters.

Only the main contributions and action of each study are reported. All boreholes and wells are reported in appendices III-4 and 5.

The first studies are dating from the end of the 19th century, with the engineers Chavannes in 1862, Cuénoud in 1866 (NCG 1992), Bridel 1868 (NCG 1992) and Develey in 1912 (NCG 1992) which proposed several remediation works at the level of the *la Grande Eau* river: levelled dams in order to cast the stream to the opposite site of the bank, a 80 meters long derivation gallery and six transversal dams completed with a protection dyke at the basement of the slide. The canalisation of the small becks spread out over the entire landslide surface was yet scheduled. In 1916 Cosendey (NCG 1992) took back the project of Develey which works were interrupted due to the First World War in 1914. He called Lugeon (Lugeon et al. 1922) which results came out from 1917 to 1922. Then, followed the studies of Bersier from 1967 to 1969 (Bersier and Weidman 1970), and finally, recently those from the EPFL (Duti 1980-1986 and De Cérenville (NCG 1992) at the origin of the main data treated in the framework of this thesis.

- The Lugeon study (1917-1922)

Two prospecting galleries were realized in the zone presenting the greatest displacements. The two so-called Lugeon galleries are totalizing 182 meters and were drilled perpendicular to the movements. The access is situated at the level of the RC 705 (Aigle-Leysin national road). From these first observations of the internal structures of the slide born the general hypothesis of triggering induced from glacial retreat. Besides the relation between the slope and the *la Grande Eau* River were analysed, conclusions about the probabilities that the river presents an aggravating factor for the stability were formulated. Propositions to isolate by means of a gallery or a dyke were yet suggested. And finally surface water drainage was scheduled.

The following works were done:
Two investigation galleries (182 meters)

- The Bersier study (1967-1969)

Three boreholes were realized. A first evaluation of the quantity of displaced material since the retreat of the glacier could be effectuated, a total volume of 125 mio. m^3 was evaluated. The first analyses of the waters permitted the first geomechanical conclusions about the causes of the high plasticity to the flysch. The priority to efficient stabilization consisting in the drainage of the underground and surface waters was given.

The following works were done:
The first boreholes (S1, S2, S3)

- DUTI "Détection et Utilisation de Terrain instable" (1986)

This was the first interdisciplinary work (geology, hydrology, hydrogeology, geotechnical analyses in laboratory and displacements measures) form the EPFL. Among all objectives, the localization of the sliding surface and the suitable instrumentation of the slide were the principal aims in order to define efficient stabilization strategies. For this purpose geophysical methods were applied; geoelectric pseudosections and seismic surveys.

The following works were done:
Boreholes FR1 to FR6

- NCG Association de bureau (1992)

This study synthesized all the previous works. A huge amount of data was grouped; geophysics, geology, core logging, inclinometer measurements, meteorology, photogrammetry, laboratory geomechanical tests. This study permitted a better knowledge about the mechanisms of the slide, and enables a zonally characterization. Besides a set of stabilization measures by stages was proposed, realized during the nineties.

The following works were done:
Boreholes LF1 to LF6 and LF8 to LF10 from 1984 to 1988 and the destructive ones LF11 to LF15 in 1989, for a total of 795 meters.

Then, in 1994 following the important activation crisis, a platform of twenty five boreholes was constructed (P1 to P22), and some important engineering works were undertaken; stabilization work of the RC 705, enlargement of the *la Grande Eau* river and reinforcement of the right shore in contact with the slide, superficial drainage works and several boreholes inside the active zone "++". Between 1998 and 2002 seven new wells (inclinometers I201 and I202, piezometers Z203, Z204 and Z205 in 1999 and I301 and P302 in 2002) were drilled in order to characterize the geological heterogeneity of the material and to install piezometers and inclinometers. Finally, in the framework of the scheduled drainage gallery work, in July and August 2001 two horizontal draining adits (LFH1 and LFH2) of 100 meters and 164 meters starting from the borehole platform were drilled into the zone "++" and "+". The main results are published in NCG+EPFL (2004). Nevertheless, it has to be noted that thanks to the crisis of the year 1994, the monitoring of the slide was significantly improved with regular data acquisitions.

The following works were done:
1994: Borehole platform (P1 to P22)
1999: Boreholes I201 and I202, Z203, Z204 and Z205
2002: Boreholes I301 and P302
2001: Horizontal drainage pipes LFH 1 and 2

- NCG+EPFL (2004)

In 2004, the *« Association technique Norbert, deCérenville Géotechnique + EPFL pour l'étude du glissement de La Frasse (2004) »* provided a complete study (period from 1995 to 2003) on the efficiency of the stabilization methods in place since 1994. This is a joint venture including several private consultants and two laboratories of the Swiss Federal Institute of Technology of Lausanne (EPFL), namely the Laboratory of Engineering and Environmental Geology (GEOLEP) and the Laboratory of Soil Mechanics (LMS) and COMSA-GEOMOD. This study had to respond to the following questions:

- *Qualitative and quantitative effects of a stabilization solution for the la Grande Eau River.*
- *Effects of the underground and superficial waters on the different established sliding surfaces.*
- *Qualitative and quantitative effects of the different stabilization solution realized until this date*

(superficial and underground drainages)

Finally, it aims at developing modelling tools allowing the characterization of the behaviour of the landslide during crises, including geological, hydrogeological and geomechanical aspects. This investigation, carried out between 2002 and 2003, has integrated all the results gathered by the numerous previous studies undertaken by the members of this association (Bonnard 1984; Vuillet and Hutter 1988; Noverraz and Bonnard 1990; Association NCG + EPFL 2004).

- NCG+EPFL (2006)

Following the study of 2004, the decision to realize the drainage gallery was took in 2006. In this framework height new boreholes were drilled in zone "++" and "+", and in addition a seismic reflection survey were undertaken. The aims were the localization of the bedrock in order to define the spatial position of the future gallery. This study, realized in the framework of this PhD thesis, describes transient hydrogeological and geomechanical models realized jointly by the GEOLEP and GEOMOD SA (NCG+EPFL, 2006). These models (presented in chapter 5 and 6) evaluate the efficiency of the drainage gallery below the sliding mass during a crisis in terms of reduction of the deformation velocities and increase of the factor of safety of the landslide.

The following works were done:

Boreholes LF401 to LF407.

4.3.2.9 ***Remediation works and observation since 1917***

In 1917, Lugeon implanted two investigation galleries (182 meters) at the level of the national road RC 705 in the most active part of the slide (zone "++"). Inflows from the sliding mass as well as from the underlying bedrock could be measured. In 1967, the first boreholes (S1, S2, S3) were drilled in the "*grand glissement supérieur*" making possible the first geological descriptions and the distinction between the sliding mass and the underlying units. Besides, these wells pointed out high water inflows from the intercalated sandy-gravely beds of the sliding mass. The project Duti (1980-1986) represents, through a multidisciplinary approach, the first developed geological and hydrogeological study. The six dug boreholes, FR1 to FR6, constitute the first wells equipped with piezometers and inclinometers. These wells are also situated inside the upper part of the slide the "*grand glissement supérieur*". The final report 1992 of NCG studies presents in details the new implemented drill-core wells (LF1 to LF6 and LF8 to LF10) from 1984 to 1988 and the destructive ones, LF11 to LF15 in 1989, for a total of 795 meters. These wells are concentrated inside the lower part of the slide.

In 1994, the borehole platform of twenty-two boreholes (P1 to P22) were drilled with a diameter of 250 mm and equipped with a strainer of 6''. This borehole platform, equipped with 16 submerged motor-driven pumps, reaches a length of 250 meters and crosses transversally the most active zone (zone "++") (appendix III-6). Each pump functions independently and discontinuously according to the water level in the well. A system of floats ensures an interlocking and an automatic release of the pumps. Below the sliding surface, the wells were prolonged with a diameter of 160 mm, without strainers, in order to test in depth the infiltration gravitating possibilities. Initially all the wells were equipped with pumps in order to extract the drained waters, but within the years, a certain number of pumps were voluntarily stopped. The pumped water volumes were too weak or the wells were bluntly dry, probably due to infiltration through

the underlying calcareous rock. Thus, in 2003 on the 22 pumps initially in service, only 15 were in function. It enables to evacuate the shallow underground waters from the sliding mass as well as from the sliding surface. In 1998, the NCG published a report presenting the main results of the borehole platform. Five new wells (inclinometers I201 and I202, piezometers Z203, Z204 and Z205) were implemented in the region of *Cergnat* above the zone "+" and "++" in order to evaluate the efficiency of the remediation method. In addition to these drainage works, Between July and August 2001, two horizontal draining adits, LFH1 and LFH2, of respectively 100 meters and 164 meters (appendix III-5), were realized from the borehole platform through the upper parts of the zones "++" and zone "+". A part its stabilization purposes, these horizontal draining adits had a value of test, aiming the establishment of the feasibility in case of positive results of a future drainage gallery located above the sliding surface.

4.3.2.10 ***Situation in 2007***

Thanks to a new sophisticated displacement monitoring tool (ROBOVEC prototype, Manetti and Steinmann 2007) installed in June 2006, the displacements could be measured every hours. Indeed, a total of eleven points (Nine on the landslide and two additional reference points outside the sliding area) were equipped with a geodetic prism and measured every hour. The ROBOVEC prototype is designed for (semi-) permanent installation in structural or geotechnical monitoring projects requiring a continuous monitoring of the 3-dimensional displacements of significant points under harsh environmental conditions.

The displacements recorded from July 2006 to January 2008 (figure 4.16) show two periods. For the first four months period (October 2006-February 2007), the point 1 and 8 present the highest displacement velocities with respectively ~4 and ~5 mm/month, starting from mid-November 2006. The averaged standard deviation of the measured distances is 1.2 mm. Note that, the maximum displacements do not concern the most active zone ("++"), but the lower right part of the zone "+". Then, since February 2007 a serious acceleration is recorded. The second period indicates an important worsening with an obvious increase of the displacements of the points 1 (up to 25 cm) and 8 (up to 70 cm).

These observations may indicate, on the one hand, that the various stabilization works undertaken on the zone "++" these last years are very efficient. On the other hand, this remediation might have translated the instability phenomenon to other neighbouring zones.

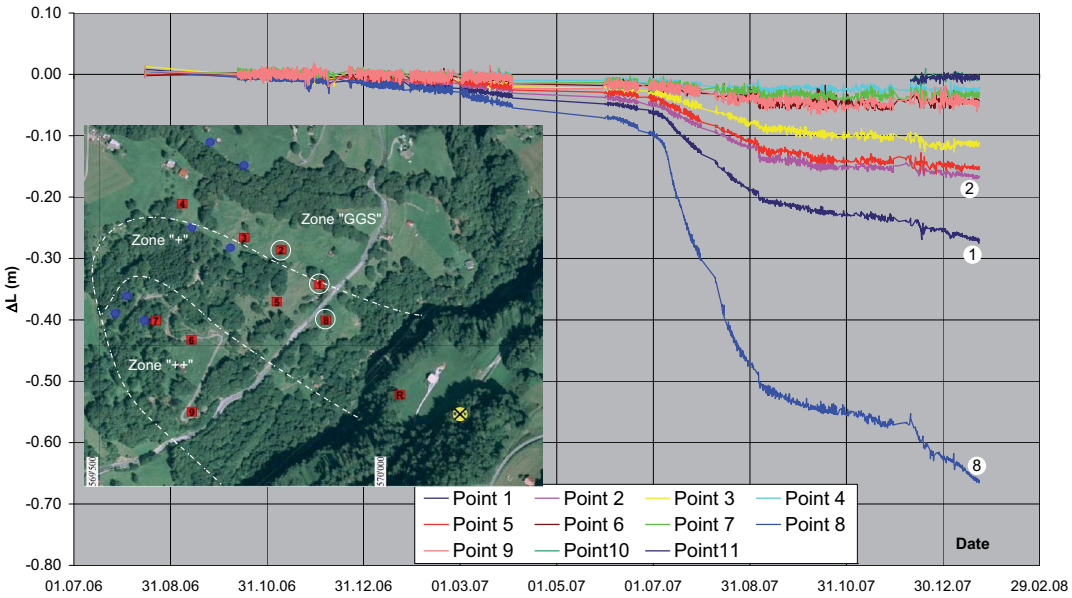

Figure 4.16: Displacements rates in 2007 in zone "++" and "+".

4.3.3 HYDROCHEMICAL HETEROGENEITY

4.3.3.1 Method

Hydrochemical and physicochemical analyses were performed on groundwaters sampled in August 2005 and 2006 from a network of 48 boreholes. These analyses were effectuated by the chemical laboratory of the GEOLEP. Water families were defined after the classification of Jäckli (1970) and compared to different alpine aquifers (Kilchmann et al. 2004). Beside this, an additional investigation performed in November 2007, enabled to measure the ^{18}O isotope, in order to confirm the defined hydrochemical families and the probable origins of the waters. This study points out the extreme heterogeneity and complexity of the circulation; hydraulic connection inside the mass and relations with the surrounding units.

The 48 wells sampled and analysed (figure 4.17, table of the results in appendix IV-1) in this study are mostly covering the active lower part of the landslide (zone"++"), 17 wells are located along the drainage borehole platform. The optimal configuration of the borehole platform enable a good representation of the chemical variation along a section crossing the active "++" zone. So-called *Piper*-diagrams (plot 4.1) (Piper and others, 1953) are used to plot the distribution of the major ions with the advantage that the dominant major element compositions are easily compared together and with the other alpine aquifers. The Jäckli (1970) water classification based on the proportions of major cations and anions is used to define water families. The water types are named using a multiple-ion designation in decreasing order of dominance. The dominant ions are determined from the percentage of milliequivalents for each major cation (Ca^{2+}, Mg^{2+}, Na^{+}, K^{+}) and anion (HCO_3^-, SO_4^{2-}, Cl^-, F^-, NO_3^-) in solution. The spatial distribution of the hydrochemical facies is given in figure 4.18, and their relative distribution and the associated hydrochemical facies are given in percents in table 4.9. In plot 4.2 and 4.3 the relations between the Na^+/Cl^- ratios, HCO_3^-/Ca^{2+} and HCO_3^-/SO_4^{2-} inform about the complexity and the heterogeneity of the underground waters.

4.3.3.2 Hydrochemical characteristics of the surrounding aquifers

In order to understand the hydrochemistry of the la Frasse aquifers, and to discuss the probable origins of the groundwaters, a general review of the hydrochemistry of water characteristic of the surrounding units is shortly presented. This summary is largely based on the AQUITYP projects, aiming the hydrogeological and lithological characterization of different alpine aquifer (Parriaux at all. 1990a, Kilchmann 2001, Basabe 1993, Dematteis 1995, Mandia 1993 and Dubois 1993) see plot 4.1. The first consideration is that the la Frasse analysed groundwaters are presenting almost all types of hydrochemical characteristics defined in the AQUITYP projects.

In detail, the **flysch groundwaters** investigated by Basabe (1993) have a low to intermediate total mineralization (median 270 mg/l) generally acquired primarily by dissolution of calcite and to a lesser degree of dolomite. The major element chemistry is dominated by Ca^{2+} alkalinity and to a minor degree by Mg^{2+}. 51% of the investigated flysch groundwaters are of the Ca-HCO_3 water type and 35% are of the Ca-(Mg)-HCO_3 water type. Flysch springwaters are generally cold (median 5.7°C) and poor in dissolved Sr^{2+}, Na^+, K^+, Cl^-, NO^{3-}, $SO4^{2-}$, and F^- is generally not detected. The poor chemical evolution of recent flysch groundwaters results from their short residence time in the fractured flysch rocks, and the absence of readily dissolving minerals except carbonates and barite. **Carbonate karst groundwaters** (Dematteis 1995) obtain their low to intermediate mineralization (161 to 547 mg/l) from the dissolution of calcite (Ca-HCO_3 waters), as well as in certain regions of dolomite (Ca-Mg-HCO_3 waters) and gypsum (Ca-Mg-HCO_3-SO_4 waters). Karst aquifers are characterised by their very permeable conduit systems, which drain

a large volume of carbonate rocks with a low permeability (e.g. Kiraly, 1975; Mangin, 1975). Therefore, the permeability of carbonate aquifers strongly depends on the extent of the development of karst systems. The major part (60 to 80%) of the groundwaters in carbonate karst aquifers flow through fissures and larger openings, whereas only a small part of the groundwater is transmitted through the pores of the carbonate rock. Groundwaters from the **crystalline rocks** are very dilute (TDS 22 to 158 mg/l). Their major element composition is dominated by Ca^{2+}, Na^{+}, Mg^{2+}, alkalinity, SO_4^{2-}, and F^{-} (Ca-Na-HCO_3-SO_4 waters) (Dubois 1993). The groundwaters from **Triassic evaporates** (Mandia 1993) in the Swiss Rhone basin are by far the most mineralised groundwaters (TDS 760 to 2788 mg/l), usually of the Ca-Mg-SO_4-HCO_3 type. Major element composition is characterised by elevated amounts of Ca^{2+}, Mg^{2+}, Sr^{2+}, SO_4^{2-}, and alkalinity (Ca-Mg-SO_4-HCO_3 waters).

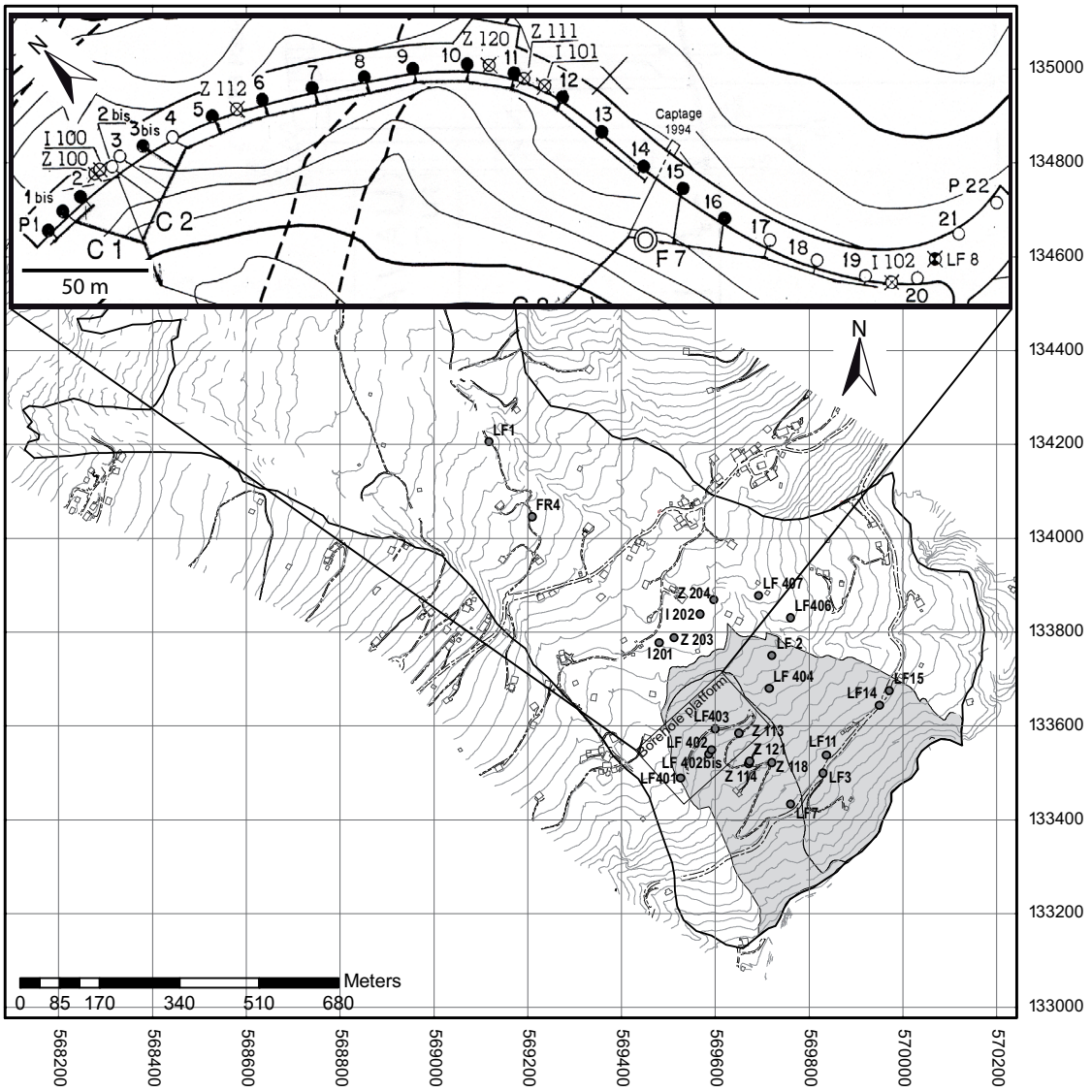

Figure 4.17: Investigated wells in the la Frasse landslide for hydrochemical analyses.

4.3.3.3 ***Physicochemical parameters***

The waters have an electrical conductivity between 233 and 1336 µS/cm (median=691µS/cm) (appendix IV-1and2) and a temperature between 8.2 and 18.2 °C (average 10.2° C). Measured pH values vary between 7.17 and 9.08. The physicochemical composition of the analysed groundwaters presents a wide

range distribution, compared to other alpine aquifers (table 4.7). For instance, median values measured are normally around 270 µS/cm in flysch aquifers, 1693 µS/cm in evaporate aquifers and 347 µS/cm in carbonate aquifers.

The high values of electrical conductivities and temperature may result from very long residence time of diffuse deep groundwater flow, while circulation through fracture system with short residence time will favour cold waters and low mineralization (Dematteis 1995). It may also locally be the result of chemical interactions with some evaporitic elements present in the heterogeneous mass.

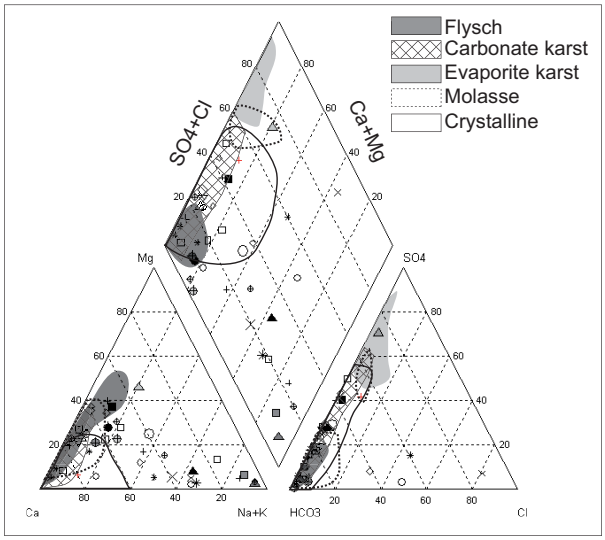

Plot 4.1: Piper-diagram illustrating the distribution of the major element compositions in the la Frasse landslide compared to different investigated aquifer types discussed in Kilchmann et al. 2004. (Milliequivalents normalised to 100%).

Parameter	Unit	CRY				CARB		EVAP		MOL		FLY	
		Gneiss		Granite									
Altitude	m	1953	n=64	1491	n=50	510	n=83	1020	n=91	650	n=96	1502	n=53
T	°C	4.7	n=63	8.9	n=46	9.8	n=86	8.7	n=91	8.7	n=96	5.7	n=50
pH	pH-units	7.6	n=17	6.5	n=35	7.2	n=85	7.0	n=20	7.2	n=94	7.0	n=46
EH	mV	439	n=6	402	n=6	440	n=72	406	n=1	391	n=94	454	n=5
O2(aq)	mg/L	13	n=1	-	-	12	n=66	7	n=1	11	n=32	12	n=1
E.C. at 20°C	µS/cm	83	n=63	79	n=55	347	n=79	1693	n=91	420	n=96	270	n=53
TDS	mg/L	75.2	n=64	69.1	n=54	345.4	n=87	1782.2	n=91	418.3	n=96	267.1	n=53

Table 4.7: Physicochemical parameters of recent groundwaters from different aquifer types (median values and the number of samples). CRY=crystallin ,CARB=carbonates, EVAP=evaporites, MOL=molasse, FLY = Flysch (After Kilchmann 2001).

4.3.3.4 Hydrochemical parameters

Average chemical compositions compared with flysch aquifers (Basabe 1993) are summarized in the table 4.8. The waters have an intermediate mineralization (median TDS = 438.8 mg/l), with total dissolved solids (TDS) values varying from 137.6 mg/l up to 938.4 mg/l. Basabe (1993) reported a TDS median value of 267.1 for flysch aquifers, while in evaporitic media it can reach 2787.5 mg/l (Kilchmann 2001). The hydrochemistry is dominated by Ca^{2+}, Mg^{2+}, SO_4^{2-} and alkalinity. Groundwaters with elevated alkalinity content (more than 50% of the total mineralization) occur principally in aquifers predominantly composed of carbonate and with part of calcium sulphate minerals. These groundwaters also show a higher mineralization than the groundwaters circulating in environments dominated by detritic rocks such as flysch or molassic deposits.

Parameters	Unit	min	med	max	var.	st. dev.	coef. of var.	n		min	med	max	n
Cond	µS/cm	233.0	691.5	1336.0	53109.0	230.5	33.3%	48		159.0	270.0	474.0	53
Temp	°C	8.2	10.1	18.2	3.6	1.9	18.6%	48		1.2	5.7	9.2	50
pH	pH-unit	7.17	7.74	9.08	0.3	0.55	7.1%	17		5.9	7.0	7.7	46
Na	mg/l	1.74	62.33	291.08	6349.0	79.68	127.8%	48		0.3	0.8	10.2	51
K	mg/l	0.75	5.76	50.29	62.0	7.87	136.6%	48		<0.2	0.4	3.0	53
Mg	mg/l	0.67	21.12	67.96	261.9	16.19	76.6%	48		1.3	3.2	23.5	53
Ca	mg/l	6.45	92.74	180.00	2028.4	45.04	48.6%	48		24.0	56.2	97.3	53
F	mg/l	0.04	0.29	1.66	0.2	0.42	143.4%	30		<0.2	<0.2	<0.2	53
Cl	mg/l	0.46	16.05	209.50	1574.1	39.68	247.3%	48		<1	<1	3.5	51
NO3	mg/l	0.05	7.78	95.29	403.3	20.08	258.2%	38		<1	2.4	8.1	53
SO4	mg/l	2.36	93.84	306.30	5649.4	75.16	80.1%	47		2.5	8.2	36.2	53
HCO3	mg/l	37.90	391.05	702.50	21812.5	147.69	37.8%	41		113.7	186.9	314.2	53
TDS	mg/l	137.6	438.77	938.4	33559.3	183.192	41.8%	48		159.7	267.1	458.8	53
water hardness	°F	2.61	28.30	67.99	284.0	16.85	59.6%	20		9.7	16.3	27.9	53

Flysch aquifers in the Niesen and Gurnigel nappes (data from Basabe, 1993)

Table 4.8: Average of chemical compositions of the la Frasse landslide waters and recent groundwaters from flysch aquifers (Basabe 1993).

The most abundant and common cations are the calcium (Ca^{2+}), magnesium (Mg^{2+}) and sodium (Na^{+}). Their concentrations largely invoke groundwater-rock interactions. Ca^{2+}, with value of 6.45 up to 180.00 mg/l, is principally produced by carbonate (limestone and dolostone) and gypsum ($CaSO_4$) dissolution. Mg^{2+}, with value of 0.67 up to 67.96 mg/l, is produced by Mg-calcite and dolomite dissolution or by de-dolomitization of dolomite to calcite by the diagenesis in high Ca/Mg groundwaters (Kilchmann 2001). Average Na^{+} concentration is anomalous with up to 60 times higher than in the others aquifers, with values varying from 1.74 up to 291.08 mg/l. Possible sources of sodium include cation exchange between groundwater and clay minerals (Ca-Na ion exchange with long residence time), dissolved minerals in water from the surrounding mesozoic carbonatic rocks (Malm and Cretaceous Sup), or anthropic activities (thawing of snow by salt, i.e. halite NaCl). On average, the cation percentage (Ca^{2+}, Mg^{+} and Na^{+}) is higher in the la Frasse groundwaters than in other typical groundwater aquifers, with exception done for evaporate aquifers. For instance in the most dilute flysch groundwaters studied by Basabe (1993), the content of dissolved Na^{+}, K^{+} is near the detection limit. These values reflect complex hydrodynamic settings and probably an alimentation from multiple sources, with strong influences of groundwaters issuing from limestone, gypsum and dolomite environment.

The most abundant and common anions are the bicarbonates (HCO_3^{-}), chloride (Cl^{-}), sulphate (SO_4^{2-}), nitrate (NO_3^{-}), and fluoride (F^{-}). HCO_3^{-} is produced by carbonate dissolution, whereas it is also produced by silicate dissolution and dissociation of water molecules. The four common water-mineral reactions are: calcite dissolution, dolomite dissolution, halite dissolution and gypsum dissolution. HCO_3^{-} average value (391.05 mg/l) is in the range of typical carbonate aquifers (median=372.1 mg/l) but higher than common flysch aquifers (median =186.9 mg/l). This concentration will be discussed later since it may probably reflect the abundance of carbonate cements and carbonate interbeds inside the flysch mass, or the recharge by waters coming from the surrounding carbonate rocks. NO_3^{-} is not common in these waters, except in some wells (i.e. well P6 with 100 mg/l). The presence of nitrate in groundwater is usually an indication of contamination by decay of organic materials, septic tanks, fertilizers (agriculture activities), or waste from farm animals, and implicates thus direct connections with surface waters. The concentration of SO_4^{2-} (median=93.8 mg/l) is significantly less than in evaporate aquifers (median=1043.3 mg/l), in the same time, significantly more than in carbonate or flysch aquifers (8.6 mg/l and 8.2, respectively). The principal sources of SO_4^{2-} have to be searched more in the surrounding carbonate rocks than in flysch units. In the meantime, inside the landslide, the oxidation of sulphides contained in the sediment (transported and incorporated blocs rich in sulphates) can occur and justify these concentrations.

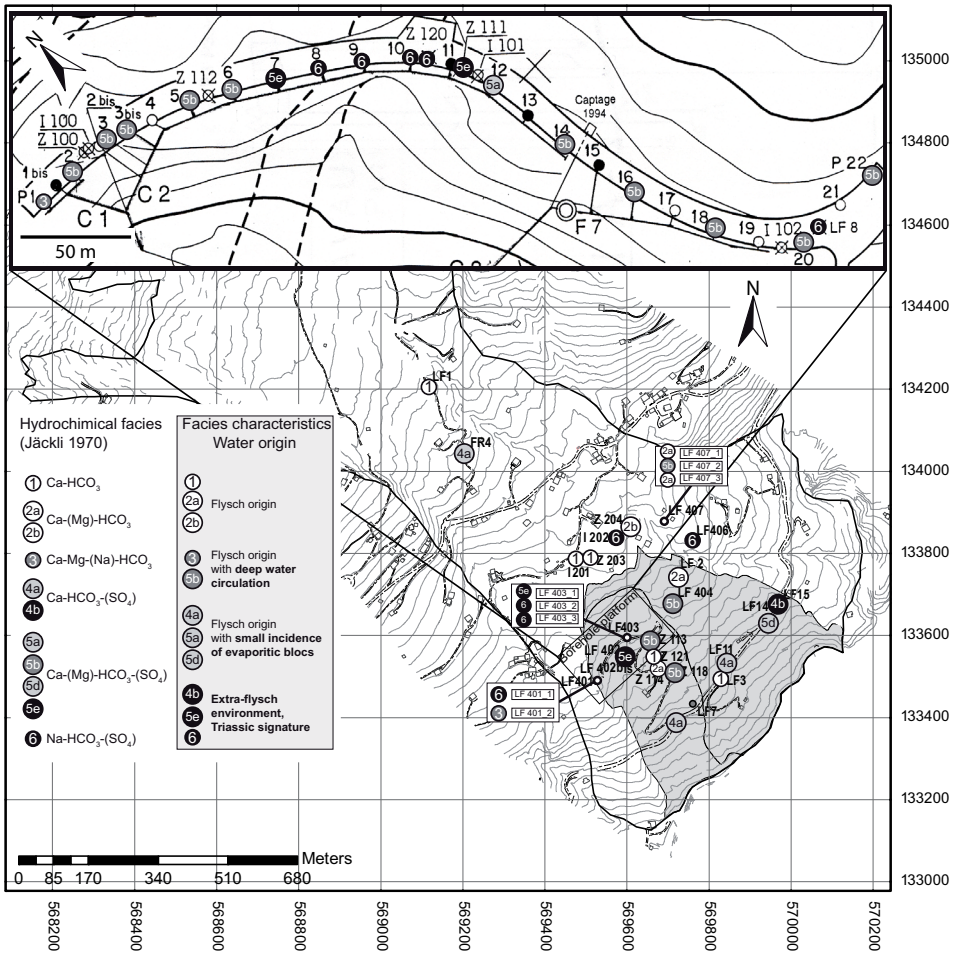

Figure 4.18: Spatial distribution of the hydrochemical facies after Jaeckli (1970), and the identified water origins.

The average concentrations of Cl^- (median =16.05 mg/l) is relatively important, and can even be locally very high (up to 209.5 mg/l in LF15). Most of the flysch groundwaters studied by Basabe (1993) indicates a content near the detection limit. Possible sources of chloride include anthropic activities (thawing of snow by salt, i.e. halite NaCl), rain water influences, cation exchange between groundwater and carbonate rocks generally more saline (Ca^{2+}/Cl^- ion exchange and Na^+/Cl^- ratios superior than in precipitation). More evolved groundwaters are characterized by high Na^+/Cl^- ratios due to additional Na^+ from Ca-Na cation exchange reactions (plot 4.2). For the wells LF14, LF15 and LF3 these chloride concentrations are probably resulting from anthropic activity according to the Na^+/Cl^- ratio equal to 1, and their geographical position (near the national road RC705).

Groundwater type (see table 4.9)**.** Thus, the dominant waters (69%) are of the Ca-(Mg)-HCO_3-(SO_4) water type with variable ratios of dissolved Ca^{2+} and Mg^{2+} and some traces of SO_4^{2-}. The second important group is controlled by the dissolved Na^+; Na-HCO_3-(SO_4) water type (23%). A third group (8% of the analyses) is represented by the strong presence of sulphate (SO_4^{2-}). These results provide a good view of the complexity of the system; chemical and spatial heterogeneity (spatial random distribution). Different provenance and sources may certainly explain this.

Jäckli chemical classification	facies	Distribution of water types
Ca-HCO_3	1	11%
Ca-(Mg)-HCO_3	2	11%
Ca-Mg-(Na)-HCO_3	3	4%
Ca-HCO_3-SO_4	4	8%
Ca-(Mg)-HCO_3-(SO_4)	5	43%
Na-HCO_3-(SO_4)	6	23%
Facies characteristics, water origin		
Flysch origin	1, 2a and 2b	**21%**
Flysch origin with deep water circulation	3 and 5b	**34%**
Flysch origin with small incidences of evaporitic blocs	4a, 5a and 5d	**11%**
Extra-flysch environment, carbonate signature	4b, 5e and 6	**34%**

Table 4.9: Water classification after Jäckli (1970), distribution of water types and origin. See figure 5 for the spatial distribution.

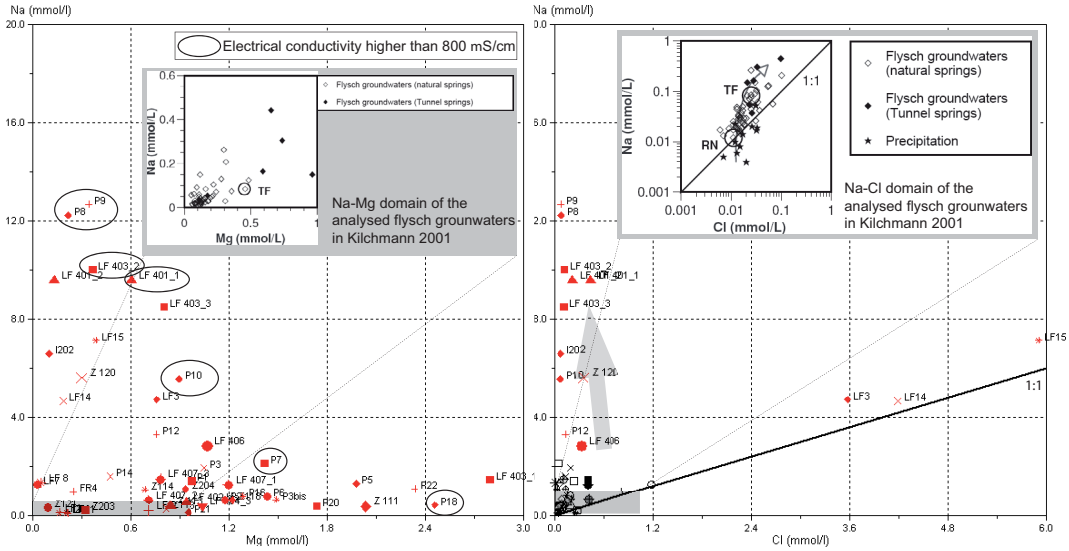

Plot 4.2: A] The comparison of average molar Mg2+, Na+ ratios compared to investigated flysch groundwaters in Kilchmann 2001. B] Average molar Na+/Cl- ratios compared to investigated flysch groundwaters in Kilchmann 2001. The arrow indicates the evolution of the Na+/Cl- ratios in the groundwaters resulting from ion exchange.

4.3.3.5 ***Hydrochemical processes and heterogeneity***

Due to this high chemical heterogeneity an accurate interpretation is difficult. In the meantime, as shown in plot 4.3 (a,b), a first group may be identified; wells P8, P9, P10, LF403_2 and 3, LF 401_1 and 2 with more evolved chemical compositions

Alkalinity/Ca^{2+}. Three tendencies are observable depending to the ratio of alkalinity/Ca^{2+}. According to the stoichiometric reaction of the calcite ($CaCO_3$(s) + H_2O + CO_2 $\leftrightarrow$$Ca^{+2}$ + 2 HCO_3), groundwaters in equilibrium with calcite have a molar alkalinity/Ca^{2+} ratio of 2 (Ca-HCO_3 water type). The groundwaters of the Ca-Mg-HCO_3 water type have higher alkalinity/Ca^{2+} ratios (ratio of 4 and more) due to their higher alkalinity from the dissolution of dolomite. The groundwaters of the Ca-Mg-HCO_3-SO_4 water type show lower alkalinity/Ca^{2+} ratios (1:1) resulting from the higher Ca^{2+} content due to gypsum dissolution. The

group formed by well P8, P9,P10, LF 403_2,3, LF 401_1,2 are characteristic of high alkalinity/Ca^{2+} ratios, and high electrical conductivities (>600 µS/cm).

Alkalinity/$SO4^{2-}$. This group is equally differentiable by its alkalinity/$SO4^{2-}$ ratios (plot 4.3b). The hydrochemical evolution of these groundwaters is governed by incipient dedolomitisation, involving dissolution of gypsum, celestite and dolomite and simultaneous precipitation of calcite. In addition, as dolomite has slower dissolution kinetics than calcite, the higher Mg^{2+} values suggest that these groundwaters are more evolved and could belong to deep slow circulations. This is also consistent with the elevated Na^{+}, and K^{+} concentrations in these groundwaters (plot 4.2). Most of the waters sampled from these wells are deep, in the meantime it has to be noted that the highest Mg^{2+} concentration is found in the water of well LF403_1 at a depth of 12 meters, thus pointing out the existence of vertical connections inside the mass. In comparison, groundwaters sampled in well Z121, Z203, I201 show a poor chemical evolution and the absence of dissolving minerals except carbonates, and are certainly to be attached to rapid subsurface flows.

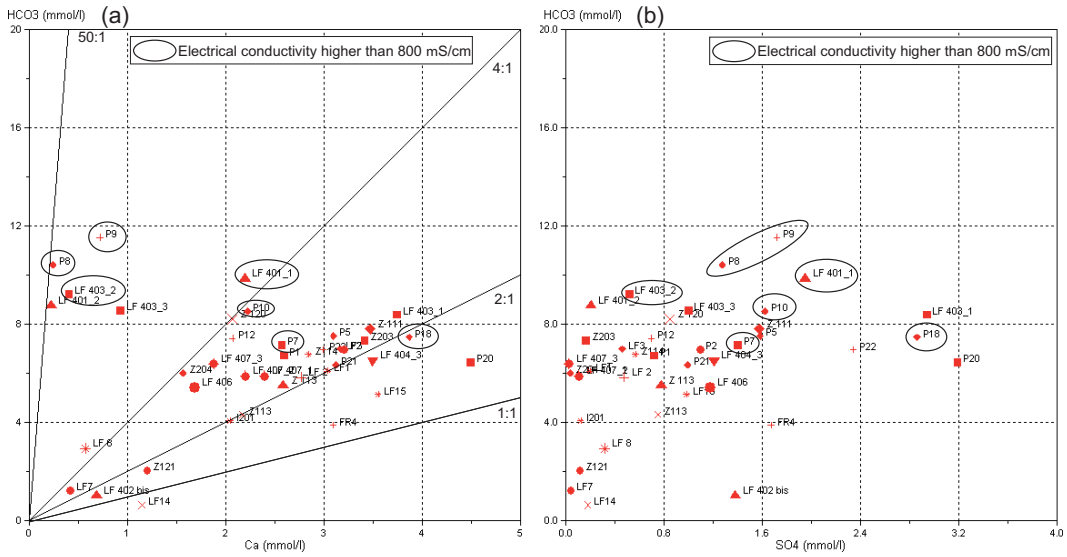

Plot 4.3: A] Average molar alkalinity/Ca2+ratios. B] Average molar alkalinity/SO42- ratios. Circled wells have an electrical conductivity higher than 800 µS/cm.

Heterogeneity observed at the borehole platform. It may be interesting to focus on the borehole platform in order to observe the heterogeneity at a local scale. The borehole platform (appendix III-6) enables to sample the water issued form the sliding surface every 10 meters (average spacing of the wells).

Results in appendix IV-5 and figure 4.19 indicate that there is no correlation between two close wells. Roughly, a group constituted by the well P7, P8, P9, P10 and P12 is showing some similitudes according to their electrical conductivity and HCO_3^-, Mg^{2+}, Na^{+} concentrations, typical of carbonate rocks circulation (i.e. low Mg^{2+} concentration and high Na^{+} and HCO_3^- concentrations). Thus, at the scale of the platform, it is possible to identify preferential zones characterized by waters coming from external units.

Direct connections with surface flows may also be identified thanks to the nitrate concentration being mostly issued from agriculture activities. In this sense the wells P6, P3, LF14 and Z121 present a poor evolved hydrochemistry and high nitrate concentration. The sampled water may directly come from the surface, i.e. 300 meters upstream of the platform where important agriculture activities are observed. In addition the concentration of chloride detected in P6 (Na^{+}/Cl^{-} ratio near 1) seems to confirm that this well is alimented by rain water. These observations at a local scale highlight that the mass is constituted by a

complex structure of isolated flow pathways, relatively thin (<10 meters), more or less connected, and draining surface water as well as extra landslides waters.

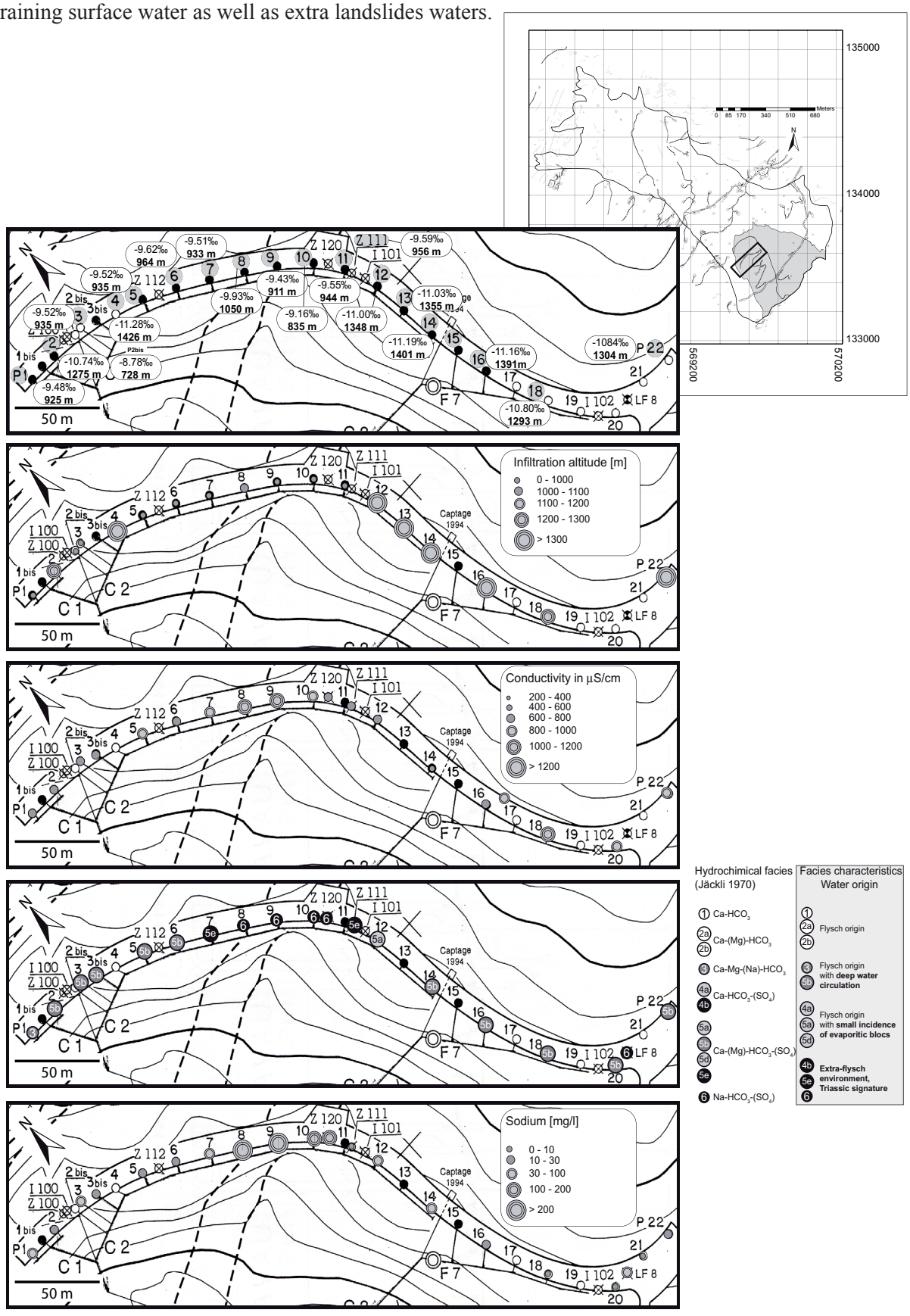

Figure 4.19: Hydrochemical analyses distribution at the borehole platform: electrical conductivity, sodium, hydrochemical facies after Jaeckli (1970), identified water origins, measured isotopic values and evaluated altitudes of infiltration.

4.3.3.6 Water classification – origin

The waters sampled during this study were chemically classified in 6 hydrochemical facies after Jäckli (1970) (see table 4.9 and figure 4.18). Within these facies, the cations and anions content can be variable, thus defining sub-facies. Each subfacies corresponds to a specific geological environment, informing about the origin of the water. The Ca-HCO_3 water type is found in pure limestone aquifers. The Ca-Mg-HCO_3 water type occurs in dolomite limestone or dolostone aquifers, while the Ca-Mg-HCO_3- SO_4 water type is found in aquifers composed of carbonate series containing evaporate beds with gypsum and other sulphate minerals. These six hydrochemical facies can be related to aquifer lithologies. Four main origins, described and discussed in Basabe 1993, are defined in this study: 1) flysch origin (*facies 1 and 2*), 2) flysch origin with deep water circulation (*facies 3 and 5b*), 3) flysch origin with small incidences of evaporitic blocs (*facies 4a, 5a and 5d*) and 4) extra-flysch environment, carbonate *karst* signature (*facies 4b, 5e and 6*).
The underground waters from the first group, defined as flysch origin water type (facies 1 and 2), are mainly characterized by waters of the calcic (-magnesium) bicarbonated (Ca-HCO_3 and Ca-(Mg)-HCO_3) family, with a concentrations in hydrogenocarbonates and calcium higher than 50% with more or less magnesium (e.g. subfacies 2a, <20% of Mg^+). The poor chemical evolution of these groundwaters and the absence of readily dissolving minerals except carbonates, results from their short residence time in the fractured flysch rocks or very permeable structures. This facies represents 21% of the analysed wells (LF1, LF2, I201, Z203, Z114, Z121, LF407_1, 3 and LF3) mainly situated in the flysch mass of the slide and sampled between 9 and 26 meters depth. The second group, representing 34% of the sampled waters, distinguishes waters from flysch environment with deeper and slower flows (facies 3 and 5b). It includes waters with higher magnesium ratio (>20%), slightly sulphated and with a significant presence (10-20%) of sodium (i.e. calcic-magnesium-(sodic)-(sulphated) bicarbonated (Ca-Mg-(Na)-HCO_3 and Ca-(Mg)-HCO_3^--(SO_4)). Huge sodium contents can be the results of different mechanisms. A mechanism of exchange of ions sodium-calcium can be evoked in the impermeable fraction of the flysch, with slow water percolation. An extra-flysch influence can also be mentioned. These waters are common to a large number of wells (LF 401_2, LF407_2, LF 404_3, Z113, Z118, P2,3,3bis,5,6,14,16,18,20 and P22). The third group (11% of the groundwaters sampled), describes waters issued from a flysch environment probably in connection with extra-flysch units because showing small incidences of evaporitic terrains (facies 4a, 5a and 5d). These waters have a calcic-bicarbonated (Ca-(Mg)-HCO_3^--(SO_4)) component more than 50% with a small presence of sulphate (10-20%). The origin of these sulphates can be either a slight influence of the evaporitic extra-flysch units, nor resulting from the oxidation of the sulphurs present in the rocks inside the flysch. Wells P12, FR4, LF7, LF11 and LF14 are forming this group. Finally, in 34% of the sampled wells, groundwaters with strong extra-flysch origin (*facies 4b, 5e and 6*), such as water signatures encountered in carbonate rocks flows. These waters show a much more moderate amount of hydrogenocarbonates (10-20%) and a higher concentration of sulphates (20 to 50%), and a consequent high concentration in sodium (sodic bicarbonated sulphated Na-HCO_3-(SO_4^{2-}) waters), i.e. wells : LF403_2,3, LF401_1, LF8, I202, LF406, P8, P9, P10, Z120 LF15 LF403_1, LF402bis, P7 and Z111. This type is similar to waters from deep flysch circulation regarding to the Na^+ compositions, but with a content of SO_4^{2-} too high to be uniquely associated to water flysch types. The argument in favour of an extra-flysch alimentation can be retained.

4.3.3.7 18O isotope characterization

Introduction. In addition to the analysis of the majors, a sampling survey was undertaken in November 2007 in order to analyse the ^{18}O isotope. Water in almost all the wells was encountered with exception of: LF2, LF8, LF15, P3bis, P20, P21, LF401_2, LF403_3, LF404_3, LF407_2, Z111 and Z120. Very rainy

meteorological conditions were recorded the previous days.
This study concerns a time-punctual sampling. Normally, as described in Tullen (2002), sampling should concern a period of at least one year in order to cover a complete hydrological cycle (snow melt season, dry and rainy periods). Our study was undertaken for comparison and characterization purposes, taking into account that isotopic values can slightly evolve during a year. In this work the defined isotopic composition are used to define altitudes of infiltration. The local gradient used to establish the relation between ^{18}O and the altitude is taken from the Hohberg isotopic study (Tullen 2002). The la Frasse and the Hohberg landslides present according to their geological, hydrological and meteorological characteristics great similitudes. The Hohberg landslide is geologically belonging to the same tectonic structure (Préalpes Externes) and geographically relatively close to the la Frasse (some kilometres), and the average altitude of the catchment area is identical. The local gradient is given by: altitude of infiltration=-279*$\delta^{18}O$-1720.

Results. The values are ranging from -8.78 to -11.74 $\delta^{18}O$ (‰) (Appendix IV-1, 3 and 4), the calculated altitudes are between 728 meters and 1573 meters. The results show that most of the sampled waters are infiltrating in the upper part of the slide (high altitudes), exception made for some wells which may indicate that the intercepted waters are rather belonging to local flow system, while their calculated altitude of infiltration corresponds more or less to the altitude of the well. Note that, the upper limit of the la Frasse landslide reaches the altitude of 1300 meters.
Four infiltration zones are thus defined; zone (1) = altitude of infiltration corresponding to the altitude of the well, zone (2) = altitude of infiltration covering an area maximum 200 meters above the altitude of the well, zone (3) = altitude of infiltration corresponding to the upper zones of the slide (>1200 meters), zone (4) = altitude of infiltration corresponding to zones above 1300 meters (outside the limits of slide).
Four water families were defined after the analyses of the majors (§4.3.3.6); family (1) flysch origin (facies 1 and 2), family (2) flysch origin with deep water circulation (facies 3 and 5b), family (3) flysch origin with small incidences of evaporitic blocs (facies 4a, 5a and 5d) and family (4) extra-flysch environment, carbonate karst rocks signatures (facies 4b, 5e and 6).
Table 4.10 present a classification of the wells according to their defined infiltration zones and their hydrochemical facies defined in §4.3.3.6.

Infiltration zones	Family (1)	Family (2)	Family (3)	Family (4)
Zone (1)	LF407_1, LF1, LF3, Z121	P1, P3, P5, P6,	FR4, LF14, LF7	P7, P9, P10, Z111
Zone (2)	LF407_3, I201, Z114			P8
Zone (3)		P18, P2	LF11	LF402bis
Zone (4)	Z203, Z204	P14, P16, P22, Z113, Z114		I202, LF406, LF401_1, LF403_1, LF403_2

Zone (1) = altitude of the infiltration zone corresponds to the altitude of the well
Zone (2) = altitude of the infiltration zone at maximum ***200 meters above*** *the altitude of the well*
Zone (3) = altitude of the infiltration zone corresponds to the ***upper zones of the slide*** *(>1200 meters)*
Zone (4) = altitude of the infiltration zone corresponds to the upper zones ***outside the limits of slide*** *(>1300 meters)*

Family (1): flysch origin (facies 1 and 2)
Family (2): flysch origin with deep water circulation (facies 3 and 5b)
Family (3): flysch origin with small incidences of evaporitic blocs (facies 4a, 5a and 5d)
Family (4): extra-flysch environment, Triassic signature (facies 4b, 5e and 6)

In grey, the waters that may infiltrate outside the boundaries of the slide

Table 4.10: Classification in zones of the different altitudes of infiltration and related to the defined water families.

- Most of the waters from the family (1) and (3) are infiltrating a zone around the well, thus with short flow distances. **Exception done for wells: Z203, 204 and LF11.**
- Waters from the family (2) are principally mostly belonging to upper zones of the landslide.
- Waters from family (4) are mostly infiltrating outside the upper boundaries of the landslide. **Exception done for wells: P7, P9, P8, P10 and Z111** all closely situated (borehole platform)

Discussion. The calculated altitudes are in part confirming the facies determination and the water origin defined by the analyses of the majors with, in the meantime, some exceptions that will be discussed in the next section. Groundwaters with an extra-flysch origin are characterized by long travel distances, while those having a flysch origin rather local infiltration zone. The waters from the family (2) are particular in the sense that they correspond to waters with long residence time. The main characteristics of these waters, high magnesium (>20%) and sodium (10-20%) ratios, are explained through different mechanisms; sodium-calcium exchanges in the impermeable fraction demanding long time residence (slow flows) or a possible extra-flysch influence. Thus, the infiltration zones can be either close to the sampled point or far away. The waters from the families 1 and 3, are corresponding to waters typical for flysch units, mostly infiltrating zones around the well and with short travel distances. The waters from well Z203, 204 and LF11, with altitudes rising above 1300 meters, are coming from upper zones. Their origin is thus to be find into the Flysch unit in contact with the landslide. The waters from family (4) have an extra-flysch provenance with a strong carbonate influence. Their origin has to be found in the surrounding units of the Cretaceous sup. or Malm.

Thus, waters recording infiltration altitudes superior than 1300 meters are infiltrating outside the upper boundaries of the landslide, near the Tour d'Aï region. Wells P7, P8, P9, P10 and Z111 are recording low altitudes. Nevertheless regards to their hydrochemistry, their origin belongs to carbonated environment. Thus, according to their altitude of infiltration, these waters are coming from the close surrounding Malm unit through lateral infiltration perpendicular to the slope.

4.3.3.8 Estimation of the inflows through the landslide boundaries

An estimation of the relative contribution of the inflow through the boundaries is done thanks to the water facies and the ^{18}O isotope study. The results indicate that at least 34% of the sampled water are infiltrating outside the upper limits of la Frasse (>1300 meters, zone 4), but without considering the waters that may infiltrate laterally at lower altitudes. If one considers that all waters situated in facies 4 and those in facies 2 and 3 of the zone 3 (table 4.10), one can estimate that around 63% of the sampled waters are infiltrating outside the boundary of the slide and recharging it through lateral boundaries. These results are in accordance with the estimation done in section 4.3.9.2 (Tacher et al. 2005).

4.3.3.9 Hydrodynamical implications

The main conclusions are the following:

- Multiple origin, 63% of exotic origin
- High local heterogeneity
- **Bimodal hydrodynamic flow system**
    - **Low flows in the impermeable fraction, with Ca-Na cation exchange reactions**
    - **Rapid flow in the permeable fraction, poorly evolved**
- High longitudinal connection to regional flow system and neighbouring watershed

- Short vertical connection to surface waters
- Local transversal inflows
- Mainly thin structures (<10meters)
- Importance of the boundary infiltrations
- The observation is **local** (punctual sampling) but provide a **regional vision** of the functioning (origin of the incomes).

4.3.4 LITHOFACIES HETEROGENEITY

4.3.4.1 Procedure

In the framework of the feasibility study of the future drainage gallery (see section 6.4), an important geological survey was undertaken from the 18th April to the 18th August 2006, including 7 boreholes (figure 4.20 and table 4.11) and a seismic reflection survey, in order to optimize the final layout of the drainage gallery and to precise the conditions of excavation (see appendix V).
The boreholes were performed by the association of SIF Groutbor SA and Stump Foratec SA, and the operation was controlled by the geological office Norbert SA. Taking advantages of these surveys, it was decided to perform an accurate sedimentological analysis of the core samples thanks to sophisticated geostatistical analyses.
It includes: *descriptive statistical analyses* on bed thicknesses and facies distribution in order to precise the lithological tendencies and organisation, *linear regressions* to test the randomness of the structures and to define if sequences are predictable, *horizontal correlation essays* to explore the lateral continuity of these facies.
Embedded Markov chain analyses and entropy estimation are then performed on facies transitions matrix to determine whether there is a preferential vertical cycle. In sedimentology, the Markov chains analysis is used to establish the prevalent pattern of vertical facies change in a stratigraphic succession. Moreover, the analysis of the entropy enables to characterize the possible symmetry of the successions (symmetric, e.g. A-B-C-B-A; asymmetric, e.g. A-B-C-A-B-C; random cycle, e.g. ACABCA).
The aims are to define the global geological architecture and to assess the degree of heterogeneity at a very *local scale.* Finally, a probalistic study of the occurrence and the distribution along the profiles of the most permeable features inside the impermeable fraction is done and the possible *hydrodynamical implications* discussed.

4.3.4.2 Description of the boreholes

These boreholes cover the main parts of the slide; LF 401, 402, 402bis and 403 are situated inside the zone "++". LF 404 and 405 are inside the zone "+". LF 406 and 407 are located in the stabilized "GGS" zone (figure 4.20).

Equipments:

- 6 deep vertical boreholes from 90 to 110 meters (LF 401, 402, 403, 405, 406, 407).
- 1 short vertical borehole of 10 meters (LF 402bis).
- 1 inclined deep borehole of 95 meters (LF 404).
- Total length: 747 meters with 191 meters inside the bedrock.
- Equipments: 6 boreholes are equipped with piezometers (3 tubes of 2'' in each borehole). 2 boreholes equipped with inclinometers in the lower part.

General lithological description. The boreholes cross successively the sliding mass, the loose stable terrains and the bedrock. The sliding mass can be divided in two parts; the active sliding mass, with a relatively constant thickness and the ancient stabilized mass with a variable thickness. In this study, the lithological sequence analyses do not differentiate these two zones; since being geologically similar. And in addition, the contact is very difficult to identify. The underlying bedrock is composed by limestone sl., greystones, schists, dolomites and cornieules. The sliding mass is mainly constituted by a very heterogeneous mass of clayey to silty weathered debris including a variable volume of gravels, stones and blocks. These abundant intercalated shale and fine-grained siltstone beds are generally thin (<1 meter). The structure and organization of these structures are not well defined; their location seems to be totally random.

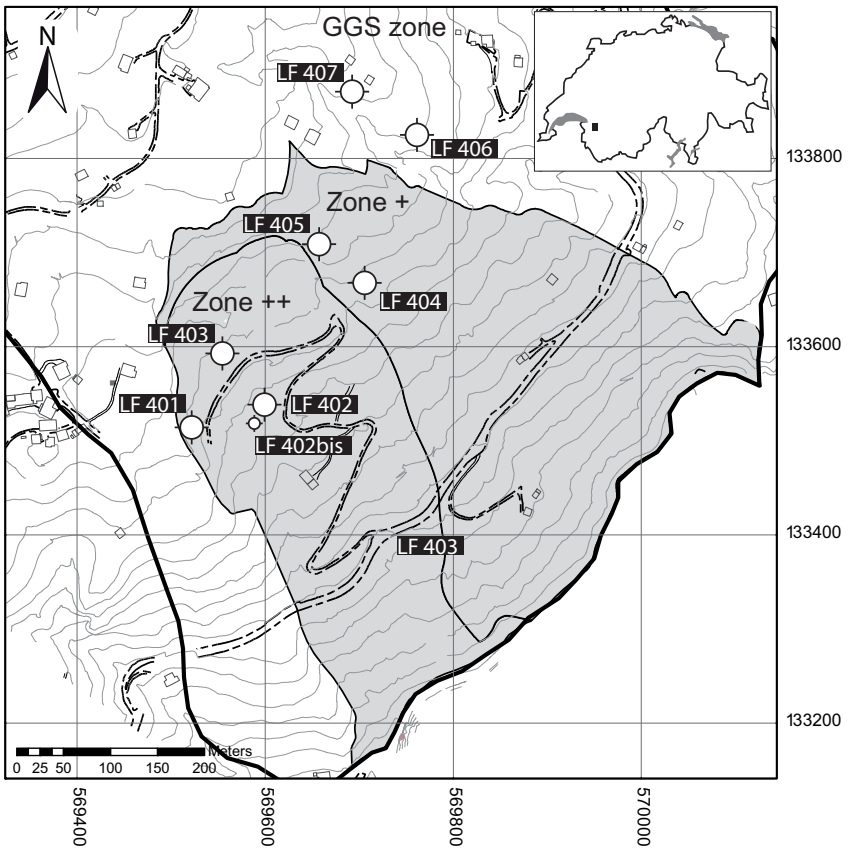

Figure 4.20: Geographical location of the new wells of 2006 in the zone "++", "+" and "GGS" of the la Frasse landslide, and table of the principal characteristics; altitudes, lengths and coordinates.

Name	Remarques	Lenght (m)	CoordY	CoordX	Alt. (m)	Equipment	Sliding surface depth (m)	Bedrock depth (m)
LF401 p	Inclination 85°	90	569'523	133'516	975	Piezo (p)	39.5 - 40	61.8
LF402 i		90	569'587	133'539	959	Inclino (i)	34.5	48,4
LF402 p		10	569'587	133'539	959	Piezo (p)	-	-
LF403 p		110	569'550	133'582	975	Piézo (p)	50.0 - 50.6	71.6
LF404 cp	Inclination 65°	90	569'715	133'679	975	CP	37.3 - 38.3	64
LF405 p		110	569'659	133'708	1000	Piezo (p)	40.8 - 43.2	74.1
LF406 i		126	569'761	133'830	992	Inclino (i)	56.7 - 58.8	116.2
LF407 p		125	569'693	133'877	1007	Piezo (p)	58.0 - 62.3	107.8

Table 4.11: Characteristics of the new boreholes LF401 to 407 (August 2006).

4.3.4.3 ***Methods***

First, the basic lithofacies have to be established. The investigated boreholes are characterized by a

succession of clayey, silty, sandy and gravely facies (see step 1 in appendix IV-6). The observed lithotypes are transcript (step 2) and classified in four facies states. Each facies state is defined by a dominant lithology and texture (i.e. grain size). Four facies state type are determined (P1 to P4), and classified (step 3) in four main permeability classes according to Freeze and Cherry (1979): P1 (Clay to silt, K ≤ E-7 m/s), P2 (Sandy silt, K=]E-7,E-5[m/s), P3 (Sand to gravely sand, K=]E-5,E-3[m/s) and P4 (Gravels, K ≥ E-3 m/s). Photos of the sediments are shown in appendix IV-6 (C), facies P1, P2 and P3 are illustrated. The clay to silt facies (P1) is actually a combination of silt-shale, clay-shale and mudstone. Sandy silt facies (P2) is a combination between silt and limy sand. Sand to gravely sand facies (P3) is composed of fine to medium-grained sandstone, infrequently with a few pebbles of quartz, feldspar, mudrock or limestone widely interspersed, and usually poorly sorted. Gravels facies (P4) consists of coarse facies to very coarse grained sandstone, sometimes pebbly to conglomeratic. The identification of these facies was done directly on field and do not necessitate laboratory test for their determination. Appendix IV-7 presents all the recorded successions for each borehole.

4.3.4.4 Vertical facies analysis

Descriptive statistics and facies distributions. Between 30 and 106 successions are recorded. Globally the thicknesses are varying from 0.03 to 13.21 meters (table 4.12) with a mean thickness around 1.33 meters, with a coefficient of variation indicating a high heterogeneity. No particular tendency is observable according to the location (i.e. inside or outside the active mass). In table 4.13; the facies P1 (clay and silt facies), with a mean value of 1.62 meters, shows the thickest beds (up to 14 meters), and thus the greatest heterogeneity.

	LF- 401	LF- 402	LF- 403	LF- 404	LF- 405	LF- 406	LF - 407	**Total**
Number of values	43	31	57	53	66	107	56	**413**
Sum	62.09	51.23	63.28	88.35	66.10	115.34	103.57	**549.97**
Minimum	0.14	0.19	0.17	0.05	0.10	0.10	0.03	**0.03**
Maximum	8.99	7.12	6.48	13.21	5.20	9.62	14.97	**14.97**
Range	8.85	6.94	6.30	13.16	5.10	9.52	14.94	**14.94**
Mean	1.44	1.65	1.11	1.67	1.00	1.08	1.85	**1.33**
Variance	3.13	3.75	1.19	6.06	0.85	1.39	6.83	**3.02**
Standard deviation	1.77	1.94	1.09	2.46	0.92	1.18	2.61	**1.74**
Coefficient of variation	122%	117%	98%	148%	92%	109%	141%	**131%**

Table 4.12: Global statistical values of the Thicknesses of the facies.

The intermediary facies P2 (Sandy silt facies) is statistically quite similar to facies P1 but less recurrent. Facies P3 and P4 are generally thin with values ranging from 0.04 to exceptionally 10.26 meters, with an average value around 1 meters. These values show that 75% of the analysed vertical successions are made of impermeable materiel (clay to sandy silt facies), 43% of P1 facies and 32% of P2 facies. The coarse and permeable fraction represents thus only 25% of the sequences. The geological medium is strongly impermeable but with intercalations of permeable features. The vertical correlation length (λz) describing the vertical maximum continuity, is around 2 meters, and locally 10 meters. The following questions may be thus formulated:

- Are these features isolated or spatially connected? Continuity of the system? Horizontal correlations?
- Does the position of these permeable features follow a deterministic/empirical law? And therefore

being predictable.

In figure 4.21 the relative proportions and the vertical distribution of each facies are presented. In grey are displayed prominently the permeable facies P3 and P4. The main observations are the following:

- The facies P1 is showing a global strong dominance especially in the active zone "++" with percentages reaching 63%.
- Inside the active zone "++": The relative proportion of facies P3 and P4 is less than 20% of the sequences
- Inside the active zone "+" and stabilized "GGS": The relative proportion of facies P3 and P4 is slightly higher (20% to 30%) exception done for LF 404 (45%) ?.
- The vertical position of the permeable (P3 and P4) features seems to be totally arbitrary and random. Their distribution is homogeneous along the vertical.

These results may demonstrate that the geological medium is globally strongly impermeable but highly heterogeneous according to the distribution of the permeable structures. These structures may be locally either concentrated at defined depth or totally absent some meters apart, as illustrated in figure In figure 4.21 (e.g. boreholes LF 404 and LF 405).

		P1 Thickness (m)	P2 Thickness (m)	P3 Thickness (m)	P4 Thickness (m)
LF 401	Number of values	14	17	9	3
	Sum	29.88	24.02	5.28	2.90
	Minimum	0.33	0.23	0.14	0.37
	Maximum	8.99	5.00	1.08	1.67
	Range	8.66	4.77	0.93	1.29
	Mean	2.13	1.41	0.59	0.97
	Variance	6.43	2.01	0.10	0.43
	Standard deviation	2.54	1.42	0.31	0.65
	Coefficient of variation	118.79%	100.39%	52.79%	67.49%
LF 402	Number of values	12	13	5	1
	Sum	16.93	28.23	3.26	2.81
	Minimum	0.20	0.26	0.19	2.81
	Maximum	6.96	7.12	1.38	2.81
	Range	6.76	6.86	1.19	0.00
	Mean	1.41	2.17	0.65	2.81
	Variance	4.43	4.38	0.21	*NA*
	Standard deviation	2.10	2.09	0.46	*NA*
	Coefficient of variation	149.10%	96.36%	70.10%	*NA*
LF 403	Number of values	27	15	11	4
	Sum	39.39	12.19	8.90	2.80
	Minimum	0.17	0.19	0.19	0.40
	Maximum	6.48	1.95	2.01	1.12
	Range	6.30	1.77	1.82	0.72
	Mean	1.46	0.81	0.81	0.70
	Variance	1.93	0.41	0.40	0.10
	Standard deviation	1.39	0.64	0.63	0.31
	Coefficient of variation	95.18%	78.46%	78.04%	44.04%
LF 404	Number of values	19	9	14	11
	Sum	38.06	10.50	16.59	23.21
	Minimum	0.11	0.05	0.17	0.32
	Maximum	13.21	6.14	3.73	10.37
	Range	13.10	6.09	3.56	10.05
	Mean	2.00	1.17	1.19	2.11
	Variance	9.77	3.91	1.28	8.14
	Standard deviation	3.13	1.98	1.13	2.85
	Coefficient of variation	156.06%	169.40%	95.60%	135.19%

		P1 Thickness (m)	P2 Thickness (m)	P3 Thickness (m)	P4 Thickness (m)
LF 405	Number of values	15	23	16	16
	Sum	19.18	27.72	10.58	8.62
	Minimum	0.32	0.10	0.00	0.11
	Maximum	3.79	5.20	1.44	1.58
	Range	3.48	5.10	1.44	1.46
	Mean	1.28	1.21	0.66	0.54
	Variance	1.04	1.40	0.25	0.20
	Standard deviation	1.02	1.19	0.50	0.44
	Coefficient of variation	79.70%	98.33%	75.47%	82.40%
LF 406	Number of values	42	40	16	9
	Sum	43.28	52.40	10.17	9.49
	Minimum	0.10	0.14	0.32	0.14
	Maximum	3.59	9.62	1.48	3.52
	Range	3.49	9.48	1.16	3.37
	Mean	1.03	1.31	0.64	1.06
	Variance	0.94	2.39	0.11	0.97
	Standard deviation	0.97	1.55	0.34	0.99
	Coefficient of variation	94.29%	118.12%	53.26%	93.62%
LF 407	Number of values	18	15	16	7
	Sum	51.86	22.52	19.01	10.18
	Minimum	0.03	0.16	0.04	0.72
	Maximum	14.97	5.40	7.12	2.08
	Range	14.94	5.24	7.08	1.36
	Mean	2.88	1.50	1.19	1.45
	Variance	16.34	1.82	2.78	0.32
	Standard deviation	4.04	1.35	1.67	0.57
	Coefficient of variation	140.29%	89.79%	140.19%	39.09%
TOTAL	Number of values	147	132	83	51
	Sum	238.58	177.58	73.79	60.02
	Minimum	0.03	0.05	0.04	0.11
	Maximum	14.97	9.62	7.12	10.37
	Range	14.94	9.57	7.08	10.26
	Mean	1.62	1.35	0.89	1.18
	Variance	5.08	2.18	0.88	2.31
	Standard deviation	2.25	1.48	0.94	1.52
	Coefficient of variation	138.89%	109.78%	105.30%	129.28%

Table 4.13: Statistical values of the Thicknesses of each type of facies (P1, P2, P3 and P4).

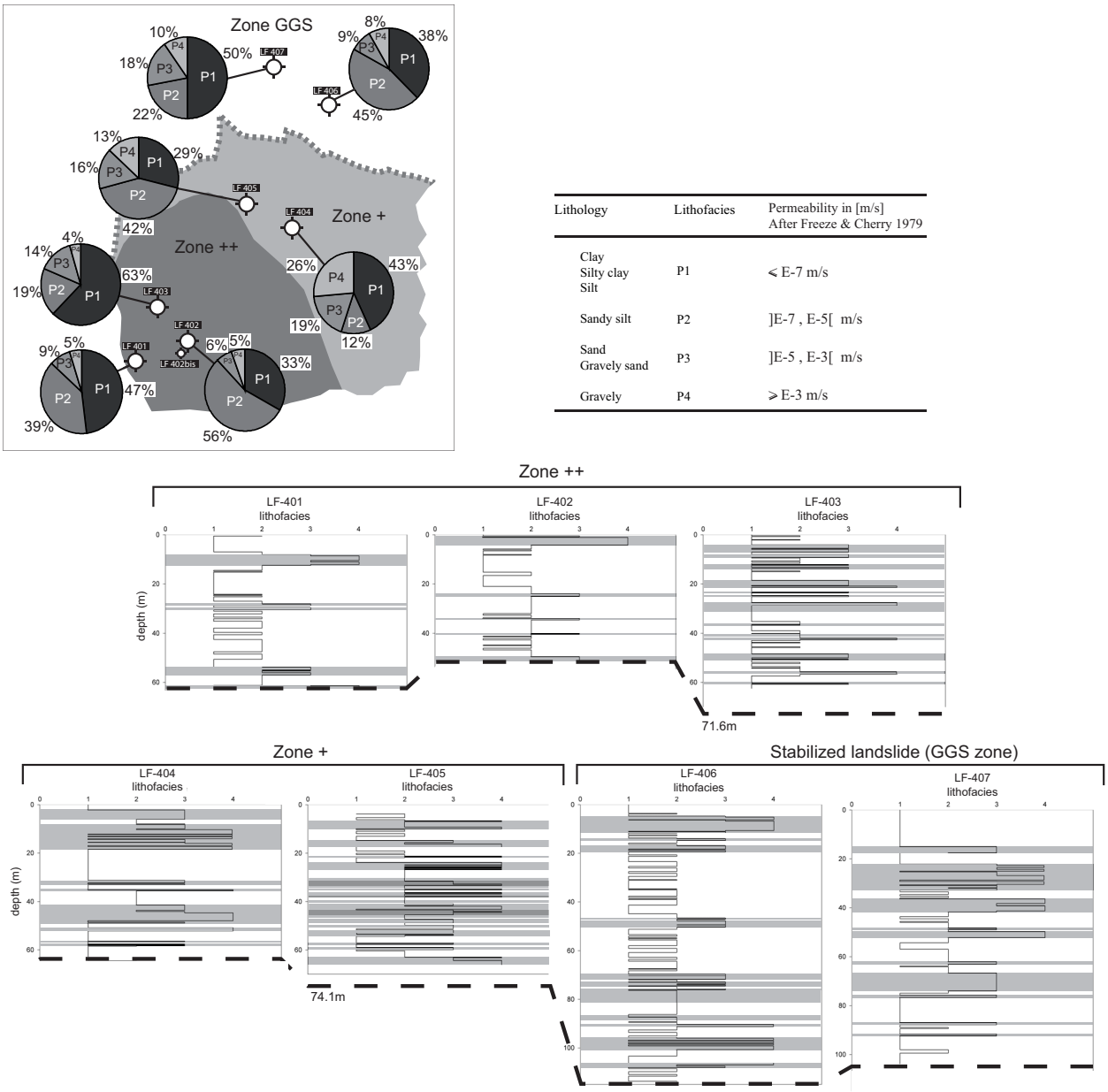

Lithology	Lithofacies	Permeability in [m/s] After Freeze & Cherry 1979
Clay Silty clay Silt	P1	⩽ E-7 m/s
Sandy silt	P2	]E-7 , E-5[m/s
Sand Gravely sand	P3	]E-5 , E-3[m/s
Gravely	P4	⩾ E-3 m/s

Figure 4.21: Spatial and vertical distribution of the identified lithofacies (P1: Clay-silt, P2: Sandy silt P3: Sand gravely sand and P4: Gravely). Vertical distribution and correlations; the permeable facies P3-P4 are isolated in grey.

4.3.4.5 ***Stratigraphic correlations***

Spatial continuity is evaluated thanks to stratigraphic correlation essays. It enables to define the extension of the structures notably of the permeable features. At first sight when looking the correlation attempted between LF 402 and LF 402bis in figure 4.22, one may notice that even 2 meters apart the correlation is not obvious, since there are many possibilities to match the horizons. The essay effectuated for the first 10 meters between the boreholes LF 402/402bis and LF 403 demonstrates that the medium is mainly constituted of discontinuous lenses, more or less connected. All possible geometrical shapes and spatial extensions for a geological horizon are illustrated in In figure 4.23. In an idealized geological environment (a), the horizons present a regular well stratified structure with a regular thickness. In reality the thickness of the geological horizons is varying (d) and often may be pinched (b). In a multi-channeled system the horizons are made

of inter-connected lenses (c) with variable thicknesses (e) or isolated (f). Ideally, accurate stratigraphic correlations of two sections S1 and S2 are only possible in example (a).

Correlation factors. To quantify the correlation of this geological system, correlation factors R^2 has been calculated (table 4.14). Considering the high heterogeneous organization of the global stratigraphy, different correlations have been considered; a global correlation (including all boreholes), a zonal ("++", "+", "GGS") permitting to reduce the distance between the wells, and to evaluate the tendencies locally. And finally, correlations according to different depths were considered; subsurface (0-15 meters), medium depth (15 – 35 meters) and deep (>35 meters). Table 4.14-A gives an overview of the obtained results; in table [B] the calculated R^2 are classified from the highest to the lowest scores. Globally (in table 4.14-A, col. 1), the correlation factors are close to zero, thus indicating that there are no obvious relations (average $R^2 < 0.01$) between the different boreholes, neither at a local scale (pair observations) according to different zones ("++", "+" and "GGS") nor at a regional scale (all boreholes). Stratigraphical correlations between boreholes according to depth, that is to say parallel to the topography, are senseless. Correlations concerning geological lenses oblique to topography are not considered in this approach.

The results of the correlations factor estimation performed on specific levels (table 4.14-A, columns 2, 3 and 4), indicate that the correlations are better (average R^2 between 0.03 and 0.11) with a maximum value of 0.3 calculated for the correlation between boreholes LF 406 and 407 at subsurface. It means that at a local scale structures might be spatially correlated.

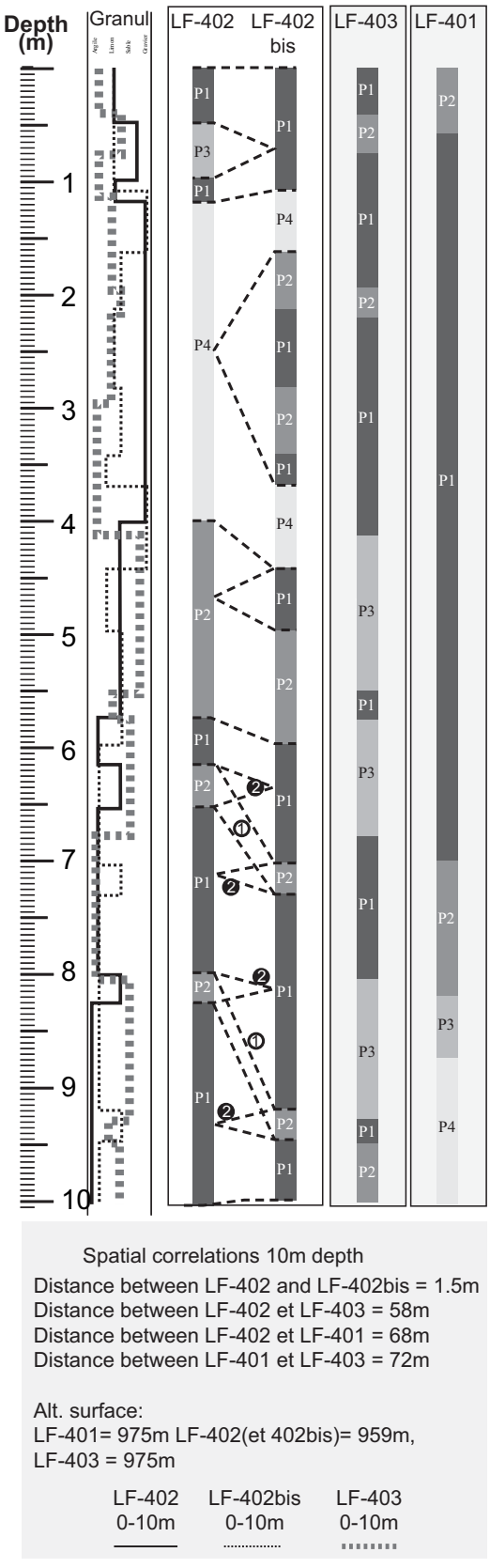

Figure 4.22: Correlation essay between LF401, 402 and 403 on the first 10 meters than 0.08.

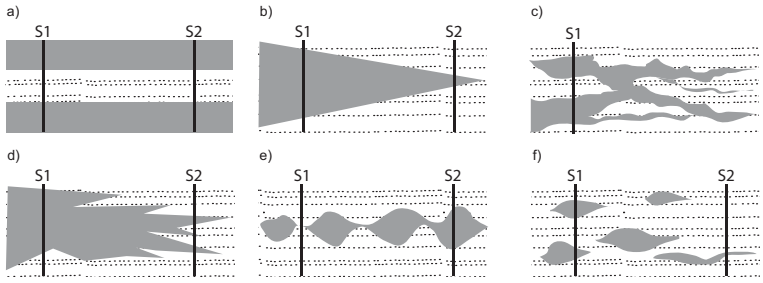

Figure 4.23: Geometrical shapes and spatial extensions for a geological horizon. (a) Regular and stratified structure horizons with a regular thickness. (b) Pinched structures. (c) Inter-connected structures. (d) multi-channelled system. (e) Structures with thickness variations. (f) Isolated lenses.

The classification of the correlation factors calculated for pair observations shows that, in a general way, the correlation factors decrease from the surface to the depth, with scores reaching 0.33 at subsurface. At intermediary depth, the correlation factors are still indicating values between 0.1 and 0.2, while in the deep underground they are less Beside this, at subsurface the zone "GGS" and "+" may show a better spatial continuity than in the active zone "++", with R^2 varying between 0.17 and 0.33 (table 4.14-B). The general tendency indicates that outside the active zone "++" the structures are longitudinally as well as transversally more continuous. The correlation factors indicate thus that in the active zone "++" the medium is globally more reworked (heterogeneous and discontinuous structures).

A]

Zonal (local scale)	Linear correlations		Entire profile (1)		0 to 15 meters (2)		15 to 35 meters (3)		> 35 meters (4)	
	Boreholes	Zones	R	R squared	R	R squared	R	R squared	R	R squared
	LF 401/402	*Zone ++*	0.08	0.006	0.14	0.022	0.37	0.140	0.13	0.017
	LF 401/403	*Zone ++*	0.04	0.001	0.12	0.014	0.14	0.022	0.20	0.042
	LF 402/403	*Zone ++*	0.11	0.012	0.16	0.027	0.13	0.016	0.09	0.009
	LF 404/405	*Zone +*	0.02	0.001	0.42	0.170	0.42	0.180	0.03	0.001
	LF 406/407	*Zone GGS*	0.01	0.000	0.57	0.330	0.16	0.026	0.05	0.002
	LF 405/407	*Zone +/GGS*	0.15	0.022	0.44	0.190	0.11	0.012	0.22	0.050
	LF 404/406	*Zone +/GGS*	0.18	0.030	0.07	0.050	0.18	0.030	0.29	0.086
	AVERAGE		0.08	**0.01**	0.27	**0.11**	0.22	**0.06**	0.14	**0.03**
	GLOBAL (regional scale)		0.01	0.012	0.31	0.090	0.19	0.037	0.16	0.025
	AVERAGE		0.07	**0.01**	0.28	**0.11**	0.21	**0.06**	0.15	**0.03**

B]

R classified

Linear correlations		Entire profile	
Boreholes	Zones	R	R squared
LF 404/406	Zone +/GGS	0.18	0.030
LF 405/407	Zone +/GGS	0.15	0.022
LF 402/403	Zone ++	0.11	0.012
LF 401/402	Zone ++	0.08	0.006
LF 401/403	Zone ++	0.04	0.001
LF 404/405	Zone +	0.02	0.001
LF 406/407	Zone GGS	0.01	0.000

Linear correlations		15 to 35 meters	
Boreholes	Zones	R	R squared
LF 404/405	Zone +	0.42	0.180
LF 401/402	Zone ++	0.37	0.140
LF 404/406	Zone +/GGS	0.18	0.030
LF 406/407	Zone GGS	0.16	0.026
LF 401/403	Zone ++	0.14	0.022
LF 402/403	Zone ++	0.13	0.016
LF 405/407	Zone +/GGS	0.11	0.012

Linear correlations		0 to 15 meters	
Boreholes	Zones	R	R squared
LF 406/407	Zone GGS	0.57	0.330
LF 405/407	Zone +/GGS	0.44	0.190
LF 404/405	Zone +	0.42	0.170
LF 402/403	Zone ++	0.16	0.027
LF 401/402	Zone ++	0.14	0.022
LF 401/403	Zone ++	0.12	0.014
LF 404/406	Zone +/GGS	0.07	0.050

Linear correlations		> 35 meters	
Boreholes	Zones	R	R squared
LF 404/406	Zone +/GGS	0.29	0.086
LF 405/407	Zone +/GGS	0.22	0.050
LF 401/403	Zone ++	0.20	0.042
LF 401/402	Zone ++	0.13	0.017
LF 402/403	Zone ++	0.09	0.009
LF 406/407	Zone GGS	0.05	0.002
LF 404/405	Zone +	0.03	0.001

Table 4.14: Results of the linear correlations of the lithofacies. A) Global correlations. B) Zonal correlations.

Spatial correlations. As discussed hereinbefore, spatial correlations are not obvious. But, in order to give a schematic representation of the general distribution of the structures, the problem was simplified at its maximum. As shown in figure 4.24, simplifying the problem in a dual permeability medium (permeable P3+P4 and impermeable P1+P2) enables to isolate the principal structures and identify some spatial correlations. Longitudinal (sect. A,B and C) and transversal (sect. D,E,F and G) sections are drawn. Globally the schematized correlations confirm the above-calculated correlation factors; the best continuity is identified near subsurface, as indicated by the transversal correlations between LF 401 to 406 and 407 (schemes D to G). The following observations may thus be done:

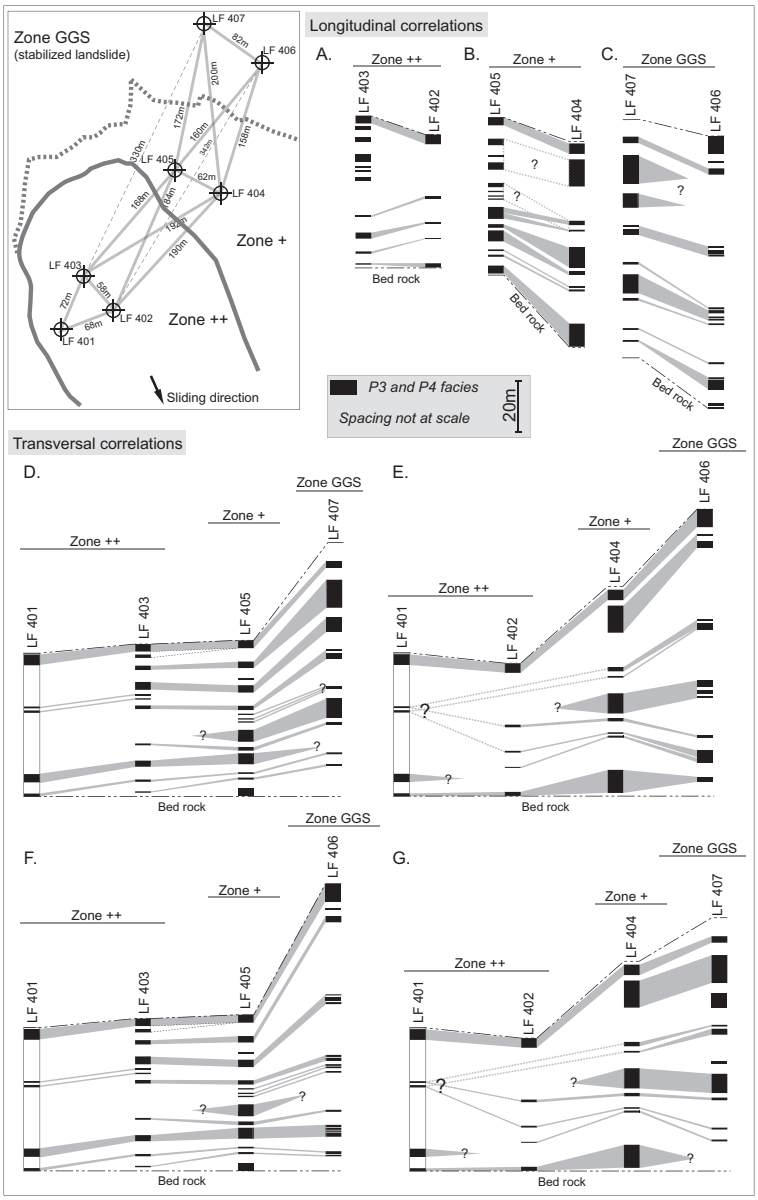

Figure 4.24: Stratigraphical correlations after facies simplification; P1+P2: impermeable, P3+P4: permeable.

Transversal correlations:

- Some horizons can reach hundred of meters, but are in general small (< 100 meters)
- Permeable members are more present and continuous in the "+" and "GGS" zones (stabilized)
- The active zone "++" is predominantly formed by impermeable material with some discontinuous

permeable structure distributed along the profiles (see figure 4.24)

Longitudinal correlations:

- The permeable horizons are more or less parallel to the sliding slope
- The structures are discontinuous and may be pinched (many horizons have no lateral correspondences)
- Thickness variations and discontinuity predominate

4.3.4.6 *Embedded Markov chains*

Embedded Markov chain analyses and entropy estimation has been performed on the facies transitions matrix to determine whether there is a preferential vertical cycle. In sedimentology, the Markov chains analysis is used to establish the prevalent pattern of vertical facies change in a stratigraphic succession (Markov 1971). Besides the analysis of the entropy enables to characterize the possible symmetry of the successions (symmetric, e.g. A-B-C-B-A; asymmetric, e.g. A-B-C-A-B-C; random cycle, e.g. ACABCA).

Embedded Markov chain analysis. The technique filters out significant facies transitions from randomly occurring facies transitions. In our case, facies transition matrices are structured on embedded Markov chains (Krumbein and Dacey 1969), which presents the advantage for calculation to have a diagonal element equal to zero. Any given facies state cannot pass upward into the same state, only the succession of lithologies are considered. Theoretical elements related to the elaboration of these matrices are presented in appendix I.
Appendix IV-8 gives the vertical and expected transitions frequency matrices (407 in total) for all boreholes. In the third column, the probability matrix of the facies transitions corresponds to the normalized difference between the transitions frequency matrix and the expected frequency matrices, where the facies in rows are overlain by facies in columns. For instance, the calculated probabilities at borehole LF 401, that facies P2 and P3 overlay P1 are respectively 0.71 and 0.22. And in this example, facies P4 is always associated to P3, since there are no transitions between P1/P4 and P2/P4 (transition frequency = 0 in column 1).

Global observations. Facies P1 are most commonly overlaid by facies P2 (or vice versa), and are less commonly by facies P4. P4 is mostly overlaid by facies P3. In LF 401-2-3 P1 and P2 are the predominant facies. Facies transitions concerning P3 and P4 are more common in boreholes LF 404 to 407 corresponding to the stabilized landslide. P3 may be rather associated to the impermeable fraction than facies P4. In boreholes LF 401 to 403, the probability that P4 is surrounded by an impermeable facies is very low. Thus, a permeable horizon will be mostly consisting in a sandy facies than a gravelly. In the meantime, in a hydrogeological point of view, the transitions between P1(or P2) and P4 are the most important, and will be further discussed.

Chi-squared X^2 test. The dependency between the observed transition matrices is tested for a first-order Markov process (independency properties) by employing a Chi-squared test. The degree of freedom is 5 ($(m\text{-}1)^2 - m$, with m the number of states =4) and the tabled Chi-squared is 11.07. The calculated values (appendix IV-9, 6th column) indicates, while far exceeding the statistic test that the successive lithologies in the *La Frasse* landslide are not independent each others, but rather exhibit a strong first-order Markovian property (dependency). Each bench is depending on the precedent. Globally the cyclical nature of the original la Simme flysch unit is preserved.
These results are not really surprising since the *la Frasse* landslide is principally made of the la Simme flysch units and that, even if it is reworked, the basic structures of the initial Bouma's cycle of the flysch may

be saved. However, local distinction may be formulated since the value of the Chi Square strongly differs from case to case. The dependency seems to be stronger for the boreholes situated outside the active zone (Chi-squared between 30 and 60). It means that the constant displacement of the mass induce, with time, the lost of the inherent structures of the flysch, in part confirmed by the percentage of the facies hereinbefore discussed. The fracturing and reworking linked to the constant displacement and water circulations change the composition of the mass. An evolution to a more and more clayey medium is recorded.

4.3.4.7 ***Hydrogeological implications***

In a hydrogeological point of view, the interesting scenario is to be in presence of a permeable structure imbricated into an impermeable medium and spatially connected to others, in order to create particular hydrodynamic conditions (overpressures or underpressure conditions). These configurations are hydrogeologically considered as being mainly confined, in opposition to free surfaces, and enable brutal variation of hydraulic pressure in response to hydrological impulses. Moreover, these variations are considered to be the main factors controlling the stability of a slide. Therefore, thanks to the facies successions, the probability that these configuration occur are evaluated (table 4.15).

	Nb of P4	Percentage of P4	P1/P4/P1	Nb of successions	**Probability that P4 embedded in P1**		*Probability of occurrence in the serie*	Degree of overpressure conditions
LF-401	3	6.8%	0	44	**0.00**		*0.000*	
LF-402	1	3.2%	0	31	**0.00**	0.17	*0.000*	
LF-403	4	7.0%	2	57	**0.50**		*0.035*	
LF-404	11	20.8%	4	53	**0.36**		*0.075*	IV
LF-405	17	26.2%	0	65	**0.00**	0.15	*0.000*	
LF-406	9	8.4%	2	107	**0.22**		*0.019*	
LF-407	7	12.7%	0	55	**0.00**		*0.000*	
Total	52	12.6%	8	412	**0.15**		*0.019*	
	Nb of P3	**Percentage of P3**	**P1/P3/P1**	**Nb of successions**	**Probability that P3 embedded in P1**		***Probability of occurrence in the serie***	
LF-401	9	20.5%	1	44	**0.11**		*0.023*	
LF-402	5	16.1%	1	31	**0.20**	0.44	*0.032*	
LF-403	11	19.3%	11	57	**1.00**		*0.193*	
LF-404	14	26.4%	6	53	**0.43**		*0.113*	III
LF-405	12	18.5%	3	65	**0.25**	0.26	*0.046*	
LF-406	16	15.0%	3	107	**0.19**		*0.028*	
LF-407	16	29.1%	3	55	**0.19**		*0.055*	
Total	83	20.1%	28	412	**0.34**		*0.068*	
	Nb of P4	**Percentage of P4**	**P2/P4/P2**	**Nb of successions**	**Probability that P4 embedded in P2**		***Probability of occurrence in the serie***	
LF-401	3	6.8%	0	44	**0.00**		*0.000*	
LF-402	1	3.2%	0	31	**0.00**	0.17	*0.000*	
LF-403	4	7.0%	2	57	**0.50**		*0.035*	
LF-404	11	20.8%	0	53	**0.00**		*0.000*	
LF-405	17	26.2%	9	65	**0.53**	0.22	*0.138*	II
LF-406	9	8.4%	2	107	**0.22**		*0.019*	
LF-407	7	12.7%	1	55	**0.14**		*0.018*	
Total	52	12.6%	14	412	**0.27**		*0.034*	
	Nb of P3	**Percentage of P3**	**P2/P3/P2**	**Nb of successions**	**Probability that P3 embedded in P2**		***Probability of occurrence in the stratigraphic succession***	
LF-401	9	20.5%	3	44	**0.33**		*0.068*	
LF-402	5	16.1%	2	31	**0.40**	0.24	*0.065*	
LF-403	11	19.3%	0	57	**0.00**		*0.000*	
LF-404	14	26.4%	2	53	**0.14**		*0.038*	I
LF-405	12	18.5%	2	65	**0.17**	0.19	*0.031*	
LF-406	16	15.0%	4	107	**0.25**		*0.037*	
LF-407	16	29.1%	3	55	**0.19**		*0.055*	
Total	83	20.1%	16	412	**0.19**		*0.039*	

Defavourable hydrodynamic conditions

Table 4.15: Probability of occurrence of facies P3 and P4 in the stratigraphic succession.

Globally, when facies P4 is present, the probabilities that P4 is embedded between two facies P1, or two facies P2, are respectively 0.15 and 0.27. When facies P3 is present, the probabilities that P3 is embedded between two facies P1, or two facies P2, are respectively 0.34 and 0.19. P3 is thus rather associated to P1 (0.34 against 0.15 for P4) and P4 associated to P2 (0.27 against 0.19 for P3). These differences are low but have to be taking into account when drawing the conceptual model.

Locally, in the active zone "++", the probability to have overpressures conditions may reach 0.5 and even 1, for instance in LF 403, if one consider that P3, when present, is only surrounded by the facies P1. In this zone, the predominant facies is P1 or secondary P2. When the facies P4 or P3 are present; their probability to be isolated vertically is thus high. In the less active areas (zone "+" and "GGS"), the better distribution between the different facies reduce the probability that P3 or P4 are vertically isolated, thus ventilating in a sense the media. In the meantime it is interesting to notice that globally, due to the low number of P4 and/or P3 facies in zone "++", the probability of such conditions is near zero. But in the case of presence the probability of worse hydrodynamical conditions would be high. In the zones "+/GGS", the homogeneity of the facies distribution maintains a constant average probability of around 0.2 (probabilities varying between 0.15 and 0.26) with the lowest probability assigned for the worst configuration (P4 in P1).

Finally, on last column of table 4.15, four degrees of "overpressure" conditions are defined and attributed. The degree IV constitutes the less favourable stratigraphic conditions (P4 pinched in P1 facies). The global degree of overpressure risk defined for the la Frasse landslide is III, with average probabilities of 0.44 (zone "++") and 0.26 ("+/GGS").

4.3.4.8 Entropy

Because of the high degree of reworking in the la Frasse mass, the entropy of the system is calculated. The methods of calculation suggested by Hattori (1976) are used. The observed sequences are compared to different sedimentary cycles in order to determine whether there is a remnant of original structures. Theoretical elements are exposed in appendix I.

Hattori (1976) applied the entropy concept to the Markov transition matrix to indicate the degree of random occurrence in a succession. Two types of entropies are calculated for every facies state: the entropy after deposition (E (post)) and the entropy before deposition (E (pre)), which together form the entropy set. Hattori (1976) analyzed and published results of several lithological sequences belonging to different environments, and classified the sedimentary cycles into six types based on entropy (figure 4.25-A). A sedimentary cycle involves a set of lithological elements (e.g. A, B, C, D) repeating in a different way through a succession. Sedimentary cycles can be classified in three ideal groups regarding to the succession order; symmetric successions (e.g. A-B-C-B-A), asymmetric successions (e.g. A-B-C-A-B-C) and random cycle (e.g. ACABCA). These successions are also called Bouma's model and are characteristics to flysch sedimentation (Bouma, 1962). The distributions A-1, A-2, A-3 and A-4 are representatives of asymmetric cycles regarding to their degree of disorganisation. Flysch sedimentary cycles with graded bedding repeating many times are recognized to belong to the asymmetric group (Hattori 1976), mostly of the cyclic sequence type A-1. However, it may happens that flysch sequences are belonging to the A-4 type or B, either when irregular migration of depositional cones or submarine erosions appeared during deposition (Simpson 1970), or when the successions are discriminated in three or four states as performed in this study. If the symmetric patterns of the cycles are preserved, an entropy distribution of type B following a diagonal line as illustrated in figure 4.25 will occur. The symmetric nature of a sedimentological succession

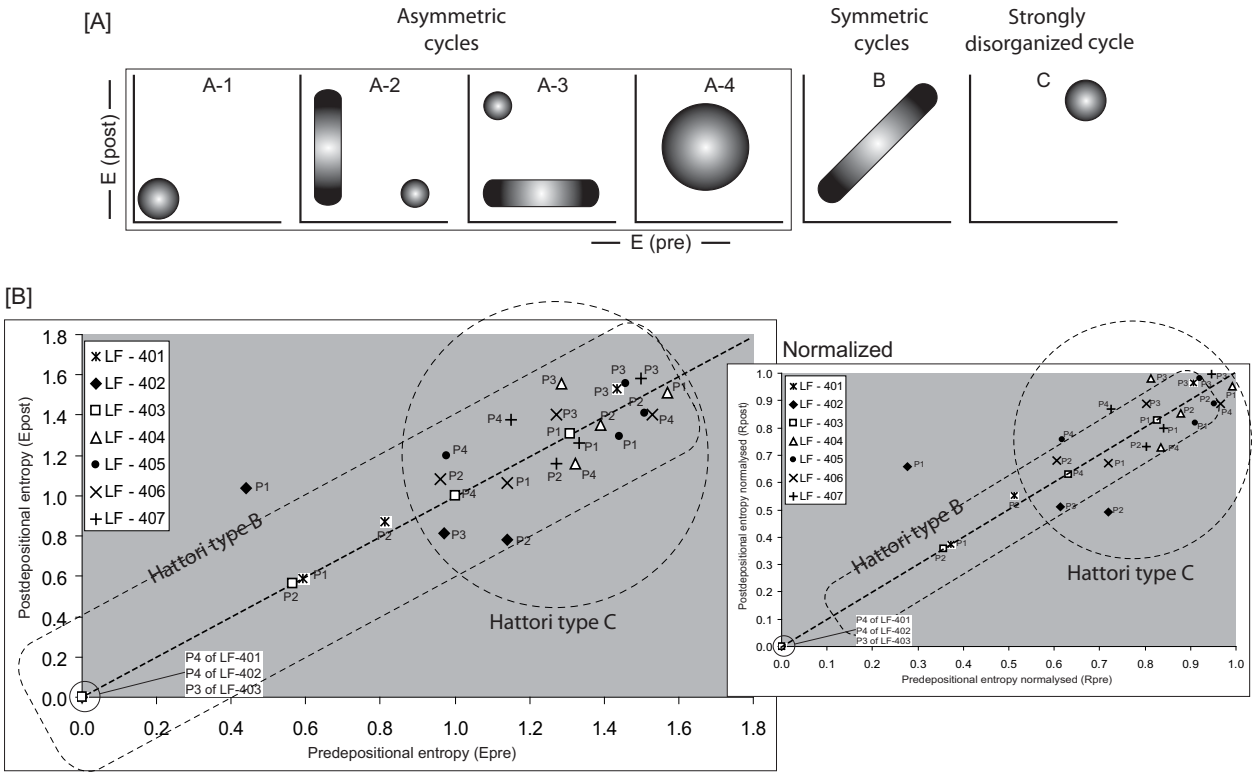

Figure 4.25: A) Entropy sets after Hattori (1976). The distributions A-1, A-2, A-3 and A-4 are representatives of asymmetric cycles. B: symmetric cycle and C: strongly disordered. B) Global calculated entropy sets.

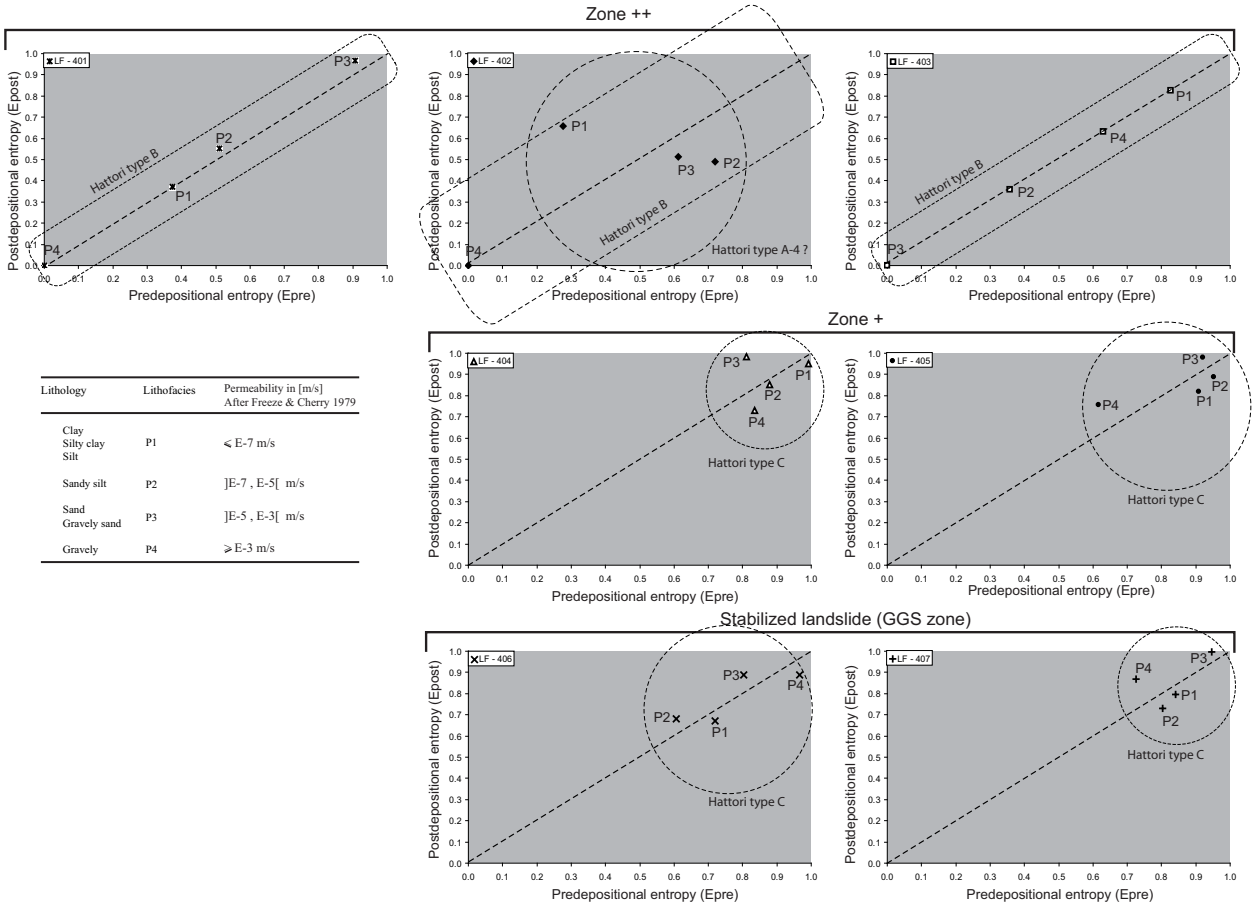

Figure 4.26: Local calculated entropy sets for each borehole and zones.

is often traducing disturbance processes in sedimentation or during tectonic settings, and can according to the degree of disturbance finally belonging to the type C. Type C represents a strongly disorganized cyclic sedimentation (random successions). Large values of both E(post) and E(pre) will be apparent. Appendix IV-9 presents all the calculated entropy sets, and figure 4.25 and 4.26 show the corresponding entropy set plots for each borehole and globally.

Results. Globally, the overall entropy set indicates that the system is rather belonging to the type C but eventually to B. The assignation is not clear because if one considers the few spread values along the central straight line, a B type distribution may correspond. Locally, the individual entropy sets show that the successions of the boreholes from the zone "++" (LF 401, 402 and 403) are rather of type B (eventually type A-4 for LF 402) while those of the zone "+/GGS" are clearly of type C with large values of both E(post) and E(pre).

Interpretation. The *la Frasse* landslide is mainly constituted by the la Simme flysch. According to the general principle of flysch sedimentation (asymmetric succession of the Bouma's series, Hattori (1976)), and due to its special neritic character (syn- and post-rift sediments deposited in a foreland basin of the alpine accretionnary prism, see Stampfli et al. 2002), the lithological succession of la Simme flysch should exhibit a A-4 cyclic sequence type with a strong deviation to the type C (strong increase in both pre- and postdepositional entropy factors E(pre) and E(post), see figure 4.25-A). This deviation is often indicating disturbance or irregular processes in sedimentation, as occurring in natural sedimentation of flyschs.
Besides, after Hattori (1976), a deviation to type B may indicate the lost of the asymmetric nature detrimental to symmetric successions. Symmetric patterns are characterizing disordered and truncated cycles. If symmetric nature is recorded the entropy set follows a diagonal line as illustrated in figure 4.25-A, because the disturbance increases both E(pre) and E(post). In the special context of flysch sedimentation, a deviation to the type B rather indicates post depositional disturbances that may be associated to tectonic processes Hattori (1976).
In this study, globally the lithological records indicate cyclic successions of type C (figure 4.25), that may vary locally to type B. In the less active zone ("+" and "GGS") the cyclic nature of type C is clearly identified, whereas in the active zone "++" intermediary states between type B and C are observed (see figure 4.26, LF401to 403).
Therefore, one may conclude that the cyclic nature of the la Simme flysch is in a part preserved, principally in the less active zones. The symmetric nature of the cycles in the active zone traduces a rearrangement of the lithological successions, and may be interpreted as post depositional reworking. The continual reworking processes and sedimentological transformation occurring inside the mass since instability may explain it.

4.3.4.9 ***Hydrodynamical implications***

- Strong impermeable dominance (75% of clayey to silty facies)
- High local heterogeneity
- Vertical correlation lengths around 2 meters
- Horizontal correlation lengths are variable, up to 100 meters
- Permeable structures (sand, gravel) might be continuous over long distances
- The probability that a permeable structure is confined in zone "++" is higher than for the other zones
- Globally, optimum overpressures probability is around 0.15

- Locally in active zone "++", optimum overpressure probability may be 0.5
- The global degree of overpressure risk is III (*max=IV!),* which is consequent
- These structures are vertically, randomly located, and complex hydraulic processes might be generated anywhere in the mass and not only at sliding surface.
- Permeable units are present at surface enabling accurate infiltration processes
- The lithofacies analysis method provides information to perform hydrogeological interpretations at a very **local scale vertically and horizontally**. Regional consideration may be done with caution, since the interpretation of the spatial correlations may be problematic.

4.3.5 GEOPHYSICAL PROPERTIES HETEROGENEITY

4.3.5.1 Method : data acquisition and processing

Three radiomagnetotelluric surveys (RMT) were undertaken in November 2005 and 2007. Three different sites are investigated and compared (figure 4.27). These zones are characterized by the same geological context but located in zones presenting different degrees of stability. Note that, the complete statistical and spatial analysis on the apparent resistivities of this case study has already been performed in section 4.2.3. The present section focuses therefore on the apparent and true resistivity distribution.

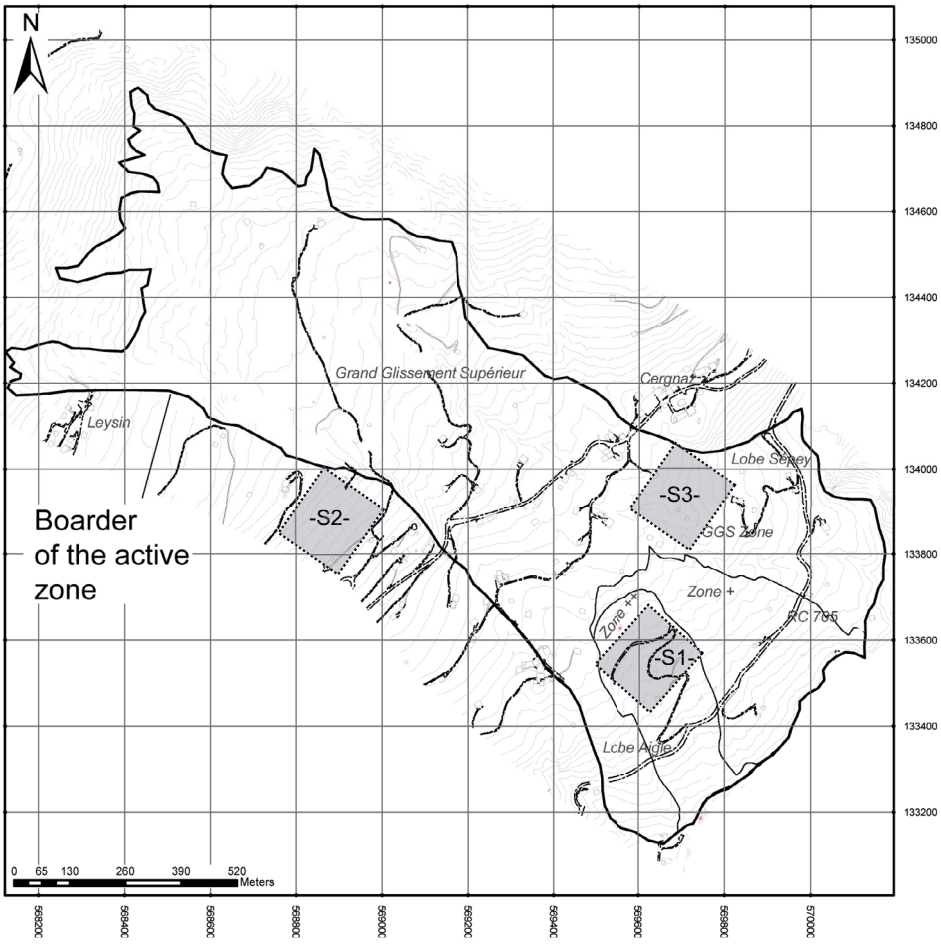

Figure 4.27: Geographical location of the studied sites for the RMT surveys.

In this study the used frequencies, (*site -S1-*: 183 kHz, 77.5 kHz and 18.3 kHz, *site -S2- and -S3-*: 183 kHz, 60 kHz, 20.3 kHz) allow, according to the crossed terrains, an investigation depths around 40 to 60 meters. Three zones presenting different degree of stability are investigated (figure 4.27); *site -S1-*: very active (zone "++"), *site -S2-*: outside the limits of the slide and *site -S3-*: stabilized "GGS" zone. Each zone covers a surface of around 0.06 km^2. The surveys are totalizing 288 measured points distributed along several profiles; *Site -S1-:* 118 measured points on 5 profiles, *site -S2-:* 94 measured points on 6 profiles and site 3: 76 measured points on 10 profiles.

The studied areas are homogeneous grids; maximum distance between the points is 20 meters. Each profile is representative of a 20 to 30 measurements, and each case study comprises between 5 and 10 profiles. From the measured variable three analyses are performed; RMT mapping, descriptive statistics and geostatistical spatial exploratory analyses. The use of the RMT contour maps obtained by ordinary kriging gives a coherent and structured image of the distribution of the subsurface and underground resistivities. Specific zones that may represent infiltration areas are discussed.

4.3.5.2 Anterior geophysical studies

In 1983 and 1985 two geophysical surveys were undertaken by the University of Lausanne aiming the geological characterisation of the mass and its basement as well as the determination of the implementation of new wells (LF 1, 2 and 3). The two campaigns comprised more than 40 electrical surveys and several seismic profiles, notably passing by the well FR2. An imposing glacial overdeepening under the sliding mass was identified, and the location of the roof of the underlying bedrock, which was not attained by the well FR2 (79 meters), defined.

Besides that, the electrical survey consisted in three pseudosections in the area of Cergnat (AB 40 m, 100 m and 200 m). The apparent resistivity values are ranging from 80 to 160 Ohm.m, the high values (> 140 Ohm.m) corresponding certainly to the underlying bedrock. A stratification of the apparent resistivities in the unstable mass corresponding to the sliding direction is apparent, with structures though not exceeding 100 meters. Recently, in November 2005, nine seismic profiles (Appendix V) were undertaken by Geo2X in the framework of the stabilization study of the la Frasse landslide (NCG+EPFL 2006). The data were treated according to the seismic reflection method in order to localize the underlying substratum and the position of the sliding surface. To complete the information in the superficial part, the first arrivals (refracted waves) were pointed and treated thanks to a seismic tomography software. The seismic profiles (Appendix V) show strong reflectors often clearly materializing the base of a slow zone (active landslide) surmounting faster layers (tectonized rock, old stabilized slide or massive rock). The zones without structured reflectors betray the presence of tectonized zones. These investigations may identify strong geological contrasts (i.e. contact flysch/limestone) but, due to the scale of acquisition, considerations about the geological internal structures are senseless. Nevertheless, the absence of spatial correlation between the profiles is obvious, and the very heterogeneous and chaotic character may be identified.

4.3.5.3 Apparent electrical resistivity and phase

Site -S1-: Globally, the measured resistivities are homogeneous and grouped around the average value of 75 Ohm.m. The coefficient of variation (around 38 %) and the dispersion are low (table 4.16). The values, varying from 15 Ohm.m up to 205 Ohm.m, correspond to a relatively strong conductive media. At frequencies 183.0 and 77.5 kHz (subsurface to intermediate depth), the apparent resistivities are homogeneous, and the average phase around 45° indicates a nearly electrical uniformity. At 18.3 kHz (maximum penetration depth) a clear increase in phase over 45° indicates a decrease in resistivity with depth, probably signifying

the presence of very low permeable deep terrains (i.e. clay conductive layer). The resistivity contour maps (appendix IV-10) at 183 kHz and 18.3 kHz show a high and relatively homogeneous conductive domain (ranging from 10 to 100 Ohm.m) divided in its north-western part (upslope) by a well developed and continuous north to south more heterogeneous resistive sub-domain (100 to 175 Ohm.m). In a north-west to south-east direction, a much more conductive second structure is observable. At 77.5 kHz (intermediate penetration depth), the medium appears to be more conductive and even more homogeneous.

	La Frasse -S1-			La Frasse -S2-			La Frasse -S3-		
Frequency	f 183	f 77.5	f 18.3	f 183	f 60	f 20.3	f 183	f 60	f 20.3
Statistics of apparent electrical resistivity data									
Number of values	118	118	118	94	94	94	76	76	76
Minimum	24	15	18.4	76	51	46	17.9	16.7	11.2
Maximum	180	205	153	665	750	1608	145	103	118
Range	156	190	134.6	589	699	1562	127.1	86.3	106.8
Mean	**77.18**	**75.82**	**65.3**	**210.9**	**239.6**	**274.88**	**57.01**	**54.44**	**63.69**
Variance	664	827	764	11150	17340	38594	639	282	458
Coefficient of variation	**33%**	**38%**	**42%**	**50%**	**55%**	**71%**	**44%**	**31%**	**34%**
Statistics of phases									
Number of values	118	118	118	94	94	94	76	76	76
Minimum	35.40	33.60	34.30	21.4	6.5	13.4	27	25.2	25.4
Maximum	58.80	67.70	57.20	63.3	65	67.9	56.9	58.5	52.3
Range	23.40	34.10	22.90	41.9	58.5	54.5	29.9	33.3	26.9
Mean	**45.03**	**45.79**	**47.48**	**36.31**	**40.27**	**44.01**	**44.51**	**40.53**	**37.56**
Variance	13.73	22.04	14.99	51.05	54.41	62.43	21.58	33.92	22.69
Coefficient of variation	**8%**	**10%**	**8%**	**20%**	**18%**	**18%**	**10%**	**14%**	**13%**

Table 4.16: Statistical values of the apparent resistivities and phases from the radiomagnetotelluric surveys in the la Frasse landslide: sites -S1- -S2- and -S3-.

Site -S2-: The average resistivities, corresponding to a high resistive media, are around 240 Ohm.m and are increasing with depth. The dispersion is relatively high (>50%) with values varying from 46 Ohm.m up to 1608 Ohm.m. The increase of the coefficient of variation (from 50% to 71%) for low frequencies (20.3 kHz) indicates an evolution of the resistivity with the depth (appendix IV-11), defining a mix of resistive and conductive sectors. These values may point out the influence of specific resistive geological bodies (up to 1600 Ohm.m) directed north-east to south-west as consolidated sandstone banks or limestone blocs. The average phase is increasing with depth; at 183 kHz and 60 kHz the phases around 36° and 40° indicate a clear increase of the resistivities with depth, and notably of the true resistivities. At 16 kHz the average phase around 45° indicates a nearly uniform situation.

Site -S3-: Regards to their magnitude and distribution, the apparent resistivity values measured are globally similar to site S1. The average resistivity is around 60 Ohm.m with a low coefficient of variation (35%). Though, at all investigated frequencies, dispersion is observable towards high values (see §4.2.3). This might been explained by strong influences of resistive blocs (reworked limestones or competent sandstone banks) yet identified by the borehole logging. Concerning the phases, a strong decrease with depth is recorded (appendix IV-12). At 183 kHz (subsurface investigations) a uniform structural situation is indicated with phases indicating nearly 45°. The medium is divided by a conductive zone extended toward south-east separating to resistive sub-domains, also observable at frequency 60 kHz. At 20.3 kHz the average phase drops to 36°, also indicating an increase of the resistivity with the depth. The spatial continuity of the sub-surface resistive structure disappears with depth; the domain is constituted by different conductive and resistive sub-domains, exhibiting thus a more chaotic distribution.

4.3.5.4 *True electrical resistivity*

To obtain a layer's resistivity model (true resistivity, layer thickness), the measured apparent resistivities and phase are simulated at each point of measurement by a uni-dimensional inversion after Fischer et al. (1981a). True resistivities and thicknesses according to three layers are calculated (see appendix IV-13,14 and table 4.17 for the overall statistics).

A)

True resistivity statistics (Ohm.m)	True rho L1	Thickness L1	True rho L2	Thickness L2	True rho L3	Thickness L3
La Frasse site S1						
Number of values	118.00	118.00	106.00	106.00	32.00	32.00
Minimum	9.00	0.00	16.00	0.10	9.00	21.36
Maximum	490.00	45.99	142.00	45.39	183.00	40.73
Range	481.00	45.99	126.00	45.29	174.00	19.37
Mean	88.72	6.99	66.66	22.55	64.84	29.10
Variance	6350	86	766	136	1570	26
Coefficient of variation	90%	132%	42%	52%	61%	17%
La Frasse site S2						
Number of values	94.00	94.00	91.00	91.00	55.00	55.00
Minimum	26.00	0.10	23.00	0.00	1.00	0.00
Maximum	1199.00	65.57	1882.00	86.85	985.00	79.71
Range	1173.00	65.47	1859.00	86.85	984.00	79.71
Mean	114.48	5.20	420.90	25.39	265.50	33.01
Variance	17925	77	128480	523	44190	473
Coefficient of variation	117%	169%	85%	90%	79%	66%
La Frasse site S3						
Number of values	76.00	76.00	66.00	66.00	37.00	37.00
Minimum	4.00	0.10	6.00	0.20	38.00	9.62
Maximum	437.00	32.87	317.00	29.31	521.00	29.85
Range	433.00	32.77	311.00	29.11	483.00	20.23
Mean	64.62	6.71	72.44	14.09	153.70	17.45
Variance	4455	88	3766	69	14320	26
Coefficient of variation	103%	139%	85%	59%	78%	29%

B) Summary

Sites	S1		S2		S3	
	Rho (Ohm.m)	Thickness (m)	Rho (Ohm.m)	Thickness (m)	Rho (Ohm.m)	Thickness (m)
L1	88.72	6.99	114.5	5.2	64.6	6.7
L2	66.66	22.55	420.9	25.4	72.4	14.1
L3	64.84	29.1	265.5	33.0	153.7	17.5

Table 4.17: Statistical values of the true resistivities and layer thicknesses from the radiomagnetotelluric surveys in the la Frasse landslide: sites -S1- -S2- and -S3-.

At **site -S1-**, the distribution of the true resistivities is homogeneous with low values (average around 70 Ohm.m) and constant for the three layers.
Site -S2- the computed resistivities indicate an evolution with depth. The intermediate layer L2 presents a strong resistive domain with an average resistivity around 421 Ohm.m.
Site -S3- is similar to site 1 at subsurface with average true resistivities around 70 Ohm.m. Higher resistivities are though calculated at depth, illustrating more pervious conditions (153 Ohm.m).
Therefore, hydrogeologically, site -S2- is showing the most favourable conditions for direct surface infiltration. On the contrary the two investigated sites inside the active area are much more conductive, and may be considered as more impermeable.

Concerning preferential zones of infiltrations, the resistive zone at high frequencies (subsurface) may be considered as preferential infiltration zones. But, observations have to be interpreted with caution. Indeed, if the medium is considered as totally saturated, a correlation between electrical resistivity and geological

material may be done (Table 4.18 after Zohdy et al. (1974), Sumner (1976), and Sharma (1997)). The problem in the type of environment such as landslides is that the saturation ratios are varying from point to point. In addition, very resistive values (>300-400 Ohm.m) may also define consolidated formations such as limestones and siltstones.

Material resistivity range

Material	Resistivity (Ohm.m)	Log resistivity
Gravel non -saturated	300 – 3000	2.5 – 3.5
Gravel saturated	150 – 300	2.2 – 2.5
Sand non -saturated	150 – 500	2.2 – 2.7
Sand saturated	80 – 150	1.9 – 2.2
Silt non -saturated	25 – 100	1.4 – 2.0
Silt saturated	10 - 25	1.0 – 1.4
Limestone	100 - 5000	2.0 – 3.7
Crystalline roc ks	1000 - 10000	3.0 – 4.0

Compiled data after: Sharma, P.V. (1997), Sumner, J.S. (1976) and Zohdy et al. (1974)

Table 4.18: Table of resistivities of several geological materials.

In the meantime some observation may still be drawn:
In the most active zone"++" (site -S1-), at surface the medium may present some local interesting infiltration capacities represented by high resistive zones. On the contrary, site -S3-, is indicating more conductive conditions at subsurface. Site -S3- may be more impermeable at surface, thus presenting very unfavourable conditions for accurate infiltration. Finally, note that these interpretations are debatable. The conditions may be, regard to the saturation ratios, very different. What is to retain? is that the distribution of the resistivity is very heterogeneous and variable. If optimum infiltration zones may exist, their location would be very local and punctual. The distribution of direct infiltration on the landslide is therefore heterogeneous.

4.3.5.5 ***Spatial analysis***

Since, the spatial analyses are well developed in §4.2.3, this section presents briefly the main results. The modelled variogram are presented in appendix II-3 and 4. Generally, the correlation lengths parallel and perpendicular (λx and λy) to the direction of the movement are small regarding to the size of the studied area. They are around 20 meters (up to 40 meters in some cases) for high frequencies and are varying with depth; λx is decreasing while λy is increasing. In appendix II-3 the modelled variograms indicates a general chaotic behaviour for site -S1-, and especially for long distances. The correlation lengths are small (10 to 20 meters) and rather developed in the direction parallel to the sliding direction. Subsurface structures are more developed than in depth, where a more heterogeneous and disconnected medium prevailed. For site -S2-, a north-east south-west anisotropy is well marked, good correlation lengths (up to 40 meters for the frequency 22.3 kHz) are calculated perpendicular to the sliding direction in accordance with the local geology and tectonic of the la Simme Nappe (strong influences of the stratification). The medium is clearly structured. For site -S3- the correlation lengths are relatively constant, between 10 and 20 meters, for both directions and at each frequency. The variograms are relatively isotropic with an initial short and rapid increase, and stabilization at sill.

4.3.5.6 ***Hydrodynamical implications***

- Strong impermeable dominance, with low apparent resistivities in the active zones (Site S1 and S3), at the scale of measurements (regional).
- Existence of decametric more permeable structures (rhoa >150 Ohm.m) oriented parallel to sliding direction relatively thin with a width of maximum 50 meters, favouring probably flow transfer

processes surface infiltration

- At surface, infiltration zones may be distributed very zonally.
- The RMT method provides information to perform hydrogeological interpretations at a **REGIONAL scale** (global assessment)

	La Frasse site S1			La Frasse site S2			La Frasse site S3		
Frequency	f 183	f 77.5	f 18.3	f 183	f 60	f 20.3	f 183	f 60	f 20.3
Investigated direction : Parallel to slide									
Orientation of lag vector (°)	135	135	135	135	135	135	135	135	135
Bandwidth (m)	30	30	30	30	30	30	30	30	30
Model	EXP	EXP	EXP	EXP	EXP	EXP	EXP	EXP	EXP
Range a (m)	63.0	27.3	12.6	48.9	69.0	102.1	50.4	65.8	65.9
Nugget	No	No	No	No	No	No	No	No	No
Correlations lengths	21.0	9.1	4.2	16.3	23.0	34.0	16.8	21.9	22.0
Semi-variance γ(h)	0.030	0.030	0.029	0.040	0.054	0.062	0.034	0.022	0.026
Investigated direction : Perpendicular to slide									
Semi-variance γ(h)									
Orientation of lag vector (°)	45	45	45	45	45	45	45	45	45
Bandwidth (m)	10	10	10	10	10	10	10	10	10
Model	EXP	EXP	EXP	EXP	EXP	EXP	EXP	EXP	EXP
Range a (m)	45.9	32.1	30.0	25.0	30.0	51.4	34.8	31.8	37.1
Nugget	No	No	No	No	No	No	No	No	No
Correlations lengths	15.3	10.7	10.0	8.3	10.0	17.1	11.6	10.6	12.4
Semi-variance γ(h)	0.022	0.030	0.030	0.040	0.054	0.062	0.034	0.022	0.026

Table 4.19: Results of the spatial analyses of the apparent resistivities at different frequencies from the radio-magnetotelluric surveys in the la Frasse landslide: sites -S1- -S2- and -S3-.

4.3.6 GEOMECHANICAL PROPERTIES HETEROGENEITY

The geotechnical characterization of the sliding mass is another important aspect in the study of instable terrains for instance for stability calculation purposes. It provides the input parameters in case of geotechnical modelling. It enables to understand the behaviour of the rock, notably during serious displacement crises. Several laboratory tests performed these last decades, allowed characterizing these parameters into the la Frasse landslide (DUTI 1986 and NCG+EPFL 2004). In DUTI (1986) an interesting geostatistical study was performed on geotechnical measures done on a series of core samples from the borehole FR2. Since this study points out the vertical heterogeneity of the geotechnical parameters, and discuss about some aspect of stability, it was decided to present. In addition to that, these observations allow an interesting correlation with the vertical geological facies described in borehole LF407 (section 4.3.4) approximately 20 meters apart from well FR2 (appendix III-5), and thus allowing relatively fair spatial correlations.

4.3.6.1 Geomechanical characteristics

In 1986, fifteen samples were carried out from the boreholes FR1, FR2 and FR6, and to complete the data, two additional boreholes were investigated in 2003; P301 (2 samples carried out into destructive from 0 to 36 m and 46 to 60 m), P302 survey (5 samples from 0 to 36 m and 46 to 140 m). The geomechanical tests were carried out at the Laboratory of soil mechanics (LMS) of FPSL and at the Laboratory of Cérenville Géotechnique SA (DCG) aiming the characterization of the geotechnical parameters and the evaluation of their resistance under shearing conditions. The tests included: triaxial compression tests on altered samples in drained conditions and on preserved samples in non drained conditions, hydraulic tests for the determination of the water retention curve and standard oedometric tests.

The principal defined parameters are: the water moisture content *w* [%], apparent wet density mass γ [kN.m^{-3}], grain density mass γ_s [kN.m^{-3}], Void ratio e_o [-], Permeability K [m/s], Young's modulus E [MPa], Poisson

ratio ν [-], friction angle ϕ [°], cohesion c [kPa or kN.m^{-2}], Dilatance angle ψ [°], Plastic compressibility λ, identification tests such as Atterberg limits w_L, w_p [%] and granulometry, direct shear resistance with the friction angle ϕ_u [°] and the cohesion c_u [kN.m^{-2}]. Note that several samples due to strong deformations or strong geological heterogeneity (i.e. reworked sediments with huge element) did not permit the shear resistance evaluation. The samples are constituted by decomposed flysch elements corresponding to gravely sands or silty clays with some big elements of undefined limestones (classification USCS: SC-CL, GC-CL, CL). The overall water saturation is about 80 to 90 %. Table 4.20 presents the average values. Globally, the analysed materials are slightly sensitive to the moisture variations and their water content is inferior to the limit of plasticity w_p, except for some samples (e.g. -19.6 meters in FR2). The granulometry is widespread contrary to the residual friction angles showing more constant values.

	Parameter	Unit	Above sliding plane	Sliding plane	Below sliding plane
Identification	Unit weight, γ	kN/m^3	19.9	19.9	21.3
	Void ratio, e_o	-	0.4	0.4	0.3
	Permeability, K	m/s	9E-8 to 1E-4	9E-8 to 1E-4	9E-8 to 1E-4
Elasticity	Young's modulus, E	MPa	80	80	100
	Poisson ratio, ν	-	0.3	0.3	0.3
Plasticity	Friction angle, ϕ	°	30	25	33
	Cohesion, c	kPa	5 to 20	2	30
	Dilatance angle, ψ	°	30	25	33
	Plastic compressibility, λ	-	-	0.07	-
	OCR	-	-	Normal	-

Table 4.20: Material parameters of the la Frasse landslide mass and slip surface.

4.3.6.2 ***Statistical analyses on FR2***

In table 4.21 the statistical results of the direct shear resistance with the friction angle ϕ_u [°], cohesion c_u [kN.m^{-2}] and apparent wet density mass γ [kN.m^{-3}] permit to appreciate the heterogeneity and dispersion of these parameters, notably of the direct shear resistance parameters (ϕ_u and c_u). It can be observed that the general dispersion around the mean is high and thus well traducing the general high geological heterogeneity, with coefficients of variation equal to: ϕ_u = 19.4% and c_u = 52.3% and γ = 2.4%. Variations of the geotechnical parameters in relation to the depth are illustrated in figure 4.28, and are analyzed thanks to linear regressions and correlations. The obtained coefficients of correlation are very low; $\rho_{\gamma z}$ = -0.16, $\rho_{\phi z}$ = -0.15 to -0.29 and ρ_{cz} = +0.18 to +0.60. There are, therefore, no relation between the depth and the mechanical characteristics. The extrapolation of these characteristic at a specified depth from defined values at other horizons are impossible and senseless. The linear correlation between the normed values of ϕ_u and c_u is in the meantime good with a coefficient varying around -0.8.

	Statistics and Dispersion at FR2		
	γ	c_u	ϕ_u
Xmin	21.3	10	20
Xmax	23.3	60	37
Mean	22.3	29.7	29.3
Standart deviation	0.55	15.5	5.7
Coefficient of variation	2.4	52.3	19.4

Table 4.21: Statistics and dispersion of geotechnical parameters at well FR2.

4.3.6.3 ***Stability***

The main factors to consider for stability evaluation are notably the direct shear resistance parameters (ϕ_u [°] and c_u [kN.m^{-2}]), while Bilgot (2007) defines a correlation factor of 85% between these parameters and the factor of security (FoS). Since then, one may observe that the measured values in FR2 are relatively low (5< c_u <60 kN.m^{-2}), thus presenting relatively high instability properties (i.e. low factor of security)

along the whole profile. The entire mass has to be considered has unstable, since no differentiated zones are identified.

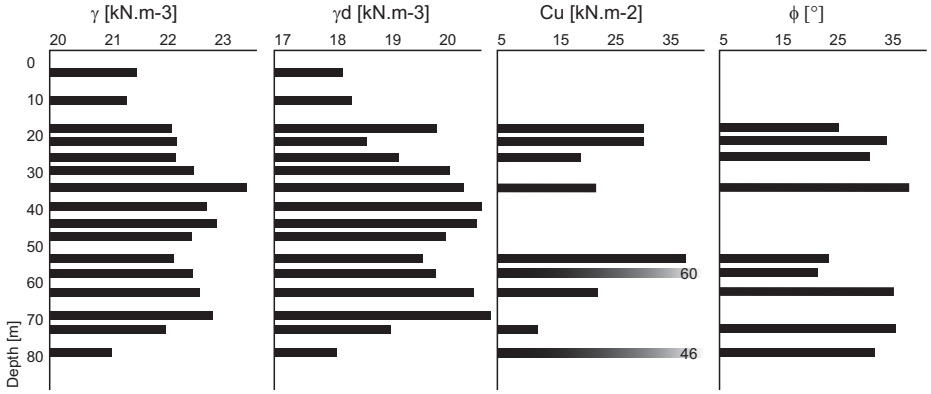

Figure 4.28: Statistics of the geotechnical measures done on a series of core samples from the borehole FR2.

4.3.6.4 ***Correlations between FR2 and LF407***

The following observations may be done on the correlation effectuated between the boreholes FR2 and LF407 in figure 4.29:

- There is no observable correlation between the facies (LF407) and the apparent wet density mass γ , since high values may correspond either to the facies P1 (clayey material) or to P4 (gravely);
- There is plausible correlation between the facies and the direct shear resistance factor c_u, since high c_u values may rather correspond to impermeable clayey-silty facies (P1 or P2);
- High friction angle may correspond to permeable facies (P3 and P4);

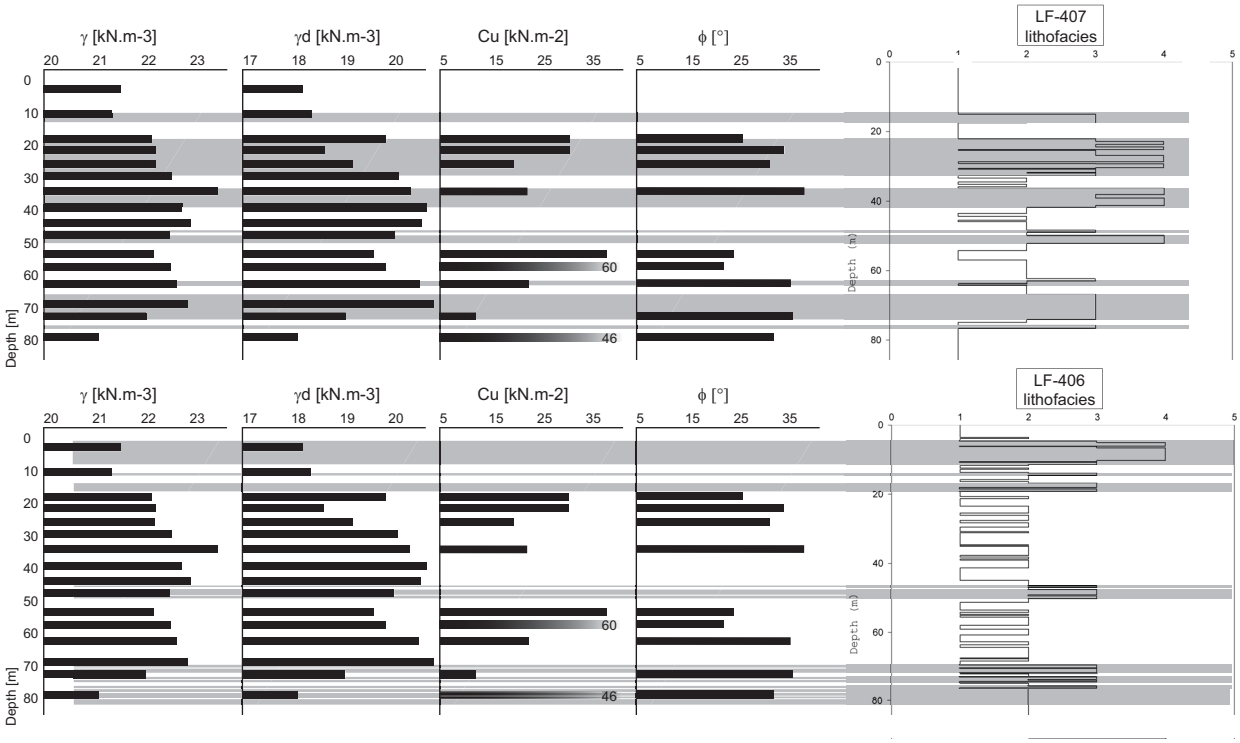

Figure 4.29: Spatial correlation between boreholes FR2 and LF407.

4.3.6.5 ***Hydrodynamical implications***

According to the **linear regression tests,** there is no obvious geomechanical stratification, and consequently no obvious geological or hydrogeological stratification, of the sliding mass that may be considered in stability evaluation **at the scale of the slide**. **The spatial correlation test** between the geological facies distribution and the geotechnical parameter 20 meters apart, seems to indicate that impermeable facies P1 and P2 may present a higher shear resistance, associated to low friction angle.
The results also indicate that there is probably a very unfavourable geological horizon near the sliding surface. According to the observed heterogeneity; the material parameters obtained at the laboratory scale (triaxial examples) are supposed to be representative of the material behaviour at the in situ scale.

- The geomechanical analyses provide information at a **REV and local scale,** but may give a global idea of the situation.

4.3.7 HYDROGEOLOGICAL PROPERTIES HETEROGENEITY

4.3.7.1 ***Introduction***

Since 1985 several hydraulic tests were performed on the la Frasse landslide (see figure 4.30 for location):

- Infiltrating tests on wells of the borehole platform (P4, P18, P19, P20, P21 , P22) (August 2002)
- Infiltrating tests on the survey wells I301 and P302 (October 2002)
- Infiltrating tests on the survey wells FR1, LF1, LF2 and LF3 (1982-1985)

This chapter presents the main results concerning the estimation of the aquifer physical parameters. Specifications about the organisation, description and the theoretical developments of the tests might be found in: Lugeon (1917-1922), Bersier (1967-1969), DUTI Détection et Utilisation de Terrains Instables (1986), NCG (1992) and NCG+EPFL (2002-2003)).

In addition to these infiltrating tests, in 2002 (12-14 November) and 2003 (24-30 September) two tests were performed directly on the wells of the borehole platform, and consisted in the momentary shutdown of the operating pumps. The test 1 (November 2002) lasted approximately 26h30, and the second (September 2003) around 165 hours. The second test was effectuated in two steps; the 24 September at 2h20 pm it began with the complete shutdown of the borehole platform, the 29 September at 4h18 pm the well P11 was switched on, and the 1st October at 11h25 am the test ended. Details on the organization and the general procedure might be found in the annexes 3.3.2 and 3.3.3 of the feasibility report 2002-2003 (NCG+EPFL, 2004).
The aims of these tests were, firstly, to evaluate the reactivity of the system and to assess the physical parameters (i.e. storage coefficient *Ss* and hydraulic conductivity *K*), and secondly, to define the spatial connectivity of the aquifer system.

4.3.7.2 ***Infiltration tests at the borehole platform***

The borehole platform is located in the upper part of the zone "++" (§4.3.2.9). It includes 22 wells equipped with submerged pumps and prolonged below the sliding surface in order to test infiltration possibilities by gravitation. In August 2002, during the annual maintenance of the pumps, infiltration tests were realized

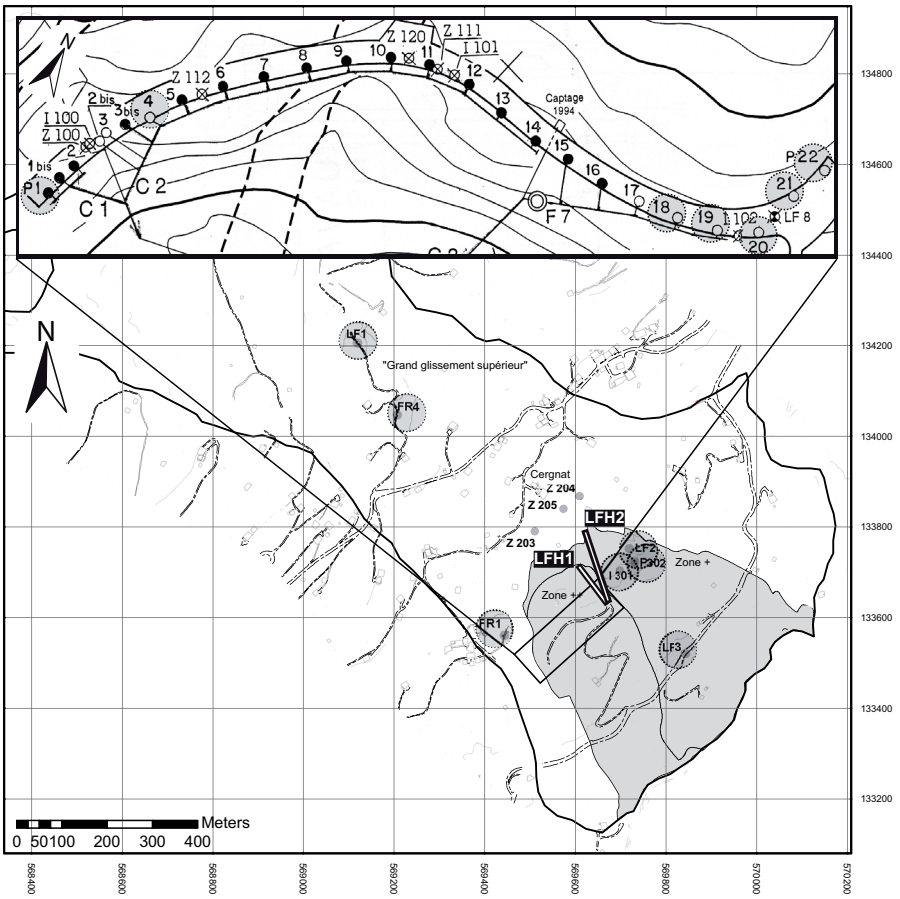

Figure 4.30: Geographical location of the studied sites for the hydraulic tests.

on a part of the wells; P4, P18, P19, P20, P21 and P22 (in grey circles figure figure 4.30). Note that, these wells were never equipped with pumps because of dry conditions meaning that, at these locations, the drained waters inside the mass directly infiltrate inside the fissured underlying limestones. Nevertheless, according to the season, equilibrium state between natural alimentation of the wells and the infiltration in the ground may exist. The tests consisted in filling the wells with a cittern and to measure the lowering during regular time intervals, as illustrated in figure 4.31.

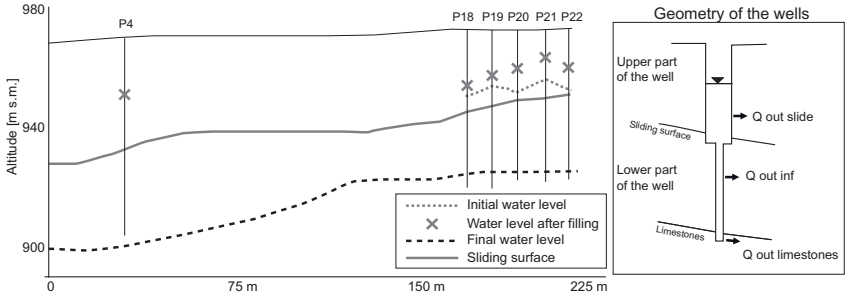

Figure 4.31: Vertical section of the borehole platform and the geometry of the wells. The various water levels during the hydraulic test are illustrated.

Filling. The filling flow rates varied from 30 l/s to 60 l/s. Calculation indicates that around 2/3 of the water is infiltrated into the ground during the filling; while the rest corresponds to the filling volume of the streamer.

Lowering in function of time. After one hour of measurement, the levels of the wells practically reached

their initial state, and the shape the lowering curves indicated that for some wells (P4 for instance), the infiltration continued beneath the sliding surface and that the equilibrium level might to be found there, instead in the upper part into the sliding mass. To facilitate the exploitation of the measurements, the following relation was fixed on the experimental values; $H = (a/(t+b))+c$, with H the water level inside the well, t the time (s) and the constants a,b,c. Constants a,b and c were defined thanks to the following boundary conditions:

$$t = \infty \Rightarrow H = Hfinal \Rightarrow c = Hfinal$$
$$t = 0 \Rightarrow H = Hinitial \Rightarrow b = a / (Hinitial - Hfinal)$$

The constant a is estimated by regression, starting from measurements of lowering. For well P4, the final water level being unknown, a multiple regression was carried out to calculate the parameters a and c (table 4.22). In (NCG+EPFL (2004) other models including logarithmic or exponential formulations were tested, but with less success unless considering additional calibration parameters. Meanwhile, note that these uni-dimensional models, whatever the number of calibration parameters used, only provides a very simplified image of reality. These models may only be used to simplify the processing of the data (i.e. fitting and interpolation). In addition to its simplicity and the relatively good agreement with the measures, the advantage of this formulation lies in the fact that it does include only one parameter to be fixed on the experimental values. Moreover, this parameter provides a general idea of the heterogeneity of the underground. The several calculated curves of tendency (appendices VI-1,-2,-3) indicate that the agreement with experimental measurements is generally very good, with exception done for wells P21 and P22 for which the convergence towards the final water level is faster experimentally. The analysis of the parameter a (table 4.22) points out the spatial heterogeneity of the hydrogeological characteristics of the underground, and demonstrates that the wells even close located, may present very different hydraulic behaviours.

Well	a	b	c	Correlation coef.
P4	7964	496.7	933.8	0.997
P18	1334	542.0	951.1	0.995
P19	115	404.0	954.7	0.996
P20	2365	279.5	952.5	1.000
P21	7946	969.0	956.8	0.988
P22	1049	118.2	952.7	0.981

Table 4.22: Constants a,b and c for the calculation of the lowering velocity of the water level inside the well.

Velocity of the hydraulic lowering in function of time. According to the hereinbefore suggested formulation the lowering velocity of the water level inside the well becomes: $v = -a/(t+b)^2$, with v = water level lowering velocity in [m/s], a and b the before-mentioned constants.
The defined tendency curves are compared to the lowering velocity calculated from the measured levels by:

$$v_{(i)} = moyenne\left[\frac{H_{(i-1)} - H_{(i)}}{t_{(i)} - t_{(i-1)}}; \frac{H_{(i-1)} - H_{(i+1)}}{t_{(i+1)} - t_{(i-1)}}; \frac{H_{(i)} - H_{(i+1)}}{t_{(i+1)} - t_{(i)}}\right]$$

with $v_{(i)}$ = experimental "instantaneous" lowering velocity at time (i)
$H_{(i)}$ = water level in the well at time (i)
$t_{(i)}$ = time variable

Note that an average value was adopted in order to smooth the observed velocities of the lowering curves. By doing this, the maximum velocities are at the beginning of the test somewhat underestimated.
The correlation between the models and the instantaneous experimental values drop down to:

P4: R^2=0.824 P19: R^2=0.972 P21: R^2=0.920
P18: R^2=0.846 P20: R^2=0.990 P22: R^2=0.769

It only remains satisfactory for well P20 and well P19. The divergence is mainly noted at the beginning of the test where the velocities are significant but also more difficult to measure. Except well P20, the velocity plots (appendices VI-1,-2,-3) include abrupt intensity variations at the beginning which exclude an infiltration in a homogeneous and continuous ground.

Average coefficient of permeability. Thanks to the Lefranc formulation, coefficients of permeabilities might be calculated: K=A/(F*T) *with K = Lefranc permeability coefficient [m/s], A=lower section of the well [m²], F= factor of cavity shape [m] and T= re-equilibrium time [s]. The calculated permeabilities are showed in figure* (figure 4.32), the average value is around 1E-5 m/s corresponding to a rather low permeable environment. Their distribution indicates that there is no clear spatial relation.

Well	Depth [m]		K in [m/s]	Mean K in [m/s]
LF1	28.5 - 32.5		3.20E-05	**1.65E-06**
	36.5 - 38		7.50E-05	
	37.5 - 38.85		2.30E-05	
	45.5 - 49		9.80E-05	
	50 - 51		3.80E-05	
	97.3 - 108		2.10E-06	
	97.3 - 111.5		4.00E-07	
	112 - 121.6		7.60E-07	
LF2	12 - 13.5		1.60E-05	**3.37E-05**
	31 - 34		8.70E-06	
	68.5 - 69		1.40E-04	
	83 - 83.5		2.30E-04	
LF3	49 - 50		5.50E-05	**9.87E-05**
FR1			3.00E-07	**5.50E-05**
			3.00E-06	
I301	34 - 36		2.00E-05	**3.01E-03**
	51 - 53		6.00E-03	
P302	56 -57		5.00E-05	**5.00E-05**
	129 - 140		5.00E-05	
	Depth upper part [m]	**Depth well total [m]**		
P4	32.2	67		**4E-6 to 1E-5**
P18	27.25	53		**2E-7 to 7E-6**
P19	24.49	53		**1E-6 to 2E-5**
P20	22.43	51		**7E-7 to 2E-5**
P21	19.92	51		**2E-7 to 6E-6**
P22	22.02	51		**2E-6 to 5E-5**

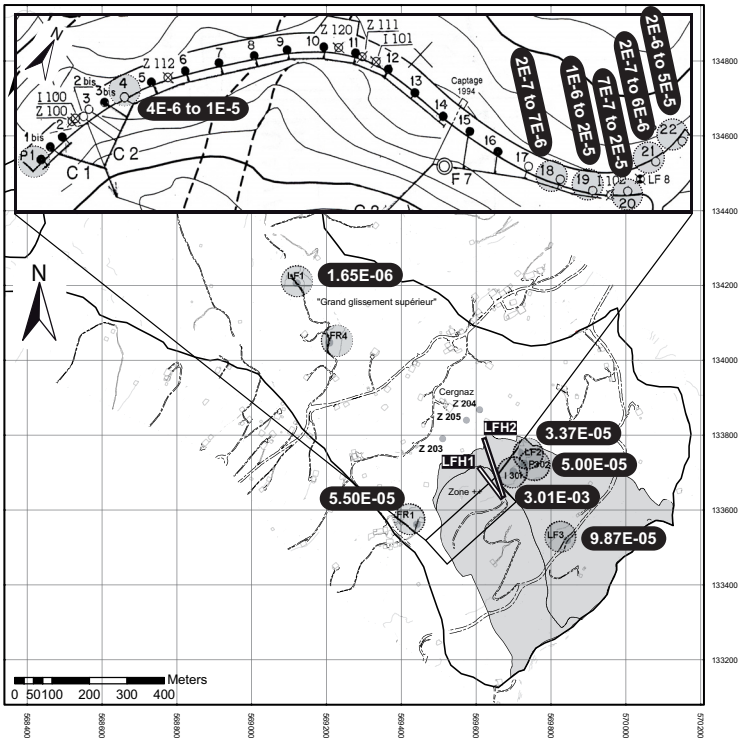

Figure 4.32: Synthesis of the calculated hydraulic conductivities of the la Frasse landslide.

4.3.7.3 *Infiltration tests at the wells FR1, LF1, LF2, LF3,I301 and P302*

Between 1981 and 1989 the following wells (FR1, LF1, LF2, LF3, I301 and P302) were installed in order to complete the existing observation system. The permeabilities calculated during the digging at different depth in LF1 and LF2 may not be correlated. For LF1 the presence of a more permeable zone situated at a medium depth as showed in plot 4.5 is identified, its extension may be very local. Note that this permeable zone corresponds to the depth of the identified sliding surface at LF2. At the depth of the identified sliding surface in LF1, permeabilities values calculated in LF2 are as well increasing. At around – 100 meters, LF2 is showing in depths, near the contact with the underlying unit, high values (> 1E-4 m/s), indicating that probably locally the bedrock is very impermeable. The average permeability is around 4.8E-5 m/s and corresponds to a limy-sand environment. Otherwise, the highest values are certainly representative of local high permeable zones, corresponding to local intercalated gravelly bodies. In addition to that, between October and November 2002, two additional wells (*I301 and P302)* were drilled in the zone "+", to supplement the existing knowledge of this area, to determine the depth of the bedrock, to locate the sliding surface, to determine displacement velocities and to study the possibilities to implant an additional draining well system in the prolongation of the existing borehole platform.

4.3.7.4 *Well test analysis at the borehole platform*

Test 1 (November 2002). The following wells were used for the observations: FR1, LF2, LF9, Z203, Z205, Z111, Z112, Z113, Z117, and Z114. The first important observation is the slow and low increase of the water level in all the observation wells, exception done for those of the borehole platform (Z111 and Z112), and the variable time evolution of the water levels for each piezometer. The following observations are schematized in figure 4.33:
Five of ten piezometers (FR1, LF9, Z113, Z117 and Z205) indicate a variation of water level lower or equal to 3 cm during the first 7 hours of the test, and less than 20 cm after 24 hours. And contrary to what expected during the test, the water level lowered in 3 piezometers (LF2, Z114 and Z203). Finally, only the water level of the two piezometers of the borehole platform (i.e. Z111 and Z112) increases significantly. The piezometer Z111 showed a traditional evolution (fast evolution at the beginning of the test with a convergence towards an asymptote) while the Z112 piezometer revealed an opposite behaviour during the first 7 hours of measurements.

Test 2 (September 2003). The choice of the observation piezometers is based on the above-discussed well test. The observation piezometers are the following: note that only the underlined wells did show a reaction to the test; P1, P2, P2b, P3, P3b, P5, P6, P7, P8, P9, P10, P11, P12, P13, P14, P15, P16, P17, P18, P19, P20, Z111, Z112, Z113, Z114, Z115, Z118, Z203 and Z204 (appendix VI-4).

In the lower part of the zone "++", the piezometer Z114 (100 meters apart from the platform) presented a regular strong decrease, as shown in figure 4.33 indicating the purging of the system around the well. A global lowering of 16 meters in 5 days was recorded; the level stabilized finally when the well P11 was switched on (see §4.3.7.1 for test description). This behaviour is once again contrary to what expected; a stop of the pumps should generate an increase of the hydraulic heads, especially downhill of the pumping system. On the contrary, the piezometers of the wells Z203 and Z204 located uphill of the platform and distant respectively 210 and 280 meters from the platform, did not record any variation until the well P11 was switched on again. Then, the water levels decrease instantaneously 0.60 m and 1.45 m respectively, in one hour, whereas the wells close to P11 practically did not react. Finally, well Z118 at the beginning

recorded a strong decrease of around 1 meter, and then stabilized until the end of the test. Z118 did not react when P11 switched on.

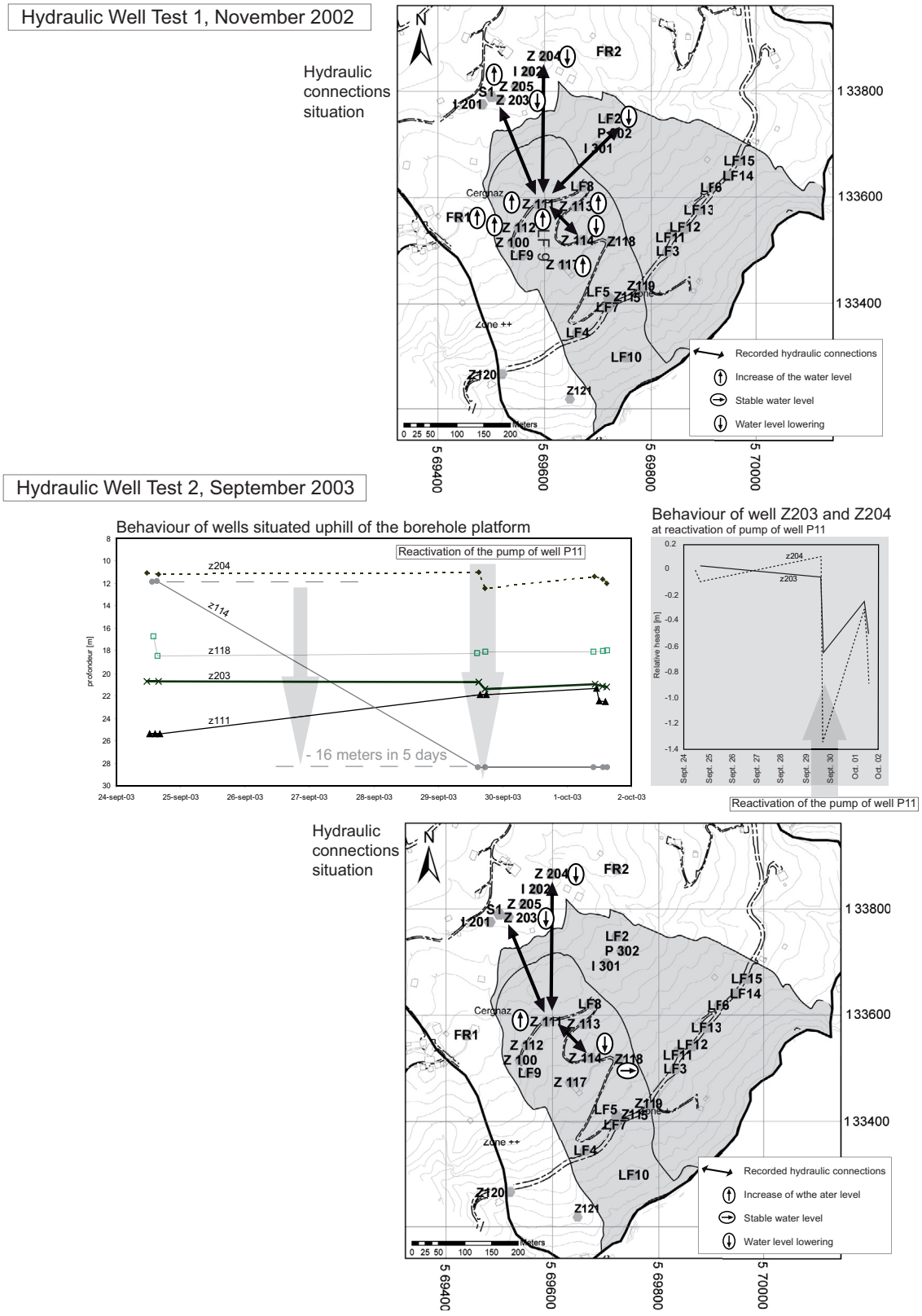

Figure 4.33: Water levels and hydrodynamical behaviours of the system under the hydraulic tests; Test 1 (November 2002) and test 2 (September 2003). The several wells are reacting differently.

4.3.7.5 Storage coefficient (Ss)

The rather contradictory results and observations obtained thanks to these tests made the interpretation and the evaluation of the storage coefficient (*Ss*) by analytical solutions very difficult. Nevertheless, in the final report NCG+EPFL (2004), the storage coefficient (*Ss*) was determined thanks to numerical simulations. A starting value was defined thanks to the application of the Theis method during increase of the well Z112, unique piezometer able to treat this case, since it showed a traditional increasing curve. Its interpretation according to Theis gives an *Ss* value = 1E-3 (m^{-1}), in the meantime overestimated due to the global increase of the aquifer water levels, which reduces the answer. Finally, several numerical modelling attempts starting from this value showed that the specific coefficient of storage (*Ss*) enabling to reproduce the test as well as possible was around 1E-4 [m^{-1}].
The numerous simulations pointed out that it is not possible to have an optimal calibration for each piezometer with the same specific storage coefficient (Ss), while certain piezometers show a better calibration with Ss = 1E-3 [m^{-1}] whereas for other, Ss = 1E-4 [m^{-1}] gives better results. Moreover, these results indicate that due to geological heterogeneity the specific storage coefficient (Ss) may probably vary locally and spatially.
The numerical method gave satisfactory results. Contrary to analytical solutions, it enables to be freed from simplifying assumptions and to consider the problem three-dimensionally; specificities of the geometry and possible boundary conditions effects.

4.3.7.6 Hydrodynamical implications

The following observations might be formulated:

- The wells, even close located, may present very different hydraulic behaviours.
- The underground, sliding mass and bedrock included, are fully heterogeneous and discontinuous, since infiltration velocity plots present abrupt intensity variations at the beginning of the tests.
- The low and slow hydraulic response during the well test analysis at the borehole platform confirms the relatively strong inertia of the aquifer.
- The hydraulic relation with the underlying unit should be studied at a very local scale (strong disparities).
- The average permeability value is around 4.8E-5 m/s corresponding to a rather low permeable environment, limy-sand environment. Their distribution indicates that there is no clear spatial relation.
- The highest values (1E-4 m/s) are certainly representative of high permeable zones, corresponding to local intercalated gravely bodies.
- Strange hydraulic behaviour during the well tests (opposite), difficult to interpret.
- Specific storage coefficient (Ss), is around 1E-3 [m^{-1}] and 1E-4 [m^{-1}], indicating strong confined properties, and may probably vary locally and spatially.
- Spatial connectivities of several hundreds of meters are possible. And according to the position of the observation wells, their orientation might be parallel to the sliding direction.
- These tests confirm that the **quantitative results** have a **LOCAL** meaning**;** however, qualitative results (global observation) may give a regional vision of the hydrodynamical behaviour and complexity.

4.3.8 FLOW HETEROGENEITY AND HYDRAULIC RESPONSE BEHAVIOUR

4.3.8.1 Water table observation

The analysis of the different piezometric levels, recorded since 1982, at different locations, indicates that the elaboration and the interpretation of a piezometric map are very questionable in such geological environments. The piezometric levels may be hardly correlated, and due to the extreme geological heterogeneity, the hydraulic equipotential surfaces have an irregular behaviour, and may be quite numerous along a vertical profile. For instance well Z205 in which three confined aquifers are observed (3 tubes with 19, 39 and 57 meters, see figure 4.34, location in figure 4.30), demonstrates that a borehole may cut through several equipotential surfaces. Under these conditions, the water level measure in the borehole neither represents the local hydraulic potential of the mass nor the upper level of the saturated zone. But, each water level represents a local isolated perched aquicludes. At a regional scale the interpretation of piezometric maps is very tricky or even impossible. In landslide aquifers, it is thus recommended to have permeability profiles, or at least to know the transmissivity of the boreholes, to draw piezometric maps and to interpret the measured water levels. Continuous measures of water levels in the boreholes may give qualitative indications on the permeability and on the spatial continuity of the medium, but locally.

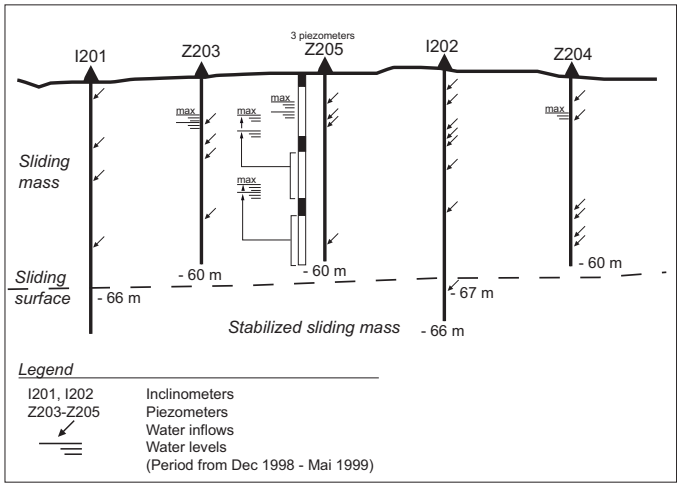

Figure 4.34: Vertical section of the boreholes I201, Z203, Z205, I202 and Z204 and location of the main water inflows measured during digging.

4.3.8.2 Vertical inflows observations

The measures in continuity from 1982 to 1985 of the water inflow and the hydraulic head distribution in the wells FR1 to FR6 at different depths provide important information about the main characteristics of the confined or free surface aquifers. The first observations indicate that the water levels are in time relatively constant but are varying in function of their vertical location.

At FR1, the cell at -54 meters shows a variation between -8.8 meters and -12 meters indicating thus obvious confined characteristics. The cell placed at -23 meters indicated in 1983 a water level at -2.73 meters to -4.65 meters. The cell placed at -13.8 meters did not indicate water inflows until end of 1982, and then a water level depth around -2 and -3.3 meters. These levels remained relatively constant until 1994. FR1 is thus showing a multi-layer system composed of confined aquifers. There are no evidences about vertical connectivity. On the contrary, in FR2, the cell placed at -19.6 meters indicates the presence of a unique unconfined aquifer (free surface) since the water level indicates a constant level around 18.3 and 19.6 meters. At the sliding surface (-60 meters), the water level varied between 41 and 46 meters, indicating a water column of 15

meters. The wells FR3 and FR5, distant of 150 meters and located inside a very impermeable zone did not indicate important water inflows. The pressure cells located at the sliding surface (around -20 meters) indicated pressures near 1.3 Bars, corresponding to a water level at -3 meters, representing moderate to high hydraulic pressure conditions. At FR5 the water level stabilized during perforation at -4 meters, and then lowered down to -9 meters when the underlying bedrock was reached, confirming the presence locally of descending flows. Artesianism could be observed in well FR6, located in the front of the active zone. A hydraulic pressure equivalent to 0.4 bar was measured at -18 meters and 0.6 bar at -42 meters. Note that these artesianism inflows correspond to water circulations inside the sliding mass, forasmuch as the perforation inside the substratum (at -51 meters) did not modify these inflows.

The wells LF1 to LF6 and LF8 to LF10, implemented from 1984 to 1989, showed that into the upper part of the active zone of the slide (i.e. well LF1) water inflows may be strongly underpressure (90 T/m^2) and may correspond to water column reaching 90 meters. Inside the lower part of the slide (i.e. LF2 to LF10) captive aquifers also may exist but with underpressures values inferior of several order of magnitude. The measured done inside the underlying units in wells LF3, LF9 and LF10, indicate leaking conditions (>20 l/min), and partly unsaturated conditions. In the same order of observation, the wells I201 and I202, Z203, Z204 and Z205, installed in 1998, recorded 4 to 6 water inflows (figure 4.34) from the more permeable zones. No spatial correlations between these water inflows are observable in figure 4.34.

4.3.8.3 ***Evolution of the water levels after 1994***

1995 corresponds to the commissioning of the borehole platform following the important crisis (1994). The plots in appendix VI-5 present the water level measurements from 1995 to 2003. The efficiency of the drainage system is well marked since, directly after the commissioning, the water levels lowered 3 meters at Z100, 14 meters at Z111. Whereas, note that first, no effects is recorded in the eastern part of the system at Z113. Afterwards, Z113 records a slight decrease between 0.2 and 3.6 meters as well as the wells P19 to P21 and Z111. Only the well P20 shows an opposite behaviour with an increase of 0.3 meters. While these variations are mostly happening during summer times, a direct relation between precipitations and water levels may exist. The following observations under the effects of this drainage system are synthesized in figure 4.35, some specificities of the spatial connectivity of the system may be observed, since the measured water levels vary strongly from point-to-point.

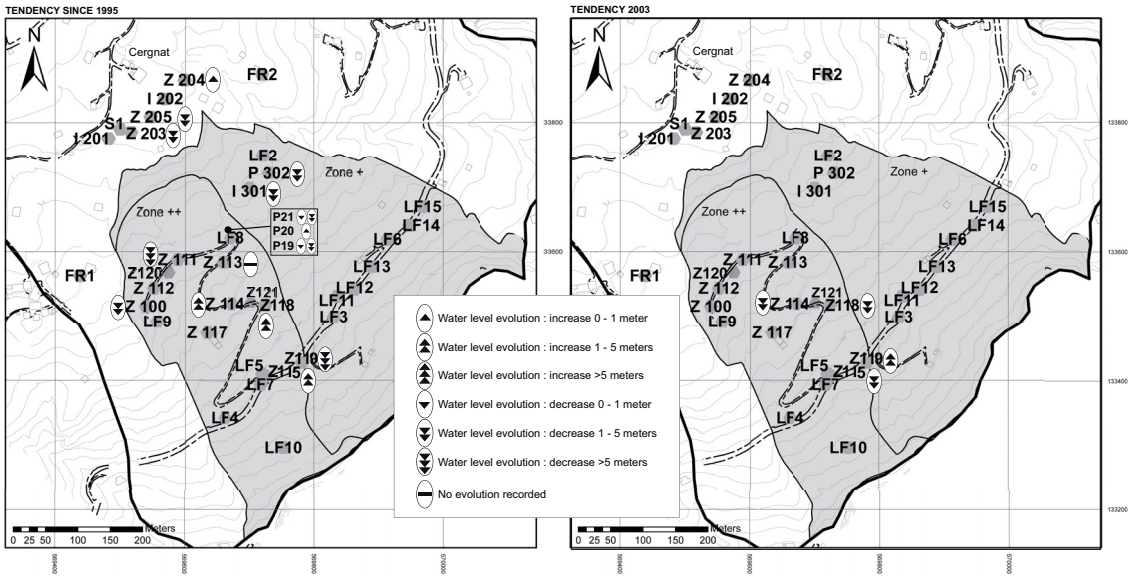

Figure 4.35: Water levels behaviour tendency since 1995 (commissioning of the borehole platform).

Lower part of the slide (between the road and the platform), the levels recorded at Z114, Z115 and Z118 show an increase from 3 to 9 meters since 1994, and at Z119 a decrease of 7 meters. Moreover, for the year 2003 (very dry summer season) a strong decrease between 0.1 to 4 meters is globally recorded, except for the piezometers Z119 showing this time a strong increase up to 3 meters from June to December 2003. Therefore, it may be noticed that the area situated between the borehole platform and the national road RC 705 is strongly influenced by the drainage, positively as well as negatively. Well Z119 shows an opposite behaviour than observed and above all expected.

In the zone "+", the influence of the drainage system is also observable at the wells P301, 302a and P302b since they indicate decreases varying from 0.25 meters up to 8.2 meters function of their location and the depth of measures.

At Cergnat, the evolution of the piezometers Z203 indicates a strong decrease between 2.2 to 3.9 meters during the year 2003, whereas the neighbouring well Z204 recorded an increase of 0.6 meters at the end of the year. Z205, equipped with pressure cell devices for measuring hydraulic pressures at three different depths, show that the water level of the intermediate aquifer (cell at - 39 meters) presents a decrease of 3.9 meters, twice bigger than for the low (-2.4 meters) and the deep aquifers (- 2.2 meters).

The year 1998 presents some particularities due to special hydrological conditions. Globally the amount of precipitation is equal to 1997 but irregularly distributed (around 60mm/month from January to May and 121 mm/months from June to December). At the borehole platform, it can be observed in almost all wells a general decrease of the water levels at the middle of the year and a strong increase at the end; between 0.1 and 3.5 meters. Besides, strong differences are observable in short distances; for instance Z100 (+ 0.1 meters) and well P1 (+ 4.71 meters). At Z120 a pressure cell placed at -24 meters indicate an increase of +2.5 meters. Between the platform and the national road, the measured levels in the piezometers increased around 1.4 meters between the beginning and the end of the year, showing an opposite behaviour. This tendency continued during the fourth first months in 1999, with a supplementary variation of 0.7 meters. At Z121 the two pressure cells placed at -22 and -28 meters recorded significant level increases respectively of +1 and +2.4 meters. At the national road, the measured levels of the piezometers increased around +1.1 meters during 1998. Finally, all piezometers indicated stabilization during 1999, except Z115 showing a very strong increase of 8.12 meters.

4.3.8.4 Flow rates analysis at the borehole platform

This chapter present the inflow rates extracted from the borehole platform from 1995 to 2003. Note that, the wells P20 to P22 are not equipped with pumps; P3 and P17 have never functioned because they are, since 1995, dry. Appendix VI-6 presents the total evacuated waters from 1995 to 2003. Figure 4.36 presents the contribution of each well for 5 selected years (1995, 1998, 2000 and 2003). The observation of these values informs about the heterogeneity of the system in time and spatially, and constitutes an excellent example of local heterogeneity.

In 1995, the first year of service record the most important evacuated water rates, notably due to the extreme hydrological conditions. The wells P2, P6, P7, P11 and P15 evacuated the most important volumes of water, with flow rates comprises between 7884 and 23652 m^3/year (15 and 45 l/min). The second group formed by the pumps P11, P12, P13, P14 and P16 evacuated average water rates between 2600 and 7900 m^3/year (5 and 15 l/min). Finally the last active pumps (P1, P4, P5, P8, P9, P10, P18 and P19) are characterized by flow rates inferior to 2000 m^3/year (< 5 l/min). The total of the evacuated waters reaches in 1995 about 60000 m^3 (164 m^3/day, 6.9 m^3/hour, 114 l/min). This total is, for comparison, three times bigger than the total in 2003.

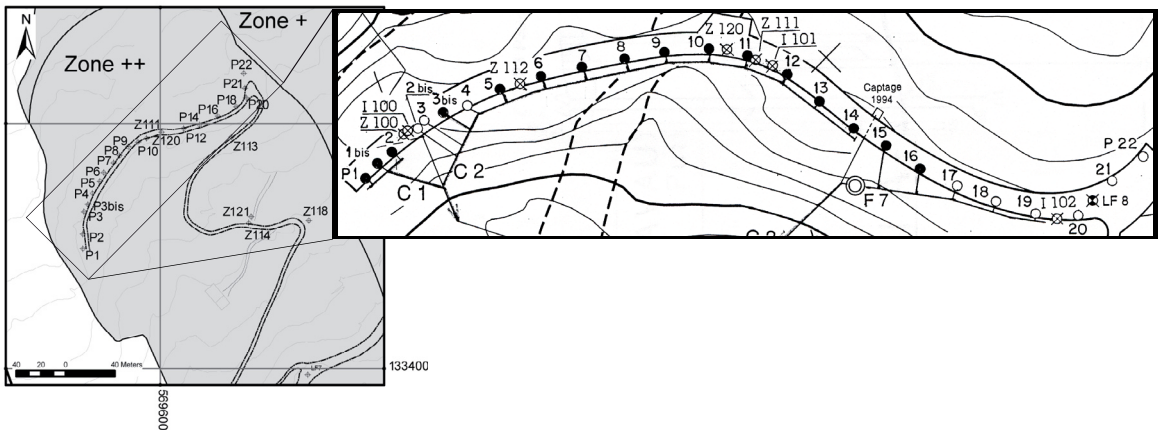

	1995	1998	2000	2003
P1	2.2		*0.7*	*0.6*
P1bis		*0.7*	*0.4*	*0.6*
P2	**25**	2.1	**7.6**	
P2bis		*0.6*		
P3				
P3bis		**8.4**	**6.9**	**7.9**
P4	4			
P5	*1.2*	*0.5*	*0.9*	
P6	**23**	**9**	**10.2**	**7.5**
P7	**24**	**9.6**	**9.2**	**7.2**
P8	*1*	*0.4*	*0.6*	*0.7*
P9	1.9	*0.3*	*0.5*	*0.6*
P10	4.5	*1.1*	*0.6*	*0.1*
P11	**18**	4.3	**11.2**	2.8
P12	**11**	4.1	**7**	**5.6**
P13	**12**	2.5	*1.5*	2.1
P14	8	2.7	**6.5**	**5**
P15	**43**	2.1	**7.1**	1.8
P16	**10**	2.8	2.1	3
P17				
P18	*1.4*			
P19	*0.9*			
P20				
P21				
P22				

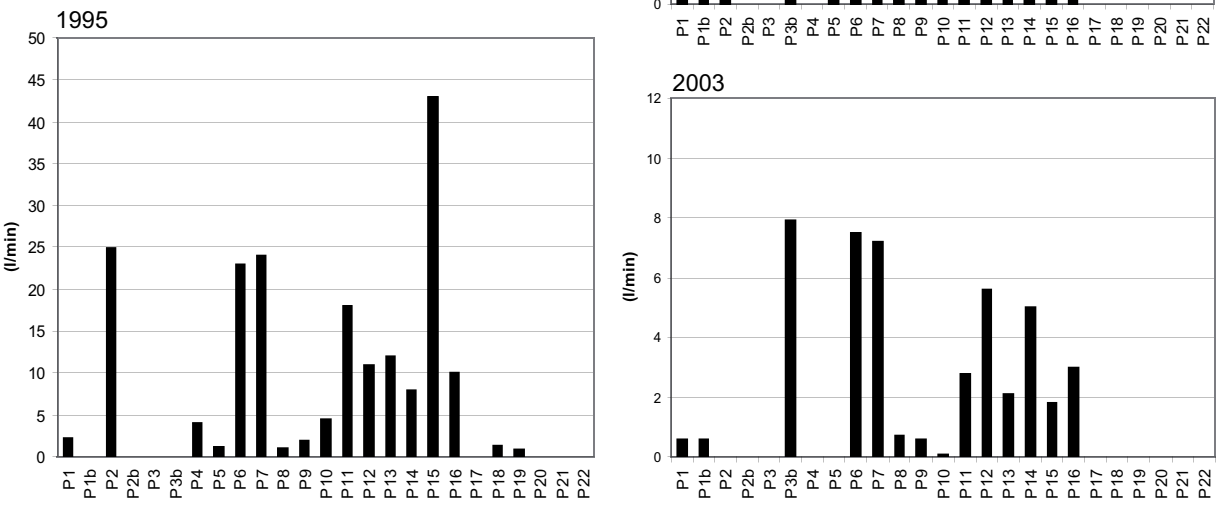

Figure 4.36: Flow rates pumped by the wells of the borehole platform for 1995, 1996, 2000 and 2003; time and spatial variation.

In 1998, the pumping wells P3bis, P6 and P7 evacuated the largest volume of water, with flow rates between 4400 and 5000 m^3/year (8.4 to 9.6 l/min). The pumping wells P2, P11 to P16 evacuated water volumes comprised between 1100 and 2300 m^3/year (2.1 to 4.3 l/min). The others wells presented very low flow rates; around 100 to 600 m^3/year. The total evacuated amount reached almost 27000 m^3 for the year 1998 (74 m^3/day, 3.1 m^3/hour, 51 l/min), for a total of approximately 1000 hours of functioning. These values are 15% lower than in 1996 and almost equal than in 1997 (+0.4%). These results are logical, since the total amount of precipitation was almost identical in 1997 and 1998 and slightly more important in 1996. It exists thus a correlation between the evacuated waters and the precipitations; a slight increase in the evacuated waters is recorded during rainy periods.

In 2000, the situation is qualitatively and quantitatively almost similar than for 1998. However note that there is a significant increase of the evacuated pumping rates in P2 (from 2 to 8 l/min), in P11 (from 4 to 12 l/min) and in P14 as well as in P15 (from 2 to 7 l/min). The total amount of evacuated water is the equal to 1998 (about 38000 m^3).

In 2003, the wells P3b, P6 and P7 evacuated the most important volumes of water, with flow rates comprises between 3700 and 4000 m^3/year (7.0 and 7.6 l/min). Already in 1998 these wells were the most prolific of the system. P12 and P14 are the second most active pumps with an average of evacuated water rates of 2700 m^3/year (5.1 l/min). Then with mean rates between 900 and 1500 m^3/year (1.7 and 2.9 l/min) arrive the pumps P11, P13, P15 and P16. Finally pumps P1, P1bis, P2, P2bis, P8, P9 and P10 are even characterized by very low inflow rates, comprise between 4 and 370 m^3/year (around 200 m^3/year, 0.4 l/min). The total of the evacuated waters reaches for 2003 about 23200 m^3 (64 m^3/day, 2.6 m^3/hour, 44 l/min). This total corresponds, for comparison, to about 57% the evacuated waters in 2001 and 74% for 2002. These results are logical according to the special dry hydrological conditions of 2003.

4.3.8.5 Water inflows in LFH1 and LFH2 and influences

Two horizontal draining adits LFH1 and LFH2 were realized between July and August 2001, and are respectively 100 meters and 164 meters long. The drilled section is equal to 3 inches (0.0762 meters), and the mean drilling velocity was around 15 meters/day. They cross successively the zones "++" and "+" (appendix III-5 and §4.3.2.9). The crossed material corresponds to the heterogeneous flysch mass; loose rocks of flysch, grey-black limestones and dolomite blocks of all sizes into a silty-clayey matrix. Some sliding surfaces could be identified. Piezometers Z203, Z204, Z205 at Cergnat, located approximately 200 meters uphill of the borehole platform are used to observe the influence of the drainage. Besides the numerous existing boreholes, these galleries allow exploring horizontally the geological heterogeneity of the mass. The measured inflow rates during digging permit to identify the hydraulic behaviours, i.e. inflow rates evolution and hydraulic head lowering at the observation wells of the system, and of course to estimate the hydraulic parameters. For this purpose sophisticated hydraulic response analysis tools are used to understand the global hydraulic behaviour. In section 5.4.6, the conceptual model of the LFH1 drain is used to test, by means of three-dimensional numerical modelling, the proposed hydrodynamical model discussed in section 4.3.11.3.

Observed water inflows in LFH1 (figure 4.37)**.** During perforation the first water inflow is located at 42 meters with an artesian discharge of 0.3 l/min. The principal inflow appeared at 57 meters and 79.5 meters (with artesian discharges respectively of 60 and 200 l/min). After perforation, the global inflow reduced to 9 l/min and finally stabilized around 6.8 l/min (September 20, 2001), and this in spite of strong rainy events (September 3 and 4).

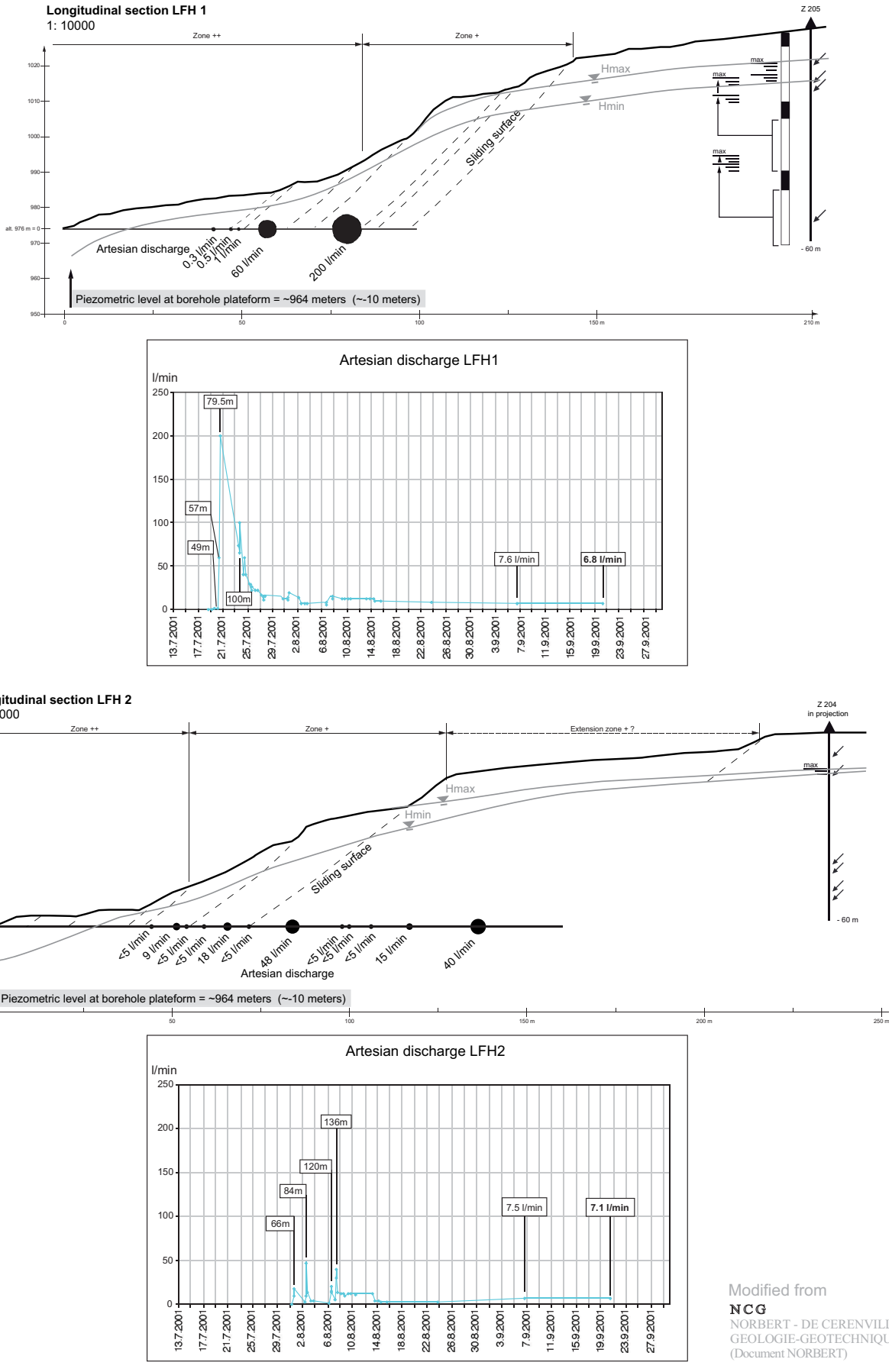

Figure 4.37: Vertical section of the LFH1 and LFH2 drains and inflow rates during digging (modified from NCG+EPFL 2004).

Observed water inflows in LFH2 (figure 4.37)**.** During perforation the first water inflow is located at 44 meters (< 5 l/min). The principal water inflow appeared at 66, 84,117 and 136 meters (with artesian discharges respectively of 18, 48, 15 and 40 l/min). After perforation, the global inflow reduced to 3 l/min since August, with a passage respectively to 7.5 and 7.1 l/min the 6 and 20 September (2001). The measured artesian discharges during perforation, up to 20 times superiors than the residual flows, may be explained by the probable presence of captive aquifers in the sliding mass, behaving as isolated water pockets which are emptied brutally during the perforation. Moreover, no correlations exist between the water inflows and the crossed zones of blocky material.

Observation at the piezometers (Z203, Z204 and Z205) in appendix VI-7**.** The piezometric levels at Cergnat (i.e. wells Z203, Z204 and Z205 which comprises 3 tubes with 19, 39 and 57 meters) were regularly measured, during and after the perforation. After a long period of decreasing since the months of April and May 2001, the five piezometric levels globally increased from the 17th to 25th of July, then dropped regularly from 38 cm to more than 3 meters. Only Z204 showed a slight increase. The piezometric level variations are thus marked but not exceptional and correspond on one hand to seasonal variations and on the other hand to a slight effect of the horizontal draining system.

Flow rates in 2003. The waters collected by these drains are controlled regularly to test the general efficiency; the results for 2003 are as follows: LFH 1: flow rates are ranging between 2.4 l/min (November 2003) and 8.2 l/min (April 2003), that is to say 1’300 and 4’300 m3/year. compared to the a single well of the borehole platform it corresponds to a low efficiency. LFH 2: flow rates are ranging between 2.2 l/min (November 2003) and 4.8 l/min (April 2003), i.e. between 1’200 and 2’500 m3/year, compared to a single well of the borehole platform it corresponds to a low to medium efficiency. 28 months after the commissioning, the system was still valuable.

4.3.8.6 Hydraulic response behaviour

The classical approach consists in the temporal observation of the inflow rates in function of the recharge during a hydrological cycle. During the digging of the drain, the encountered inflows evolve in function of the time, sometimes during relatively long periods according to hydrogeological and geological characteristics of the massif. Several mathematical formulas are available in literature for the calculation of the hydraulic permeability from the measured inflow rates at the scale of the massif or even from a specific zone, hydrogeologically differenced. In Maréchal (1998) these methods are fully tested, and in this work, we will use for steady calculations the Goodman (1965) formulation and for the unsteady conditions, the Jacob and Lohman (1952) (see appendix I for the theoretical elements).

Typical inflow rate behaviour. When a water inflow is intercepted by an underground work, the evolution of its rate in function of time has generally the aspect illustrated in figure 4.38. The initial flow rate *Qi* decrease very fast under the decompression effects and the depletion of the massif until a *Qf* value, which is permanent and traduce the equilibrium state between the drainage of the work and the recharge conditions. The ratio *Qi/Qf* depends on several factors; i.e. the hydraulic conductivity *K* of the massif, the storage compressibility *Ss* and the recharge conditions *I.* A permeable zone will tend to liberate more easily its water and will be characterized by a higher ratio, comprises between 1 and 5 after Heuer (1995).
During the decrease phase and then during the equilibrium state, the water inflows may react to external impulsions, such as heavy rain events or snow melt, in the form of principal floods *Qp* or secondary

Qs. The ratios *Qp/Qf* and *Qs/Qf* depend on the permeability *K* of the massif, the recharge *I*, the size of the reservoir and the depth of the underground work (elevation of the phreatic level). The flow rate vary therefore strongly in function of time, especially during the first instants. The water inflows encountered in the two drainage galleries (LFH1 and LFH2), for which we dispose instantaneous measures, illustrate the behaviour at the first instants, as discussed.

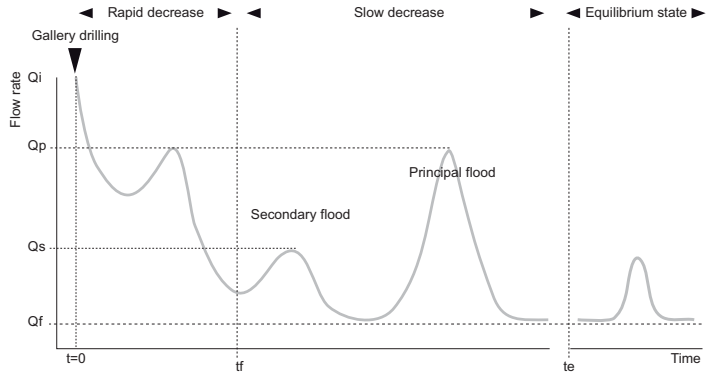

Figure 4.38: Typical inflow rate behaviour in function of time when a water inflow is intercepted by an underground work.

These inflows are characterized by a logarithmic decrease of the flow rates (i.e. $Q(t)= -a\ln(t)+b$), where *a* characterizes the intensity of decrease. *a* is function of the permeability of the drained zone, its porosity and of the size of its watershed (figure 4.39a). Note that these observations are not adjustable with classical decrease function (exponential of Maillet (1905)) presenting to slow decreases. The formulation of Maillet is adapted to a pure depletion whereas in the problematic of underground works, the storage compressibility intervenes. The observed decreases are faster than the Maillet exponential at the beginning and then slower. *Qf/Qi* is linked to the available recharge for the considered zone. For instance in LFH1 the strong decrease (high *a*) and the low final inflows (strong *Qi/Qf*) are the expression of a low available recharge in relation to the existence of local high permeable zones. LFH2 shows mainly the same behaviour, the initial inflow is slightly lower; orders of magnitude are though similar. These adjustments are in the meantime purely indicative. Compared to what occurred in crystalline zones (i.e. Maréchal 1998, figure figure 4.66b), the LFH drainage galleries are presenting similitude with the tectonized zone of the Mont-Blanc. Nevertheless, the *Qi/Qf* ratio is twice more important. This ratio may be representative of large isolated water reservoir, formed by high permeable zones. The depletion curve seems to indicate that these reservoir are disconnected, thus, presenting very low spatial connectivity. Their extension as well as their content in water may be important, as illustrated by the high water inflows during perforation with an artesian discharge up to 200 l/min (20 times superiors than the residual flows). In the meantime, this discontinuous character does not allow satisfactory recharge. These permeable features are thus drained out, and a resulting very slow basal flow persists. Therefore, these observations compared to those done for the Mont-Blanc or Simplon zone, indicate that most of the permeable structures may have a very local importance and a poor alimentation.

4.3.8.7 ***Estimation of hydraulic conductivities***

Numerous analytical solutions allow the calculation of drained inflow rates by an underground work. The two most commonly used solutions are the Goodman (1965) for the steady state and Jacob and Lohman (1952) assumptions for unsteady conditions. The hypothesis and the theoretical developments of theses formulation are exposed in appendix I. In this study both formulations are used and compared.

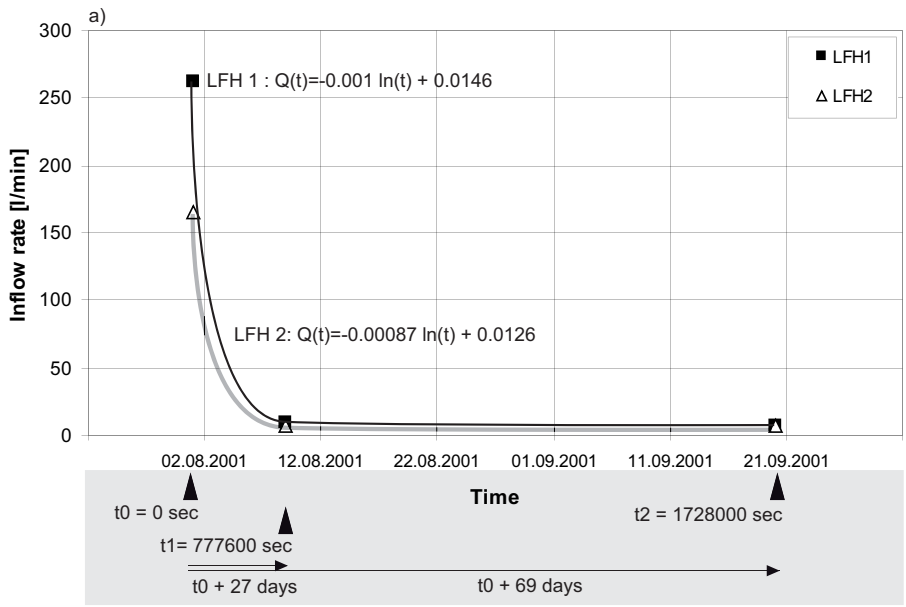

b) Calculated ratios

	Qi [m3/s]	Qf [m3/s]	Qi/Qf	a
LFH1	0.00436	0.00015	29	0.0010
LFH2	0.00275	0.00012	23	0.0009
Data from Maréchal 1998				
Tectonized zone of the Mont-Blanc tunnel	*0.03*	*0.003*	*10*	*0.0026*
Granit zone Mont-Blanc tunnel	*0.035*	*0.015*	*2*	*?*
Veglia zone of Simplon tunnel	*0.0035*	*0.001*	*4*	*0.0003*
Antigorio zone of Simplon tunnel	*0.05*	*0.005*	*10*	*0.0077*

Figure 4.39: a) Inflows characterized by a logarithmic decrease of the flow rates (i.e. Q(t)= -aln(t)+b), where a characterizes the intensity of decrease. a is function of the permeability of the drained zone, its porosity and of the size of its watershed. b) Values calculated in Maréchal 1998 in Alpine crystalline contexts.

Goodman (1965) formulation demands the knowledge of the piezometric heights above the underground work H_o, i.e. distance between the centre of the tunnel and the groundwater table. This is and remains a critical problem in landslide problems. Usually, due to the complex underground heterogeneity distribution, the hydrogeological system may be split in numerous aquifers, perched, confined or unconfined. A borehole thus always cuts through several equipotential surfaces as indicated by the piezometer Z205. The water level measure in the borehole represents neither the local hydraulic potential of the mass nor the upper level of the saturated zone. It represents the level of a local perched aquicludes. Under these conditions several assumptions have to be made. Generally, it is admitted that at the scale of the slide, the entire mass may be considered as a unique aquifer (Tacher et al. 2005), thus considering the system as a saturated system, i.e. water level nearby the surface. For the calculations a subsurface water level varying between 0 and -10 meters is considered. Table 4.23 presents the calculated hydraulic conductivities (*Kmin* and *K max*), the differences are insignificant.

Jacob and Lohman (1952) formulation demands the knowledge of the storage compressibility coefficient Ss, rarely known. In Tacher et al. (2005) and NCG+EPFL (2004), the interpretation of the pumping tests suggests that ,except at the top of the aquifer, the heterogeneities are captive and therefore a storage compressibility coefficient Ss of 1E-4 (m-1) may be adopted. This value expresses a fast response of the pressure field to temporal variations of the boundary conditions, which is plausible according to the hydraulic behaviour of the system.

						Goodman estimations		Jacob Lohman estimations		
LFH1	**length in [m]**	**INFLOW in [l/min]**	**INFLOW in [m3/s]**	**dH min [m]**	**dH max [m]**	**K min [m/s]**	**K max [m/s]**	**T [m2/s]**	**K [m/s]**	**Ss [1/s]**
Measured values	42.0	0.3	5.00E-06	7.12	8.9	3.36E-05	4.35E-05			
radius:	48.9	0.5	8.33E-06	7.2	9	5.67E-05	7.35E-05			
0.0381	51.2	1	1.67E-05	7.2	9	1.13E-04	1.47E-04			
	57.0	60	1.00E-03	8	10	7.69E-03	9.97E-03			
	79.5	200	3.33E-03	12.8	16	4.42E-02	5.72E-02			
				estimated mean dH in [m]		**K mean [m/s]**				
Total during perforation	100.0	261.8	4.36E-03	7.2		2.97E-02				
Total after perforation	100	6.8	1.13E-04	7.2		**7.71E-04**		2.69E-05	1.79E-06	0.0001
						Goodman estimations		***Jacob Lohman estimations***		
LFH2	**length in [m]**	**INFLOW in [l/s]**	**INFLOW in [m3/s]**	**dH min [m]**	**dH max [m]**	**K min [m/s]**	**K max [m/s]**	**T [m2/s]**	**K [m/s]**	**Ss [1/s]**
Measured values	44.0	5	8.33E-05	4	5	2.84E-04	3.69E-04			
radius:	50.0	9	1.50E-04	8	10	1.15E-03	1.50E-03			
0.0381	55.0	5	8.33E-05	9.6	12	7.92E-04	1.03E-03			
	60.0	5	8.33E-05	10.4	13	8.69E-04	1.13E-03			
	66.0	18	3.00E-04	13.6	17	4.27E-03	5.51E-03			
	70.0	5	8.33E-05	16	20	1.43E-03	1.85E-03			
	84.0	48	8.00E-04	20	25	1.77E-02	2.29E-02			
	95.0	5	8.33E-05	26.4	33	2.53E-03	3.26E-03			
	100.0	5	8.33E-05	26.4	33	2.53E-03	3.26E-03			
	105.0	5	8.33E-05	28	35	2.71E-03	3.49E-03			
	117.0	15	2.50E-04	29.6	37	8.65E-03	1.11E-02			
	136.0	40	6.67E-04	37.6	47	3.03E-02	3.90E-02			
				estimated mean dH in [m]		**K mean [m/s]**				
Total during perforation	164.0	165	2.75E-03	19.13		5.79E-02				
Total after perforation	164	7.1	1.18E-04	19.13		**2.49E-03**		2.83E-05	1.49E-06	0.0001

Table 4.23: Hydraulic conductivities calculated after Goodman and Jacob and Lohman for drains LFH1 and LFH2.

The estimated hydraulic conductivities are presented in table 4.23. Globally, considering the two galleries, hydraulic conductivities calculated thanks to the Goodman formulation of the measured inflows during perforation are varying from 1.11E-2 [m/s], for the most permeable structures, to 3.36E-5 [m/s]. The global hydraulic conductivity for the massif calculated after perforation, considering a global flow rate of 6.8 l/min for LFH1 and 7.1 l/min for LFH2 are respectively of 7.71E-4 m/s and 2.49E-3 m/s. The global hydraulic conductivity for the massif calculated after Jacob and Lohman is around 1.5E-6 m/s for both galleries. This value represents an average value and defines a global permeability in accordance with those estimated in section 4.3.7.

4.3.8.8 ***Hydrodynamical implications***

- At a regional scale the interpretation of piezometric maps is very tricky or even impossible.
- Water levels vary strongly from points to points
- The landslide is constituted vertically by a succession of aquifers, each water level represents a local isolated perched aquicludes
- Strong underpressure (90 T/m^2) zones are recorded
- The measured artesian discharges during perforation, up to 20 times superiors than the residual flows, may be explained by the probable presence of captive aquifers in the sliding mass, behaving as isolated water pockets which are emptied brutally during the perforation
- The global hydrodynamic may be characterized by a system with a low available recharge in relation to the existence of local high permeable zones
- The global hydrodynamic is presenting similitude with the tectonized zone of the Mont-Blanc system (crystalline aquifers), permeable structures with local importance and a poor alimentation
- *Qi/Qf* ratio representative of large isolated water reservoir (spatially disconnected as shown by the depletion curve), formed by high permeable zones
- A storage compressibility coefficient Ss of 1E-4 (m-1) may be adopted, expressing a fast response of the pressure field to temporal variations of the boundary conditions

- The estimated hydraulic conductivities with Goodman formulation are between 1.11E-2 and 3.36E-5 (m/s), and consider the permeable conductive fraction at a **LOCAL scale**
- The estimated hydraulic conductivities with Jacob and Lohman are around 1.5E-6 m/s, and may rather express the capacitive function of the reservoir at a **REGIONAL scale**

Therefore, **globally** results of section 4.3.7 and 4.3.8 indicate that the flysch terrains of the unstable mass is generally characterized by a low hydraulic conductivity around 1E-6 to 1E-5 m/s with locally gravely levels showing higher values around 1E-3 to 1E-2 m/s, while the flysch corresponding to the underlying stabilized mass present lower values varying between 1E-7 and 1E-6 m/s. These results based on very local measures allow giving a global definition of the hydrogeological conditions of the slide, but the calculated values still have a very local meaning. These chapters call for two main questions:

1. How does the hydraulic conductivity K vary with scale?

This question means how to transpose local hydraulic conductivities in a global scale. Generally speaking, by equivalent permeability we mean a constant permeability tensor taken to represent the heterogeneity. A complete equivalence between the real heterogeneous medium and the fictive homogeneous one is impossible. Therefore the before-discussed values of hydraulic conductivity at the scale of the slide (i.e. 1E-6 to 1E-5 m/s) may either underestimate or overestimate the hydrodynamic conditions locally. Due to the complex geological processes involved in the instability, aquifer properties of la Frasse, and in particular hydraulic conductivity (K), exhibit a large degree of heterogeneity, which governs the flows. The lack of K data hampers the complete determination of the K field and introduces local strong uncertainties. This study has shown that in such medium the calculated hydraulic conductivity is only valuable at a specific location (place of measure).
According to the number of values, several methods may be applied to characterize the hydraulic conductivity fields, namely; (1) the determinist approach, (2) the zoned heterogeneity and (3) the geostatistical approach. The homogeneous zones method is the only way to model distributed systems within a deterministic framework. Applying the zonation method, the model area is divided into a number of zones; each is characterized by a constant value of permeability. Here the structure (the number and the shape) of the zones is defined according to the available information from aquifer pumping tests, hydraulic gradient and geologic mapping. The zonation method is considered superior to other approaches in case of limited and poor quality data.
It has long been known that strictly deterministic description of the environment does not seem feasible. It has been argued that, in reality, information about the hydrogeologic environment is incomplete and subject to measurement as well as interpretative error. Geostatistical methods are developed mainly to account for or quantify spatial uncertainty. In this work (see chapter 5), geostatistics is conducted to generate on the basis of these measured data stochastic fields that may represent a plausible image of reality.
In the meantime, one may recognize that due to the high degree of heterogeneity identified in the la Frasse case, methods allowing to define with certitude the distribution of these parameters are since yet not existing. Thus, the problem may be approached thanks to one of the three before-mentioned methods.

2. The role of spatial connectivity?

The observations have shown that inside this mass, complex flowpaths may connect distinct zones. These zones may consist in isolated aquifers or spatially well developed flow systems. These spatial connections

represent thus preferential flowpaths taking place either in more permeable zones (sand, gravel levels) of the heterogeneous medium or in structural discontinuities. In the first case, the fluid flow seeks the less resistive pathways and therefore the flow through a heterogeneous medium takes place in channels. These channels are not physical entities, contrary to structural discontinuities, meaning that if the direction of the hydraulic gradient is changed the locations of the channels are also changed (Tsang and Tsang, 1989). The emergence of channeling as a function of the degree of the heterogeneity will be shown is chapter 5. The hydraulic responses to the several well tests confirm that intense channeling is occurring in the la Frasse system. In the meantime, it is quite difficult to identify the cause of this channeling (heterogeneity or discontinuity), however, both may play a role in the distribution of the flows in the system. If this phenomenon is linked to the geological context, it may thus be a general behaviour for aquifers in landslide taking place in these particular environments (Quaternary or flysch deposits).

4.3.9 HYDROGEOLOGICAL BOUNDARY CONDITIONS

4.3.9.1 ***Hydraulic conditions of the underlying units***

In 1984 a tracing test with uranine (10 kg) was effectuated in the le *Gouffre du Chevrier*, which entry is situated at 1700 m s.m. in the *Combe de Brion* (Lutz et al. 1987). It is an important karstified network descending in the direction of the "*cirque des Rouvènes"* (see figure 4.40*)*. The bottom of this network is situated at 1200 m s.mm, 260 meters below the surface behind the "*Couches Rouges"* cliffs, situated at the front of the landslide. During four months, twenty four sources were controlled. The results indicated that the quasi-totality of the injected uranine went out at the "*Fontaney"* source near "*Aigle"* after a rapid circulation of 30 to 40 hours through the karstic network. Concerning the other sources, a slight signal was identified between two and four weeks after injection, notably for those situated nearby the sliding area. In the meantime, the classical simple analysis by spectrometry of fluorescence method used at that time could not establish with certitude the presence of uranine. Besides, the results show that the uranine was absent in the entire analysed sources concerning the la Frasse sliding mass, and equally at well FR3. A slight low signal was present inside the FR1 at -54 meters inside the stable flysch unit. The relation between the Jurassic karst and the slide are thus very limited; even if the le "*Gouffre du Chevrier"* is not representative of the entire karst. It has to be recognized that the waters are naturally and rapidly flowing in the direction of the *Rhône* valley following the structures of the "*Leysin synclinal"*. Therefore these waters may not present high hydraulic pressures conditions, and thus are not infiltrating the impermeable "*marnes rouges éocènes"* to reach the sliding mass. Therefore, the water from the karsts of *"Aï"*, have no or very low and local relations with the top of the la Frasse landslide. The absence of very captive water inside the underlying units is confirming in a part these observations. One can think that the *"Couches Rouges"* play the role of a first impermeable barrier between the karstic limestones of the Malm and the Flysch itself very impermeable transversally of the bedding. In the meantime an existing slight sufficient fissural permeability with an increase of hydraulic heads can explicate the existence of uranine at the lower half-part of the slide (FR1). Even now, the development and the structure of this karstic network enabling this connection through this impermeable unit, 2.5 km wide, are totally unknown.

As already discussed, the hydraulic conditions of the underlying units remain unknown. Neither the presence of under-pressure conditions inside this one have been established nor the existence of fissural high permeable conditions. However, the existence of hydrogeological conditions less unfavourable in the underlying bedrock than in the sliding mass seems to be established by the fact that the deepest sliding surface is always located inside the ancient sliding mass and not at the contact with the underlying bedrock.

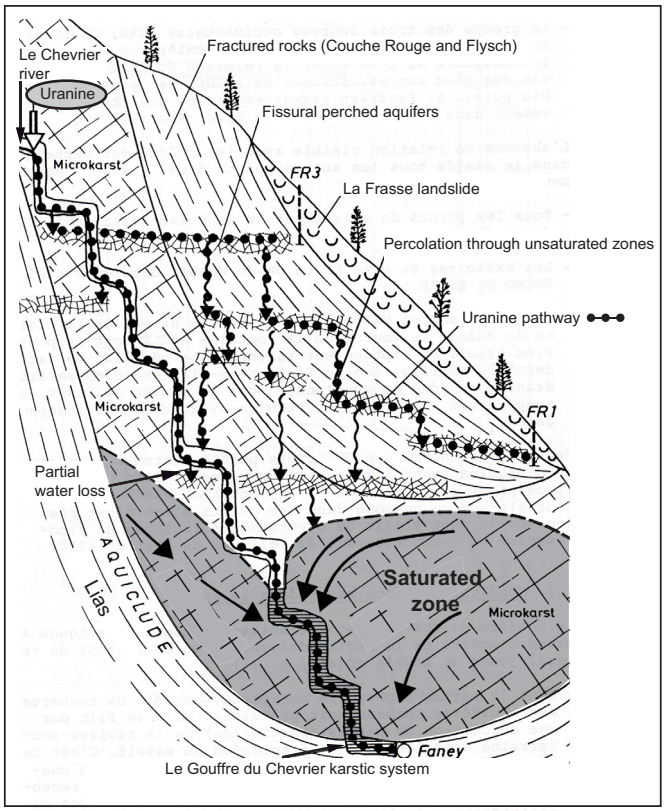

Figure 4.40: Scheme of the tracing test of the « Gouffre du Chevrier »; possible flowpaths. Modified from Lutz et al. 1987.

4.3.9.2 ***Recharge estimation***

The correlation of rough precipitations with the movements of the slide is bad in the la Frasse landslide (figure 4.41), so that the calculation of the effective infiltration as a fraction of the precipitations (Primault, Turk or Coutagne formulas) ultimately does not permit the simulation of the crises at the right time. It is thus necessary to use a more complete model of infiltration, namely a coupled 1-D model of the hydrological and thermal processes in the system ground-plant-atmosphere (COUP model, Jansson, 2003). This tool allows to estimate the evolution in time of the various variables of the moisture balance (effective infiltration, real evapotranspiration and runoff) by taking into consideration, in particular, the saturation of the ground, the removed water by the roots and the occasional snow cover formation. Calculations were effectuated by the Technical Office Norbert SA (in NCG+EPFL (2004)), by introducing the following data:

- The daily climatological data at the station *"Le Sépey"* from 1977 to 1995 (i.e. Precipitation, average temperature, average relative humidity, average wind speed and average snow cover).
- The intrinsic soil characteristics; i.e. 2 meters of sandy-clayey lime with an average hydraulic conductivity of 7E-7 m/s).
- The characteristics of the plants; i.e. vegetation of type grassland, with a maximum depth of 1 meter for the roots.

Note that the accurate calibration of the infiltration is slightly reduced because of the lake of measurements of the evolution in time of the moisture conditions. However, the heights of the snow cover calculated and measured from 1977 to 1995 present a good coherence (figure 4.42)

Effective infiltration thus calculated corresponds to approximately 40% of the annual precipitations and underlines satisfactorily the natural phenomena (figure 4.43) namely: effective infiltration peaks dependent

on the snow melting or to rainy events lasting several days. The isolated rain events (1 to 2 days) following a dry period do not take part or very little in the recharge of underground waters (evacuated by runoff).

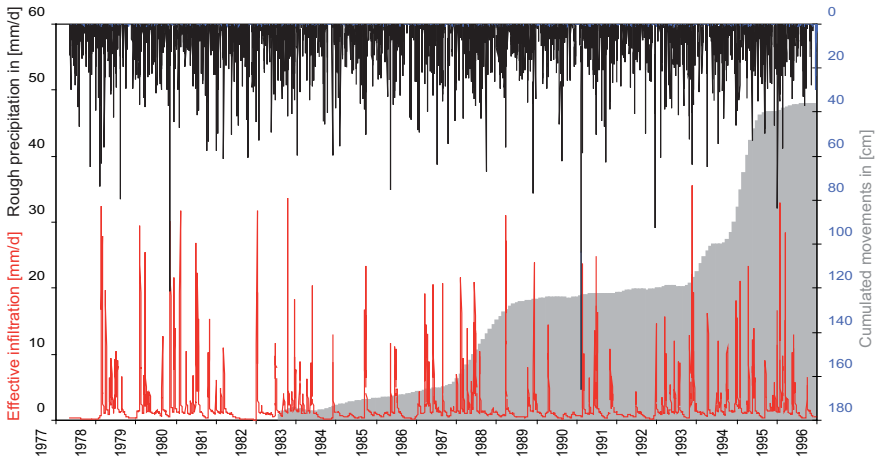

Figure 4.41: Rough precipitation, cumulated movements and effective infiltration calculated thanks to the COUP model (Jansson 2003).

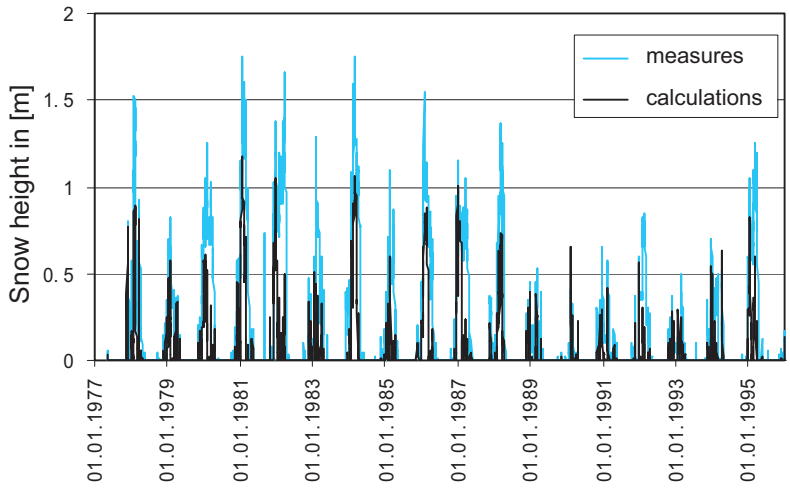

Figure 4.42: Comparisons between simulation of the snow cover and the observations.

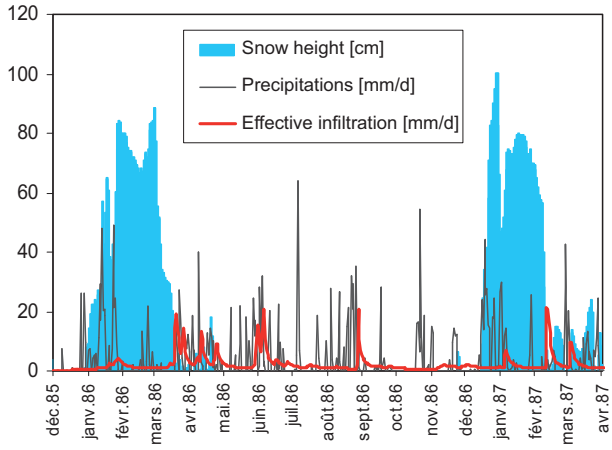

Figure 4.43: Daily calculated effective infiltration, observations of the daily precipitations and of the snow cover for the period end 1985 up to early 1987.

Because of its encased topography, the landslide receives also water infiltrating in the surrounding units thanks to lateral inflows. This component proves to be very important, and even dominant. Numerical simulations have shown manifest water balance deficits when this contribution was omitted (Tacher et al. 2005), for that matter, it is introduced into the conceptual model under flux flow boundary conditions entering by the lateral limits. To evaluate the intensity of the inflows, the following factors are taken into account:

- The area and geology of the catchment area alimenting the relevant section of the lateral boundary
- The transit of this water in the surrounding units before arriving into the slide. Consequently the intensity of the infiltration peaks has to be plugged

The total catchment area of the slide is difficult to estimate because of the karst which covers a considerable part of the topographic catchment area. Moreover, following the tracing test carried out at the "*Gouffre du Chevrier"* (see §4.3.9.1), this karstic surface is not actively taking part in the alimentation of the slide. Therefore, the total hydrogeological basin is approximately of 2.1 km^2, sliding surfaces not included. The flysch located near the sliding surface being more permeable, the temporal fluctuations of the alimentation are there stronger. Thus, the entering flow is constant in time for the entire domain except concerning the sliding surface. For this last, its calculation is carried out as follows:

- A data set of moving average is applied to the daily effective infiltration to represent the buffer effect of the water transit through the surrounding units before entering the slide.
- A multiplicative factor is applied to the result to hold account of the surface and geology of the catchment area alimenting the considered section of lateral boarder.

The weighting method used to balance the effective infiltration is exposed in the following figure (figure 4.44).

4.3.9.3 Relations between lateral inflows and slide movements

The study DUTI (1986) showed the poor relation between the estimated effective infiltration and the landslide velocities and movements, idem for rough precipitations (See figure 4.45). NCG+EPFL (2004) proposes a relation between the flow entering by the lateral boundaries and its velocity, relation permitting to validate the estimated inflows for the lateral boundaries.
Figure 4.46 shows the cumulated movements in the zone "++" (grey surface area) and two series of two curves, which correspond to the cumulated normed flow entering the boarder (dotted grey line) and the cumulated effective infiltration (solid grey line). The two lower curves are obtained by removing before cumulation, the values lower than 2 mm/day; namely to erase the background noise of the small events. The plot shows that the cumulated displacements fit well with the normed flux truncated at 2 mm/day. Thus, the slide is mainly controlled by the strong infiltration events rather than by the weak ones. The quality of this adjustment is good between July 1982 and January 1994. Between January and December 1994, the separation of the curves indicates a probable nonlinear behaviour of the movements according to the entering inflows. From December 1994, due to the commissioning of the borehole platform, the adjustment is not any more required. In addition, the observations show that for the crisis of 1981 (not represented on the plot) this correlation is not valuable, concluding that it works for the crises of low and medium intensity

Weighting method for the effective infiltration
Evaluation of the lateral boundaries alimentation

The surrounding rocks have two functions:

1) A capacitive function (slow discharge) --- climatic conditions from the pas years
2) A transmissive function (fast through fracture network) --- climatic conditions from the previous days

For each days the balanced sum of the effective infiltration is calculated until J - 2 years, thanks to two normal distributions of standard deviation equal to one year and three days:

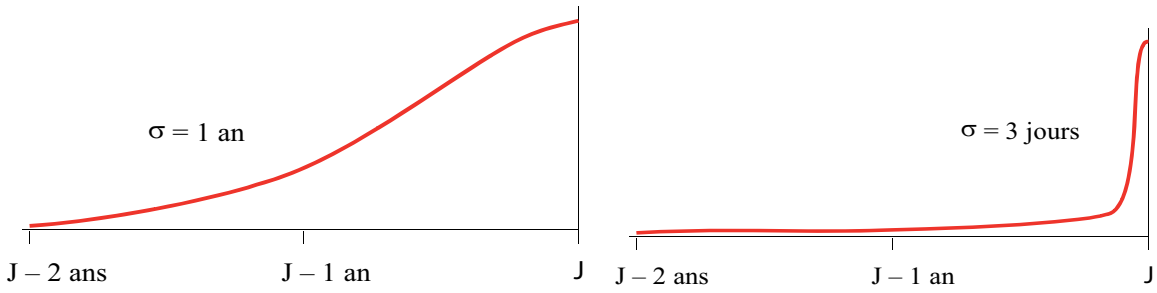

Then the results are summed :
1/3 fast alimentation + 2/3 slow alimentation

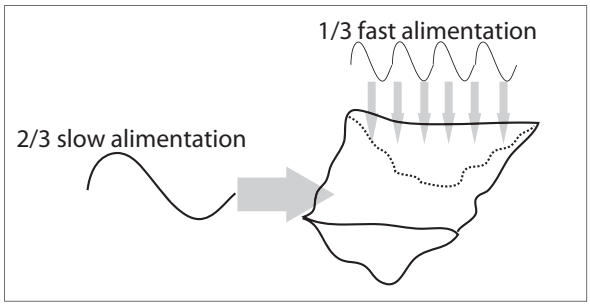

Correlation between movements and balanced effective infiltration and truncated

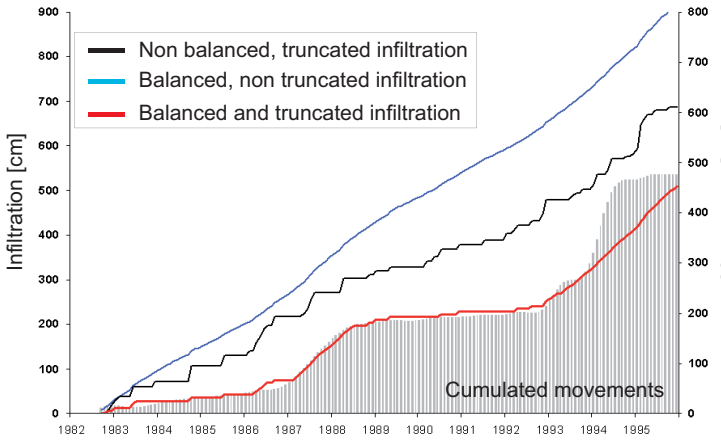

All infiltration inferior to 1.9 mm/day are suppressed

Weighting parameters:

- 15% of the weight for the latest infiltrations (σ = 10 days)

- 85% of the weight for the previous infiltrations (σ = 450 days)

Figure 4.44: Weighting method for the effective infiltration. Evaluation of the lateral boundaries alimentation. See text for explanations.

(e.g. 1987). The crises of 1966, 1981 and to a lesser extent 1994 integrate other factors (erosion, rupture ...). The adjustment being better with the flow entering from the lateral limits than with the effective infiltration, underlines the need for considering, in the conceptual model, the pluviometric events of the past, which is coherent with the hydrogeological functioning of these structured masses.

Appendices VI-8 and 9 present in details the distribution of the estimated infiltrations along the lateral limits, as well as the values considered for the zone nearby the sliding surface. Due to particular geological and hydrogeological behaviours, these values are varying in time. The weighting method is exposed in figure 4.44. The estimation is based on the hydrological conditions of the period August 1993 to December 1995, which represent an important crisis.

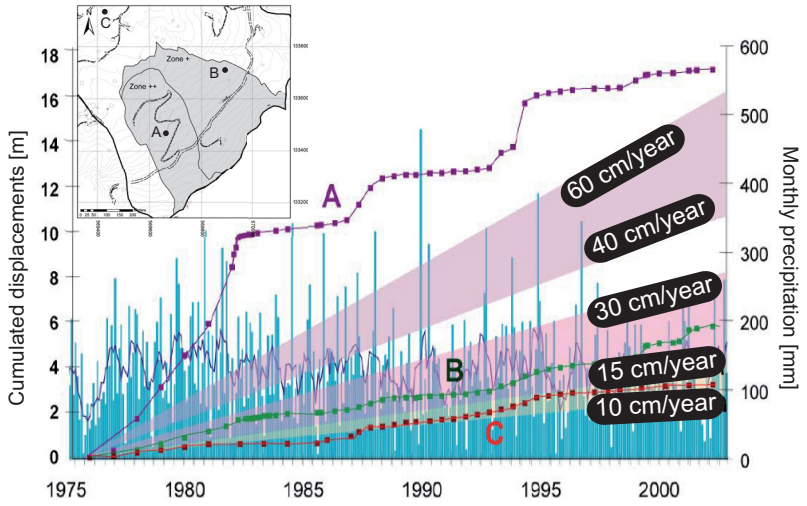

Figure 4.45: The poor relation between the estimated effective infiltration and the landslide velocities and movements, idem for rough precipitations after DUTI 1986.

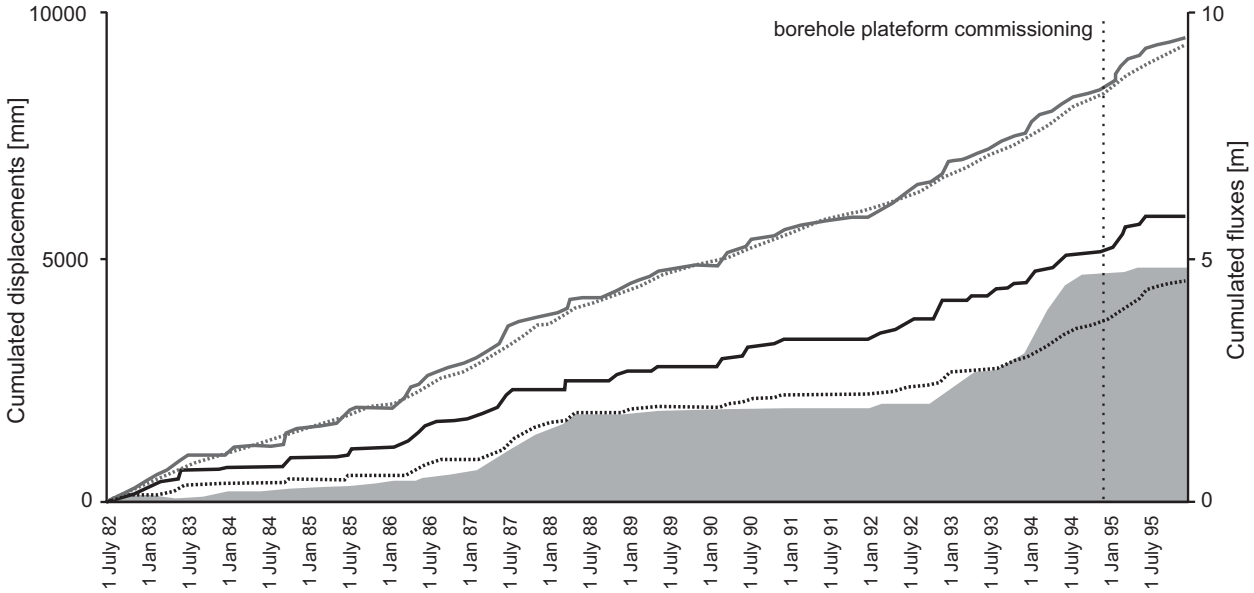

Figure 4.46: Cumulated movements in the zone "++" (grey surface area) and two series of two curves, corresponding to the cumulated normed flow entering the boarder (dotted grey line) and the cumulated effective infiltration (solid grey line).

4.3.9.4 ***Hydrodynamical implications***

- The existence of hydrogeological conditions less unfavourable in the underlying bedrock than in the sliding mass seems to be established
- The slide is mainly controlled by the strong infiltration events rather than by the weak ones
- Effective infiltration calculated may only correspond to 40% of the annual precipitations
- The adjustment is better with the flow entering from the lateral limits than with the effective infiltration
- The pluviometric events of the past, have to be considered in the conceptual model

4.3.10 DISPLACEMENT RATES DISTRIBUTION HETEROGENEITY

The numerous observations made on the deformations of the cantonal road RC705 indicate that the velocities of the landslide mass are not uniform, neither in time nor spatially. The characterisation of the displacements distribution into the landslide, horizontally as well as vertically, allows drawing important conclusions about the structural properties of the mass at the scale of the landslide (regional). Indeed the several activation episodes generated the partitioning of the whole mass in individual structural compartments. Finally, hydrodynamical considerations may be formulated since the contacts between these zones are the seat of important flow transfers.
This chapter is the results of the compilation of various documents; aerial photography, photogrammetry, geodesic measurements, comparison between cadastral measurements, as well as analysis done within the framework of the DUTI project (1986).

4.3.10.1 ***Vertical displacement distribution***

The continuous measurements and observations effectuated since decades of the numerous inclinometers allow detecting the principal and the secondary sliding surfaces in all investigated drills. This information permits the establishment of an instability map and of several movement sections of the different zones of the unstable mass (figure 4.47 and 4.48). These measurements allow in certain cases to locate sliding surface levels that are not directly detected by borehole core analyses. The various sliding surfaces are either localized at lithological contacts (flysch/limestone) or within the formation (flysch/flysch).

For instance in wells FR1 and FR2 the main movements are located at respectively 43 meters and between 56 and 59 meters, it is to say within the unstable mass. In these cases they do not correspond to the contact with the bedrock. The annual average velocity obtained for instance in spring 1982 reached 26 and 13 cm/year respectively. Secondary movements are also detected in the well FR2 between 31 and 33 meters where a displacement of 1 cm was recorded in 20 months between 1982 and 1984, reaching afterwards more than 5 cm. Whereas, in the upper part of the slide (*"Grand glissement supérieur"*), no significant movements were observed in FR3. The inclinometer in well FR4, installed in the first 30 meters of the borehole, detected a sliding surface at low depth between 8 and 9 meters where a displacement of 2 cm in 8 months was observed.
The inclinometers installed in spring 1985 in FR5 and FR6 revealed tidy movements around 2 cm in 7 months in the FR5 between 20 and 24 meters. Whereas in FR6, three shearing surfaces were detected, between 17 and 18 meters, 40 and 41 meters and between 49.5 and 51 meters, giving a total displacement of 4 cm in five months.

The examination of these deformations shows that the movements are taking place on very definite levels and limited ground slices. For instance, 1 meter maximum within the well FR1 between 42.7 to 43.9 meters and approximately 0.5, 2.0 and 2.5 meters within the well FR2 (59.1 to 59.7 meters, 55.5 to 57.3 meters and 30.5 to 32.9 meters), and 2 meters within the well FR4 (7.3 to 9.1 meters). No significant displacements are observed within these shear levels, corresponding to a general creep the instable mass. Moreover it is confirmed that the most active sliding levels are the deepest.

4.3.10.2 ***Horizontal displacement distribution***

The instability map in figure 4.47 gives a general overview of the superficial average velocity distribution. It shows that the slide is characterized of mainly 6 zones of velocities rather oriented parallel to the sliding direction and traducing an appreciable great heterogeneity. Globally, three main zones are identifiable; the zone "++", the zone "+" and the main body ("*Grand glissement supérieur");* velocities from 7 to 8 cm/year for the zone "++", 5 to 6 cm/year for the zone "+" and 2 to 6.4 cm/year for the "*Grand glissement supérieur).* Note that, since 2003 an inversion of the velocity ratios compared to the initial situation between the zones "+" and "++" is mainly observed, certainly due to the effects of the borehole platform. On the long range one notes that since 1996 a progressive acceleration of the zone "+", whereas in the zone "++" the velocities remain constant. The situation in 2007 even got worse with an important acceleration of the zone "+" (see § 4.3.2.10). Concerning the upper part of the slide, the average velocities are still lower than those of the lower zone. In the meantime, as shown in figure 4.47, the landslide is divided in several independent entities, and given that the acceleration/deceleration phases are not simultaneous, these entities are evolving separately.

Zone "++", initially very fast, this zone is since 1999 characterized by very low movements, less than 10 mm/year, with some short acceleration peaks (2000 and 2001: 30-40 mm/year, 2002: 30 mm/year, 2003: 32 to 48 mm/year with a peak recorded in April 2003: 100 mm/year). This zone is calm compared to 1999 (100 mm/year) and beginning of 1994 (300 mm/year).

Zone of Cergnat (*"Grand glissement supérieur"),* approximately 7 mm/year were recorded in 2001 in inclinometer I201. In 2002, the movements were relatively weak, and reached 13 mm at 5 meters of depth and 8 mm at 63 meters of depth. In 2003, the movements were relatively weak, and reached 21 mm at 5 meters of depth and 12 mm at 63 meters of depth. A slight acceleration is thus actually recorded in this zone.

Zone "+" inclinometer I301 located a main sliding surface at 38.5 meters deep and a second at 5 meters. In 2003, movements of 9 mm (5 meters deep) and 5 mm (38 meters deep) were measured in 10 months. On the other hand, topographic measurements made on the field situated on the right of I301 recorded surface displacements around 54 mm, concluding that it exists, locally, faster movements on the surface.

Also, the analyses of the numerous displacements data indicate that it can exist big differences from a year to another, notably depending on meteorological conditions and seasonal snow melt ratio. For instance movements in 2003 are higher of 15% to 60% than those observed in 2002 (i.e. zone"++": 15%, zone"+": 60% and upper part: 50%).

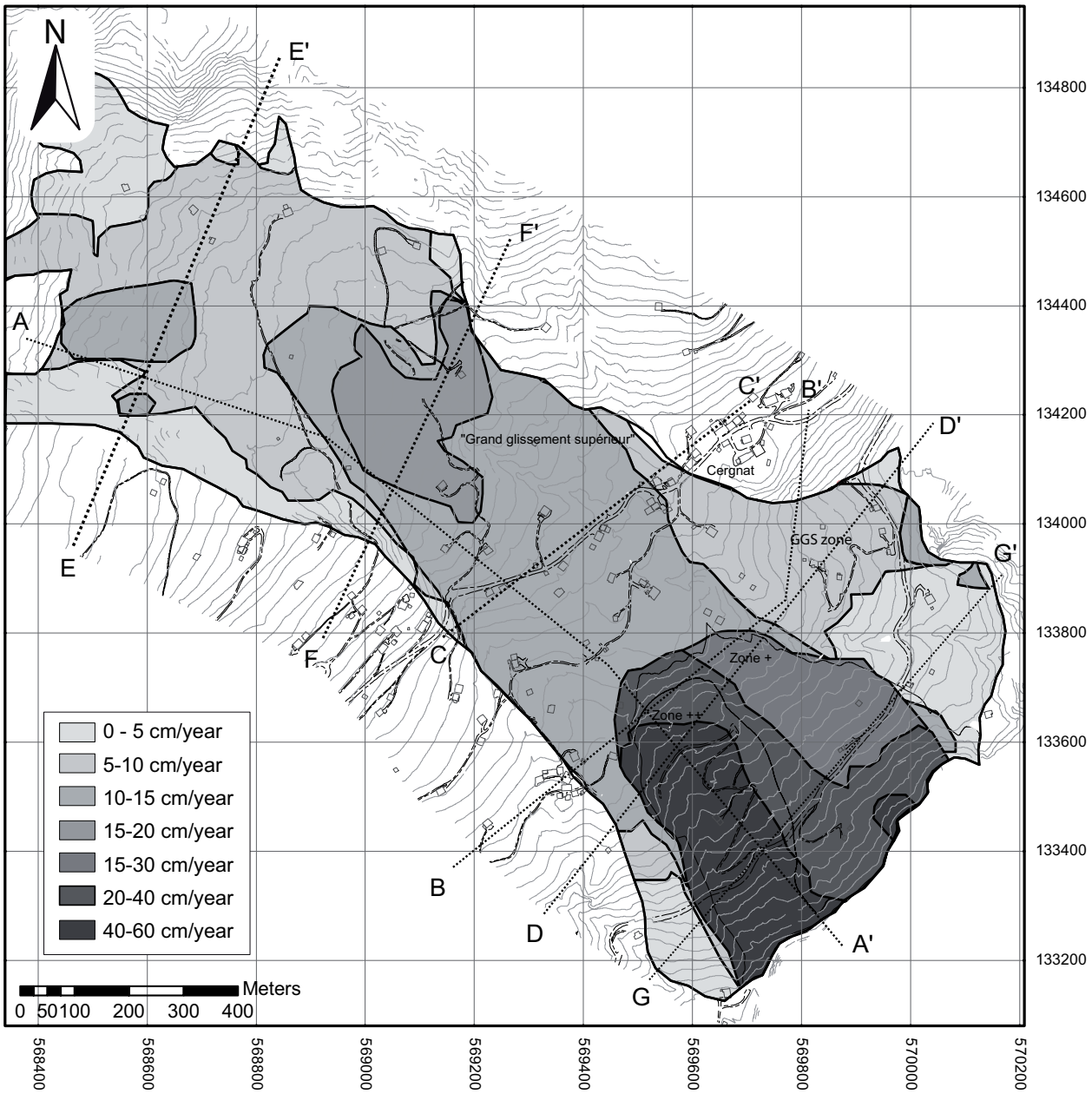

Figure 4.47: Map of the recorded movements showing different zones. See vertical sections figure 4.48.

Figure 4.48: Vertical sections of the movement (see figure location 4.47).

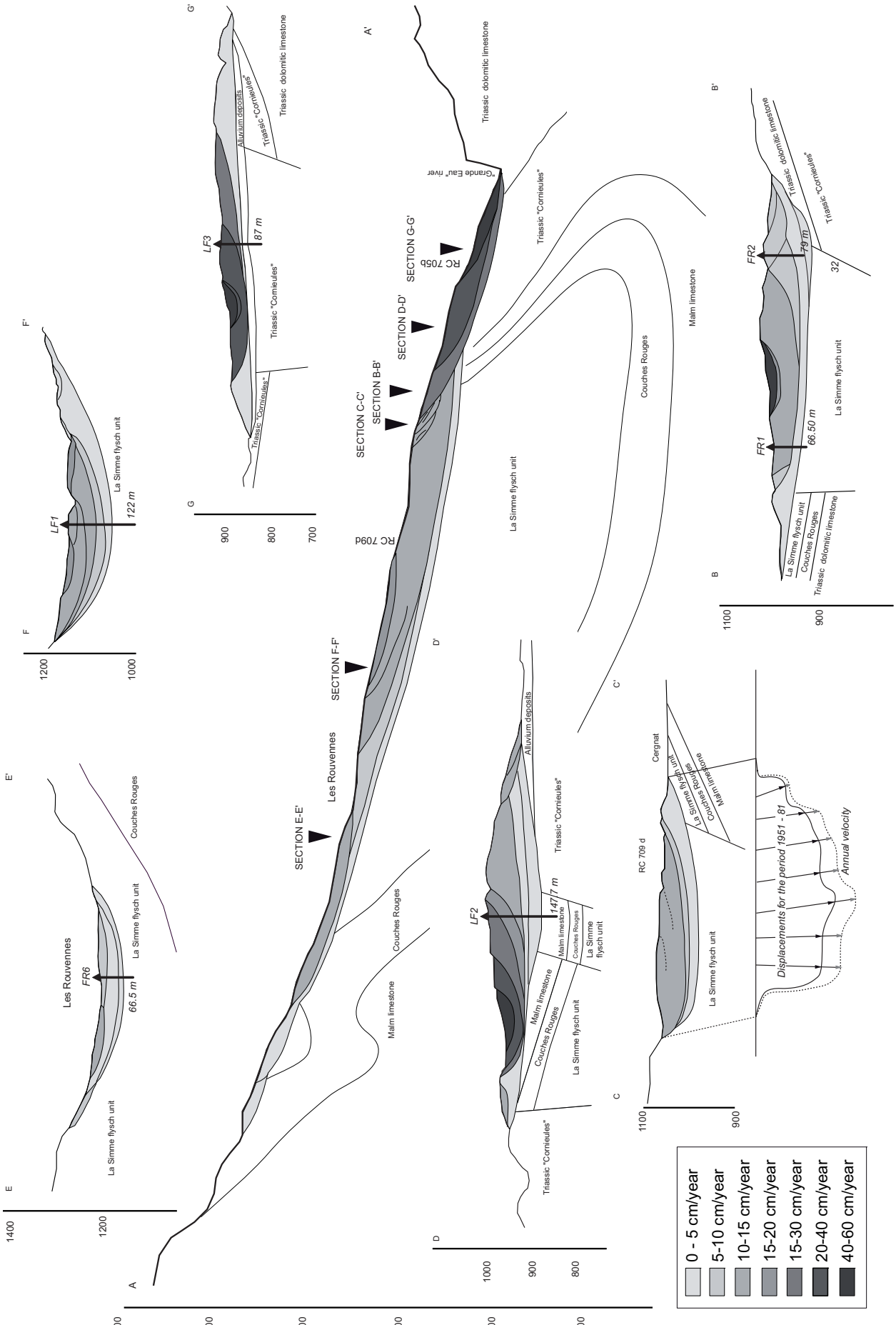
A
A'
B
B'
C
C'
D
D'
E
E'
F
F'
G
G'
SECTION E-E'
SECTION F-F'
SECTION C-C'
SECTION B-B'
SECTION D-D'
SECTION G-G'
Les Rouvennes
"Grande Eau" river
RC 709b
RC 709d
LF1
122 m
LF2
147 m
LF3
87 m
FR1
66.50 m
FR2
79 m
FR6
66.5 m
32
La Simme flysch unit
Couches Rouges
Malm limestone
Triassic "Cornieules"
Triassic dolomitic limestone
Alluvium deposits
Cergnat
Displacements for the period 1951 - 81
Annual velocity
0 - 5 cm/year
5-10 cm/year
10-15 cm/year
15-20 cm/year
15-30 cm/year
20-40 cm/year
40-60 cm/year

4.3.10.3 ***Hydrodynamical implications***

- Multitude of flowpaths.
- Fracture channelling occurs anywhere in these shearing planes.
- Complex 2D and 3D flow distribution.
- Formation of discontinuous hydrogeological system with perched aquifer more or less connected.

4.3.11 SYNTHESIS

4.3.11.1 ***Geological architecture***

The *la Frasse* deep-seated mass movements currently result in a large spectrum of different slope failures, depending on the type of movement and the nature of the mass. The horizontal and vertical displacement mapping as well as the various comparative studies enable a global view of the dynamics and the development of these failures. A principal sliding surface ranging from 20 to 80 meters and multiple secondary surfaces are randomly distributed within the mass.

Thus, **the global geological architecture** of the slide, observed in figures 4.47 and 4.48, indicates that the landslide is made up by several compartments, horizontally as well as vertically delimited, and rather independent regards to their displacements velocities. The horizontal organization may indicate that these zones are oriented in the direction of the sliding direction. Vertically, these compartments are superposed with an "onion-like" layered structure, with variable kinetic behaviours (displacements velocities, see figure 4.49). These blocks may be assimilated to prominent material rafts flowing independently. The thickness of these compartments may vary from some meters to 50 meters for the more important zones. The main factors influencing their development must be the local lithology (clay, gravel) varying from point to point due to heterogeneity and the faulting by the flysch-bloc separations (which enabled further weakening through deep weathering and water flow transfers), the geomorphic setting (slope) and heterogeneous infiltration zone distribution. In addition the geotechnical analyses correlated with the facies distribution indicate that the competent sandstone zones may constitute weak layers (susceptible to shearing) that may evolve in sliding surface. Besides the lithofacies analysis pointed out the random character of these features, while their vertical position inside the sliding mass seems to be totally arbitrary.

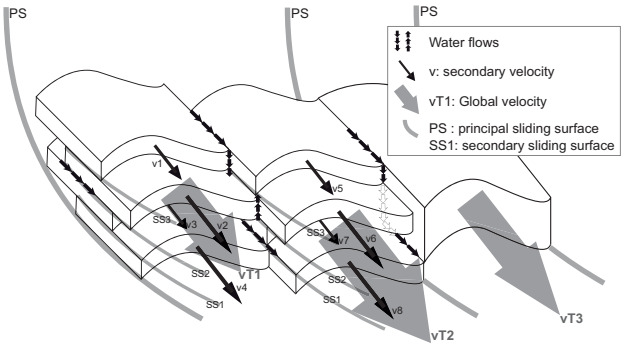

Figure 4.49: Block diagram illustrating the different superposed compartments with an "onion-like" layered structure, and presenting variable kinetic behaviours.

Considering **the geological material**, the strong impermeable dominance (clayey to silty facies) is demonstrated since representing 75% of the total. At the scale of the slide (regional), the radiomagnetotelluric surveys indicate that globally the mass is a non homogeneous impermeable mass, with a structured heterogeneity. The mean thickness of the bodies is 1.33 meters, though impermeable facies (clay and silt) with a mean value of 1.85 meters can locally reach 14 meters. Horizontal correlations even at the metric scale are impossible other than proceeding in facies simplification (i.e. permeable/impermeable). The lithological analysis units show a very complex and discontinuous structure, representing local "channelized" bodies or individual isolated lenses (see block diagram in figure 4.50). These observations fit with the presence of a global low permeability media in which small permeable lenses and channels can occur. Each bench is depending on the precedent (strong Markovian property of first degree). In the sliding mass, the asymmetric cyclic nature recorded in the boreholes of the active zone traduces a rearrangement of the facies successions, resulting directly from the continual reworking processes and sedimentological transformation occurring inside the mass.

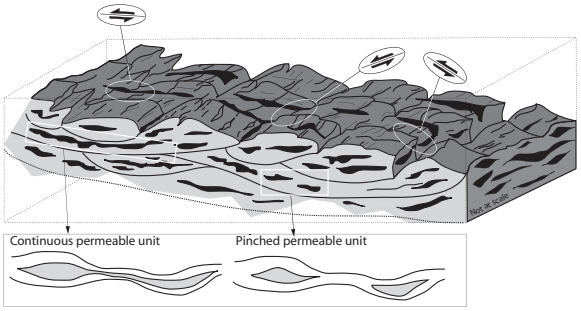

Figure 4.50: Block diagram illustrating the very complex and discontinuous structure of the la Frasse landslide, representing local "channelized" bodies or individual isolated lenses. The different superposed compartments are represented and permit to appreciate the general reworked and discontinuous character.

4.3.11.2 Hydrogeological functioning

Hydrogeological properties. The presented analyses permit to define at least two degrees of permeabilities as illustrated in figure 4.51:

1. *Primary permeability: Impermeable flysch mass (clay and silt)*

It is represented by the strong impermeable mass of clayey to silty facies (i.e. representing 75% of the total). This mass corresponds to the capacitive function of the system. The results indicate that the flysch terrains of the unstable mass is generally characterized by a low hydraulic conductivity (§ 4.3.7) around 1E-6 to 1E-5 m/s and the flysch corresponding to the underlying stabilized mass present lower values varying between 1E-7 and 1E-6 m/s.

2. *Secondary permeability :*

   a. *Permeable features (sand and gravel lithofacies)*

In a hydrodynamical point of view, these features, being very permeable, correspond to the conductive function and thus may be the seat of critical hydraulic pressures variation. They may act as a braking factor and in a sense probably control the activation of the movements. The permeability of the local gravely levels may be around 10-3 to 10-2 m/s.

b. Fracture channels (structural discontinuity)

Hydrological field evidences (i.e. performed hydraulic tests in §4.3.7 and 4.3.8) show that the flow inside the *la Frasse* system may be often concentrated to flowpaths in fractures and thus may favourite channeling phenomena. The complex recorded behaviour under the several well tests, may indicate that these flowpaths occur within the numerous shearing plane at the intersection of the several compartments resulting from the differential kinetic behaviour of the whole slide. The permeability of these fracture systems has not been defined, but may be around 1E-2 to 1E-1 m/s.

Finally, the underlying bedrock constituted of triassic Cornieules, is characterized by a hydraulic conductivity around 5E-5 m/s which confers a good absorption capacity (e.g. active zone "++").

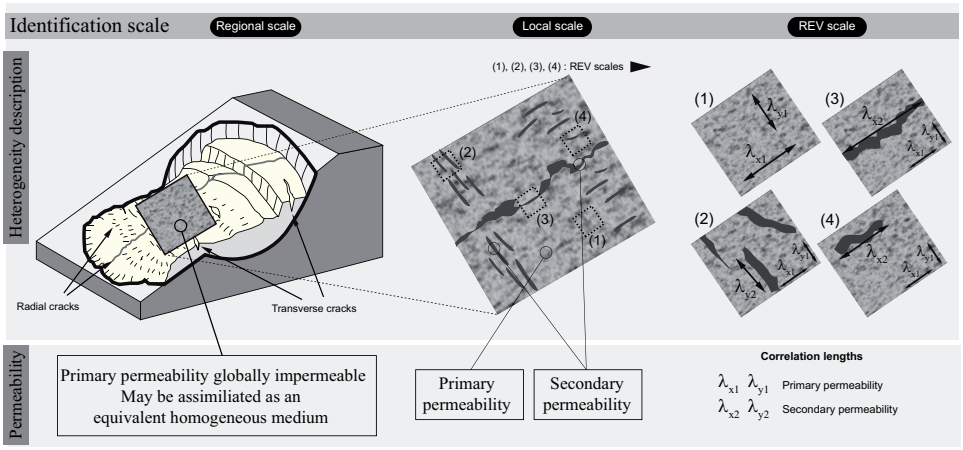

Figure 4.51: Diagram illustrating the degree of heterogeneity at different scales. Two families of permeability are represented. The system presents a bimodal permeability: Low hydraulic conductivities characterizing the global matrix (flysch mass) and defining the capacitive functions, and high permeable features (HPF), with high hydraulic conductivities. When these features are spatially connected, they are playing the role of the conductive function.

Aquifer behaviour heterogeneity. The observation of the water levels and inflows, presented in section 4.3.8, shows that the effects of drainage system being in office since 1994 are mostly significant in the two-third of the western part of the zone "++", while in the eastern part of the zone "++" a contrary effects is observed (i.e. Z119 indicating a lowering of -11 meters).

This contradiction claims for the existence of more developed spatial hydraulic connections, notably in a longitudinal direction, parallel to the sliding direction. One noticed that the wells Z114, Z115 Z118 and Z119 are concordant; when an increase is observed in wells Z114, Z115 and Z118 a decrease is recorded in Z119 and inversely. In figure 4.52A, a section linking the borehole platform to the south boundary of the landslide has been considered, namely the "La Grande Eau" river, and passing by the wells Z114, Z118 and Z119. A hypothetic piezometric line controlled by upper and lower boundary conditions has been drawn. This piezometric had initially *(wl init),* before the commissioning of the platform, a parabolic shape. The introduction of this platform has generated new hydraulic constrains modifying the initial piezometric level *(wl fin),* and especially in the confined features of the aquifer system. Therefore an important groundwater lowering may cause in the direct neighbourhood local groundwater increases. Similarly in the lower part of the landslide (at the level of RC 705) the strange reactions; between Z115 and Z119 (figure 4.52B) are evidences of important vertical flows, that may linked two confined aquifers (i.e. perched).

It results that the nature of the flows are extremely complex and must be locally assimilated as a complex inter-connected system of perched water tables. Besides, the situation is not stable in time and changes

constantly as shown in well Z115. From 1995 to 2000 the measured levels were comprised between 17 and 22 meters, then during 2 years from 13 to 17 meters, and in 2003 between 8 and 9 meters. In the meantime, the flow rate analysis at the borehole platform shows in the guideline, that the flowpaths are temporally more or less stable. The most efficient pumps are generally the same from year to year. Finally, the analysis indicates that the upper part of the slide shows important water circulations and over-pressures zones (LF1=90 T/m^2), while almost dry conditions may be found in the lower part of the active zone of the slide (LF2 and 3).

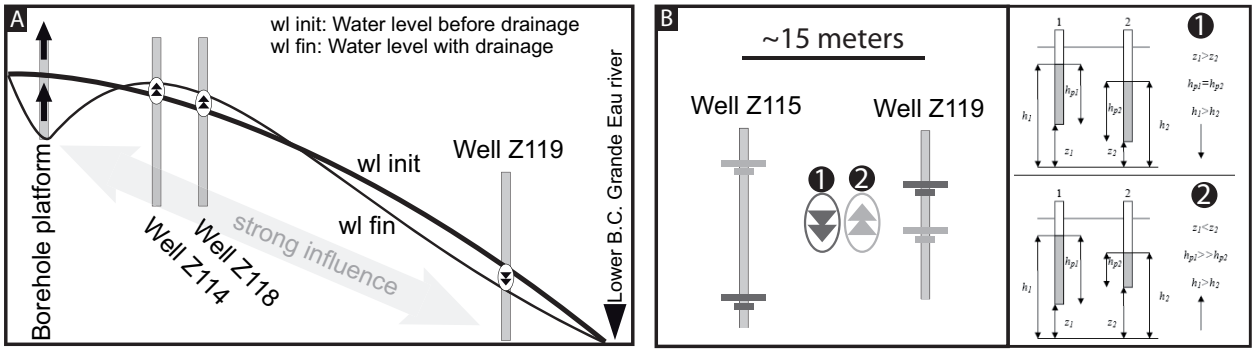

Figure 4.52: A) Illustration of the effects of the borehole platform in the lower part of the slide; positive and negative effects (water rise in wells Z118 and Z114). B) Opposite behaviour of two close wells; illustrating important vertical flows.

Hydrodynamical organisation and flow origin. Independently of the origin of the waters, the flows inside the la Frasse landslide are characterized by a bimodal hydrodynamic flow system (figure 4.53). The first one and predominant one (45% of the sampled wells, i.e. hydrochemistry), is defined by slow and locally deep flow through the impermeable shale matrix of the landslide mass (n°2 in the scheme C, n°6 in the scheme D). These conditions permit cation exchanges (i.e. Ca-Na cation exchange reactions) and in particular, the presence of blocs bearing gypsum may modify the chemistry of the waters (n°7 in the scheme D) by SO_4^{2-} dissolution. Locally, inflows from surrounding units can also change the chemistry (hydrochemical melanges, n°3 and n°4 in the scheme C) and enrich the water with sulphated waters. These waters are hydrochemically evolved and constitute the capacitive fraction of the slide. The second water system is characterized by poorly evolved waters. It is occurring in the permeable structures, more or less connected (n°5 in the scheme D) in which cation exchange is almost impossible. These permeable structures enable fast circulations, and their extension is only controlled by developed internal connections. These fast circulations may be locally shallow (n°1 in the scheme C) or very deep. In addition these circulations may drive surface water deep into the mass through subvertical connections, or inversely, and are in part alimented by rain infiltrations. These waters are hydrochemically poorly evolved and constitute the conductive fraction of the slide (see chapter 5, conceptual model).

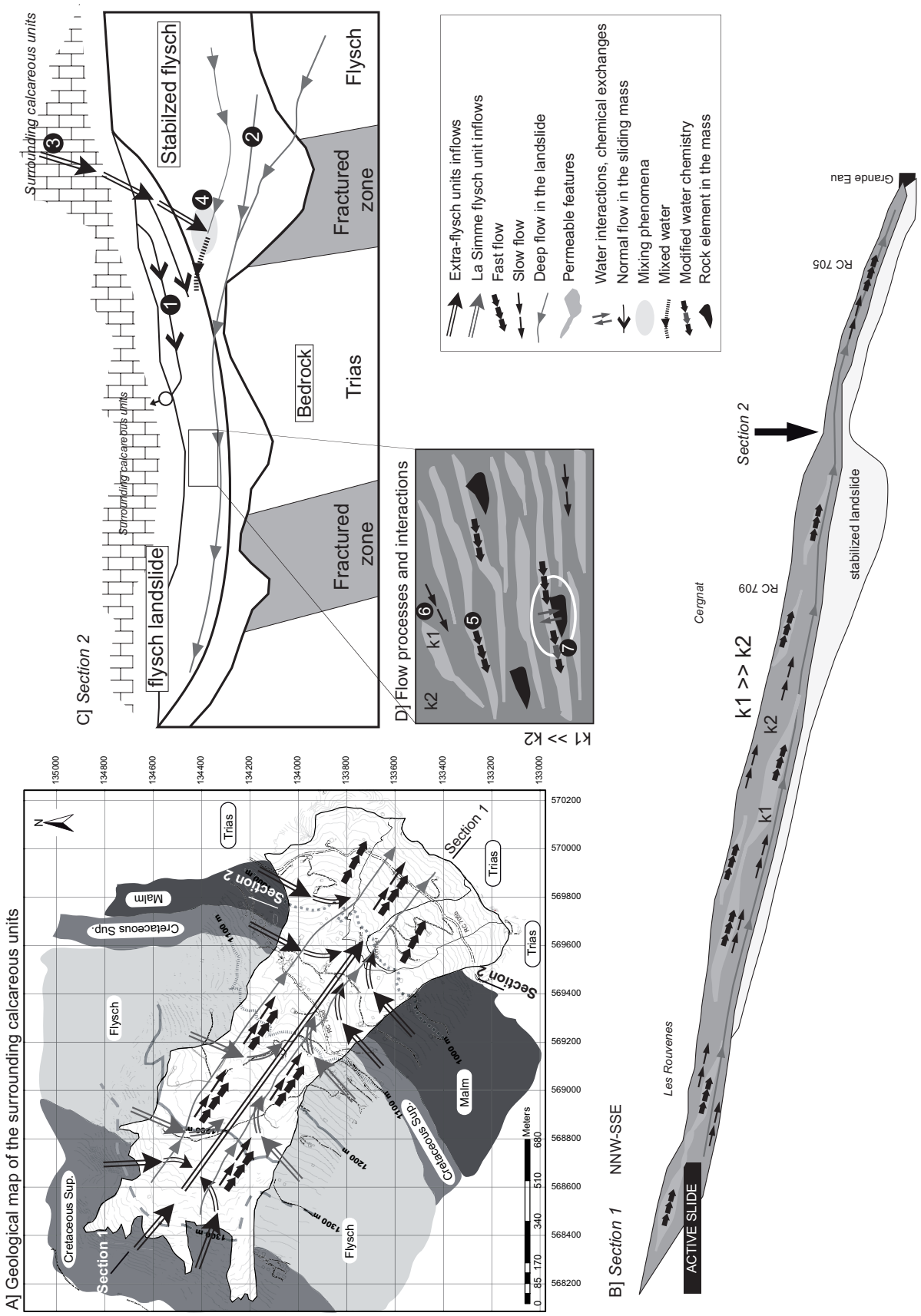

Figure 4.53: Conceptual model of the la Frasse landslide hydrodynamic system. A) Regional scale: global map representing the contribution of the several boundary conditions and the different water origin. B) and C) Longitudinal and transversal sections showing the different flowpath; Deep and surface flows. D) Illustration inside the mass; flows and cation exchanges.

The origin of the water has to be searched mainly in the surrounding units, since the results (i.e. ^{18}O isotope study) indicate that at least 60% of the sampled water are infiltrating outside the upper limits of la Frasse and laterally at lower altitudes. These results are in accordance with the infiltration estimation done in section 4.3.9.2 (Tacher et al. 2005). The scheme A in figure 4.53, show the plausible flowpaths in the system, both long and short distance travels are characterizing the connections between the different aquifers.

The system presents thus a bimodal permeability:

- *Low hydraulic conductivities characterizing the global matrix (flysch mass) and defining the* **capacitive fraction**.
- *High permeable features (HPF), with high hydraulic conductivities. When these features are spatially connected, they are playing the role of the* **conductive fraction**.

4.3.11.3 ***Hydrodynamical model***

The hydraulic conductivities estimated by the Goodman and the Jacob and Lohman formulations in section 4.3.8.6 are different of a factor 2. In that case; which formulation is the most adapted to estimate the hydraulic conductivities into a system such as the la Frasse landslide: Goodman or Jacob and Lohman? And what is the hydrodynamical meaning of this difference?
The estimated hydraulic conductivities after Goodman are rather high at the scale of the massif. Indeed they are principally influenced by the permeable fraction of the massif rather than from the impermeable matrix, hence showing the high permeable character that may locally prevail. On the contrary, the low values estimated after Jacob and Lohman are closer from the expected values at the regional scale. This can be explained by the fact that contrary to the Goodman formulation, Jacob and Lohman formulation is strongly influenced by the storage compressibility coefficient. As suggested in figure 4.54, initially, the system may rather be adjusted thanks to the Goodman solution, while finally after equilibrium, the inflow rate behaviour seems to follow a Jacob and Lohman adjustment. The Jacob and Lohman solution, on the contrary to Goodman, considers the effect of the decompression, which plays a major role in differing the depletion of the massif. In addition to that, this formulation supposes an aquifer with an infinite extensions, which might not been the case when draining out the water of isolated confined permeable features. The water quantities are provided by the transmissivity and by the effect of the hydraulic pressure decrease into the massif induced by the drilling of the drain, causing the relaxation of the massif and the water. During this phase a cone of depression around the work which radius increase with time may be observable, and at surface, will slightly influence the hydraulic head distribution.

The hydrodynamic system is thus characteristic of two phases (figure 4.54):

- **The depletion of the massif (Goodman solution) controlled by the permeable fraction**
- **The decompression of the massif (Jacob and Lohman solution) controlled by the massif itself (impermeable fraction)**

In figure 4.55 the hydrodynamical mechanism is presented. *At stage 1*, before perforation, the permeable fractions are saturated, and since the system is locally confined inside the impermeable mass, the hydraulic load is important. *At stage 2*, the perforation of these structures by the work liberates the confined waters, and due to the high permeability of the structures, the inflows inside the drain are at the first moments very high. In the meantime since this permeable zone is most of the time isolated, spatially limited and

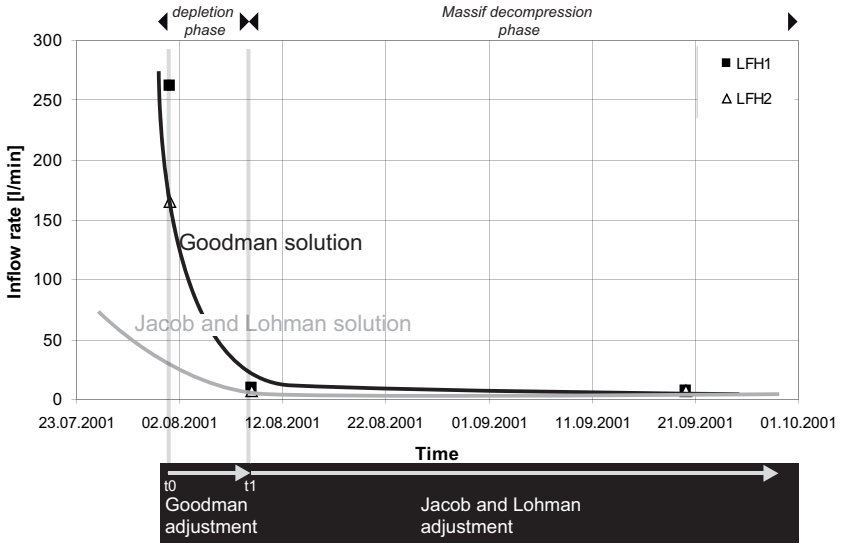

Figure 4.54: Global hydrodynamical functioning of the la Frasse landslide after the inflows measured at LFH1 and LFH2; Goodman adjustment for short times and Jacob and Lohman for long times.

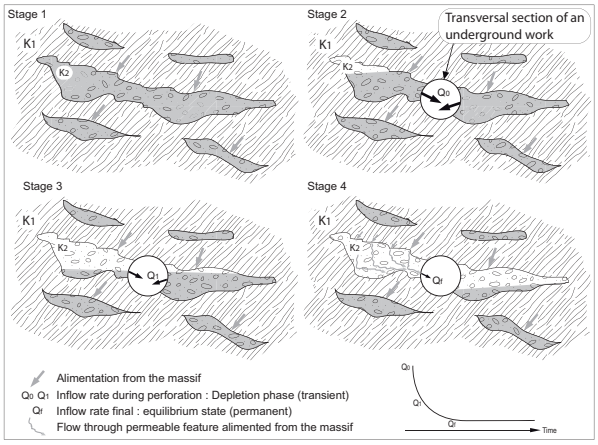

Figure 4.55: Hydrodynamical mechanism. At stage 1, the permeable fractions are saturated. At stage 2-3, the perforation of these structures by the work liberates the confined waters. The hydraulic permeabilities estimated at these stages, concern only the permeable zone and not the massif itself. The system finally reaches an equilibrium state, with a final flow rate (Qf), when the permeable zone is totally drained out (stage 4).

disconnected from the others permeable zone, the magnitude of the flow rates decrease very quickly (Q_0 to Q_1, stage 2 to stage 3). The hydraulic permeabilities estimated at this stage, concern only the permeable zone and not the massif itself. The system finally reaches an equilibrium state, with a final flow rate (Q_f), when the permeable zone is totally drained out.

This resulting flow rate (Q_f) might characterize the impermeable fraction, and since this moment and in normal hydrological conditions, the permeable fraction will only play a conductive role. However, during critical hydrological events, i.e. intense rain period, these structures might refill again according to their spatial connectivity, and cause locally hydraulic overpressure stress. These strong and brisk pore pressure variations are greatly influencing the stability of the slide. This phenomenon will be handled in detail in chapters 5 and 6. Finally, it is interesting to note that the observations done in this case study differ from those made in Maréchal (1998), in the sense that in Alpine crystalline system the major phenomenon controlling the hydraulic behaviour of the system is the decompression phase rather than the depletion phase.

4.4 CONCLUSIONS ON THE CHARACTERIZATION

Finally, in guise of conclusions, several additional constructive remarks on the different used methods may be formulated. This multidisciplinary approach enables to propose a complex and precise geological-hydrogeological model, but had allowed as well to test different characterization methods and to define their domain of application (observation and interpretation scales, see table 4.26).

4.4.1 HYDROCHEMICAL METHODS

Finally, it is important to notice that the sampling of the underground waters was realized during three different campaigns (August 2005, 2006 and 2007). This constitutes thus a negative point for the interpretation, in the sense that we are not 100% secure that the caught water at a well in 2007 belongs to the same flow system than in 2005. In figure 4.56 thanks to a simple 3D numerical simulation in a heterogeneous medium, it is show that a single well can, functions of the spatial connectivity of the heterogeneities, being the arrival point of numerous flowpaths.

4.4.2 GEOLOGICAL METHODS

The lithofacies analysis enabled the identification of the geological facies (e.g., clays, sands, silts, and gravels), distribution, thickness and correlation. Potential aquifers and confining formations may be identified, and the units that may create unusual hydraulic pressures distribution delineated. In fact, the lithofacies analysis defines the geometry and the general frame of the ground-water flow system. Therefore, the knowledge of the stratigraphy is necessary in order to identify potential pathway zones in the mass, and to estimate the vertical and horizontal extent of critical structures. Function of the scale, correlations might be possible. In system presenting the degree of heterogeneity such as the la Frasse landslide, linear correlations at a regional scale may be possible if some facies simplification is effectuated. The study further suggests that the use of entropy principles together with Markov chain analysis may reveal important characteristics and features in the geological succession, like the structural disorganisation and the geological inheritance. The entropy of the system is thus evaluated and may be useful for incertitude evaluation.

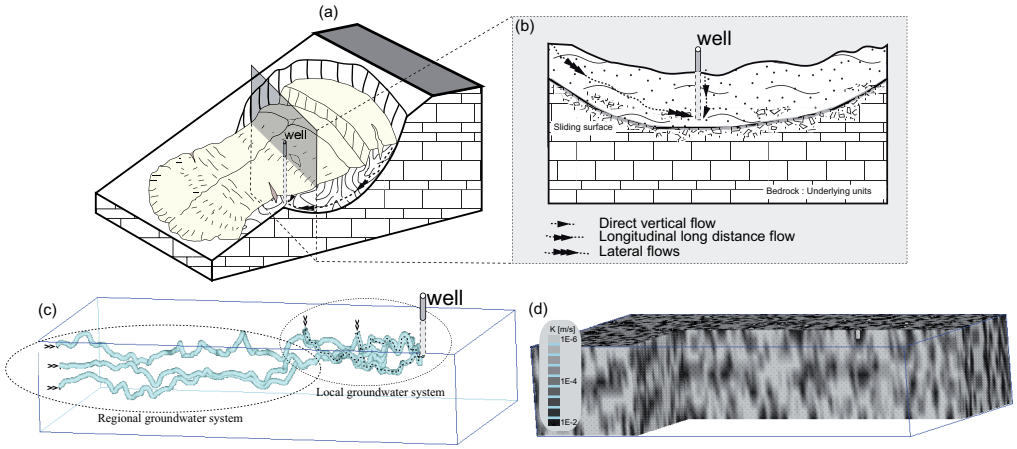

Figure 4.56: Diagram illustrating some hydrodynamic properties in heterogeneous media. a) General 3D view of a landslide area. b) 2D section with schematized underground flows; lateral flow from boundary units and direct vertical flow from the surface. c) Calculated flow pathlines in a random high heterogeneous medium (d) Hydraulic conductivity field constituted by a low permeable matrix (1E-6 m/s) with permeable structures. A single well can, functions of the spatial connectivity of the heterogeneities, being the arrival point of numerous flowpaths.

4.4.3 GEOPHYSICAL METHODS

Because of the rugged nature and complex geology of landslide areas, geophysical investigation is frequently considered as a non-productive operation. In sections 4.2.3 and 4.3.5 the RMT method is presented and several case studies for which this method was successfully applied. The different application have demonstrated that the RMT method is a light enough method to be applied to such field conditions and an accurate tool to define three dimensionally (vertical and horizontal prospecting) the geological heterogeneity of the underground, allowing thus the detection of geophysical resistive and conductive structures. In the meantime it has to be noted that the exact petrographic nature of the resistive units detected by RMT still needs to be documented because of the possible electrical equivalences existing between different geological formations. Exploration boreholes and groundwater monitoring may greatly help to determine the geological and hydrogeological characteristics of these resistive structures, as well as to confirm their aggravating role in the landslide's process. RMT method has to be further tested on different types of landslides and may be specifically developed to assess local subsurface conditions in order to provide more effective remediation strategies. Besides the geostatistical study of the apparent resistivities, may constitute a new approach for drainage design (§4.2.3.8).

4.4.4 HYDROGEOLOGICAL METHODS

In most of the cases, the evaluation of the hydraulic conductivity *K* into the drilling wells is based on tests lasting only a few hours (less than one hour for the FR1), and requesting thus the water contained in the more permeable levels without waiting their purging. The refilling from the surrounding impermeable mass being not anticipated, the hydraulic conductivity *K* is therefore over-estimated. Consequently, it is the lowest permeability of the mass which controls the flows on the scale of the landslide, and which authorizes to consider in the conceptual models, field parameters lower than that of the reality. The geological conditions make the interpretation of the hydraulic response very difficult. The observation made at a very local scale (site scale; one dimensional observation) permits nevertheless to propose a hydrodynamic concept at a regional scale (landslide scale). The observation done under the influence of a borehole platform, inform about the spatial relations of the aquifers; spatial connectivity. The record of the pumped water volumes points out the degree of heterogeneity and the evolution in space and time of the physical parameters of the system at a local scale.

4.4.5 OBSERVATION AND INTERPRETATION SCALE

A summary of the different used methods is presented in table 4.24, following considerations may be done:

Radiomagnetotelluric. The RMT method provides information to perform hydrogeological interpretations at a *regional scale* (global vision). The seismic reflection investigation provides a very regional resolution. It enables to perform 2D tomography, and according to the number of performed profiles, sophisticated 3D models.
Hydrochemistry. The observation is *local* (punctual sampling) but provide a *regional vision* of the functioning (origin of the incomes).
The Lithofacies analysis. This method provides information to perform hydrogeological interpretations at a very **local scale** vertically and horizontally. Regional consideration may be done with caution, since the interpretation of the spatial correlations may be problematic.
The geomechanical analyses provide information at a *REV and local scale,* but may give a global idea of

the situation. In the meantime, function of the number of investigations, an interesting tool for correlations, and define landslide instability.

Hydraulic tests and inflow rates analyses confirm that the *quantitative results* have a *local* meaning**;** however, qualitative results (global observation) may give a regional vision of the hydrodynamical behaviour and complexity.

Scale of observation of the different methods used in this PhD thesis									
	Investigation methods		*Chapters*	Observation scale			Interpretation		
				Regional	Local	REV	1D	2D	3D
ological and flow heterogeneity	Hydrochemistry		*4.3.3*	x	**X**			**X**	
	Borehole analyses	Vertical facies analysis	*4.3.4*		**X**		**X**		
		Stratigraphic correlations		x	**X**			**X**	x
	Radiomagnetotelluric		*4.3.5 and 4.2.4*	**X**				**X**	x
	Seismic		*4.3.5*	**X**				**X**	x
	Geomechanical Lab tests		*4.3.6*			**X**	**X**	x	
	Well tests	Single well observation	*4.3.7*		**X**		**X**	x	
		Multiple well observation			**X**			**X**	x
	Inflow rates	Well	*4.3.8*		**X**		**X**	x	
		Drainage gallery		**X**	**X**			**X**	x

Table 4.24: Synthesis of the scale of investigation, observation and interpretation of the used methods.

Finally, these contrasted permeabilities often pose in an acute way the problem of the representativeness of the field measures. The spacing between the measured or sampled boreholes must be based on a priori knowledge of the extension and the dimension of the geological heterogeneities.

In the same way, the equipment of the piezometers must permit to inform about the connectivity (i.e. spatial correlations) of the most permeable structures. Indeed, if well tests are effectuated, they should be able to check if the strong permeabilities correspond either to isolated lenticular structures without significant refill, or if on the contrary they are taking part of a more general flow system. This is a major aspect of the hydrogeological recognition of a landslide, when it requires the determination of an equivalent homogeneous permeability, whether it acts of a conceptual or a numerical model. In the case of spatially connected permeable structures, the equivalent homogeneous permeability will have a value close to that of these structures, whereas in the absence of connections (i.e. isolated lenses), the system is controlled by the impermeable fraction (i.e. permeability of the matrix).

Therefore, according to the studied problem, the use of an appropriate method of characterization either for geological or hydrodynamical purposes is necessary. The interpretation of these field measures will be facilitated since a difference is made between the local and regional behaviour.

5. HOW TO USE GEOLOGICAL HETEROGENEITY

5.1 FOREWORD

The information gathered thanks to the geological characterization are used for flow modelling purposes; several general and specific numerical analyses are performed. The role of the geological heterogeneity on the distribution and behaviour of the hydraulic pressures is investigated. The generation of preferential flow paths (channeling effects) is also precisely studied. The lessons obtained from the previous investigations (chapter 4) as well as from the following theoretical flow simulations will find a direct application in the study of the efficiency of a drainage system in the la Frasse landslide, scheduled for end 2008 (chapter 6).

First, the general notion of conceptual model is introduced. Thanks to the funding of chapter 4 and the conclusions in Tullen (2002) and Oswald (2003); the main characteristics of landslides occurring in these specific contexts (i.e. low permeable porous environments) are presented. A methodological approach is proposed, and boundary conditions discussed. The conceptualization concludes finally with the presentation of stochastic field parameter generations. A direct application is done on the la Frasse landslide data set.

5.2 GEOLOGICAL-HYDROGEOLOGICAL CONCEPTUAL MODEL

5.2.1 INTRODUCTION

In the specific context of landslides, the objective of geological and hydrogeological studies is to understand the effect of the underground water in the unstable mass in order to assess the risk and to elaborate remediation works or actions leading to an improvement of the stability. These studies result in the definition of a conceptual model; a schematic representation of the geological and hydrogeological conditions. This model synthesizes all the phases of recognitions; preliminary studies, borehole surveys, hydrogeological monitoring, hydrochemistry, and guides the nature of the investigations, if necessary numerical modelling, and then finally the design of efficient remediation solution. Finally it enables to understand the fundamental and principal processes occurring for each case study.

The elaboration of the conceptual model integrates:

- Lithological and geometrical characteristics (structure) of the geological units;
- General behaviour of the system;
- The effect of the geological properties on the underground waters; modification of permeability due to postglacial decompression for instance, or slide movements;
- Hydrological conditions: surface and lateral recharge, water losses of the rivers;
- Analysis of the hydraulic response of the system: piezometric variation, sources flow rates, geochemical signature of underground waters, vertical circulations;
- Hydrogeological structure: confined or unconfined aquifers, perched aquifers etc;

5.2.2 CONCEPTUAL MODEL IN LANDSLIDE ENVIRONMENTS – BASIC PRINCIPLES

The following section presents the most important parameters that a conceptual model should integrate for numerical modelling purposes. These parameters are defined thanks to the characterization study

performed in chapter 4, and thus is applied to the considered landslide type, namely occurring in very low permeable porous environments. Nevertheless, this global approach may be applied to other type of instability problems.

The studies performed in chapter 4 as well as the characterization undertaken in Tullen (2002) and Oswald (2003) enabled to define the most relevant characteristics of landslides occurring in these types of medium. Globally, they are defined by a heterogeneous environment with fracture flow and discontinuity porosity. The overall hydraulic conductivity is low, and locally very high permeable zones exist. Regional groundwater circulations are limited and are forming local interconnected aquicludes organised in thin aquifers, and presenting saturated and unsaturated zones. At the scale of the slide (regional scale) the entire mass can be considered as a unique aquifer and the equivalent homogeneous permeability representation is more or less valuable. At a local scale these heterogeneous structures have to be taking into account to enhance the accuracy of the model. Indeed inside the landslide, rapid groundwater flow through open failure networks are occurring. In addition to surface infiltration, the particular *"bowl shaped"* geometry allows important inflows of water from the neighbouring units (hydrogeological). The estimation of these contributions is often problematic and approximated. Besides the water balance may also integrate the outflows of the system.

The hydraulic gradient is generally high (several percents) principally due to the low permeability, and secondary to the slope and to the important difference of altitude between the infiltration zones (inlet) and the outlet areas (river, sources). For comparison, mean hydraulic gradients in alluvial aquifers are around some ‰. In addition, a reduction of the section of the slide is regularly observed at its foot, favouring the increase of the hydraulic head gradients. The seepage forces, which are proportional to the gradient, are intense and can give place to underground erosion and slope rupture. In depth, the movements are governed by the geomechanical laws of the sliding mass and its substratum, as well as by the local hydrogeological conditions. During a phase of activation, surface fractures in the traction zone enable the infiltration of important quantities of water in the mass or directly to the sliding surface through open scarps. In the compression zone a reduction of permeability will induce an increase in the pore water pressures.

Finally, the geological, structural and hydrogeological characteristics make that the landslides are three dimensional systems and their studying is rather senseless in two dimensions except for the test of some hypothesis (see section 2.1.5.3). The scale of study may be defined according to the considered problem. For instance, a local remediation work will necessitates a focused model on the zone of interest enabling to represent the main details of the zone, while for a global hydrodynamical behaviour evaluation, the whole landslide with its lateral limits must be represented in order to integrate the contribution of all the existing boundary conditions.

Thus, with the aim of flow modelling, the important parameters to consider, sum up in figure 5.1-a, are the following:

a. The three-dimensional shape and geometry of the sliding mass; **topography** and the **altitudes of the bedrock**.
b. An serious assessment of the boundary conditions:
    - **Surface recharge**; effective infiltration of the precipitations
    - **Lateral infiltration** from the boundary units
    - **Outlet** zones; source, rivers.

c. Distribution of the **physical parameters** integrating the observed or supposed heterogeneity.

Concerning the limit at the bottom of the model with the underlying units, some additional remarks have to be formulated. If during the geological characterization it is recognized that no water is alimenting the slide from the underlying units (bedrock), a no-flux boundary may be imposed at this limit. Nevertheless, its delimitation is often problematic, since its spatial differentiation with the lateral infiltration zone may not be clearly determined. In fact, a landslide is defined by an active mass sliding on a stable substratum. This substratum is constituted by a bedrock and in many cases covered with an older prehistoric mass, which is stabilized or latent. Thus, two principal configurations, schematized in figure 5.1-b, are possible; active mass on bedrock or active mass on stabilized or latent mass. Besides, field observations have shown that this stabilized or latent mass has to be incorporated in the models, since playing a important hydrogeological role. Therefore, in the first case the bottom limit of the model will correspond to the sliding surface, whereas in the second case, the sliding surface may be located inside the three-dimensional model. This configuration will be applied and discussed in section 5.4.2. Finally, in chapter 7 the synthesis on the global functioning model of these landslide types precisely presents these geological and structural configurations.

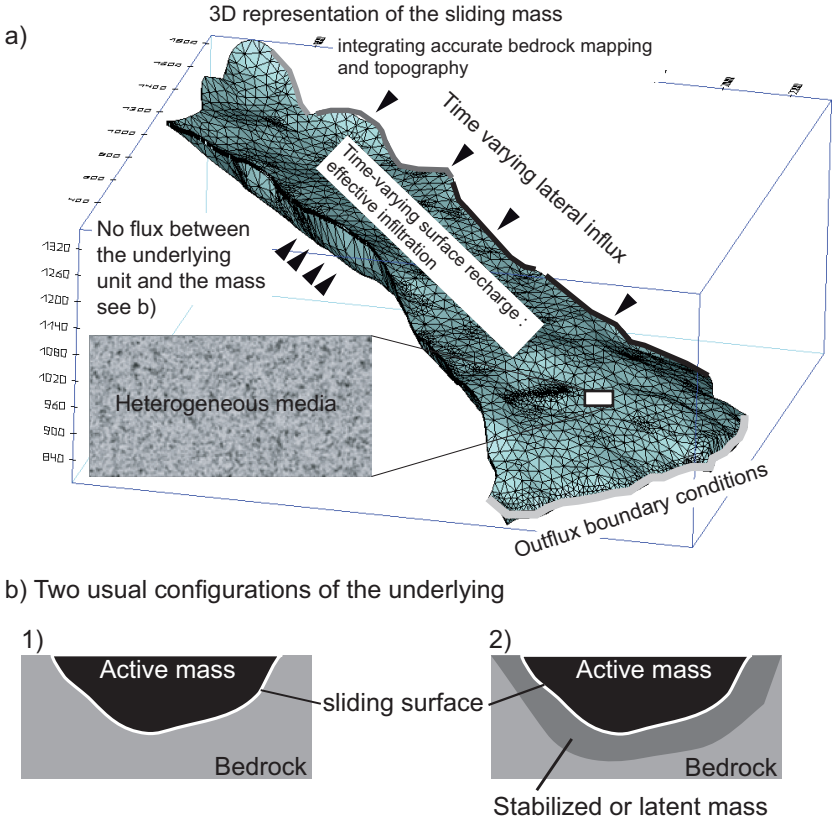

Figure 5.1: a) Summary of the most important parameters to consider during the conceptualization of a numerical model in the case of instability problems; three-dimensional shape and geometry of the sliding mass, an accurate assessment of the boundary conditions, and the distribution of the physical parameters integrating the observed variability (heterogeneity). b) Two configurations representing the relations between the sliding mass and the underlying units. In 1) the active mass is directly lying on the bedrock, in 2) the stabilized or latent mass is separating the active mass from the bedrock.

5.3 FIELD PARAMETER GENERATION

5.3.1 HOW TO REPRESENT THE GEOLOGICAL HETEROGENEITY

In classical flow modelling, the underground properties are usually described as an equivalent homogeneous medium with an average hydraulic conductivity which is not assumed to exactly represent the real medium, but to generate results that fit the observed data (e.g. observed hydraulic head). The homogeneous assumption is the oldest one and also the least valuable for most cases. Nonetheless, most hydrogeological studies still represent the subsurface structure as a homogeneous domain, or at least consisting of a set of homogeneous layers. Therefore the resulting hydraulic pressure heterogeneity is severely neglected. It will be shown in chapter 6 that especially in the case of instability problems, incorporating the geological heterogeneity in the numerical models is essential for the accuracy of the study. The evaluation, for instance, of the efficiency of drainage configurations requires that the main aspects of the structure of the flow domain are integrated into the model.

The use of geostatistical methods permits to represent the spatial heterogeneity (Isaaks and Srivastava 1989) of the physical parameters. The heterogeneity of the local hydraulic conductivity K (m/s) is typically described as a random field with a given statistical distribution (often assumed to be lognormal) and a covariance function (Gelhar 1993, Shvidler 1985, Fogg 1986, Dagan 1989), the statistical domain is presented in figure 5.2. Since the natural logarithm of the hydraulic conductivity ($\ln K$) is a stochastic process, it can be written as:

$$\ln K(x) = F + f(x)$$

Mean: $E[\ln K] = F$

Autocovariance function: $C(\xi) = \sigma_f^2 \left[\frac{|\xi|}{\lambda} \right]$

Where F denotes the mean of ln K, which is constant in space and f(x) is the perturbation (or the random part) about the mean. Note that ln K(x) is a dimensionless quantity.

Where:

σ_f^2 = variance of ln K

λ = correlation scale

In this study the three dimensional physical parameters distributions, i.e. hydraulic conductivity fields, are generated thanks to the Hydro_gen® code (Bellin A. and Rubin Y. 1996). Normally, the transcription of the observed heterogeneity into statistic parameters (mean μ, variance σ^2, correlation length $\lambda x,y,z$), is done after detailed borehole descriptions, well tests and geophysical soundings. In order to respect the values observed locally, conditioning values are introduced. Figure 5.3 illustrates some realizations.

These generated fields will finally be imported into the three-dimensional finite element model Feflow®. During the calibration steps, manual adjustments of the hydraulic conductivities are, in the meantime, effectuated.

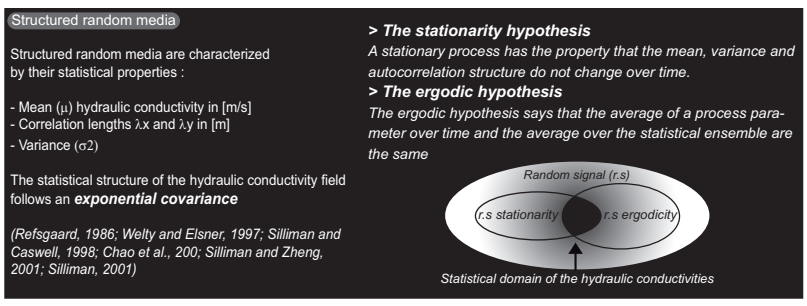

Figure 5.2: Statistical domain of the used geostatistical method permitting to represent the spatial variability. The variability of the local hydraulic conductivity K (m/s) is typically described as a random field with a given statistical distribution (often assumed to be lognormal) and a covariance function. The theory is based on two hypothesis; stationarity and ergodicity.

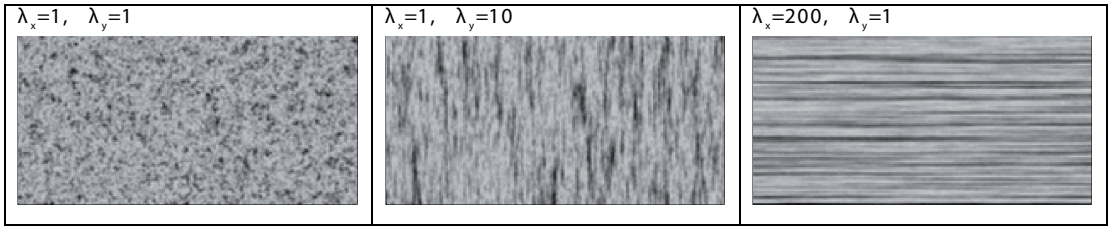

Figure 5.3: Examples of stochastic field data realization.

5.3.2 APPLICATION TO THE LA FRASSE LANDSLIDE

Geological data issued from the borehole investigations (§4.3.4) show a high heterogeneity between boreholes spaced some 10 meters apart, indicating that 10 meters may be the maximum width of the permeable structures. The permeability values calculated from Lefranc tests (§4.3.7) indicate an overall low shale matrix permeability of ca E-7 m/s, with locally intercalated high permeability structures (> E-3 m/s).

The statistical data used for the field data generation in Hydro-Gen® are summarized in figure 5.4. The mean and variance are equal to -4.69 and 1.08 (logarithmic values). Therefore the hydraulic conductivities K (m/s) introduced in the hydrogeological model range from 9E-8 to 1E-4 m/s, with a mean value around 4E-6 m/s (variance=2.56E-11 m^2/s^2). Maximal spatial continuities of 50 meters parallel to the sliding direction (correlation length λx) and 10 meters perpendicularly (λy) are fixed. These correlation lengths are defined after the detailed geostatistical analyses performed on the apparent resistivities acquired thanks to the radiomagnetotelluric surveys (§4.3.5). The analyses of the modelled variograms enable to characterize statistically the spatial structures (§4.3.5.5). These values are compatible with the observations, since the various well tests (§4.3.7.4) indicated possible connections between wells reaching locally hundred meters. A vertical correlation length (λz) of 2 meters is determined on the basis of mean thicknesses of the permeable bodies (gravel and sand) identified by the lithofacies analysis (§4.3.4). In order to respect the in-situ measured hydraulic conductivities, conditioning data are imposed during the data generations (figure 5.4). These generated field data are compatible with the measured parameters in flysch environment. The destructured flysch matrix of the la Frasse landslide has a global very low hydraulic conductivity (1E-6 m/s to 1E-7 m/s). The high permeable gravely intercalations in the mass, have locally a very high value (1E-3m/s).

Finally, during the calibration steps, some adjustments are done. In order to calculate the imbalances calculated in NCG-EPFL (2004) and Tacher et al. (2005), the global values are divided by a factor 10. Some structures, representing a coarser system of channels, are added on the slipping surface in order to match the calculated and measured hydraulic heads. This schematization, imposed by the calibration of the model, does not underestimate the connectivity of the real structures. These permeable channels are interrupted before their exit at the lower boundary (i.e. Grande-Eau River) in order to avoid a too-fast emptying of the hydrogeological system. This configuration allows a fast balancing of pressures (transfer time) in the channels rather than a fast velocity field (transit time) as discussed in NCG+EPFL (2004). These layers at the bottom of the sliding mass were recognized in DUTI (1986) being particularly heterogeneous, and represent well the discontinuous and disorganized structure that may exist close the principal sliding surface. In section 5.4.5, the importance of these permeable structures on the general hydrodynamic behaviour of the slide is discussed through various numerical tests.

Figure 5.5 sums up the attributed hydraulic conductivities for the 11 layers composing the conceptual model of la Frasse (§5.3.2.2) used for the numerical simulations. Layers 1 to 7 represent the active landslide, layer 8 and 9 the zone of the slip surface, layer 10 to 12 the stabilized landslide. Regarding to the assigned hydraulic conductivities, layers 1 to 7 and 10 are conform to the three-dimensional generated field values. The layers 8 and 9 are situated above the sliding surface; a system of channelized structures is incorporated as further discussed. The layers 10 and 11 represent the stabilized slide, and are constituted of various loose terrains (flysch, couches rouges and moraines) very heterogeneous. No data concerning these zones are available, statistic data equal to the sliding mass (layer 1 to 9) are attributed. Layer 11 includes the alluvium zone due to the Grande-Eau River at its lower part (NCG+EPFL 2004). A well test in LF10 indicated a *K*value of 5.5E-5 m/s, brought back to 1E-4 m/s after calibration. This zone is very important regards to the simulation. Being in the lower part of the slide, and in contact with the boundary conditions representing the river La Grande Eau, it plays the role of a water gate, regulating the in and outflows.

I)

	x-coordinate	y-coordinate	altitud	K mesured	LOG K	depth (m) from	depth (m) to
LF2	569675.20	133689.40	984.30	1.60E-05	-4.80	-12.00	-13.50
				8.70E-06	-5.06	-31.50	-34.50
				1.40E-04	-3.85	-68.50	-69.00
				2.30E-04	-3.64	-83.00	-83.50
LF3	569574.80	133434.90	946.67	5.50E-05	-4.26	-49.00	-50.00
P302	569659.60	133659.70	980.25	5.00E-05	-4.30	-56.00	-57.00
				5.00E-05	-4.30	-129.00	-140.00
I301	569623.60	133661.90	984.21	2.00E-05	-4.70	-34.00	-36.00
				6.00E-03	-2.22	-51.00	-53.00

II)

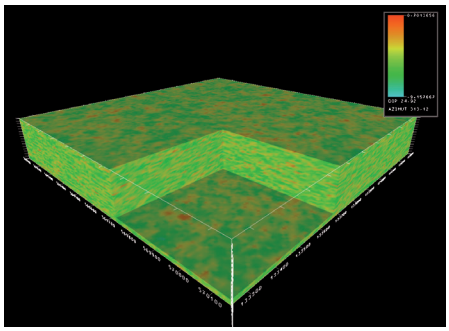

III)

Grid dimension (m)			Model dimension (m)			Statistical parameters			Correlation lengths		
dx	dy	dy	dimX	dimY	dimZ	Covariance type	Variance	Mean	λx (m)	λy (m)	λz (m)
10	10	10	1050	1050	-160	Exponential	1.08	-4.69	10	50	2

Figure 5.4: Parameters used in Hydro_Gen® for the generation of the physical parameters. I) Conditioning values. II) Three-dimensional field of the generated permeabilities. III) Statistical parameters used in Hydro_Gen®. See figure 1 for the location of the used piezometers.

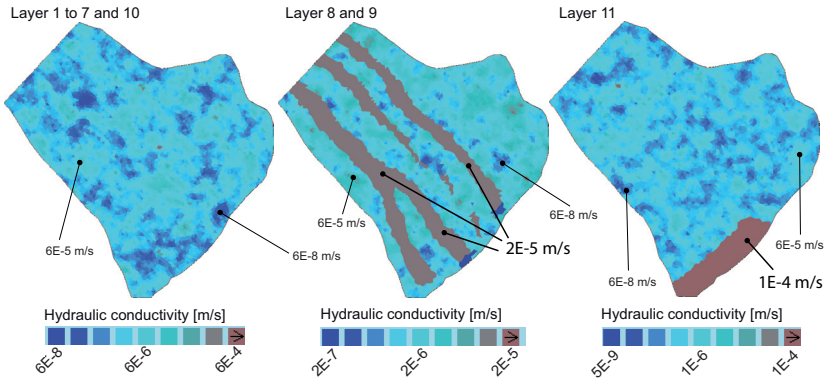

Figure 5.5: Hydraulic conductivities attributed to the 11 layers of the numerical model in Feflow. Layers 1 to 7 represent the active landslide, layer 8 and 9 the zone of the slip surface, layer 10 to 12 the stabilized landslide.

5.4 FLOW MODELLING

5.4.1 INTRODUCTION

Four different numerical models (figure 5.6) are used to investigate the effects of the spatial heterogeneity of the hydraulic conductivity on the underground flows; i.e. hydraulic pressures and velocity distributions. The following quantities are investigated: mean, variance (heterogeneity), correlation length (anisotropy). The role of the connectivity in generating flow channelling is examined thanks to the observation of close relations between the permeability and the hydraulic pressures. Flow pathlines and velocity analyses in a vertical (drainance effects) and horizontal direction are examined. The study consists thus in four approaches:

1. Sensitive analyses on theoretical 2D models (*2DT*) are performed to test the sensibility of the distribution of the calculated hydraulic pressures according to heterogeneity. The following sensitivity analyses are performed:
    - Sensitivity analysis in heterogeneous media with changing correlation lengths
    - Sensitivity analysis in heterogeneous media with changing variance
    - Sensitivity analysis in dual permeability models with changing correlation lengths
2. 3D theoretical models (*3DT*) allow studying the behaviour of the hydraulic pressures under the effects of new boundary conditions, for instance simulating the assignment of a drainage gallery.
3. Thanks to the 3D model of the la Frasse landslide (*3DFrasse*), an estimation of the uncertainties in relation with the distribution of the physical parameter is done. The model is used to test several heterogeneity scenarios. Compared to the calibrated model, the importance in considering the local heterogeneity is discussed. Finally this study allows a better understanding of the structure and the heterogeneity distribution of the sliding surface area.
4. A pseudo 3D model (*3DLFH1*) representing a "vertical slice" is performed on the base of the conceptual model of the drain LFH1 presented in section 4.3.8.5. It permits to validate the hydrodynamical model proposed in section 4.3.11.3.

5.4.2 NUMERICAL FLOW MODELS

5.4.2.1 ***Theoretical 2D and 3D models(2DT and 3DT)***

Principle

One solves the problem of a uniform flow in 2D and 3D heterogeneous media. In 2D, within the framework of the Dupuit assumption (Dupuit 1863) the flow is independent to the depth. This assumption holds that groundwater moves horizontally in an unconfined aquifer, and that the groundwater discharge is proportional to the saturated aquifer thickness. It was first designed by Jules Dupuit in 1863 to simplify the groundwater flow equation for analytical solutions. It requires that the water table is relatively flat, and that the groundwater is hydrostatic (i.e., the equipotential lines are vertical):

Law of Dupuit (1863)

$$\frac{\partial P}{\partial z} = -\gamma = -\rho g \quad \text{and} \quad \frac{\partial h}{\partial z} = 0$$

with:
- $\partial P / \partial z$ is the is the vertical pressure gradient,
- γ the specific weight ρ is the density of water,
- g is the standard gravity,
- $\partial h / \partial z$ is the vertical hydraulic gradient

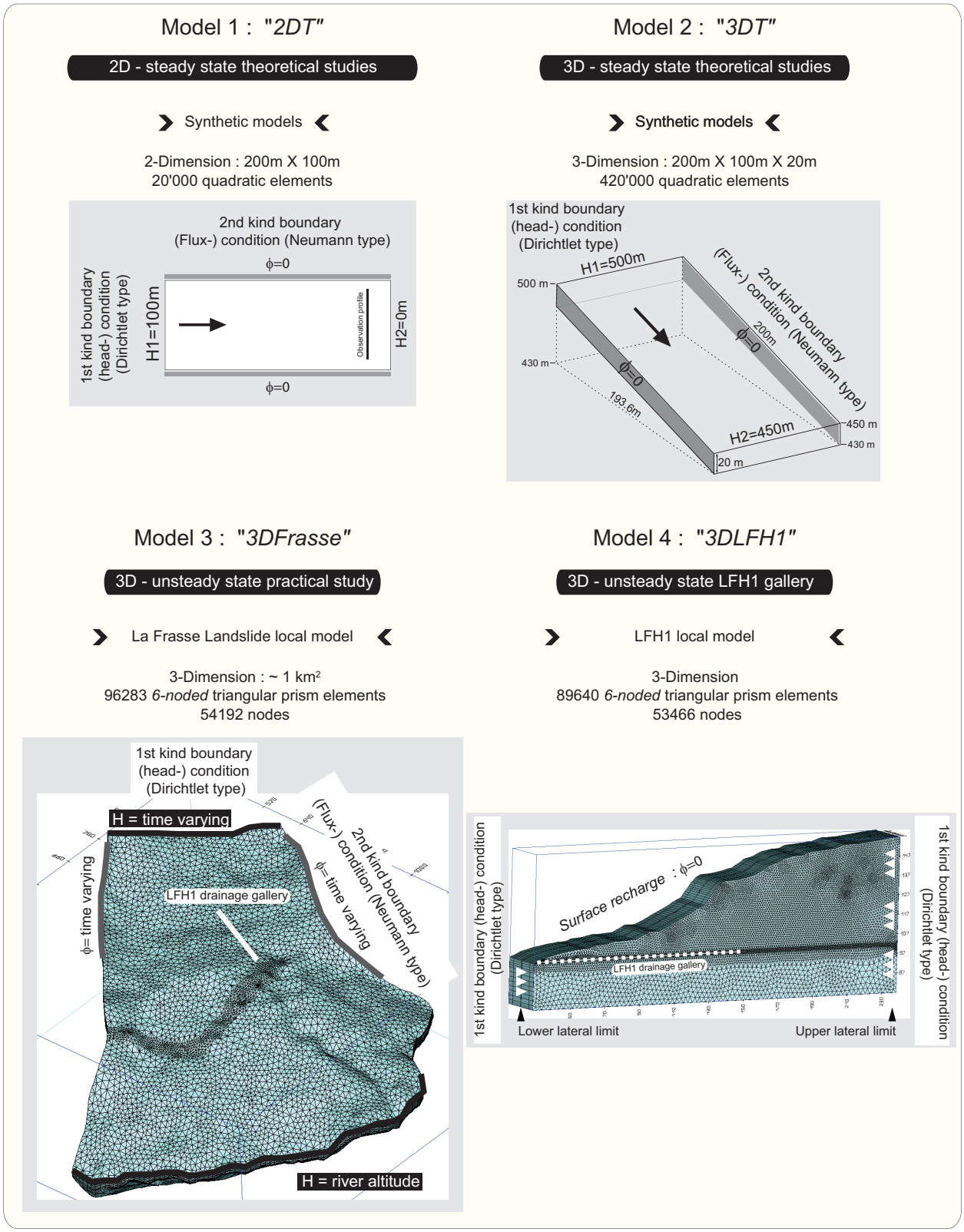

Figure 5.6: The four numerical models used in the framework of this PhD thesis; geometrical description (nodes, elements) and boundary conditions (1st and 2nd kinds).

The physical parameter of flow becomes the transmissivity, the vertical integral of the hydraulic permeability of an aquifer. By simplification a unit height (thickness) of layer is defined, which allows, except for the unit, confusing transmissivity and permeability on the one hand, velocity and linear flow on the other hand. Porosity intervenes by modifying the microscopic velocities compared to the Darcy velocity. However, in this study, the heterogeneity of the porosity is not analyzed. Note that, when it is constant, it changes simply the time scale. The problem does not lose of anything of its generality by taking a constant porosity.

The 3D model (*3DT*) represents a vertical extension of the 2D models (*2DT),* see figure 5.6. It allows studying vertical phenomena and velocity fields in three dimensions. The shape of the models, i.e. elevation and boundary conditions (BC's), permits to consider very strong hydraulic gradients, representative of landslide aquifers.
The models are representing a rectangular surface. The 2D model (*2DT)* is 200 meters on 100 meters and composed of 20'000 quadratic elements. The 3D model (*3DT*) is 200 meters on 100 meters with a thickness of 20 meters, and composed of 420'000 quadratic elements. The longitudinal, transversal and vertical discretization is 1 meter. This discretization scheme provides accurate flow calculations.
A random field simulator discussed in section 5.3.1 is used to create various permeability realizations of aquifers. The purpose here is to use the simulator to create a single realization (i.e. a heterogeneous aquifer) rather than to create many realizations from which probabilistic inferences could be made. The simulator is used to construct three-dimensional models, but three-dimensional random fields are not generated per se. Rather, two-dimensional random fields are stacked to create a three-dimensional random field. Each two dimensional field has a thickness of 1 meter, which is a typical correlation length in the vertical direction in such heterogeneous porous environments (§ 4.3.4.4). Thus, perfect vertical correlation existed within a single layer, and no vertical correlation existed between layers. This simplified approach is used for practical reasons. Proper accounting for boundary effects and accurate simulation of flow requires a very large grid, with very fine grid spacing in portions of the domain. Incorporating the discretization necessary to properly represent vertical correlation would have increased the number of cells by at least a factor of five, which is not practical with the computing resources that are available. Consequently, a compromise is made by creating a model with the fine discretization necessary to properly simulate flow, as well as correlation structure in the aquifer in directions parallel and perpendicular to flow. This compromise results in a less realistic simulation of vertical aquifer structures, but nonetheless provides a reasonable representation of natural systems.
Finally note that in order to avoid numerical inferences; a homogeneous permeability zone of 1E-4 m/s (2 meters large, i.e. 2 cells) is assessed at the "entry" of the model; i.e. the cells including the boundary conditions nodes (BC). It allows separating the heterogeneous field and the BC's, and thus to reduce numerical inferences.

Boundary conditions (BC's)
First kind boundary conditions (Dirichtlet type) are imposed on the upper and lower limits, and no flux is considered from the lateral boundaries. In additions, neither second kind boundary condition (Neumann type) nor surface recharge are imposed. Head conditions on the upper limit of the 2D models are H1=100 meters and H2=0 meters, concerning the 3D models; H1=500 meters and H2=450 meters. Hydraulic gradient are respectively 0.5 and 0.25.

5.4.2.2 La Frasse landslide model: model 3DFrasse

Principle

This model is originally designed for the drainage evaluation performed in chapter 6; coupling hydrogeological and geomechanical modelling. Nevertheless, it is used in this chapter to perform several additional theoretical studies and validations. The model is built in 3D in order to represent both the vertical and lateral heterogeneity of the parameters and boundary conditions (figure 5.6). It extends over a surface of around 1 km^2, it is composed of 96283 6-noded triangular prism elements (54192 nodes) distributed on 12 finite element slices (11 layers). The pressure field is computed in a transient mode. Feflow® is based on the general three dimension (3D) form of the governing differential equation for flow in heterogeneous isotropic media. The Boussinesq differential equation described below is the principal functions in it:

$$\frac{\partial}{\partial x}\left(Kh\frac{\partial H}{\partial x}\right)+\left(Kh\frac{\partial H}{\partial y}\right)+W(x,y,t)=\mu\frac{\partial H}{\partial t} \quad (1)$$

$$H(x,y,t)|_{t=0}=H_0(x,y) \quad with\ (x,y)\in D \quad (2)$$

$$\frac{\partial H}{\partial n}|_{\Gamma_2}=q(x,y,t) \quad with\ (x,y)\in \Gamma_2 \quad (3)$$

Where H is the saturated hydraulic head [L], h is the water table elevation above the impermeable barrier [L], H0 is the initial hydraulic head [L], q is the flux to recharge [LT-1], K is the hydraulic conductivity [LT-1], μ is the specific yield, W is the water balance, i.e., discharge minus recharge [LT-1], D is the study area, Γ2 is the second kind boundary condition, t is time [T] and n is the normal direction.

The flow regime is saturated, which implies that the slide body is saturated up to the surface. Thus, suction in the unsaturated zone is not considered, which represents a pessimistic hypothesis for stability calculations. The parameters (hydraulic conductivity *K* and specific storage *Ss*) and boundary conditions are initially tuned according to natural conditions. The physical parameters remain constant (e.g. no temporal change of the permeability field). Once the calibration is obtained, boundary conditions specific to remediation scheme are added. The simulation period ranges on the well documented crisis between August 1993 and December 1995 (i.e. 884 days).

Boundary and initial conditions

The major difficulty in assessing boundary conditions is the evaluation of the rates of infiltration. Although groundwater is recognized to be the cause of the sliding, there is no clear relationship between the acceleration phases and either gross rainfall or net infiltration computed by simple formulas (see section 4.3.9). Even the correlation of movements with accurately computed infiltration (COUP model, Jansson and Karlberg 2001) is poor. However, in Tacher et al. (2005) a correlation has been found weighting the COUP infiltration data in the past and then considering only the daily values above a threshold value (truncation process, figure 4.44) (see section 4.3.9.2). Elaborated algorithmic correlation functions enabled to reproduce the infiltration dynamic, taking into account the capacitive as well as the conductive function of the in-situ flysch enclosing the landslide. On the one hand, the fractured flysch layers are able to quickly transfer an infiltration event to the sliding mass. On the other hand the flysch, also made of low permeability rocks, stores and smoothes out events far back in the past. It means finally that only the most important feeding events contribute to the increase of pore pressures and those events of the past intervene in the present behaviour. Since the long-term component is dominant, one must conclude that the slide is fed by the geological bodies enclosing it rather than by direct infiltration from the surface. Indeed, the hydraulic balance of the system shows that about 1/3 of the inflow is supplied by superficial infiltration and the sold by the borders of the landslide.

The ***boundary conditions*** for the hydrodynamic modelling are distributed as follows and summarized in figure 5.6:

- On the surface, flux represents the direct infiltration, changing daily and computed according to the weighting process discussed in section 4.3.9.2.
- First kind boundary conditions (Dirichtlet type) are imposed on the upper and lower limits. Head conditions on the upper limit correspond to water level varying in time of piezometer LF1 adjusted to FR4. The lower limit corresponding to the outlet of the model is characterized by the La Grande-Eau river, head values corresponding to the altitude of the river bed are attributed ($h = z$ *(m)* i.e. zero pressure). Heads along the Grande-Eau are assigned to slice 1 to 10. The fact to stop head boundary conditions at layer 9 along the Grande-Eau is arbitrary and leading to a satisfactory calibration of the model. This tuning is very sensitive on the result since it means to open more or less the main outlet of the system.
- Second kind boundary conditions (Neumann type) are imposed on lateral limits in form of flux conditions varying in time according to the weighting process described in section 4.3.9.2, , and presented in appendices VI-8 and VI-9. These conditions extend to the whole model thickness.

The ***initial conditions*** come from steady state computations at time 0 (i.e. 1st August 1993).

Storage coefficient: compressibility Ss

In transient regime, the compressibility governs the amplitude and velocity of the response of the model on the variations of infiltrations. Interpretation of the pumping tests (see section 4.3.7) suggests that except at the top of the aquifer, heterogeneities are captive. The Ss value issued from the calibration, 1E-4 (m-1) characterizes an aquifer locally confined and expresses a fast response of the pressure field to temporal variations of the boundary conditions (see section 4.3.7.5).

5.4.2.3 ***Horizontal drainage work: model 3DLFH1***

Principle

This model consists in a three-dimensional slice through the zone"++" and "+" of the la Frasse landslide, and is designed after the conceptual model of the LFH1 drainage work (see sections 4.3.2.9 and 4.3.8.5). It represents a pseudo three-dimensional domain 12 meters thick and around 200 meters long. Composed of 89640 6-noded triangular prism elements (53466 nodes) distributed on 6 finite element slices; two meters large. Refinement is done along the drainage work, crossing the model in its middle part, along 160 meters (figure 5.6).

The flow regime is unsaturated (van Genuchten), thus suction in the unsaturated zone is considered. The parameters (hydraulic conductivity *K* and specific storage *Ss*) are distributed according to the la Frasse model (§5.3.2). The physical parameters remain constant (e.g. no temporal change of the permeability field). The simulation runs on 365 days.

Boundary and initial conditions

The boundary conditions for the hydrodynamic modelling are distributed as follows and summarized in figure 5.6:

- No flux is attributed on the surface
- First kind boundary conditions (Dirichtlet type) are imposed on the lateral limits (lower and upper). Head conditions on the lower limit correspond to water level measured in well LF8 and values 964 meters (= topography - 10 meters). The upper limit corresponds to the measurements in well Z205: 1018m.

5.4.3 ANALYSIS 1 : EFFECTS OF THE GEOLOGICAL HETEROGENEITY ON THE HYDRAULIC PRESSURES

5.4.3.1 ***Procedure – Scenario***

Thanks to numerical models in two dimension (model *2DT* presented in §5.4.2.1), sensitivity analyses are effectuated on two cases; (1) *heterogeneous media* (appendices VII-2 to VII-23), and (2) *dual-permeability media* (appendices VII-24 to VII-45). With K1=1E-2 m/s and K2=1E-6 m/s, the effect of strong permeability contrasts may be investigated.

A series of tests (81 tests for each case) are effectuated by varying the correlation lengths (λx and λy). The statistical properties of the heterogeneous media and the explored correlation lengths are presented in table 5.1. The 81 scenarios allow exploring the anisotropy longitudinally and transversally to flows, on the entire 2D spatial dimension. Although, note that the last two rows and columns highlighted in grey (table 5.1) must be considered with caution. According to the size of the model, the ergodic hypothesis for the correlation lengths; λx=200 meters and λy =50, 100 meters may not be anymore valid (Gehlar 1993).

Additional analyses are performed on the case 1 (*i.e. heterogeneous media*) by modifying the variance. The average value for the hydraulic conductivities remains constant.

a)

Number of values	20301
Minimum	-17.14
Maximum	-5.60
Range	11.54
Mean	-7.54
Variance	1.07
Coefficient of variation	-13.69%

b)

λ_x/λ_y	1	2	5	7	10	15	20	50	200
1	■								
2		■							
5			■						
7				■					
10					■				
15						■			
20							■		
50								■	
100									■

Table 5.1: a) parameters used in Hydro_Gen® for the generation of the physical parameters for the 2D and 3D flow modelling theoretical studies. b) the correlation length pairs (λx and λy) used in the framework of this study.

Observation of the results

This study consists mainly in a comparative qualitative study, aiming identifying one- and two-dimensional spatial behaviours (hydraulic pressure distribution, velocity fields and flowpaths).

Appendices VII-2 to VII-45 present all the performed one-dimensional observations. The straight relations between the hydraulic conductivity and the computed hydraulic pressures along a one-dimensional profile are compared. This profile is selected arbitrarily and transversally across the lower part of the model, as illustrated in figure 5.6. It enables to have for each realization an observation at the same position. In the homogeneous case, the potential head isolign computed along this profile equal 7 meters (P=68.5kPa). In appendices VII-2 to VII-9 (heterogeneous media) and appendices VII-24 to VII-31 (dual-permeability media), the computed hydraulic pressures are represented under a "*box-plot"* representation, allowing

evaluating the induced heterogeneity.
The overall mass balances are showed in appendices VII-8 and VII-30. Note that for each case, the two-dimensional generations of the hydraulic conductivity fields are also illustrated. The hydraulic conductivities are ranging from 1E-3 m/s (red-yellow colors) to 1E-5 m/s (blue colors).

5.4.3.2 ***Results***

The following relations are studied:

- *General observations*
- *One dimensional observation of the heterogeneity*
- *Channeling effects when varying correlation lengths*
- *Channeling effects when varying variance*

General observations

Heterogeneity. The link between the geological heterogeneity, the heterogeneity of the flowpaths and the hydraulic head distribution is not a commonplace. The gradient of the hydraulic head is spatially variable; the relation between permeability and flow velocity is thus not direct. For instance, the plot 5.1 shows the results of five numerical simulations.
The statistical framework (mean, variance and correlation lengths) of the hydraulic permeabilities is identical, the data are issuing from five independent data generations (random distribution). The computed hydraulic pressures indicate differences up to 25% between the five realizations.

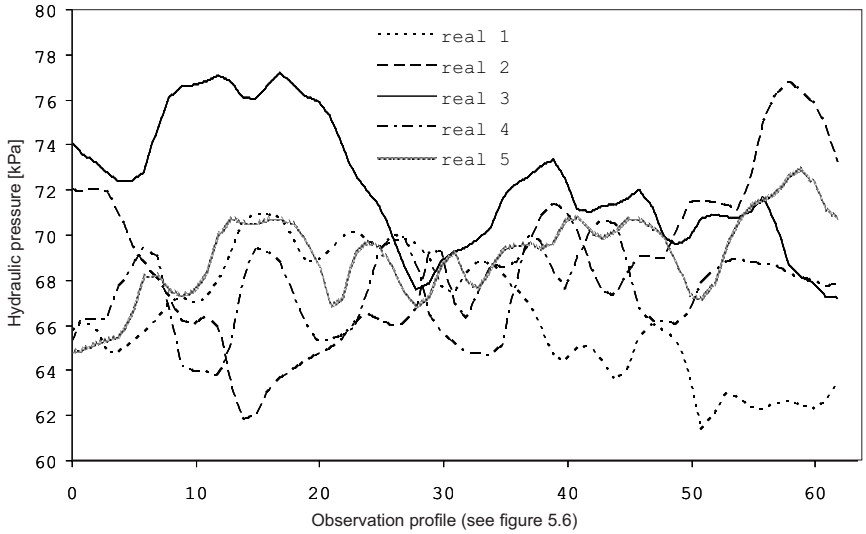

Plot 5.1: Results of five numerical simulations. The statistical framework (mean, variance and correlation lengths) of the hydraulic permeabilities is identical, the data are issuing from five independent data generations (random distribution). The computed hydraulic pressures indicate differences up to 25% between the five realizations.

This first test highlights the importance of the geological heterogeneity on the flows. The flow rate satisfies the equation of continuity and is connected to the permeability, the gradient of pressure and porosity, as indicated by the empirical law of Darcy (Darcy 1856):

Law of Darcy (1856)

$$q = \frac{-K}{\eta} \cdot \nabla p$$

and the modified form: $$Q = -K \frac{A}{\eta} \cdot \frac{dP}{dz}$$

with:
Q = Discharge of the fluid
K = Hydraulic conductivity (m/s)
A = Surface (m^2)
dP/dz = Hydraulic gradient
η= the viscosity of the fluid

Connectivity. A system of permeable structures may present diverse degree of importance function of its spatial connectivity. For instance, in the realization of figure 5.7, a one dimensional comparison indicates that the relation between the hydraulic pressures and the permeability is not straight. That is to say that the hydraulic pressures are not automatically decreasing when the flow is passing through high permeable structures and vice versa. The computed hydraulic pressures along this profile are strongly variable (variation up to 25%). In this model, a two dimensional observation of the distribution of the permeabilities indicates the presence of two areas. The permeable features are rather disconnected in area 1, and connected in area 2. These structural differences play a major role in the control of the distribution of the hydraulic pressures. Function of the connectivity of the system, local zones may stay head loaded while others are discharging.

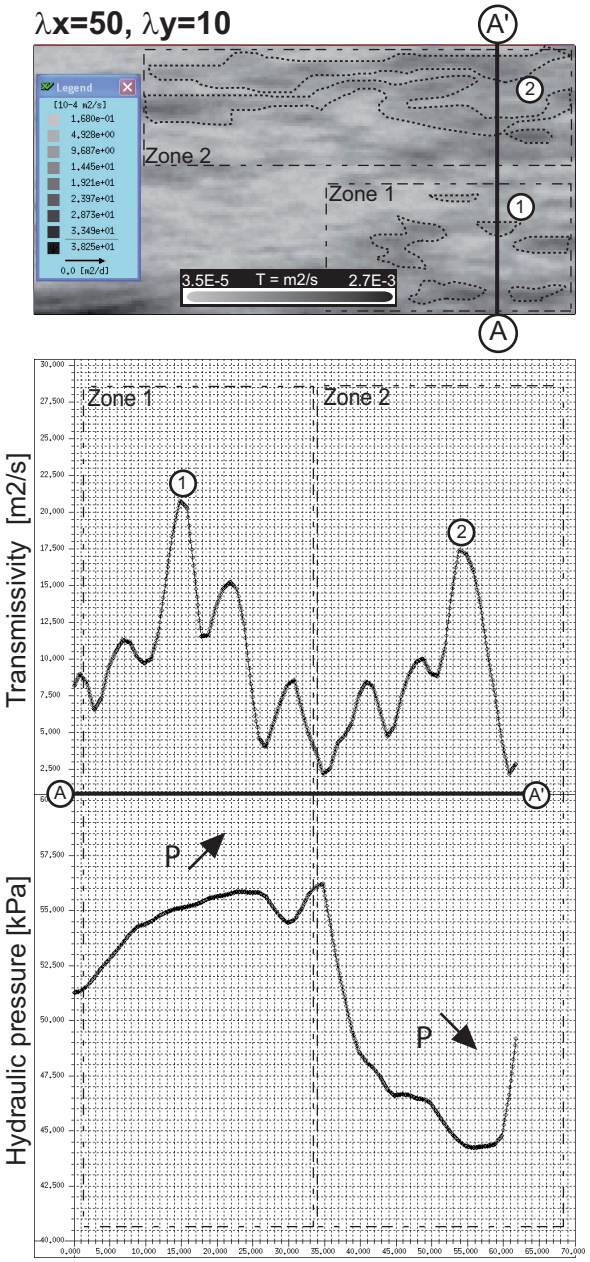

Figure 5.7: Flow modelling in a 2D heterogeneous model showing the high variability of the computed hydraulic pressures along a profile A-A'. A one dimensional comparison indicates that the relation between the hydraulic pressures and the permeability is not straight; the hydraulic pressures are not automatically decreasing when the flow is passing through high permeable structures and vice versa. In this model, a two dimensional observation of the distribution of the permeabilities indicates the presence of two areas. The permeable features are rather disconnected in area 1, and connected in area 2. Function of the connectivity of the system, local zones may stay head loaded while others are discharging.

In the second example of figure 5.8, the one-dimensional profile of the permeabilities shows three main principal peaks and a variable computed hydraulic pressure, partly constant and finally strongly decreasing. A two dimensional observation shows that the third peak is spatially well connected, since the two first are representing isolated lenses. This model is therefore constituted by connected channels (primary channels: C_p) and secondary disconnected (isolated) channels (C_s). The flows through the primary channels (C_p) generate a low hydraulic pressures, whereas, the flows through the "disconnected" isolated lenses (C_s) strongly increase it. In the same way, the connected channels are presenting high velocity flow paths as indicated in the right schemes of figure 5.8 with velocities reaching 102 m/s.

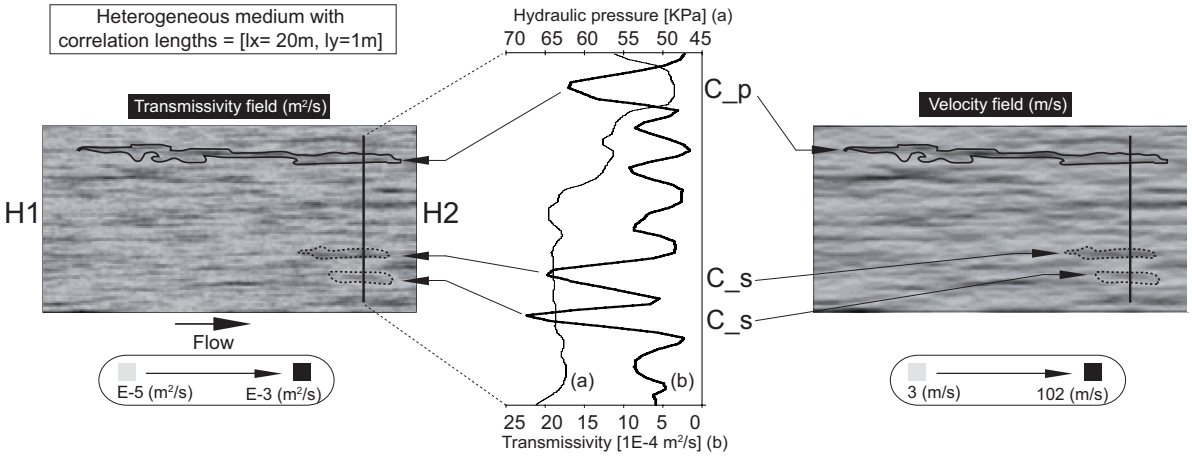

Figure 5.8: Computed hydraulic pressures along a transversal section and associated transmissivity. Transmissivity map (on the left). Velocity map (on the right). C_p : primary channel system, C_s: secondary channel system. Curve (a): Hydraulic pressures. Curve (b): Transmissivity. Domain size: 200x100m. Boundary conditions: H1=100m, H2=0m.

Note that, the distribution of the velocity field is also strongly heterogeneous, with values ranging from 3 m/s up to 102 m/s. Connected permeable features are thus allowing an aquifer system to drain the waters and to buffer the hydraulic pressures. These structures control the distribution of the hydraulic pressures of a system.

Additionnal examples showing the relations between the computed hydraulic pressure and these structures are illustrated in figure 5.9. These simulations, according to various spatial correlations, show that the occurrence of these channels, primary or secondary, is not function of the degree of connectivity (i.e. correlation lengths); even if the probability to have a system governed by primary channels is higher in well developed media. Thus, the organization of the flows depends on the heterogeneity of the hydraulic properties and their spatial correlation, i.e. the spatial connectivity of zones of similar hydraulic properties. Be it reminded, that the spatial connected permeable structures tend to decrease groundwater pressures

One dimensional observation of the heterogeneity
(Box plot representation of the computed hydraulic pressures appendices VII)

In *heterogeneous media* (appendices VII-2 to VII-9), the simulations show that when the correlation lengths are very small, the heterogeneity of the hydraulic pressure is low and more or less equal to the isotropic and homogeneous case. The heterogeneity of the hydraulic pressures increases with the correlation lengths λx or λy. For a given λx, an increase of λy also increases the heterogeneity of the hydraulic pressures. When

λx is high (i.e. good longitudinal connectivity) an increase of λy facilitates the flows and thus reduce the hydraulic pressure. Likewise, for a given value of λy, an increase of λx improves the water flow.
Concerning the calculated water balances (appendix VII-7), no great differences are recorded between the various studied cases. For instance, for λx=1 and λy=1 meters, the total fluid flux mass equal 2.72E-3 m^3/days and raises up to 2.81E-3 m^3/days for λx=15 meters and to 2.86E-3m^3/days for λx=50 meters. However, a strong increase is shown towards high λx values. These cases may be influenced by the BC's since the correlation length is almost equal to the dimension of the model.

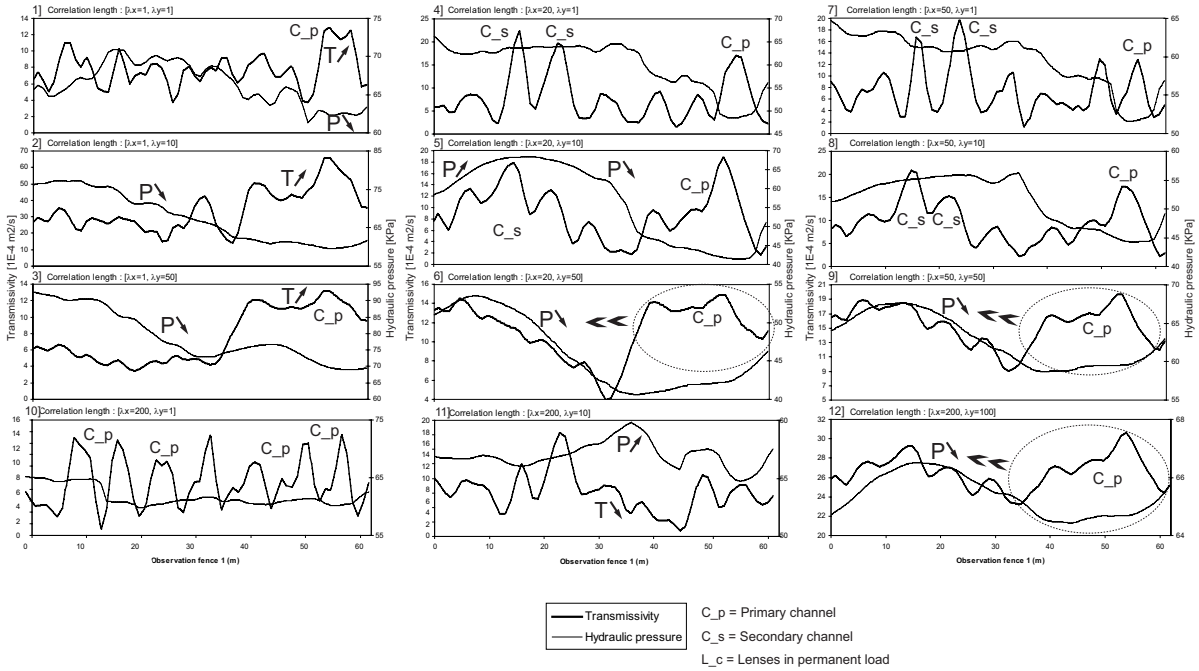

Figure 5.9: Computed hydraulic pressures along a transversal section and associated transmissivity for 12 different spatial structures (correlation lengths). C_p : primary channel system, C_s: secondary channel system. These simulations, according to various spatial correlations, show that the occurrence of these channels, primary or secondary, is not function of the degree of connectivity.

In the case of dual-permeability media (K1=1E-2 and K2=1E-6 m/s, see appendices VII-24 to VII-31), due notably to the strong permeability contrasts, the relations between the structures and the computed hydraulic pressures are blurred. The hydraulic pressures show a very strong heterogeneity and a perturbed behaviour. It is therefore quite impossible to draw a general tendency since the hydrodynamic conditions may change from point to point. These hydrodynamical behaviours may be, in a sense, roughly compared to karst system or fractured network.
As shown by others (Wu 1973; Aiken 1993; Jussel et al. 1994a; Moreno and Tsang 1994; Scheibe and Cole 1994; Webb and Anderson 1996; Riemersma 1996 and Riemersma et al. 1996), the spatial location and connectivity of regions with higher hydraulic conductivity strongly influence advective transport in the aquifer. As above-indicated, the simulations indicate that if the system is poorly structured (very low λx or λy), that is to say nearly isotropic, the heterogeneity of the hydraulic pressures is also rather low. Concerning the water balances (appendix VII-29), for low λy (thin structures) an increase of the longitudinal correlation (λx) tends to increase the fluxes. For instance for λx=λy=1 meters, the total fluid flux mass equal 18.8 m^3/days and rises to 237.4 m^3/days for λx=15 meters, and finally reaches 3764.6 m^3/days for λx=50 meters. Whereas, the differences are significantly lower for λy=15 meters with a total fluid flux mass equal to 10.3 m^3/days for λx=1 meter, and rising to 13.8 and 23.5 m^3/days respectively for λx=15 and λx=50 meters. The

system, regards to the computed water balances, show an enhanced hydraulic homogeneity, in the case of large transversal structures.

Thus, a better longitudinal and transversal continuity improves the flows and reduces the risk of overpressures. In figure 5.10 two examples with ideal longitudinal continuity are presented; λx=200/λy=1 meters (case 1) and λx=200/λy=10 meters (case 2). The calculated hydraulic pressures indicate an appreciable heterogeneity with values ranging from 5 to 70 kPa for case 1, and from 0 to 175 kPa for case 2. For instance in case 1, differences up to 65 kPa may be observed 10 meters apart. In case 2 the recorded hydraulic pressures are globally lower, reflecting the importance of the transversal correlation length (λy). Finally note that as illustrated by the dotted line, the hydraulic pressure of the homogeneous case rates 68.5kPa, in both case the hydraulic pressures are lower.

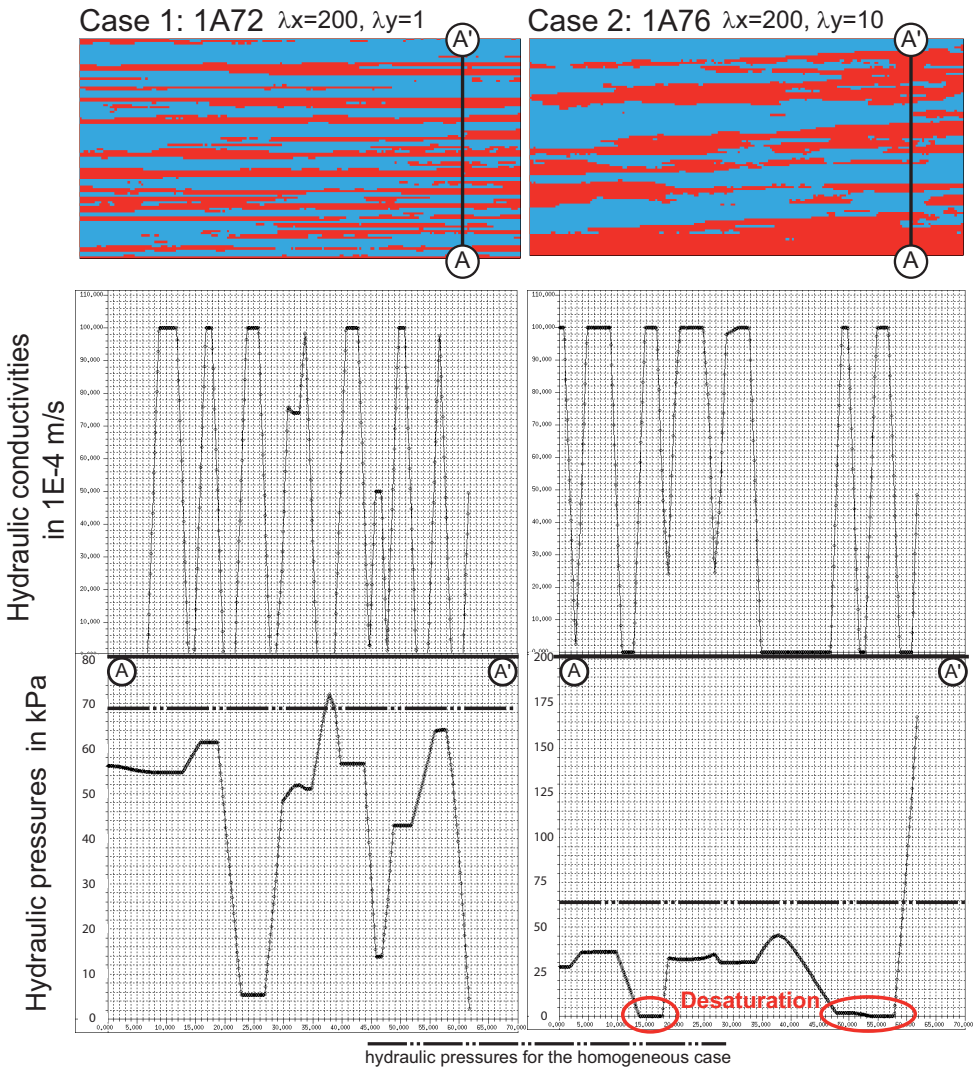

Figure 5.10: Flow modelling in a 2D dual-permeability model showing the high variability of the computed hydraulic pressures along a profile A-A'. The calculated hydraulic pressures indicate an appreciable variability with values ranging from 5 to 70 kPa for case 1, and from 0 to 175 kPa for case 2. For instance in case 1, differences up to 65 kPa may be observed 10 meters apart. In case 2 the recorded hydraulic pressures are globally lower, reflecting the importance of the transversal correlation length (□y). Finally note that as illustrated by the dotted line, the hydraulic pressure of the homogeneous case rates 68.5kPa, in both case the hydraulic pressures are lower.

Channeling effects when varying correlation lengths

This analysis is realized on the base of 12 selected cases representing the principal spatial structures; correlation length pairs in meters: 1] λx=1, λy=1; 2] λx=1, ly=10; 3] λx=1, λy=50; 4] λx=20, λy=1; 5] λx=20, λy=10; 6] λx=20, λy=50; 7] λx=50, λy=1; 8] λx=50, λy=10; 9] λx=50, λy=50; 10] λx=200, λy=1; 11] λx=200, λy=10 and 12] λx=200, λy=100. The results are presented in figure 5.11 and 5.12.

The flows in heterogeneous media tend to be organized in channels more or less independent. This phenomenon of channeling is often evoked like one of the principal reasons of the incapacity of the traditional models to reproduce the observations (Moreno and Tsang 1994, Tsang and Neretnieks 1998; Bruderer-Weng et al. 2004 and Tiedeman and Hsieh 2004). The movement of water through natural earth materials is influenced not only by the distribution of inflow in time and space (i.e. boundary conditions), but also by the nature of the material through which the water flows. Basically, increasing λ*x* and λ*y* generate channelling. In figure 5.11 it is shown that flow channeling depends on the spatial correlation range. For small correlation range, λ*x*= λ*y*=1, channeling occurs, but the channels are closely spaced, and there are many of them over the flow domain. Increasing the correlation length favours the channeling. Therefore, channelling may depend on the λ*x*/λ*y* ratios:

- If the λ*x*/λ*y* ratio is superior 1, representing a spatial continuity expanded in the direction of the flow, channelling may be well developed with good differentiation of the flow paths. More this ratio is important the more the channelling effects will be strong.
- If the λ*x*/λ*y* ratio is equal to 1 the flow field tends to a homogenization as illustrated by the models 1 and 9; λ*x*=λ*y*=1 meters *and* λ*x*=λ*y*=50. The channeling effect is "averaged out".
- If the λ*x*/λ*y* ratio is inferior to 1 no channelling occurs (see model 2, 3 and 6).

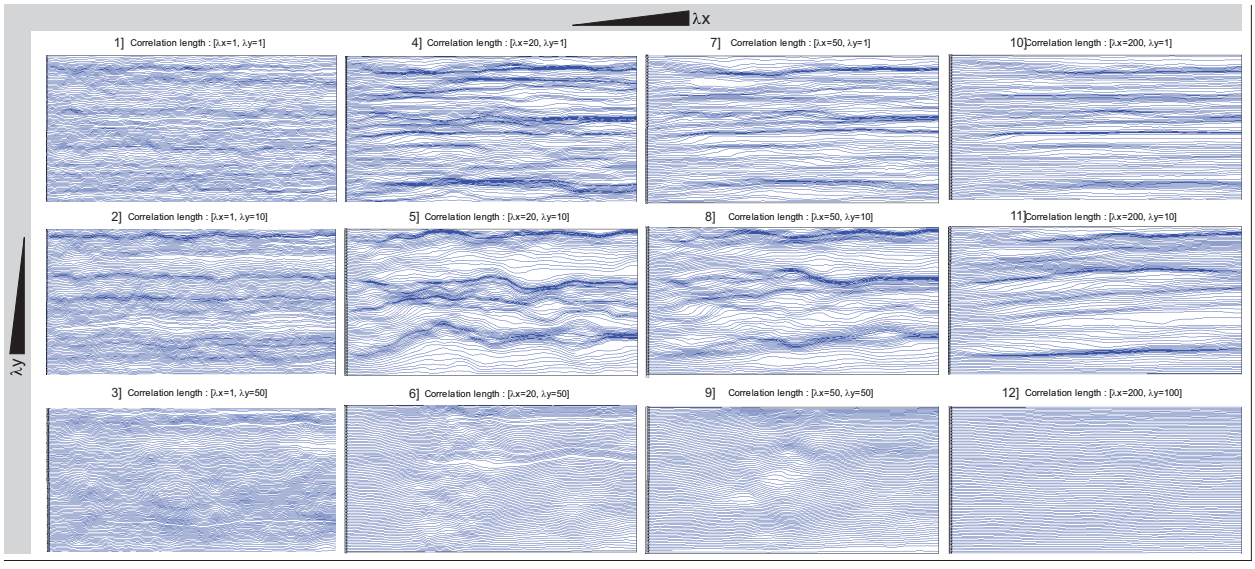

Figure 5.11: Flow paths and flow channeling effects in 12 selected cases (2D numerical heterogeneous models) representing the principal spatial structures (correlation lengths). See

In addition, the various flow paths transit through the medium with different velocities due to the heterogeneity of the permeability. As indicated in figure 5.12, the variation of the velocities is dependent on the correlation lengths factors. For low λ*x* and λ*y* values, the velocities are more or less homogeneous

and low (i.e. model 1). High velocity zones are appearing with channelling (i.e. λx=200 m/λy=1 m), with values reaching 100 m/day, and increasing with λy (i.e. λx=200 m/λy=50 m), with values reaching 160 m/day. The homogenization of the distribution of the velocity is function of these correlation lengths, and especially of λy. It is interesting to observe in the middle of model 6 the existence of a very heterogeneous zone that is certainly created thanks to special local heterogeneity distribution.

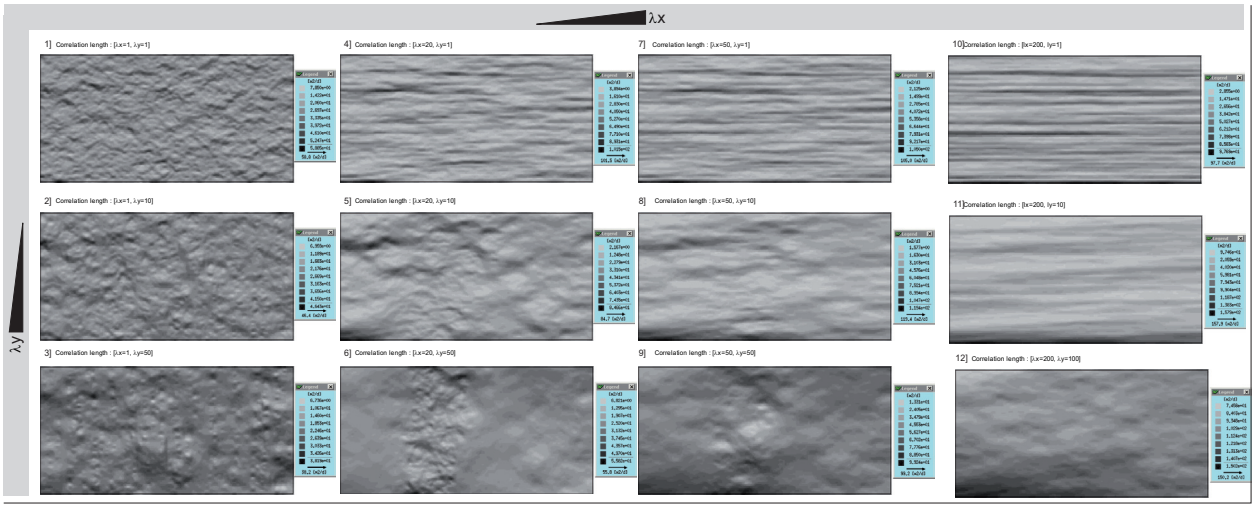

Figure 5.12: Velocity distribution in 12 selected cases (2D numerical heterogeneous models) representing the principal spatial structures (correlation lengths). See figure 5.11 for the distribution of the flow paths.

Channeling effects when varying variance

The development of strong channeling effects may also be observed as a function of the variance σ^2 of the natural log permeability values. The emergence of channeling as a function of the degree of the heterogeneity is shown in figure 5.13 for six realizations. The studied model presents a $\lambda x/\lambda y$ ratio equal to 10 (λx=20 m/λy=2 m), and a variance σ^2 varying from 0.25 to 8.

For a small variance of permeability, $\sigma^2 = 0.25$ in natural log, flow is essentially vertical with little contrast between fast and slow flows. However, as σ^2 is increased to 1 and 8, flow becomes highly channelized, with exit flow on the right boundary concentrated at a few discrete locations. Increasing the heterogeneity influences considerably the organisation of the flows. In extreme heterogeneous distribution and for large heterogeneities, the flow is transported through few fast paths. The flows may thus be concentrated in only one bearing structure according to the structural complexity of the medium.

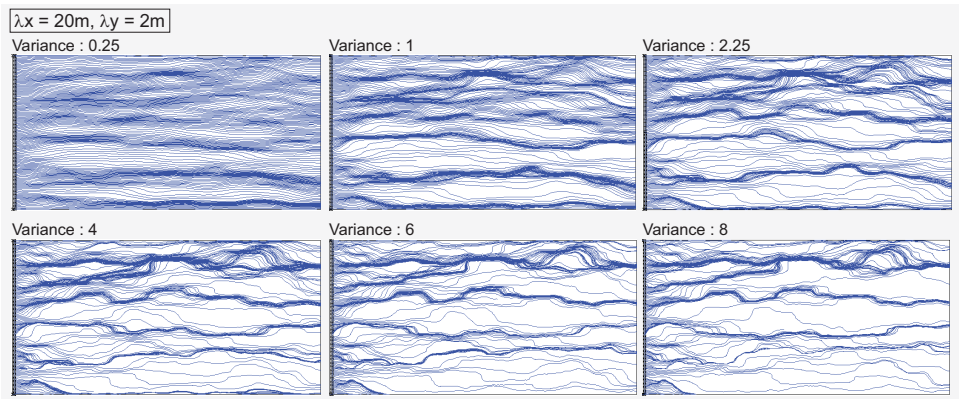

Figure 5.13: Development of strong channeling effects as a function of the variance σ2 of the natural log permeability values for six realizations. The studied model presents a $\lambda x/\lambda y$ ratio equal to 10 (λx=20 m/λy=2 m), and a variance σ2 varying from 0.25 to 8.

5.4.3.3 ***Discussions***

Flow through porous heterogeneous media is affected by the heterogeneity of the medium permeability (i.e. variance) and the way this heterogeneity is distributed in the system (i.e. correlation lengths). The highest fluid rates are found along the least-resistive pathways and vice versa. The development of flow channelling as a function of the variance and the correlation length is demonstrated.

According to the degree of anisotropy and the heterogeneity of the medium; three types of flows are distinguishable: *"homogeneous" distributed flows*, *strongly channelized flows* and the *intermediate flows*. Note that, these types of flow have already been recognized and described in karstic and fractured systems in de Marsily et al. 2005). The structure of the generated flows, as well as the hydraulic properties of the medium, is strongly influenced by the connectivity of the medium.

"Homogeneous" distributed flows. The "homogeneous" distributed flows are rather characteristic of homogeneous porous media or slightly heterogeneous. After de Marsily et al. (2005) they may mostly be encountered in fractured media with a strong density of fracturation. In our studies, these flows appear when $\lambda x/\lambda y$ ratios are more or less equal or inferior to 1; i.e. structures rather developed transversally to flows with small longitudinal correlation lengths. The velocity fields are likewise homogeneous and relatively low.

Strongly channelized flows. The simulations performed in this study showed that channeling may not only occur in fractured or karstic media, but also in porous aquifers, which seemed sufficiently homogeneous to not envisage such "organized" flows. In fact, in porous aquifers, clay and inter-connected sand zones constituted broad structures of flows, however if being relatively homogeneous. Often, these permeable structures are concentrating the flows, and may be characterized by very high flow rates. In the studied cases, channeling rather appears when the spatial connectivity is longitudinal to the flow direction (i.e. x-direction) with $\lambda x/\lambda y$ ratios superior to 1. More this ratio is important, the more the channelling effects will be strong. Likewise, the velocities are organised and separated in fields, and may be locally very important. Thus, the flows are organized by the network structure of the high permeable features:

- Flows are localised in mono and two-dimensional zones formed by the high permeable features, and always tend to follow them.
- Flows are, in very porous media, strongly structured in principal channels separated by "small islands" from very slow flow, representing thus bi-modal systems.

Intermediate flows. Finally, between the strongly channelized flows and the "homogeneous" distributed flows, exist intermediate flows, partially channelized and distributed along many channels. These flows are representing an intermediary system and are typical of natural systems presenting a low to medium heterogeneity.

In addition to these three types of flows, two types of permeable structures are identified: ***type 1) primary structures*** *(connected structures)* and ***type 2) secondary structures*** *(disconnected structures, i.e. isolated lenses)*. In a hydrodynamical point of view, these structures behave differently. The first type acts mostly positively on the system, driving efficiently the flows and lowering the hydraulic pressures. And thanks to optimal spatial connectivity may drain the system. The second type rather generates negative effects on the system, concentrating the flows and increasing locally but strongly the hydraulic pressures (overpressures effects).

5.4.4 Analysis 2: Behaviour of the hydraulic pressure under new boundary conditions

5.4.4.1 ***Procedure – Scenario***

Thanks to theoretical three-dimensional numerical models (3DT, §5.4.2.1), the behaviour of the hydraulic pressure distribution under constraints of new boundary conditions is investigated. These new boundary conditions are representing in this case a drainage system permitting to extract water from the system. The hydrodynamic equilibriums are thus modified. The drainage system represents a drainage gallery with vertical pipes (see chapter 6 for basic principles) with several spacing: 5, 10 and 20 meters.
The different media are heterogeneous with a mean hydraulic conductivity in logarithmic values equal to -7.6 and a variance equal to 2.25. The considered correlation length pairs λx and λy are in meters: [1,1]; [20,2]; [20,10]; [50,2] and [50,10]. A second series of realization is performed to test the effects of strong contrasted media; for this purpose dual-permeability models with K1=1E-2 m/s and K2=1E-7 m/s are created. The correlation lengths (in metres) equal to: [20,2] *y* and [50,2]. All results are showed in appendix VIII, the following chapter presents the basic funding.

5.4.4.2 ***Results***

In function of the degree of heterogeneity and continuity of the medium, simulations reveal that, before drainage, the development of preferential pathways is increasing strongly the hydraulic pressures locally. Furthermore, in media presenting strong permeability contrasts (dual-permeability models), the concentration of water flux in permeable channels even tends to dry out and dewater locally certain zones (negative hydraulic pressures), resulting in a very heterogeneous distribution of the hydraulic pressure field. Consequently, the efficiency of a drainage adit in a system in which mass volumes remain isolated from preferential flow paths will be extremely reduced. Modelling also indicates that in such highly heterogeneous medium, some pipes are strongly participating in the global lowering of the hydraulic pressures while others are remaining totally inactive and useless. Moreover, according to the global connectivity of the system, some pipes could have only a very local effect, draining isolated and disconnected lenses, and being active the time the system is drained out.

Besides, in some cases, the simulations clearly demonstrate that, the drainage system could have the opposite effect as expected. Drainage pipes connect units of higher hydraulic conductivity that are initially discontinuous. That is to say, the drainage pipes may cause a short circuit (hydraulic bypass) by forming preferential flow paths that connect more conductive units. Locally, the hydraulic pressures distributions may thus be changed. Overpressures or even dewatered zones, initially absent, appear therefore in some regions.

Evidence in support of this hypothesis is shown in figure 5.14. These profiles show that the initial distributions of hydraulic pressures before drainage (A) has a maximum of 284 KPa, and after drainage, according to the adopted drainage system (B: spacing between pipes = 5 meters or C: spacing between pipes = 20 meters), the pressures reach respectively 397.7 and 212.2 kPa. In case B, too close pipes produce an opposite effect, increasing locally the pressures up to 100 kPa. The drainage efficiency evaluation is therefore depending on the physical parameter model. A practical application of the la Frasse landslide is presented in the following section.

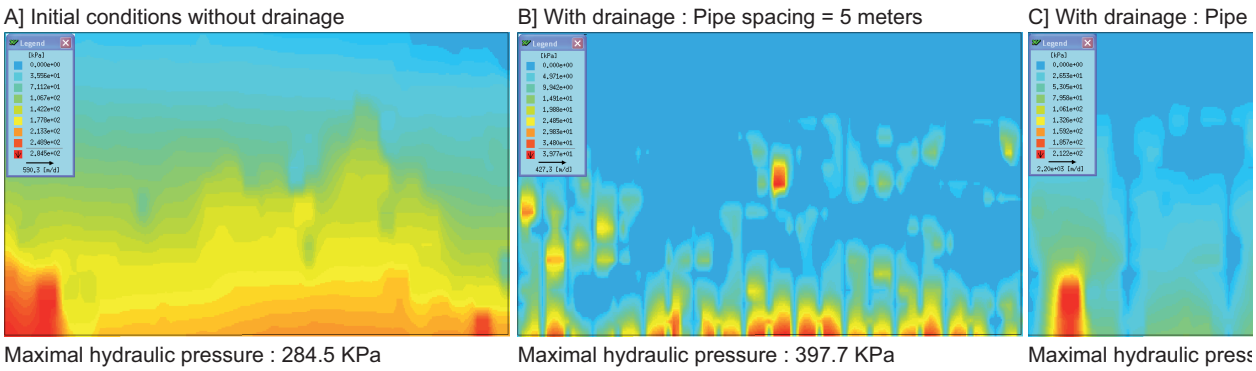

Figure 5.14: A transversal 2D profile at the drainage system through a 3D system. The medium is represented by a dual-permeability (K1:1E-3 m/s, K2:1E-7 m/s) and is highly channelled. The flux is perpendicular to the profile. A] Initial conditions before drainage, B] and C] with drainage.

5.4.5 Analysis 3: Heterogeneity and structure of the sliding surface area

5.4.5.1 ***Procedure – Scenario***

Thanks to the three dimensional model of la Frasse landslide (3DFrasse, §5.4.2.2) several tests are effectuated. 10 different geological heterogeneity scenario applied on the slice corresponding to the sliding surface (slice 9) are evaluated. The explored scenarios are presented in table 5.2, and consist in varying the hydraulic conductivity of the matrix (capacitive impermeable fraction) and those from the special permeable channels (conductive permeable fraction). For each scenario, a complete run is performed (i.e. 882 days), the computed hydraulic pressures at five observation points (figure 5.17) are then compared to the calibrated la Frasse model (i.e. *3*DFrasse model *KV09* in table 5.2 and §5.4.2.2). The simulation period ranges on the well documented crisis between August 1993 (t=180-200 days) and December 1995 (t=550-600 days). These two crises (§4.3.2.7) are characterize by strong water inflows on short time (figure 5.15).

Id.	Scenario: geological heterogeneity
KV09	La Frasse 3D model with the physical parameter distribution as discussed in **chapter 5.2** and special features on the sliding surface (channel structures)
KV09D	Homogeneous K = 1E-7 m/s, and special features on the sliding surface (channel structures)
KV09E	Homogeneous K = 3.79E-6 m/s corresponding to the mean value of KV09, and special features on the sliding surface (channel structures)
KV09F	KV09 without the special features on the sliding surface (channel structures)
KV09G	KV09E without the special features on the sliding surface (channel structures)
KV09H	KV09 with special features extremely permeable (1E-2 m/s) on the sliding surface (channel structures)
KV09I	KV09 with an extremely impermeable sliding surface with K=1E-10 m/s
KV09J	KV09I with special features on the sliding surface (channel structures) extremely permeable (1E-2 m/s)
KV09K	KV09 with an extremely permeable sliding surface with K=1E-2 m/s, without the special features on the sliding surface (channel structures)
KV09L	KV09F, with discrete features elements, K=1E-1, section: 0.314 m2 (r=5cm)
KV09M	KV09 --- special features on S8-S9 interrupted, see figure 5.17

Table 5.2: Geological heterogeneity scenarios of the three-dimensional model of la Frasse landslide, tested by means of numerical simulations. For each scenario, a complete run is performed (i.e. 882 days); the computed hydraulic pressures at five observation points (figure 5.17) are then compared to the calibrated model.

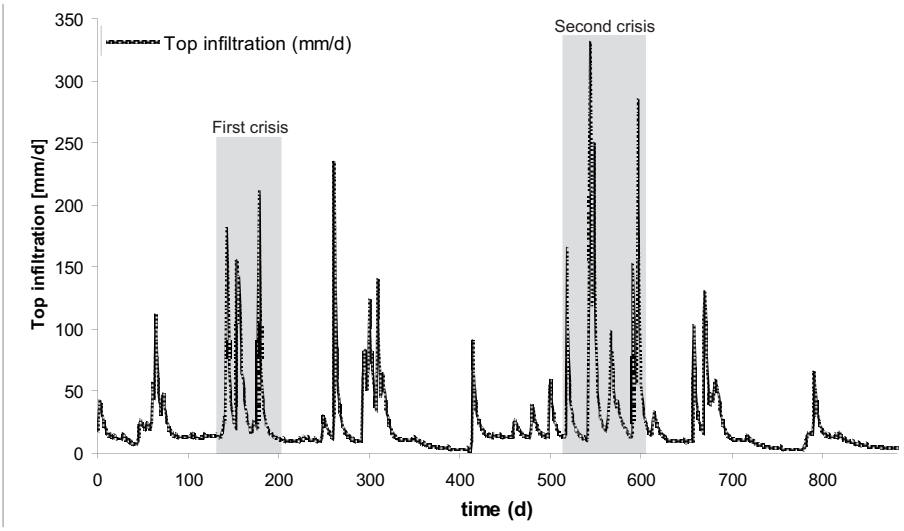

Figure 5.15: Top "effective" infiltration assigned in the la Frasse model. The simulation period (882 days) ranges on the well documented crisis between August 1993 (t=180-200 days) and December 1995 (t=550-600 days). These two crises (§4.3.2.7) are characterize by strong water inflows on short time.

The aims of this study are, first, to identify structural characteristics of the sliding surface, and secondly, to pointed out the importance of considering the geological heterogeneity in flow modelling.
The following parameters of the hydraulic response are discussed (figure 5.16): the peak intensity, the heterogeneity of the response, the synchronization between the hydraulic stress and the response of the model and finally the peak intensity duration. The physical parameters of the calibrated la Frasse model are presented in section 5.2, as well as the configuration of the special permeable channels added on the sliding surface during calibration.

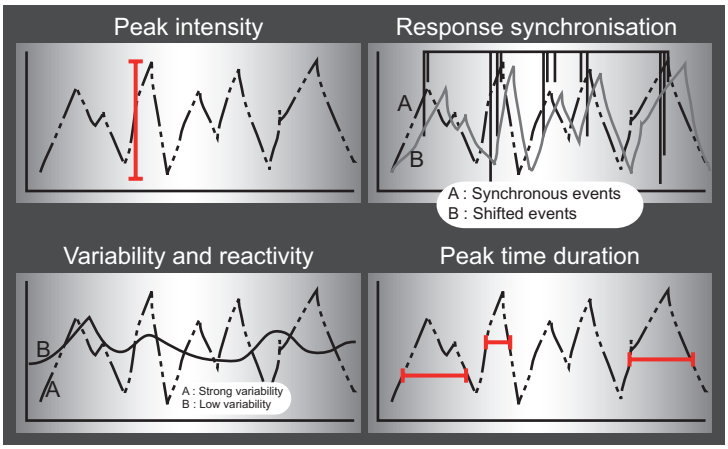

Figure 5.16: The analysed and discussed characteristics of the hydraulic response: the peak intensity, the variability of the response, the synchronization between the hydraulic stress and the response of the model and the peak intensity duration.

Observation of the results.
Five observation points are considered (see figure 5.17). Observation points *LF8* and *Obs4* are situated in the upper part of the model, and *LF10*, *Obs5* and *Obs6* in the lower part. *Obs4* and *Obs5* are placed into the permeable structures, *LF8* and *LF10* in the capacitive matrix. *Obs6* is placed in an isolated lens.
In figure 5.17, the scheme a) show the distribution of the permeabilities at the layer corresponding to the sliding surface as discussed in section 5.3.2. The scheme b) represents the permeability model used for case

KV09M, showing the disconnected characteristics of the permeable structures.

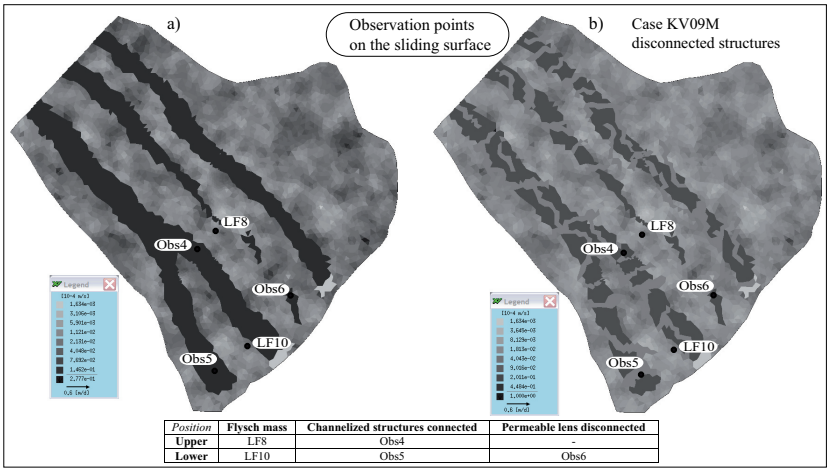

Position	Flysch mass	Channelized structures connected	Permeable lens disconnected
Upper	LF8	Obs4	-
Lower	LF10	Obs5	Obs6

Figure 5.17: Distribution of the five observation points. Observation points LF8 and Obs4 are situated in the upper part of the model, and LF10, Obs5 and Obs6 in the lower part. Obs4 and Obs5 are placed into the permeable structures. LF8 and LF10 are situated in the capacitive fraction (impermeable mass). Obs6 is placed in an isolated lens. a) Show the distribution of the permeabilities at the layer corresponding to the sliding surface as discussed in chapter 5.3.2. The scheme b) represents the permeability model used for case "KV09M", showing the disconnected characteristics of the permeable structures.

5.4.5.2 ***Results***

The initial hydrogeological situation

The water balance (table 5.3) is principally negative (outflows superior than inflows) and globally around 3800 m3/day. This tendency inverts during important precipitation periods, showing the importance of surface infiltration in the dynamic of the model. The major modelling results on a period of 884 days show that, in accordance with observations (Norbert and deCérenville S.A 1979), daily hydraulic heads vary with time from some meters in the upper part of the landslide to some tens of meters downhill. The computed hydraulic heads (appendix IX-1) at sliding surface decrease regularly from top (1100 m) to bottom (850 m) of the slide (*dh=250 m*), constraint by the important slope gradient (17°). The calculated hydraulic pressures show values from 200 KPa to 600 KPa.

Fluxes in m^3/day	
Inflow	**3770.1**
Outflow	**3790.2**
Top surface infiltration	**1613.4**
Upper limit inflow	**2011.3**
Lateral limit inflow	**146.3**
Lower limit outflow (Grande Eau river)	**3785.7**

Table 5.3: Water balance for the la Frasse model.

Analyses of the scenarios

The left plots on appendices IX-2 to IX-11 show the computed hydraulic pressures for each case study over 882 days (i.e. years 1993-1995 including two main crises). The horizontal axis gives the days of simulation; the vertical axis the computed hydraulic pressures. The right plots show the differences between

the reference case *KV09* and the considered case studies; *KV09D* to *KV09M.* The differences are positive when the computed hydraulic pressures in the reference case *KV09* are superior to the scenarios.

- ***Homogeneous distribution with the permeable features***

*In models **KV09D** – **KV09E** the capacitive fraction is homogeneous (respectively K=1E-7 m/s and 3.79E-6 m/s, i.e. mean value of KV09). The spatial connected permeable channels (K=2E-5 m/s) are maintained as discussed in section 5.4.2.2.*

KV09E. The computed hydraulic pressures in model *KV09E* are globally lower than in *KV09*. The differences between the two models is higher in the upper part (between 80 and 120 kPa) than in the lower part (30 to 50 kPa), whether if the observation points are situated into or outside the permeable features (i.e. conductive fraction). The observation point situated inside the isolated lens (i.e. Obs6) is slightly influenced (<25kPa).
This homogeneous distribution of 3.79E-6 m/s, corresponding to the mean value of the heterogeneous distribution, is not representative of the hydraulic conductivities of the system, since the responses are too weak.

KV09D. The behaviour of the resulting hydraulic pressures in model *KV09D* is different than for model *KV09E*. The main recorded differences concern the periods of strong hydrological events (i.e. the period of crises at t=180 and 550 days) generating brisk and important water inflows into the model on short time. The calculated differences may reach 200 kPa in the upper part. However, two tendencies are observable:

1. In the upper part of the slide (i.e. LF8 and Obs4) the computed hydraulic pressures are higher than those from the reference model *KV09*
2. In the lower part (i.e. LF10, Obs5 and 6) the computed hydraulic pressures are lower

On the one hand this homogeneous very impermeable medium (i.e. 1E-7 m/s) smoothes and buffers in the upper part of the model the responses of the hydraulic pressure, mainly during the crisis events. The magnitude and the breadth (i.e. time duration) of the peaks of hydraulic pressures are reduced; the importance of the hydraulic event is underestimated. The inertia and the reactivity of the system are not considered. On the other hand, in the lower part, the system is more reactive and sensitive to these low permeabilities and generates strong overpressures (up to 80 kPa). These differences seem to be proportional to the water inputs. This constitutes thus a very important observation, since the aim of numerical modelling in landslides principally focuses on the periods of crisis.

- ***Heterogeneous distribution without the permeable features***

*The model **KV09F** corresponds to the reference model KV09 but without spatial connected permeable channels.*

The computed hydraulic pressures in *KV09F* are globally slightly lower than in *KV09.* The differences are not important, but may reach 50 kPa in the lower part (e.g. Obs5).
Two tendencies are observable:

1. In the upper part of the slide (i.e. LF8 and Obs4) the overall differences are mainly recorded between the main hydrological events with differences reaching 25 kPa. No significant differences are recorded during the crises!

2. In the lower part (i.e. LF10, Obs5 and 6) a global shift of around 15 to 50 kPa is observable between models KV09F and KV09. No special behaviour is observed during or between the crises.

Therefore, one may note that the absence of these permeable features is largely felt between the hydrological crises. The important crises are well computed, but the distribution of the hydraulic pressures is slightly underestimated between these periods.

- ***Homogeneous distribution without the permeable features***

*The model **KV09G** corresponds to KV09E (homogeneous: K*=3.79E-6 m/s), *but without the spatial connected permeable channels.*

The computed hydraulic pressures in *KV09G* are globally lower than in *KV09*. No special behaviour is noticeable during or between the various hydrological events, a global shift is observed. The difference is important and may reach 140 kPa in the upper part (e.g. LF8). Note that the observation points situated in the lower part the system (i.e. Obs5 and LF10) may be slightly more sensitive to the differences, since the peaks of hydraulic pressure during the crises are more marked.
The computed hydraulic pressures are globally lower and thus strongly underestimated. This overall homogeneous low permeable distribution does not allow an accurate representation of the dynamic of the system.

- ***Heterogeneous distribution with "very permeable" features***

*In model **KV09H** the spatial connected permeable channels are extremely permeable (1E-2 m/s). The global heterogeneous distribution of KV09 is respected.*

Strong differences between *KV09H and KV09* are recorded. Three tendencies are observable:

1. In the upper part of the slide (i.e. LF8 and Obs4) the overall differences are mainly recorded during the main hydrological events (i.e. t=180 and 550 days) with differences reaching +200 kPa. The hydraulic response in model *KV09H* to these important water inputs is totally buffered. No significant differences are recorded between the crises!
2. In the lower part (i.e. LF10, Obs5) an opposite behaviour is observed, during crises the computed hydraulic pressures in model *KV09H* are superior to those in model *KV09* (differences up to –70 kPa at Obs5). Whereas, between crises, the hydraulic pressures are strongly lower.
3. The observation point inside the isolated lens (i.e. Obs6) does not record important differences.

Therefore, the permeability of these permeable features (1E-2 m/s) is overestimated; the water is too quickly driven to the lower boundary limits (outlet zones), where it is concentrated. The computed hydraulic pressures are low and smoothed (no heterogeneity; no reactivity of the system) in the upper part,

and increase strongly in the lower part, generating strong overpressures. The magnitude of the computed hydraulic pressures is thus in the lower zone much higher than in model *KV09*, with differences ranging from -60 kPa (during crises) to +40kPa (between crises). The simulations indicate that the imposed outflow boundary conditions are not adapted to drain out suitably the concentrated water.

- ***Homogeneous (very impermeable) distribution with permeable features***

*In model **KV09I** the capacitive fraction is homogeneous and extremely impermeable with K=1E-10 m/s. The spatial connected permeable channels (K=2E-5 m/s) are maintained as discussed in section 5.4.2.2.*

The calculated hydraulic pressure profiles at observation points inside the impermeable matrix (i.e. LF8 and LF10) are flat, no heterogeneity is recorded. The observation points inside the permeable channels are showing some differences; the computed hydraulic pressures are slightly higher than in model *KV09* (between -25 and -70 kPa). Obs4 in the upper part is more sensitive since presenting a difference around -70 kPa again -25 kPa recorded at Obs5. The observation point inside the isolated lens is not influenced by this impermeable distribution.
Therefore, the impermeable capacitive fraction smooth totally the reaction inside the mass (LF8 and LF 10). The distribution of the hydraulic pressures is homogeneous; the reactivity of the system is lost.

- ***Homogeneous (very impermeable) distribution with the very permeable features***

*In model **KV09J** the capacitive fraction is homogeneous and extremely impermeable with K=1E-10 m/s, with very permeable spatial connected permeable channels (1E-2 m/s).*

The calculated hydraulic pressure profiles at observation points inside the impermeable matrix (i.e. LF8 and LF10) show a strange behaviour. The values are rising endlessly as if the system were accumulating the water without draining it out; no heterogeneity is recorded.
Strong differences are observable for the points situated inside the permeable channels (i.e. Obs4 and Obs5). As previously observed in *KV09H*, in the upper part of the slide (i.e. Obs4) the strongest differences are recorded during the main hydrological events (i.e. t=180 and 550 days), with differences reaching +200 kPa, while between the crises the computed hydraulic pressures are identical to model *KV09.* In the lower part (i.e. Obs5) an opposite behaviour is observed, during crises the computed hydraulic pressures in model *KV09J* are superior to those in model *KV09* (-60 kPa). Between crises, the hydraulic pressures are lower (around +40 kPa). The very permeable channels tend to concentrate the flux in the lower part of the model. The water are not correctly drained out, the hydraulic pressures are rising too much. The observation point inside the isolated lens (i.e. Obs6) does not show important differences, except that a strongest decrease is observed at the end of the crises (i.e. t=200, 300, 600).

- ***Homogeneous "very permeable" (K=1E-2m/s) distribution without the permeable features***

*In models **KV09K** the distribution is homogeneous with K=1E-2 m/s. No special features are considered.*

The computed hydraulic pressures are showing very flat and smoothed values; no heterogeneity is recorded. The reactivity of the system is lost. This model is totally unrealistic.

- ***Heterogeneous distribution with interrupted (disconnected) permeable features***

*The model **KV09M** corresponds to the reference model KV09 but the permeable channels are disconnected.*

Some few differences are observable between the two configurations. Prima facie the disconnected character of the permeable structures might not influence the distribution of the hydraulic pressures. But in details one may observe that, for instance LF8, the computed hydraulic pressures during the crises are slightly higher (between 10 and 20 kPa) in the case of disconnected channels. These differences are of course small, but represent a column of water of 2 meters (1 kilopascal = 0.01 bars, and 1 bar = 10 meters of water), with a weight of 0.2 kg/cm^2, which is important in terms of landslide stability. In the lower part, the computed hydraulic pressures are globally slower than those for the reference model (i.e. KV09), with an accentuation during the crises (up to +40 kPa).
The observation point inside the isolated lens (i.e. obs6) indicates differences essentially between the crises (up to 20 kPa). The decrease of the hydraulic pressures is stronger and extends on a shorter period. The base flow is lower.

- ***Special case: Heterogeneous distribution with permeable features represented by discrete features elements***

*Model **KV09L** corresponds to **KV09**, but the connected permeable channels are represented by discrete features elements. In FEFLOW, 1D or 2D discrete feature elements can be inserted interactively for the modelling. Different laws of fluid motion can be defined for these discrete feature elements: 1) Darcy, 2) Hagen-Poiseuille or 3) Manning-Strickler. Discrete feature elements represent finite elements of lower dimensionality which can be inserted at edges, faces and node-connections of an existing mesh. They are useful to describe fractures in rocks, faults, boreholes, tunnels, rivers, channels, mining rooms and slopes, drainage elements, overland flows and others. For detailed information on the theoretical background see chapter 9 (p. 147) of the FEFLOW White Papers called 'Discrete feature modelling of flow, mass and heat transport processes by using FEFLOW'.*
*Thus, in model **KV09L**, the permeable features were replaced by these discrete features elements. The Darcy fluid motion law was chosen, with the following variable: K=1E-1 and section: 0.314 m2 (r=5cm). The results are purely qualitative and informative; the differences between these two ways of representation are briefly commented. This type of representation should be investigated and developed more in details.*

One may observe that the computed hydraulic pressures in model *KV09L* are lower for the upper part of the model. For the observation point situated outside these features (i.e. LF8) the differences are reaching 200 kPa during the crises, the point situated inside these features (i.e. Obs4) 350 kPa.
This tendency is totally inversed in the lower part where the calculated pressures are superior (around 50 kPa*)* in model *KV09L.* These permeable "tubes", with K=1E-1 and a section equal to 0.314 m^2, drain the water too quickly from the upper part to the lower boundary conditions, and thus generating some overpressure zones. These parameters are not representative of the system, since representing too permeable conditions. Additional parametrical adjustment have shown that with a K=1E-3 m/s and a section = 0.157 (i.e. r=2.5 cm), the hydraulic pressures are fitting better with those calculated in model *KV09.* It means that the "permeable" features may not be considered as open channels enabling fast flows. These features may rather have an intermediate permeability around 1E-3 or 1E-4.

5.4.5.3 ***Discussion***

Globally these various tests show that:

1. The models are very sensitive to the distribution of the parameters
2. The differences are very marked during the periods presenting strong hydraulic inputs; i.e. high effective infiltration
3. The upper and the lower part of the model present different hydraulic behaviours. The lower part is directly dependent on the hydrodynamical conditions of the upper part; i.e. distribution of the physical properties

The geometrical configuration of the model, the thin layer and the important differences in altitude between the BC's is a reason. These models illustrate the hydrodynamical consequences of the strong hydraulic gradients characterizing landslide areas.

Characteristics of the capacitive fraction

1. ***If Homogeneous*:** The magnitude and the breadth (i.e. time duration) of the peaks of hydraulic pressures are reduced; the importance of the hydraulic event is underestimated. The inertia and the reactivity of the system are disregarded. The computed hydraulic pressures are globally lower and thus strongly underestimated; an overall homogeneous medium does not allow representing the dynamic of the system.
2. ***If too impermeable**:* The reactivity of the system is lost (test *KV09I* with K=1E-10 m/s). Besides, the effects of an impermeable medium are also reflected inside the conductive fraction, lowering slightly hydraulic pressures.
3. ***If too permeable:*** The computed hydraulic pressures are showing very flat and smoothed values; no heterogeneity is recorded. The reactivity of the system is lost. This model is totally unrealistic.
4. ***If unsaturated conditions**:* Additional tests have shown that the reactivity of the system is strongly smoothed when simulating in unsaturated conditions. Saturated medium and confined conditions reproduce the observed nervousness of the system.

Characteristics of the conductive fraction

1. ***If conductive fraction neglected***: The differences between the models with and without permeable channels are low, but the computed hydraulic pressures may be 50 kPa smaller in the lower part of the system (model without). In terms of stability, this difference play a major role, since 50 kPa represents a column of water of 5 meters and a weight of 0.5 kg/cm^2.
2. ***If too permeable***: The dynamic of the system in the upper part is lost; too smooth reactions and no reactivity (i.e. model *KV09J, KV09H and L*). The flows are driven to the lower part and increase strongly the hydraulic pressures, as illustrated in figure 5.18. The permeability of this conductive fraction may be situated around 1E-4 m/s.
3. ***If not connected:*** The reactivity on strong hydrodynamical inputs is lost. The connectivity of the system plays an important role and mainly in the lower part. The water inputs in the upper part are not reflected in the lower part. The system is not correctly drained, and overpressure zones are generated.

The conductive fraction fills an important hydrodynamical role essentially between the main hydrological events, controlling the hydrological balance. Extremely heterogeneous media and slightly connected, smooth the effects of the strong permeabilities. Thus the low permeabilities govern the system. That is to say, if the permeable structures are isolated and disconnected (i.e. non organised in channels), it is the low permeability of the capacitive fraction (matrix) who governs the system, the lenses functioning as small reservoir slightly alimented.

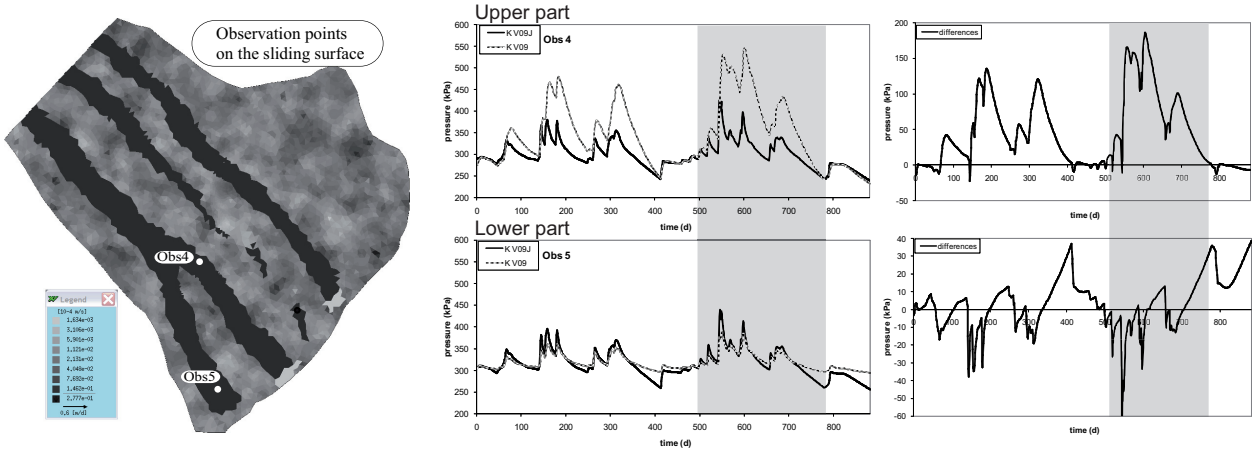

Figure 5.18: Computed hydraulic pressures at Obs4 and Obs5. The results indicate that if the permeable features are too permeable the dynamic of the system in the upper part is lost; too smooth reactions and no reactivity. The flows are driven to the lower part and increase strongly the hydraulic pressures.

On the structure of the sliding surface

Thus, the surface must be constituted by a very heterogeneous distribution of the permeability, since a homogeneous distribution buffers the hydraulic responses. The permeability of this surface may be situated between 1E-5 and 1E-7 m/s, corresponding to an intermediate to low permeability. The surface may also be constituted by permeable features, representing a coarser system of channels, with a permeability situated between 1E-3 and 1E-4 m/s. These structures may be well spatially connected, longitudinally to the sliding direction. If these structures are disconnected the flows are perturbed, and the main water inputs in the upper part are not reflected in the lower part.

5.4.6 ANALYSIS 4: VALIDATION OF THE HYDRODYNAMICAL MODEL OF THE LA FRASSE CASE

5.4.6.1 ***Procedure – Scenario***

For this analysis the horizontal draining system LFH1 presented in sections 4.3.8.5 and 4.3.8.6 is chosen. It crosses successively the zones "++" and "+" (see appendix III-5, §4.3.2.9) over 100 meters. The crossed material corresponds to the heterogeneous flysch mass; loose rocks of flysch, grey-black limestones and dolomite blocks of all sizes into a silty-clayey matrix. Some sliding surfaces could be identified. Piezometers Z205 at Cergnat, located approximately 200 meters uphill of the borehole platform is used to observe and assign the upper boundary conditions. This drainage work allows exploring horizontally the geological heterogeneity of the mass. The measured inflow rates during digging permit to identify the hydraulic

behaviours, i.e. inflow rates evolution and hydraulic head lowering at the observation wells of the system, and of course to estimate the hydraulic parameters. For this purpose sophisticated hydraulic response analysis tools are used to understand the global hydraulic behaviour (see section 4.3.8.5). The conceptual model of this drainage adit is used to perform the following simulations. The boundary conditions are discussed in section 5.4.2.3. The assigned physical parameters (i.e. hydraulic conductivity) are those of the la Frasse model.

Drainage work simulation

The simulation of this drainage work consists in the introduction of additional boundary conditions representing the layout of the drain through the model (see section 6.2.2). Each nodes intercepted by the drain corresponds a node with an assigned head boundary condition. The value corresponds to its altitude (i.e. H = z (m) =973 meters), thus corresponding to a pressure equal to zero, simulating atmospheric conditions. In addition, flux constraints are imposed to prevent from any water inflow, in order that the work is only draining and not infiltrating.

5.4.6.2 ***Results***

The total water balance, according to the size of the model, is in good agreement with the 3DFrasse model, that is to say an inflow/outflow average value equal to **220 m^3/day.** The simulated inflows are compared to the measures in figure 5.19. The results indicate that the model is well simulating the second part of the observed dynamic, that is to say the decompression phase. The residual flows are in the same order of magnitude. After 27 days the simulated outflows are around 3 l/min against 9 l/min and after 69 days 1.5 against 6.8 l/min. The difference is of a factor 3, which is relatively reasonable.

The model was nevertheless not able to reproduce the first part of the hydraulic response; the depletion phase. In the reality, the observed depletion may be due to one or two very local inflows from isolated permeable lenses, producing this first arrival.

The model allows reproducing the global hydrodynamic behaviour (figure 5.19). And except the order of magnitude of the first arrival, the decrease of the computed inflow curve is characteristic to the hydraulic response defined in section 4.3.8.6; namely a strong decrease (high *a*) and a low final inflows (strong $Qi/Qf = 6$). The logarithmic decrease of the flow rates, i.e. $Q(t) = -a\ln(t)+b$, is similar to what is observed. The factor *b* is in the meantime 10 times inferior. The expression of a low available recharge in relation to the existence of local high permeable zones is respected by the model.

Some observation may be done on the general behaviour of the system under the drainage conditions:

The system at equilibrium (without the drain) shows hydraulic heads ranging from 1018 to 964 meters and distributed from the upper boundary to the lower boundary, with computed hydraulic pressures ranging from 8443 to 9231 kPa, as illustrated in figure 5.20. Some perturbation may be observed, traducing the effect of local heterogeneity contrasts. The velocity field indicates, due to the low permeabilities, low values around 0.5 m/day (max = 1.3 m/day). Note that, a preferential flowpaths crossing the model in its centre is generated due to the permeability field distribution. The zones where the velocities may be considered null are in white shaded; they are distributed more or less randomly and local. These hydraulic properties represent a plausible realization of the reality. In this sense the generated permeability field in section 5.3.2 is satisfactory.

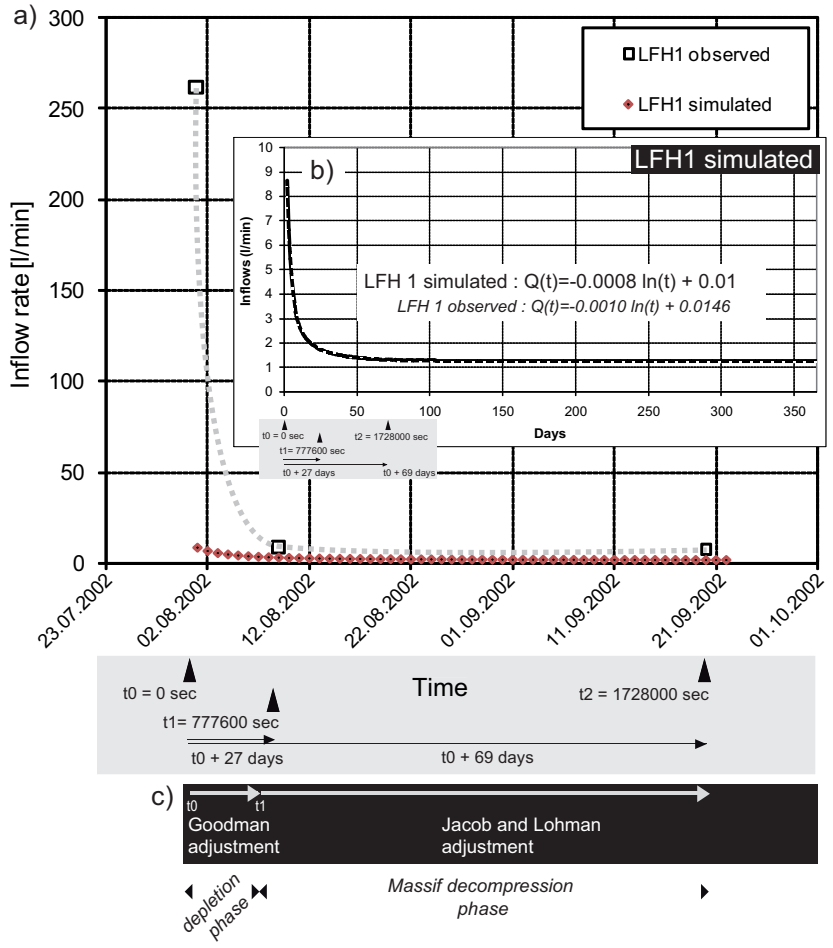

d) Calculated ratios

	Qi [m3/s]	Qf [m3/s]	Qi/Qf	a
LFH1 observed	0.00436	0.00015	29	0.0010
LFH1 simulated	0.00014	0.00002	6	0.0008
Data from Maréchal 1998				
Tectonized zone of the Mont-Blanc tunnel	*0.03*	*0.003*	*10*	*0.0026*
Granit zone Mont-Blanc tunnel	*0.035*	*0.015*	*2*	*?*
Veglia zone of Simplon tunnel	*0.0035*	*0.001*	*4*	*0.0003*
Antigorio zone of Simplon tunnel	*0.05*	*0.005*	*10*	*0.0077*

Figure 5.19: a) Comparison of the observed and computed inflow rates in the drainage work LFH1. Inflows characterized by a logarithmic decrease of the flow rates (i.e. Q(t)= -aln(t)+b). b) Computed inflow rates for 3DLFH1. c) Logarithmic adjustments. d) Calculated ratios and compared to case studies in Alpine crystalline contexts (Maréchal 1998)

The numerical results with the introduction of the drain indicate a redistribution of the hydraulic parameters. The hydraulic heads are strongly influenced by the drainage effects of the drain, attracting the underground flow (right schemes in figure 5.20). The hydraulic pressures are ranging from 8299 to 9231 kPa, and indicate a lowering of around 200 kPa at the level of the drain. The velocity field are presenting the most important differences; the model indicates that in the most part of medium the flow may be considered as insignificant. In the meantime, the redistribution has generated a high velocity zone extending from the north extremity of the drain towards the upper boundary condition, with an average value of 10 m/day. This preferential flowpath is likewise surely corresponding to a more permeable zone of the permeability field. The effects have on the one hand reduced the hydraulic pressures in the lower zone, but on the other hand allowed a considerable increase in the upper zone (ten times), thus creating new overpressure zones. These new flowpaths may generate unexpected serious instability phenomena; such as local settlings,

concentration of overpressures, or more severely, generation of new sliding surfaces. The response of the system under the introduction of new boundary conditions, as already discussed in section 5.4.4, may generate opposite negative effects.

Validations:

- The generated hydraulic conductivity field in section 5.3.2 is validated
- The proposed hydrodynamic model in section 4.3.11.3 is validated

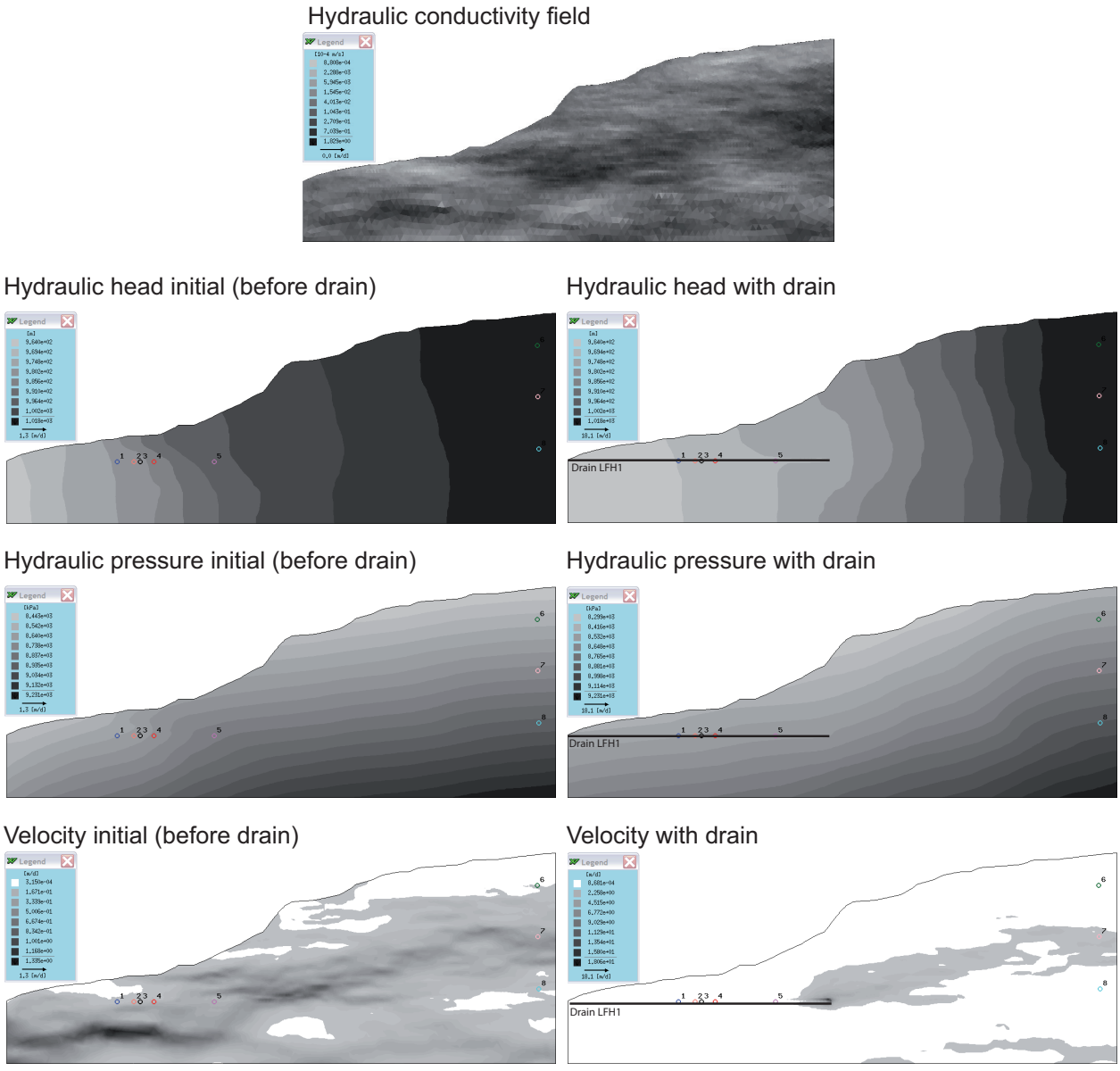

Figure 5.20: Results of the flow modelling for 3DLFH1 model. Computed hydraulic pressures distribution, computed hydraulic heads distribution and computed velocity fields, without and with the drain

5.4.7 SYNTHESIS ON FLOW MODELLING

5.4.7.1 Importance of the integration of the geological heterogeneity

Heterogeneity and connectivity. One of the principal consequences of geological heterogeneity is that it can lead to significant variations of the fluid velocities on short distances and create preferential pathways more or less independent. The existence of spatial heterogeneity of the hydraulic conductivities involves a spatial heterogeneity of the field velocities, and also a heterogeneous distribution of the resulting hydraulic pressures fields. The organization of the flows depends on the heterogeneity of the hydraulic properties and their spatial correlation. Flow channeling occurs in aquifers at all scales, from centimetre- to kilometre-scale, and strongly affects the distribution of hydraulic pressures. The various 2D and 3D simulations have shown that the heterogeneous media may be characterized by three types of fluxes: distributed, channelized and intermediary. The obtained results emphasized the importance of including heterogeneous distribution of the permeabilities and the spatial correlation structure in groundwater flow simulations, since the hydraulic heads and the permeability are linked. The head variance is strongly dependent on the correlation distance of the log conductivity covariance function. Connectivity of high conductivity (K) paths is important because it can lead to channeling which can reduce or increase the computed hydraulic pressures significantly. Finally, connectivity of high permeability paths is recognized as important but still has not been properly quantified in the groundwater literature (Knudby and Carrera 2005 and 2006).

5.4.7.2 On the la Frasse case

The two analyses performed on the la Frasse case studies permitted to:

1) To show the importance of serious hydrological events on the distribution of the flows
2) To show the importance of the spatial connectivity
3) To identify the main hydrogeological and structural characteristics of the sliding surface
4) To show the importance of considering the observed heterogeneity in flow modelling
5) The incidences of the particular geometrical characteristics (i.e. strong hydraulic gradients)
6) To validate the generated hydraulic conductivity field in section 5.3.2
7) To validate the proposed hydrodynamic model in section 4.3.11.3

5.4.7.3 Implications for flow characterization

In this study two types of permeable structures are identified: type 1) *primary structures (connected structures)* and type 2) *secondary structures (disconnected structures, i.e. isolated lenses)*. The first one drives efficiently the flows and the second rather concentrates the flows and increases locally the hydraulic pressures (overpressures effects). Thus, for site characterization purposes, these observations likewise lead to some fundamental questions:

1. ***How could these structures be identified one-dimensionally during the digging of a tunnel for instance?***

Thanks to hydraulic response analysis tools exposed in section 4.3.8. If the inflows, directly after digging, decreases briskly, the perforated structure may be of type2, i.e. isolated lenses, slightly alimented. If after

digging an important base flow is maintained the type1 is to be favoured, meaning that the structure is permanently alimented. In that case direct connections with surface have to be considered transporting the water directly to the underground structures. The system will be sensitive to the precipitation rates.

2. Recharge? How are these structures alimented?

Type1 is rather sensitive to the inputs provided by the BC's of the system (lateral and/or surface infiltration). While, type 2 is rather linked to the impermeable fraction of the mass (i.e. capacitive function). It is characterized by a low recharge, absence of direct connections with the surface, and will not be sensitive to strong precipitation events.

Finally, these studies on two and three dimensional heterogeneous models allowed the observations of some interesting phenomena concerning the relations *"or non-relations"* between hydraulic conductivity structures and hydraulic pressures. It permits to draw some important considerations in relation with the previous chapters (i.e. geological characterization in chapter 4).

5.5 Conclusions

This chapter presented how to use the information got from the geological characterization; how to conceptualize a problem, and how to integrate the information in flow modelling. This chapter allows clarify the following demands:

What is a hydrogeological conceptual model? And how to use it?

Many scientists have still difficulties finding consensus on defining terminology and guiding principles on hydrogeological conceptual modelling. A conceptual model is a simplification of a problem, where the associated field data are organised in such a way, that the system can be analysed more readily. A hydrogeological model may be describe as a framework that serves to analyse, qualitatively and quantitatively, subsurface flow at a site in a way that is useful for review and performance evaluation. Thus, when numerical modelling is considered, the conceptual model should define the hydrogeological structures relevant to be included in the numerical model given the modelling objectives and requirements, and help to keep the modeller tied into reality and exert a positive influence on his subjective modelling decisions. The nature of the conceptual model determines the dimensions of the model and the design of the grid. Therefore, an important part of the conceptual model for groundwater modelling is related to the geological structure and how this is represented in the numerical model.

How to represent the reality? Notion of stochastic field generation

The spatial distribution of rock properties in porous media, such as permeability, is often strongly variable. Therefore, these properties may be considered as a random field. However, this heterogeneity is correlated frequently on correlation length scales comparable to geological lengths (for example, scales of sand bodies or facies). To solve various engineering problems, numerical models of a porous medium are often used. The use of geostatistical methods permits to represent the spatial heterogeneity of the physical parameters.

The heterogeneity of the local hydraulic conductivity K (m/s) is typically described as a random field with a given statistical distribution (often assumed to be lognormal) and a covariance function. The transcription of the observed heterogeneity into statistic parameters is done after detailed geological characterisation. These methods were applied on the la Frasse case study, and the generated permeability fields were validated thanks to numerical tests.

Flow modelling, 2D or 3D?

Two-dimensional modelling (2D) of a three-dimensional natural system (3D) constitutes an advantageous simplification (e.g. preparation of input data and iteration velocities), but can be unacceptable concerning the accuracy of the results. In this study, two- and three dimensional models were used. On the one hand, sensitivity analyses to define the link between input and output data (i.e. hydraulic conductivity and hydraulic pressures) were performed thanks to two-dimensional theoretical models. On the other hand, a three-dimensional model of the la Frasse landslide was used to test several scenarios of heterogeneity, to define some important characteristics of the geological structures of the mass. And finally, it is used in chapter 6 to evaluate the efficiency of a drainage gallery, presenting thus a direct application.
In table 5.4, the four different numerical models used in this chapter are briefly summed up. According to the purchased objectives, a model is conceptualized and designed. Each model is characteristic to a specific investigation scale. The difficulties in the elaboration of the model (e.g. model building, boundary conditions assessment, etc) may also vary seriously from case to case. And besides the simulation times may equally be various, ranging from 1 minute to 1 week. Thus, the choice of the dimension of the model depends on the problems to be solved, on its size, on the capacity and the speed of the computers, and the financial aspects. Various experiences in modelling natural environment problem, such as unstable mass, showed that the problem must be handled in three-dimension and may be treated thanks to transient saturated/or unsaturated models.

Sensibility of the models?

The various numerical tests, have clearly demonstrated that to simulate accurate responses, the main features of the medium have to be represented; i.e. heterogeneity and connectivity of the hydraulic conductivities. The connectivity of the system may be represented roughly thanks to arbitrary channels, but is essential for the dynamic of the system.

6. Incidences on slope stabilization techniques

6.1 Introduction

6.1.1 Effects of hydraulic pressure on the mechanical behaviour of the slope

Groundwater flow usually causes a worsening of the slope stability condition. The principal reasons for the water influence on slope stability are: the variation of the pressure acting on the joint and the pores of the geomaterial (i.e. rock fabric), and the destruction, transport or change in the consistence degree of this fabric. The water pressure reduces the available shear resistance on the discontinuities and determines active forces which tend to induce sliding. The increased pore pressure reduces the normal stress and thus the frictional strength. Internal friction is due to the grains of the material rubbing against each other. The friction depends on (1) how slick the grains are (i.e. the coefficient of friction or angle of internal friction), which depends on the particular material, and (2) how hard the grains are being forced against each other by gravity (i.e. the normal stress). In addition, the moisture variations of some rocks may also decrease the strength and deformation features of the intact rock.

Thus, the equilibrium condition of a slope depends on the field water pressure distribution, i.e. the spatial distribution of potentials, flows and hydraulic conductivities. Landslides occur when the driving forces tending to pull the soil and the rock downhill equal or exceed the resisting forces holding it in place. The driving forces are either that part of the weight of the soil and rock acting parallel to the slope, or that part of the weight that tries to rotate the material out of the slope. The driving forces increase with increasing slope steepness and rock density, and, in the case of rotational failures, with increasing slope height. The resisting forces are due to: (1) the strength of the slope materials; (2) strength added by roots; and (3) buttressing of the lower part of the slope by materials that have to be pushed or rotated out of the way before the upper part of the slope can move.

Pore-water pressure increases may be directly related to rainfall infiltration and percolation, or may be the result of the build-up of a perched or groundwater table (Terlien 1998). The response of the material involved is largely dependent on its permeability. In high-permeability soils the build-up and dissipation of positive pore pressures during intense precipitation events could be very rapid (Johnson and Sitar 1990). In these cases slope failures are caused by high intensity rainfall and antecedent rainfall has little influence on landslide occurrence (Corominas 2001). On the contrary, in low-permeability soils slope failures are caused by long duration-moderate intensity rainfall events. The reduction in soil suction and the increase in pore water pressures due to antecedent rainfall is considered as a necessary condition for landslide occurrence (Sanderson et al. 1996; Wieczorek 1987).

6.1.2 Landslide remedial measures

Terzaghi (1950) has written that “if a slope has started to move, the means for stopping movement must be adapted to the processes which started the slide”. For example, if erosion is a causal process of the slide, consideration regarding remediation would include armoring the slope against erosion, or removing the source of erosion. An erosive spring can be made non-erosive by either blanketing with filter materials or drying up the spring with horizontal drains, etc. Landslides are so varied in type and size and always dependent upon special local circumstances, that for a given landslide problem there is more than one method of prevention or correction that can be successfully applied. The success of each measure depends to a large

extent on the degree to which the specific soil and groundwater conditions are correctly recognized in investigation and applied in design. As many of the geological features, such as sheared discontinuities, are not well known in advance, it is better to put simple or temporary remedial measures; i.e. the design has to be flexible enough for changes to be made during or subsequent to construction of the remedial works.

Correction of an existing landslide or the prevention of a pending landslide is a function of a reduction in the driving forces or an increase in the available resisting forces. Any used remedial measure must provide one or both of the above results. Many general reviews of the methods of landslide remediation have been made. The interested reader is particularly directed to Hutchinson (1977), Zaruba and Mencl (1982), Bromhead (1992), Schuster (1992), Fell (1994) and Popescu (1996). In order to help include relevant information on landslide remediation in a standard format in the Landslide Report (WP/WLI 1990), the IUGS WG/L Commission on Landslide Remediation has prepared a short checklist of landslide remedial measures (see table 6.1). The measures are arranged in four practical groups, namely: modification of slope geometry, drainage, retaining structures and internal slope reinforcement. Hutchinson (1977) has indicated that drainage is the principal measure used in the remediation of landslides, with modification of slope geometry the second most commonly used method. These are also generally the least costly of the four major categories, which is clearly a factor in their wide use. Experience shows that while one measure may be dominant, most landslide remediation involves the use of a combination of two or more from the major categories.

During the early part of the post-war period, landslides were generally seen to be "engineering problems" requiring "engineering solutions", involving correction by the use of structural techniques. This structural approach initially focused on retaining walls, but has subsequently been diversified to include a wide range of more sophisticated techniques including passive piles and piers, cast-in situ reinforced concrete walls and reinforced earth retaining structures. When properly designed and constructed these structural solutions can be extremely valuable, especially in areas with high loss potential or in restricted sites. However, fixation with structural solutions has in some cases resulted in the adoption of over-expensive measures that proved to be less appropriate than alternative approaches involving slope geometry modification or drainage (Jones and Lee 1994).

Over the last several decades there has been a notable shift towards "soft engineering" non-structural solutions including classical methods such as drainage and modification of slope geometry but also some novel methods such as lime/cement stabilization, grouting or soil nailing (Powel 1992).

1. Modification of slope geometry
1.1 Removing material from area driving the landslide (with possible substitution by lightweight fill)
1.2 Adding material to area maintaining stability (counterweight berm or fill)
1.3 Reducing general slope angle
2. Drainage
2.1 Surface drains to divert water from flowing onto slide area (collecting ditches and pipes)
2.2 Shallow or deep trench drains filled with free-draining geomaterials (coarse granular fills and geosynthetics)
2.3 Buttress counterforts of coarse-grained materials (hydrological effect)
2.4 Vertical (small-diameter) boreholes, pumped or self draining
2.5 Vertical (large-diameter) wells with gravity draining
2.6 Sub-horizontal or sub-vertical boreholes
2.7 Drainage tunnels, galleries or adits
2.8 Vacuum dewatering
2.9 Drainage by siphoning
2.10 Electro-osmotic dewatering
2.11 Vegetation planting (hydrological effect)
3. Retaining structures
3.1 Gravity-retaining walls
3.2 Crib-block walls
3.3 Gabion walls
3.4 Passive piles, piers and caissons
3.5 Cast-in-situ reinforced concrete walls
3.6 Reinforced earth-retaining structures with strip/sheet- polymer/metallic-reinforcement elements
3.7 Buttress counterforts of coarse-grained material (mechanical effect)
3.8 Retention nets for rock slope faces
3.9 Rock fall attenuation or stopping systems (rock trap ditches, benches, fences and walls)
3.10 Protective rock/concrete blocks against erosion
4. Internal slope reinforcement
4.1 Rock bolts
4.2 Micropiles
4.3 Soil nailing
4.4 Anchors (pre-stressed or not)
4.5 Grouting
4.6 Stone or lime/cement columns
4.7 Heat treatment
4.8 Freezing
4.9 Electro-osmotic anchors
4.10 Vegetation planting (root strength mechanical effect)

Table 6.1: A brief list of landslide remedial measures after Popescu (2001).

The cost of non-structural remedial measures is considerably lower when compared with the cost of structural solutions. On the other hand, structural solutions such as retaining walls involve opening the slope during construction and often require steep temporary cuts. Both these operations increase the risk of failure during construction, due to oversteeping or increased infiltration from rainfall. In contrast, the use of soil nailing as a non-structural solution to strengthen the slope avoids the need to open or alter the slope from its current condition.

6.1.3 Drainage: a "soft engineering" solution

Drainage is often a crucial remedial measure due to the important role played by pore-water pressure in reducing shear strength. Because of its high stabilization efficiency in relation to cost, drainage of surface water and groundwater is the most widely used and generally the most successful stabilization method. As a long-term solution it suffers greatly because the drains must be maintained if they are to continue to function (Bromhead 1992). Surface water is diverted from unstable slopes by ditches and pipes. Drainage of the shallow groundwater is usually achieved by networks of trench drains. Drainage of the failure surfaces, on the other hand, is achieved by counterfort or deep drains which are trenches sunk into the ground to intersect the shear surface and extending below it. In the case of deep landslides, often the most effective way of lowering groundwater is to drive drainage tunnels into the intact material beneath the landslide. From this position, a series of upward-directed drainage holes can be drilled through the roof of the tunnel to drain the toe of the landslide. Alternatively, the tunnels can connect up a series of vertical wells sunk down from the ground surface. In instances where the groundwater is too deep to be reached by ordinary trench drains and where the landslide is too small to justify an expensive drainage tunnel or gallery, bored sub-horizontal drains can be used. Another approach is to use a combination of vertical drainage wells linked to a system of sub-horizontal borehole drains. Schuster (1992) discusses recent advances in the commonly used drainage systems and briefly mentions less commonly used, innovative means of drainage, such as electro-osmotic dewatering, vacuum and siphon drains. Buttress counter forts of coarse-grained materials placed at the toe of unstable slopes are often successful as a remedial measure. They are listed in table 6.1, under both "Drainage" when used mainly for their hydrological effect and "Retaining Structures" when used mainly for their mechanical effect.

6.2 La Frasse case study drainage evaluation

6.2.1 Introduction

The technical association «NCG+EPFL pour l'étude du glissement de la Frasse» provided in 2004 a final report concerning the stabilization of the La Frasse landslide (NCG+EPFL 2004). Transient hydrogeological and coupled hydro-mechanical modelling allowed the simulation of the behaviour of the La Frasse landslide mass during a crisis and the evaluation of several remediation designs (vertical boreholes equipped with pumps or pipes drilled from a gallery). The main results concerning the potential effect of a drainage system during a crisis showed that a drainage gallery reduces horizontal displacements down to 5% of the values modelled during the crisis without any confortation works. Spacing between the pipes limited to about 10 meters was recommended. These previous models incorporated roughly the heterogeneous character of the slide, but due to the scale of study (regional scale of the landslide), the size of the geological structures was fairly too large. Therefore, while the results only had a meaning at a global scale, it was recommended to perform a second analysis at a local scale, in order to define the optimum spacing between the pipes.

The final decision of the conception of a drainage gallery below the sliding surface of the landslide was taken in 2005. In 2006, the Geolep/EPFL was mandated for the hydrogeological modelling in collaboration with GeoMod SA, who was in charge with the geomechanical aspects. In comparison with the simulations undertaken in the previous report (NCG+EPFL 2004), the outline of the drainage gallery, the spatial distribution of the underground permeabilities with the integration of the geological heterogeneity, and the position of the substratum were adjusted.
A key element of this study is the incorporation of the geological heterogeneity into models, treated at the scale of a drainage work (local scale). This new local model is presented and largely discussed in sections 5.3.2 and 5.4.2.2.

This study presents the new hypothesis admitted in the calculation of the impact of the gallery execution project as well as the main results. These models evaluate the efficiency of the drainage gallery below the sliding mass during a crisis in terms of reduction of the deformation velocities and increase of the factor of safety of the landslide. While the present study represents the continuation of the final report concerning the stabilization of the La Frasse landslide, references to NCG+EPFL (2004) and Tacher et al. (2005) will be regularly made.

6.2.2 PRESENTATION OF THE PROJECT

The projected gallery will run over a total length of 725 meters. The estimated costs are around 16 mio CHF. The work began the 20th of August 2007, and in April 2008 yet 75% (550 meters) were realized, corresponding to a daily average velocity of 3 m/days. The several stakeholders are the followings:
Municipality of Leysin (R. Calderini), of Ormont-Dessus (Ph. Grobety), of Ormont-Dessous (Ph. Blatti)an of Aigle (J. Devaud). The « Voyer 3° arrondissement » (J. Francey). De Cérenville SA (C.Tartuffi, engineer), Norbert Géologues SA (E. Marclay, geologist), Groupe d'experts Crottaz-Giacomini-Kälin, EFA+C Ingénieurs géomètres officiels S (E. Borloz), ECF – SESA (Ph. Hohl, president),C.-A. Davoli, secrétaire ECF – SESA, ECF – SR (J.-P. Bruand), métré et suivi financier (P.-A. Franzosi), SR (A. Giovannoni), resp. internet site SESA (J.-M. Zellweger), SDBEG (P.-F. Décoppet, project leader), SDBEG (M. Soldini, project engineer), SDBEG (F. Philippossian, geologist), SDBEG (G.Grosjean, geologist), E. Borloz (official geometer), M. Meury (consortium project leader), J.-D. Gugger (consortium technical director), G. De Gasperis (consortium agent), P. Echenard (consortium work comity), P. Cartagenova (consortium geometer), COMSEC gaz (M. Vercelloni, coordinator) and G. Hauri, (security).

6.2.3 DRAINAGE GALLERY

The efficiency of the drainage gallery to lower pore waters pressures and stabilize unstable slopes has been widely documented in a number of case studies; Dutchman' s Ridge (Moore and Imrie (1995), the Taren slide (Martin and Warren, 1992), Campo Valle Maggia (Bonzanigo et al. 2000 and 2001) and the Pacific Palisades area (Krohn, 1992). Similarly, the decision was made to construct an 725 meters long drainage adit in the bedrock below the La Frasse slide mass (see design in figure 6.1). Underground water is evacuated from unstable slope through a network of pipes connected to a drainage gallery. This gallery is situated below the sliding surface, into the intact or stabilized material, in order not to be affected by the landslide movements. The pipes directed upward are thus draining naturally the water thanks to gravity, avoiding the use of pumping systems. This configuration enables an optimal stabilization while the water from the shear surface is intercepted and evacuated. In addition to that it is possible at any moment to add pipes and so to increase the drainage effect.

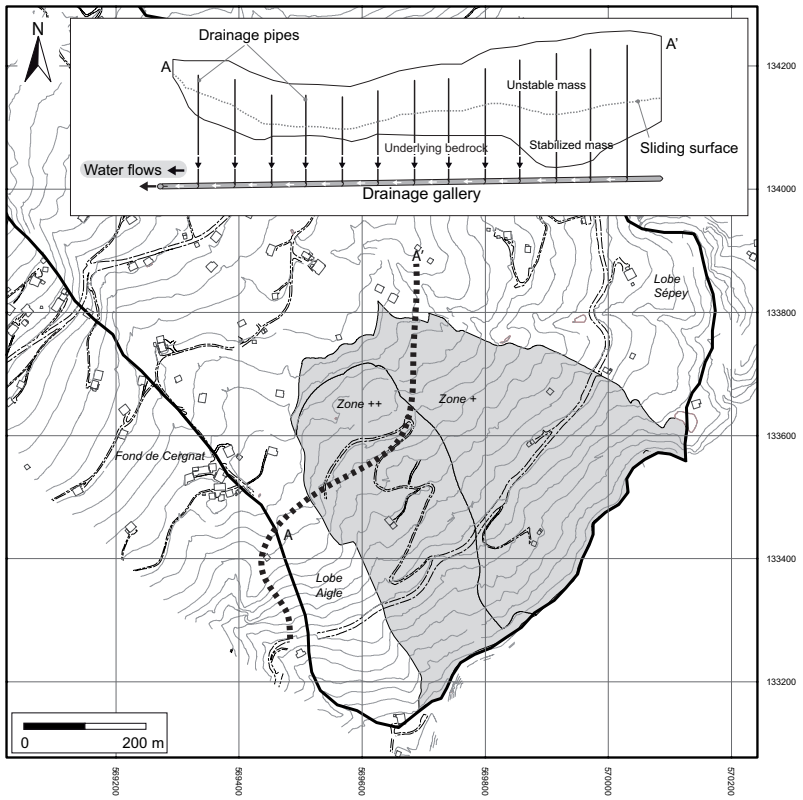

Figure 6.1: Location and principle of the projected drainage gallery. Underground water is evacuated from unstable slope through a network of pipes connected to a drainage gallery situated below the sliding surface, into the underlying bedrock.

The simulation of this drainage gallery consists in the introduction of additional boundary conditions representing the pipes through the model (figure 6.2). The drainage gallery is not represented in the model because it is situated outside the physical limits. At each slice intercepted by a pipe corresponds a node with an assigned head boundary condition. The value corresponds to the altitude of this node on this slice $H = z$ *(m),* i.e. zero pressure, simulating atmospheric conditions.

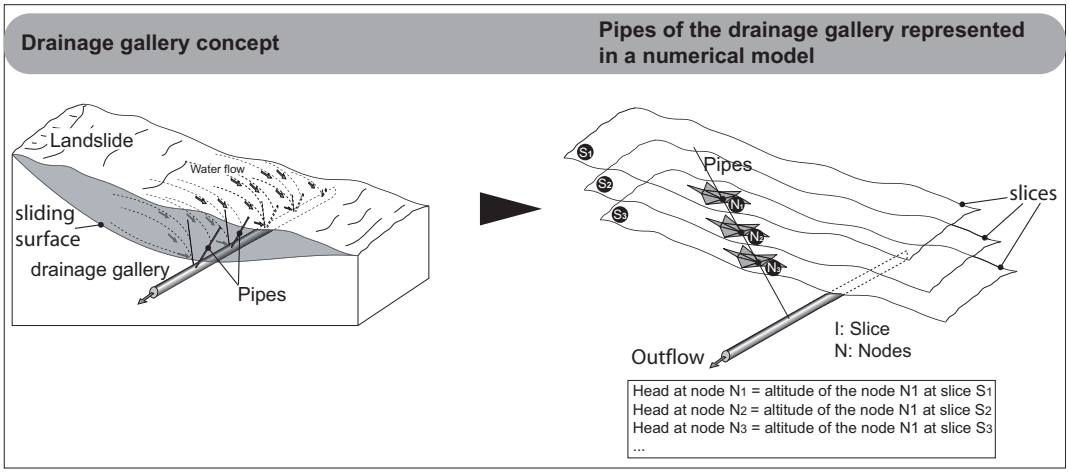

Figure 6.2: Principle of boundary conditions attribution for the simulation of a drainage gallery. For principle see also figure 2.

6.2.4 HYDROGEOLOGICAL MODELLING

The conceptual model as well as the boundary and initial conditions are presented in section 5.4.2.2, since this model was already used for numerical sensitivity tests.

6.2.5 HYDRO-MECHANICAL MODELLING

The geometry, the physical parameters and the constitutive laws used in the present model are identical to the hydro-mechanical coupling models of la Frasse 2002-2003 except the hydraulic permeabilities and the position of the bedrock. As the theoretical framework is largely discussed in Tacher et al. (2005) and Commend et al. (2004), it won't be developed in this section. The finite element geomechanical calculation was carried out with Z_Soil v6 (2007). A 30'000 finite element mesh distributed on 9 layers is used to perform the hydromechanical analyses: The sliding mass (1 to 6), the stabilized mass (7 and 8) and the bedrock (9). Drucker-Prager and Cap models are the elastoplastic constitutive laws. In order to conserve the mass and momentum of the fluid and solid phases in a two-phase saturated medium, interactions between the pore-water pressures and the mechanical behaviour of the solid skeleton may be obtained with a Biot-type mathematical formulation (Biot 1956). Pressure boundary conditions are interpolated from the hydrogeological model. The bedrock located under the flysch is considered fixed.

6.2.6 FACTOR OF SAFETY

The factor of safety (FoS) of a slope is the ratio of resisting forces to driving forces. If the factor of safety is less than or equal to 1 (i.e. FoS $\leq$1), the slope will fail. If FoS is significantly greater than 1, the slope will be quite stable. However if FoS is only slightly greater than 1, small disturbances may cause the slope to fail. For example, if FoS = 1.05, the slope's strength is only 5% greater than the driving forces, and heavy rain for example or seismic shaking, may easily cause it to fail.

6.2.7 HYDRO-MECHANICAL MODEL DESCRIPTION

Concerning the hydro-mechanical (HM) modelling, an initial state of stress induced by the soil weight at rest is first computed in the HM model. The initial hydraulic conditions are those induced by the groundwater table. The groundwater pressures resulting from the hydrogeological simulation are introduced as nodal boundary conditions in the geomechanical model. They vary over time at the edge of all layers of the model, except the first one, and therefore induce displacements.

6.2.7.1 Geomechanical parameters distribution

On the basis of the geotechnical investigations, it was decided to consider that all soil layers apart from the slip surface (layer located between 35 and 45 meters depth in the lower part of the slide) would follow a Drucker-Prager law. The behaviour of the slip surface was carefully considered and two elastoplastic constitutive models were adopted: the Drucker-Prager and Caps models as further discussed. In order to calibrate the model parameters, laboratory tests including drained and undrained triaxial tests were carried out on the samples obtained from two additional boreholes drilled in 2002. In Tacher et al. (2005) the numerical simulations of triaxial tests compared to the experimental results are presented. The material parameters obtained at the laboratory scale (triaxial examples) are supposed to be representative of the material behaviour at the in situ scale. The geomechanical parameters based on a series of laboratory and in situ tests are summarized in table 6.2.

	Parameter	Unit	Above sliding plane	Sliding plane	Below sliding plane
Identification	Unit weight, γ	kN/m^3	19.9	19.9	21.3
	Void ratio, e_o	-	0.4	0.4	0.3
	Permeability, K	m/s	9E-8 to 1E-4	9E-8 to 1E-4	9E-8 to 1E-4
Elasticity	Young's modulus, E	MPa	80	80	100
	Poisson ratio, ν	-	0.3	0.3	0.3
Plasticity	Friction angle, ϕ	°	30	25	33
	Cohesion, c	kPa	5 to 20	2	30
	Dilatance angle, ψ	°	30	25	33
	Plastic compressibility, λ	-	-	0.07	-
	OCR	-	-	Normal	-

Table 6.2: Material parameters of the landslide mass and sliding surface.

6.2.8 RESULTS

Water balances and computed hydraulic heads and pressures with and without drainage are presented in table 6.3 and appendix IX-1. Figure 6.3 presents the computed hydraulic heads and pressures along two sections: a) Along the drainage gallery layout and b) north-south across the whole model. All observations are made at the sliding surface (layer 9 in the hydrodynamic model). Figure 6.4 presents the computed displacements at the end of the crisis with and without drainage. Finally, figure 6.7 presents the computed factor of security (FoS).

Fluxes in m^3/day	**Without drainage**	Variant 1 (15m)	Variant 2 (30m)	Variant 3 (60m)
Inflow	**3770.1**	4623.4	4545.1	4439.7
Outflow	**3790.2**	4617.9	4558.7	4454.9
Top surface infiltration	**1613.4**	1614.4	1614.4	1614.4
Upper limit inflow	**2011.3**	2859.4	2781.2	2671.2
Lateral limit inflow	**146.3**	149.6	149.5	154.1
Lower limit outflow (Grande Eau river)	**3785.7**	2460.3	2564.6	2736.9
Outflow from pipes	**-**	2157.6	1986.4	1705.2
Contribution of the pipes	**-**	46.7%	43.6%	38.3%

Table 6.3: Water balances from the undrained model and the three drainage variants.

6.2.8.1 Without drainage

Hydrogeological situation – water balance. In transient modelling the inflows are not necessary equal to the outflows. The difference comes from the storage capacity of the aquifer. The global hydraulic budget shows that the peaks of outgoing flow in the la Grande-Eau river occur only a few days after the peaks of inflow. More than a third (43%) of the inflow results from the surface infiltration, the sold from the borders of the slide. This proportion clearly inverts during important precipitation periods or snow melting. During these periods, the hydraulic budget is more chaotic since buffer effect of the flysch substratum is dominated by the unsmoothed surface infiltration signal (Tacher et al. 2005). The water balance is principally negative (outflows superior than inflows) and globally around 3800 m3/day. This tendency equally inverts during important precipitation periods, showing the importance of surface infiltration in the dynamic of the model. The major modelling results on a period of 884 days show that, in accordance with observations (Norbert and deCérenville S.A 1979), daily hydraulic heads vary with time from some meters in the upper part of the landslide to some tens of meters downhill. The computed hydraulic heads at sliding surface (figure 6.3, plot III) decrease regularly from top (1100 m) to bottom (850 m) of the slide (dh=250 m), constraint by the important slope gradient (17°). The calculated hydraulic pressures show values from 200 kPa to 600 kPa. Along the drainage work (figure 6.3, plot I), hydraulic heads are around 1000 m, and the computed hydraulic pressures are distributed around 400 kPa (figure 6.3, plot II).

The computed displacement fields in figure 6.4 (A) show a maximum displacement of 101 cm reproducing in that way the order of magnitude of the in situ measured displacement histories at the RC 705 (2.04 meters). The comparison between computed and observed values shows a good agreement qualitatively, in the meantime, the models underestimate the in situ displacements by a factor of two. The continuous nature of the model, as no sliding interfaces have been introduced in the mesh, can explain it (Commend et al. 2004). The spatial displacements of the landslide are reproduced satisfactorily and the model is ready to estimate the influence of a drainage gallery work on its behaviour.
The factor of safety evaluated at the end of the crisis (figure 6.7) by decreasing progressively the cohesion and the tangent of the internal soil friction angle, gives a reference value of 1.05.

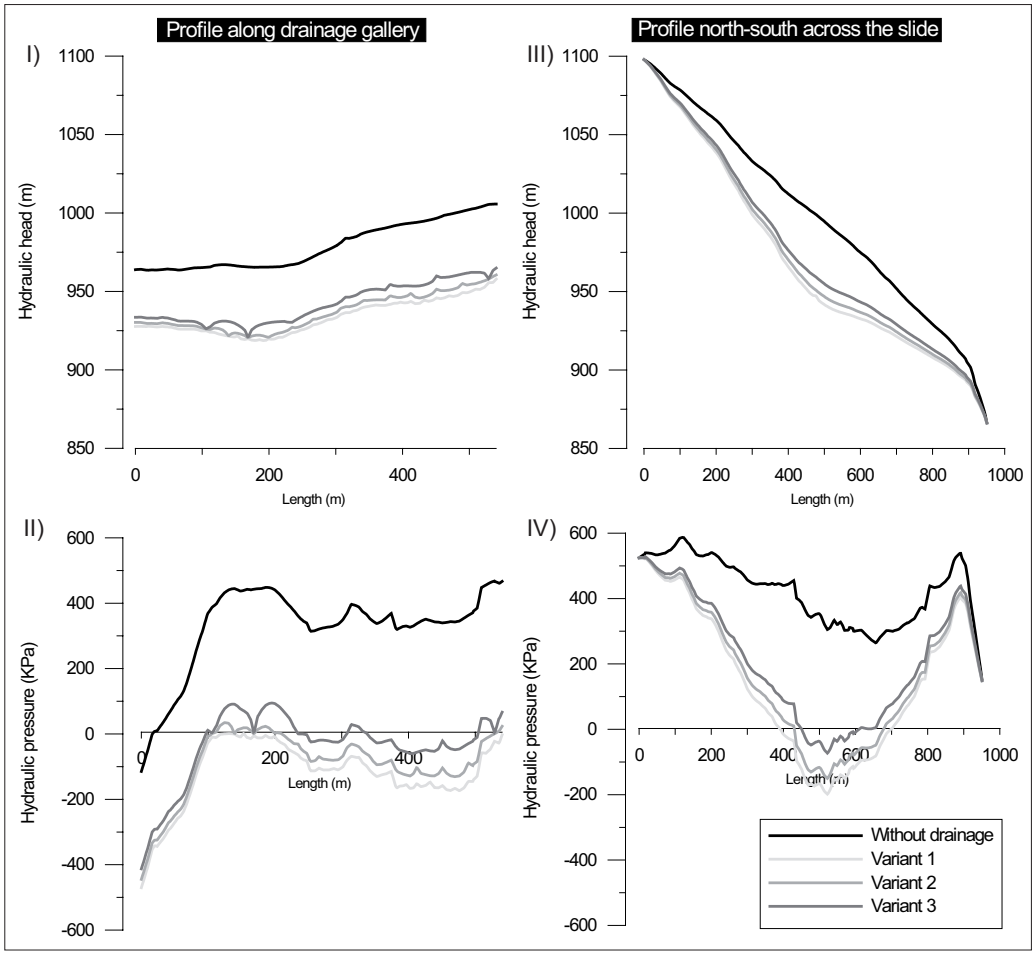

Figure 6.3: Computed hydraulic heads and pressure of variant 1 to 3 at sliding surface for two profiles. See figure 6.1 for the location of the profile along the drainage gallery (A-A'). The second profile (North-South) is passing through piezometers LF3 and I301.

6.2.8.2 ***With drainage***

Influence of drainage on the hydraulic heads and pressures
In Tacher et al. (2005) a sensitivity analysis is carried out in order to estimate the optimum spacing between wells or drains with a schematic 3D model in which connected heterogeneities are about 10 meters wide. The results show that 10 meters spacing is able to control the temporal head fluctuations between the wells within a range of some meters. This range increases quickly with the spacing. 10 meters spacing is thus considered as the most favourable mean value. In practice, wells or drains will have a larger spacing in a

first construction stage and others will be added depending on the real encountered conditions. In this study three variants are considered:

1. Variant 1: 32 pipes with a mean spacing of 15 meters
2. Variant 2: 16 pipes with a mean spacing of 30 meters
3. Variant 3: 8 pipes with a mean spacing of 60 meters

Regarding the water budget (table 6.3) we can observe that the global water balance increases as soon as the new boundary conditions representing the pipes are introduced. Functions of the number of pipes introduced (8, 16 or 32), the water budget increase from 3770.1 to 4623.4 m3/day (+19%). From hydrogeological point of view these values represent an aberration. The model tends, for numerical reasons, to overestimate the in/outflows where the head is fixed, in order to maintain the imposed heads (upper limit boundary and drainage pipes). Figure 6.5 illustrates this phenomenon, the addition of new boundary conditions (scheme 2) modifies the hydraulic gradient i (i2>>i1). In numerical models, the results are highly sensitive to boundary conditions, even when in reality; hydraulic gradients at limits don't change. In terms of discharge, the contribution of the pipes in the outflows can seem consequent (38.3% to 46.7%), but due to the geometry and mesh dimension of the model, the simulated drainage adit presents an important hydraulic barrier. The differences between the variant 1 (32 pipes) and variant 3 (8 pipes) in terms of evacuated discharges by the pipes is low, around 550 m3/day (21%), which is valueless in comparison to the global discharges. In spite of that, excluding this sensibility in terms of discharge, what is to consider is the relative low difference in hydraulic heads and pressures distribution existing between the variant 1, 2 and 3. In fact, the purchased objective is not to dress a hydraulic barrier catching the entire water flows, but to reduce the hydraulic pressure (see figures 6.3 and 6.6). In that point of view the objectives are reached. In terms of hydraulic heads and pressures, the efficiency of the different variants is illustrated in figures 6.3 and 6.6. The results show that a mean spacing of the order of 15 meters between the pipes is capable to reduce the hydraulic heads of around 36 meters along the drainage work at the sliding surface and to intercept around 46% of the hydraulic fluxes from the sliding mass. Variants bringing the spacing to 30 meters then to 60 meters indicate hydraulic head lowering of respectively 34 and 30 meters. Across the slide, the profile of hydraulic head indicates maximal lowering of respectively 53 meters, 48 meters and 40 meters. The hydraulic head fluctuations are more significant for a large inter-pipes spacing. Contrary to variant 3, the variant 1 and 2 permit the desaturation (i.e. negative hydraulic pressures) of the section above the drainage work. In variant 3, high pressures (>100 kPa) are remaining.

Finally, the results after drainage (variant 1, 2 and 3) indicate a correlation between the fluctuations of the drained discharge and the infiltration rates (plot 6.1). The intensity of these fluctuations is in the meantime very low. The pipes seem to maintain a constant mean discharge whatever the infiltrated water is. The relationship between infiltration and drained water is important from the moment that the principal causes of sliding are the surface infiltrations.

Influence of drainage on the displacements and on the factor of safety (FoS)

The efficiency of a drainage gallery can be evaluated in term of displacements (figure 6.7). The presence of the drainage gallery induces a strong diminution of the predicted displacements (from 101cm for the model without drainage to around 15-20 cm for the drained models (i.e. variant 1, 2 and 3)). The influence of the pipe spacing on the maximal predicted horizontal displacements is very low (14 cm for the variant 1 and 19 cm for the variant 3). In the meantime, only a spacing of 15 meters enables a significant gain of security. The variant 1 indicates a FoS=1.30, again FoS =1.15 for the two other variants. For memory, the non remediate model has a FoS of 1.05. The drainage work enables a reduction of about 85% of the displacements.

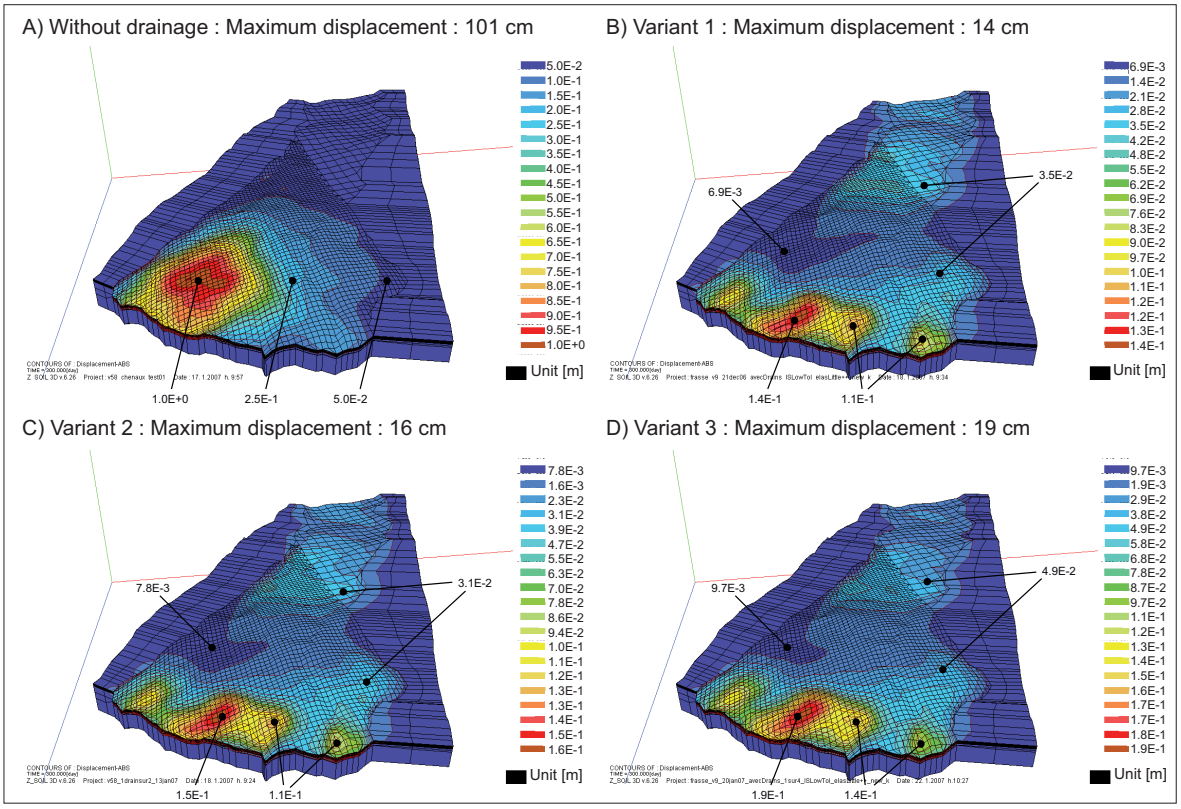

Figure 6.4: Absolutes Displacements, 3D view.

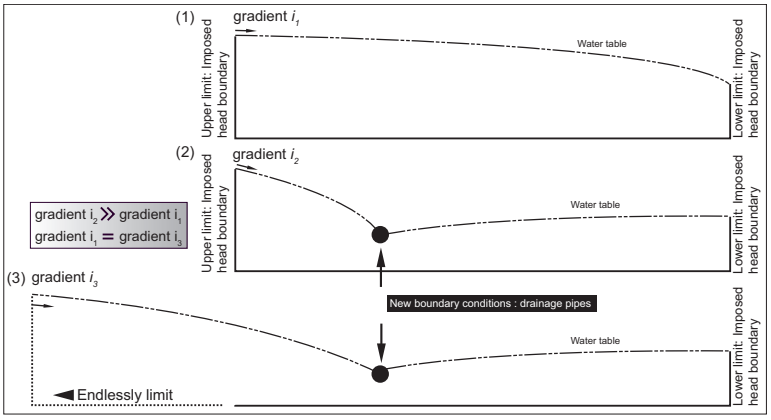

Figure 6.5: Effects of new boundary limits on the hydraulic gradient. (1) Hydrodynamic system with two boundary limits, imposed heads. (2) Hydrodynamic system with new boundary conditions. (3) The upper limit position in the reality.

6.2.9 Discussions

The proposed drainage design scheme with boreholes drilled from a deep gallery excavated in the bedrock is in a hydraulic point of view very efficient. The results show that a mean spacing between the pipes of the order of 15 meters (variant 1) is capable to lower the hydraulic head about 36 meters along the work at the sliding surface, and to intercept around 45% of the hydraulic flux of the sliding mass. The variants increasing the spacing to 30 meters (variant 2) and then to 60 meters (variant 3), indicate a lowering of the hydraulic head from 34 and 30 meters respectively. Concerning the deformation (hydro-mechanical coupled calculation) the presence of the drainage gallery induces a strong diminution of the predicted displacements (from 101cm for the model without drainage to around 15-20 cm for the drained models (i.e.

variant 1, 2 and 3)). The influence of the pipe spacing on the maximal predicted horizontal displacements is very low (14 cm for the variant 1 and 19 cm for the variant 3).

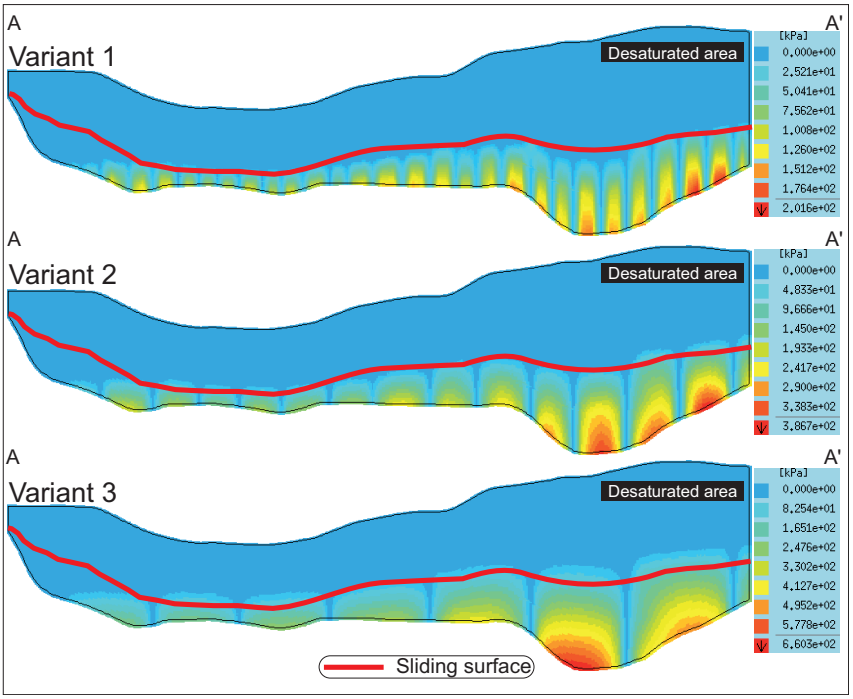

Figure 6.6: 2D-profile (A-A') along the drainage gallery layout illustrating the effects of drainage on the hydraulic pressure distribution. See figure 2 for the location of the profile A-A'.

These differences are low from a hydraulic point of view, in return, present implications more obvious in terms of factor of safety (FoS). Only a spacing of 15 m enables a significant gain of security. The variant 1 indicates a FoS=1.30, again FoS =1.15 for the two other variants. For memory, the non remediate model has a FoS of 1.05.

The results obtained prove that a well-designed drainage scheme may provide a substantial stabilising effect during a crisis, although this type of work requires spacing between the pipes with a maximum of 15 meters.

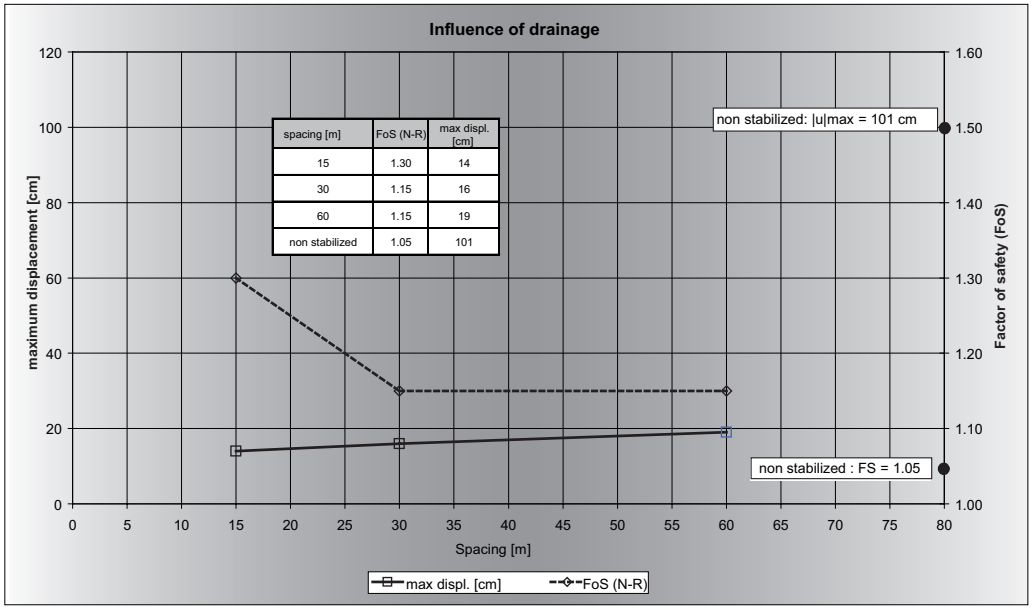

Figure 6.7: Summary of displacements and FoS.

Finally, the construction of a drainage gallery still represents an important work, as well economically as technically. The geological conditions are often very complicated (variable bedrocks, tectonized, loose material) from which long ascending pipes should be dug through instable and loose material. This material being strongly heterogeneous, the geotechnical parameters will be variable in space. In the meantime, this solution, presents, apart high stabilization efficiencies as demonstrated in this paper, also technical advantages, and this despite of the costs, clearly higher than a classical drainage system issued from a well platform.

- Absence of operating and maintenance costs due to drainage by gravity.
- The risk of shearing of the drainage work limited only to the drainage system (pipes), and are not affecting the gallery.
- The possibility to add complementary pipes in case of necessity, without an intervention from the surface (facilitated procedure, absence of impacts).
- The possibility to extend the drainage gallery with a minimum of surface interventions, which would be limited to the construction of air shafts.
- The guaranty, in case of a brutal reactivation of the slide (even local), to preserve the main work (drainage gallery) from which the drainage system (pipes) could be fastly and without difficulties reconstructed. For a system based on a well-platform drainage, such a reactivation could definitively ruin the entire system.
- The artificial increase of the connectivity of the heterogeneities in the mass slide, as well in the stabilized mass.
- The drainage of the bedrock, in case of an exceptional raise of water pressures.

6.2.10 Conclusion

The integration of the heterogeneous character of the landslide mass in the hydrogeological and geomechanical modelling of the La Frasse landslide has supplied a significant contribution to increase the reliability of the computed hydraulic pressures and movements during crises. Due to the size of the heterogeneities (Degree of details) the results have a meaning at a local scale and not only at a global scale. This study enables to validate and confirm the recommended solution in (NCG+EPFL 2004), namely a drainage gallery equipped with pipes with a mean spacing of 10 m (pipes mean spacing of the execution project). Indeed the fineness of the mesh used in the numerical models did not enable to insert as many pipes. The results of variant 1 – with a mean spacing of 15 meters – are considered to be representative of the expected efficiency of the execution project.

6.2.11 Acknowledgements

The authors express their thanks first for the financial support by the Office for Water, Soil and Sewage of the Canton of Vaud and by the Swiss Federal Office for Water and Geology for allowing the fulfilment of this research project. Then they wish to express their acknowledgements to all the private consultant partners for a positive collaboration, in particular to De Cérenville Géotechnique and Norbert Géologues-conseils SA Bureau technique which contributed in an essential way to the project by its technical support and critical discussions.

7. GLOBAL MODEL OF THE HYDROGEOLOGICAL FUNCTIONING

The observations of geological heterogeneity and flow behaviours in chapter 4, 5 and 6 are integrated to develop and propose a conceptual model of the hydrogeological functioning. The main field test site of the *La Frasse* landslide makes it possible to identify and to explain some important geological and hydrogeological characteristics that are also recognized and recorded in other landslides occurring in low permeable environments, namely those presented and analysed in chapter 4.2. This chapter synthesises and concludes this PhD thesis, but first, the relations between geological heterogeneity and hydrogeological behaviour of some relevant cases are presented.

7.1 RELATIONS BETWEEN GEOLOGICAL HETEROGENEITY AND HYDROGEOLOGY

The observations of the geological structures and the observed hydrogeological behaviours of the selected landslides discussed in chapter 4.2 are synthesized in figure 7.1 (pages 176 and 177). This approach allows the identification of the principal characteristics, and opens the discussion about the role of the geological and structural heterogeneity, as well as the relations between the underlying substratum and the active sliding mass.

The observation is done thanks to borehole data, from the upper and the lower part of the slide. The hydrogeological observations (i.e. water level, hydraulic pressure variations, inflow rates…) are often sparse, but nonetheless allow some conclusions to be drawn. In figure 7.1, each case study comprises three columns; a one-dimensional projection of the geological structure, the corresponding permeabilities and the hydrogeological observations.

The considered geological entities are: the active sliding mass and the substratum, which comprises the stabilized or latent mass and the bedrock. In some cases the active sliding mass is directly lying on the bedrock. Each case study is discussed individually and then synthesized. The observations are the following:

***La Lécherette* landslide.** The active sliding mass is directly in contact with the bedrock. Water level measures in the upper part of the slide were continuously taken since end 1995 in borehole “L2” at the level of the sliding surface. Globally, the observations illustrate the scalable character of the mass. Three periods may be identified. (1) From October 1995 to July 1997 the fluctuations are regular and may be correlated with the precipitations. A reaction to precipitations is felt from the first day. The response of the hydraulic pressure is delayed; its maximum is recorded one or two days after the event, and presents a decrease relatively slower than the increase. The magnitude is relatively low and never exceeds 25 cm; making it possible to assume a low permeable medium. (2) From July 1997 to August 1998 the system is characterized by variations with higher magnitude (i.e. metric). The hydraulic pressure increases relatively slowly and regularly over several days, whereas the decrease is very quick (some hours!). Often this decrease occurs directly after a strong rainy event, generating a threshold effect. This threshold effect confirms the impermeable character of the media, and its poor and sparse connectivity. The hydraulic connection is done thanks to a plug-flow effect from the surface to the sliding surface, linking a multitude of small water pockets (permeable reservoir) inside the impermeable capacitive fraction of the mass.

Figure 7.1: Geological and hydrogeological observations of several case studies (see page 176-177).

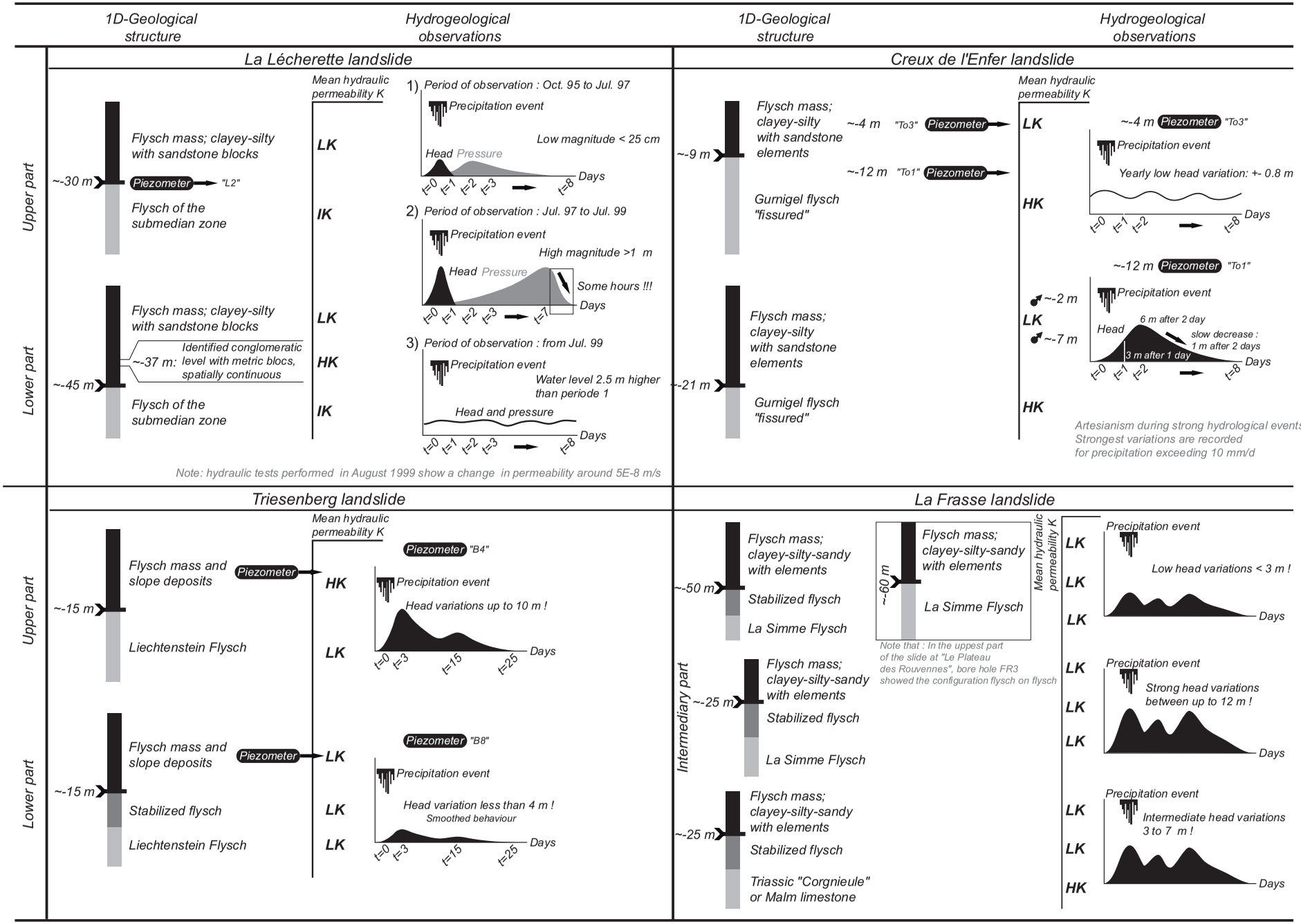
1D-Geological structure
Hydrogeological observations
La Lécherette landslide
Upper part
Lower part
Flysch mass; clayey-silty with sandstone blocks
~-30 m
Piezometer
"L2"
Flysch of the submedian zone
Flysch mass; clayey-silty with sandstone blocks
Identified conglomeratic level with metric blocs, spatially continuous
~-37 m:
~-45 m
Flysch of the submedian zone
Mean hydraulic permeability K
LK
IK
LK
HK
IK
1) Period of observation : Oct. 95 to Jul. 97
Precipitation event
Low magnitude < 25 cm
Head Pressure
Days
t=0 t=1 t=2 t=3 t=8
2) Period of observation : Jul. 97 to Jul. 99
Precipitation event
High magnitude >1 m
Head Pressure
Some hours !!!
Days
t=0 t=1 t=2 t=3 t=7
3) Period of observation : from Jul. 99
Precipitation event
Water level 2.5 m higher than periode 1
Head and pressure
Days
t=0 t=1 t=2 t=3 t=8
Note: hydraulic tests performed in August 1999 show a change in permeability around 5E-8 m/s
1D-Geological structure
Hydrogeological observations
Creux de l'Enfer landslide
Flysch mass; clayey-silty with sandstone elements
~-9 m
Gurnigel flysch "fissured"
~-4 m "To3" Piezometer
~-12 m "To1" Piezometer
Flysch mass; clayey-silty with sandstone elements
~-21 m
Gurnigel flysch "fissured"
Mean hydraulic permeability K
LK
HK
LK
HK
~-4 m Piezometer "To3"
Precipitation event
Yearly low head variation: +- 0.8 m
Days
t=0 t=1 t=2 t=8
~-12 m Piezometer "To1"
~-2 m
~-7 m
Precipitation event
Head
6 m after 2 day
slow decrease : 1 m after 2 days
3 m after 1 day
Days
t=0 t=1 t=2 t=8
Artesianism during strong hydrological events.
Strongest variations are recorded
for precipitation exceeding 10 mm/d
Triesenberg landslide
Upper part
Lower part
Flysch mass and slope deposits
Piezometer
~-15 m
Liechtenstein Flysch
Flysch mass and slope deposits
Piezometer
~-15 m
Stabilized flysch
Liechtenstein Flysch
Mean hydraulic permeability K
Piezometer "B4"
HK
LK
Precipitation event
Head variations up to 10 m !
Days
t=0 t=3 t=15 t=25
Piezometer "B8"
LK
LK
LK
Precipitation event
Head variation less than 4 m !
Smoothed behaviour
Days
t=0 t=3 t=15 t=25
La Frasse landslide
Flysch mass; clayey-silty-sandy with elements
~-50 m
Stabilized flysch
La Simme Flysch
Intermediary part
Flysch mass; clayey-silty-sandy with elements
~-25 m
Stabilized flysch
La Simme Flysch
Flysch mass; clayey-silty-sandy with elements
~-25 m
Stabilized flysch
Triassic "Corgnieule" or Malm limestone
~-60 m
Flysch mass; clayey-silty-sandy with elements
La Simme Flysch
Note that : In the uppest part of the slide at "Le Plateau des Rouvennes", bore hole FR3 showed the configuration flysch on flysch
Mean hydraulic permeability K
LK
LK
LK
LK
LK
LK
LK
HK
Precipitation event
Low head variations < 3 m !
Days
Precipitation event
Strong head variations between up to 12 m !
Days
Precipitation event
Intermediate head variations 3 to 7 m !
Days

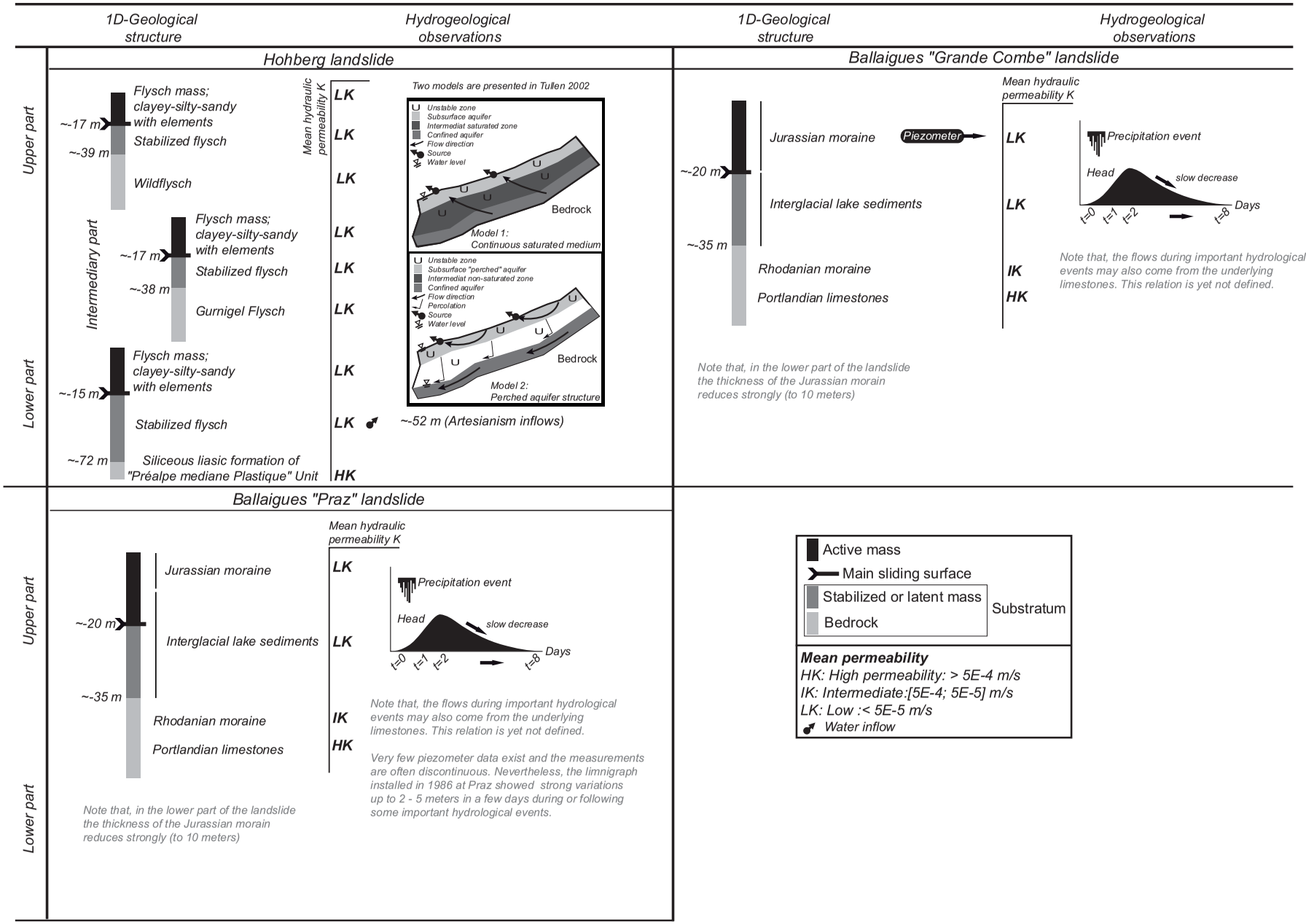
1D-Geological structure
Hydrogeological observations
Hohberg landslide
Upper part
Intermediary part
Lower part
~-17 m
~-39 m
Flysch mass; clayey-silty-sandy with elements
Stabilized flysch
Wildflysch
~-17 m
~-38 m
Flysch mass; clayey-silty-sandy with elements
Stabilized flysch
Gurnigel Flysch
~-15 m
~-72 m
Flysch mass; clayey-silty-sandy with elements
Stabilized flysch
Siliceous liasic formation of "Préalpe mediane Plastique" Unit
Mean hydraulic permeability K
LK
LK
LK
LK
LK
LK
LK
HK
Two models are presented in Tullen 2002
Unstable zone
Subsurface aquifer
Intermediat saturated zone
Confined aquifer
Flow direction
Source
Water level
Bedrock
Model 1: Continuous saturated medium
Unstable zone
Subsurface "perched" aquifer
Intermediat non-saturated zone
Confined aquifer
Flow direction
Percolation
Source
Water level
Bedrock
Model 2: Perched aquifer structure
~-52 m (Artesianism inflows)
1D-Geological structure
Hydrogeological observations
Ballaigues "Grande Combe" landslide
~-20 m
~-35 m
Jurassian moraine
Piezometer
Interglacial lake sediments
Rhodanian moraine
Portlandian limestones
Mean hydraulic permeability K
LK
LK
IK
HK
Precipitation event
Head
slow decrease
Days
t=0
t=1
t=2
t=8
Note that, the flows during important hydrological events may also come from the underlying limestones. This relation is yet not defined.
Note that, in the lower part of the landslide the thickness of the Jurassian morain reduces strongly (to 10 meters)
Ballaigues "Praz" landslide
Upper part
Lower part
~-20 m
~-35 m
Jurassian moraine
Interglacial lake sediments
Rhodanian moraine
Portlandian limestones
Mean hydraulic permeability K
LK
LK
IK
HK
Precipitation event
Head
slow decrease
Days
t=0
t=1
t=2
t=8
Note that, the flows during important hydrological events may also come from the underlying limestones. This relation is yet not defined.
Very few piezometer data exist and the measurements are often discontinuous. Nevertheless, the limnigraph installed in 1986 at Praz showed strong variations up to 2 - 5 meters in a few days during or following some important hydrological events.
Note that, in the lower part of the landslide the thickness of the Jurassian morain reduces strongly (to 10 meters)
Active mass
Main sliding surface
Stabilized or latent mass
Bedrock
Substratum
Mean permeability
HK: High permeability: > 5E-4 m/s
IK: Intermediate:[5E-4; 5E-5] m/s
LK: Low :< 5E-5 m/s
Water inflow

The absence of direct connections is an acceptable explanation for the observed delay. Finally since August 1998, the third period (3) shows that the system has recovered more or less the behaviour of period 1, but with lower variations, and an overall water level 2.5 meters higher. The permeability seems to have seriously decreased. For instance, no reactions were recorded during and after the strong rainy events of August 1999. It is relatively difficult to explain this change of permeability and where it occurs exactly. It may be a local change around the borehole, or even a more global change. The facts are that the permeability of the media has temporally and spatially changed. A well test performed in August 1999 indicated a permeability of around 5E-8 m/s. Finally, in this case study, the relations between the mass and the substratum have not been established, but there are certainly no water inflows coming from the underlying bedrock.

This example illustrates perfectly the complexity of this hydrological system and the incidences on stability. Effectively, the hydraulic head gains after period 2 present very unfavourable conditions for stability. Moreover, 8 months after this period, the slide sustained an important reactivation, and this might not be related to any especial hydrological crisis. In these regions (Alpine and Préalpes regions) the snow melt is often evoked as representing a serious factor for instability (see *les Peillettes* case study, Alpgeo 2006). Snow melt effectively conduces to threshold effects accelerating instability processes.
In addition, it is also often observed that directly after reactivation phases, the hydraulic pressures decrease strongly. The movements thus temporarily favour a global or local increase of the permeability of the mass or of the sliding surface. Finally, observation indicates that the most important hydraulic pressure variations are recorded when the connectivity is developed. Numerical tests in chapter 5 for la Frasse case study have demonstrated that in order to reproduce the global hydrological behaviour, the structures on the sliding surface have to be connected, and with a good overall permeability. In very impermeable media, numerical tests performed in chapter 5 have showed that the hydraulic pressures may be important but totally smoothed.

***Creux de l'Enfer* landslide.** The active sliding mass is directly in contact with the bedrock, with a relatively low thickness (around 9 meters). Water level measures in the upper part of the slide were realized in continuous at two locations; subsurface (*To3*) and in the bedrock (*To1*). Globally, the highest hydraulic variations (up to 6 meters!) are observed in the piezometer placed in the bedrock (*To1*). These fluctuations are characterized with a strong increase, up to 3 meters after one day, after serious rainy events. The reactivity is high with strong and fast responses occurring just hours after the precipitation. The maximum of fluctuation happens one day after the event. The decreases are generally slower but still well marked; up to 1 meter in two days. Some artesianism is observed during important rainy events. In *To3* placed in the active mass, the variations are low (< 80 cm), the subsurface shows therefore a yearly constant saturation. The strongest variations are recorded when the precipitation exceeds 10 mm/d. Note that this value is indicative since dependent upon past events. The response to strong hydrological events thus concerns both surface and bedrock. Generally, the beginning of increase of the hydraulic pressure in *T03* precedes (some hours) that of *To1*. The peak of intensity also appears earlier in the sliding mass than in the bedrock. This characteristic illustrates the behavioural independence of the two media. Besides, sometimes artesianism is observed in *To1* whereas in *To3* no particular variations are recorded. Had the contrary been observed, the reaction in *To3* would have been considered as an influence of the hydraulic pressure increase in the underlying bedrock. Therefore, hydraulic variations recorded in the sliding mass are influenced by direct effective infiltration. In the bedrock, the reaction is differed by several hours, since the infiltration zones are far apart. These zones may be located outside the landslide at higher altitude. Thus, the location of these infiltration zones explains the observed artesianism. Finally, the observation shows that the system is

very reactive with important magnitudes. There is a straight correlation between water level variation and climatic conditions.

***Triesenberg* landslide.** In the upper part of the slide the active mass is overlying the bedrock, whereas in the lower part a stabilized mass is present between these two units. The mean thickness is around 15 meters. Hydrogeological observations are available for both the lower and the upper part (i.e. B8 and B4 piezometers). Stormy events result in double peaks in piezometric observations. After some hours, a first peak occurs and corresponds to the direct infiltration. Some days later (around 10 days), a smoother peak appears and is attributed (François et al. 2007) to the inflow from the *Valüna* valley through the sandstone covering the Arosa zone. Note that part of the *Valüna* valley (Arosa zone) groundwater flows feed the landslide. This double feeding is also effective outside of intensive infiltration periods. Bernasconi (2002b) suggests that about one half of the inflow in the landslide is supplied by the *Valüna* valley. In the upper part of the slope, the piezometric behaviour is directly influenced by the inflow from the neighbouring units (i.e. Valüna valley). The hydraulic head is rather constant close to 1101 meters suggesting a base flow due to the capacitive function of the sandstones. After snowmelt and storm events, however, sharp peaks of more than 10 meter high are recorded. In the lower part of the slide, the inflow peaks are smoothed by the landslide aquifer with piezometric variations inferior to 4 meters. This behavioural difference may be explained by the permeabilities. In fact it is recognized that in the upper part, the old deep-seated zone, the system shows a higher permeability and, above all, a more developed continuity thanks to the numerous sandy and gravely facies. In the lower part a strong impermeable character is observed. This is also partly confirmed by observation of the water table, which is located about 20-30 meters below surface in the upper part, whereas in the lower part it almost reaches the surface. The underground is thus correctly drained out in the upper part. As defined for the *la Frasse* case, it is admitted that there are no hydraulic relations between the underlying bedrock and the active mass.

***La Frasse* landslide.** Since this case is developed in chapter 4, it is only briefly presented. Three observation points are considered: upper, lower and intermediate. Local geological configurations vary from part to part. The slide is composed of the following three entities; active sliding mass, stabilized mass and bedrock. The main hydrogeological observations that can be noted down are the opposite of hydrological behaviour that is observed for the *Triesenberg* landslide, namely low reaction in the upper part. Strong variations are recorded in the intermediate and lower part, up to 12 meters. Structural and geological characteristics may explain this. First, geophysical and hydrogeological surveys have identified in the area of the most active zone "++" permeable characteristics parallel to the sliding direction certainly resulting from the various intense deformation processes. Secondly, the dimension of the mass in this location may play a primary role. In fact, the location is characterized by both vertical and horizontal tightening of the mass. The average thickness is only around 25 meters against 55 meters observed higher. The increase of spatial connectivity along with the decrease of the flow section gives a satisfactory explanation of the strong hydraulic responses. Besides, some well analyses showed very impermeable conditions in boreholes of the upper part (i.e. FR1).

***The Hohberg* landslide.** Very few observations exist concerning water table variations and hydraulic pressure distribution into the slide, since most of the hydrological studies concentrated on the various sources. The particularity of this slide is the relation between the stabilized mass and the active mass. In Tullen (2002) two aquifer models are proposed. The first model consists in three independent systems; a subsurface aquifer, an intermediate semi-permeable and a confined aquifer located in the stabilized mass.

The two aquifers are connected thanks to vertical drainage through the semi-impermeable formation. The overall system is saturated. The second model conserves the same structure, but the lower and the upper aquifers are disconnected. This model represents a perched aquifer system, the intermediate zone is considered as unsaturated. Isotopic data have shown that the flow transit times are very short; Tullen (2002) explains it thanks to superficial flows. However, since very resistive zones (permeable) were recognized (see radiomagnetotelluric surveys in section 4.2), the very short flow transit times may also be explained by the local presence of an organized and connected system. Reality may be situated between these two models; namely an aquifer system composed by deep internal flows and perched aquifers.

***Ballaigues "Grande Combe" and "la Praz"* landslides.** Since similar hydrogeological observations were done for both cases, they are treated together. These landslides are geologically composed of very impermeable quaternary material (section 4.2.2). Since very little hydrological information is available, only basic observations are down. The system, as yet recognized in the flysch cases, shows a good reactivity (instantaneous reaction, one or two days), relatively strong magnitude and a slow but constant decrease. This observation traduces relatively good capacitive characteristics; locally the aquifer may be considered as confined. Internal developed connections were also recognized thanks to radiomagnetotelluric surveys. Note that, the flows during important hydrological events may also come from the underlying limestones; nevertheless, this relation is not yet well defined.

7.2 SYNTHESIS OF HYDROLOGICAL BEHAVIOURS

In most of the case studies, the landslide mass is composed of an old prehistoric stabilized mass, pinched between the active sliding mass and the bedrock, and playing an important hydrologic role. The stabilized mass and the bedrock form the substratum of the landslide. Observations indicate that the older the slide is, the more this stabilized mass is important (i.e. extension and thickness).

Hydrogeological relations between the bedrock and the landslide mass (active and stabilized) are not obviously observed. At the *La Frasse* landslide, as shown in some boreholes, artesian inflows were met inside the mass, indicating that there are certainly local tendencies to recharge from the bedrock and showing that local excess of hydraulic pressures is not only present at the main slip surface but also inside the sliding mass. Indeed the hydraulic relations with the substratum are still not well defined, as there is no clear information about water inflows. Generally, the observations rather indicate that the underlying karstified substratum of Trias and Malm drains the water out of the slide. At the *Creux de l'Enfer* landslide behavioural independence is clearly confirmed, even if strong hydraulic pressure variations and artesianism are recorded in the bedrock. These overpressures are not caused by the overlying mass, but are rather conditioned by the boundary conditions of the bedrock, that is to say the difference of altitude between the observation point and its infiltration zone. Note that, generally due to the special geomorphologic and geological configuration, the catchment area of the underlying bedrock is always situated higher than the highest point of the slide.

Hydrogeological relations between the stabilized and the active mass may be observed in some cases (e.g. *La Frasse* and *Hohberg* landslides). But usually the stabilized zone presents very impermeable characteristics, preventing important water flows. This impervious character is mainly inherited from its

long instability history. And in addition it is often considered as representing an impermeable barrier between the bedrock and the active sliding mass, avoiding any flow transfer (e.g. *La Frasse*). Hydrochemical and lithological observations at *La Frasse* have shown that the constant movements of the mass and slow flows with long residence time favour the cation exchange (Ca-Na) between groundwater and the mass and the generation of clay minerals. Thus, since it belongs entirely to the geological structure of the slide, the conceptual model, for instance used for numerical purposes, has to integrate it. In that case the sliding surface will not correspond to the bottom interface of the model, but rather to a slice enclosed inside the model.

Hydrogeological relations between the surface and the active mass. In most of the cases a good hydraulic connection between the surface and the active mass is observed through the unsaturated sub-system. Often the hydraulic response to a hydrological event is instantaneous (some hours). Due to the geological heterogeneities (low permeability and connectivity) the reactivity and the intensity of the reaction are very high. Nevertheless, it doesn't mean that each important hydrological event corresponds to a reactivation of the slide. The flow and pressure transfer inside the mass are much more complex. Complex storage capacities and plug-flow effects may record past events and reactivate sliding processes several months after the last important rainy event, for instance up to 8 months at the *La Lécherette* landslide.

Finally, this study demonstrated that the conductive fraction fills an important hydrodynamical role essentially between the main hydrological events, controlling the hydrological balance of the system. The observations were confirmed by the numerical tests performed in chapter 5.4.5.3. The observation indicated also that the upper and the lower part of the slide often present different hydraulic behaviours. And according to the structure of the medium (degree of connectivity), the lower part may be dependent on the hydrodynamical conditions of the upper part.

7.3 GLOBAL MODEL OF THE HYDROGEOLOGICAL FUNCTIONING

7.3.1 INTRODUCTION

The proposed conceptual model for landslides occurring in low permeable environments is based on the principle of reservoir systems. After reviewing literature, and especially studies in the karst (Jeannin 1998 and Perrin 2003), it appears that the hydrological phenomena and behaviour observed in these case studies present many similarities with karstic networks; namely the *organized heterogeneity* and the *duality of the aquifers*. The organized heterogeneity may be schematized by a high permeability, generally unknown channel network, which is immersed in a low permeability, often discontinuous volume, and connected to local discharge areas; sources and rivers. The duality of the aquifers is a direct consequence of this structure:

- Duality of the infiltration processes (diffuse or slow infiltration into the low permeability volumes, concentrated or rapid infiltration into the permeable network);
- Duality of groundwater flow field (low flow velocities in the impermeable fraction, high flow velocities in the permeable network);
- Duality of the discharge conditions (diffuse seepage from the low permeability volumes, like fissure aquifers and concentrated discharge from the channel network), as shown by the discharge rates measured at several sources (e.g. *Hohberg, la Frasse*);

This approach of reservoir models presents the advantage of simplicity and allows most of the various observed behaviours discussed in section 7.1 to be represented and explained. The classical "porous model", presented in chapters 5 and 6, provided satisfactory results, but does not allow simulation of particular responses proper to specific areas inside the mass. The approach used for simulating the flows, and mainly based on a homogeneous or heterogeneous distribution of the physical parameters over the entire model, is valuable since it made it possible to simulate the observed water balances and the global water level variations. This approach, which considers a global saturated media with confined conditions, allows reproduction of the nervousness of the system. Nevertheless, it does not consider unsaturated and isolated areas, which may play an important role in the stability. Finally, it does not incorporate temporal variations of permeabilities and plug-flow effects.

7.3.2 THE FLOW SYSTEM CONCEPTION

The observations made, especially at the *La Frasse* test site (chapter 4), combined with the hydrogeological and lithological data of the several case studies discussed in sections 4.2 and 7.1, led to the proposal of a global synthesis (section 4.3.11). The numerical tests performed in chapters 5 and 6 made it possible to understand the effects of the geological heterogeneities on the flows. Thus, the following assumptions are considered to enable the subsequent quantification of flow components:

- The flow occurs under confined to leaky conditions, with leakage varying in space;
- The flow framework is controlled by a complex multi-layer system, isolated lenses or perched aquifer;
- The aquifer system is divided into interconnected hydrological zones presenting various degrees of saturation;
- Each hydrological zone may function individually from the others;
- Horizontally and vertically, the flow direction in the porous matrix is affected by prevailing structural patterns generating channeling effects;
- The flow is multidirectional, free and channelized, and is affected by temporal and spatial changes;
- The aquifer is under a unsteady flow regime due to seasonal variation of natural gradients;

7.3.3 FUNCTIONING OF THE SYSTEM – A CONCEPTUAL MODEL

The considered cascading sub-systems of the conceptual model presented in figure 7.2 try to take into account all the presented geometrical, structural, geological and hydrogeological characteristics. The model is vertically represented from the top to bottom by the following hydrogeological zones: the surface and soil, the unsaturated zone and the phreatic zone. And by the following structural zones of the landslide: the active sliding mass, the sliding surface, the stabilized mass and the bedrock. The top of the active sliding mass (i.e. surface and soil) is situated in the unsaturated sub-system, while the underlying structural zones are entirely comprised in the phreatic sub-system. The phreatic sub-system is considered as mostly saturated, however, according to local hydrological conditions, unsaturated areas may exist.

The stabilized mass and the bedrock constitute the substratum of the active sliding mass. The model takes into account water transfer between the stabilized mass and the active sliding mass through the sliding surface. However, transfers between the bedrock and the landslide mass (active and stabilized mass) are omitted, because of the lake of justifiable information. The phreatic sub-system is split into a network of

high permeability features (conductive fraction) and low permeability mass (capacitive fraction) with a high storage capacity.

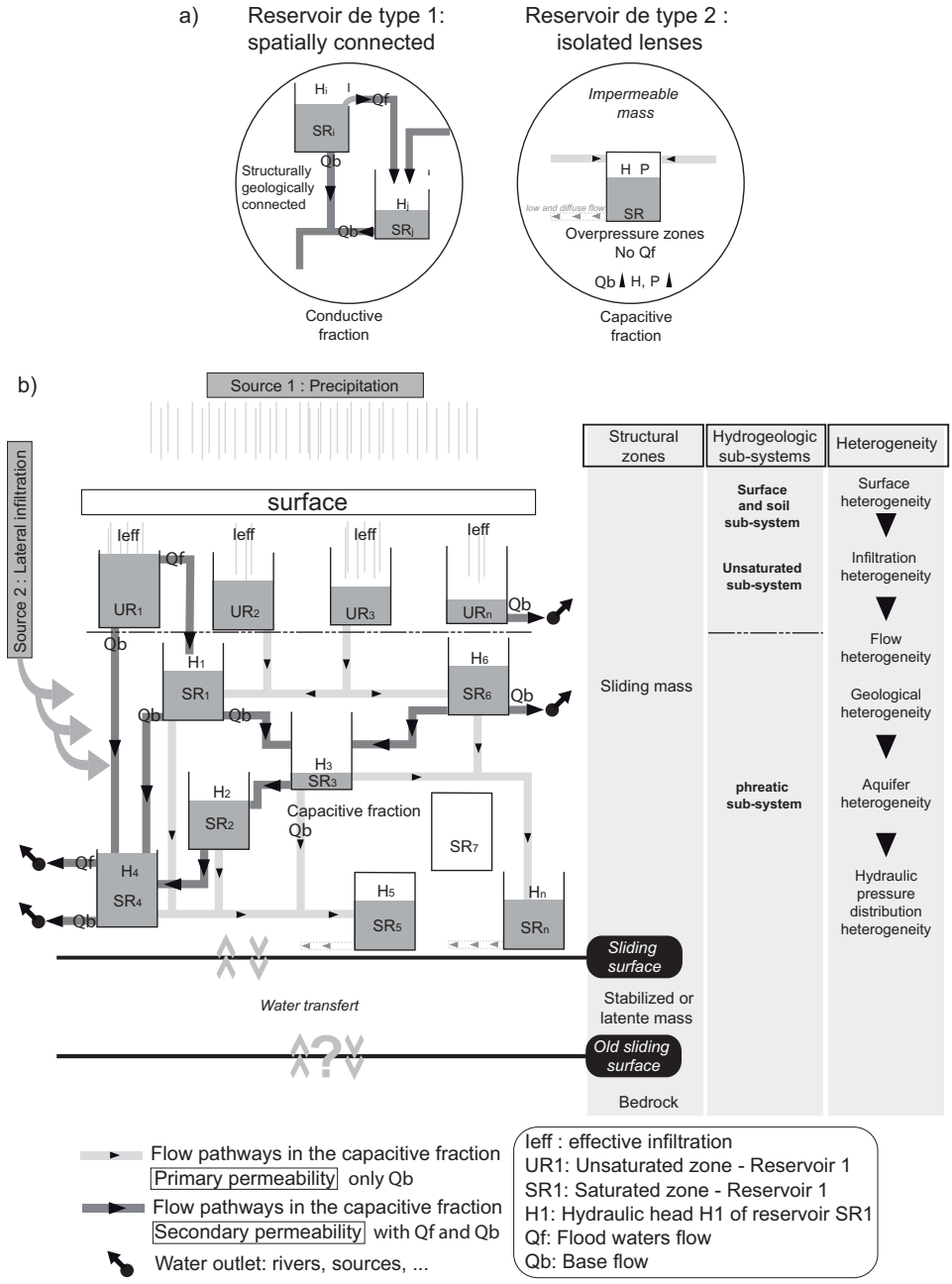

Figure 7.2: Conceptual model based on a simple reservoir approach (b). The two types of reservoirs considered in the system are representative of the conductive and the capacitive fraction (a).

The system is constituted by two fractions; a conductive and a capacitive, and two types of reservoir (groundwater store); connected and disconnected (figure 7.2-a). The reservoirs of the conductive fraction are connected each other thanks to permeable features, representing either permeable zones (sand or gravel layers of the primary permeability) or structural discontinuities (secondary fracture permeability inherited by the deformation processes). In the first case, as discussed in section 4.3.3.8 and chapter 5, the less resistive pathways of the primary permeability may change temporally and spatially the function of the hydraulic gradient. In the second case, the structural discontinuities represent physical entities, but, in the special context of landslide, may also change temporally and spatially according to the activity of the slide, i.e. deformation processes. Therefore the channeling direction produced by the geological heterogeneities

and contrasted permeability may constantly change. This may explain the strange hydraulic behaviour observed during the well tests at *La Frasse* (section 4.3.7) and *La Lécherette* landslides.
The reservoirs (isolated lenses, water pockets or perched aquifers) of the conductive fraction are composed by two types of flows; one of which is a base flow (Qb), the part of the flow that is not attributable to rapid infiltration and generally sustained by groundwater storage. Storage can exist in the low permeability fraction of the phreatic and in the unsaturated sub-systems. This flow is mainly diffused, and equally described as seepage flow or percolation water through the low permeable mass. The flood flow (Qf) is a high-discharge through the permeable structures and may be due to important precipitations, or to the reservoirs being "full". When a reservoir is saturated, it will discharge. Thanks to plug-flow effects the water is briskly liberated in the system flowing to the next unsaturated reservoir. Note that it does not necessarily generate a flooding downstream of the spring. In the *La Frasse* case for instance, the pumped water rates of the platform system (section 4.3.8.4) illustrate perfectly this phenomenon; with variable inflow rates.

At each level of the system, from input to output, a water molecule will be submitted to heterogeneous conditions. The surface infiltration, where recharge is diffuse or concentrated, represents the first of the heterogeneous zones. The soil sub-systems which store part of the infiltrated water are also heterogeneous. The unsaturated zone sub-system connects the former subsystem to the phreatic zone by drainage through a complex vertical network. Thus from an initial precipitation, a succession of zones distributes the water inside the system in a heterogeneous manner. Each reservoir in Figure 7.2-b (*URi* of unsaturated zone and *SRi* of phreatic zone) is finally represented by a proper hydraulic head (Hi), function of the degree of saturation. This is partly confirmed by the variable distribution of the water level maps.

Two input sources have to be considered; lateral infiltration and effective infiltration from the surface. As observed at the *Triesenberg* and *La Frasse* landslides, lateral inputs from neighbouring zones are the main recharge (i.e. > 60% at the *la Frasse* landslide and one half of the inflow at *Triesenberg*).

The water finally issues from the system thanks to variably distributed outlet zones. (i.e. sources, rivers or seepage areas). The hydrogeological observations have shown that these zones are a determining factor in the functioning and the stability of the system. Their distribution, density and behaviour are variable for each case. Some outlets will have a long delayed reaction to hydrological events, whereas others, directly connected to surface, record instantly each water input. Note that each landslide will show different characteristics, but the sources tend to drain surface waters, while rivers discharge deeper flows. For instance, at *La Frasse*, the numerous springs scattered over the landslide show a total rate of the order of some liters per second, leading to a total of about 1000 m^3/day. In the NW, a humid area occurs close to El.1200 m a.s.l. About 1,000 m^3/day are also drained by the Bonne-Eau and Le Bay streams. But the hydraulic connection of all these outlets with the aquifer is in that case doubtful since nearby boreholes show systematically that the aquifer is some meters below, mainly in the downward part of the landslide. Thus, springs correspond to very shallow local aquifers that influence the bulk hydraulic balance of the slide by reducing the direct infiltration through the surface. The main outlet of the system is the Grande-Eau River; the discharge at the toe of the slide is estimated by means of balance computations at about 4000 m^3/day.

Flow transit times depend on the structure of the system and may be very variable. As shown in chapter 4, the hydrochemistry identified water that may belong either to very slow flow or to very low mineralized flows. For instance, at the *Hohberg* landslide, the flow transit time is varying from 0.3 to 3 years (Tullen 2002).

7.3.4 FUNCTIONING DURING A HYDROLOGICAL CRISIS

Figure 7.3 presents a schematic evolution during an important hydrological crisis based on the proposed conceptual model. The resulting piezometric level variations are sketched in figure 7.3-b for observation points located at different place inside the system.

In steady-state conditions (**phase 1**) the system is fed by waters stored in both the conductive and capacitive fraction. The reservoirs discharge and recharge according to local hydraulic gradients. Flow rates are stable at the springs as well as the mass displacements. The system is not saturated even after an important precipitation. Thanks to the role of each reservoir, the system manages these hydrological events (precipitation, snow melt ...). This hydraulic equilibrium may last over long period; however, the degree of saturation of the system is slightly and constantly increasing.

During **phase 2**, rainfall has started; the surface heterogeneity associated with runoff concentrates the effective infiltration in the most permeable zones. The soil becomes variably saturated (zones into the unsaturated sub-system may be kept dry, for instance *URn in* figure 7.3 stage 2). The pore pressure is increasing; the water is pushed into the landslide mass nappe. The hydraulic stress on the system causes a discharge increase in the system, observable at the sources or rivers. The system is fed at the same time by the lateral inflows. Inside the phreatic zone, some reservoirs are becoming saturated, hydraulic pressure is seriously increasing.

During **phase 3**, rainfall continues, more soil water is pushed into the phreatic nappe. Part of the soil water bypasses the phreatic reservoirs and flows directly to the outlet points (C1). Discharge still rises at the springs. At this stage, and according to local geological conditions, shallow landslide activation may be generated due to high pore-pressures. Inside the active mass, structural failures may occur; rupture of connections (decrease of permeability) or reservoir burst, schematized by the black lightning in Figure 7.3. Note that, depending on the degree of connectivity of the system, zones may remain unsaturated.

During **phase 4**, rainfall continues, the soil is entirely at field capacity. Some fresh water bypasses the soil reservoir and flows directly to the phreatic zone. Discharge is near maximum at the spring. Structural failures have modified the flow distribution. For instance, the rupture of the connections C1 and C2 concentrates the waters to reservoirs *SR2* and *SR3* and thus entirely saturates the system. The pore-pressures undergo a global increase. According to the connectivity of the system, localized geological modifications (variation of permeability, reservoir burst...) may produce a chain reaction generating failures at unexpected places.

The resulting piezometric level variations located at different places inside the system are sketched in Figure 7.3-b. Each sketch is referenced to a real context, observed and discussed in section 7.1.

The piezometer located at **point 1** (*behaviour observed at la Frasse*), is directly connected to the surface and nearby an outlet zone. The water is flowing directly through this zone, which is connected to the surface. Each hydrological event is instantly recorded (fast increase), and while the water is directly drained out, the decrease is also very quick.

At **point 2** (*observed at Creux de l'Enfer*), near the surface, the water level is also strongly influenced by effective infiltration. But according to the degree of saturation of the downstream system, the variation (i.e. discharge) may be lower than at point 1. A slow and constant decrease of the water may occur.
The piezometer of **point 3** (*observed at Ballaigues "Grande Combe" and "Praz"*) is situated in a permeable zone in the system; if the system is well connected it may react to water infiltration. If the system is complex, formed by the succession of various reservoirs, its hydraulic response (increase and decrease) will be lower and/or delayed.
In the capacitive fraction (**point 4,** *observed at La Lécherette and Triesenberg*) the head is constant with low magnitude throughout the whole cycle. The overall low permeabilities smooth all hydraulic response.

7.4 CONCLUSIONS

Landslides in these special contexts are characterized by two important inflows, namely effective infiltration and lateral inflows from the neighbouring units (e.g. *Triesenberg* and *la Frasse* landslides). Water transfer between the stabilized mass and the active mass may be important (e.g. *Hohberg*) and thus have to be considered. The existence of water transfer between the bedrock and the landslide mass (stabilized and active) is not well established. The bedrock and the landslide mass present a hydrological behavioural independence. Thus, artesianism observed in the bedrock is not linked to special hydrological conditions occurring in the sliding mass, but is a function of the boundary limit, namely the altitude of its infiltration area.

A conceptual model based on a simple reservoir approach is proposed. It enables representation of most of the field observations and the main characteristics, namely the *organized heterogeneity* and the *duality of the aquifers.* The system is represented by various water pockets with different degrees of saturation. Complex storage capacities and plug-flow effects may record past events and reactive sliding processes several months after the last important rainy event. The analysis shows that until all the reservoirs are full and according to the downstream capacity of the system, even during a strong hydrological crisis the water is drained out. An important hydrological event is not necessarily associated with a reactivation.

According to the degree of complexity of the system (saturation, connectivity...) a very localized geological modification (variation of permeability, reservoir burst...) may produce a chain reaction, and generate failures in unexpected places.

The conductive fraction favours the drainage of the system, whereas the capacitive fraction controls the distribution of the hydraulic heads. For instance, concerning the role of the conductive fraction, Cardinali et al. (1994) found that in the flysch complex, drainage density is negatively correlated to landslide density, namely areas characterized by a high percentage of impermeable rock. Meaning that zones through which the water flows with difficulty may present a higher probability of instability.
The role of the phreatic nappe, through the conductive fraction, is to drain and control the hydrological equilibrium of the system. Therefore landslide remediation done thanks to deep drainage gallery, as discussed and presented in chapter 6, is obviously the most valuable method for this type of landslides. It supports and enhances the natural effects of the conductive fraction in draining the system.

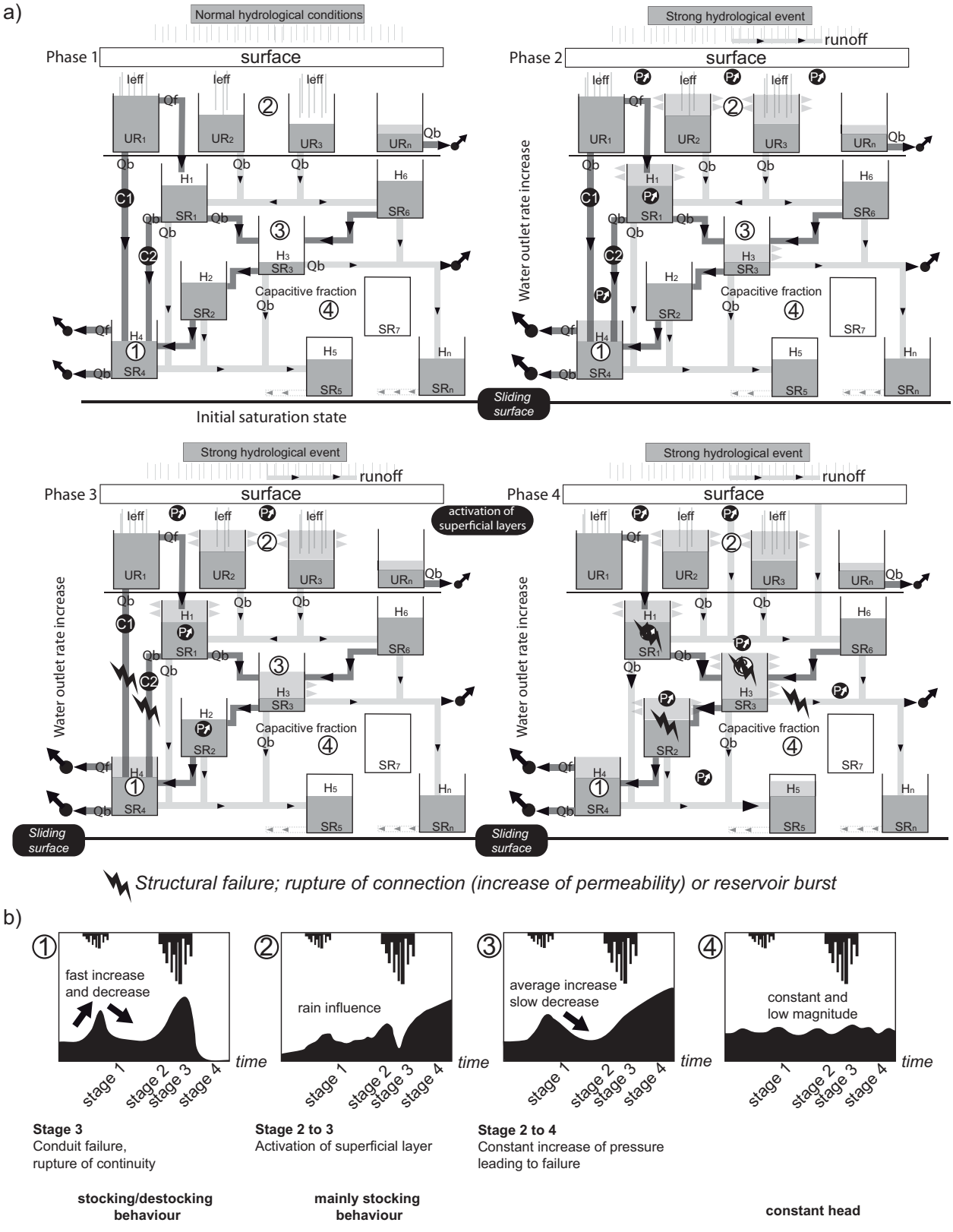

Figure 7.3: Conceptual model based on a simple reservoir approach (b). The two types of reservoirs considered in the system are representative of the conductive and the capacitive fraction (a).

8. General conclusions and perspectives

Intermediary detailed conclusions and syntheses are presented at the end of each chapter of this PhD thesis. In addition, chapter 7 presents an overall synthesis on global hydrogeological observations and proposes a conceptual model. The present chapter synthesizes the used approach and presents the main conclusions as well as the key results. It shows the progress supplied by the developed analyses in the general problematic of landslide characterization and flow modelling, in answering several pending questions. Finally the perspectives that open this work are presented.

In a first step, an integrated multidisciplinary characterization study on the internal structure of landslide taking place in low permeable porous environments is performed. The term of "low permeable porous environments (LPPE)" has been defined to describe all landslides occurring in environments of loose sediments. It includes all landslides in flysch zones (i.e. Gurnigel, la Simme and Niesen) and those taking place in Quaternary deposits (i.e. morainic terrains and fluvio-glacial drifts). They are different in terms of geological settings and inheritance, but hydrogeologically (i.e. physical parameter distribution and hydrogeological behaviour) they are very similar. The following case studies are selected: *La Frasse, Triesenberg, Hohberg, La Lécherette* and *Creux de l'Enfer* landslides in flysch environment, and *Travers* and *Ballaigues* landslides in Quaternary deposits. *La Frasse* landslide constitutes the core of this thesis, a complete multidisciplinary investigation integrating numerous geological, geophysical, hydrochemical and hydrogeological data is performed.

Depending on the scale of the study, the use of multiple data sets is required to constrain the interpretations of geological heterogeneity at a site. Several direct or indirect field investigation methods are thus applied in order to define the main characteristics of these environments. It includes; geophysics, borehole surveys, hydrochemical analyses, hydraulic well and infiltration tests, displacement measures, geotechnical laboratory testing. These methods allow the heterogeneity to be described, qualitatively and quantitatively, vertically in 1D, horizontally in 2D and according to several scales; at a local scale as well as a more regional scale. Thus, some may delineate large-scale features, such as permeable channels, others may detect finer-scale facies transition.

In a second step, the incidences of this heterogeneity on the hydrogeological behaviour of the landslide is evaluated thanks hydrogeological field observations and numerical flow modelling. 2D and 3D theoretical numerical tests allow studying the effects of heterogeneity on the flow, and thus identifying basic concepts. Thanks to the three dimensional model of *la Frasse* landslide several tests are effectuated. Ten different geological heterogeneity scenarios applied on the slice corresponding to the sliding surface are evaluated. It consists in varying the hydraulic conductivity of the matrix (capacitive impermeable fraction) and those from the special permeable features (conductive permeable fraction).
These various tests compared to the calibrated model allow a better understanding of the structure and the heterogeneity of the sliding surface and secondly on the importance in considering the local heterogeneity in flow modelling.

8.1 MAIN CONCLUSIONS

Observation and characterization of the geological heterogeneity demonstrated that:

1. **The heterogeneity is organised in…**
    - Connected structures
    - Isolated lenses
2. **The medium (nature of the material) is bimodal with…**
    - A capacitive fraction
    - A conductive fraction
3. **Duality of the aquifers…**
    - Saturated, confined or free
    - Unsaturated

Hydrogeological observations and numerical tests indicated that:

- The models are very sensitive to the distribution of the parameters;
- The geological heterogeneity has to be connected;
- The geological heterogeneity generate channelling effects;
- The upper and the lower part of the model present different hydraulic behaviours;
- The lower part and the upper part are linked according to the degree of continuity of the system; the spatial continuity of the physical properties;
- The conductive fraction favours the drainage of the system and fills an important hydrodynamic role essentially between the main hydrological events;
- The capacitive fraction controls the distribution of the hydraulic heads;
- The differences (hydraulic pressures) may be small;
- Incidence on slope stability evaluation;

8.2 KEY RESULTS

The geological heterogeneity

General characteristics. The strong impermeable dominance of the geological material is demonstrated. Geological surveys identified thin stratifications of gravely, sandy, silty and clayey banks, varying from point to point. At the *la Frasse* from instance the impermeable sediments (silty and clayey banks) represents 75% of the total of the investigated borehole cores. In other case studies, at *la Lécherette*, the ratio of permeable/ impermeable material varies from 1:3 to 1:9, and at *Creux de l'Enfer* from 1:1 to 1:4. In Quaternary sequences, at *Ballaigues La Praz*, the ratio is around 1:9, and present thus a more impervious character than in flysch environment; around 15% against 20-30 %. In addition, the lithofacies study at *la Frasse* shows a clear decrease of the percentage of the permeable material inside the most active zone "++" compared to the stabilized areas, indicating thus a decrease of the average permeability. The overall hydraulic conductivities are low with average values around 1E-5 to 1E-7 m/s. Permeabilities up to 1E-8 m/s are also measured at the *La Lécherette* and at *Ballaigues La Praz* (Quaternary deposits). In the meantime, note that at the *la Frasse,* data from two boreholes show an increase with depth, indicating that nearby the sliding surface the permeabilities are probably more permeable (i.e. 1E-4 m/s). These geological environments present thus a bimodal permeability; (i) low hydraulic conductivities characterizing the matrix (i.e. the flysch mass) and defining the capacitive fractions, and (ii) high permeable features, with high hydraulic conductivities. When these features are spatially connected, they are playing the role of the conductive fraction. On the contrary when these structures are disconnected, they fill the role of permeable isolated lenses.

Finally, the apparent resistivities measured thanks to radiomagnetotelluric surveys indicate very low values ranging from 15 to 150 Ohm.m. The highest values indicate the presence of sandy to gravely permeable structures.

The structures. Observations indicate that the structures are mainly discontinuous, representing either "channelized" bodies or individual isolated lenses. Various geometrical shapes and spatial extensions for a geological horizon are identified, including: pinched structures, inter-connected structures and multi-channelled system with strong thickness variations. For instance, the lithological facies analysis performed on the *la Frasse* borehole cores, indicate that thickness variations and discontinuity predominate. The mean thicknesses of the geological beds is around 2 meters, with gravely beds even thinner (mean value around 1 meter). Nevertheless, impermeable layers constituted by the clayey to silty material may be more important, up to 15 meters. Finally, the apparent resistivity maps indicate that these structures present interesting spatial continuity mainly oriented parallel to the sliding direction.

The organisation, spatial continuity. The organisation and spatial continuity of these structures is evaluated thanks to lithofacies analyses, well tests and vertical geomechanical characterization performed on the *la Frasse* case, as well as thanks to radiomagnetotelluric surveys effectuated on the selected case studies. These investigations permit to identify the vertical and horizontal organisation.

Vertical organisation

At a first sight, embedded Markov chain analyses and entropy estimation performed on the facies transitions matrix at *la Frasse* indicate that the heterogeneity is vertically defined by a random lithological succession without any organization. Each identified facies may be present anywhere in the sequence. In the meantime, a comparative study between the seven boreholes, indicate that the permeable structures may be preferentially concentrated at subsurface or near the sliding surface.

In the same order, the vertical investigation of the geotechnical parameters performed at the well FR2 (*la Frasse* landslide) indicated that no geomechanical stratification is identifiable. The entire mass has to be considered as unstable, since the measures indicated very high instability properties along the whole profile. No differentiated zones are thus identified. The radiomagnetotelluric surveys indicate a global increase of the apparent resistivities with depth, confirming also a more permeable character for the area near the sliding surface.

Horizontal organisation

Horizontally, at *la Frasse* lithofacies investigations indicated that spatial correlations even at the metric scale are often impossible. Globally, calculated correlation factors (i.e. pair correlations) indicate that there is no obvious relation between the boreholes, with $R^2 < 0.01$. Nevertheless, at a local scale (zonal correlations according to depth) some structures might be spatially correlated, with average R^2 between 0.03 and 0.11. A maximum value of $R^2 = 0.3$ for the boreholes situated outside the active zone "++" and at subsurface is calculated. In fact, observations show that outside the active zone "++", the structures are longitudinally as well as transversally more continuous. The medium is thus globally in the active zone "++" more reworked, due to intense deformation. As discussed hereinbefore, spatial correlations are not obvious. But a schematic representation of the spatial extension of the lithofacies is possible by simplifying the problem in a dual permeability medium; permeable and impermeable facies. Globally, the schematized correlations confirm the above-calculated correlation factors; transversal and longitudinal continuity identified near subsurface and at sliding surface. Finally, variogram analyses performed thanks to the geophysical investigation on the numerous apparent resistivity data acquired at different frequencies indicate the presence of continuous structures mainly oriented parallel to the sliding direction and presenting a maximum length of 40 meters. The width of these heterogeneous structures is rarely exceeding 10 to 20 meters. This defined width is partly confirmed by the hydrochemical and geological observation done at the *la Frasse* borehole platform (1995), where a high variability between boreholes spaced some 10 meters apart is observable. This is considered as the width of the permeable structures.

On the other hand, hydrogeological observations done thanks to pumping tests carried out in 2002 and 2003 from this borehole platform (complete shutdown); show that connectivity of the permeable structures is higher in a direction parallel to the landslide and reaches hundreds of meters. Typically, stopping the entire pumping platform and restarting only the P11 pump five days later showed that piezometers Z203 and Z204 situated more than 200 meters away reacted strongly whereas others much closer do not show any response. The observed behaviours are in the meantime relatively contrary to what expected, with strong decreases in the lower part. For instance the piezometer Z114 situated 100 meters apart from the platform, presented a regular strong decrease up to 16 meters in 5 days.

The role of spatial connectivity

The observations have shown that inside this mass, complex flowpaths may connect distinct zones. These zones may consist in isolated aquifers or spatially well developed flow systems. These spatial connections represent thus preferential flowpaths taking place either in more permeable zones (sandy and gravely levels) of the heterogeneous medium or in structural discontinuities. In the first case, the fluid flow seeks the less resistive pathways and therefore the flow through a heterogeneous medium takes place in channels. These channels are not physical entities, contrary to structural discontinuities, meaning that if the direction of the hydraulic gradient is changed the locations of the channels are also changed. The emergence of channelling as a function of the degree of the heterogeneity is shown in chapter 5. The hydraulic responses

to the several well tests confirm that intense channelling is occurring in *la Frasse* landslide system. In the meantime, it is quite difficult to identify the cause of this channelling (heterogeneity or discontinuity), however, both may play a role in the distribution of the flows in the system. If this phenomenon is linked to the geological context, it may thus be a general behaviour for aquifers in landslide taking place in these particular environments (Quaternary or flysch deposits).

Incidences on the hydrogeological behaviour of the landslide

Field observations. Incidences of this heterogeneity on the hydrogeological behaviour of the landslide are obvious when observing the distribution of vertical inflows inside a well. In fact, the analysis of the different piezometric levels at *la Frasse*, recorded since 1982 at different locations, indicates that the elaboration and the interpretation of a piezometric map are very questionable in such geological environments. The piezometric levels may be hardly correlated, and due to the extreme geological heterogeneity, the hydraulic equipotential surfaces have an irregular behaviour, and may be quite numerous along a vertical profile. For instance well Z205, in which three confined aquifers are observed, demonstrates clearly that a borehole may cut through several equipotential surfaces. Under these conditions, the water level measure in the borehole neither represents the local hydraulic potential of the mass nor the upper level of the saturated zone. The nature of the flows is extremely complex and must be locally assimilated as a complex inter-connected system of perched water tables. Each water level represents a local isolated perched aquicludes. In the same order since 1995 (commissioning of the borehole platform) strange hydrogeological behaviours are observed; in the lower part of the slide (between the road and the platform), the recorded water levels show an increase from 3 to 9 meters. Exception done for well Z119 presenting a decrease of 7 meters. This well is obviously showing an opposite behaviour than observed, and above all expected. In the meantime, in the upper part of the slide expected decreases varying from 0.25 meters up to 8.2 meters are observed. Note that vertically also, the behaviours may strongly change. For instance Z205 equipped with pressure cell devices for measuring hydraulic pressures at three different depths, show that the water level of the intermediate aquifer (cell at - 39 meters) presents a decrease of 3.9 meters, twice bigger than for the low (-2.4 meters) and the deep aquifers (- 2.2 meters). The aquifers are thus rather confined. This may equally be confirmed by the calculated specific storage coefficients (Ss) at la Frasse; around 1E-3 [m-1] and 1E-4 [m-1]. These values vary locally and spatially.

Finally the heterogeneous distribution of the flows is clearly showed thanks to hydrochemical analyses. Cation and ^{18}O isotopic analyses indicate that the flows inside *la Frasse* are characterized by a bimodal hydrodynamic flow system. The first one, and predominant, is defined by slow and locally deep flow through the impermeable matrix of the landslide mass, allowing cation exchanges (i.e. Ca-Na cation exchange reactions and SO_4^{2-} dissolution). Locally, inflows from surrounding units can also change the chemistry and enrich the water with sulphated waters. These waters are hydrochemically evolved and are characteristic of the capacitive fraction. The second water system is characterized by hydrochemical poorly evolved waters, which mainly flow through the conductive fraction. These permeable structures enable fast circulations, and their extension is only controlled by developed internal connections. These fast circulations may be locally shallow or very deep. These circulations may drive surface water deep into the mass through subvertical connections, and are in part, alimented by rain infiltrations. The origin of the water has to be searched mainly in the surrounding units, since the results (i.e. ^{18}O isotope study) indicate that at least 60% of the sampled water are infiltrating outside the upper limits of *la Frasse* and laterally at lower altitudes.

2D and 3D numerical modelling. First, theoretical two- and three-dimensional flow models are used to investigate the effects of the spatial variability of the hydraulic conductivity on the underground flows; i.e. hydraulic pressures and velocity distributions. The role of the connectivity in generating flow channelling is examined thanks to the observation of close relations between the permeability and the hydraulic pressures. Flow pathlines and velocity analyses in a vertical and horizontal direction are examined. The sensitivity analysis shows clearly that the organization of the flows depends on the heterogeneity of the hydraulic properties and their spatial correlation, i.e. the spatial connectivity of zones of similar hydraulic properties. The relation between local permeability and hydraulic pressures is not straight. Strong channelling effects are observed in highly heterogeneous porous media. The development of flow channelling as a function of the variance of the natural log permeability values and the correlation lengths is demonstrated. In addition, this study shows that, in a three-dimensional porous media with strongly variable hydraulic properties, the flow seeks the less resistive pathways (high hydraulic conductivity) generating sometimes vertical drainance. According to the anisotropy (ratio between the correlation lengths λx and λy) and the degree of heterogeneity (variance) of the medium; three types of flows are distinguishable: (1) "homogeneous" distributed flows, (2) strongly channelized flows and the (3) intermediate flows. In addition to these three types of flows, two types of permeable structures are identified: 1) Primary structures (connected structures) and 2) secondary structures (disconnected structures, i.e. isolated lenses).

In a hydrodynamical point of view, these structures behave differently. The first one acts mostly positively on the system, driving efficiently the flows and lowering the hydraulic pressures. And thanks to optimal spatial connectivity may drain the system. The second rather generate negative effects on the system, concentrating the flows and increasing locally strongly the hydraulic pressures (overpressures effects).

Then, thanks to the three-dimensional flow model of *la Frasse* several different geological heterogeneity scenarios applied on the slice corresponding to the sliding surface allow evaluating the roles and the characteristics of the capacitive and conductive fraction. Globally, these various tests show that, the models are very sensitive to the distribution of the parameters. The geological heterogeneity has to be considered, and structurally connected. Especially, the sliding surface must be constituted by a structured heterogeneity of the hydraulic permeabilities, since a homogeneous distribution buffers the computed hydraulic responses. The permeability of this surface corresponds to an intermediate to low permeability. Outside this range of values, the computed hydraulic pressures are showing very flat and smoothed values. The surface is constituted by permeable features (conductive fraction), representing coarser system of channels. These structures are spatially connected, longitudinally to the sliding direction. In the case of disconnected structures, the flows are perturbed, and the main water inputs in the upper part are not reflected in the lower part of the model. The system is not correctly drained, and overpressure zones are generated.

If this conductive fraction is neglected, the differences in the computed hydraulic pressures between the models with and without permeable channels are low, but may in terms of stability, play a major role. For instance, an overpressure of 50 kPa applied on a geological layer 10 meters thick won't cause severe instability, while applied on a layer 1 meter thick, the resulting seepage force will generate strong instable behaviour. The upper and the lower part of the model present thus different hydraulic behaviours, and are linked according to the degree of continuity of the system; the spatial continuity of the physical properties. This is also confirmed by the before-mentioned hydrogeological field observations. This behavioural difference is well observable at Triesenberg. Strong hydrological reactions in the upper part and smooth piezometric variation in the lower part are recorded. Nevertheless, the opposite behaviour is observed at *la Frasse*, namely low reactions in the upper part. In that case, strong hydraulic variations are recorded in the intermediate and

lower part, up to 12 meters. Finally, models show that the conductive fraction of the medium favours the drainage of the system and fills an important hydrodynamic role essentially between the main hydrological events. The capacitive fraction controls the distribution of the hydraulic heads. In a hydrodynamical point of view, these features may be the seat of critical hydraulic pressures variation, especially when confined, and may control the activation of the movements of the slide. In a hydrogeological point of view, the interesting scenario is to be in presence of a permeable structure imbricated into an impermeable medium and spatially connected to others, in order to create particular hydrodynamic conditions (overpressures or underpressure conditions). These configurations are hydrogeologically considered as being mainly confined, in opposition to free surfaces, and enable brutal variation of hydraulic pressure in response to hydrological impulses. Moreover, these variations are considered to be the main factors controlling the stability of a slide. For instance, at *la Frasse* thanks to the lithofacies successions, the probability to have a confined permeable structure pinched between impermeable layers is calculated. Globally, when facies P4 is present, the probabilities that P4 is embedded between two facies P1, or two facies P2, are respectively 0.15 and 0.27. Locally, in the active zone "++", the probability to have overpressures conditions may reach 0.5.

Temporal evolution of the system

The observations indicate that the aquifer systems in these landslide contexts are under unsteady flow regimes. For instance, the temporal evolution of the inflow rates of the pumping rates at the borehole platform of *la Frasse* from 1995 illustrates it. One may observe that during the first years of commissioning the pump P2 very active, while since 2003 no flow rates are recorded anymore. Two pumps, P6 and P7, are maintaining constant flow rates. On the contrary, pumps situated at the extremity of the system (P18 to P22) never recorded influxes.

Conceptual model

Globally, landslides occurring in these types of media are defined by a heterogeneous environment with "fracture" flows and discontinuity porosity. The overall hydraulic conductivity is low, and locally high permeable zones exist. Regional groundwater circulations are limited and are forming local interconnected aquicludes organised in thin aquifers, and presenting saturated and unsaturated zones. Landslides in these special contexts are characterized by two important inflows, namely effective infiltration and lateral inflows from the neighbouring units. Water transfer between the stabilized mass and the active mass may be important and thus have to be considered. The existence of water transfer between the bedrock and the landslide mass (stabilized and active) is not well established. The bedrock and the landslide mass present a hydrological behavioural independence.

A conceptual model based on a simple reservoir approach is proposed. It allows representing most of the field observations and the main characteristics, namely the organized heterogeneity and the duality of the aquifers. The system is represented by various water pockets more or less saturated (reservoirs). Complex storage capacities and plug-flow effects may record past events and reactive sliding processes several months after the last important rainy event. An important hydrological event is not necessarily associated to a reactivation.

According to the degree of complexity of the system (saturation, connectivity...) localized geological modification (variation of permeability, reservoir burst...) may produce a chain reaction, and generate failures at unexpected places. The conductive fraction favours the drainage of the system, whereas the capacitive fraction controls the distribution of the hydraulic heads.

The role of phreatic nappe, through the conductive fraction, is to drain and control the hydrological equilibrium of the system. Therefore landslide remediation done thanks to deep drainage gallery, as discussed and presented in chapter 6, is obviously the most valuable method for this type of landslides. It supports and enhances the natural effects of the conductive fraction in draining the system.

Incidences on slope stabilization techniques

All these previous tests are not only of academic value but were designed to give answer to practical questions to engineering problems. In this context the efficiency of civil engineering works was evaluated according to the heterogeneity of the medium. This study describes transient hydrogeological and geomechanical models realized in the framework of the stabilization work of the *la Frasse* landslide. These models evaluate the efficiency of the drainage gallery below the sliding mass during a crisis in terms of reduction of the deformation velocities and increase of the factor of safety of the landslide.

First, based on the conceptual hydrogeological model, a flow computation including geology and transient hydraulic conditions has been carried out with FEFLOW. The model has been used to evaluate the impact of a deep drainage gallery with subvertical pipes towards the surface in terms of hydraulic pressure on the behaviour of the landslide. Thanks to a coupled elastoplastic 3D finite element model (Z_SOIL, 2004) the hydro-mechanical behaviour of the landslide under drainage during a crisis could be evaluated and factors of safety calculated. As suggested in this study, the hydrogeological models are very sensitive to the geometry of the field heterogeneities, principally to the connectivity of the permeable structures. In these conditions of particular high heterogeneity and of complex hydraulic relations, the remediation design has to be able to intercept both the water from the sliding surface and the waters in the whole mass. In this context, the models cannot in principle define the exact location of the pipes, but enable to establish the mean spacing which should be adopted in function of the local geological conditions encountered during the execution.

The results show that a mean spacing between the pipes of the order of 15 meters (variant 1) is capable to lower the hydraulic head about 36 meters along the work at the sliding surface, and to intercept around 45% of the hydraulic flux of the sliding mass. The variants increasing the spacing to 30 meters (variant 2) and then to 60 meters (variant 3), indicate a lowering of the hydraulic head from 34 and 30 meters respectively. These differences are low from a hydraulic point of view, in return, present implications more obvious in terms of factor of safety (FoS). Concerning the deformation (hydro-mechanical coupled calculation) the presence of the drainage gallery induces a strong diminution of the predicted displacements (from 101cm for the model without drainage to around 15-20 cm for the drained models (i.e. variant 1, 2 and 3)). The influence of the pipe spacing on the maximal predicted horizontal displacements is very low (14 cm for the variant 1 and 19 cm for the variant 3). In the meantime, only a spacing of 15 meters enables a significant gain of security. The variant 1 indicates a FoS=1.30, again FoS =1.15 for the two other variants. For memory, the non remediate model has a FoS of 1.05. In conclusion, this study enables to validate and confirm the recommended solution namely a drainage gallery equipped with pipes with a mean spacing of 10 meters (pipes mean spacing of the execution project). Indeed the fineness of the mesh used in the numerical models did not enable to insert as many pipes. The results of variant 1 – with a mean spacing of 15 meters – are considered to be representative of the expected efficiency of the execution project.

Importance of the integration of the geological heterogeneity in flow modelling

In conclusion, a lesson learned from these studies is that proper aquifer characterization is necessary for safe and effective design of hydraulic stabilization works, such as a drainage gallery. The findings also suggest that the simulation of an aquifer represented as an equivalent porous medium will neglect the effects of the heterogeneity. Thus, the general geological heterogeneity has to be taken into account when evaluating aquifer systems and constructing groundwater flow models.

8.3 PENDING QUESTIONS

Finally, this PhD Research helps to answer the following questions:

Q1: Do these types of landslides share a common geological structure? Or should each case be considered individually?

YES at a regional scale, NO at a local scale; each case may be handled individually.

Q2: Concerning the influence of the heterogeneity on the hydraulic pressure distributions, is it possible to deduce a general behaviour from the geological context?

YES, if the heterogeneity of the permeability (degree of heterogeneity) is assessed and the correlation lengths (connectivity and anisotropy) identified, even roughly.

Q3: According to the geological context and the degree of heterogeneity, how efficient a given stabilization method will be?

Instability occurs when the pre-existing hydrological equilibriums are disturbed. The aim of remediation is to stabilize and thus to bring back the system to its initial state of equilibrium. The design of such stabilization methods is only possible if one has the fullest possible advance knowledge of the natural state of equilibrium of the area before the activation. Hence the design and therefore the construction of any underground work must be preceded by activity, termed the survey phase, to obtain that knowledge and this is performed by acquiring all possible information on the morphology, structure, tectonics, stratigraphy, hydrogeology, geotechnics, geomechanics and stress states, which characterise the geology of the body.

Thus the efficiency will be function of the dimensioning of the stabilization method based on this field characterization (i.e. conceptual model). For instance in case of drainage systems of the localisation and spacing of the pipes. An adequate conceptual model, elaborated after detailed and integrated pluridisciplinary field investigations allows defining which method should be the most appropriate to each case study: limited works (boreholes precisely located, or in reason of the underground structure complexity, more expensive general works (e.g. gallery with multiple drains).

In the case of drainage systems, a sustainable remediation solution must drawdown and stabilise hydraulic heads in the all thickness of the system. This study has demonstrated that the efficiency of this type of work is closely linked to the geological and hydrogeological characteristics of the medium, since spatial connectivity drains and controls the hydrological equilibrium of the system. Therefore landslide remediation done thanks to deep drainage gallery should support and enhances this natural effect. Dimensioning implies the full knowledge of the hydrogeological conditions, for instance, if the aquifer is globally captive (small

specific storage coefficient), wells or drains will have fast and long distance effects on the heads. However, drawdown and hydraulic variations may be observable at a distance of several hundreds of meters. In that sense, the captive nature of the aquifer, due to its high heterogeneity, is an aggravating factor since head fluctuations are higher and faster, but on the other hand, gives a much larger radius of influence to remediation wells or drains. The dimensioning is thus influenced by the assumed initial conditions; the effects of drains can be overestimated according to the results obtained considering the observed variably saturated initial conditions.

Finally, drainage is a principal physical measure used in mitigation of landslides because it is an economical and efficient way to alleviate positive pore-water pressures that promote slope failure. Nevertheless, drainage systems are usually designed from practical experience, and the real effect of this mitigation system on slope stability is seldom quantified.

8.4 PERSPECTIVES

Considerable progress has been made during the last decades in understanding and describing the geological and hydrogeological behaviours of unstable masses. Most processes are now reasonably well understood at the scale of the slide (regional), since most studies have been carried out at that scale. But, there is an evident lack of observations at a largest scale, arising primarily from the local heterogeneity of the medium with parameters changing from point to point and the difficulty in collecting data.

The data should include uppermost: measures of the hydrodynamic conditions (water table level, hydraulic pressures) and displacements, in addition to the classical hydrological measures (precipitation, evapotranspiration, temperatures, etc.). Ideally, the points of measurement should be spatially close, including a complete monitoring in continue over a period of one or two years. This configuration would provide very indicative data. Spatially, a three-dimensional observation network would allow a complete "scanning" of the entire mass horizontally and vertically, and thus accurate spatial correlations.

In our opinion, future work should take advantage of the *la Frasse* drainage gallery that is actually in progress (commissioning end-2008). This case could represent a test site for experimental observations. This drainage gallery allows, thanks to the perforated pipes, the investigation of the entire mass, and an ideal location from which various hydraulic tests could be performed. The aim of the hydrogeological monitoring network is to provide continuous information on the effects, regularities, and trends of the natural processes taking place in this special context of instability.

Thus, in order to complete the present PhD thesis, future study will concentrate on the close relations between the hydraulic parameters and the geological heterogeneity on a very local scale.

It will emphasize the following topics:

Data acquisition

(a) A water sampling for hydrochemistry characterization purposes (at least one sample per week for each pipe, during one or two years), including ^{18}O (natural tracer) and cations analyses;

(b) Installation of water pressure cells on different places inside the pipes, to cover the maximum area;

(c) Installation of inclinometers on different places inside the pipes, to cover the maximum area;

(d) Hydraulic well tests;

(e) A campaign of artificial tracers to locate precisely preferential flow paths, or at least preferential areas;

(f) A geophysical survey, including borehole diagraphy (e.g. resistivity, spectral gamma…) and borehole seismic diagraphy (i.e. cross-hole type);

Data Processing

(g) The development of a local numerical model to simulate local-scale processes, incorporating the measured data, in addition to the yet existing three-dimensional model;

(h) The application of direct current electrical resistivity inverse modelling, including resistivity imaging methods, will allow testing several electrical resistivity distribution models, and to discuss about plausible heterogeneity images of the landslide mass.

An interesting correlation between hydrochemistry and hydraulic pressure variations (change of hydrochemistry according to pressures) will inform about the temporal and spatial dynamic of the system; modification of flow paths and contribution of the various boundary limits. Thus, this characterisation will allow the calibration and validation of several numerical models of both groundwater flow and electrical resistivity models.

Besides, this investigation may inform about the scope of action of the drainage pipes. According to the geological setting around each pipe, the scope of action may vary strongly. This variation will inform about the internal structures of the medium.

Finally, the evaluation of the efficiency of the drainage gallery will then be determined locally for each pipe, and not only globally. Dimensioning criteria will be formulated for future drainage works.

9. References

Aiken J. (1993): A three-dimensional characterization of a coarse glacial outwash deposit used for modeling contaminant movement, M.S. thesis, Dep. Of Geol., Univ. of Wis.-Madison, Madison.

Ambrosi and Thüring (2004): Geotechnical modeling of large rock slope movements – the Cerentino landslide (Ticino,Switzerland). 2nd Swiss Geoscience Meeting, Lausanne, 2004.

ALPGEO (2006) : Glissement des Peillettes, projet de défense N° 431-VS9'032 - Campagne de forages (2002), assainissement des drainages (2001-2004) et suivi hydrogéologique (1998-2005) - Rapport final pour l'Etat du Valais, DTEE - SRCE - SFP - Géologue cantonal, avril 2006, 41 p., 14 annexes et 1 dossier photos, inédit.

Bakr AA., Gelhar L.W., Gutjahr A.L. and MacMillan JR. (1978): Stochastic Analysis of Spatial Variability in Subsurface Flows. 1. Comparison of one-and three-Dimensional Flows. Water Resources Research Vol. 14, No. 2, p 263-271.

Basabe P. P. (1993): Typologie des eaux souterraines du flysch de la nappe tectonique du Niesen (Préalpes Suisses). Thèse de doctorat, EPF Lausanne, Dép. Génie Civil.

Bellin A, Rubin Y. (1996): Hydro_gen, a spatially distributed random field generator for properties. Stochastic Hydrogeology and Hydraulics, 10(4), pp. 253-278

Bernasconi R., Turberg P., Müller I., Tullen P. and Parriaux A. (2001): Investigation of landslide areas with radiomagnetotelluric geophysics: The case of Triesenberg (Liechtenstein). Proceeding of the Landslides Conference in Davos.

Bernasconi R. (2002b): Tiefbauamt des Fürstentums Liechtenstein - Hangsanierung Triesenberg-Hydrogeologische Überwachung – Messdaten 1999-2001. Hydrogeologischer Bericht No. 1124-03.

Bernasconi-GEOLEP-LMS_final report (2006): Geologische, Hydrogeologische und Geomechanische Modellierung des Erdrutsches von Triesenberg (Fürstentum Liechtenstein), auftrag des Tiefbauamtes vom 12.dezember 2003, Schlussbericht 2006. GEOLEP-LMS Dr. Riccardo Bernasconi "Beratender Geologe und Hydrogeologe" (sargans).

Bersier A. et Weidman M. (1970): Le glissement de terrain de Cergnat – La Frasse (Ormont-Dessous, Vaud). Bull. Soc. vaud. Sc. nat., 33, 70.

Beylich A.A., Kolstrup E., Linde N., Pedersen L.B., Thyrsted T., Gintz D. and Dynesius L. (2003): Assessment of chemical denudation rates using hydrological measurements, water chemistry analysis and electromagnetic geophysical data. Permafrost Periglac., 14, 387-397.

Beylich A.A., Kolstrup E., Thyrsted T., Linde N., Pedersen L.B. and Dynesius L. (2004): Chemical denudation in arctic-alpine Latnjavagge (Swedish Lapland) in relation to regolith as assessed by radio magnetotelluric-geophysical profiles. Geomorphology, 57, 303-319

Bilgot S. (2007) : Application de la méthode des géotypes à la cartographie des secteurs de protection des eaux souterraines ainsi qu'à la détermination de la susceptibilité aux instabilités de versants. Travail de master effectué au Geolep (EPFL).

Biot M.A. (1956): General solutions of the equations of elasticity and consolidation for a porous material. J Appl Mech 78:91–96.

Bollinger D. And Noverraz F. (1996): Pilotstudie Karte der Bodenbewegungsgefahren 1:25000, Blatt 1247 Adelboden. Rapport géologique No 20, Service hydrologique et géologique national (OFEFP) OCFIM

310.022d, 1-40.

Bonnard Ch. (1984): Determination of slow landslide activity by multidisciplinary measurements techniques. In: International symposium on field measurements in geomechanics, Z_rich, Balkema edn, 1:619–638

Bonomi T. and Cavallin A. (1999) : Three-dimensional hydrogeological modelling application to the Alverà mudslide (Cortina d'Ampezzo, Italy). Geomorphology. Volume 30, Issues 1-2, Pages 189-199.

Bonzanigo L. Eberhardt E. and Loew S. (2000): Measured Response to a Drainage Adit in a Deep Creeping Slide Mass. Landslides in research, theory and practice. Ed. by E.Bromhead, N.Dixon and ML. Ibsen. Proceedings of the 8th International Symposium on Lanslides held in Cardiff on 26-30 June 2000. Thomas Telford editions.

Bonzanigo L., Eberhardt E. and Loew S. (2001): Hydromechanical Factors controlling the Creeping Campo Vallemaggia Landslide. Davos, UEF.

Bossy F. (1999): Etude hydrogéologique des glissements de terrain du «Creux de l'Enfer» et de «La Lécherette». Travail de Diplôme du Postgrade en Hydrogéologie de Neuchâtel.

Bouma A.H. (1962): Sedimentology of Some Flysch Deposits: A Graphic Approach to Facies Interpretation. Ed. Elsevier.

Bromhead E.N. (1992): The stability of slopes. Blackie Academic and Professional, London, 411 pp.

Bruderer-Weng C., Cowie P., Bernabe Y. and Main I. (2004): Relating flow channelling to tracer dispersion in heterogeneous networks - advances in water resources, 27, 843-855.

Cardinali M., Galli M., Guzzetti F., Reichenbach P. and Borri G. (1994): Relazioni fra movimenti di versante e fenomeni tettonici nel bacino del Torrente Carpina: Geografia Fisica e Dinamica Quaternaria, Vol. 17, pp. 3-18.

Cagniard L. (1953): Basic theory of magnetotelluric method of geophysical prospecting; Geophysics 18 605–635.

Commend S., Geiser F. and Tacher L. (2004): 3D numerical modelling of a landslide in Switzerland, in Proc. of NUMOG IX, Ottawa.

Corominas J. (2001): Landslides and Climate, Keynote Lectures from the 8th International Symposium on Landslides, No 4, pp 1–33.

Crosta G.B. (2001): Failure and flow development of a complex slide : the 1993 Sesa landslide. Engineering Geology, Elsevier Science, n° 59, pp. 173-199.

CSD (1980): Etude hydrogéologique, Rapport technique, VD 97, AR N9b Vallorbe – Chavornay, section 362-368 Ballaigues-Montcherand, Département des Travaux Publics Service des Eaux et de la Protection de l'Environnement.

Dagan G. (1989): Flow and Transport in Porous Formations. Springer, New York. 465 pp.

Dagan G. and Neuman Sh. P. (1997): Subsurface flow and transport: A stochastic Approach. International Hydrology series. 241p.

De Marsily Gh. (1986): Quantitative hydrogeology - groundwater hydrology for engineers. academic press, inc.

De Marsily Gh., Delay F., Gonçalvès J., Renard Ph., Teles V. and Violette S. (2005): Dealing with spatial heterogeneity. Hydrogeol J (2005) 13:161–183.

Dematteis A. (1995): Typologie géochimique des eaux des aquifères carbonatés des chaînes alpines d'Europe centrale et méridionale. Thèse EPFL, no 1419, Dép. Génie Civil.

Desai C.S., Samtani N.C. and Vuillet L. (1995): Constitutive modelling and analyses of creeping slopes. Journal of Geotechnical Engineering, ASCE, 121(1): 43-56.

Desvarreux P. (1988) : Le reconnaissance géologique des mouvements de terrain. Stage

ENCP, Stabilité des pentes, Grenoble.

Dounias G.T., Potts D.M. and Vaughan P.R. (1988): Finite element analyses of progressive failure: two case studies. Computers and Geotechnics, 6: 155-175.

Dubois J.-D. (1993): Typologie des aquifères du cristallin: Exemple des massifs des Aiguilles Rouges et du Mont Blanc (France, Italie et Suisse). Thèse de doctorat, Nº 950, EPFL, Dép. Génie Civil.

Dupuit J. (1863) : Etudes théoriques et pratiques sur le mouvement des eaux dans les canaux découverts et à travers les terrains perméables, Second Edition, Paris: Dunod, 304 p.

DUTI Détection et Utilisation de Terrains Instables (1986),

Eberhardt E., Thuro K. and Luginbuehl M. (2005): Slope instability mechanisms in dipping interbedded conglomerates and weathered marls- the 1999 Rufi landslide, Switzerland. Engineering Geology, 77: 35-56.

Elmi C., Fini A., Francia R., Lizzani A. and Genevois R. (1993): Large landslides in flysch formations in the Northern Apennines, Italy: analysis and comparison of the geomorphological features and geotechnical behaviour. In Chowdury and Sivakumar (editors), Environmental Management, Geo-Water &Engineering Aspects, Balkema, Rotterdam, pp. 299-304.

Fabre R., Lebourg T. & Clement B. (2000): Les dépôts morainiques holocènes de la zone axiale pyrénéenne : approche déterministe de leur instabilité à Verdun sur Ariège, (Pyrénées centrales, France). Bulletin of Engineering Geology and the Environment, Springer Verlag, vol. 58, n°2, pp. 133-143.

Feflow groundwater modelling software, Wasy AG, Berlin

Fell R. (1994): Stabilization of soil and rock slopes. In: Proc East Asia Symp and Field Worksh on Landslides and Debris Flows, Seoul, Rep 1, pp 7–74.

Fischer G., Schnegg P.-A., Peguiron M.and Le Quang B.V. (1981): An analytic one-dimensional magnetotelluric-resistivity (RMT-R 12–240 kHz), Geophys. J. R. Astron. Soc. 67 (1981), pp. 257–278.

Fogg G. E. (1986): Groundwater Flow and Sand Body Interconnectedness in a Thick Multiple-Aquifer. System, Water Resources Res. 22 (5), 679–694.

François B., Tacher L., Bonnard Ch., Laloui L. and Triguero V. (2007) : Numerical modelling of the hydrogeological and geomechanical behaviour of a large slope movement : the Triesenberg landslide (Liechtenstein). Can. Geotech. J. 44 : 840-857.

Frenette M. (1964): Etude de colmatage dans un milieu poreux dde granulométrie

étendue.Thèse de l'Université de Grenoble, France.

Gelhar L. W. (1993): Stochastic Subsurface Hydrology, Engelwood Cliffs, New Jersey.

Gervreau E. (1991): Elude de l'évolution des versants naturels en mouvement : prévoir, alerter. Thèse. Paris. 244 p.

Grivas D.A. and Chowdhury R.N. (1988): Two and three dimensional progressive failure of slope : Model development and implementation. Landslides. Proceeding of the fifth international symposium on landslides, 10-15 July 1988, Lausanne, Balkema, Rotterdam, Netherlands, vol. 1, pp. 643-648.

Goodman R.E., Moye D.G., Van Schalkwyk A. And Javandel I. (1965): Groundwater inflows during tunnel driving. Eng. Geol., 2, 39-56.

Goovaerts P. (1997): Geostatistics for Natural resources evaluation. Applied geostatistics series, Oxford university press, Inc. 481 p.

Guzzetti F., Cardinali M. And Reichenbach P. (1996): The influence of structural setting and lithology on landslide type and pattern. Environmental & Engineering Geoscience, Vol. II, No. 4, Winter 1996, pp. 531-555.

Hattori I. (1976): Entropy in Markov Chains and Discrimination of Cyclic Patterns in Lithologic Successions. Mathematical Geology, Vol. 8, No. 4.

Harbaugh J. W. and Bonham-Carter G. F. (1970): Computer simulation in geology: John Wiley & Sons, New York, 575 p.

Heuer R.E. (1995): Estimating rock tunnel water inflow. Proceedings of Rapid Excavation and Tunneling Conference, San Francisco, 41-60.

Hutchinson JN (1977): The assessment of the effectiveness of corrective measures in relation to geological conditions and types of slope movement. Bull IAEG 16: 131–155.

Isaaks E. H. and Srivastava R. M. (1989): An Introduction to Applied Geostatistics. Oxford Univ. Press, New York, Oxford.

Jäckli, H. (1970): Kriterien zur Klassifikation von Grundwasservorkommen. Eclogae Geol. Helv., Vol. 63/2, 389-434.

Jacob C.E. and Lohman S.W. (1952): Nonsteady flow to a well of constant drawdown in an extensive aquifer. Am. Geophys. Union Trans., v. 33, no. 4,p. 559-569.

Jansson P.E. (2003): Physical Processes. In:Bendi, D.K. & Nieder, R. (Eds.) Handbook of Processes and Modeling in the Soil-Plant-System. Haworth Press, New York, pp.5-26.

Jansson P.E. and Karlberg L. (2001): Coupled heat and mass transfer model for soil-plant atmosphere systems., Division of Land and Water Resources, Departement of Civil and Environmental Engineering, Royal Institute of Technology. TRITA-AMI REPORT 30 87.

Jeannin P.-Y. (1998): Structure et comportement hydraulique des aquifères karstiques, PhD thesis,

Neuchâtel, 237 pp.

Johnson K. A. and Sitar N. (1990): Hydrologic conditions leading to debris-flow initiations, Can. Geotechnical J., 27, 789–801.

Jones D.K.C. and Lee E.M. (eds) (1994): Landsliding in Great Britain. Department of the Environment, HMSO, London, 361 pp.

Jussel P., Stauffer F. and Dracos T. (1994a): Transport modeling in heterogeneous aquifer, 1, Statistical description and numerical generation of gravel deposits, Water Resour. Res., 30(6), 1803– 1817.

Kilchmann S. (2001): Typology of recent groundwaters from different aquifer environments based on

geogenic tracer elements. Thèse EPFL, no 2411, Dép. Génie Civil.

Kilchmann S., Waber H. N., Parriaux A. and• Bensimon M. (2004): Natural tracers in recent groundwaters from different Alpine aquifers. Hydrogeology Journal vol. 12/6.

Kiraly L. (1975): Rapport sur l'état actuel des connaissances dans le domaines des caractères physiques des roches karstiques. In: Burger A. and Dubertret L. (Eds), Hydrogeology of karstic terrains, Int. Union of Geol. Sciences, B, 3, 53- 67.

Koltermann C. E. and Gorelick S. M. (1996): Heterogeneity in sedimentary deposits: A review of structure-imitating, process-imitating and descriptive approaches, Water Resour. Res., 32, 2617–2658.

Krähenbühl S. (2007) : Prévision de la sensibilité locale d'un versant aux mouvements de terrain par l'analyse des indices topographiques, géologiques et hydrogéologiques. Cas du glissement de terrain de Travers (Canton de Neuchâtel, Suisse). Mémoire de Master en Science et Ingénierie de l'Environnement (SIE), EPFL LASIG GEOLEP.

Krohn J.P. (1992): Landslide mitigation using horizontal drains, Pacific Palisades area, Los Angeles, California. In Landslides/Landslide Mitigation. Eds. J.E. Slosson, A.G. Keene and J.A. Johnson, Geological Society of America, 63-68.

Krumbein W.C. and Dacey M.F. (1969): Markov chains and embedded Markov chains in geology,Journal of Mathematical Geology 1 79–96.

Lacube, J. & Durville, J.-L. (1989): Un essai de fichier informatique sur les mouvements de terrain. Bulletin LCPC, n° 161, pp. 86-89.

Lambe T.W. And Whitman R.V. (1969): Soil Mechanics. JohnWiley & Sons, Inc., 553p.

Lateltin O., Beer C., Raetzo H. and Caron C. (1997) : Instabilités de pente en

terrain de flysch et changements climatiques. Rapport final du Programme National de

Recherche : Changements climatiques et Catastrophes naturelles. PNR 31, 168 p.

Locher D. and Tacher L. (2008): An evapo-transpiration controlled landslide in Switzerland: The Steinernase case. Geophysical Research Abstracts, Vol. 10, EGU General Assembly 2008.

Long JCS, Billaux D.M (1987): From field data fracture network modeling: an example incorporating spatial structure. Water Resource Research 23:1201-1216.

Louis (1976): Introduction à l'hydraulique des roches. PhD thesis, Paris.

Lugeon M., Paschoud E. et Rothpletz F. (1922): Rapport d'expertise sur le glissement des Frasses, Etat de Vaud, Département des Travaux Publics, Service des Routes.

Lutz T., Parriaux A. et Tissières P. (1987): Traçage au gouffre du Chevrier (Préalpes vaudoises) et méthodes d'identification de l'uranine à faible concentration. Tiré à part du Bulletin du Centre d'Hydrogéologie de l'Université de Neuchâtel, n°7.

Maillet E. (1905): Essais d'Hydraulique Souterraine et Fluviale. Herman, Paris, France.

Mandia Y. (1993): Typologie des aquifères évaporitiques du Trias dans le Bassin lémanique du Rhône (Alpes occidentales). Thèse de doctorat, EPF Lausanne, Dép. Génie Civil.

Mangin A. (1975): Contribution à l'étude hydrodynamique des aquifères karstiques. Thèse de doctorat ès

science, Univ. de Dijon (publié dans Ann. Spéléol. C.N.R.S. T. 29/3, pp. 283-332, T. 29/4, pp. 495-601, T. 30/1, pp. 21-124). In Paris.

Manetti L. and Steinmann G. (2007): 3DeMoN ROBOVEC – Integration of a new measuring instrument in an existing generic remote monitoring platform .7th International Symposium on Field Measurements in Geomechanics, 24-27 September 2007, Boston, MA.

Maréchal J.C. (1998): Les circulations d'eau dans les massifs cristallins alpins et leurs relations avec les ouvrages souterrains.. Thèse EPFL, no 1769, Dép. Génie Civil.

Mari J.-L., Sequeira J. and Guiard C. (1999): Caractérisation de volumes numériques binaires par surfaces implicites. In 12braes journées de I4FIG, AFIG'99, pages 49-58, Reims, France.

Martin P.L. and Warren C.D. (1992): The design and performance of drainage measures installed for the stabilization of Taren Landslide, South Wales, UK. In Proc. 6th Int. Symp. On Landslides, Christchurch. Ed.. D.H. Bell, A.A. Balkema, 777-784.

Matzarakis A., Mayer H., Schindler D. and Fritsch J. (2000): Wasserhaushalts eines Buchenwaldes mit dem forstlichen Wasserhaushaltsmodell WBS3. Berichte des Meteorologischen Institutes der Universität Fraiburg, 5, 137-146.

Mizell, S.A., Gutjahr A.L. and Gelhar L.W. (1982): Stochastic analysis of spatial variability in two{dimensional steady groundwater ow assuming stationary and nonstationary heads, Water Resources Research, 18(4), 1053{1067, .

Moore D.P. and Imrie A.S. (1995): Stabilization of Dutchman's Ridge. In Proc. 6th Int. Symp.on Landslides, Christchurch. Ed.. D.H. Bell, A.A. Balkema, 1783-1788.

Moreno L. and Tsang, C.-F. (1994): Flow channeling in strongly heterogeneous porous media: A numerical study, Water Resources Research, 30 (5), 1421-1430.

Mosar J., Stampfli G.M. and Girod F. (1996): Western Préalpes médianes: timing and structure. A review. Eclogae geol. Helv. 89(1), 389-425.

NCG (1992) - Norbert SA, de Cérenville SA « NCG, association de bureaux »: Glissement de la Frasse. Rapport final.

NCG+EPFL (2004) - Association technique Norbert, deCérenville Géotechnique + EPFL pour l'étude du glissement de La Frasse: Glissement de La Frasse, modélisation et étude de faisabilité, unpublished report.

NCG+EPFL (2006) - Association technique « NCG+EPFL pour l'étude du glissement de la Frasse »: Glissement de la Frasse, communes d'Ormont-dessous et de Leysin. Travaux d'assainissement : Galerie de drainage. Projet de détail, octobre 2006.

Norbert SA, de Cérenville SA « NCG, association de bureaux » (1999) : Travaux d'assainissement et suivi des mesures de contrôle depuis 1979. Glissement de la Frasse. Rapport d'activité.

Noverraz F. (1990): Essai de recensement cartographique des glissements de terrain et écroulements rocheux sur le territoire Suisse. Hydrology in Mountainous Répons. Il'- Artificial Reservoirs; Water and Slopes(Proceedings of two Lausanne Symposia, August 1990). IAHS Publ. no. 194,1990.

Noverraz F. & Bonnard C. (1990): Technical Note on the Visit of La Frasse Landslide. – In: BONNARD, C. [ed.], Proc. 5th Int. Symp. on Landslides, Vol. 3: 1549-1554; Rotterdam (Balkema).

Oswald D. (2003): Analyse de l'activité de glissements de terrain et relation avec les conditions climatiques:

Exemples dans les Préalpes fribourgeoises (Suisse). Thèse présentée à la Faculté des Sciences de l'Université de Fribourg (Suisse). Geofocus, 2003, vol.8, 132 p.

Parasnis D.S. (1997): Principles of applied geophysics. Published by Chapman & Hall. 5th edition.

Parriaux A., Dubois J.-D., Mandia Y., Basabe P., & Bensimon M. (1990a): The AQUITYP Project:Towards an aquifer typology in the alpine orogen. In A. Parriaux (Ed.), Proceedings of the 22nd Congress of IAH: Water Resources in Mountainous Regions, 1 (pp. 254-262). Lausanne, EPFL

Parriaux A., Tullen P., Tacher L. & Turberg P. (2001a): The Hydrogeological Modeling of Slopes : a Tool for Movement Forecasting. Proceeding of the International Conference on Landslides, Davos, June 2001, pp. 179-188.

Perrin J. (2003): A conceptual model of flow & transport in a karst aquifer based on spatial & temporal variations of natural tracers. PhD thesis, Neuchâtel, 188 pp.

Piper A. M., Garret A. A., & Others (1953): Native and contaminated groundwaters in the Long Beach-Santa Ana area, California (Water Supply Paper 1136, 320p.). U.S. Geol. Survey.

Popescu M.E. (2001): A suggested method for reporting landslide remedial measures. International Union of Geological Sciences Working Group on Landslides, Commission on Landslide Remediation. Bull Eng Geol Env 60 : 69–74.

Popescu M.E. (1996): From landslide causes to landslide remediation. Special lecture. In: Proc 7th Int Symp on Landslides, Trondheim, Rep 1, pp 97–114.

Powel G.E. (1992): Recent changes in the approach to landslip preventive works in Hong Kong. In: Proc 6th Int Symp on Landslides, Christchurch, Rep 3, pp 1789–1795.

Prina E. (2000): Analisi del rischio rispetto ai pericoli naturali di una strada di montagna. Tesi di Laurea, Politecnico di Milano, 333 p.

Reid M.E. (1997): Slope instability caused by small variations in hydraulic conductivity.''

Journal of Geotechnical and Geoenvironmental Engineering, vol. 123, n° 8, pp. 717-725.

Riemersma P. (1996): Geostatistical characterization of heterogeneity, simulations of advective transport, and evaluation of pump-and-treat systems in braided stream deposits, Ph.D. dissertation, Dep. of Geol., Univ. of Wis.-Madison. Madison,

Riemersma P., Bahr J. , and Anderson M. (1996): A comparison of geological and stochastic approaches to characterization of heterogeneity and their effects on simulations of pump-and-treat systems, in Uncertainty in the Geologic Environment: From Theory to Practice, edited by C. Shackelford, P. Nelson, and M. Roth, pp. 1003–1018, Am. Soc. of Civ. Eng., New York.

Rubin Y. and Bellin A. (1997): Conditional Simulation of Geologic media with Evolving Scales of Heterogeneity, In: G. Sposito (ed.), Scale Dependence and Scale Invariance in Hydrology, Cambridge University Press.

Sanderson F., Bakkehøi S., Hestenes E. and Lied K. (1996): The influence of meteorological factors on the initiation of debris flows, rockfalls, rockslides and rockmass stability, in: Landslides. Proceedings 7th International Symposium on Landslides, edited by: Senneset, K., A.A. Balkema, 1.

Scheibe T. and Cole C. (1994): Non-Gaussian particle tracking: Application to scaling of transport processes in heterogeneous porous media, Water Resour. Res., 30(7), 2027–2039.

Schuster R.L. (1992): Recent advances in slope stabilization. Keynote paper. In: Proc 6th Int Symp on Landslides, Christchurch, Rep 3, pp 1715–1746.

Schwarzacher W. (1969): The use of Markov chains in the study of sedimentary cycles: Jour. Math. Geology, v. 1, no. 1, p. 17-39.

Simpson F. (1970): Sedimentation of the middle Eocene of the Magura series, Polish western Carpathians: Roczn. Pol. Tow. Geol., v. 40, no. 2, p. 209-286.

Sharma P.V. (1997): Environmental and Engineering Geophysics: Cambridge University Press, New York. 475 p.

Shvidler M.I. (1985): Stochastic Hydrodynamics of Porous Medium, Nedra, Moscow (in Russian).

Stampfli G.M., von Raumer J. and Borel G.D. (2002): Paleozoic evolution of pre-Variscan terranes: from Gondwana to the Variscan collision: Geological Society of America Special Paper, v. 364, pp. 263-280.

Sudicky E.A. (1986): A natural gradient experiment on solute transport in a sand aquifer: Spatial variability of hydraulic conductivity and its role in the dispersion process. Water Resources Research 22:2069-2082.

Sumner J.S. (1976): Principles of induced polarization for geophysical exploration: Elsevier, 277 p.

Tacher L. ,Bonnard C., Laloui L. and Parriaux A. (2005): Modelling the behaviour of a large landslide with respect to hydrogeological and geomechanical parameter heterogeneity. Landslides journal, vol. 2, num. 1, 2005, p. 3-14.

Tercier P., Knight R. and Jol H. (2000): A comparison of the correlation structure in GPR images of deltaic and barrier-spit depositional environments. Geophysics, vol. 65, N°4; p.1142-1153.

Terlien M. T. J. (1998): The determination of statistical and deterministic hydrological landslide-triggering thresholds, Environ. Geology, 35, 2–3.

Terzaghi K. (1950): Mechanisms of landslides. Geological Societyof America, Berkley Vol, pp 83–123.

Tezkan B., Goldman M., Greinwald S., Hördt A., Müller I., Neubauer F.M. and Zacher G. (1996): A joint application of radiomagnetotellurics and transient electromagnetics to the investigation of a waste deposit in Cologne (Germany). J. Appl. Geophys., 34, 199-212.

Tezkan B., Hördt A. and Gobashy M. (2000): Two-dimensional radiomagnetotelluric investigation of industrial and domestic waste sites in Germany. J. Appl. Geophys., 44, 237-256.

Tiedeman C.R. and Hsieh P.A. (2004): Evaluation of longitudinal dispersivity estimates from simulated forced- and natural-gradient tracer tests in heterogeneous aquifers: Water Resources Research, v. 40, no. 1, 15 p.

Troncone A. (2002): Numerical analysis of a landslide in soils with strain-softening behaviour. Géotechnique, 55(8): 585-596.

Tullen P. (2002): Méthodes d'analyse du fonctionnement hydrogéologique des versants instables. Thèse n°2622 présentée à la faculté ENAC, section Génie Civil, Ecole Polytechnique Fédérale de Lausanne.

Tullen P., Turberg P. and Parriaux P. (2006): Radiomagnetotelluric mapping, groundwater numerical modelling and 18-Oxygen isotopic data as combined tools to determine the hydrogeological system of landslide prone area. Engineering Geology 87, 195-204.

Turberg P. (1994): Apport de la cartographie radiomagnétotellurique (RMT) à l'hydrogéologie des milieux

fracturés. Thèse Université de Neuchâtel, Centre d'hydrogéologie.

Turberg and Müller (1997): Colloque GEOFCAM, Géophysique des sols et des formations superficielles, BRGM, INRA, ORNSTOM, UPMC) exposes the good potential of the RMT method for the detection of infiltration zones, and presents a classification inferred from this surveying technique.

Turrian F. (2003): Etude du fonctionnement hydrogéologique des glissements de la Praz et de la Grande Combe, Ballaigues (VD). Diplôme de Géologue, Université de Lausanne.

Tsang C.-F. and Neretnieks I. (1998): Flow Channeling in Heterogeneous Fractured Rocks, Reviews of Geophysics, 36 (2), 257-298.

Tsang Y.W. and C.F. Tsang (1989): Flow channeling in a single fracture as a two-dimensional strongly heterogeneous permeable medium, Water Resourc. Res., 25(9), 2076-2080.

VARIOWIN - Software for Spatial Data Analysis in 2D: Pannatier, Yvan (1996): Springer Verlag, 91p., ISBN: 0-387-94679-9, Hardcover DM 78.00

Vulliet L. and Hutter K. (1988): Set of constitutive models for soils under slow movement. J. of Geotech. Div., ASCE, 114(9):1022-1041.

Vuillet L. (2000): Natural slopes in slow movement. In Modelling in geomechanics. Edited by M.Zaman, J.R. Booker, and G.Gioda. John Wiley & Sons, Chchester, UK. Pp. 654-676.

Webb E. and Anderson M. (1996): Simulation of preferential flow in three-dimensional, heterogeneous conductivity fields with realistic internal architecture, Water Resour. Res., 32(3), 533– 545

Wieczorek G. F. (1987): Effect of rainfall intensity and duration on debris flows in central Santa Cruz Mountains, California, Geolog. Soc. Amer., Reviews in Engineering Geology, 7.

WP/WLI (1990): International Geotechnical Societies' UNESCO Working Party on World Landslide Inventory (Chairman: DM Cruden) (1990). A suggested method for reporting a landslide. Bull IAEG 41: 5–12.

Wu T. (1973): Probabilistic analysis of seepage, J. Soil Mech. Found. Div. Am. Soc. Civ. Eng., SM4, 323–340.

Zaruba Q. and Mencl V. (1982): Landslides and their control. Elsevier, Amsterdam, 324 pp.

Zohdy, A.A.R., Eaton, G.P. and Mabey D.R. (1974): Application of Surface Geophysics to Ground-Water Investigations: Techniques of Water-Resources Investigations of the U.S. Geological Survey, Book 2, Chapter D1, 116 p.

Z_Soil v6 (2007): User manual, www.zace.com, Elmepress

APPENDICES

1. RADIOMAGNETOTELLURIC METHOD (RMT)

The RMT method is an emerging geophysical mapping technique for waste-site characterization and groundwater investigations. The method is an extension of the very-low-frequency (VLF) EM induction method (10–30 kHz) to frequencies as high as 1 MHz The principle of the method is demonstrated in the following figure I-1.

In the far-field of a radio transmitter, the EM field can be viewed as a propagating plane wave where the horizontal electric and magnetic field components are altered by variations in the subsurface electrical conductivity. In the method, the horizontal magnetic field is measured along with an orthogonal component of the horizontal electric field. With this measurement the impedance, which is a ratio between particular components of the magnetic and electric field, can be estimated. Because impedance data are ratios of electric to magnetic field, the source location and strength need not be considered further, which greatly simplifies data interpretation. The impedance is usually converted to apparent resistivity and phase at each measurement site using the Cagniard formula in magnetotellurics (Cagniard, 1953). This transformation allows the measurements to be related more easily to the subsurface geology. Nevertheless, the same information content is present in the impedance data. Because of the use of several frequencies between 10 kHz and 1 MHz, a quick sounding is possible by this method; such soundings using VLF frequencies are impractical because of the method's limited frequency range (10–30 kHz). RMT surveys have been successfully applied in a number of hydrological and environmental investigations. For field measurements, the RMT instrument was developed from a prototype built at the Hydrogeological Institute of the University of Neuchatel (CHYN) by Mueller in 1983. The horizontal component of the magnetic field is measured with a coil (0.4 m diameter), and the horizontal component of the electric field is measured with two grounded electrodes 5 m apart. The frequency range of this instrument is limited to 10–300 kHz. The apparent resistivity ρ*a* (Ohm.m) is calculated from the ratio *Ex/Hy* according to Cagniard; the phase shift between *Ex* and *Hy* is also measured. The depth of penetration *Pi*, according to the skin depth formula (see figure I-1), can be changed by using different radio-frequencies (different transmitters) at the same point; in this way a simple and rapid frequency sounding is carried out. The data acquisition was made in a unidirectional mulitifrequency mode.

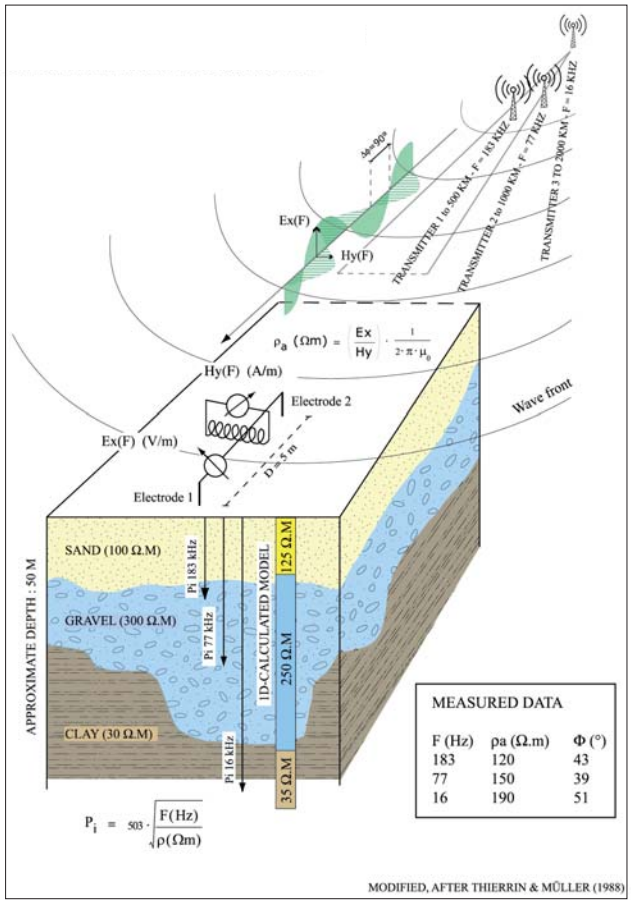

Figure I-1: Principle of radio-magnetotellurics (RMT). Example of a 3 frequencies uni-directional sounding.

The instrument is lightweight and easy to use — one important reason for its emerging popularity in environmental applications. Measurements (i.e. apparent resistivity and phase observations from a single radio transmitter) can be carried out in a relatively short time. About two minutes are necessary to measure apparent resistivities and phase values for four frequencies at one fixed location. Because of the large number of radio transmitters (especially in Europe), it is possible to cover the entire frequency range required for a sounding with selected frequency pairs arising from two orthogonal transmitters. In an ideal case, each pair of transmitters should operate at similar frequencies, where the electric-field polarization of one transmitter

is parallel and the other is perpendicular to the general strike direction of the geological or anthropological structure. Assuming a 2D resistivity structure in the survey area, the data can then be associated with the transverse electric and transverse magnetic modes and interpreted using standard 2DMT inversion algorithms. Because the instrument treats the data arising from each transmitter, in a given pair, as separate, the *Zxy* and *Zyx* impedance measurements are assumed to be independent of each other and the *Zxx* and *Zyy* impedances are assumed to be zero and are not measured. In practice, the strike direction of the target is often unknown.

2. HYDROCHEMISTRY

Hydrochemical characterization permits to highlight the nature of the waters. It includes the study of the physicochemical parameters (electrical conductivity, temperature and PH), the analysis of the major cations and the isotopes (^{18}O). Chemical groundwater analyses were performed in the chemistry laboratory of the GEOLEP, under the direction of Dr. M. Bensimon. In each sample 10 major and minor anions (Cl^-, SO_4^{2-}, NO_3^-, F^-, and alkalinity) and cations (Na^+, K^+, Mg^{2+}, Ca^{2+}, and Sr^{2+}) were analysed by means of high-pressure liquid ion chromatography (HPLC-IC, Dionex DX 120, equipped with an auto-suppressor). Alcalinity was analysed thanks to titration (0.1 N HCl titration to pH 4.3) and titration (EDTA) for the total hardness. The variations of isotope contents are analyzed by mass spectrometry. The isotopic ratios expressed are in δ and the relative variation in ‰ between the sample and the standard (the VSMOW - Standard Vienna Mean Ocean Toilets), (IUPAC, 1994).

A. 018 Isotope

The isotopes of the water behave like ideal natural tracers to describe the hydrogeological phenomena. The stable isotopes of water (i.e. oxygen and hydrogen) are strictly conservative parameters. The majority of the elements constituting the matter contain a melange of stable or radioactive isotopes which differs the ones from the others by the number of neutrons contained in their atomic nucleus. The difference in mass causes an isotopic fractionation during physicochemical processes, the light isotopes being overall more mobilizable than the heavy isotopes. Isotopic analyses are approached by the measurement of the relative difference between the content of isotope of a sample and a standard:

$$\delta^{18}O = \frac{\left(^{18}O / {}^{16}O\right)_{sample} - \left(^{18}O / {}^{16}O\right)_{VSMOW}}{\left(^{18}O / {}^{16}O\right)_{VSMOW}} \cdot 1000$$

The systematic study of the isotopic fractionation of the precipitations enables to identify various effects which influence the variation of this fractionation; i.e. the altitude, the continentality, the latitude and the quantity of precipitations.

Elementary Definitions. Every element consists of an assemblage of different types of atoms, termed nuclides, each constituted of protons, neutrons and electrons. Even though the atomic number Z, representing the nuclear charge and the number of protons, is the same for all nuclides of a given element, the number (N) of neutrons may vary. Thus the mass number A, an integer represented by the sum of Z + N, will also vary among the nuclides comprising that element. Nuclides of an element that have different values of A are termed isotopes, and are represented by the appropriate chemical symbol preceded by a superscript indicating the mass number. For example, a rare stable isotope of oxygen, called oxygen-18, has 8 protons and 10 neutrons, and is denoted by the symbol 180. Properties of the approximately 2500 known nuclides, most of which are artificial radionuclides with short half lives, have been tabulated. Only about 270 nuclides are stable, and these are

classified as being either radiogenic or nonradiogenic, depending on whether they are, or are not, the daughter products of radioactive atoms that underwent nuclear decay, respectively. Nonradiogenic stable nuclides, a group including all atoms discussed below, have been present since nucleosynthesis.

Natural Abundance. The masses and natural abundances of stable isotopes are generally determined by sensitive mass spectrometers. The atomic weight of the element which is the quantity one finds in an ordinary Periodic Table is not a fundamental physical quantity but rather the sum of the masses of the constituent isotopes weighted by their abundances. In contrast, the atomic weights of the individual nuclides are intrinsic. Isotopes with an odd mass number tend to have lower abundances than those with an even mass number, although hydrogen is an exception. If the abundances of the stable isotopes were truly invariant, their measurement would have very limited application. In fact, the abundances given above are averages, and in detail the values vary from sample to sample. This implies, of course, that the atomic weight of these elements will also vary slightly from sample to sample.

A. **Relation between the oxygen-18 and the infiltration altitude**

Oxygen-18 is a stable isotope which has the effect of being depended on the temperature, itself dependent on the altitude and the season. It indirectly records the altitude to which water infiltrates the ground. Consequently, a relation between oxygen-18 and the altitude of infiltration can be established. For that, it is necessary to establish a local gradient, equivalent to: altitude of infiltration = f(δ18O), on which the measured isotopic compositions are reported.

3. Borehole surveys

Boreholes surveys are a direct method to obtain information on the underground geological material and structure vertically of a given point. Various types of measurements are possible either directly on site; i.e. in-situ geological core samples description and geophysical borehole logging, or in laboratory through geomechanical tests. The boreholes are then often equipped with inclinometers to follow the displacements of the mass and with piezometers to observe in time the variation of water levels. Finally, it enables also to sample underground waters for hydrochemical analyses. Boreholes surveys bring essential and detailed information of the geological medium of the mass but at a very restricted scale. The one-dimensional character of the method do not enable a direct two dimensional or either three dimensional representation of the mass. An indirect representation is regardless possible thanks to spatial correlations, but often in very heterogeneous medium, such as landslides, the interpretation may be problematic and erroneous. Consequently, there is necessary to remain attentive with the representativeness of this type of investigation at the scale of the landslide (regional scale).

4. Markov matrix and entropy

In mathematics , a Markov chain, named after Andrey Markov, is a stochastic process with the Markov property. Having the Markov property means that, given the present state, future states are independent of the past states. In other words, the description of the present state fully captures all the information that could influence the future evolution of the process. Future states will be reached through a probabilistic process instead of a deterministic one.

At each instant the system may change its state from the current state to another state, or remain in the same state, according to a certain probability distribution. The changes of state are called transitions, and the probabilities associated with various state-changes are termed transition probabilities. Homogeneous first order Markov

chains have been used in modelling stratigraphy in the vertical direction. The paper by Krumbein and Dacey (1969) form the state of the art of modelling stratigraphy in one dimension.

Two types of Markov chains are commonly employed. The first approach considers the stratification at discrete points that are spaced equally along a vertical profile. The points are numbered consecutively, and the use of the Markov chain is based on the assumption that the lithology or state at point n depends upon the lithology at the preceding point (n - I). Because the same lithology may be observed at successive points, the transition matrix that gives the probability of going from one lithology to another generally has non-zero dements on the main diagonal. This type of Markov chain is known as a conventional or ordinary Markov chain. If stratigraphy follows a first order conventional Markov chain, then the thicknesses of lithologies should follow geometric distributions (Krumbein and Dacey, 1969). This important property can be used in testing whether a stratigraphy follows a first order conventional Markov chain. The second approach considers only the succession of lithologies, and because each transition is to a different lithology within the system, the diagonal elements are all zero. This Markov chain is known as an embedded Markov chain. In this case, the distributions for lithologic thicknesses need not follow geometric distributions. Thus, some stratigraphic sequences may be modelled by using an embedded Markov chain to describe the transitions between different lithologies, and using different probability distributions to describe thicknesses of different lithologies. Such a process is known as a semi-Markov process.

Entropy. The concept of cyclic sedimentation is accepted widely and applied in a variety of sedimentary environments (Hattori 1976). Sedimentary cycles are so-called because of the occurrence of many lithologies in a sedimentary sequence which seems to be cyclic to some extent. As ideal patterns of unit cycles, the following two types can be considered theoretically; a symmetric pattern (ABCDCBA) and an asymmetric pattern (ABCDABCD). Cyclic patterns exhibited in actual lithologic sequences, however, are complicated because probabilistic effects share with deterministic effects in the formation of lithologic successions. This standpoint enables us to describe and analyze reasonably a lithologic sequence with effective use of Markov matrices, and the geologic application of Markov chains has been accumulated rapidly since the pioneering work by Vistelius in 1949, and the mathematical background and technique were summarized by Harbaugh and Bonham-Carter (1970). Schwarzacher (1969) equated logically cyclic sedimentation with the recurrence times in Markov chains. In the natural system, the physical and random processes advance hand in hand, and consequently produce intricate patterns in lithologic successions observed in fields. As a parameter indicative of the degree of random occurrence in a succession which can be regarded as a Markov chain, the concept of entropy can be applied to the Markov matrix expressing the succession. Allègre (1964), probably first, extended the concept to real lithologic sequences and successfully divided the Hell6nides and the Lod6ve Series of European Alps into some zones according to the entropy. In this thesis, sedimentary cycles are classified from the aspect of entropy in Markov chains, and the result is applied to real sequences which have been described with Markov matrices.

5. Linear regressions

If Y is the random variable, and *X* the fixed variable, the problem is to define the possibility to predict *Y* from *X*. Having agreed on the characteristics of the desired trend line, some terms have to be defined. The variable being examined is the dependent or regressed variable, designed *Y*; individual observations of the dependent variable are indicated as y_i. Deviations of y_i from the fitted line will be minimized. The other variable is independent or regressor variable and is denoted *X*, with individual observations, x_i. The fitted line will cross the Y-axis at a point b_o (the intercept), and will have a slope, b_1. The equation of the line is: $y_{i\,est.} = b_o + b_1 x_{i.}\, y_{i\,est.}$ Is the estimated value of y_i at specified values of x_i. The deviations we are considering, therefore, are $y_{i\,est} - y_i$ and our problem becomes one of finding a method.

6. Water level analyses

In a saturated zone, the hydraulic head, H, is measured at a point using a piezometer and is defined as the elevation (pressure head) at which the water surface stands in an open piezometer tube terminated at a given point in the porous medium. Hydraulic head is a combination of pressure head and elevation head (distance of the measuring point above a reference level. The reference level chosen for measurement of H is arbitrary. The hydraulic head is a potential function, the potential energy per unit weight of the ground water. Hydraulic head can vary temporally at any given well. The variation may be the result of an aquifer's response to a known stress (e.g., a pumping well or seasonal changes in recharge) and may demonstrate a temporal relationship between hydraulic head and displacement rates. In addition, piezometric observations bring a means of calibration for the numerical models in addition to the precious indications which they provide for the establishment of the conceptual models which represent the hydrogeological functioning of the unstable slope.

7. Well test analyses

The aquifer properties considered here include storage properties and hydraulic conductivity. In addition, methods are considered for estimating the spatial variability of hydraulic conductivity. These methods, including slug tests and pumping tests, can be used to measure storage values for unconfined or confined aquifers and test a relatively large volume of the aquifer. The determination of aquifer properties begins with identifying a known stress to the ground-water system, and then measuring the response to that stress over space and/or time. Given the system geometry and boundary conditions representing the stress, a mathematical description and corresponding solution (computed response) can be determined for a range of parameters. The observed aquifer response is matched to a computed response, and the corresponding parameters are determined. Thus, aquifer properties are not measured directly, but instead are determined through this curve-matching process. Using more than one method to determine aquifer properties is recommended. Results then can be weighted toward the best performed tests with the greatest stress to the aquifer system.

A. Lefranc method

Variable-head tests provide only the local *K* value in either an aquifer or an aquitard. They are performed by gravity injection of water, either through the lower opening of a casing or through a cavity located below the end of the casing and filled with a filtering material. Alternatively, they can be performed by injecting water in monitoring wells. An injection cavity is called a lantern or a gravel pack. The flow occurs in saturated conditions, conditions, at positive water pressures, within a zone of limited extent where neither consolidation nor storage take place. The equations for these tests are well established (Lefranc 1936) gathered shape factors for a variety of injection-zone geometries and either
isotropic (hydraulic conductivity *K*) or anisotropic (horizontal and vertical hydraulic conductivity *K*h and *K*v, respectively) hydraulic conductivities. Variable-head tests can be carried out using falling or rising head. The latter should not be performed in cased boreholes: inward seepage forces destabilize the soil around the intake, thus causing internal erosion, washing fines towards the casing, and eventually inducing soil heave in the casing. Rising tests may be run in a piezometer or monitoring well, given a correct gravel-pack design (filtration) and an adequate development. The estimated *K* value is then representative of a soil that has lost some fines around the gravel pack, with associated skin effects.

8. Analysis methods of hydraulic responses

In the general context of landslide remediation, drainage works are often undertook. They may consist in

drainage wells or galleries. In both cases inflow and pumping rates are recorded, and studied through analytical solutions may provide important information about the hydrodynamical characteristics of the aquifer system. The classical approach consists in the temporal observation of these flow rates in function of the recharge during a hydrological cycle. These flow rates evolve in function of the time, sometimes during relatively long periods according to hydrogeological and geological characteristics of the massif. Several mathematical formulas are available in literature for the calculation of the hydraulic permeability from the measured flow rates at the scale of the massif or even from a specific zone, hydrogeologically differenced. In this work the Goodman (1965) formulation is used for steady calculations, and for unsteady conditions, the Jacob and Lohman (1952).

A. Goodman (1965)

In steady state, the solution of Goodman corresponds to the drainage of an aquifer which phreatic level is supposed constant. The equation itself resembles Thiem's well formula, but it assumes a special geometry with respect to the drawdown. Goodman's formula is probably the most commonly used approximation for calculating early tunnel inflow rates:

$$Q = 2\pi K \cdot \frac{\Delta h}{\ln\left(\frac{2 \cdot \Delta h}{r}\right)} \quad \text{or} \quad K = \frac{Q \cdot \ln\left(\frac{2 \cdot \Delta h}{r}\right)}{2\pi \cdot \Delta h}$$

With Q= tunnel inflows [m3/s], K=Hydraulic conductivity [m/s], Δh= distance between the centre of the tunnel and the groundwater table [m] and r=tunnel radius [m].

B. Jacob and Lohman (1952)

Jacob and Lohman (1952) derived an analytical solution for a constant-head test in a homogeneous, isotropic confined aquifer assuming a fully penetrating well. The Laplace transform solution for dimensionless discharge is as follows:

$$\overline{q}_\rho = \frac{K_1\left(\sqrt{\rho}\right)}{\sqrt{\rho}\,K_0\left(\sqrt{\rho}\right)}$$

$$q_0 = \frac{Q}{2\pi T H_w}$$

$$t_0 = \frac{Tt}{Sr_w^2}$$

where

- H_w is the constant head in the test well [L]
- K_i is modified Bessel function of second kind, order i
- p is the Laplace transform variable
- Q is discharge rate [L^3/T]
- r_w is well radius [L]
- S is storativity [dimensionless]
- t is time [T]
- T is transmissivity [L^2/T]

Jacob and Lohman (1952) also presented a straight-line method for estimating T and S as follows:

$$\frac{Hw}{Q} = \frac{2.303}{4\pi T}\log\frac{2.25Tt}{Sr_w^2}$$

$$T = \frac{2.303}{4\pi\Delta(H_w / Q) / \Delta\log(t / r_w^2)}$$

$$S = 2.25T\left(\frac{t}{r_w^2}\right)_0$$

The straight-line is matched to a data plot of H_w/Q versus t/r_w^2 on semi-log axes.

- *This formulation calls for several assumptions:*
- *aquifer has infinite areal extent*
- *aquifer is homogeneous, isotropic and of uniform thickness*
- *aquifer potentiometric surface is initially horizontal*
- *well is fully penetrating*
- *flow is unsteady*
- *aquifer is confined*
- *water is released instantaneously from storage with decline of hydraulic head Data*

9. GEOSTATISTICS AND SPATIAL ANALYSES

As it is always the case, the important hydrogeological properties and parameters such as piezometric head, transmissivity or hydraulic conductivity, storage coefficient, yield, thickness of aquifer, hydrochemical parameters, etc. are all functions of space. According to De Marsily (1986) these variables (known as the regionalized variables) are not purely random, and there is some kind of correlation in the spatial distribution of their magnitudes. The spatial correlation of such variables is called the structure, and is normally defined by the variogram. The experimental variogram measures the average dissimilarity between data separated by a vector h (Goovaerts 1997). It is calculated according to the following formula:

$$\gamma(h) = \frac{1}{2N(h)}\sum_{i=1}^{N(h)}\left[Z(x+h) - Z(x)\right]^2$$

h = separation distance between two points, also called the lag distance.

A (semi)-variograms is one of the significant functions, representing a graph that shows the variance in measure with distance between all pairs of sampled locations. Like this, the experimental variograms is calculated by averaging one-half the difference squared of the z-values over all pairs of observations with the specified separation distance and direction**.** It is plotted as a two-dimensional graph; the mathematical formulas used to calculate the experimental variogram are developed in Isaaks and Srivastava (1989). The variogram model is chosen from a set of mathematical functions that describe spatial relationships**.** The appropriate model is chosen by matching the shape of the curve of the experimental variogram to the shape of the curve of the mathematical function. The exponential model is used since the spatial continuity of geologic units seems to follow an exponential correlation function type (Gelhar 1993). The exponential model is a thus commonly used in hydrogeophysical studies. Its equation is given by:

$$\gamma(|h|) = c \cdot \exp_a(|h|) = c \cdot \left[1 - e^{-\frac{3|h|}{a}}\right]$$

Where c is the covariance contribution or sill value and a is the practical range, that is, the distance at which the variogram value is 95% of the sill. This model reaches its sill asymptotically and has linear behaviour at the origin. The calculated spatial correlation lengths are one-third of the practical range. In conclusion, a variogram analysis consists of the experimental variogram calculated from the data and a variogram model fitted to the data.

In a given direction a, the variogram may become stable beyond some distance $|h|=a$ called the range, cf. Figure I-2 VARIOGRAM. Beyond this distance a, the mean square deviation between two quantities Z(x) and Z($x+h$) no longer depends on the distance $|h| = a$ between them and the two quantities are no longer correlated. The range a gives a precise meaning to the intuitive concept of the zone of influence of a sample z(x). However, there is no reason for the range to be the same in all directions a of the space. For a given distance $|h|=a$, the horizontal variogram may presents a weaker variability than the vertical variogram or vice versa: this expresses the horizontal sedimentary character of the phenomenon considered.

10. Tracing test

Hydrological tracing techniques use tracers to follows underground flowpaths. Tracing tests are commonly used for evaluating mean velocities, retention effects and hydrodynamic dispersion. It consists in creating a circulation of substance from a given point of a hydrological watershed to an outlet point or an observation point within the aquifer. A concentrated mixture of water and tracer (uranine, eosin …) is profuse during a very short time and then the tracer is analyzed at the points of expected appearances. The curve of restitution (relation of the concentration of the tracer according to the time) allows expressing the concentration of the tracer at the outlet. The ratio of the reappeared mass with the infiltrated mass gives the coefficient of restitution of the tracer. The analysis of the restitution curve provides information on flow characteristics in the aquifer between the point of injection and the point of observation. In the meantime, tracing methods are rather regarded as a tool permitting to validate conceptual assumptions based on other hydrogeological or geological investigations.

11. Software

A. FEFLOW

Feflow® is a software package for modelling fluid flow and transport of dissolved constituents and/or heat transport processes in the subsurface. It contains pre- and post processing functionality and an efficient simulation engine. A user-friendly graphical interface provides easy access to the extensive modeling options. In contrast to some of the competing products - is not a graphical front end for a separately developed simulation kernel. It is a completely integrated system from simulation engine to graphical user interface. It includes a public programming interface for user code. Feflow® is developed by WASY GmbH, a German company. WASY's areas of expertise encompass groundwater hydrology, surface water hydrology and geographic information systems. In these fields, WASY provides software, training and consulting services.

Feflow® is based on the general three dimension (3D) form of the governing differential equation for flow in heterogeneous isotropic media. The Boussinesq differential equation described below is the principal functions in it:

$$\frac{\partial}{\partial x}\left(Kh\,\frac{\partial H}{\partial x}\right)+\left(Kh\,\frac{\partial H}{\partial y}\right)+W(x,y,t)=\mu\,\frac{\partial H}{\partial t} \quad (1)$$

$$H(x,y,t)|t=0 = H0(x,y) \quad with \quad (x,y)\in D \quad (2)$$

$$\frac{\partial H}{\partial n}|\Gamma 2 = q(x,y,t) \quad with \quad (x,y)\in \Gamma 2 \quad (3)$$

Where *H* is the saturated hydraulic head [L], *h* is the water table elevation above the impermeable barrier [L], *H0* is the initial hydraulic head [L], *q* is the flux to recharge [LT-1], *K* is the hydraulic conductivity [LT-1], μ is the specific yield, *W* is the water balance, i.e., discharge minus recharge [LT-1], *D* is the study area, Γ2 is the second kind boundary condition, *t* is time [T] and *n* is the normal direction.

B. Variowin

This is a brief introduction to the exploration and modeling of variograms using Yvan Pannatier's Variowin 2.21 software package. This packages is freely available from *http://www-sst.unil.ch/research/variowin/index.html*. However, there is no manual available on the web. The "official" manual is the book by Pannatier (Springer Verlag, 1996) that contains a disk with an older version.
Variowin consists of a collection of four programs (as .exe files) that need to be run separately: Prevar2D (a utility to construct a distance matrix for all point pairs in the data set), Vario2D with PCF
(exploring variograms) and Model (fitting theoretical variogram models).
The data input files for Variowin need to be in a specific format (Geo-EAS), common to many geostatistical software packages. Each data file starts with a header line containing a descriptive title. Next follows a line with the number of variables. The following set of lines contains the variable names, one per line. Next are the actual values, with a new line for each observation, and the values separated by tabs or spaces, but not by commas. The last line in the file should be a blank line.

C. Hydrogen

Hydro gen (Bellin and Rubin, 1996; Rubin and Bellin, 1997) is a computer code for generating two-and three-dimensional space random functions with an assigned covariance structure. The code is written in Ansi Fortran 77 with a quite standard implementation that allows the use of a wide class of computers. The computations are performed in double precision and the actual configuration has been tested on the workstation IBM RISC/6000 mod. 320H.
The code contains the following files:

hydro gen.f: the main program containing the definitions of the arrays and variables, the calls for the computation of the kriging coefficients, the selection of the path followed during the field generation, the calls for the linear combination of suitable kriging points, and the generation of the field;
coefcy.f: subroutine which computes the kriging coefficients used in the coarse grid generation step and in the first level of the refinement process;
coe2.f: subroutine which computes the kriging coefficients used in the second level of the refinement process;
comb.f: subroutine which computes the conditional mean at the generic point x;
covariance.f: subroutine which computes the covariance matrix with reference to the larger search neighborhood;
covar.f: collection of covariance function options. This file can be modified by users who would like to use

covariance functions different from the preloaded ones. The calling command for the function is cov(itype; rx; ry) where itype identifies the covariance function and rx,ry are the lag distances at which the covariance is computed. The following options are possible:

itype=0 discrete covariance function. It is read from a file;
itype=1 exponential covariance function;
itype=2 Gaussian covariance function;
itype=3 Whittle isotropic covariance function;
itype=4 Mizell isotropic covariance function (type B) (Mizell et al. 1982);
itype=5 Power law semivariogram;

bessik.f : functions that compute the modified zero and first order Bessel functions of third kind.
linpack.f: contains the Linpack library subroutines *dspfa* (to factor a double precision packed symmetric matrix) and *dspsl* (to solve the double precision symmetric system a*x=b using the factors computed by *dspfa*);
blas.f: contains the Blas library subroutines and functions *daxpy*, *dswap*, *idamax*, and *ddot*. These are linear algebra routines used by the Linpack routines;
ranlib.f: contains the necessary subroutines and functions from the Ranlib package to initialize the seed for and to generate normally distributed random variables. The above routines can be replaced by corresponding routines from different packages. In that case, however, the authors do not guarantee the accuracy of the reproduced field. Specifically, the generation of the normally distributed random values requires a particular attention. The user intending to substitute the Ranlib package is strongly advised to perform tests for normality of the generated numbers and convergence of the mean and
variance.
According to the user's choice the generation is performed in two ways: 1) direct generation on the selected grid; 2) generation over a coarse grid followed by up to three nested refinements. At each refinement step the block size is reduced by a factor of 2. We advise the user to respect the limit of three nested refinement levels in order to avoid appreciable reduction in accuracy. During the input session the user will be required to provide the number of nested refinement levels. Note that 0 reference levels imply no refinement. The refinement step can be useful when the search neighborhood area is large. In these situations the computational effort for the coarse grid generation can be reduced without an appreciable impact on the accuracy. At the beginning of the main program, values of integer variables are assigned to reserve space for the arrays used in the code. These variables are:
igrid1: maximum number of grid points in the x direction.
igrid2: maximum number of grid points in the y direction.
icond: maximum number of points inside the search neighborhood area that can be used to compute the conditional mean and variance.
iptmx: maximum dimension of the array storing the independent kriging coefficients. The exact number of independent kriging coefficients is computed at each run and printed to standard output.
iptmxcv: maximum dimension of the vector storing the independent conditional variances. In analogy with the previous point the exact number of vector positions required at each run is computed and printed to standard output.
idim: maximum dimension of the matrix containing the covariance function.

The main advantage of the program's method is that the kriging coefficients depend on the field geometry and grid spacing but not on the actual field values. To capitalize on this advantage the user can choose between two options: 1) Compute the interpolation coefficients and store them in a file, 2) Read the interpolation coefficients from the file where previously generated interpolation coefficients have been stored. The option 2 is selected

when the interpolation coefficients have been computed in a previous simulation using the same grid spacing and autocorrelation function. For additional information we refer to the example Section of this document.

gset: decision variable for setting the random number generator seed. If y, the user is prompted for the seed number; if any other letter, the clock is used to set the seed. The code for the latter option is written for use with Unix systems and must be modified by DOS users (see the main program at the line labeled 1001).
dx; dy: grid dimension in the x and y directions;
np: number of independent Monte Carlo replicates;
lx; ly : field dimensions;
sigy: field variance (the unconditional one);
cond10 : mean (the unconditional one);
imark : integer variable which indicates whether the kriging coefficients have already been computed and stored in the file filecoef (from a previous run; option 2 above) or need to be computed and stored (option 1 above). A value of 1 indicates that the values have already been computed and stored, and any other value indicates otherwise. (Note: the coefficients are stored in the file in unformatted binary format.);
itype: integer variable which indicates the type of autocorrelation function. If *itype=0* the autocovariance is read from a file specified by the user. The file must contain the discretized autocovariance function on a subgrid of dimensions *(xsp+xspa)_ysp* with grid spacing equal to the coarse grid spacing. The matrix is written in free format row by row without empty lines. The discretized covariance function used for the two levels of refinement must be introduced immediately after the coarse grid covariance function
sclx; scly: integral scales in the x and y directions. The integral scales are read only if the autocovariance function is given analytically. In the case of an isotropic function, sclx=scly and only one value is read. For the fractal fields *sclx* and *scly* assume the meaning of reference scales since integral scales cannot be defined.
xsp; ysp: main dimensions of the search neighborhood area in the x and y directions. Suggested values, based on the chosen covariance function and integral/correlation scales, are calculated and printed to standard output. The search neighborhood dimensions must be reasonably smaller than the field dimensions or a segmentation fault will result. The code tests for this possibility and issues a warning to the user, who may then opt to enter search neighborhood dimensions smaller than those suggested by the author or to stop the program and begin again with a larger field. Because the suggested search neighborhood dimensions are based on the authors' numerical tests for covariance structure reproduction, use of dimensions much smaller than those suggested is not recommended; it is better to work with a larger field if possible. In case of fractal fields the search neighborhood is automatically fixed equal to the field dimension. The number of nested refinement stages should be sufficiently large to avoid segmentation fault, but at the same time, enough to preserve an acceptable level of accuracy of the generated fields. The number of refinement stages depends on the ratio between the resulting coarse grid spacing and the integral scales. Numerical tests performed by the authors suggest that for regular random fields the coarse grid spacing should not exceed two integral scales. For this reason the optimal coarse grid spacing should be fixed according to tests performed by the user using different number of multistage refinements.
xspa: secondary dimension of the search neighborhood area in the x direction. As with the main dimensions, a suggested value is calculated and printed to standard output;
filecoef: name of the file in which kriging coefficients are stored (if imark is 1) or should be stored once computed (if imark is not 1). Storage is in unformatted binary format;
ilevref: number of nested refinement stages. The generation is first performed on a coarse grid and then subsections of the grid are refined by increasing the density of nodes. At each refinement stage, which is performed in two steps, the grid density increases by a factor of two. As an example, to obtain a final grid spacing of 0.25, the coarse grid spacing should be 0.50 and 1.0, for one and two refinement stages respectively. The latter is more computationally efficient; file1: name of the output file containing the generated fields for

all Monte Carlo replicates;

iformat: integer variable indicated whether the field values should be output in 3{column x,y,z format (iformat=1) or matrix format (iformat=0). In addition to the output files filecoef and file1, the file stats: out, which shows the mean and variance for each replicate, is generated with each run.

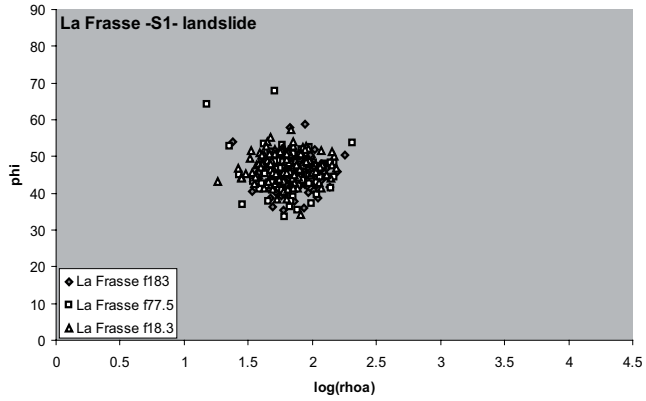
La Frasse -S1- landslide
phi
log(rhoa)
La Frasse f183
La Frasse f77.5
La Frasse f18.3

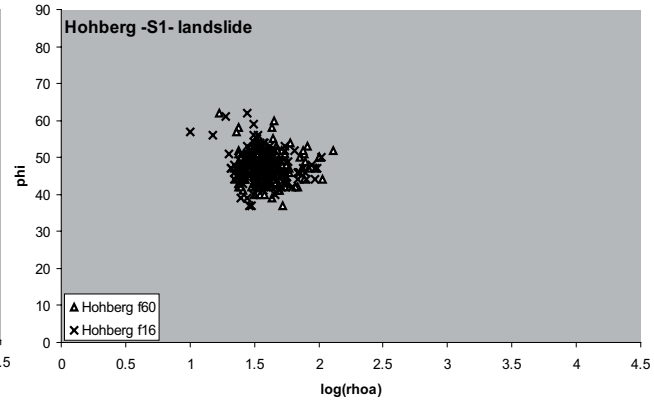
Hohberg -S1- landslide
phi
log(rhoa)
Hohberg f60
Hohberg f16

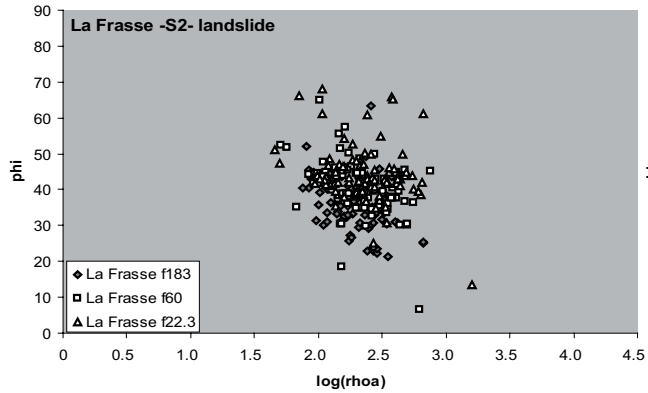
La Frasse -S2- landslide
phi
log(rhoa)
La Frasse f183
La Frasse f60
La Frasse f22.3

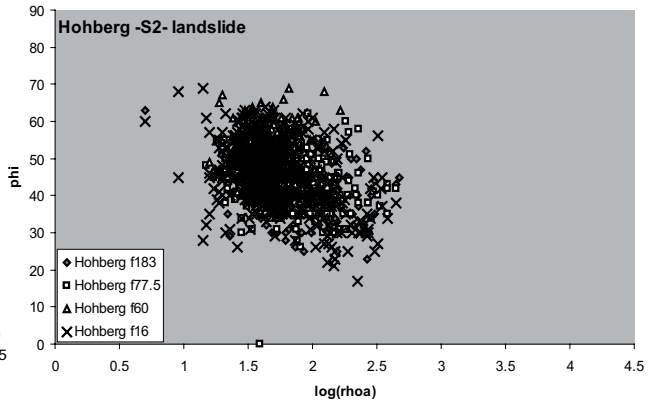
Hohberg -S2- landslide
phi
log(rhoa)
Hohberg f183
Hohberg f77.5
Hohberg f60
Hohberg f16

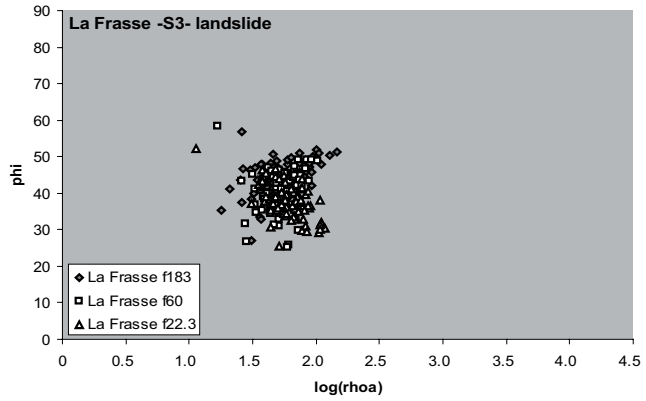
La Frasse -S3- landslide
phi
log(rhoa)
La Frasse f183
La Frasse f60
La Frasse f22.3

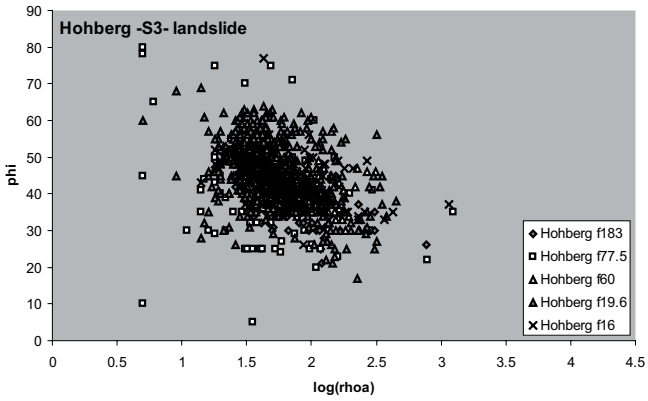
Hohberg -S3- landslide
phi
log(rhoa)
Hohberg f183
Hohberg f77.5
Hohberg f60
Hohberg f19.6
Hohberg f16

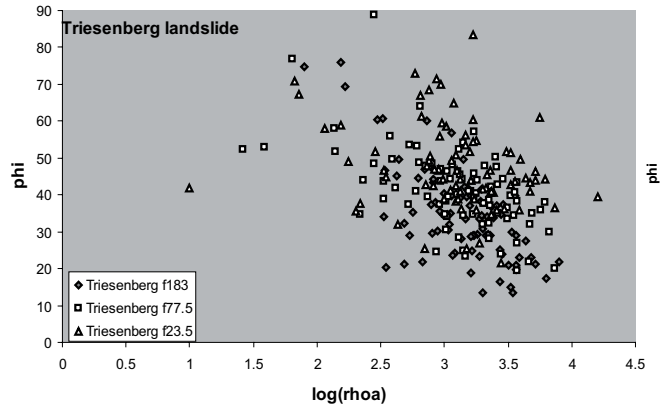
Triesenberg landslide
phi
log(rhoa)
Triesenberg f183
Triesenberg f77.5
Triesenberg f23.5

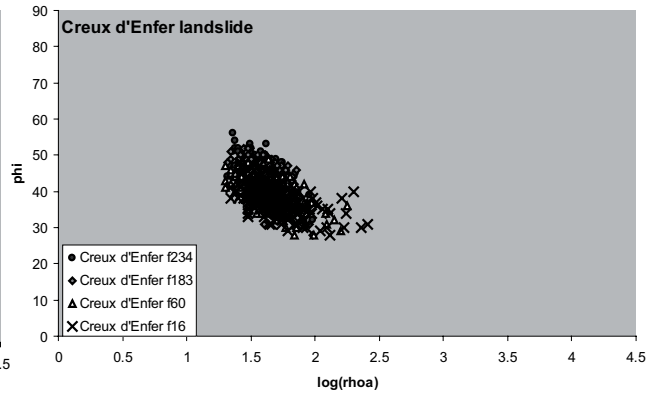
Creux d'Enfer landslide
phi
log(rhoa)
Creux d'Enfer f234
Creux d'Enfer f183
Creux d'Enfer f60
Creux d'Enfer f16

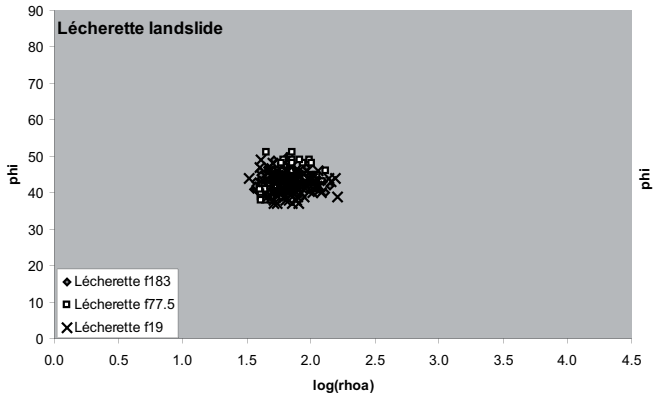
Lécherette landslide
phi
log(rhoa)
Lécherette f183
Lécherette f77.5
Lécherette f19

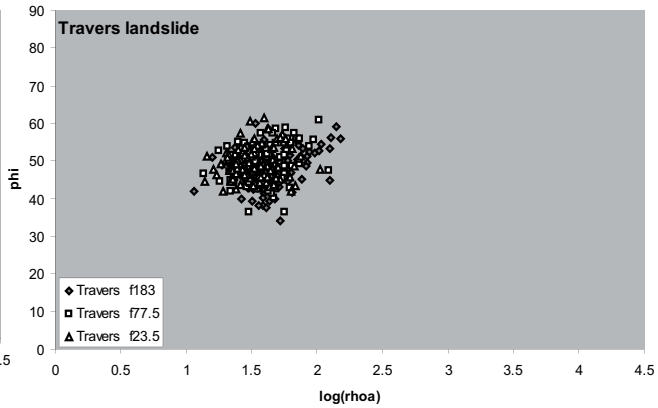
Travers landslide
phi
log(rhoa)
Travers f183
Travers f77.5
Travers f23.5

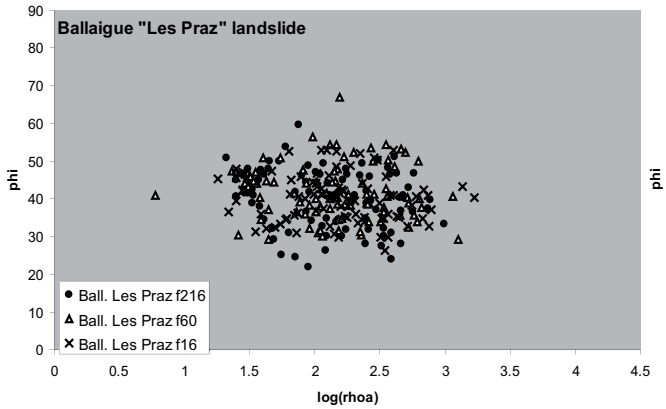
Ballaigue "Les Praz" landslide
phi
log(rhoa)
Ball. Les Praz f216
Ball. Les Praz f60
Ball. Les Praz f16

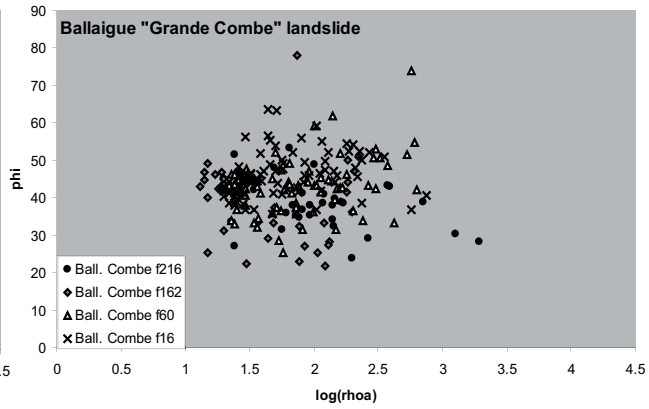
Ballaigue "Grande Combe" landslide
phi
log(rhoa)
Ball. Combe f216
Ball. Combe f162
Ball. Combe f60
Ball. Combe f16

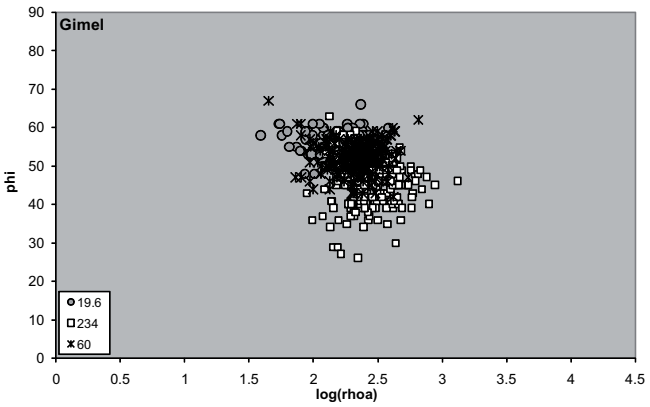
Gimel
phi
log(rhoa)
19.6
234
60

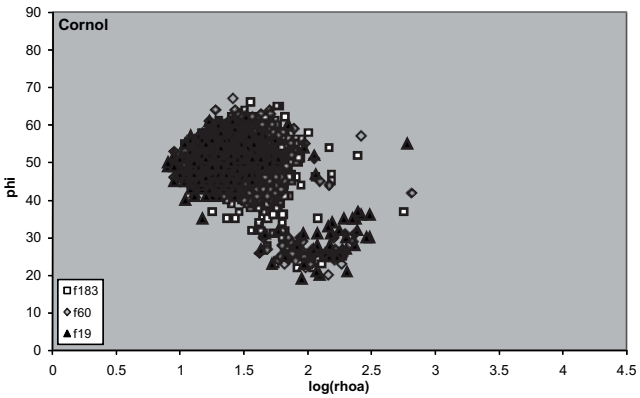
Cornol
phi
log(rhoa)
f183
f60
f19

Frasse landslide -S1-

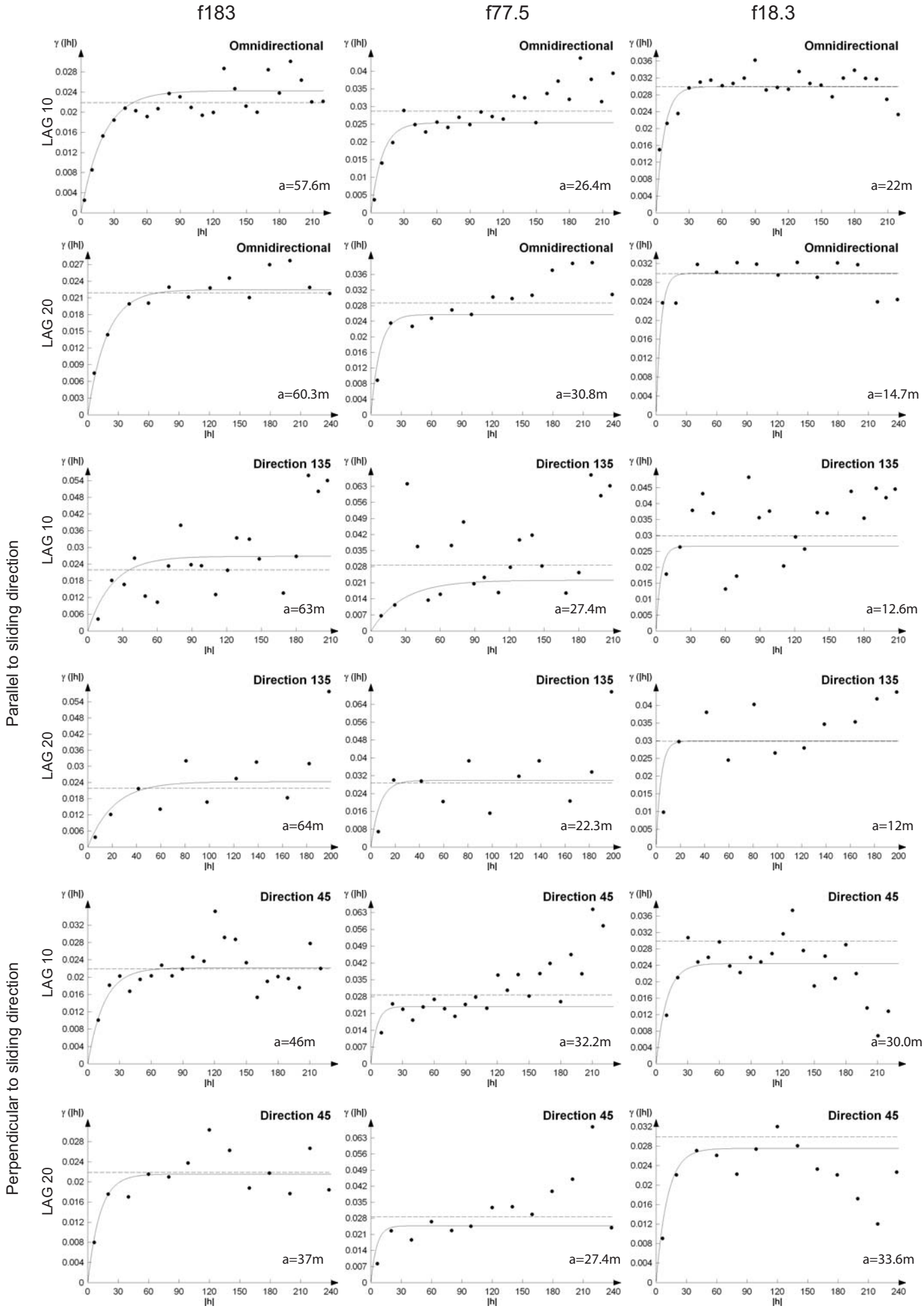

Frasse landslide -S2-

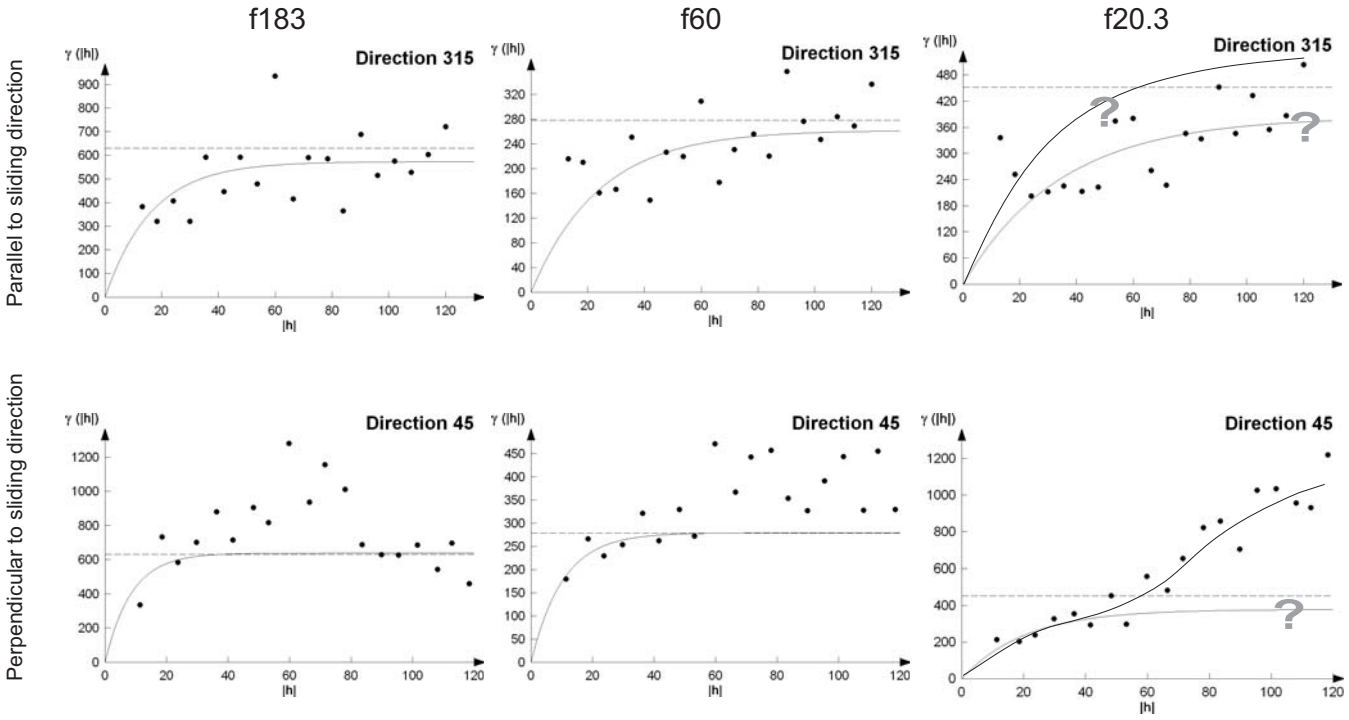

Frasse landslide -S3-

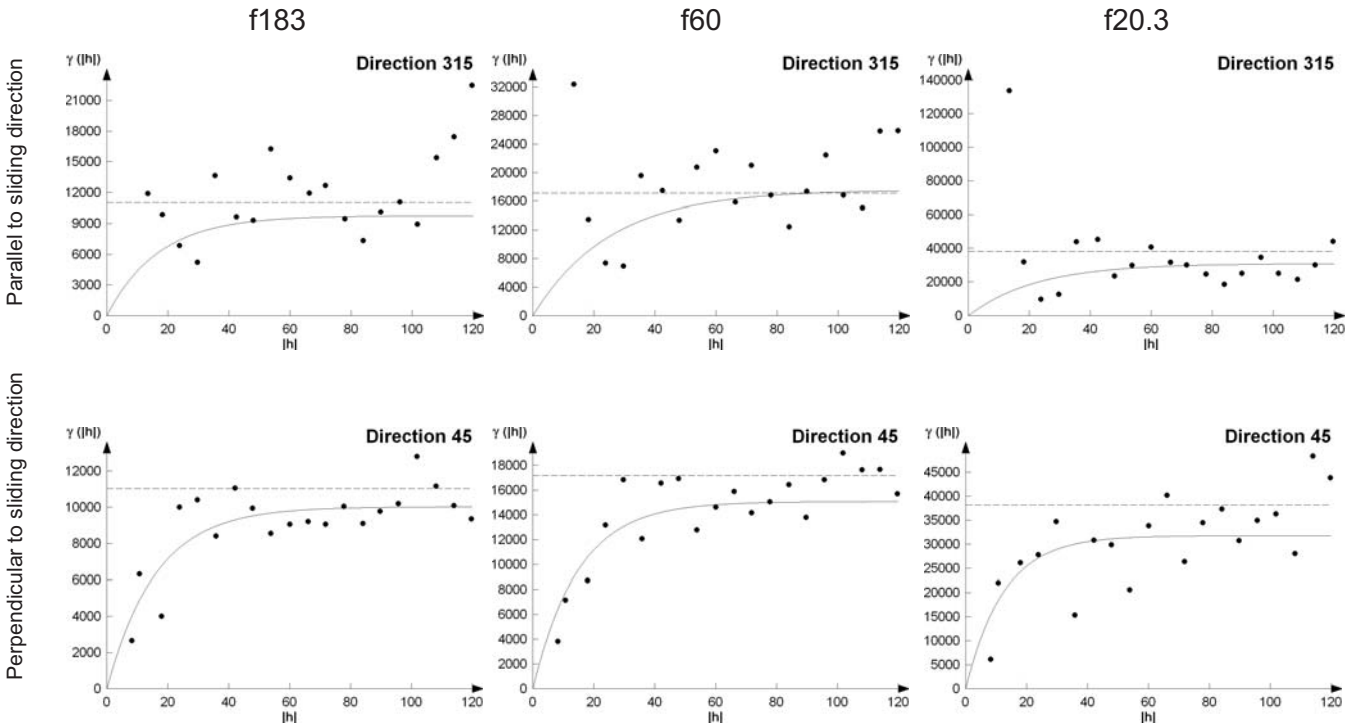

Gimel

f234

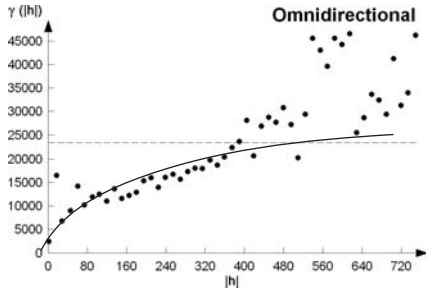

f60

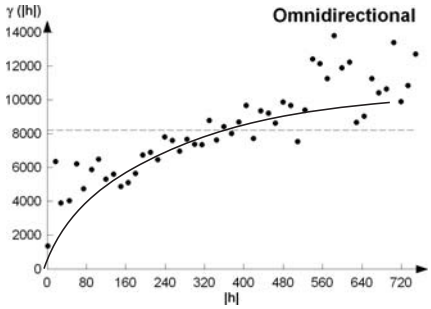

f19.6

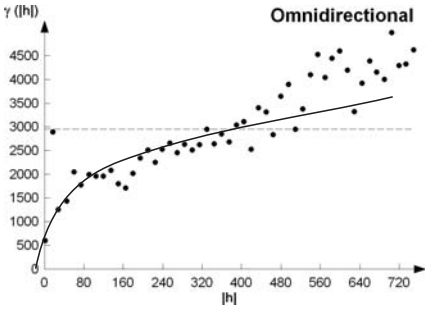

Cornol

f183

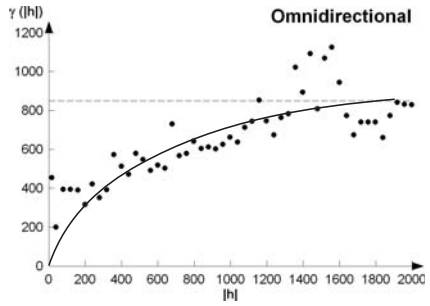

f60

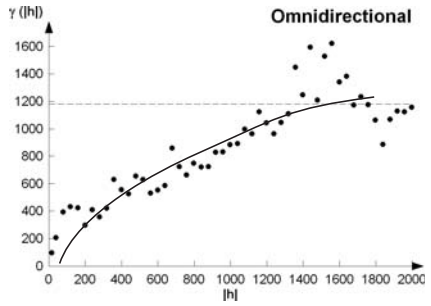

f19

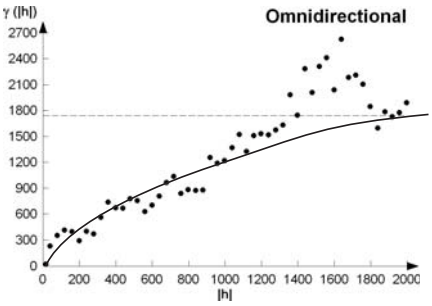

Creux de l'enfer

f234

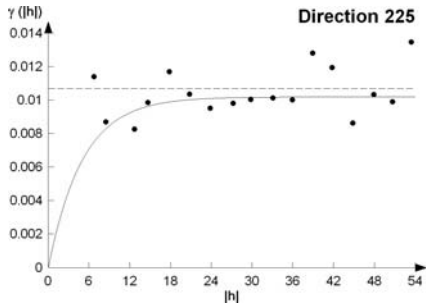

f183

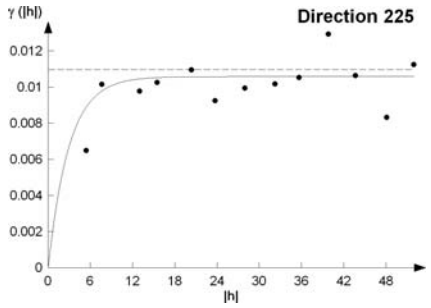

f60

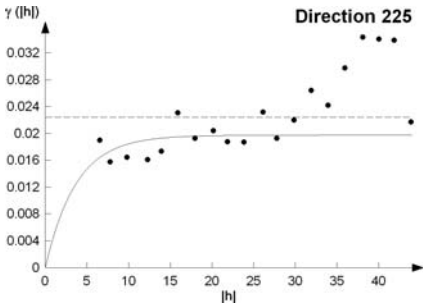

Parallel to sliding direction

Perpendicular to sliding direction

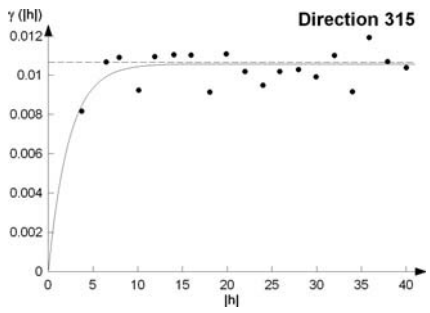

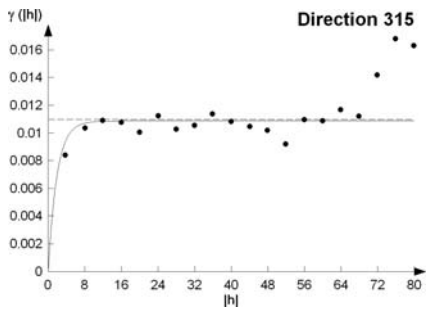

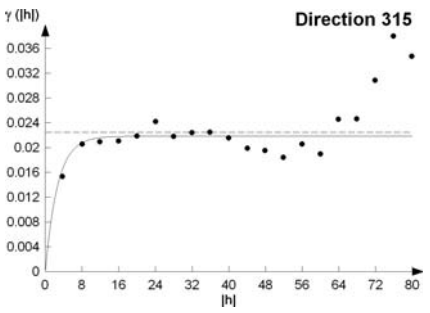

f16

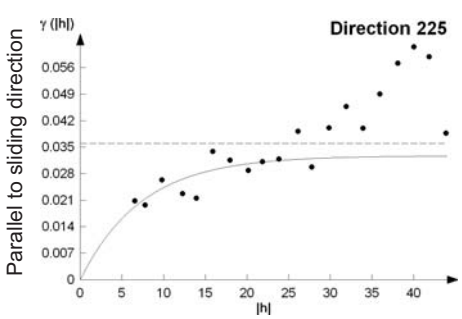

Parallel to sliding direction

Perpendicular to sliding direction

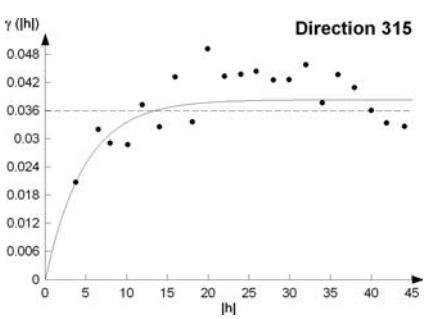

Ballaigue Grande Combe

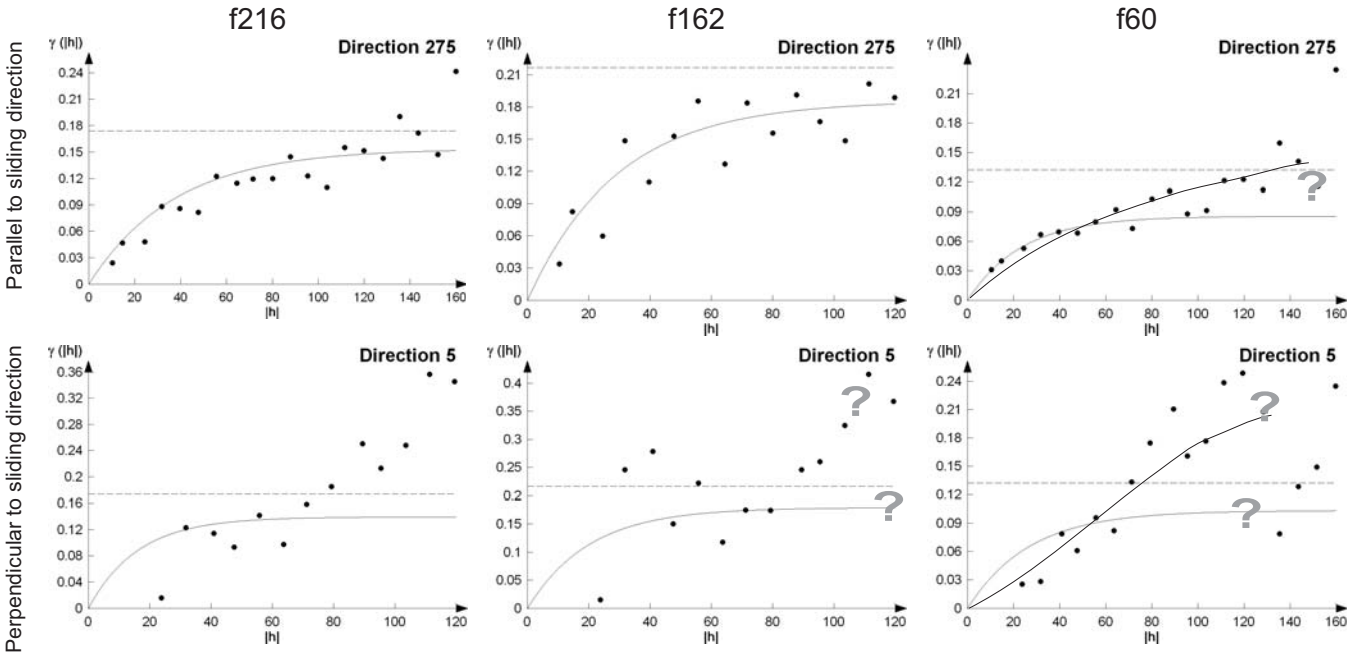

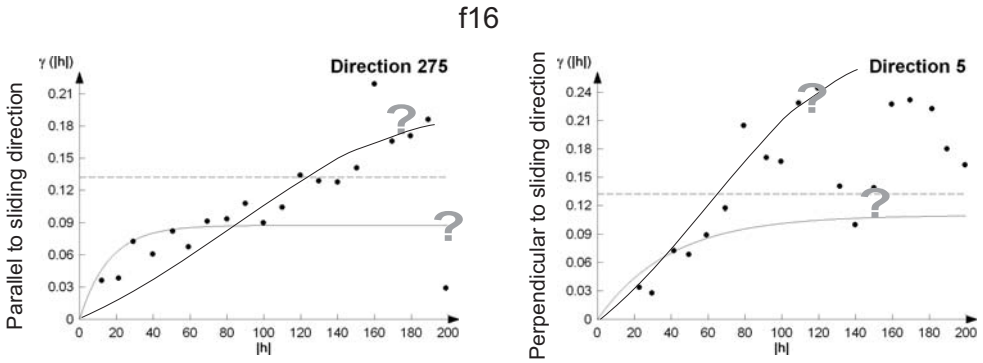

Ballaigue Praz

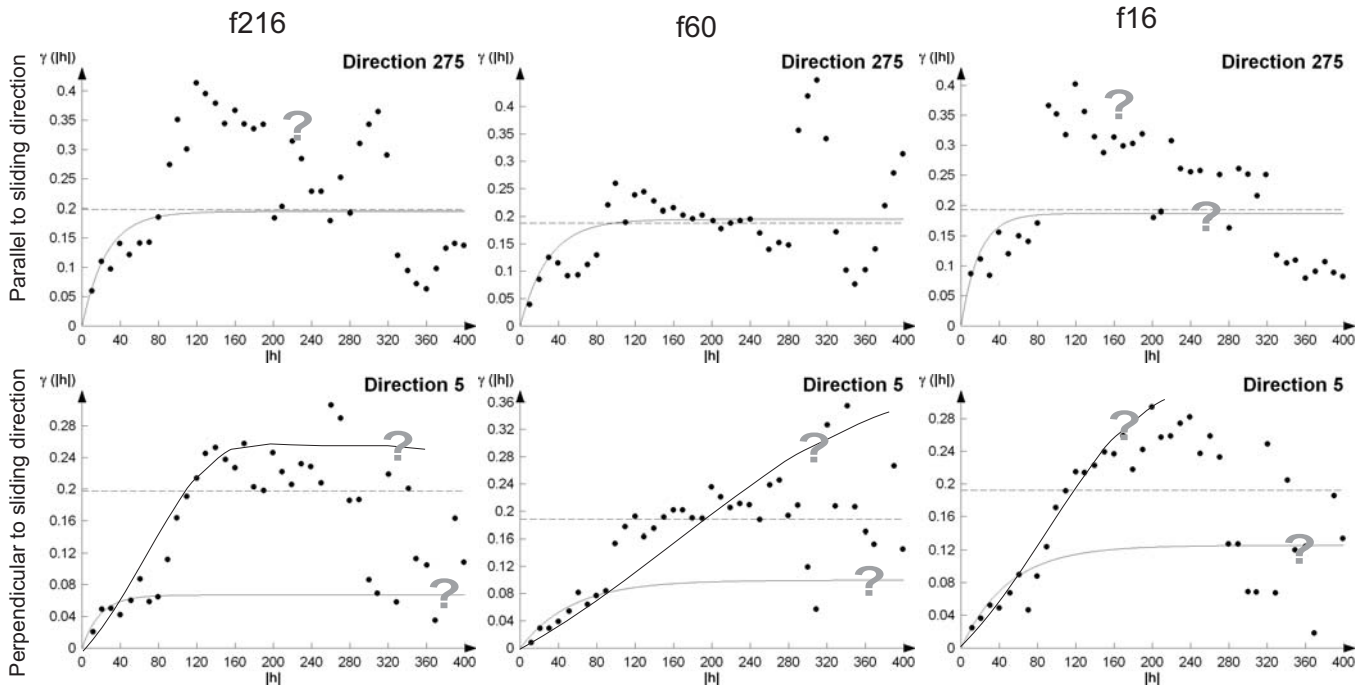

Hohberg landslide -S1-

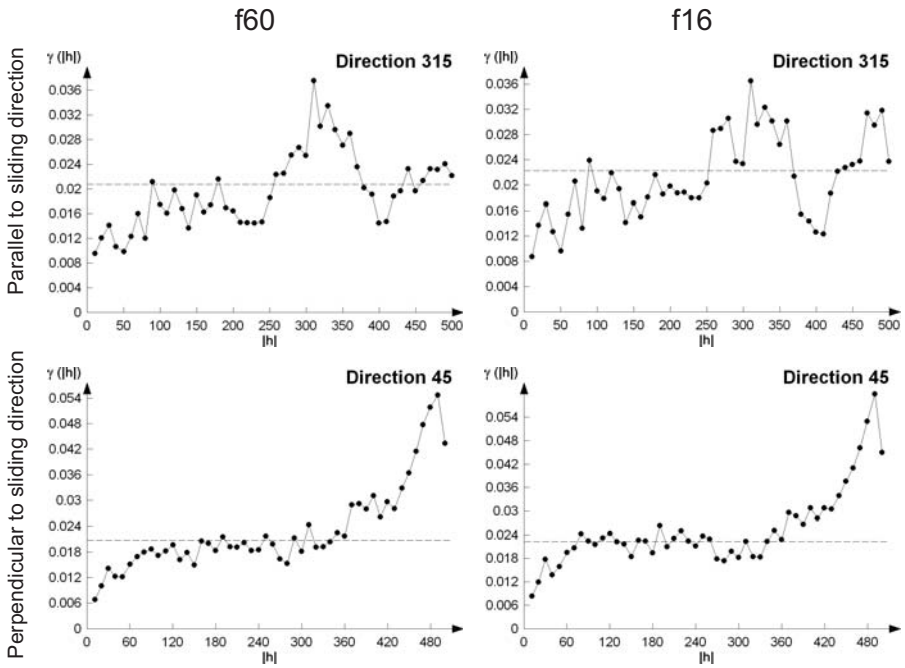

Hohberg landslide -S2-

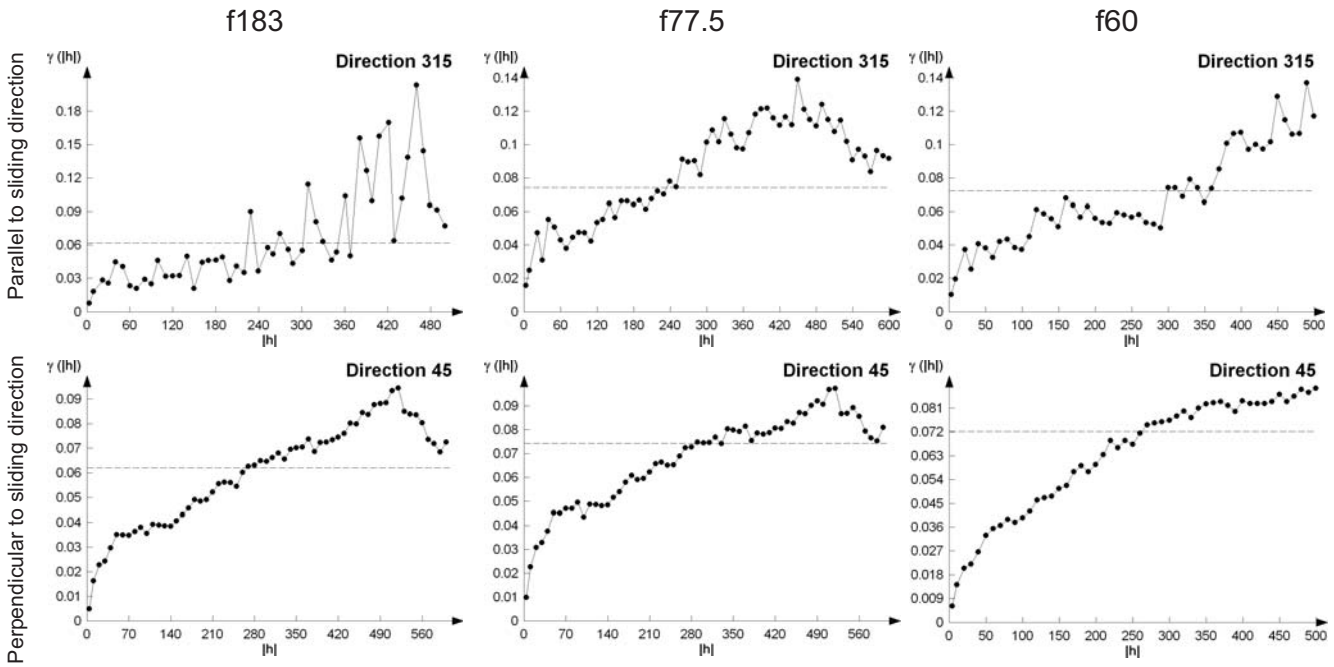

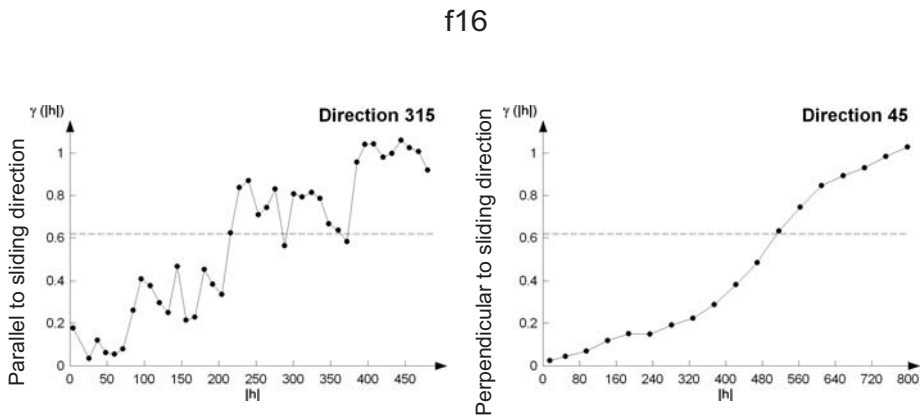

Hohberg landslide -S3-

f183

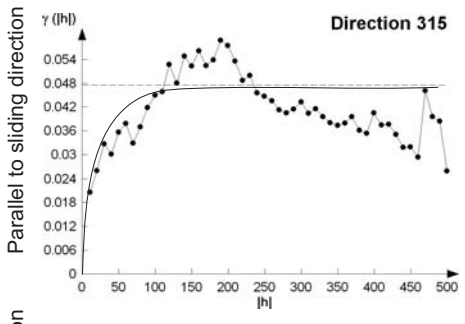

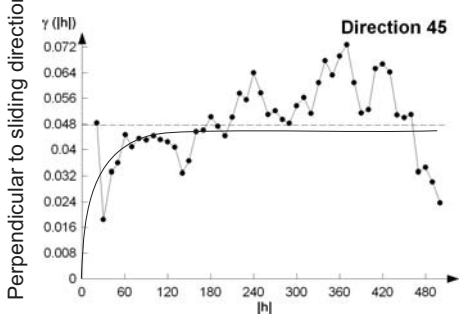

f77.5

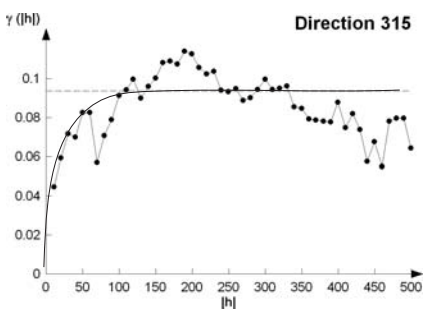

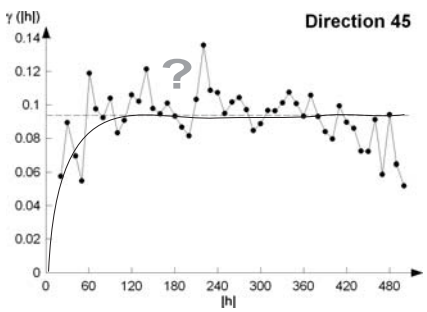

f60

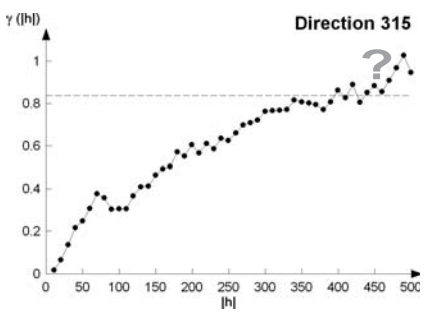

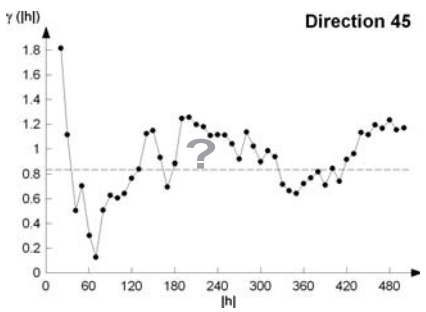

f19.6

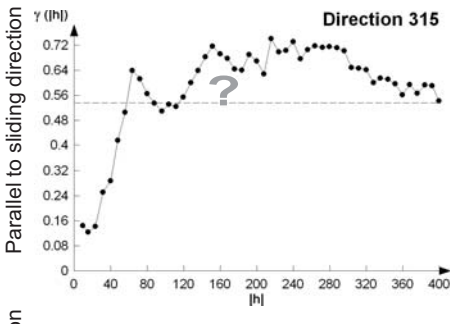

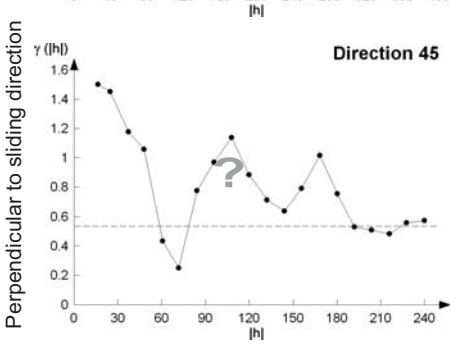

f16

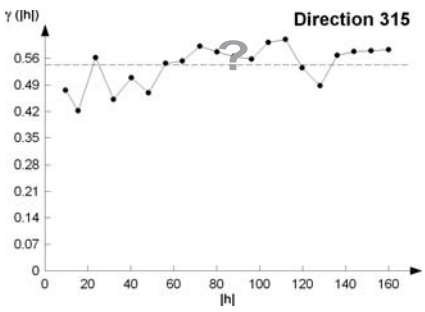

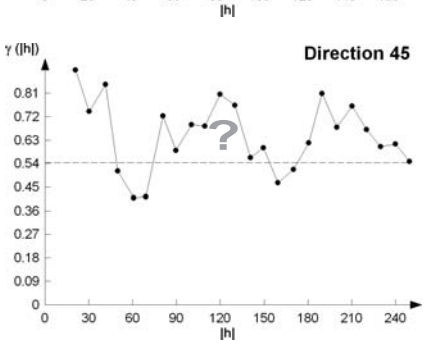

La Lécherette landslide

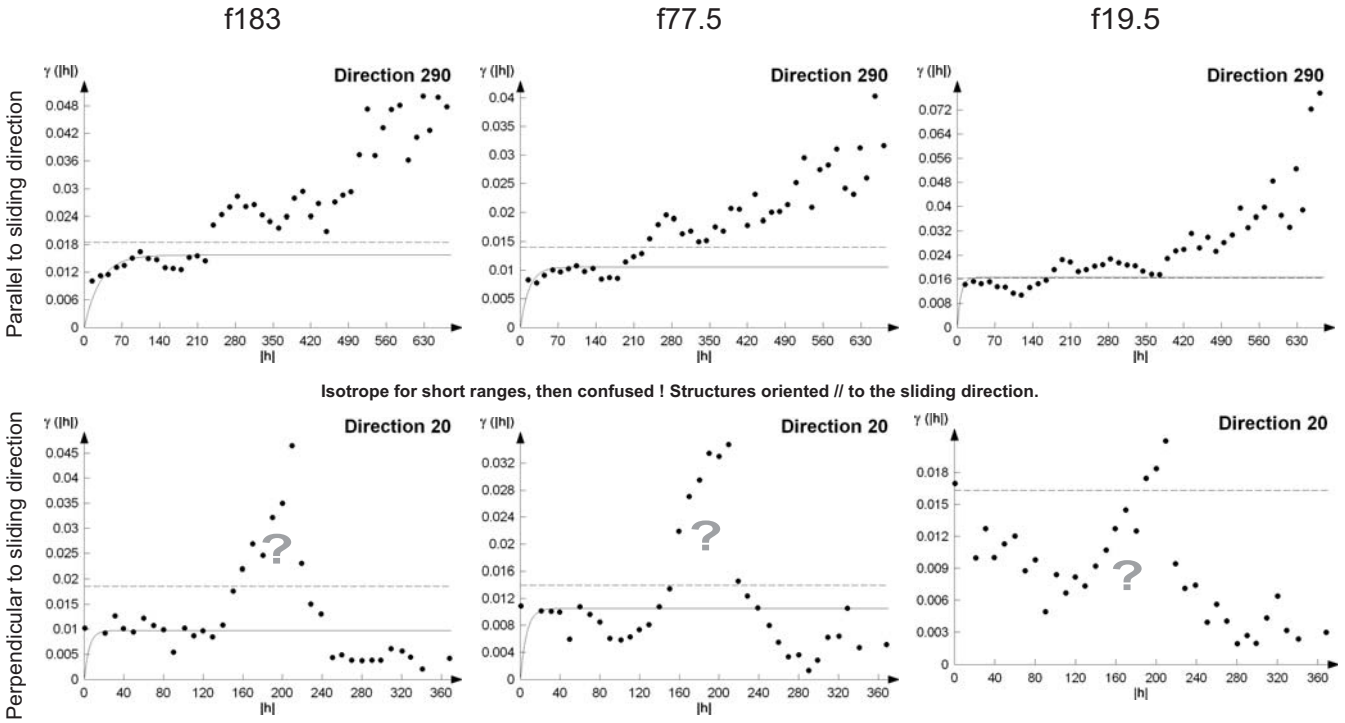

Travers landslide

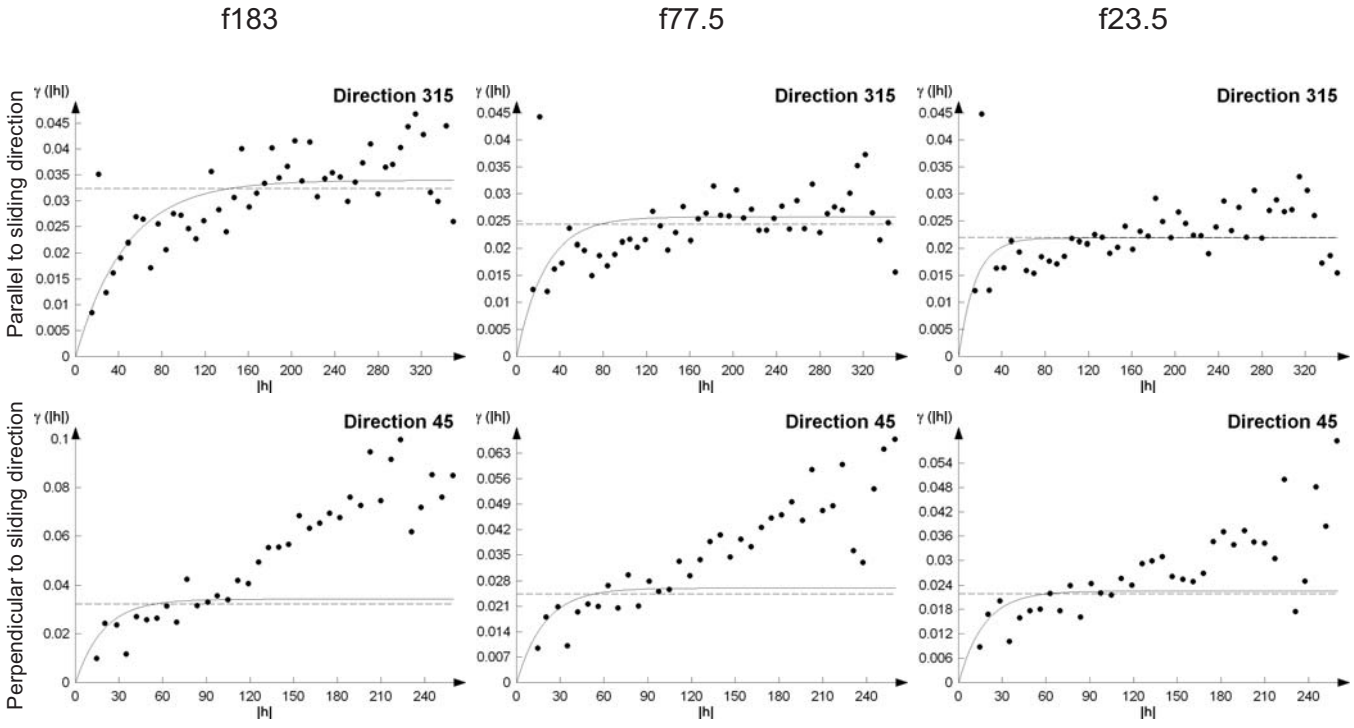

Triesenberg landslide

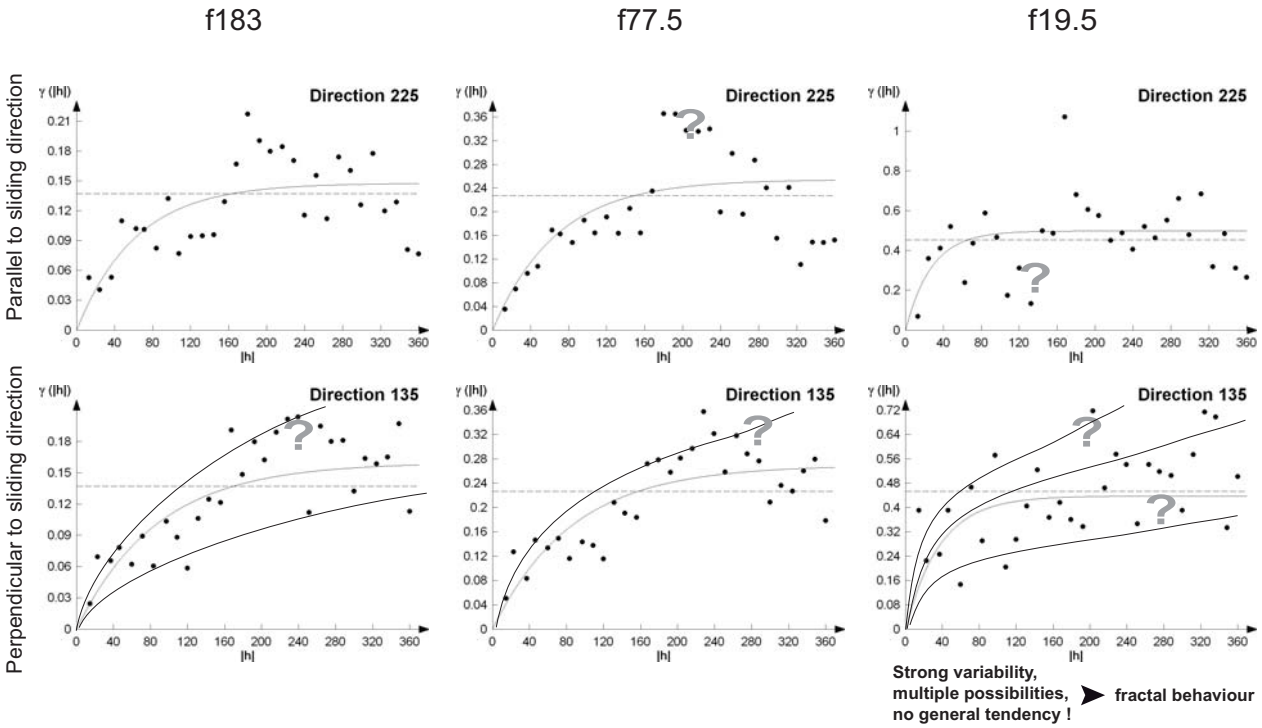

Distribution of the altitudes

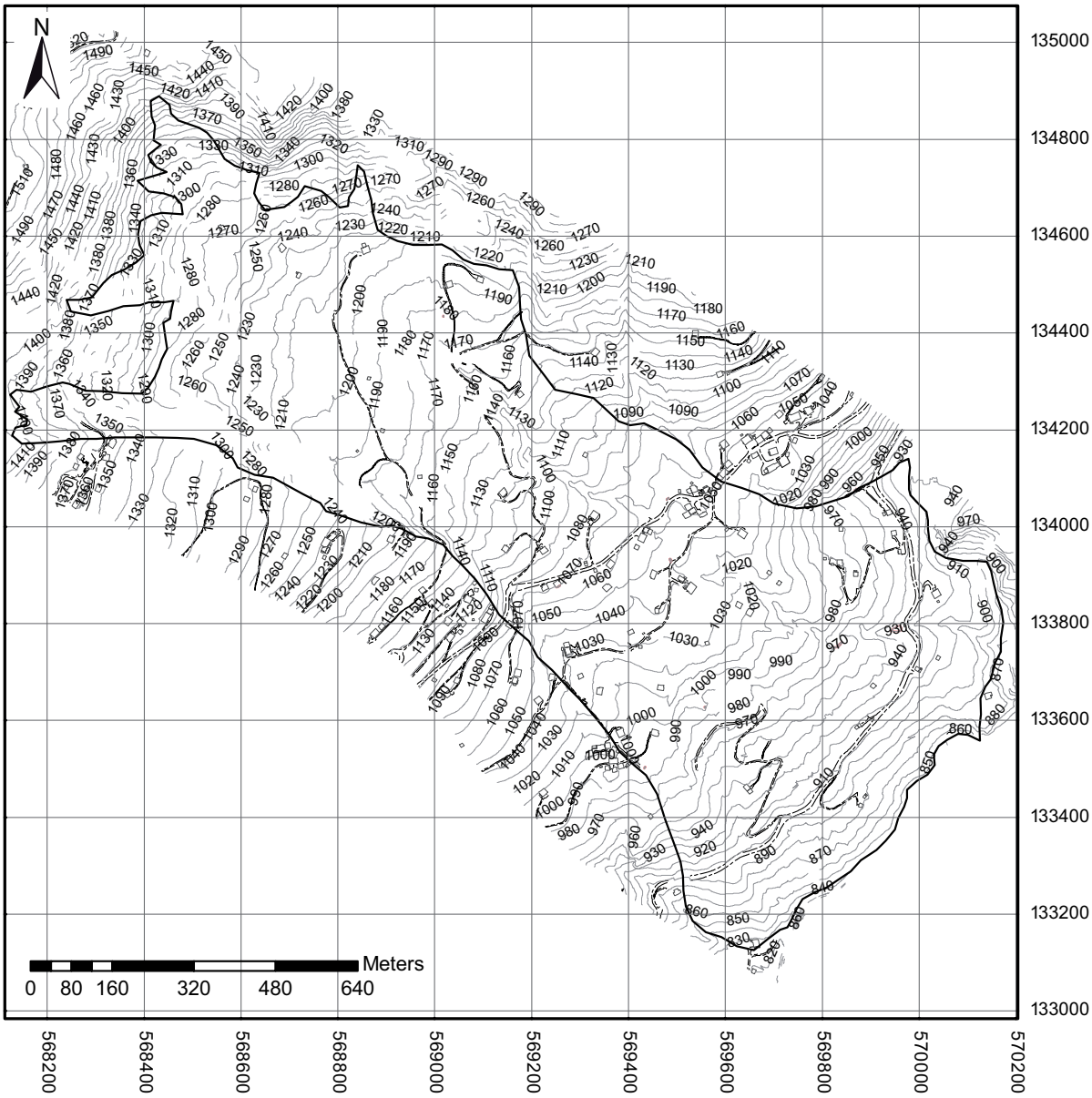

Geology of the surrounding units of the la Frasse region

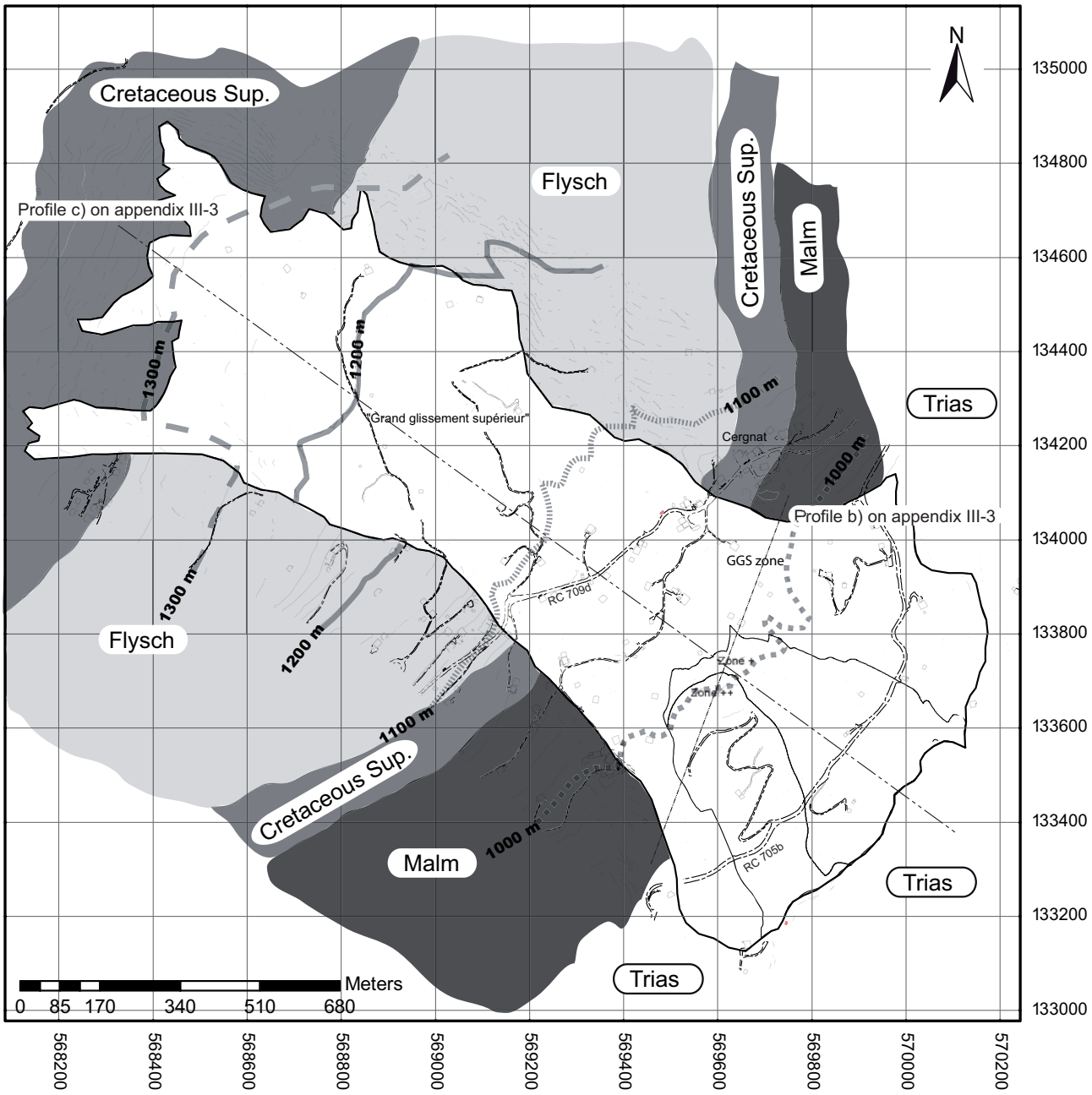

(a) Geological context and (b) transversal and (c) longitudinal profiles

a)

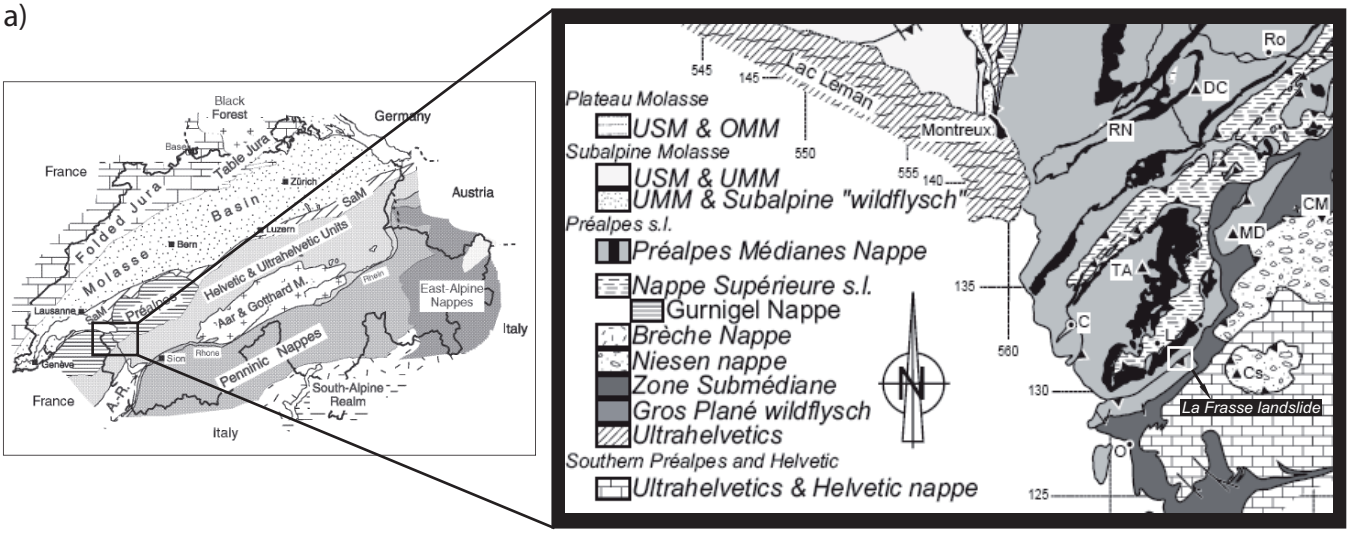

UMM = Lower Marine water Molasse; USM = Lower Fresh water Molasse; OMM = Upper Marine water Molasse; OSM = Upper Fresh water Molasse. RN : Rochers de Naye, DC : Dent de Corjon, Ro : Rossinière, TA : Tours d'Aï L : Leysin, CM : Col des Mosses

b)

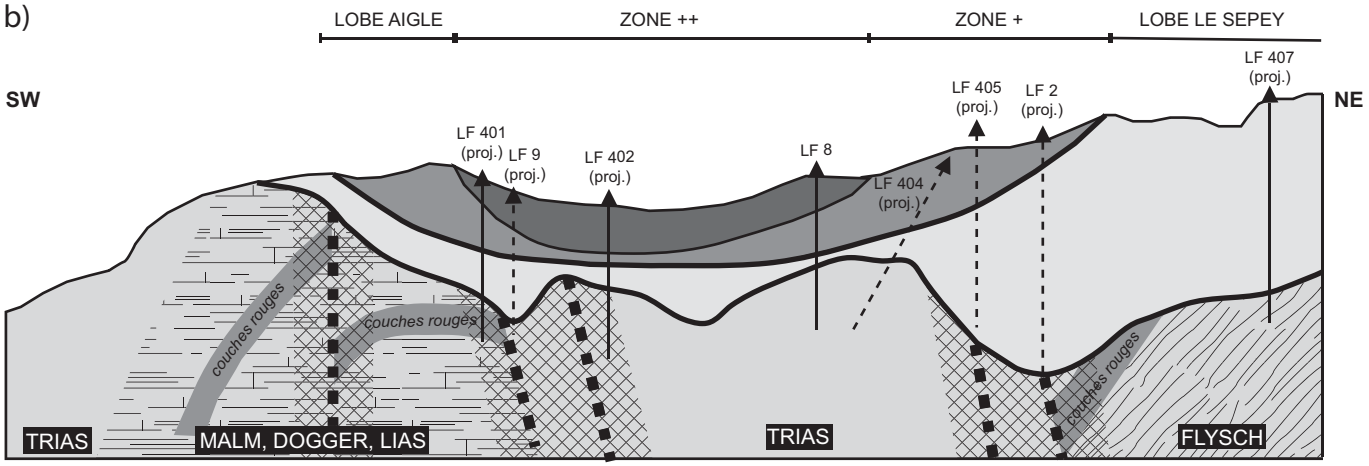

ACTIVE SLIDE : flysch

Glacial till sediments or flysch stabilized

Fractured zones

Supposed faults

FLYSCH : sandstones and clay schists, consisting of strongly weathered to plastic black clay including sandy blocks.

COUCHES ROUGES : Platy marly limestones

MALM, DOGGER, LIAS : Sandy limestones

TRIAS : Brecciated cornieules and dolomites

c)

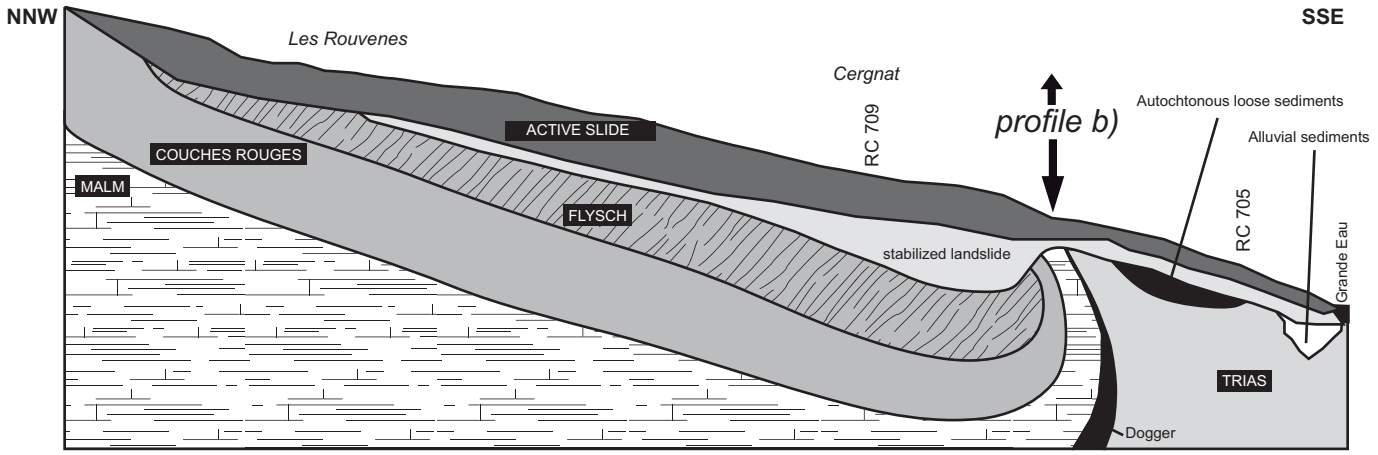

Boreholes and wells characteristics of the la Frasse landslide

Name	Date	Coord.			Length.	Type	Bedrock		Sliding surface		Equipment	Study
		Y	X	Z			Depth	alt.	Depth	alt.		
S1	1967	569'500	133'790	1034	77.50	Drilling core	-	-	*49.6 ??*	*984.4 ??*		Bersier
									61.5 ??	972.5 ??		
S2	1967	569'082	134'100	1135	81.60	Drilling core	-	-	*6.0 ??*	*1129.0 ??*		Bersier
									13.5 ??	*1121.5 ??*		
									39.8 ??	*1095.2 ??*		
									79.0 ??	1056.0 ??		
S3	1967	568'375	134'325	1305	30.35	Drilling core	-	-	-	-		Bersier
FR1	1981-82	569'438	133'563	995	66.50	Drilling core	55.80	939.20	43.90	951.10	Inclino/piezo	DUTI
FR2	1982	569'720	133'875	1011	79.00	Drilling core	-	-	59.70	951.30	Inclino/piezo	DUTI
FR3	1983	568'565	134'568	1261	54.90	Drilling core	-	-	*16.35*	*1244.65*	Inclino/piezo	DUTI
FR4	1983	569'211	134'044	1105.6	104	Destructive	88	1017.6	*9*	*1096.6*	Inclino/piezo	DUTI
FR5	1984	568'516.9	134'646.2	1282.8	30.30	Drilling core	25.50	1257.30	*13.60*	*1269.20*	Inclino/piezo	DUTI
									22.90	1259.90		
FR6	1984	568'742.7	134'457.9	1208.6	65.50	Drilling core	51.20	1157.40	50.25	1158.35	Inclino/piezo	DUTI
LF1	1984	569'118	134'205	1145.25	122.00	Drilling core	94.50	1050.75	78.00	1067.25	Inclino/piezo	NCG
LF2	1985	569'722	133'749	995.08	147.70	Drilling core	118.50	876.58	44.00	951.08	Inclino/piezo	NCG
LF3	1984	*569'830.8*	*133'499.1*	*909*	87.00	Drilling core	52.60	856.40	18.00	891.00	Inclino/piezo	NCG
LF4	1986	569'662	133'343	900	48.00	Drilling core	43.80	856.20	19.00	881.00	Inclino/piezo	NCG
LF5	1986	569'721	133'410	902	44.00	Drilling core	37.20	864.80	22.00	880.00	Inclino/piezo	NCG
LF6	1986	569'914	133'619	918	100.00	Drilling core	80.95	837.05	20.50	897.50	Inclino/piezo	NCG
LF7	1988	*569'718.3*	*133'393.8*	*900*	30	Destructive	-	-	27	873	Inclinometer	NCG
LF8	1988	569'670.5	133'621.0	973.66	87.00	Drilling core	50.00	923.66	21.00	952.66	Inclino/piezo	NCG
LF9	1988	569'557.0	133'491.6	960.58	73.20	Drilling core	63.00	897.58	51.90	908.68	Inclino/piezo	NCG
LF10	1988	569'753.2	133'296.9	865.81	55.50	Drilling core	41.00	824.81	18.50	847.31	Inclino/piezo	NCG
LF11	1989	569'836	133'531	*913*	25 ??	Destructive	- ??	- ??	12.50	900.50	Inclinometer	NCG
LF12	1989	569'863	133'542	*910*	25 ??	Destructive	- ??	- ??	19.50	890.50	Inclinometer	NCG
LF13	1989	569'890	133'577	*910*	25 ??	Destructive	- ??	- ??	18.00	892.00	Inclinometer	NCG
LF14	1989	569'948	133'640	*921*	25 ??	Destructive	- ??	- ??	17.50	903.50	Inclinometer	NCG
LF15	1989	569'968	133'669	*924*	25 ??	Destructive	- ??	- ??	17.50	906.50	Inclinometer	NCG
I 100	1994	569'540.074	133'516.553	969.676	51	Destructive	- ??	- ??	40	930	Inclinometer	NCG
I 101	1994	569'592.744	133'589.138	971.444	50.5	Destructive	- ??	- ??	32	939	Inclinometer	NCG
I 102	1994	569'667.648	133'611.041	973.674	55	Destructive	48 ??	926 ??	25	949	Inclinometer	NCG
I 103	1994	569'668.630	133'521.470	944.330	41	Destructive	34 ??	910 ??	28	916	Inclinometer	NCG
I 104	1994	569'712.160	133'395.483	900.281	30	Destructive	- ??	- ??	25	875	Inclinometer	NCG
Z 100	1994	569'539.650	133'515.606	969.647	49	Destructive	- ??	- ??	40	930	Piezometer	NCG
Z 111	1994	569'588.770	133'587.710	971.526	35	Destructive	- ??	- ??	31	941	Piezometer	NCG
Z 112	1994	569'551.812	133'543.581	971.705	90	Destructive	57 ??	915 ??	39 ??	933 ??	Piezometer	NCG
Z 113	1994	569'659.043	133'583.705	964.104	45	Destructive	42.5 ??	921.5 ??	30 ??	934 ??	Piezometer	NCG
Z 114	1994	569'672.385	133'519.760	943.992	30	Destructive	- ??	- ??	28	916	Piezometer	NCG
Z 115	1994	569'725.379	133'406.689	900.763	30	Destructive	- ??	- ??	25	876	Piezometer	NCG
Z 116	1994	569'664.600	133'340.301	897.851	30	Destructive	- ??	- ??	19	879	Piezometer	NCG
Z 117	1994	569'634.203	133'473.901	941.768	42	Destructive	41 ??	901 ??	- ??	- ??	Piezometer	NCG
Z 118	1994	569'724.865	133'517.765	938.003	34	Destructive	- ??	- ??	- ??	- ??	Piezometer	NCG
Z 119	1994	569'781.461	133'427.430	905.643	30	Destructive	- ??	- ??	20 ??	886 ??	Piezometer	NCG
Z 120	1995	569'582.007	133'584.648	971.753	36	Destructive	- ??	- ??	32 ??	940 ??	Piezometer	NCG
Z 121	1994	569'668.481	133'521.589	944.622	32	Destructive	- ??	- ??	28	917	Piezometer	NCG
P1	1994	569'540.874	133'500.868	969.493	80	Destructive	69 ??	900 ??	40 ??	929 ??	Pump	NCG
P1bis	1995	569'541.580	133'505.310	969.000	44	Destructive	- ??	- ??	40 ??	929 ??	Pump	NCG
P2	1994	569'541.028	133'509.828	969.838	75	Destructive	70 ??	900 ??	41 ??	929 ??	Pump	NCG
P2bis	1995	569'542.500	133'518.250	970.000	45	Destructive	- ??	- ??	40 ??	930 ??	Pump	NCG
P3	1994	569'541.377	133'520.896	970.756	70	Destructive	70 ??	901 ??	40 ??	931 ??	Pump	NCG
P3bis	1995	569'544.060	133'525.320	970.000	43	Destructive	- ??	- ??	40 ??	930 ??	Pump	NCG
P4	1994	569'546.444	133'530.811	971.732	67	Destructive	- ??	- ??	38 ??	934 ??	Pump	NCG
P5	1994	569'549.326	133'539.297	972.042	62	Destructive	- ??	- ??	36 ??	936 ??	Pump	NCG
P6	1994	569'554.023	133'548.580	972.194	60	Destructive	- ??	- ??	34 ??	938 ??	Pump	NCG
P7	1994	569'559.824	133'556.883	972.165	59	Destructive	- ??	- ??	32 ??	940 ??	Pump	NCG
P8	1994	569'565.640	133'565.157	972.193	58	Destructive	- ??	- ??	32 ??	940 ??	Pump	NCG
P9	1994	569'571.447	133'573.218	972.168	57	Destructive	- ??	- ??	32 ??	940 ??	Pump	NCG
P10	1994	569'578.384	133'581.351	972.083	56	Destructive	- ??	- ??	32 ??	940 ??	Pump	NCG
P11	1994	569'586.281	133'586.796	972.041	56	Destructive	- ??	- ??	32 ??	940 ??	Pump	NCG
P12	1994	569'596.553	133'590.163	972.145	43	Destructive	- ??	- ??	32 ??	940 ??	Pump	NCG
P13	1994	569'606.736	133'591.006	972.349	42	Destructive	- ??	- ??	32 ??	940 ??	Pump	NCG
P14	1994	569'617.009	133'592.332	972.437	54.5	Destructive	48.5 ??	924 ??	31 ??	941 ??	Pump	NCG
P15	1994	569'625.835	133'594.785	972.856	54	Destructive	49 ??	924 ??	31 ??	942 ??	Pump	NCG
P16	1994	569'635.515	133'596.605	973.468	54	Destructive	49 ??	924 ??	30 ??	943 ??	Pump	NCG
P17	1994	569'644.813	133'600.112	973.820	54	Destructive	49 ??	925 ??	29 ??	945 ??	Pump	NCG
P18	1994	569'653.933	133'603.753	974.117	53	Destructive	48.5 ??	925.5 ??	28 ??	946 ??	Pump	NCG
P19	1994	569'662.684	133'608.101	974.306	53	Destructive	48 ??	926 ??	26 ??	948 ??	Pump	NCG
P20	1994	569'670.406	133'614.875	974.226	51	Destructive	47.6 ??	926.6 ??	24 ??	950 ??	Pump	NCG
P21	1994	569'669.945	133'626.536	974.364	51	Destructive	47.5 ??	926.9 ??	23 ??	951 ??	Pump	NCG
P22	1994	569'671.734	133'636.426	975.172	51	Destructive	46 ??	929 ??	22 ??	953 ??	Pump	NCG
I 201	1998	*569'482.13*	*133'775.80*	*1030*	80	Destructive	-	-	> 78	< 952	Inclinometer	NCG
I 202	1998	*569'569.06*	*133'837.38*	*1034*	80	Destructive	-	-	67.0	967.0	Inclinometer	NCG
Z 203	1998	569'516.67	133'785.19	1'032.81	60	Destructive	-	-	- ??	- ??	Piezometer	NCG
Z 204	1998	*569'598.84*	*133'866.29*	*1031*	60	Destructive	-	-	- ??	- ??	Piezometer	NCG
Z 205	1998	*569'546.90*	*133'809.33*	*1033*	60	Destructive	-	-	- ??	- ??	Piezometer	NCG
LFH 1	2001	*569'670*	*133'635*	*975*	100	Destructive	-	-	62* ??	975	Drain horiz.	NCG
									97* ??	975		
LFH 2	2001	*569'670*	*133'635*	*975*	164	Destructive	-	-	42* ??	975	Drain horiz.	NCG
									71* ??	975		
I 301	2002	569'701.06	133'697.48	986.45	60	Destr/core	-	-	39.0	947.5	Inclino/piezo	NCG
P 302	2002	569'730.79	133'721.06	989.95	140	Destr/core	125.00	864.95	??	??	Piézo/TDR	NCG
LF401 p	2006	569'523	133'516	975	80						Piezometer	NCG
LF402 i	2006	569'587	133'539	959	80						Inclinometer	NCG
LF403 p	2006	569'550	133'582	975	100						Piezometer	NCG
LF404 cp	2006	569'715	133'679	975	90						CP	NCG
LF405 p	2006	569'659	133'708	1000	140						Piezometer	NCG
LF406 i	2006	569'761	133'830	992	110						Inclinometer	NCG
LF407 p	2006	569'693	133'877	1007	110						Piezometer	NCG

Geographical location of the boreholes and wells of the la Frasse landslide

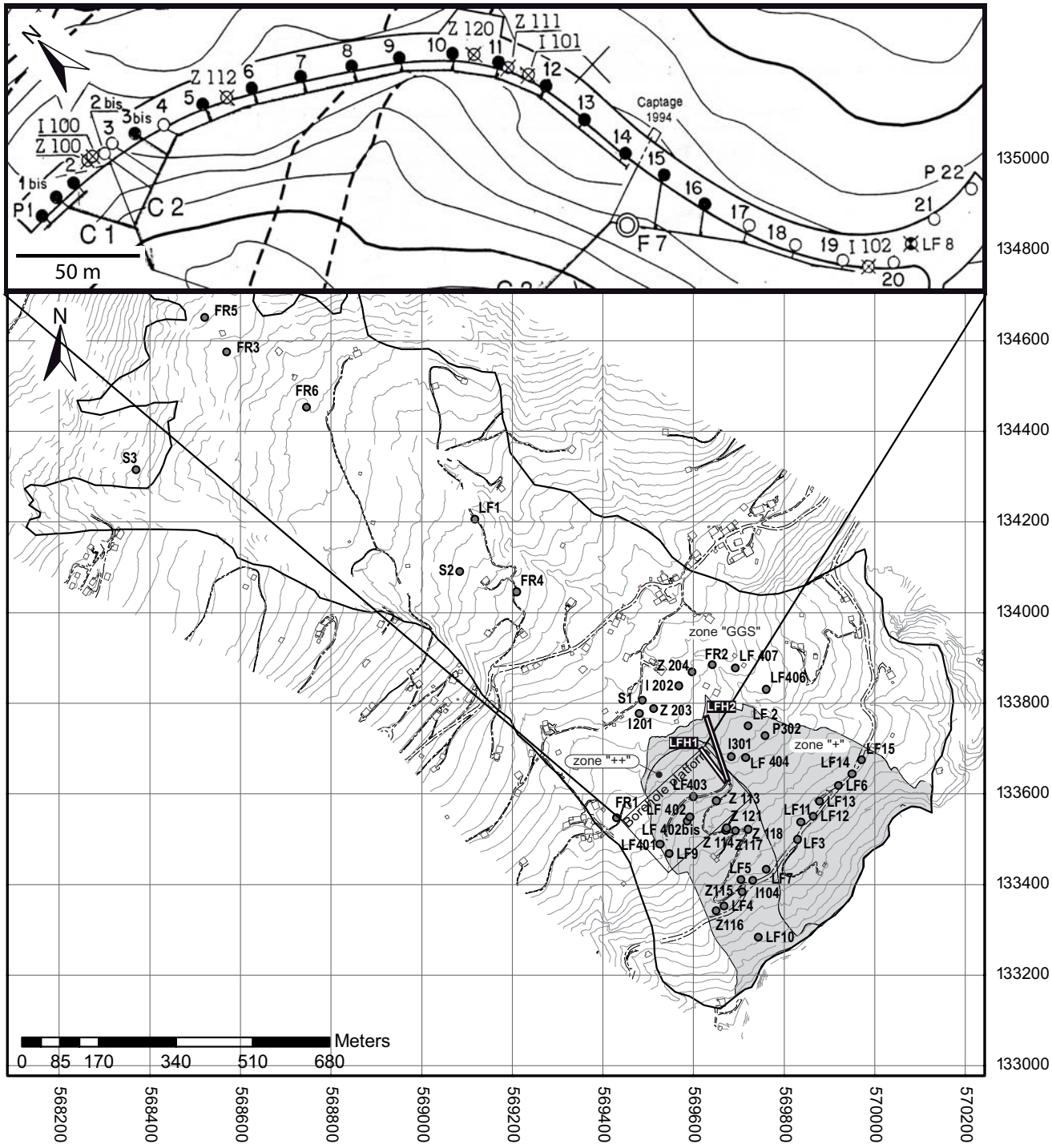

Borehole platform commissioned in 1995; transversal section. *See Appendix III-5 for geographical location.*

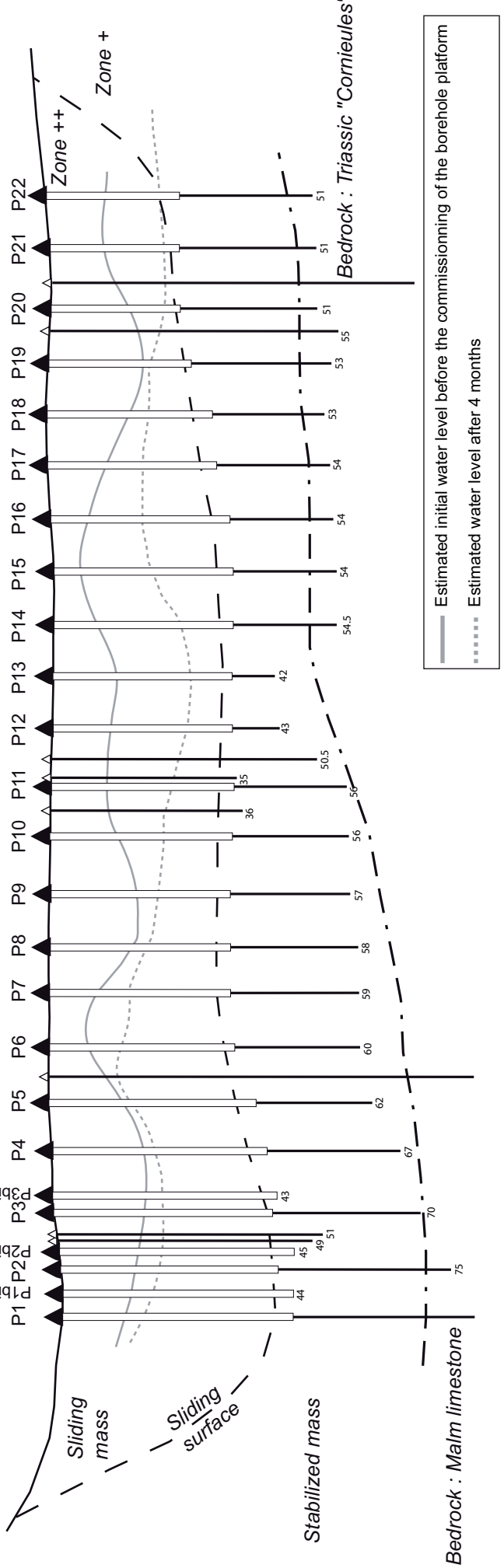

Hydrochemical analyses of the la Frasse landslide

Well	Coord. X	Coord. Y	Zone	Depth (m)		Substratum	Water level (m) 08.2006	cond. (mS/cm)	temp. (°C)	pH	Na (mg/l)	K (mg/l)	Mg (mg/l)	Ca (mg/l)	F (mg/l)	Cl (mg/l)	NO3 (mg/l)	SO4 (mg/l)	HCO3 (mg/l)	TDS (mg/l)	water hardness	$d^{18}O$ (‰)	Water TYPE	Jäckli type
				Well	Sliding surface																			
LF1	569118	134205	GGS	122	78	Flysch	20.2	579	8.2	*n.m*	2.37	1.31	4.02	121.76	-	1.30	0.93	18.91	371.20	331.30	*n.m*	-10.18	$Ca\text{-}HCO_3$	1
LF3	569830	133499	+	87	18	Trias	9.5	1071	9.7	*n.m*	108.66	4.02	18.41	126.40	-	126.73	1.44	44.16	426.40	637.80	*n.m*	-10.73	$Ca\text{-}Na\text{-}HCO_3\text{-}Cl$	1
LF7	569720	133395	++	?	?	?	1.4	233	18.2	*n.m*	28.73	17.19	0.67	16.80	-	41.84	4.10	3.93	74.80	137.60	*n.m*	-9.48	$Ca\text{-}HCO_3\text{-}(SO_4)$	4a
LF11	569837	133537	+	?	?	?	5.3	541	8.9	*n.m*	1.74	1.55	5.23	128.21	-	1.55	0.51	24.18	*Precipitate*	*163.00*	*n.m*	-10.59	$Ca\text{-}HCO_3\text{-}(SO_4)$	4a
LF14	569950	133643	+	?	?	?	15.4	738	10.1	*n.m*	107.16	3.21	4.58	46.08	-	148.59	64.95	17.41	37.90	429.90	*n.m*	-9.65	$Ca\text{-}(Mg)\text{-}HCO_3\text{-}(SO_4)$	5d
LF15	569972	133674	+	?	?	?	11.9	1336	10.3	*n.m*	164.06	2.52	9.43	142.33	-	209.50	2.75	94.68	313.19	938.40	*n.m*	*dry*	$Ca\text{-}HCO_3\text{-}(SO_4)$	4b
FR4	569210	134045	GGS	104	(30?)	Flysch	2.3	473	12	*n.m*	22.16	3.13	6.08	124.09	0.06	28.88	11.15	160.80	236.20	456.70	33.46	-10.17	$Ca\text{-}HCO_3\text{-}(SO_4)$	4a
I 201	569481	133777	GGS	74	?	?	24.1	411	12.3	*n.m*	2.23	0.75	5.11	82.00	0.05	8.83	1.26	11.76	247.90	359.90	*n.m*	-10.43	$Ca\text{-}HCO_3$	1
Z 203	569513	133787	GGS	60	?	?	*n.m*	607	11.1	*n.m*	4.58	11.25	7.84	136.68	0.04	9.51	2.53	15.80	447.70	402.30	37.33	-10.84	$Ca\text{-}HCO_3$	1
I 202	569568	133838	GGS	74	67.5	?	*n.m*	562	10.7	*n.m*	151.70	1.84	2.43	6.45	0.85	2.52	0.32	-	445.20	611.30	2.61	-11.17	$Na\text{-}HCO_3\text{-}(SO_4)$	6
Z 204	569598	133868	GGS	60	?	?	*n.m*	471	9.7	*n.m*	24.76	2.46	22.74	62.77	0.15	4.72	-	3.41	366.90	269.00	25.02	-11.57	$Ca\text{-}(Mg)\text{-}HCO_3$	2b
$Z\ 113_1$	569658	133589	++	45	30	Trias	14.6	547	8.5	7.6	5.74	3.00	19.78	87.00	-	4.49	1.34	72.18	263.70	377.70	*n.m*	-11.04	$Ca\text{-}(Mg)\text{-}HCO_3\text{-}(SO_4)$	5b
$Z\ 113_2$	569658	133589	++	45	30	Trias	14.6	548	9.3	7.6	8.78	3.49	20.39	103.60	0.04	6.64	1.31	74.59	336.23	457.20	35.98	-11.04	$Ca\text{-}(Mg)\text{-}HCO_3\text{-}(SO_4)$	5b
Z 114	569672	133519	++	30	28	?	10.6	662	8.7	*n.m*	24.09	1.50	16.71	114.00	-	1.19	0.77	54.61	412.50	390.70	*n.m*	-9.99	$Ca\text{-}(Mg)\text{-}HCO_3$	2a
Z 118	569721	133521	++	34	?	?	12.8	714	9.4	*n.m*	14.47	3.90	29.65	129.51	-	2.75	0.71	101.08	*Precipitate*	*282.10*	*n.m*	-11.11	$Ca\text{-}(Mg)\text{-}HCO_3\text{-}(SO_4)$	5b
Z 121	569674	133524	++	32	28	?	26.0	287	9.9	*n.m*	6.83	16.64	2.32	48.08	0.08	1.41	56.53	11.08	123.80	266.80	*n.m*	-9.35	Ca-HCO3	1
P1	569537	133498	++	80	40	?	*n.m*	628	9	*n.m*	32.45	4.13	23.61	103.88	-	8.34	1.21	69.06	409.90	413.30	*n.m*	-9.48	$Ca\text{-}Mg\text{-}(Na)\text{-}HCO_3$	3
P2	569536.63	133510	++	75	42	?	*n.m*	683	9.1	*n.m*	14.49	4.24	28.54	128.46	-	5.47	1.85	105.20	424.70	485.30	*n.m*	-10.74	$Ca\text{-}(Mg)\text{-}HCO_3\text{-}(SO_4)$	5b
P3	569538.19	133528.23	++	70	40	?	*n.m*	723	9	*n.m*	44.52	3.96	25.43	114.26	0.20	6.87	22.35	108.33	*Precipitate*	*325.90*	*n.m*	-9.52	$Ca\text{-}(Mg)\text{-}HCO_3\text{-}(SO_4)$	5b
P3bis	569540.75	133533.95	++	43	?	?	*n.m*	763	9.6	*n.m*	14.85	4.26	36.23	137.81	0.08	7.25	1.79	116.38	*Precipitate*	*318.60*	*n.m*	dry	$Ca\text{-}(Mg)\text{-}HCO_3\text{-}(SO_4)$	5b
P5	569544.81	133542.78	++	62	35-36	?	24.9	843	9.3	*n.m*	29.81	3.32	48.07	124.09	0.14	1.90	1.15	151.94	458.40	369.90	*n.m*	-9.52	$Ca\text{-}(Mg)\text{-}HCO_3\text{-}(SO_4)$	5b
P6	569551.06	133552.72	++	60	33-34	?	*n.m*	743	10.4	*n.m*	18.09	3.03	34.84	129.93	0.83	6.50	95.29	116.32	*Precipitate*	*404.80*	*n.m*	-9.62	$Ca\text{-}(Mg)\text{-}HCO_3\text{-}(SO_4)$	5b
P7	569554.5	133559.7	++	59	32	?	*n.m*	804	8.8	*n.m*	49.03	2.50	34.47	103.00	-	1.56	0.95	134.57	435.80	481.30	*n.m*	-9.51	$Ca\text{-}(Mg)\text{-}HCO_3\text{-}(SO_4)$	5e
P8	569562	133568	++	58	32	?	*n.m*	1023	9.2	*n.m*	280.84	1.21	5.27	9.76	0.30	2.83	1.62	122.62	635.70	424.40	*n.m*	-9.93	$Na\text{-}HCO_3\text{-}(SO_4)$	6
P9	569566.63	133573.95	++	57	32	?	*n.m*	1132	10.7	*n.m*	291.08	1.40	8.36	28.88	0.41	2.70	1.44	165.39	702.50	499.70	*n.m*	-9.43	$Na\text{-}HCO_3\text{-}(SO_4)$	6
P10	569573.63	133581.36	++	56	32	?	*n.m*	890	9.8	*n.m*	127.89	2.37	21.74	89.00	0.12	2.41	1.23	155.89	519.70	490.20	*n.m*	-9.16	$Na\text{-}HCO_3\text{-}(SO_4)$	6
P12	569600.94	133593.44	++	43	32	?	*n.m*	685	10.7	*n.m*	75.57	2.84	18.42	83.00	0.09	4.79	0.88	67.19	451.60	380.50	*n.m*	-11.00	$Ca\text{-}(Mg)\text{-}HCO_3\text{-}(SO_4)$	5a
P14	569619	133596	++	54.5	31-32	Trias	*n.m*	421	11.9	*n.m*	36.40	2.89	11.57	70.56	0.06	4.79	-	44.55	*Precipitate*	*170.80*	*n.m*	-11.19	$Ca\text{-}(Mg)\text{-}HCO_3\text{-}(SO_4)$	5b
P16	569631.81	133599.45	++	54	30-31	Trias	*n.m*	692	9.5	*n.m*	17.92	2.92	31.24	123.46	0.11	4.97	0.78	94.33	*Precipitate*	*275.70*	*n.m*	-11.16	$Ca\text{-}(Mg)\text{-}HCO_3\text{-}(SO_4)$	5b
P18	569646.63	133606.27	++	53	27-28	Trias	22.4	1010	9	*n.m*	9.95	3.44	59.74	155.00	-	2.02	-	274.83	455.40	712.80	*n.m*	-10.80	$Ca\text{-}(Mg)\text{-}HCO_3\text{-}(SO_4)$	5b
P20	569664.25	133620.36	++	51	24	Trias	21.2	928	8.6	*n.m*	9.12	3.01	42.22	180.00	-	1.65	-	306.30	393.50	724.60	*n.m*	*dry*	$Ca\text{-}(Mg)\text{-}HCO_3\text{-}(SO_4)$	5b
P21	569669.25	133628.89	++	51	23	Trias	17.6	672	9.8	*n.m*	2.66	2.35	23.10	125.00	-	1.01	-	95.36	386.00	434.10	*n.m*	*dry*	$Ca\text{-}(Mg)\text{-}HCO_3\text{-}(SO_4)$	5b
P22	569668	133641	++	51	21	Trias	21.3	949	9.1	*n.m*	24.52	4.07	56.80	120.00	-	1.07	-	225.15	424.10	610.80	*n.m*	-10.84	$Ca\text{-}(Mg)\text{-}HCO_3\text{-}(SO_4)$	5b
LF406	569761	133830	GSS	110	56.7	Flysch	*n.m*	627	12.3	7.9	65.24	6.72	25.93	67.29	0.47	11.67	1.42	112.76	331.47	385.80	27.46	-11.17	$Na\text{-}HCO_3\text{-}(SO_4)$	6
LF 407_1	569693	133877	GGS	20	60	Flysch	*n.m*	604	11.9	7.4	28.76	4.79	29.05	95.81	0.11	2.94	4.97	30.74	449.20	542.20	35.86	-9.79	$Ca\text{-}(Mg)\text{-}HCO_3$	2a
LF 407_2	569693	133877	GGS	65	60	Flysch	*n.m*	451	9.2	7.4	14.30	12.70	17.18	88.02	-	14.55	-	10.13	359.17	324.70	29.03	*dry*	$Ca\text{-}(Mg)\text{-}HCO_3\text{-}(SO_4)$	5b
LF 407_3	569693	133877	GGS	125	60	Malm	*n.m*	501	10.1	7.5	34.01	3.56	19.02	75.30	-	3.62	-	2.36	388.94	296.10	26.98	-10.23	$Ca\text{-}(Mg)\text{-}HCO_3$	2a
LF 8	569670.5	133621	++	87	21	Trias	*n.m*	310	9.6	7.5	30.31	50.29	1.24	22.95	0.06	0.46	4.08	30.59	178.73	158.30	6.24	*dry*	$Na\text{-}HCO_3\text{-}(SO_4)$	6
Z 111	569588.77	133587.71	++	35	31	?	*n.m*	788	9.8	7.2	8.50	3.74	49.48	139.00	0.08	2.57	0.46	151.34	476.78	831.40	56.89	*dry*	$Ca\text{-}(Mg)\text{-}HCO_3\text{-}(SO_4)$	5e
LF 2	569721.51	133748.79	+	147.7	44	Malm	*n.m*	503	12.3	7.2	3.91	2.04	17.19	110.98	0.04	2.39	0.74	45.66	355.63	538.50	34.76	*dry*	Ca-(Mg)-HCO3	2a
LF 401_1	569523	133516	++	13	39.5	Flysch	*n.m*	1036	9.9	7.5	220.04	5.92	14.69	87.90	0.10	15.50	0.41	187.21	601.58	582.70	28.62	-11.18	$Na\text{-}HCO_3\text{-}(SO_4)$	6
LF 401_2	569523	133516	++	45	39.5	Flysch	*n.m*	657	9.4	8.5	220.31	3.38	3.18	8.88	1.14	7.64	-	19.77	535.09	273.10	3.52	*dry*	$Ca\text{-}Mg\text{-}(Na)\text{-}HCO_3$	3
Z120	569582.01	133584.65	++	36	32	Flysch	*n.m*	750	9.8	7.5	128.75	12.17	7.30	82.94	0.07	12.31	0.84	81.33	500.20	417.10	27.21	*dry*	$Na\text{-}HCO_3\text{-}(SO_4)$	6
LF 402bis	569587	133539	++	10	34.4	Flysch	*n.m*	428	9.4	9.1	12.05	12.44	22.76	27.41	0.08	5.01	0.25	132.57	62.46	227.00	16.20	-10.78	$Ca\text{-}(Mg)\text{-}HCO_3\text{-}(SO_4)$	5e
LF 403_1	569550	133582	++	12	50	Flysch	*n.m*	982	8.5	7.3	33.54	18.68	67.96	150.00	0.07	14.31	0.05	282.31	511.30	782.90	67.99	-10.97	$Ca\text{-}(Mg)\text{-}HCO_3\text{-}(SO_4)$	5e
LF 403_2	569550	133582	++	110	50	Flysch ?	*n.m*	765	8.7	8.8	230.30	1.44	8.88	16.10	1.66	4.07	-	49.65	562.05	327.10	8.17	-11.51	$Na\text{-}HCO_3\text{-}(SO_4)$	6
LF 403_3	569550	133582	++	28	50	Flysch	*n.m*	797	8.6	8.1	195.38	2.38	19.53	37.14	1.26	3.88	0.10	96.00	521.67	399.50	17.30	*dry*	$Na\text{-}HCO_3\text{-}(SO_4)$	6
LF 404_3	569715	133679	+	20	37.3	Flysch	*n.m*	624	16.7	7.7	9.00	6.62	25.23	140.08	0.07	2.70	1.11	115.91	397.96	698.60	45.33	*dry*	$Ca\text{-}(Mg)\text{-}HCO_3\text{-}(SO_4)$	5b

Remarks: [*n.m*] = non mesured, [*dry*] : means that at the day of sampling the well was dry. [-]= element absent

Spatial distribution of the electrical conductivity

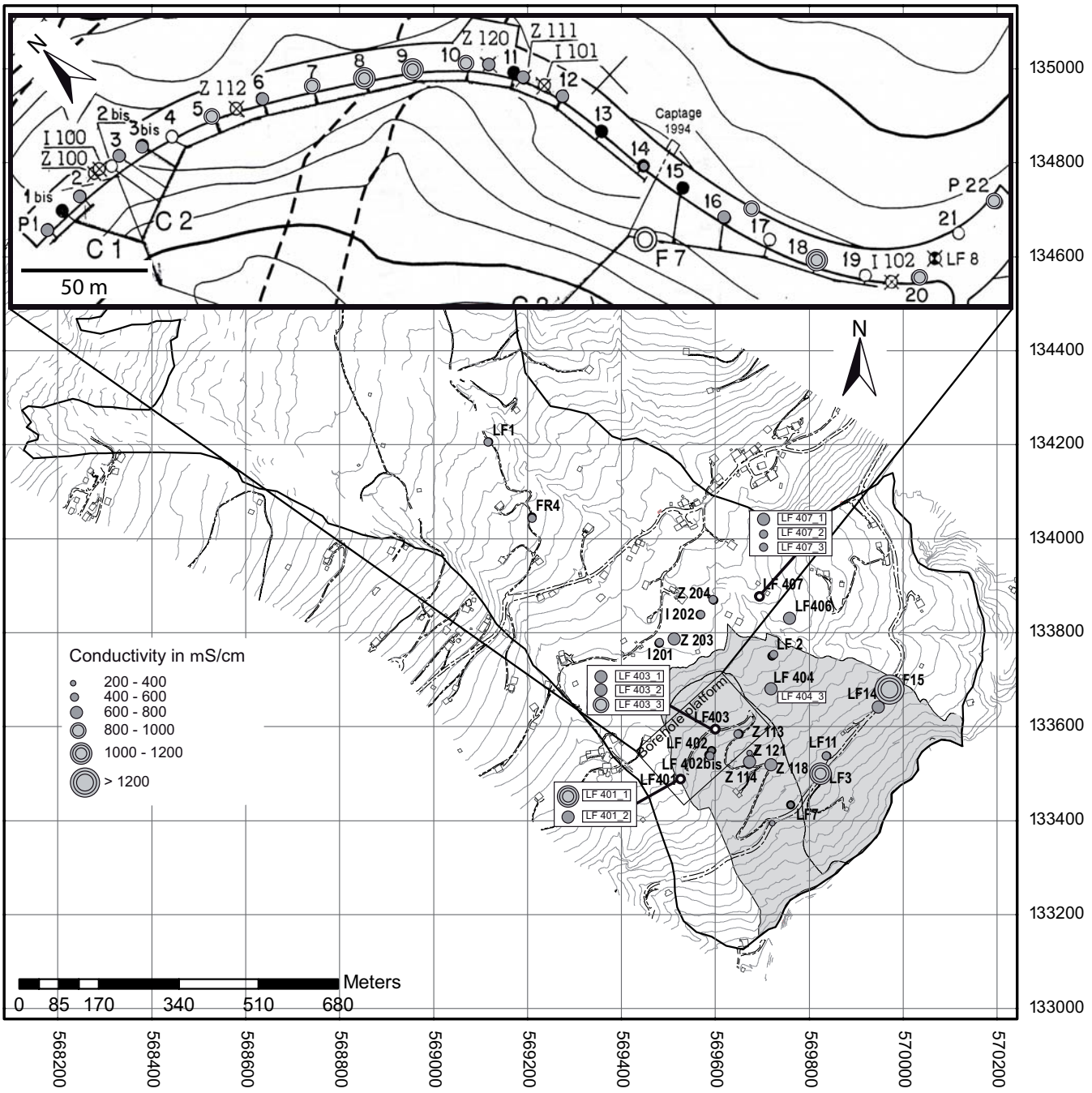

Spatial distribution of the measured isotopic values

Spatial distribution of the calculated altitudes of infiltration

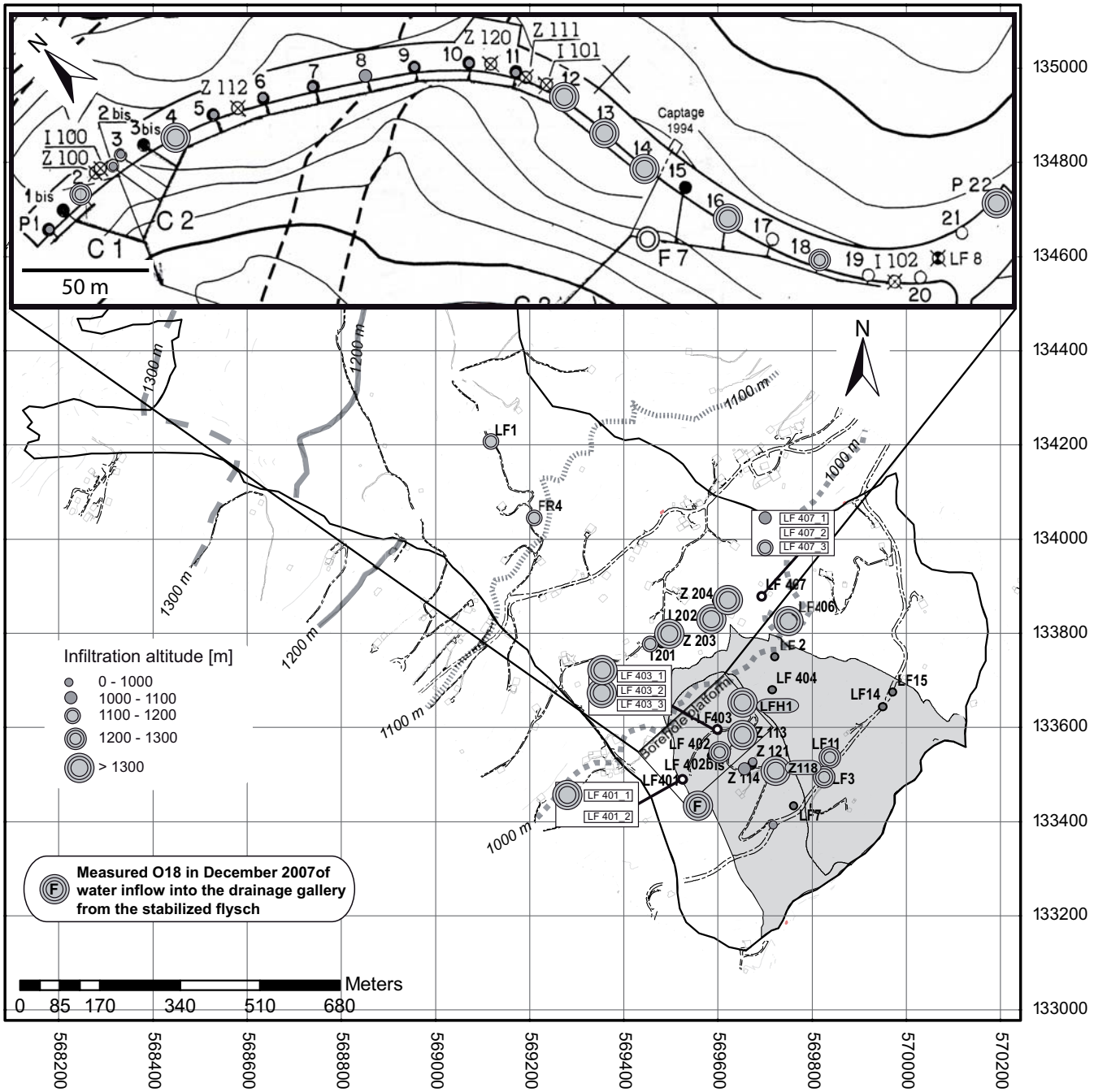

Hydrochemical analyses at each well of the borehole platform;
representation of the strong spatial variability

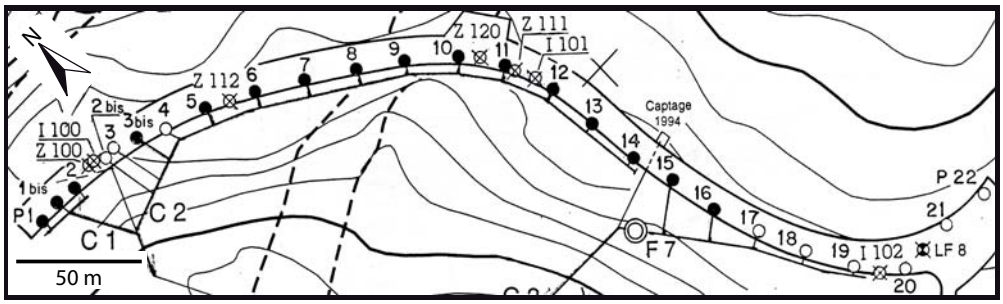

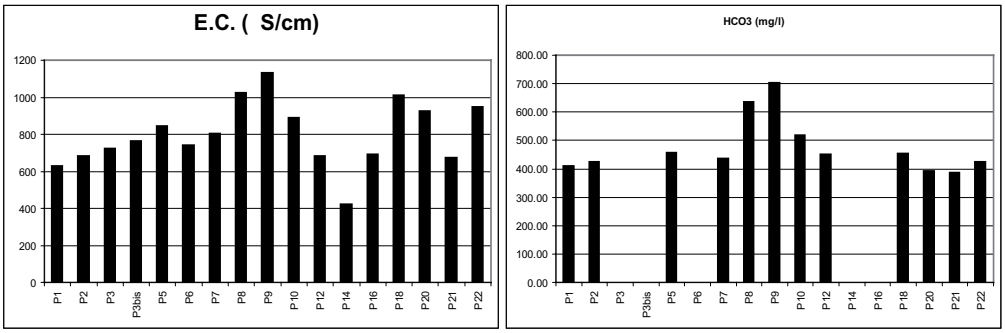

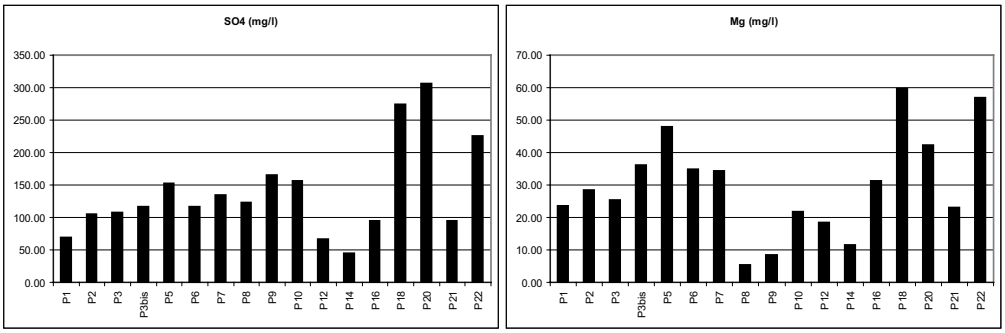

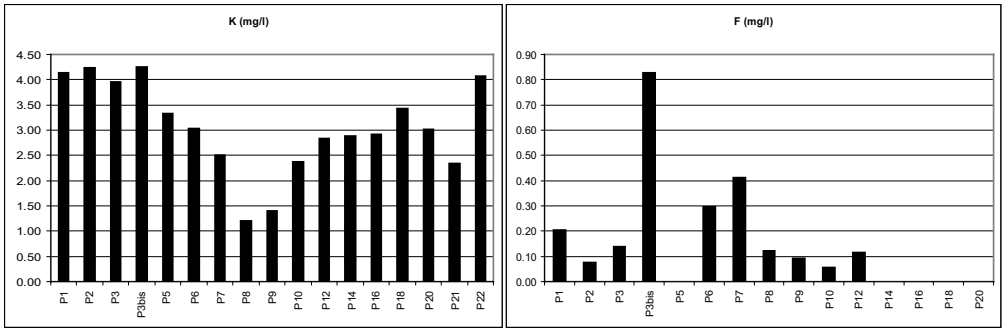

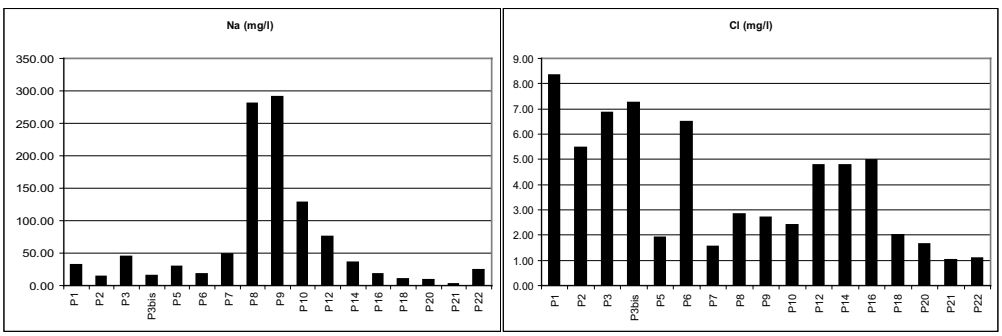

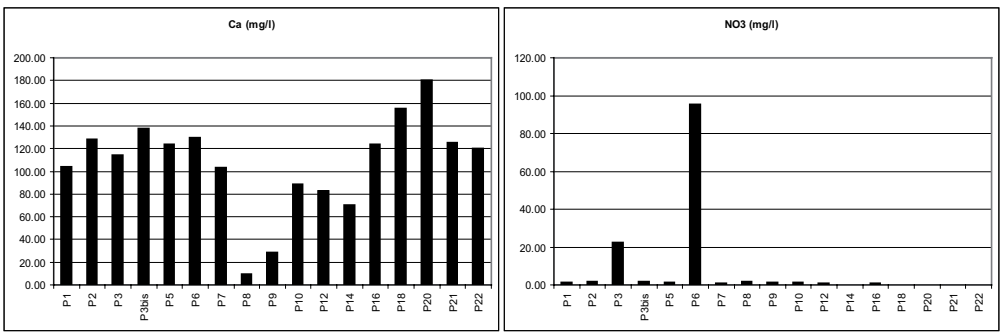

[A]

Drainage gallery
Boring 2006

Example of bore logging

Document translated from NCG + EPFL (Document Norbert SA)

Well LF 402
Zone ++
Length : 90.00 m
X : 133539.0
Y : 569587.0
Z : 959.0 m
09.06.2006 to 23.06.2006

Scale : 1 / 50

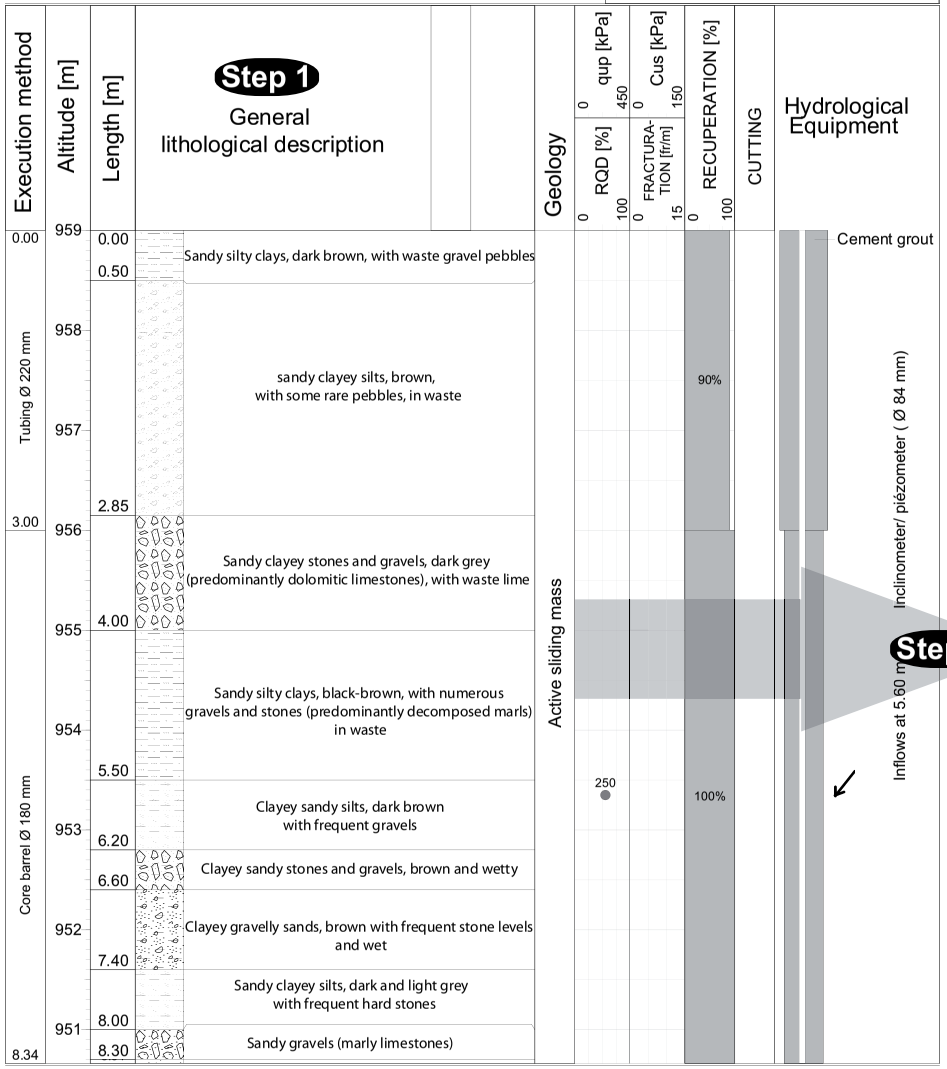

[C]

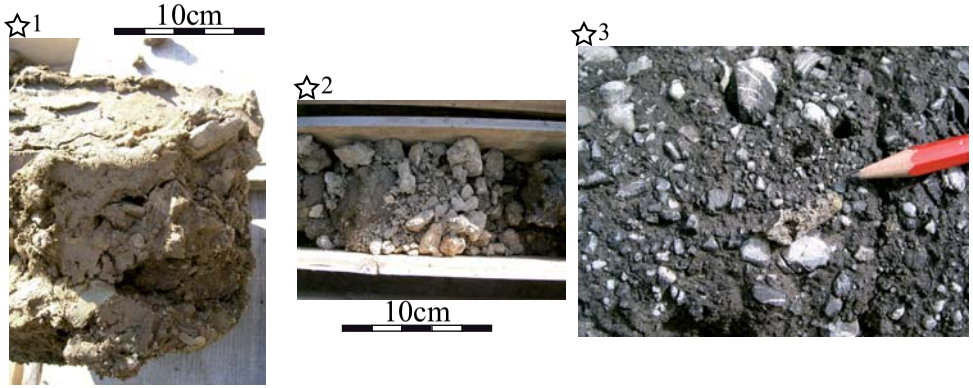

[B]

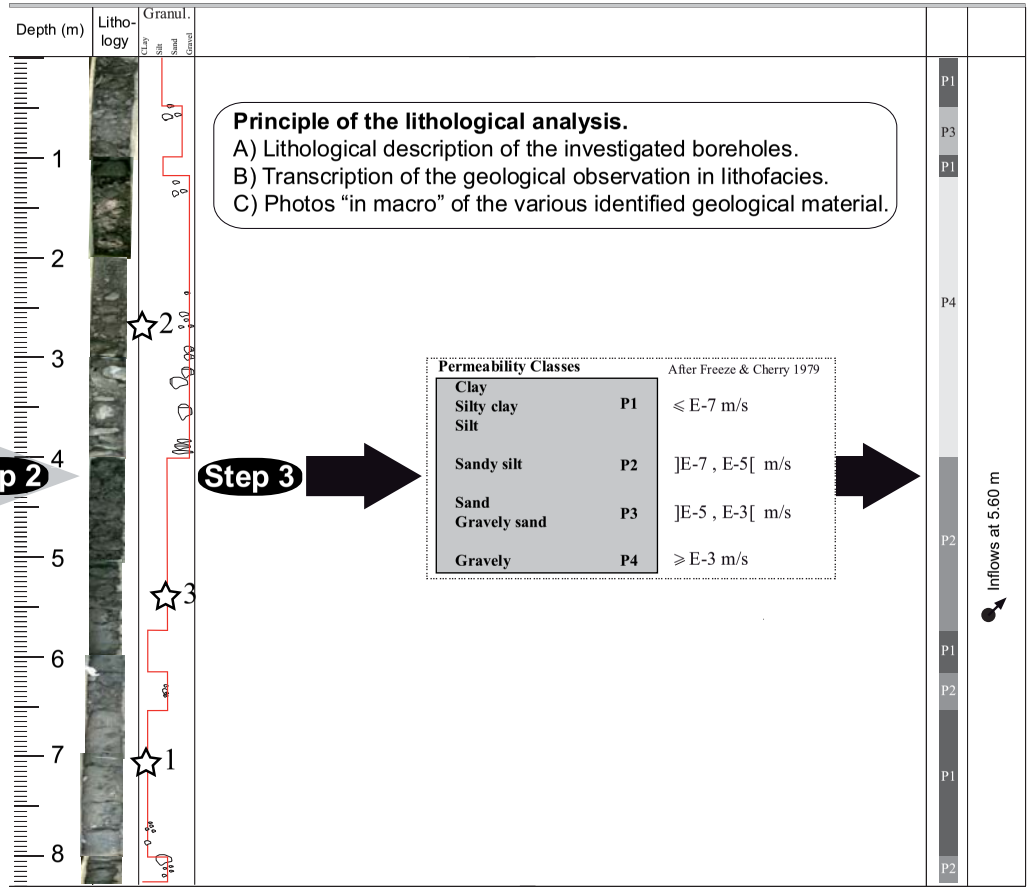

Lithofacies successions of the well LF401 to 407

		(1) Transition frequency matrix					(2) Expected Frequency matrix				(3) Transition probability matrix					(4) Marginal vector	(5) Expected frequency vector				(6) Chi-square test				
		P1	P2	P3	P4		P1	P2	P3	P4	P1	P2	P3	P4			P1	P2	P3	P4	P1	P2	P3	P4	
LF-401	P1	0	12	2	0	14	5.71	10.32	3.09	0.60	0.00	0.86	0.14	0.00	1	0.33	5.71	10.32	3.09	0.60	5.71	0.27	0.39	0.60	
	P2	12	0	5	0	17	10.32	18.64	5.59	1.08	0.71	0.00	0.29	0.00	1	0.40	10.32	18.64	5.59	1.08	0.27	18.64	0.06	1.08	
	P3	2	4	0	3	9	3.09	5.59	1.67	0.32	0.22	0.44	0.00	0.33	1	0.21	3.09	5.59	1.67	0.32	0.39	0.45	1.67	22.15	
	P4	0	0	2	0	2	0.60	1.08	0.32	0.06	0.00	0.00	1.00	0.00	1	0.05	0.60	1.08	0.32	0.06	0.60	1.08	8.69	0.06	
		14	16	9	3	42																			**62.1**
LF-402	P1	0	9	2	1	12	6.80	0.11	0.11	1.08	0.00	0.75	0.17	0.08	1	0.40	6.80	0.11	0.11	1.08	21.15	8.445	3.616	0.33	
	P2	10	0	3	0	13	0.00	14.93	0.19	0.55	0.77	0.00	0.23	0.00	1	0.43	0.00	14.93	0.19	0.55	7.274	24.82	2.815	1.909	
	P3	1	3	0	0	4	0.21	0.19	0.37	0.09	0.25	0.75	0.00	0.00	1	0.13	0.21	0.19	0.37	0.09	5.191	2.815	2.35	0.587	
	P4	0	1	0	0	1	0.37	0.38	0.09	0.02	0.00	1.00	0.00	0.00	1	0.03	0.37	0.38	0.09	0.02	1.762	0.433	0.587	0.147	
		11	13	5	1	30																			**25.5**
LF-403	P1	0	13	11	2	26	73.78	12.90	9.05	3.08	0.00	0.50	0.42	0.08	1	0.46	73.78	12.90	9.05	3.08	73.78	8E-04	0.42	0.381	
	P2	13	0	0	2	15	12.90	2.26	1.58	0.54	0.87	0.00	0.00	0.13	1	0.27	12.90	2.26	1.58	0.54	8E-04	2.256	1.582	3.957	
	P3	11	0	0	0	11	9.05	1.58	1.11	0.38	1.00	0.00	0.00	0.00	1	0.20	9.05	1.58	1.11	0.38	0.42	1.582	1.11	0.378	
	P4	2	2	0	0	4	3.08	0.54	0.38	0.13	0.50	0.50	0.00	0.00	1	0.07	3.08	0.54	0.38	0.13	0.381	3.957	0.378	0.129	
		26	15	11	4	56																			**90.7**
LF-404	P1	0	4	9	6	19	22.60	8.71	8.20	3.09	0.00	0.21	0.47	0.32	1	0.37	22.60	8.71	8.20	3.09	22.6	2.547	0.077	2.727	
	P2	5	0	3	1	9	8.71	3.36	3.16	1.19	0.56	0.00	0.33	0.11	1	0.17	8.71	3.36	3.16	1.19	1.581	3.358	0.008	0.031	
	P3	6	4	0	4	14	8.20	3.16	2.98	1.12	0.43	0.29	0.00	0.29	1	0.27	8.20	3.16	2.98	1.12	0.592	0.222	2.979	7.364	
	P4	7	1	2	0	10	3.09	1.19	1.12	0.42	0.70	0.10	0.20	0.00	1	0.19	3.09	1.19	1.12	0.42	4.928	0.031	0.684	0.424	
		18	9	14	11	52																			**50.2**
LF-405	P1	0	7	6	1	14	3.16	7.62	2.61	3.78	0.00	0.50	0.43	0.07	1	0.22	3.16	7.62	2.61	3.78	3.161	0.05	4.421	2.044	
	P2	6	0	4	13	23	7.62	18.35	6.28	9.11	0.26	0.00	0.17	0.57	1	0.35	7.62	18.35	6.28	9.11	0.343	18.35	0.827	1.666	
	P3	4	5	0	3	12	2.61	6.28	2.15	3.12	0.33	0.42	0.00	0.25	1	0.18	2.61	6.28	2.15	3.12	0.746	0.26	2.148	0.004	
	P4	3	11	2	0	16	3.78	9.11	3.12	4.52	0.19	0.69	0.13	0.00	1	0.25	3.78	9.11	3.12	4.52	0.161	0.394	0.4	4.519	
		13	23	12	17	65																			**39.5**
LF-406	P1	0	32	7	4	43	27.81	25.87	10.3	5.17	0.00	0.74	0.16	0.09	1	0.40	27.81	25.87	10.35	5.17	27.81	1.455	1.082	0.266	
	P2	29	0	8	3	40	25.87	24.06	9.62	4.81	0.73	0.00	0.20	0.08	1	0.37	25.87	24.06	9.62	4.81	0.38	24.06	0.274	0.682	
	P3	8	6	0	2	16	10.35	9.624	3.85	1.92	0.50	0.38	0.00	0.13	1	0.15	10.35	9.62	3.85	1.92	0.532	1.365	3.85	0.003	
	P4	4	3	1	0	8	5.173	4.812	1.92	0.96	0.50	0.38	0.13	0.00	1	0.07	5.17	4.81	1.92	0.96	0.266	0.682	0.444	0.962	
		41	41	16	9	107																			**64.1**
LF-407	P1	0	8	8	1	17	8.49	6.82	7.59	2.60	0.00	0.47	0.47	0.06	1	0.31	8.49	6.82	7.59	2.60	8.487	0.204	0.023	0.98	
	P2	10	0	4	1	15	6.82	5.48	6.10	2.09	0.67	0.00	0.27	0.07	1	0.27	6.82	5.48	6.10	2.09	1.483	5.48	0.72	0.565	
	P3	5	6	0	5	16	7.59	6.10	6.78	2.32	0.31	0.38	0.00	0.31	1	0.29	7.59	6.10	6.78	2.32	0.881	0.001	6.78	3.098	
	P4	2	1	4	0	7	2.60	2.09	2.32	0.79	0.29	0.14	0.57	0.00	1	0.13	2.60	2.09	2.32	0.79	0.136	0.565	1.218	0.794	
		17	15	16	7	55																			**31.4**

Entropy matrices

LF-401

Transition frequency matrix

	P1	P2	P3	P4	
P1	0	12	2	0	14
P2	12	0	5	0	17
P3	2	4	0	3	9
P4	0	0	2	0	2
	14	16	9	3	42

Transition probability matrix

	P1	P2	P3	P4	
P1	0.00	0.86	0.14	0.00	1
P2	0.71	0.00	0.29	0.00	1
P3	0.22	0.44	0.00	0.33	1
P4	0.00	0.00	1.00	0.00	1

Upward Transition matrix P_{ij}

	P1	P2	P3	P4	
P1	0.00	0.86	0.14	0.00	1
P2	0.71	0.00	0.29	0.00	1
P3	0.22	0.44	0.00	0.33	1
P4	0.00	0.00	1.00	0.00	1

Downward Transition matrix Q_{ij}

	P1	P2	P3	P4
P1	0.00	0.75	0.22	0.00
P2	0.86	0.00	0.56	0.00
P3	0.14	0.25	0.00	1.00
P4	0.00	0.00	0.22	0.00
	1	1	1	1

Independent Trial Matrix R_{ij}

	P1	P2	P3	P4
P1	0.000	0.286	0.048	0.000
P2	0.286	0.000	0.119	0.000
P3	0.048	0.095	0.000	0.071
P4	0.000	0.000	0.048	0.000

LF-402

Transition frequency matrix

	P1	P2	P3	P4	
P1	0	9	2	1	12
P2	10	0	3	0	13
P3	1	3	0	0	4
P4	0	1	0	0	1
	11	13	5	1	30

Transition probability matrix

	P1	P2	P3	P4	
P1	0.00	0.75	0.17	0.08	1
P2	0.77	0.00	0.23	0.00	1
P3	0.25	0.75	0.00	0.00	1
P4	0.00	1.00	0.00	0.00	1

Upward Transition matrix P_{ij}

	P1	P2	P3	P4	
P1	0.00	0.75	0.17	0.08	1
P2	0.77	0.00	0.23	0.00	1
P3	0.25	0.75	0.00	0.00	1
P4	0.00	1.00	0.00	0.00	1

Downward Transition matrix Q_{ij}

	P1	P2	P3	P4
P1	0.00	0.69	0.40	1.00
P2	0.91	0.00	0.60	0.00
P3	0.09	0.23	0.00	0.00
P4	0.00	0.08	0.00	0.00
	1	1	1	1

Independent Trial Matrix R_{ij}

	P1	P2	P3	P4
P1	0.000	0.300	0.067	0.033
P2	0.333	0.000	0.100	0.000
P3	0.033	0.100	0.000	0.000
P4	0.000	0.033	0.000	0.000

LF-403

Transition frequency matrix

	P1	P2	P3	P4	
P1	0	13	11	2	26
P2	13	0	0	2	15
P3	11	0	0	0	11
P4	2	2	0	0	4
	26	15	11	4	56

Transition probability matrix

	P1	P2	P3	P4	
P1	0.00	0.50	0.42	0.08	1
P2	0.87	0.00	0.00	0.13	1
P3	1.00	0.00	0.00	0.00	1
P4	0.50	0.50	0.00	0.00	1

Upward Transition matrix P_{ij}

	P1	P2	P3	P4	
P1	0.00	0.50	0.42	0.08	1
P2	0.87	0.00	0.00	0.13	1
P3	1.00	0.00	0.00	0.00	1
P4	0.50	0.50	0.00	0.00	1

Downward Transition matrix Q_{ij}

	P1	P2	P3	P4
P1	0.00	0.87	1.00	0.50
P2	0.50	0.00	0.00	0.50
P3	0.42	0.00	0.00	0.00
P4	0.08	0.13	0.00	0.00
	1	1	1	1

Independent Trial Matrix R_{ij}

	P1	P2	P3	P4
P1	0.000	0.232	0.196	0.036
P2	0.232	0.000	0.000	0.036
P3	0.196	0.000	0.000	0.000
P4	0.036	0.036	0.000	0.000

LF-404

Transition frequency matrix

	P1	P2	P3	P4	
P1	0	4	9	6	19
P2	5	0	3	1	9
P3	6	4	0	4	14
P4	7	1	2	0	10
	18	9	14	11	52

Transition probability matrix

	P1	P2	P3	P4	
P1	0.00	0.21	0.47	0.32	1
P2	0.56	0.00	0.33	0.11	1
P3	0.43	0.29	0.00	0.29	1
P4	0.70	0.10	0.20	0.00	1

Upward Transition matrix P_{ij}

	P1	P2	P3	P4	
P1	0.00	0.21	0.47	0.32	1
P2	0.56	0.00	0.33	0.11	1
P3	0.43	0.29	0.00	0.29	1
P4	0.70	0.10	0.20	0.00	1

Downward Transition matrix Q_{ij}

	P1	P2	P3	P4
P1	0.00	0.44	0.64	0.55
P2	0.28	0.00	0.21	0.09
P3	0.33	0.44	0.00	0.36
P4	0.39	0.11	0.14	0.00
	1	1	1	1

Independent Trial Matrix R_{ij}

	P1	P2	P3	P4
P1	0.000	0.077	0.173	0.115
P2	0.096	0.000	0.058	0.019
P3	0.115	0.077	0.000	0.077
P4	0.135	0.019	0.038	0.000

LF-405

Transition frequency matrix

	P1	P2	P3	P4	
P1	0	7	6	1	14
P2	6	0	4	13	23
P3	4	5	0	3	12
P4	3	11	2	0	16
	13	23	12	17	65

Transition probability matrix

	P1	P2	P3	P4	
P1	0.00	0.50	0.43	0.07	1
P2	0.26	0.00	0.17	0.57	1
P3	0.33	0.42	0.00	0.25	1
P4	0.19	0.69	0.13	0.00	1

Upward Transition matrix P_{ij}

	P1	P2	P3	P4	
P1	0.00	0.50	0.43	0.07	1
P2	0.26	0.00	0.17	0.57	1
P3	0.33	0.42	0.00	0.25	1
P4	0.19	0.69	0.13	0.00	1

Downward Transition matrix Q_{ij}

	P1	P2	P3	P4
P1	0.00	0.30	0.50	0.06
P2	0.33	0.00	0.33	0.76
P3	0.22	0.22	0.00	0.18
P4	0.17	0.48	0.17	0.00
	1	1	1	1

Independent Trial Matrix R_{ij}

	P1	P2	P3	P4
P1	0.000	0.108	0.092	0.015
P2	0.092	0.000	0.062	0.200
P3	0.062	0.077	0.000	0.046
P4	0.046	0.169	0.031	0.000

LF-406

Transition frequency matrix

	P1	P2	P3	P4	
P1	0	32	7	4	43
P2	29	0	8	3	40
P3	8	6	0	2	16
P4	4	3	1	0	8
	41	41	16	9	107

Transition probability matrix

	P1	P2	P3	P4	
P1	0.00	0.74	0.16	0.09	1
P2	0.73	0.00	0.20	0.08	1
P3	0.50	0.38	0.00	0.13	1
P4	0.50	0.38	0.13	0.00	1

Upward Transition matrix P_{ij}

	P1	P2	P3	P4	
P1	0.00	0.74	0.16	0.09	1
P2	0.73	0.00	0.20	0.08	1
P3	0.50	0.38	0.00	0.13	1
P4	0.50	0.38	0.13	0.00	1

Downward Transition matrix Q_{ij}

	P1	P2	P3	P4
P1	0.00	0.78	0.44	0.44
P2	0.71	0.00	0.50	0.33
P3	0.20	0.15	0.00	0.22
P4	0.10	0.07	0.06	0.00
	1	1	1	1

Independent Trial Matrix R_{ij}

	P1	P2	P3	P4
P1	0.000	0.299	0.065	0.037
P2	0.271	0.000	0.075	0.028
P3	0.075	0.056	0.000	0.019
P4	0.037	0.028	0.009	0.000

LF-407

Transition frequency matrix

	P1	P2	P3	P4	
P1	0	8	8	1	17
P2	10	0	4	1	15
P3	5	6	0	5	16
P4	2	1	4	0	7
	17	15	16	7	55

Transition probability matrix

	P1	P2	P3	P4	
P1	0.00	0.47	0.47	0.06	1
P2	0.67	0.00	0.27	0.07	1
P3	0.31	0.38	0.00	0.31	1
P4	0.29	0.14	0.57	0.00	1

Upward Transition matrix P_{ij}

	P1	P2	P3	P4	
P1	0.00	0.47	0.47	0.06	1
P2	0.67	0.00	0.27	0.07	1
P3	0.31	0.38	0.00	0.31	1
P4	0.29	0.14	0.57	0.00	1

Downward Transition matrix Q_{ij}

	P1	P2	P3	P4
P1	0.00	0.53	0.50	0.14
P2	0.59	0.00	0.25	0.14
P3	0.29	0.40	0.00	0.71
P4	0.12	0.07	0.25	0.00
	1	1	1	1

Independent Trial Matrix R_{ij}

	P1	P2	P3	P4
P1	0.000	0.145	0.145	0.018
P2	0.182	0.000	0.073	0.018
P3	0.091	0.109	0.000	0.091
P4	0.036	0.018	0.073	0.000

Postdepositional entropy E^{post}

-	0.19	0.40	-	P1	0.59
0.35	-	0.52	-	P2	0.87
0.48	0.52	-	0.53	P3	1.53
-	-	0.00	-	P4	0.00
					3.00

-	0.31	0.43	0.30	P1	1.04
0.29	-	0.49	-	P2	0.78
0.50	0.31	-	-	P3	0.81
-	0.00	-	-	P4	0.00
					2.63

-	0.50	0.53	0.28	P1	1.31
0.18	-	-	0.39	P2	0.57
0.00	-	-	-	P3	0.00
0.50	0.50	-	-	P4	1.00
					2.88

-	0.47	0.51	0.53	P1	1.51
0.47	-	0.53	0.35	P2	1.35
0.52	0.52	-	0.52	P3	1.56
0.36	0.33	0.46	-	P4	1.16
					5.57

-	0.50	0.52	0.27	P1	1.30
0.51	-	0.44	0.47	P2	1.41
0.53	0.53	-	0.50	P3	1.55
0.45	0.37	0.38	-	P4	1.20
					5.46

-	0.32	0.43	0.32	P1	1.06
0.34	-	0.46	0.28	P2	1.08
0.50	0.53	-	0.38	P3	1.41
0.50	0.53	0.38	-	P4	1.41
					4.95

-	0.51	0.51	0.24	P1	1.26
0.39	-	0.51	0.26	P2	1.16
0.52	0.53	-	0.52	P3	1.58
0.52	0.40	0.46	-	P4	1.38
					5.38

Predepositional entropy E^{pre}

P1	P2	P3	P4	
-	0.31	0.48	-	
0.19	-	0.47	-	
0.40	0.50	-	0.00	
-	-	0.48	-	
0.59	**0.81**	**1.44**	**0.00**	2.84

P1	P2	P3	P4	
-	0.37	0.53	0.00	
0.13	-	0.44	-	
0.31	0.49	-	-	
-	0.28	-	-	
0.44	**1.14**	**0.97**	**0.00**	2.55

P1	P2	P3	P4	
-	0.18	0.00	0.50	
0.50	-	-	0.50	
0.53	-	-	-	
0.28	0.39	-	-	
1.31	**0.57**	**0.00**	**1.00**	2.88

P1	P2	P3	P4	
-	0.52	0.41	0.48	
0.51	-	0.48	0.31	
0.53	0.52	-	0.53	
0.53	0.35	0.40	-	
1.57	**1.39**	**1.29**	**1.32**	5.57

P1	P2	P3	P4	
-	0.52	0.50	0.24	
0.53	-	0.53	0.30	
0.48	0.48	-	0.44	
0.43	0.51	0.43	-	
1.44	**1.51**	**1.46**	**0.98**	5.39

P1	P2	P3	P4	
-	0.28	0.52	0.52	
0.35	-	0.50	0.53	
0.46	0.41	-	0.48	
0.33	0.28	0.25	-	
1.14	**0.96**	**1.27**	**1.53**	4.90

P1	P2	P3	P4	
-	0.48	0.50	0.40	
0.45	-	0.50	0.40	
0.52	0.53	-	0.35	
0.36	0.26	0.50	-	
1.33	**1.27**	**1.50**	**1.15**	5.25

Entropy for the whole sedimentation system

-	0.52	0.21	-	0.73
0.52	-	0.37	-	0.88
0.21	0.32	-	0.27	0.53
-	-	0.21	-	0.00
				2.14

-	0.52	0.26	0.16	0.95
0.53	-	0.33	-	0.86
0.16	0.33	-	-	0.50
-	0.16	-	-	0.16
				2.46

-	0.49	0.46	0.17	1.12
0.49	-	-	0.17	0.66
0.46	-	-	-	0.46
0.17	0.17	-	-	0.34
				2.59

-	0.28	0.44	0.36	1.08
0.32	-	0.24	0.11	0.67
0.36	0.28	-	0.28	0.93
0.39	0.11	0.18	-	0.68
				3.36

-	0.35	0.32	0.09	0.76
0.32	-	0.25	0.46	1.03
0.25	0.28	-	0.20	0.74
0.20	0.43	0.15	-	0.79
				3.32

-	0.52	0.26	0.18	0.96
0.51	-	0.28	0.14	0.93
0.28	0.23	-	0.11	0.62
0.18	0.14	0.06	-	0.38
				2.90

-	0.40	0.40	0.11	0.91
0.45	-	0.28	0.11	0.83
0.31	0.35	-	0.31	0.98
0.17	0.11	0.28	-	0.55
				3.27

Number n of facies	4				
Entropie max E_m	1.58		E^{post}	E^{pre}	R^{post}	R^{pre}
Clay - Silty clay - Silt		P1	0.59	0.59	0.37	0.37
Sandy silt		P2	0.87	0.81	0.55	0.51
Sand - gravely sand		P3	1.53	1.44	0.97	0.91
Gravel		P4	0.00	0.00	0.00	0.00
Clay - Silty clay - Silt		P1	1.04	0.44	0.66	0.28
Sandy silt		P2	0.78	1.14	0.49	0.72
Sand - gravely sand		P3	0.81	0.97	0.51	0.61
Gravel		P4	0.00	0.00	0.00	0.00
Clay - Silty clay - Silt		P1	1.31	1.31	0.83	0.83
Sandy silt		P2	0.57	0.57	0.36	0.36
Sand - gravely sand		P3	0.00	0.00	0.00	0.00
Gravel		P4	1.00	1.00	0.63	0.63
Clay - Silty clay - Silt		P1	1.51	1.57	0.95	0.99
Sandy silt		P2	1.35	1.39	0.85	0.88
Sand - gravely sand		P3	1.56	1.29	0.98	0.81
Gravel		P4	1.16	1.32	0.73	0.83
Clay - Silty clay - Silt		P1	1.30	1.44	0.82	0.91
Sandy silt		P2	1.41	1.51	0.89	0.95
Sand - gravely sand		P3	1.55	1.46	0.98	0.92
Gravel		P4	1.20	0.98	0.76	0.62
Clay - Silty clay - Silt		P1	1.06	1.14	0.67	0.72
Sandy silt		P2	1.08	0.96	0.68	0.61
Sand - gravely sand		P3	1.41	1.27	0.89	0.80
Gravel		P4	1.41	1.53	0.89	0.97
Clay - Silty clay - Silt		P1	1.26	1.33	0.80	0.84
Sandy silt		P2	1.16	1.27	0.73	0.80
Sand - gravely sand		P3	1.58	1.50	1.00	0.95
Gravel		P4	1.38	1.15	0.87	0.72

La Frasse RMT site -S1- : Apparent resistivity and phases

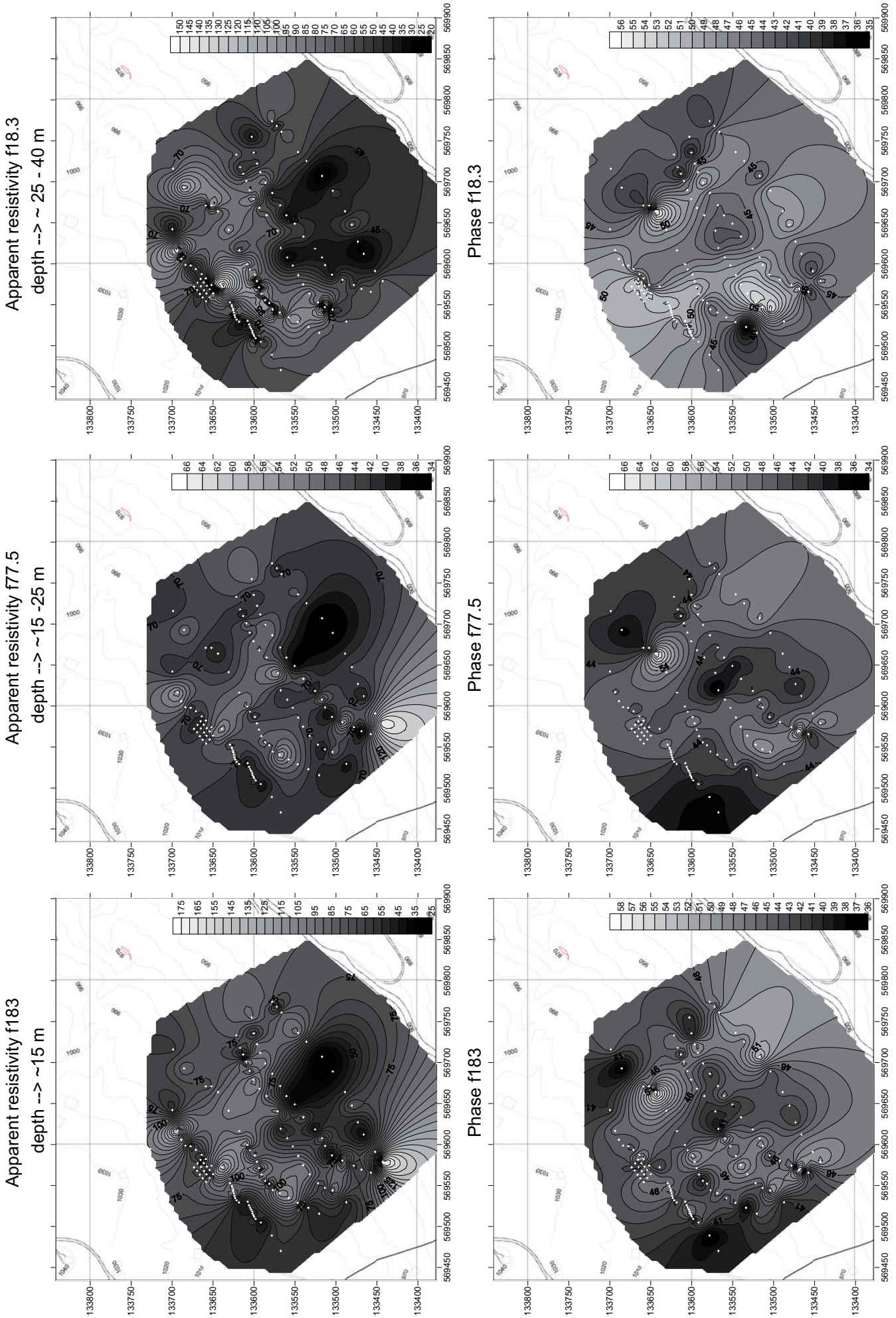

La Frasse RMT site -S2- : Apparent resistivity and phases

La Frasse RMT site -S3- : Apparent resistivity and phases

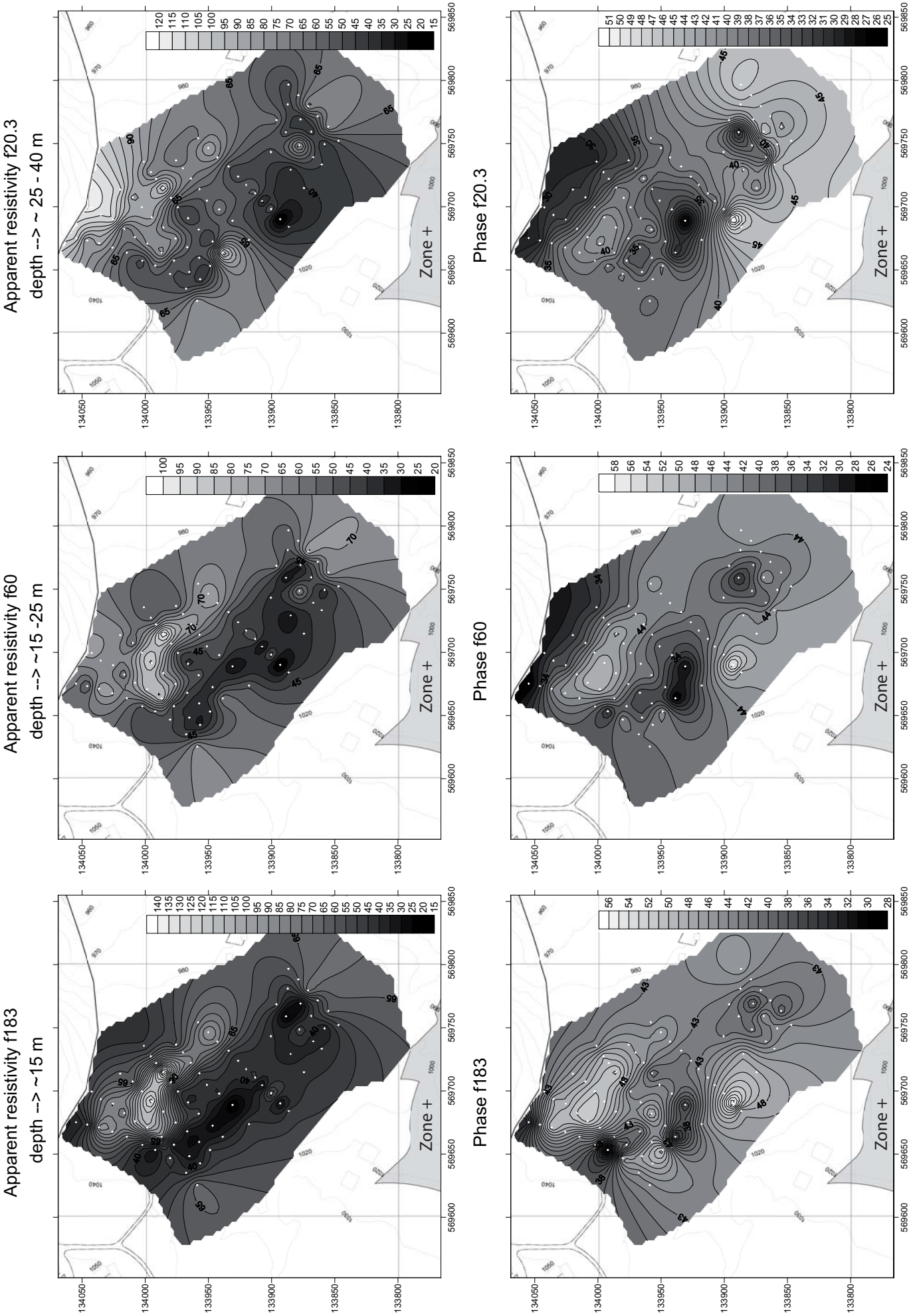

La Frasse RMT site -S1- : True resistivity and thickness layer

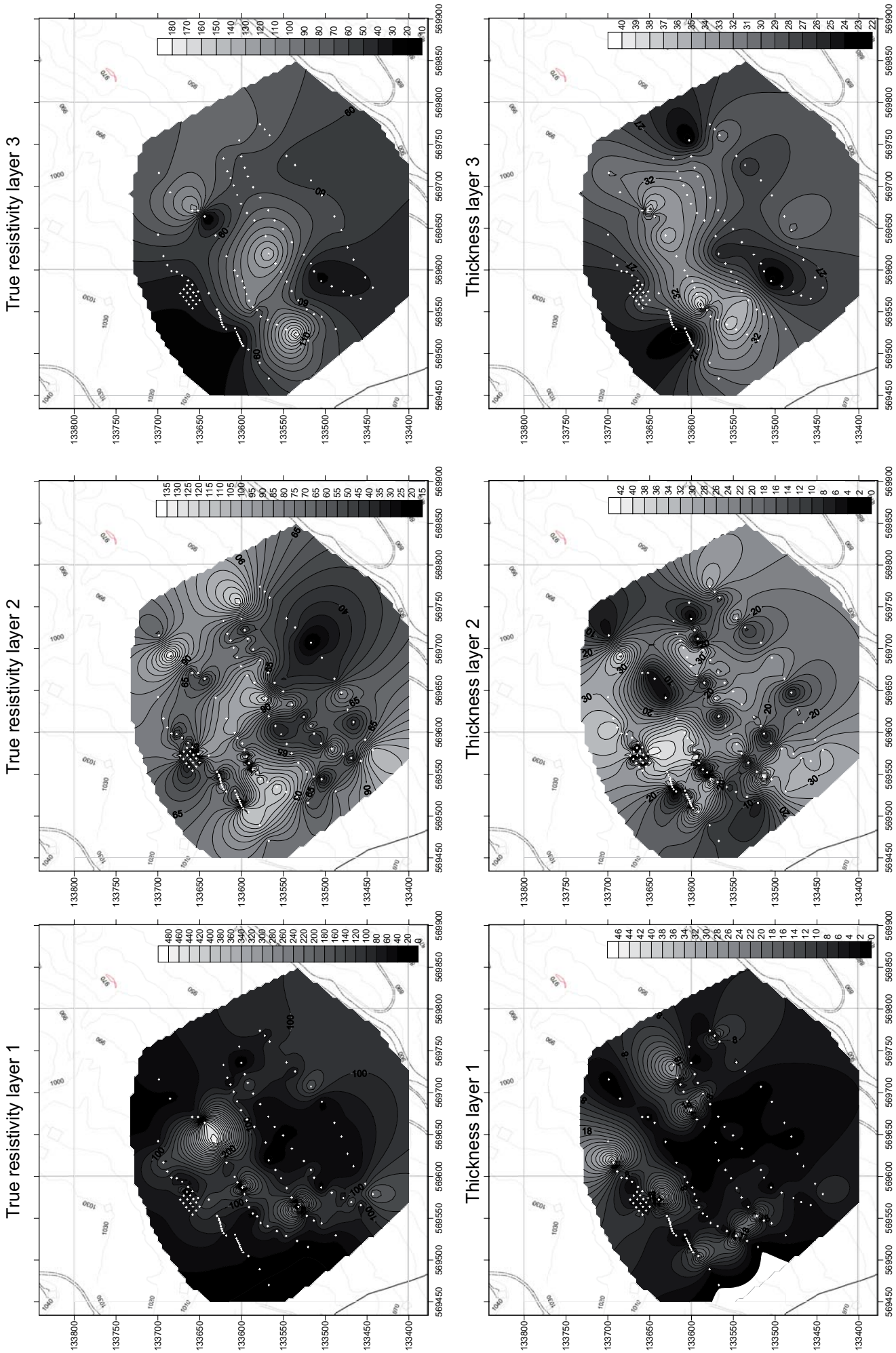

La Frasse RMT site -S2- : True resistivity and thickness layer

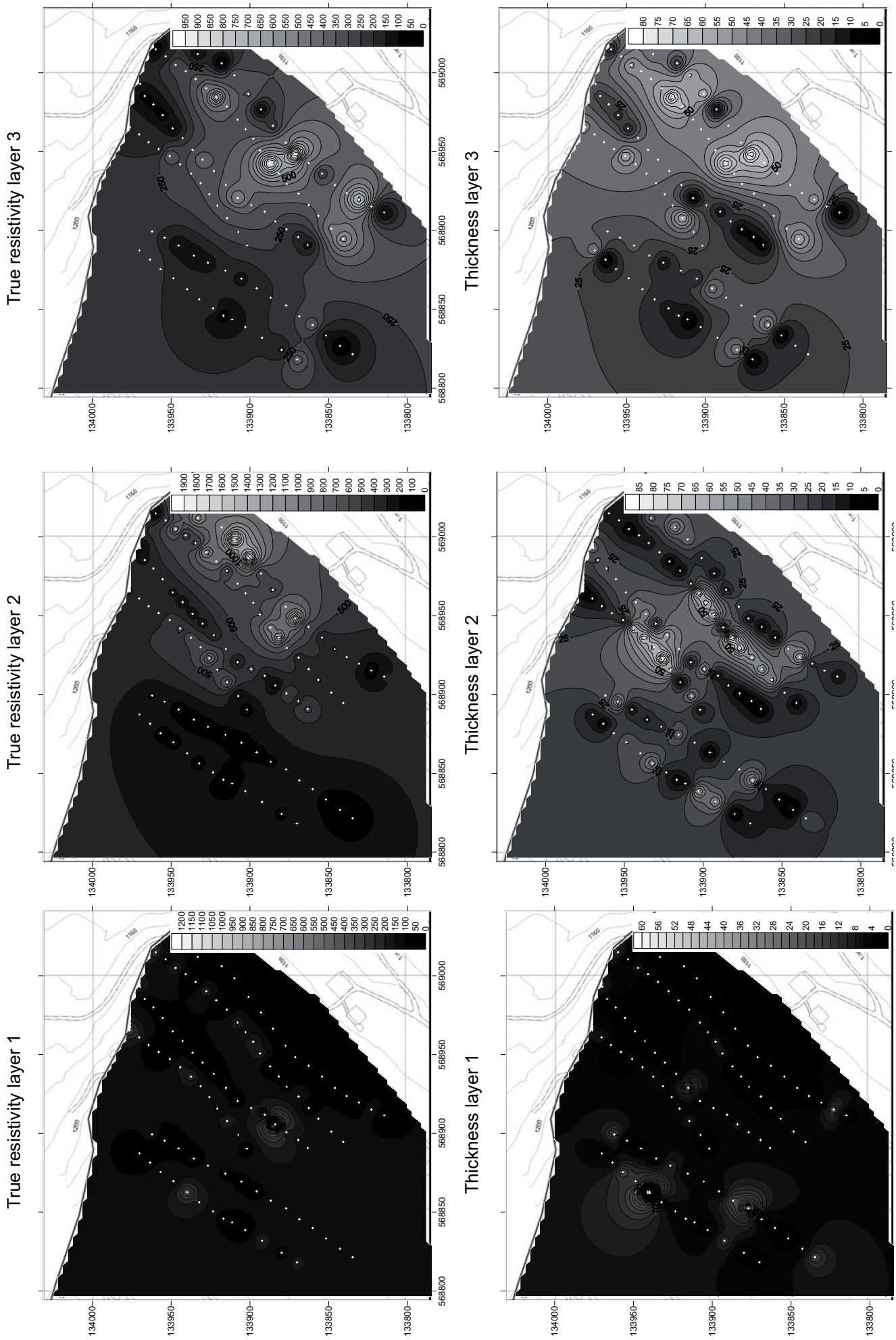

La Frasse RMT site -S3- : True resistivity and thickness layer

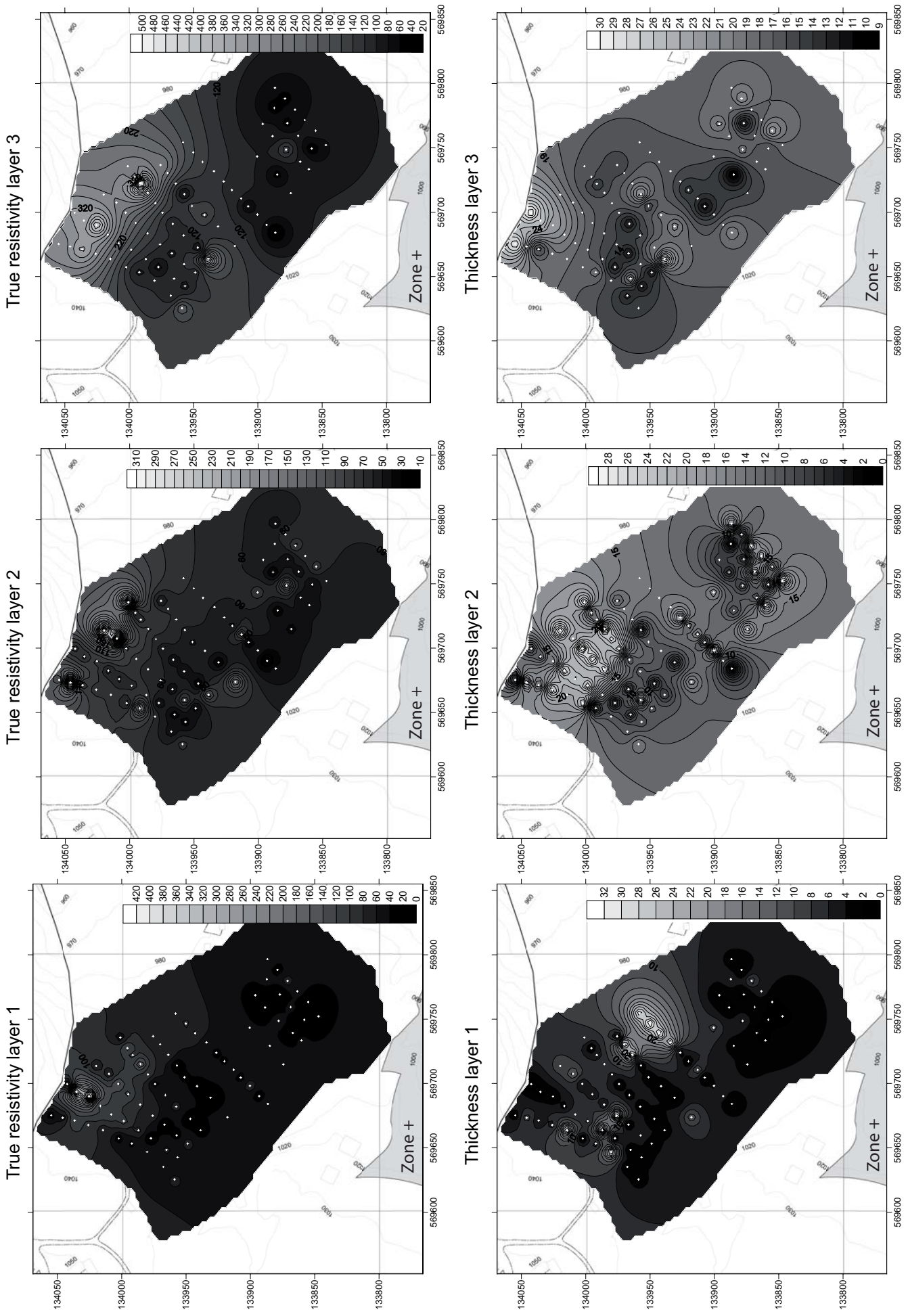

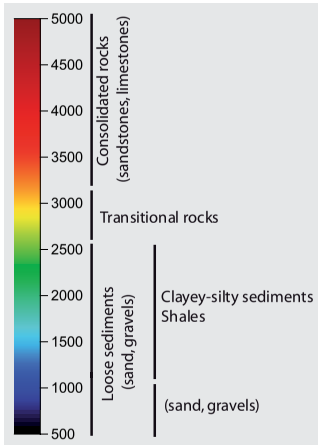
5000
4500
4000
3500
3000
2500
2000
1500
1000
500
Consolidated rocks (sandstones, limestones)
Transitional rocks
Loose sediments (sand, gravels)
Clayey-silty sediments Shales
(sand, gravels)

Profile 7
Profile 6
Profile 5
Profile 4
Profile 3
Profile 2
Profile 1
Profile 9
Profile 8
0 50 100m

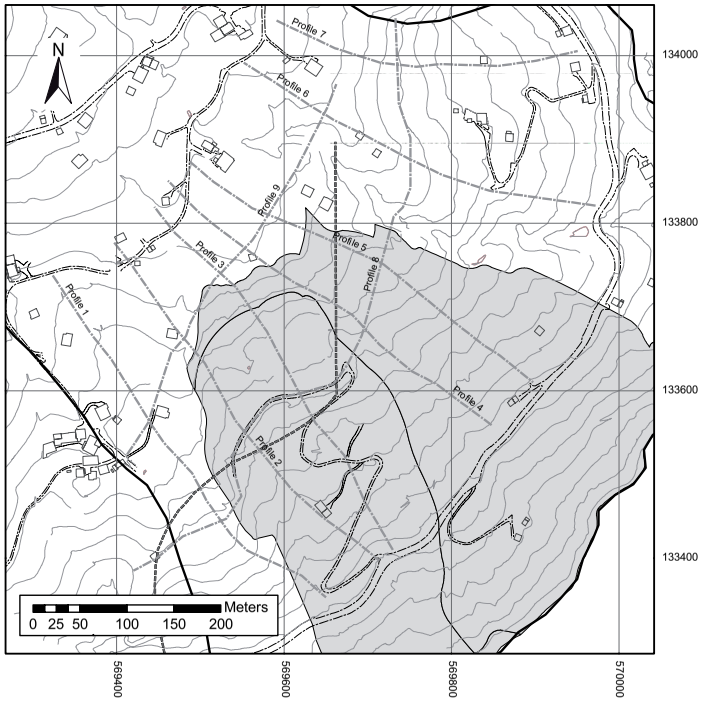
N
Profile 7
Profile 8
Profile 9
Profile 3
Profile 5
Profile 6
Profile 1
Profile 4
Profile 2
Meters
0 25 50 100 150 200
134000
133800
133600
133400
569400
569600
569800
570000

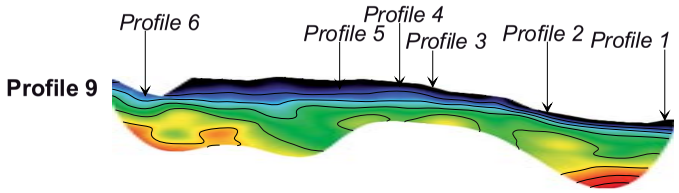
Profile 9
Profile 6
Profile 5
Profile 4
Profile 3
Profile 2
Profile 1

Profile 8
Profile 7
Profile 6
Profile 5
Profile 4
Profile 3
Profile 2
Profile 1

Infiltration tests at the borehole platform

Infiltration measures processing

Well data

	Upper part of the well (inside the active mass)				Lower part of the well (below sliding surface)	
	Depth [m]	Well volume [l]	Streamer volume [l]	Filter volume [l]	Depth [m]	Well volume [l]
P4	32.20	1581	587	993	34.80	700
P18	27.25	1338	497	841	25.75	518
P19	24.49	1202	447	755	28.51	573
P20	22.43	1101	409	692	28.57	574
P21	19.92	978	363	614	31.08	625
P22	22.02	1081	402	679	28.98	583

Hypothesis : Filter void percentage = 40%

Infiltration measures

	Introduced volume [l]	Filling duration [s]	Filling flow rate [l/min]	Initial water level [m]	Final water level [m]	Initial water height [m]	Final water height [m]	filled height [m]
P4	1000	1860	32.3	32.20	21.15	0.00	11.05	11.05
P18	180	~360	~30	22.12	19.81	5.13	7.44	2.31
P19	200	197	60.9	19.10	15.77	5.39	8.72	3.33
P20	1000	874	68.6	21.01	12.50	1.42	9.93	8.51
P21	600	1012	35.6	16.75	8.60	3.17	11.32	8.15
P22	1000	881	68.1	21.12	14.00	0.90	8.02	7.12

	Steamer filling [l]	Sup. filter filling [l]	Max. infiltred volume [l]	Inf. filter filling [l]	Min. infiltred volume [l]	Mean infiltred flow rate Minimum [l/min]	Mean infiltred flow rate Maximum [l/min]
P4	202	136	662	280	382	12.3	21.4
P18	42	29	109	0	109	~18.2	~18.2
P19	61	41	98	0	98	29.9	29.9
P20	155	105	740	0	740	50.8	50.8
P21	149	101	351	0	351	20.8	20.8
P22	130	88	782	0	782	53.3	53.3

Measures of water lowering in function of time

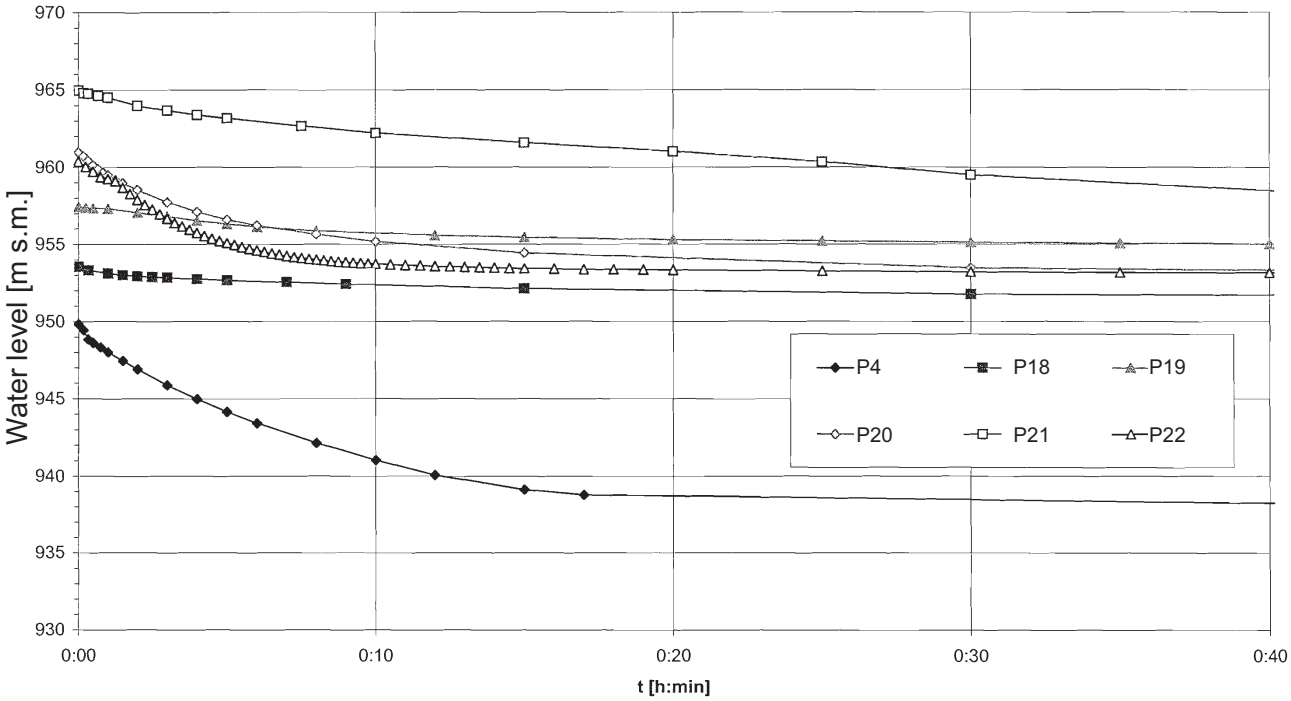

Infiltration tests at the borehole platform

Measures of water lowering in function of time - P4 -

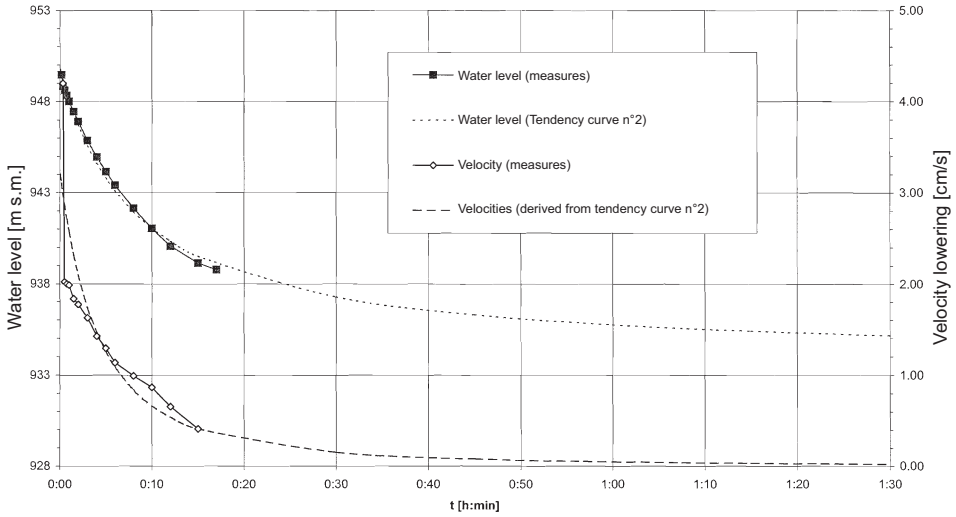

Measures of water lowering in function of time - P18 -

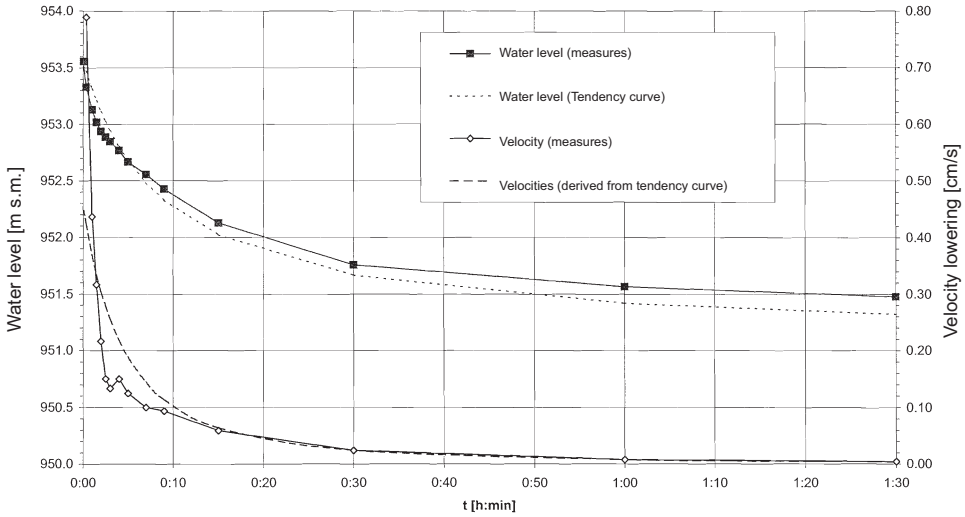

Measures of water lowering in function of time - P19 -

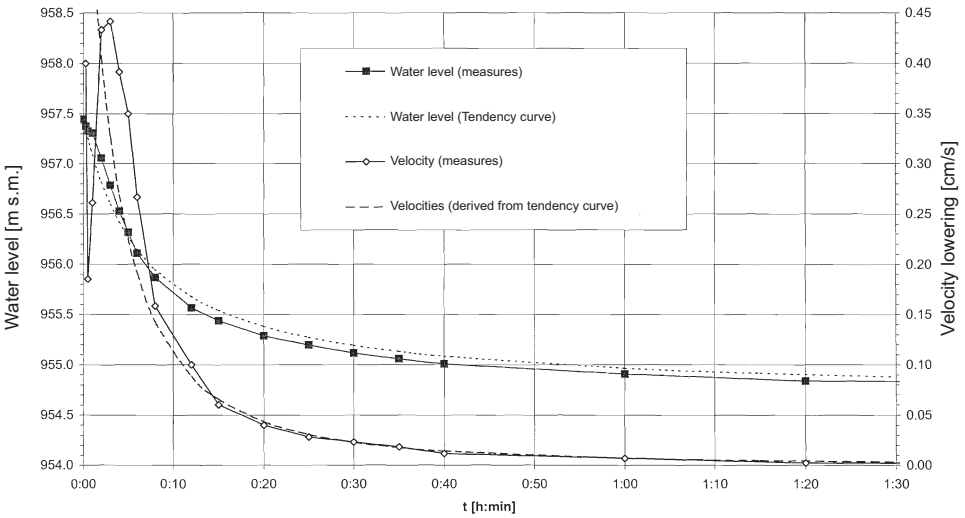

Infiltration tests at the borehole platform

Measures of water lowering in function of time - P20 -

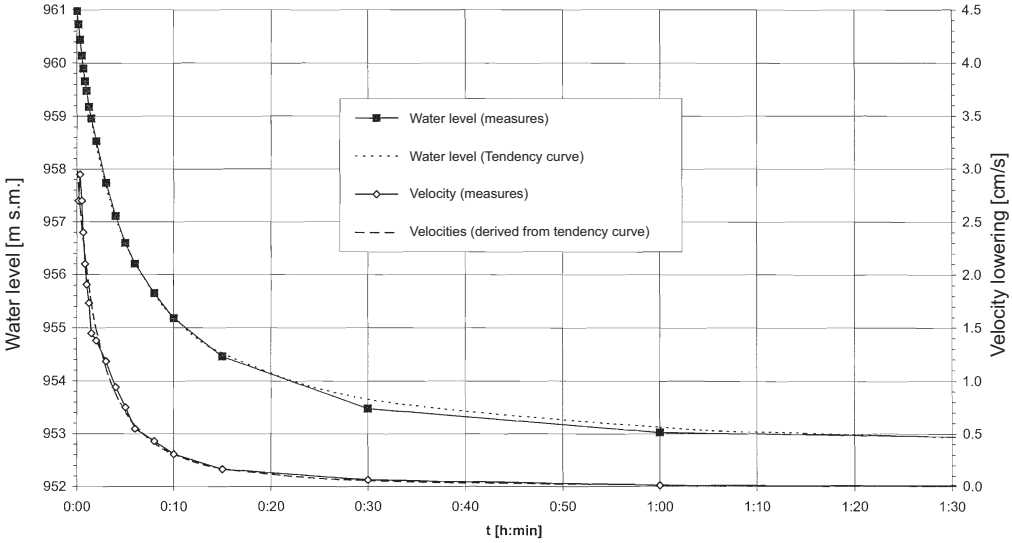

Measures of water lowering in function of time - P21 -

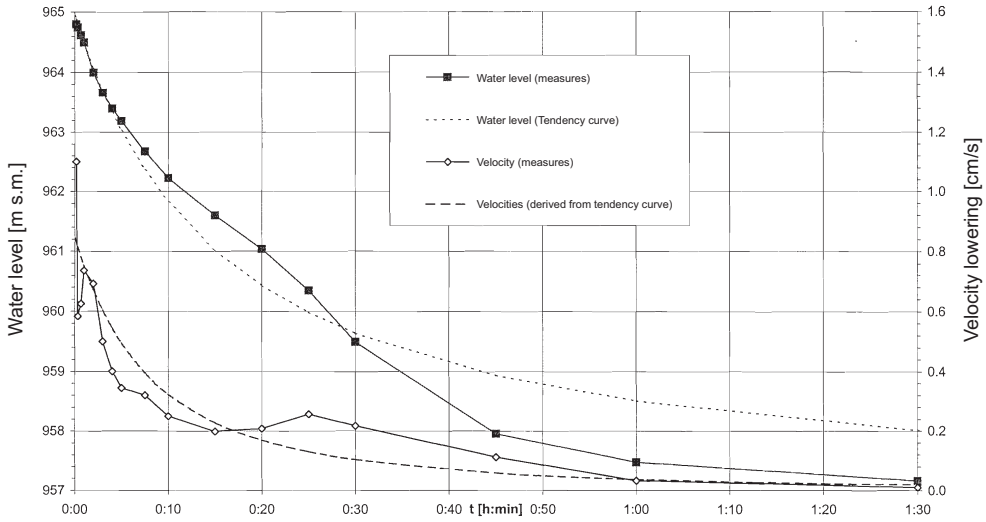

Measures of water lowering in function of time - P19 -

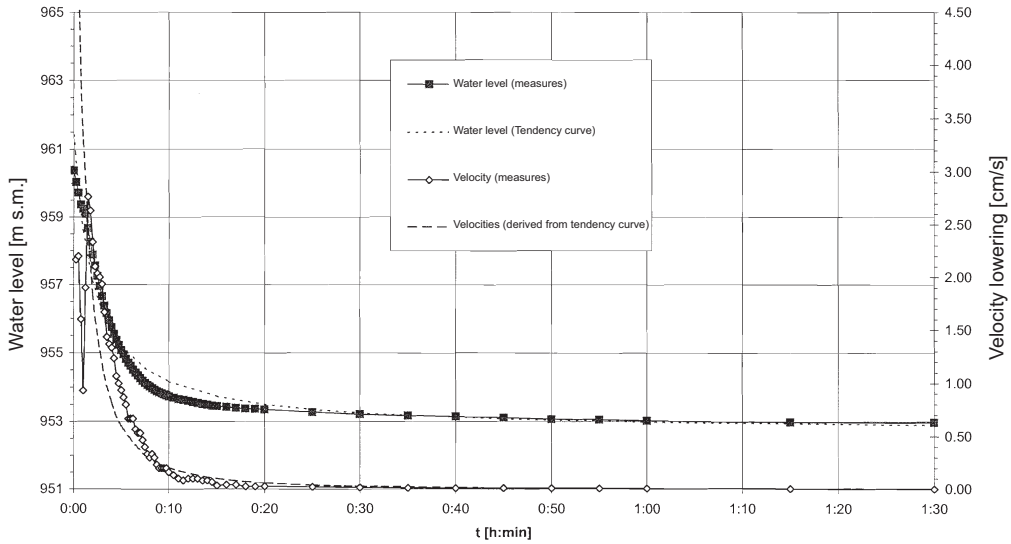

Hydraulic test 2 (September 2003)

24-sept-03						
	Before shutdown		Just after the shutdown		After the shutdown	
piezometers	Hours	Measures [m]	Hours	Measures [m]	Hours	Measures [m]
P1	13:12	32.34	14:57	32.44	16:42	>30
P2	13:06	28.28	14:54	28.33	16:38	28.53
P3	13:09	35.36	14:56	33.11	16:40	>30
P2b	13:00	35.35	15:36	34.65	16:36	>30
P3b	12:58	29.36	14:49	29.36	16:34	29.36
P5	12:55	24.59	14:48	24.64	16:33	24.64
P6	12:50	24.97	14:46	22.62	16:29	19.02
P7	12:47	16.88	14:45	17.28	16:27	17.18
P8	12:45	27.74	14:43	26.84	16:25	26.09
P9	12:42	32.42	14:42	31.22	16:23	28.22
P10	12:36	21.13	14:40	21.13	16:21	21.18
P11	12:33	29.8	14:38	28.1	16:19	26.27
P12	12:25	30.54	14:37	28.29	16:15	25.24
P13	12:11	28.77	14:35	27.32	16:12	26.97
P14	12:08	22.98	14:33	22.28	16:10	22.28
P15	12:05	25.44	14:31	25.09	16:08	24.14
P16	12:02	24.82	14:29	24.82	16:06	24.72
P18	11:58	23.14	14:27	23.19	16:05	23.24
P19	11:53	21.99	14:26	22.04	16:03	21.99
P20	11:50	21.09	14:25	21.09	16:00	21.04
z111	12:29	25.36	14:39	25.36	16:17	25.36
z112	12:53	13.32	14:47	13.37	16:30	13.35
z113	13:26	15.31	15:19	15.16		
z114	13:37	11.88	15:25	11.83		
z115	13:48	9.4	15:32	9.45		
z118	14:02	16.7	15:28	18.5		
z203	11:21	20.73	15:53	20.7		
z204	11:30	11.08	15:49	11.18		

Water level measurements from 1995 to 2003

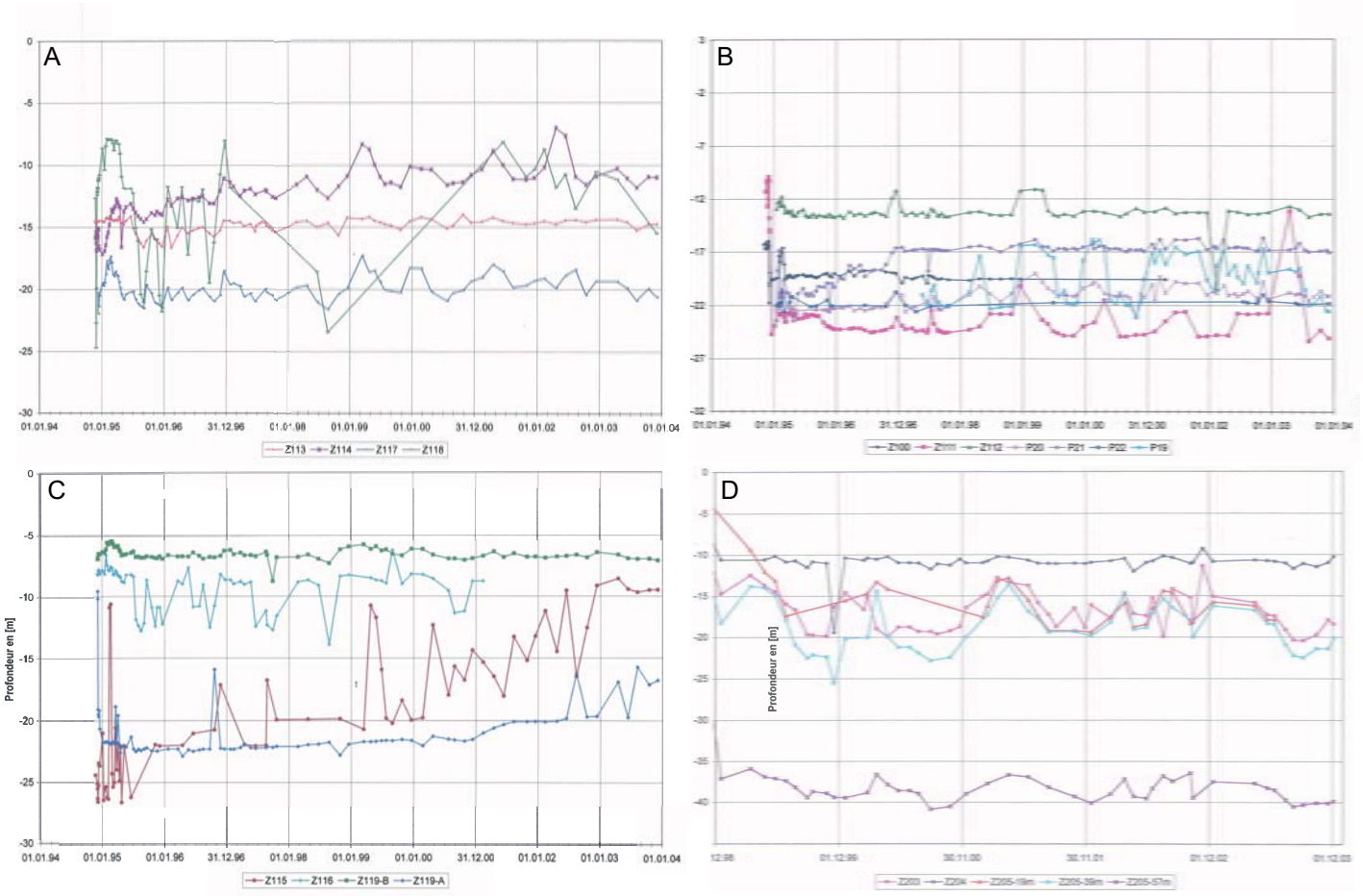

A) Between the national road RC 705 and the borehole platform
B) At the borehole platform
C) At the national road RC 705
D) At Cergnaz

Inflow rates of the borehole platform

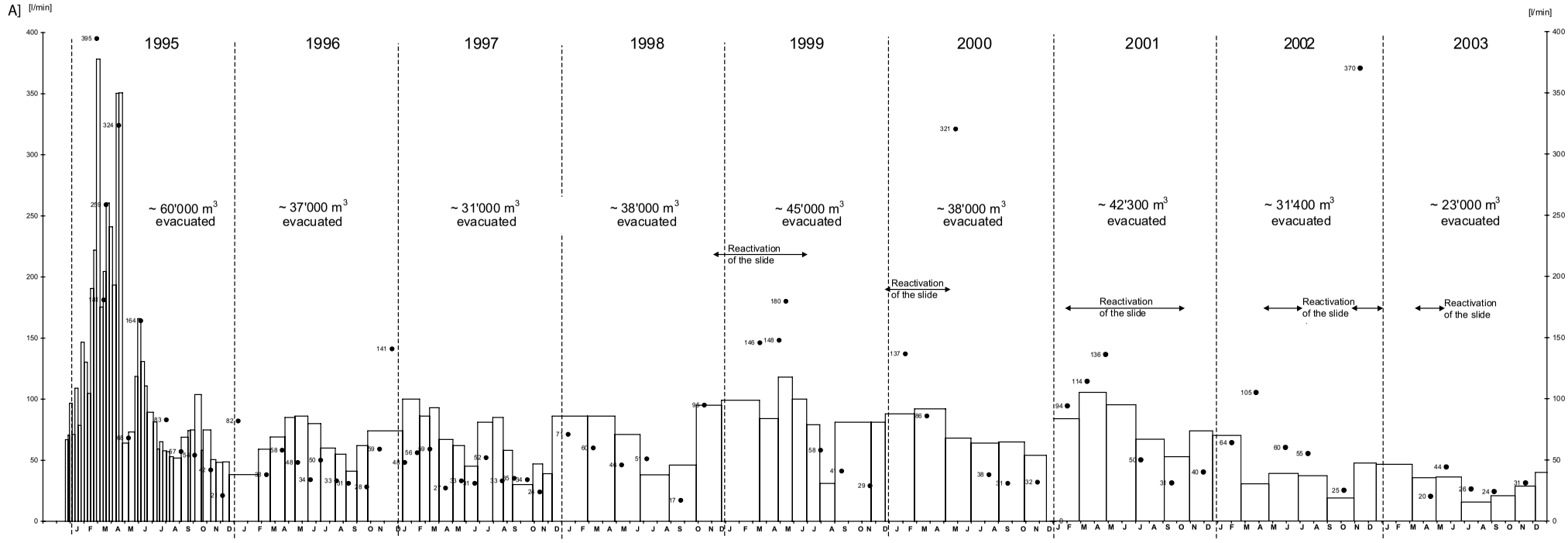

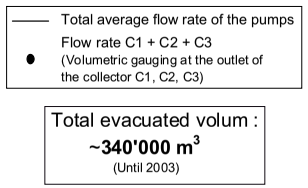

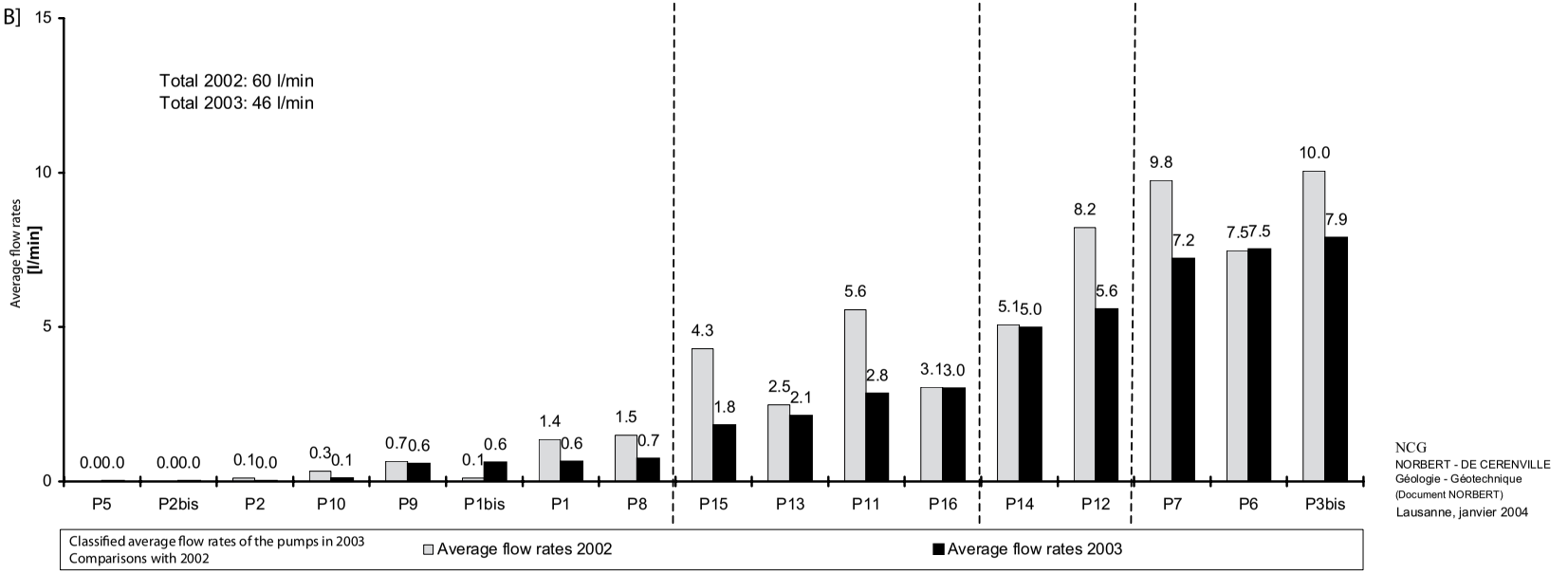

NCG
NORBERT - DE CERENVILLE
Géologie - Géotechnique
(Document NORBERT)
Lausanne, janvier 2004

Observation at the piezometers (Z203, Z204 and Z205)

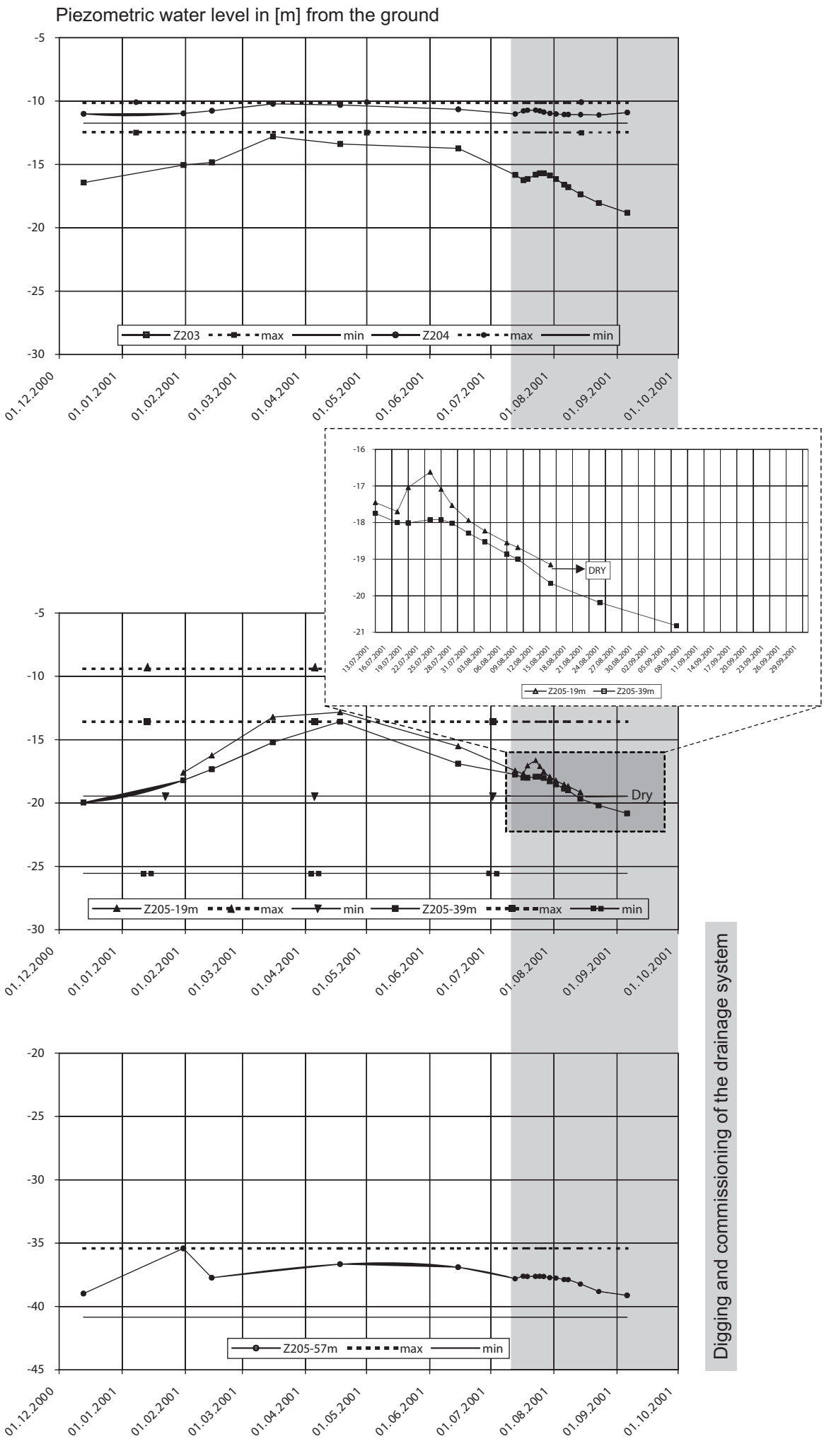

Mean estimated inflow at lateral limits

Mean estimated inflow at lateral limits: Mean estimated inflow in [m/d] values entering the lateral boundaries of the conceptual model. The unity m/d designs m3 of water per m2 of vertical boarder and per day. These values are estimated being constant a part for the zones of the sliding surface, where the differential permeability of the flysch interacts

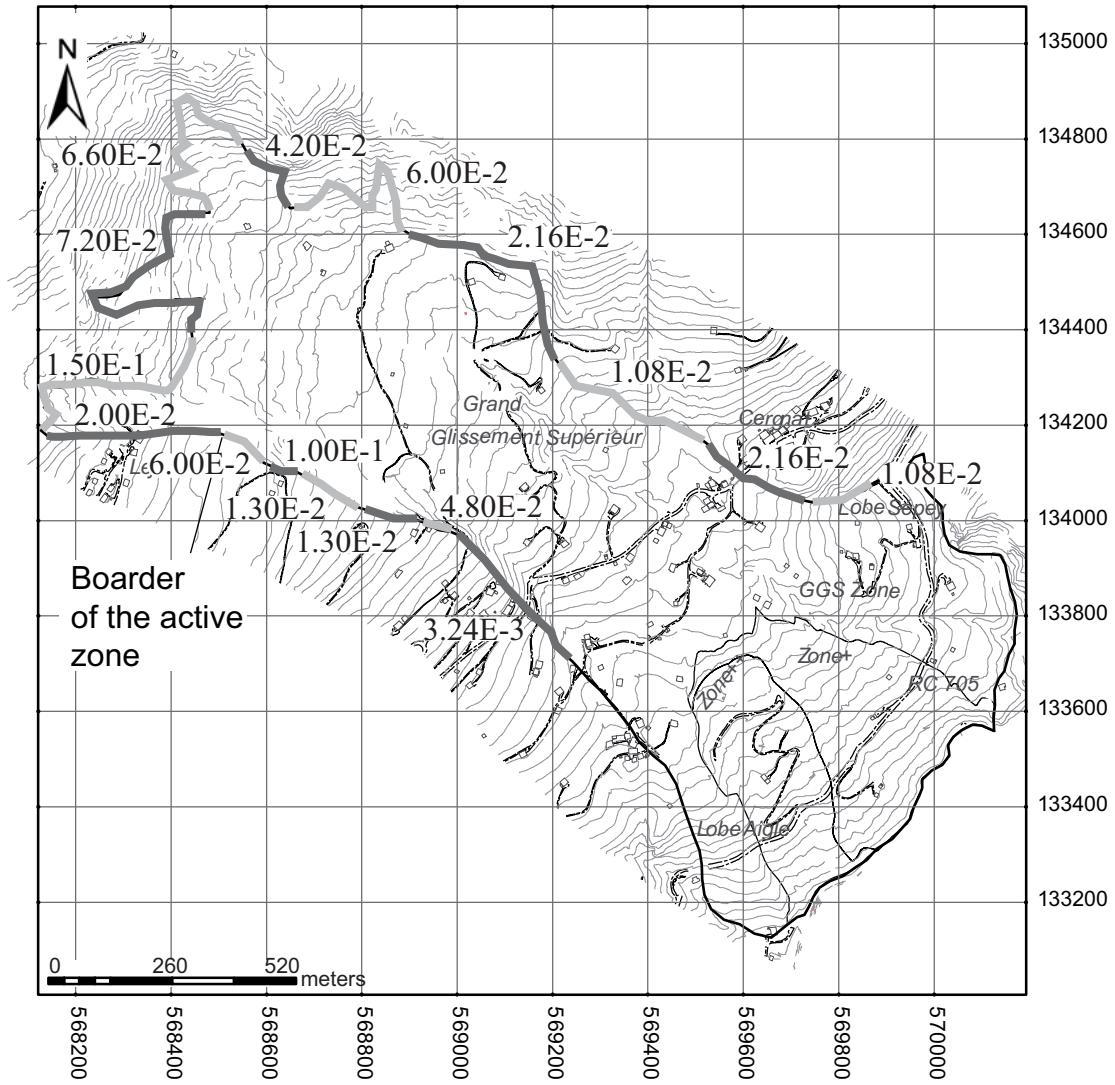

Transient inflow at lateral limits

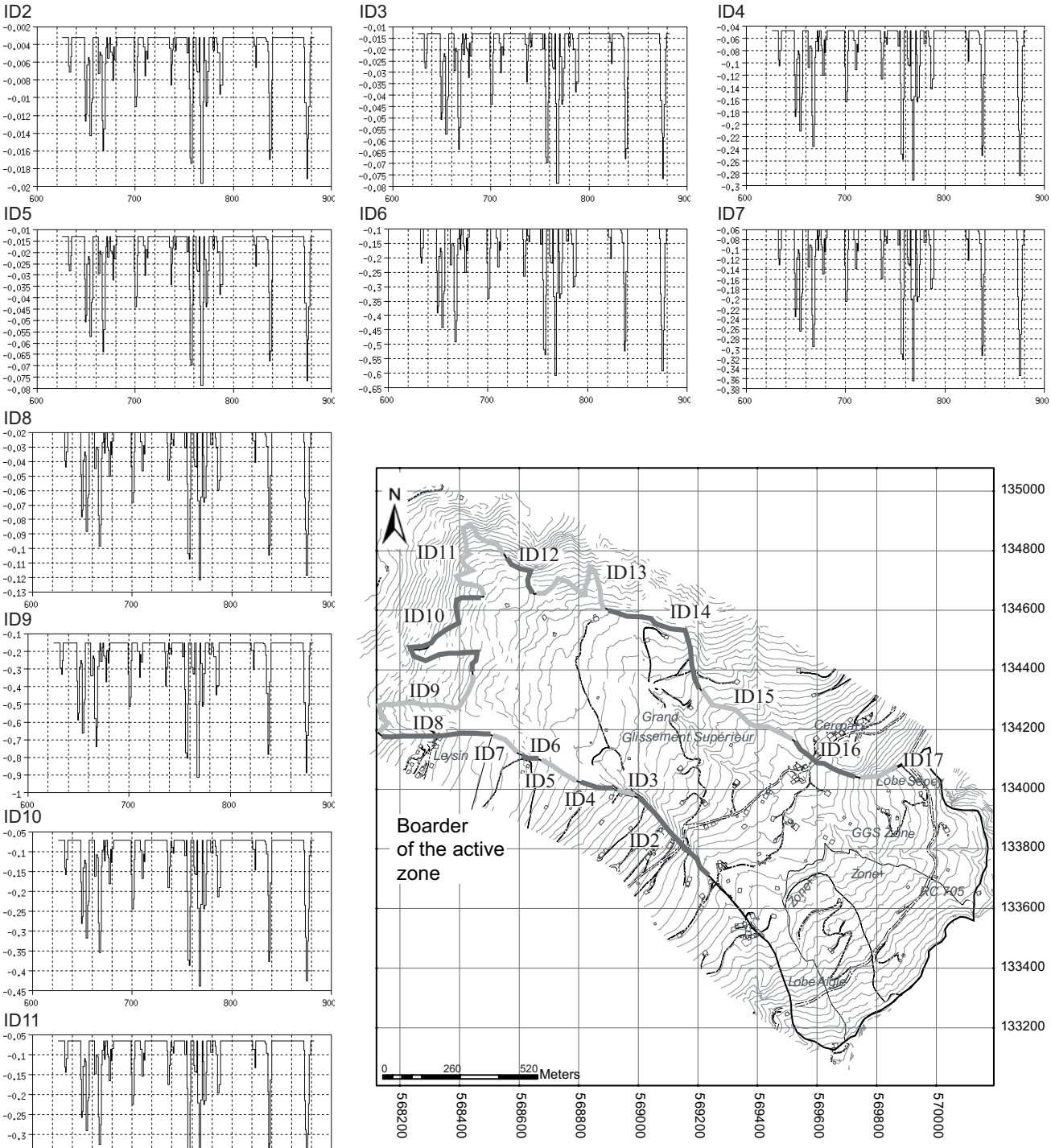

xcorrelation length

ycorrelation lengths (m) X/Y	1	2	5	7	10	15	20	50	200
1	1A1	1A42	1A2	1A49	1A3	1A56	1A4	1A63	1A72
2	1A36	1A43	1A18	1A50	1A19	1A57	1A20	1A64	1A73
5	1A37	1A44	1A21	1A51	1A22	1A58	1A23	1A65	1A74
7	1A38	1A45	1A24	1A52	1A25	1A59	1A26	1A66	1A75
10	1A39	1A46	1A27	1A53	1A28	1A60	1A29	1A67	1A76
15	1A40	1A47	1A30	1A54	1A31	1A61	1A32	1A68	1A77
20	1A41	1A48	1A33	1A55	1A34	1A62	1A35	1A69	1A78
50	1A81	1A82	1A83	1A84	1A85	1A86	1A87	1A70	1A79
100	1A88	1A89	1A90	1A91	1A92	1A93	1A94	1A71	1A80

Case where ergodic hypothesis may not be anymore valid (Gehlar 1993), correlation lengths >= 1/2 dimension of the domain

The study is performed on two series of simulations;

1) Heterogeneous permeability field (appendices VII-2 to VII-23)
2) Dual-permeability realizations (appendices VII-24 to VII-45).

The correlation lengths are indicated in the table hereinbefore.

To have accurate observations, a one dimensional profile is arbitrary selected transversally across the lower part of the model. It enables to have for each realization an observation at an identical position, this profile corresponds in the homogeneous case to the potential head isolign equal to 7 meters
The following appendices present all the results obtained from the 81 performed simulations.

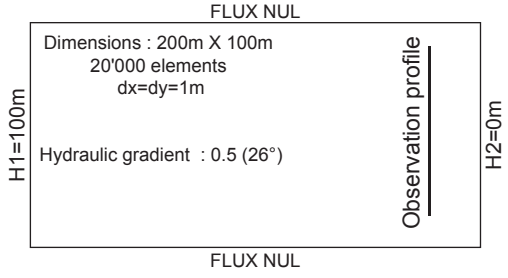

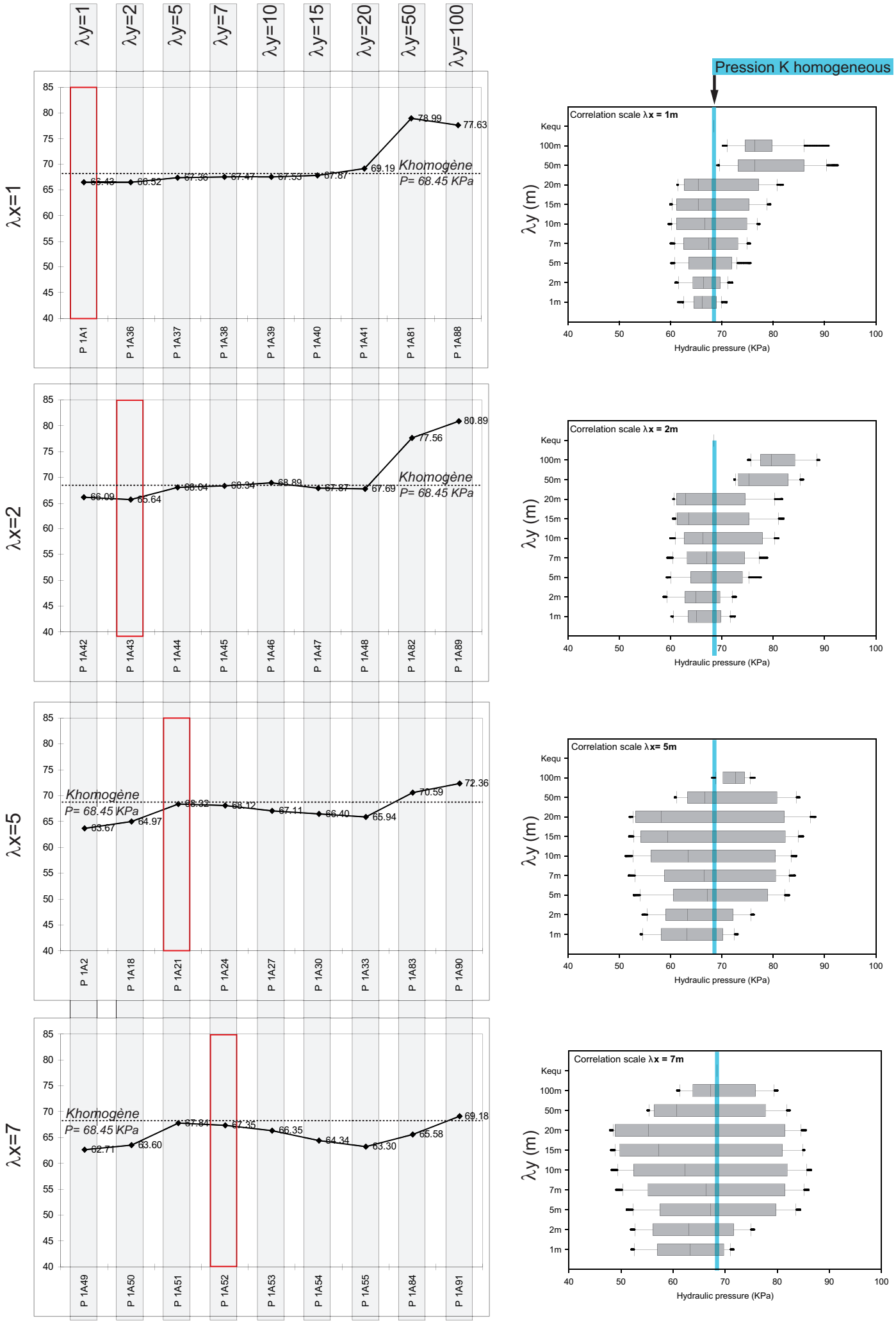
λy=1
λy=2
λy=5
λy=7
λy=10
λy=15
λy=20
λy=50
λy=100
λx=1
λx=2
λx=5
λx=7
Khomogène
P= 68.45 KPa
P 1A1
P 1A36
P 1A37
P 1A38
P 1A39
P 1A40
P 1A41
P 1A81
P 1A88
P 1A42
P 1A43
P 1A44
P 1A45
P 1A46
P 1A47
P 1A48
P 1A82
P 1A89
P 1A2
P 1A18
P 1A21
P 1A24
P 1A27
P 1A30
P 1A33
P 1A83
P 1A90
P 1A49
P 1A50
P 1A51
P 1A52
P 1A53
P 1A54
P 1A55
P 1A84
P 1A91
Pression K homogeneous
Correlation scale λx = 1m
Correlation scale λx = 2m
Correlation scale λx= 5m
Correlation scale λx = 7m
Kequ
100m
50m
20m
15m
10m
7m
5m
2m
1m
λy (m)
Hydraulic pressure (KPa)

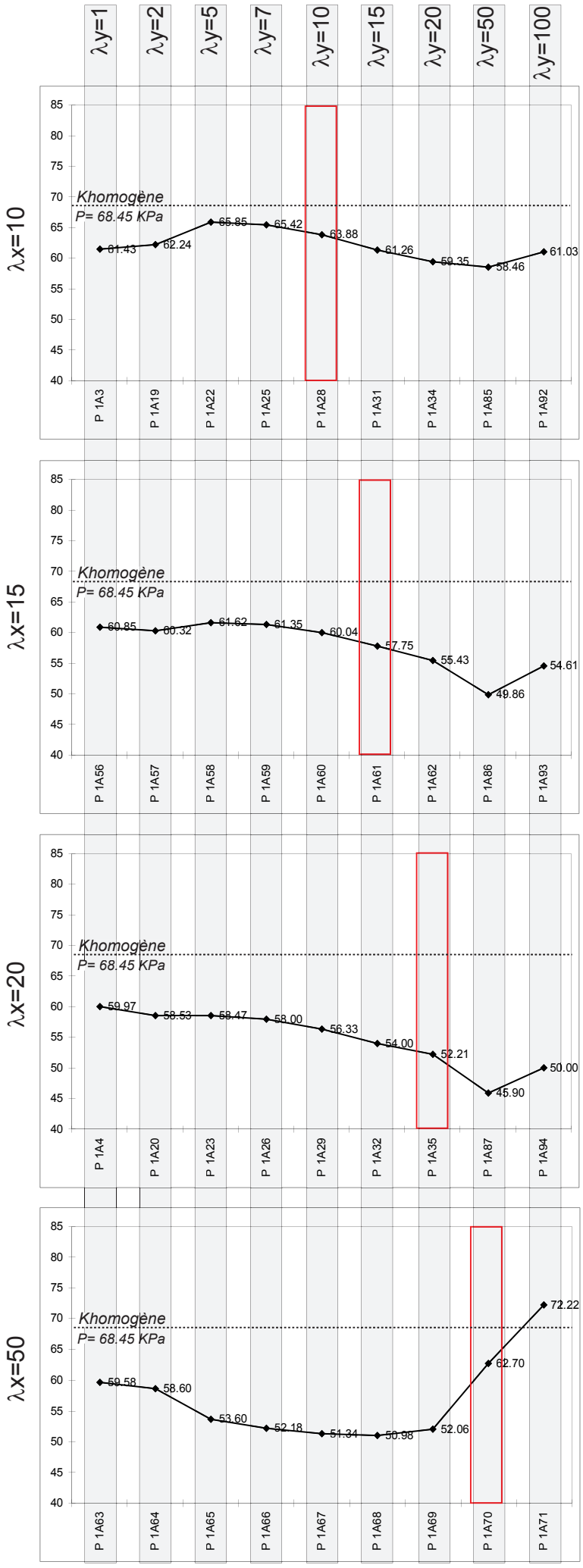
λy=1
λy=2
λy=5
λy=7
λy=10
λy=15
λy=20
λy=50
λy=100
λx=10
λx=15
λx=20
λx=50
Khomogène
P= 68.45 KPa
61.43
62.24
65.85
65.42
63.88
61.26
59.35
58.46
61.03
60.85
60.32
61.62
61.35
60.04
57.75
55.43
49.86
54.61
59.97
59.53
58.47
58.00
56.33
54.00
52.21
45.90
50.00
59.58
58.60
53.60
52.18
51.34
50.98
52.06
62.70
72.22
P 1A3
P 1A19
P 1A22
P 1A25
P 1A28
P 1A31
P 1A34
P 1A85
P 1A92
P 1A56
P 1A57
P 1A58
P 1A59
P 1A60
P 1A61
P 1A62
P 1A86
P 1A93
P 1A4
P 1A20
P 1A23
P 1A26
P 1A29
P 1A32
P 1A35
P 1A87
P 1A94
P 1A63
P 1A64
P 1A65
P 1A66
P 1A67
P 1A68
P 1A69
P 1A70
P 1A71

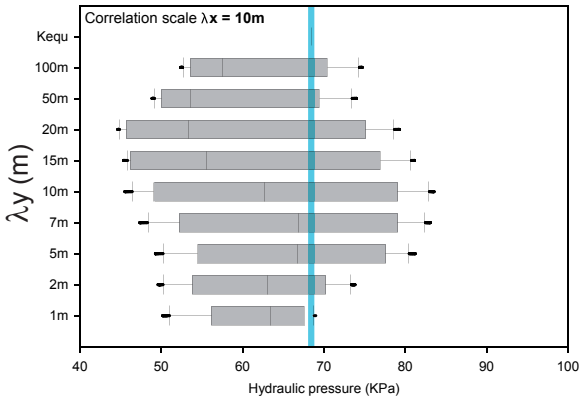
Correlation scale λx = 10m
λy (m)
Kequ
100m
50m
20m
15m
10m
7m
5m
2m
1m
Hydraulic pressure (KPa)

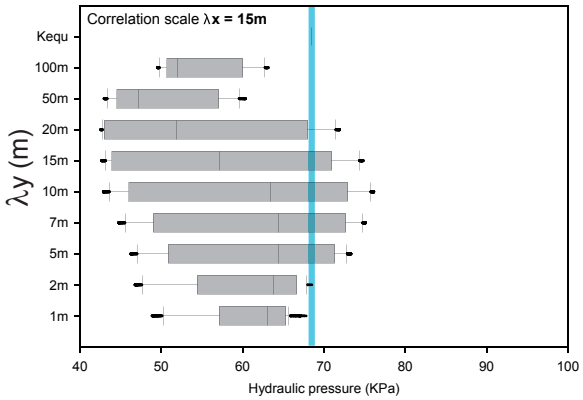
Correlation scale λx = 15m
λy (m)
Kequ
100m
50m
20m
15m
10m
7m
5m
2m
1m
Hydraulic pressure (KPa)

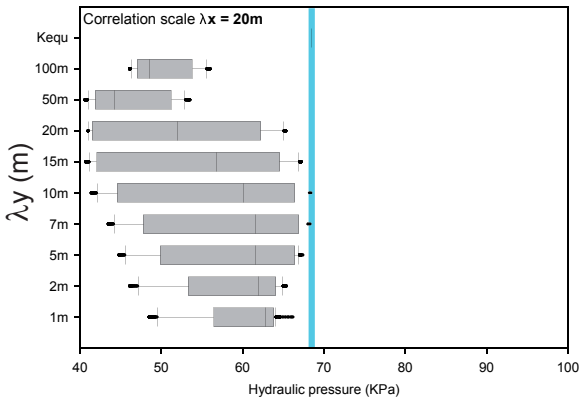
Correlation scale λx = 20m
λy (m)
Kequ
100m
50m
20m
15m
10m
7m
5m
2m
1m
Hydraulic pressure (KPa)

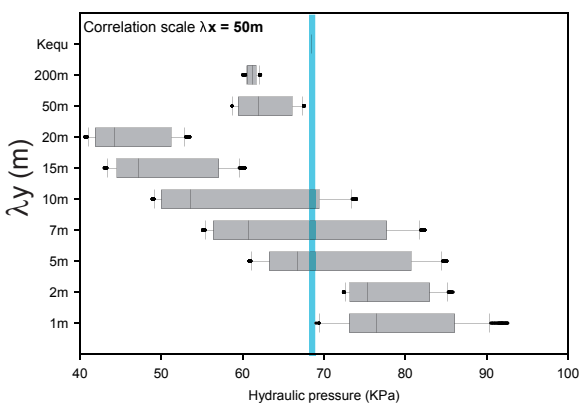
Correlation scale λx = 50m
λy (m)
Kequ
200m
50m
20m
15m
10m
7m
5m
2m
1m
Hydraulic pressure (KPa)

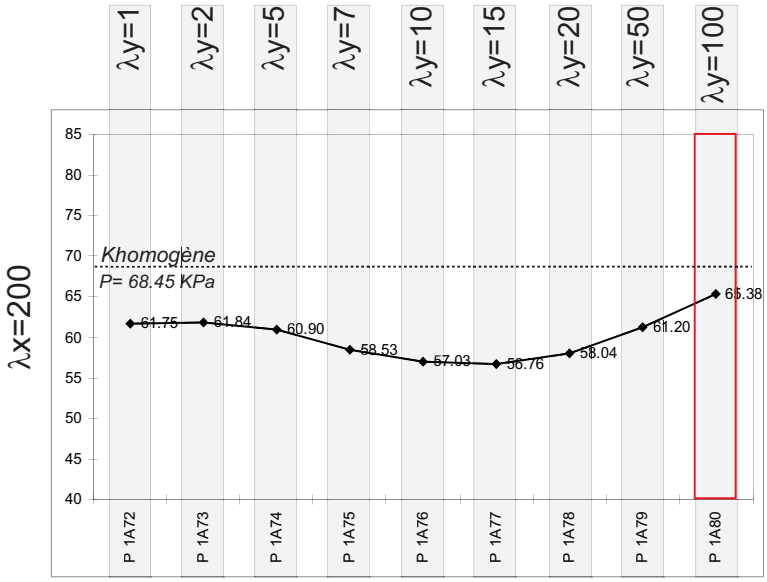
λy=1
λy=2
λy=5
λy=7
λy=10
λy=15
λy=20
λy=50
λy=100
λx=200
Khomogène
P= 68.45 KPa
61.75
61.84
60.90
58.53
57.03
56.76
58.04
61.20
65.38
P 1A72
P 1A73
P 1A74
P 1A75
P 1A76
P 1A77
P 1A78
P 1A79
P 1A80

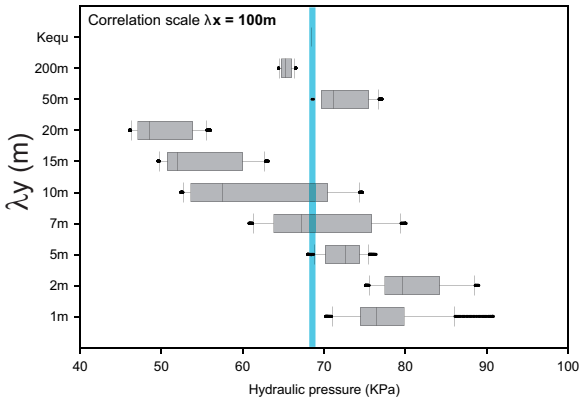
Correlation scale λx = 100m
λy (m)
Kequ
200m
50m
20m
15m
10m
7m
5m
2m
1m
Hydraulic pressure (KPa)

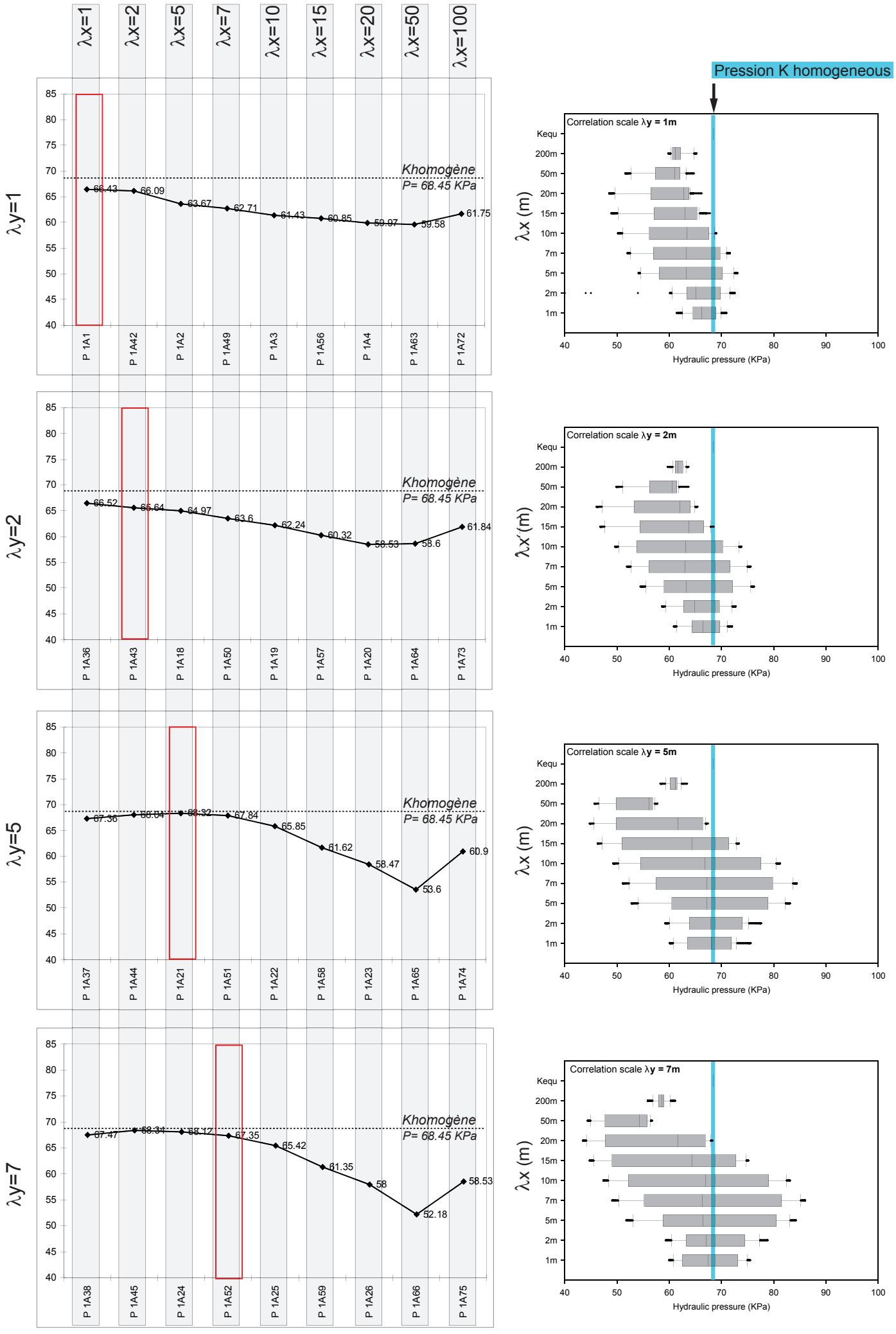
λx=1
λx=2
λx=5
λx=7
λx=10
λx=15
λx=20
λx=50
λx=100
λy=1
λy=2
λy=5
λy=7
Khomogène
P= 68.45 KPa
66.43
66.09
63.67
62.71
61.43
60.85
59.97
59.58
61.75
66.52
65.64
64.97
63.6
62.24
60.32
58.53
58.6
61.84
67.36
68.04
68.32
67.84
65.85
61.62
58.47
53.6
60.9
67.47
68.34
68.12
67.35
65.42
61.35
58
52.18
58.53
P 1A1
P 1A42
P 1A2
P 1A49
P 1A3
P 1A56
P 1A4
P 1A63
P 1A72
P 1A36
P 1A43
P 1A18
P 1A50
P 1A19
P 1A57
P 1A20
P 1A64
P 1A73
P 1A37
P 1A44
P 1A21
P 1A51
P 1A22
P 1A58
P 1A23
P 1A65
P 1A74
P 1A38
P 1A45
P 1A24
P 1A52
P 1A25
P 1A59
P 1A26
P 1A66
P 1A75
Pression K homogeneous
Correlation scale λy = 1m
Correlation scale λy = 2m
Correlation scale λy = 5m
Correlation scale λy = 7m
λx (m)
Kequ
200m
50m
20m
15m
10m
7m
5m
2m
1m
Hydraulic pressure (KPa)

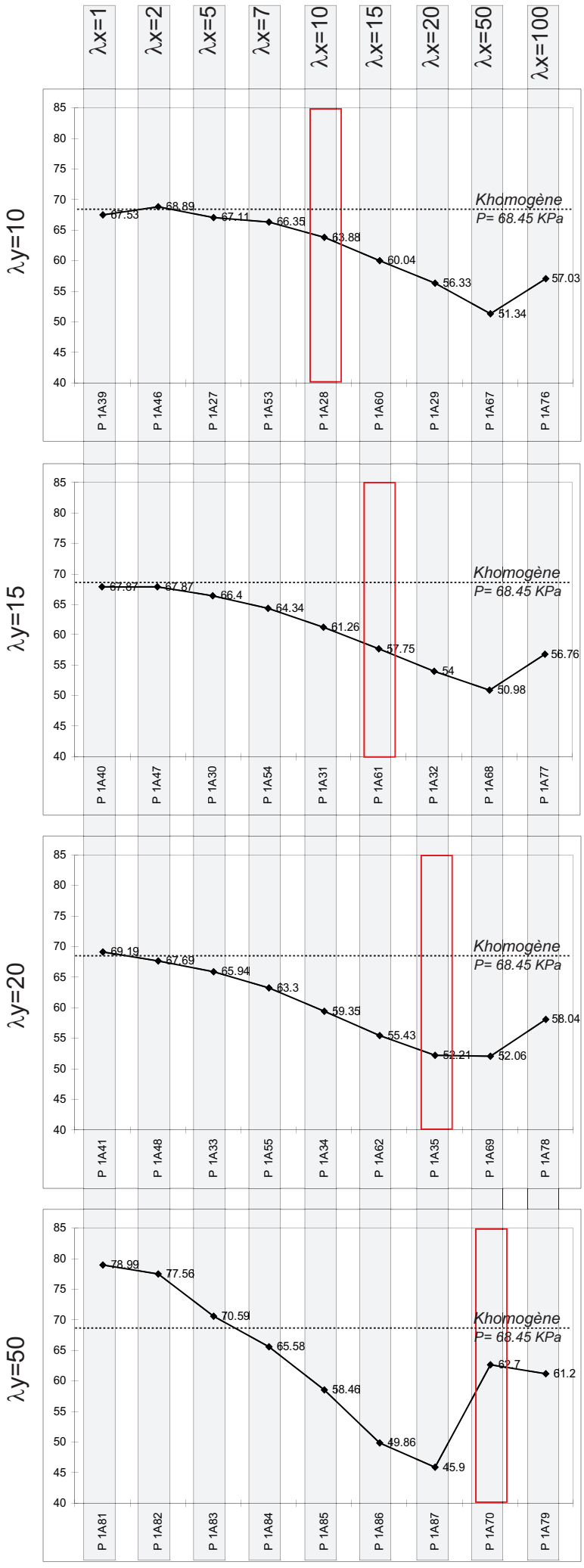
λx=1
λx=2
λx=5
λx=7
λx=10
λx=15
λx=20
λx=50
λx=100
λy=10
λy=15
λy=20
λy=50
Khomogène
P= 68.45 KPa
67.53
68.89
67.11
66.35
63.88
60.04
56.33
51.34
57.03
67.87
67.87
66.4
64.34
61.26
57.75
54
50.98
56.76
69.19
67.69
65.94
63.3
59.35
55.43
52.21
52.06
58.04
78.99
77.56
70.59
65.58
58.46
49.86
45.9
62.7
61.2
P 1A39
P 1A46
P 1A27
P 1A53
P 1A28
P 1A60
P 1A29
P 1A67
P 1A76
P 1A40
P 1A47
P 1A30
P 1A54
P 1A31
P 1A61
P 1A32
P 1A68
P 1A77
P 1A41
P 1A48
P 1A33
P 1A55
P 1A34
P 1A62
P 1A35
P 1A69
P 1A78
P 1A81
P 1A82
P 1A83
P 1A84
P 1A85
P 1A86
P 1A87
P 1A70
P 1A79

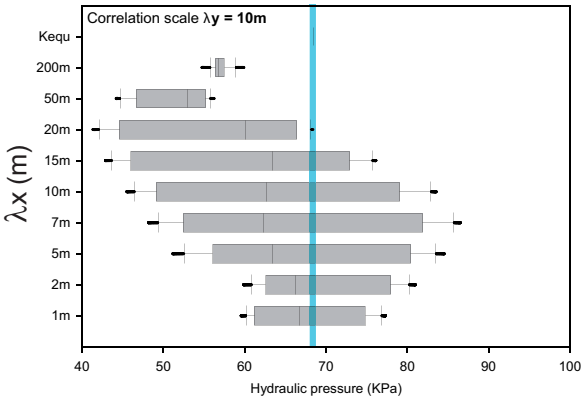
Correlation scale λy = 10m
Kequ
200m
50m
20m
15m
10m
7m
5m
2m
1m
λx (m)
Hydraulic pressure (KPa)

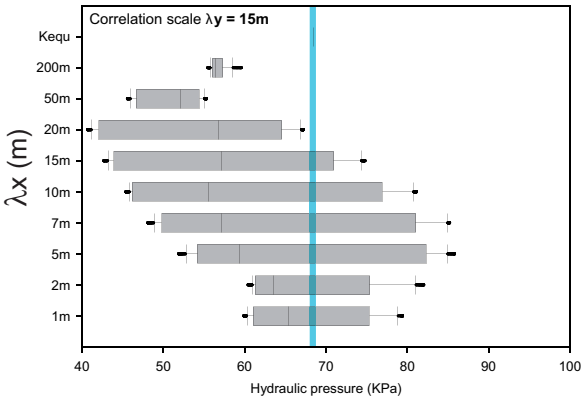
Correlation scale λy = 15m
Kequ
200m
50m
20m
15m
10m
7m
5m
2m
1m
λx (m)
Hydraulic pressure (KPa)

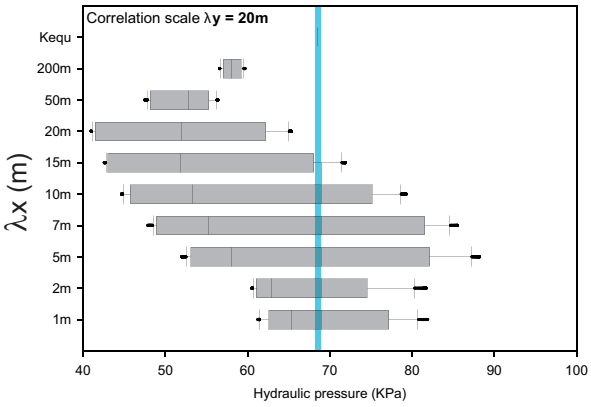
Correlation scale λy = 20m
Kequ
200m
50m
20m
15m
10m
7m
5m
2m
1m
λx (m)
Hydraulic pressure (KPa)

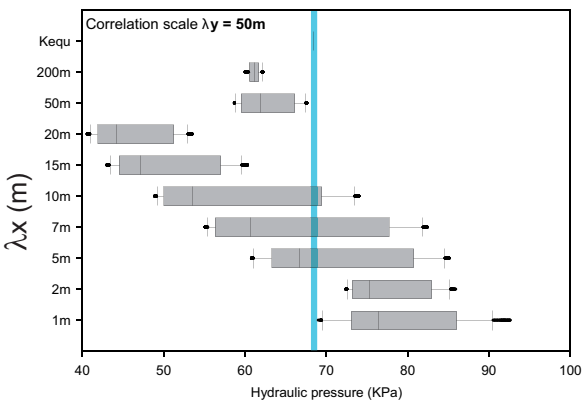
Correlation scale λy = 50m
Kequ
200m
50m
20m
15m
10m
7m
5m
2m
1m
λx (m)
Hydraulic pressure (KPa)

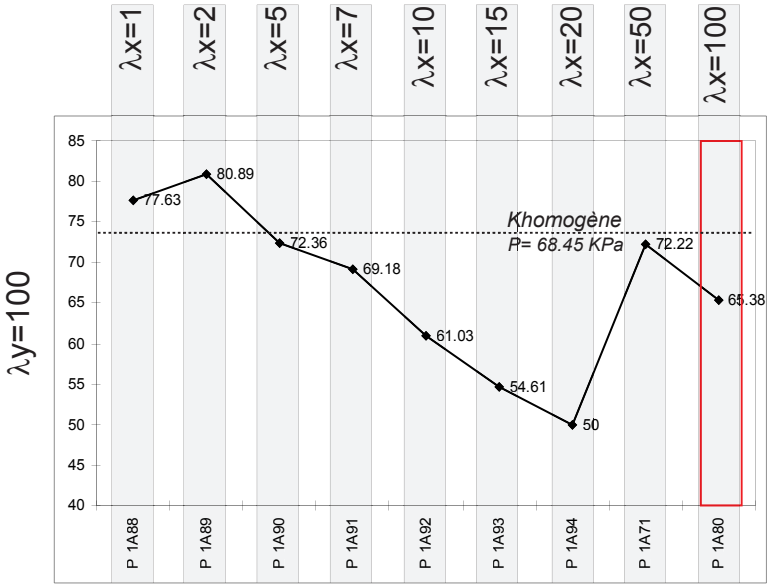
λx=1
λx=2
λx=5
λx=7
λx=10
λx=15
λx=20
λx=50
λx=100
λy=100
85
80
75
70
65
60
55
50
45
40
77.63
80.89
72.36
69.18
61.03
54.61
50
72.22
65.38
Khomogène
P= 68.45 KPa
P 1A88
P 1A89
P 1A90
P 1A91
P 1A92
P 1A93
P 1A94
P 1A71
P 1A80

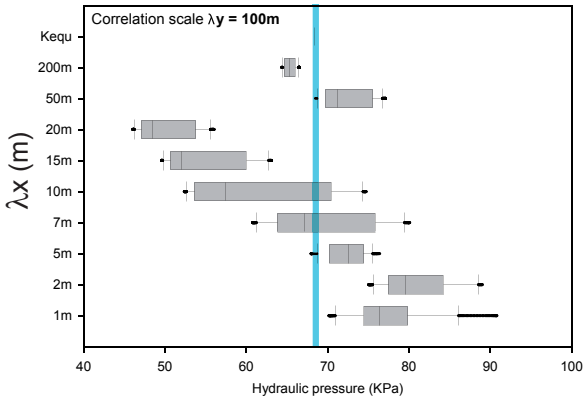
Correlation scale λy = 100m
λx (m)
Kequ
200m
50m
20m
15m
10m
7m
5m
2m
1m
40
50
60
70
80
90
100
Hydraulic pressure (KPa)

Fluid Flux Mass Balance (m3/day)

λx/λy	λx=1m	λ x=2m	λ x=5m	λ x=7m	λ x=10m	λ x=15m	λ x=20m	λ x=50m	λ x=200m
1	*1A1* 2.72E-03	*1A42* 2.71E-03	*1A2* 2.75E-03	*1A49* 2.77E-03	*1A3* 2.81E-03	*1A56* 2.81E-03	*1A4* 2.84E-03	*1A63* 2.86E-03	*1A72* 2.91E-03
2	*1A36* 2.62E-03	*1A43* 2.61E-03	*1A18* 2.64E-03	*1A50* 2.66E-03	*1A19* 2.73E-03	*1A57* 2.71E-03	*1A20* 2.77E-03	*1A64* 2.83E-03	*1A73* 2.91E-03
5	*1A37* 2.45E-03	*1A44* 2.41E-03	*1A21* 2.46E-03	*1A51* 2.50E-03	*1A22* 2.54E-03	*1A58* 2.58E-03	*1A23* 2.60E-03	*1A65* 2.82E-03	*1A74* 2.93E-03
7	*1A38* 2.39E-03	*1A45* 2.34E-03	*1A24* 2.38E-03	*1A52* 2.43E-03	*1A25* 2.49E-03	*1A59* 2.55E-03	*1A26* 2.60E-03	*1A66* 2.91E-03	*1A75* 3.04E-03
10	*1A39* 2.34E-03	*1A46* 2.26E-03	*1A27* 2.29E-03	*1A53* 2.36E-03	*1A28* 2.43E-03	*1A60* 2.53E-03	*1A29* 2.59E-03	*1A67* 3.11E-03	*1A76* 3.31E-03
15	*1A40* 2.29E-03	*1A47* 2.19E-03	*1A30* 2.18E-03	*1A54* 2.26E-03	*1A31* 2.35E-03	*1A61* 2.50E-03	*1A32* 2.59E-03	*1A68* 3.48E-03	*1A77* 3.91E-03
20	*1A41* 2.27E-03	*1A48* 2.17E-03	*1A33* 2.11E-03	*1A55* 2.19E-03	*1A34* 2.31E-03	*1A62* 2.48E-03	*1A35* 2.61E-03	*1A69* 3.88E-03	*1A78* 4.60E-03
50	*1A81* 2.26E-03	*1A82* 2.23E-03	*1A83* 2.20E-03	*1A84* 2.23E-03	*1A85* 2.30E-03	*1A86* 2.43E-03	*1A87* 2.63E-03	*1A70* 5.64E-03	*1A79* 8.13E-03
100	*1A88* 2.25E-03	*1A89* 2.23E-03	*1A90* 2.16E-03	*1A91* 2.15E-03	*1A92* 2.17E-03	*1A93* 2.38E-03	*1A94* 2.61E-03	*1A71* 6.50E-03	*1A80* 1.08E-02

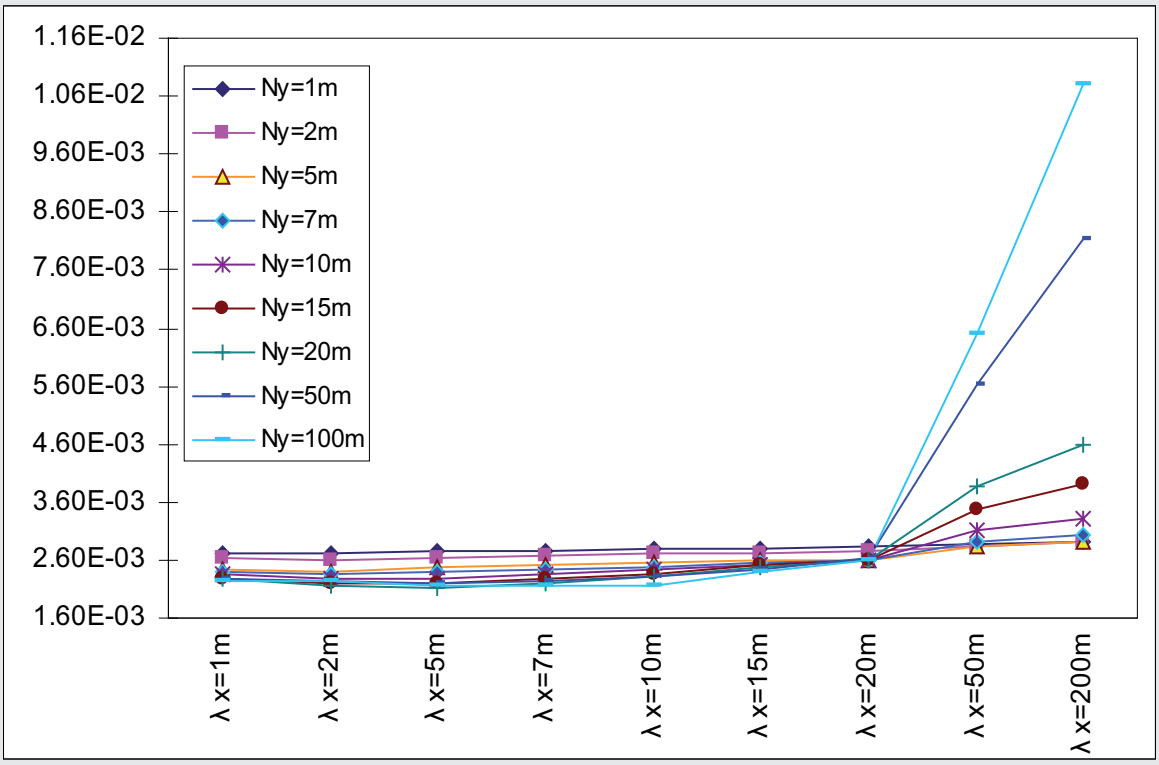

λx=λy

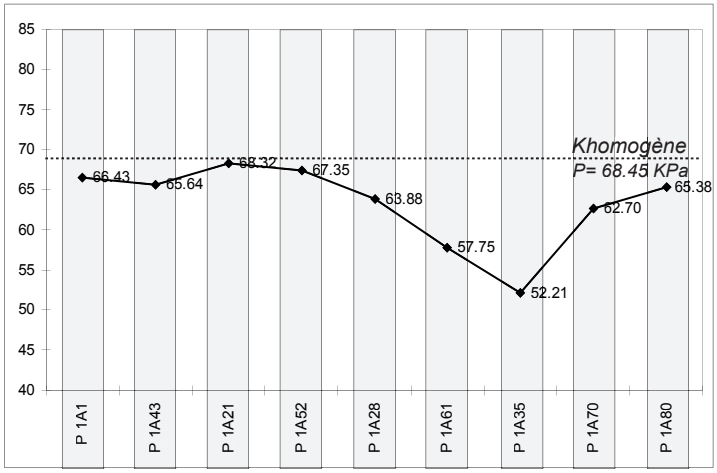

Exception for y=100m : x=200m

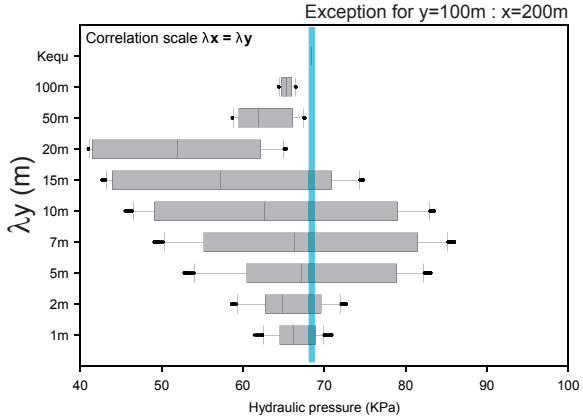

λx inv λy

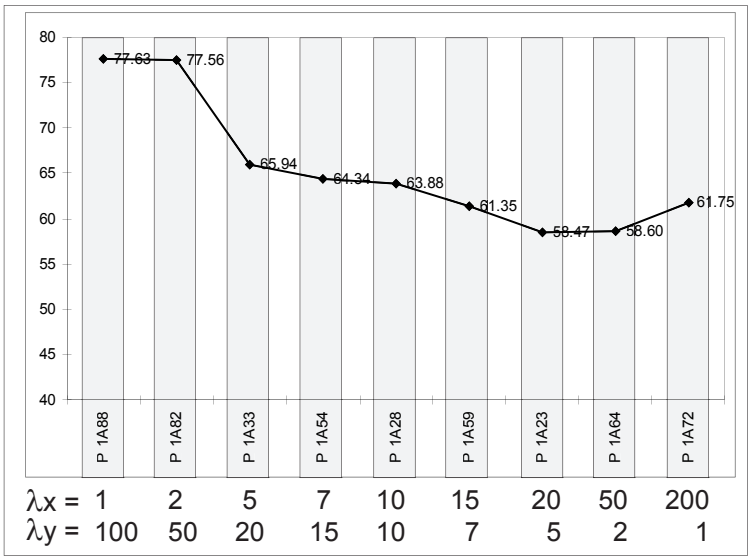

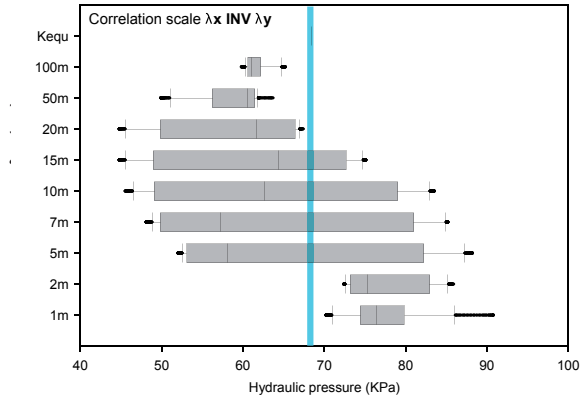

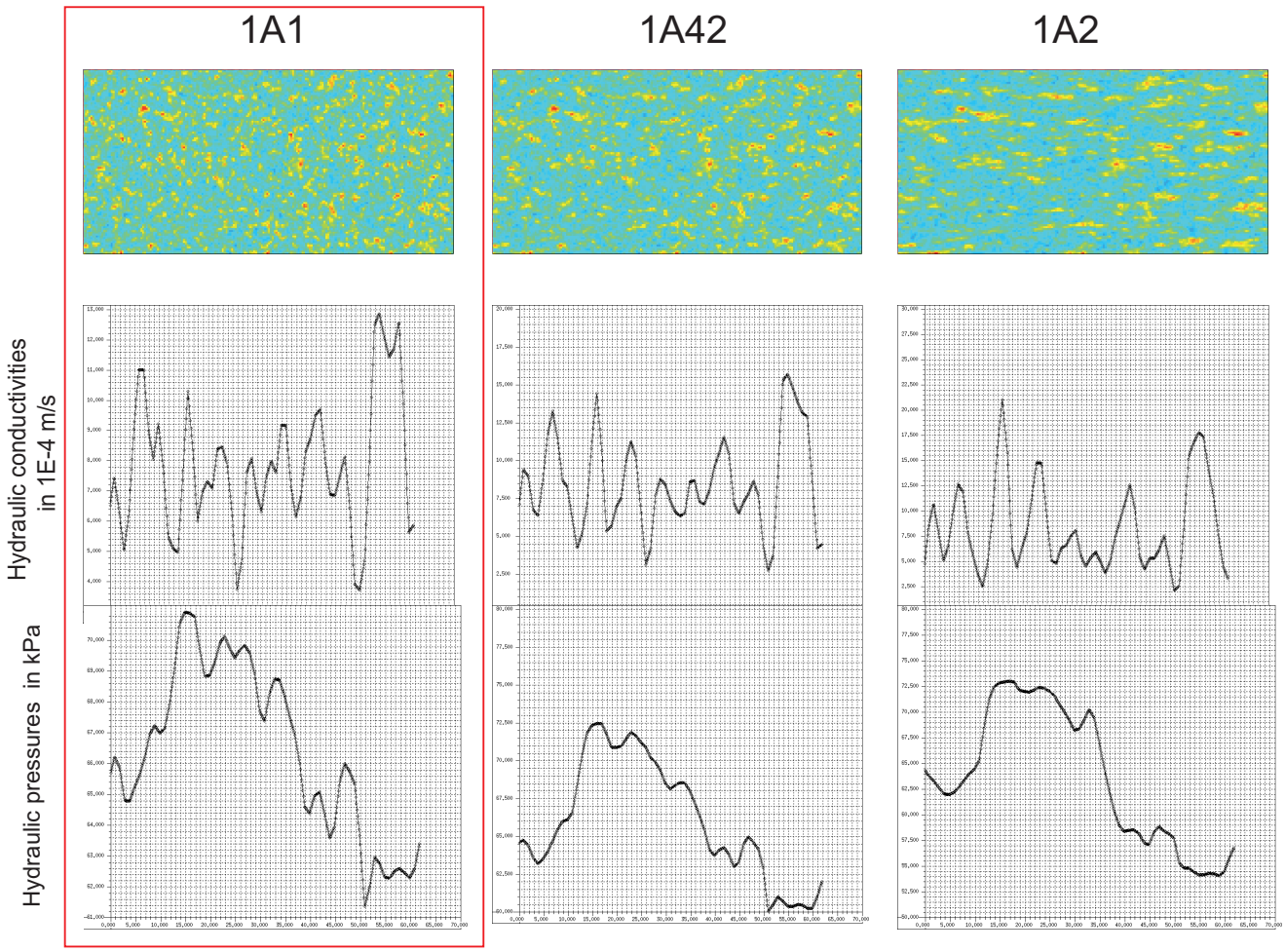
1A1
1A42
1A2
Hydraulic conductivities in 1E-4 m/s
Hydraulic pressures in kPa

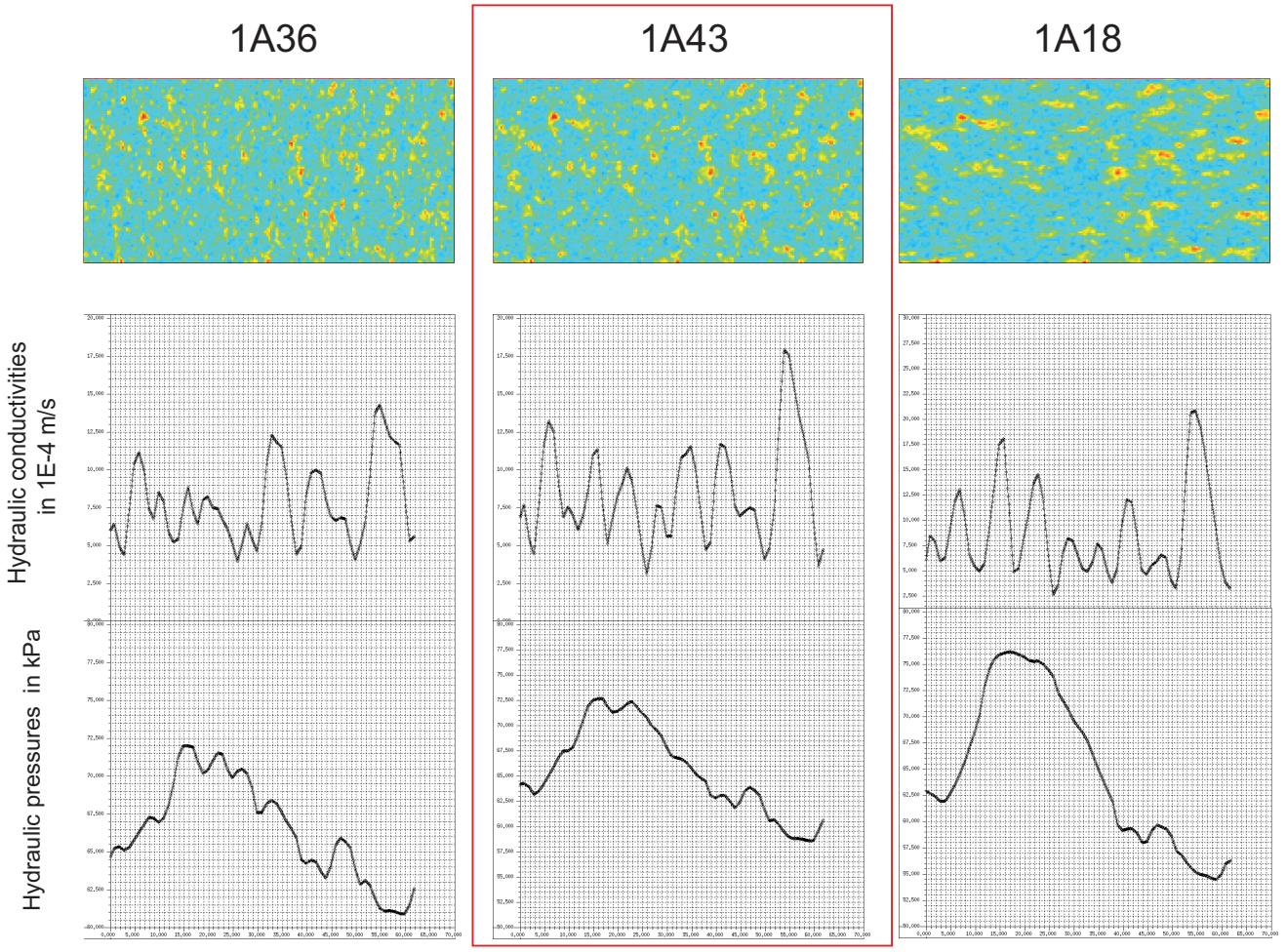
1A36
1A43
1A18
Hydraulic conductivities in 1E-4 m/s
Hydraulic pressures in kPa

1A49 1A3 1A56

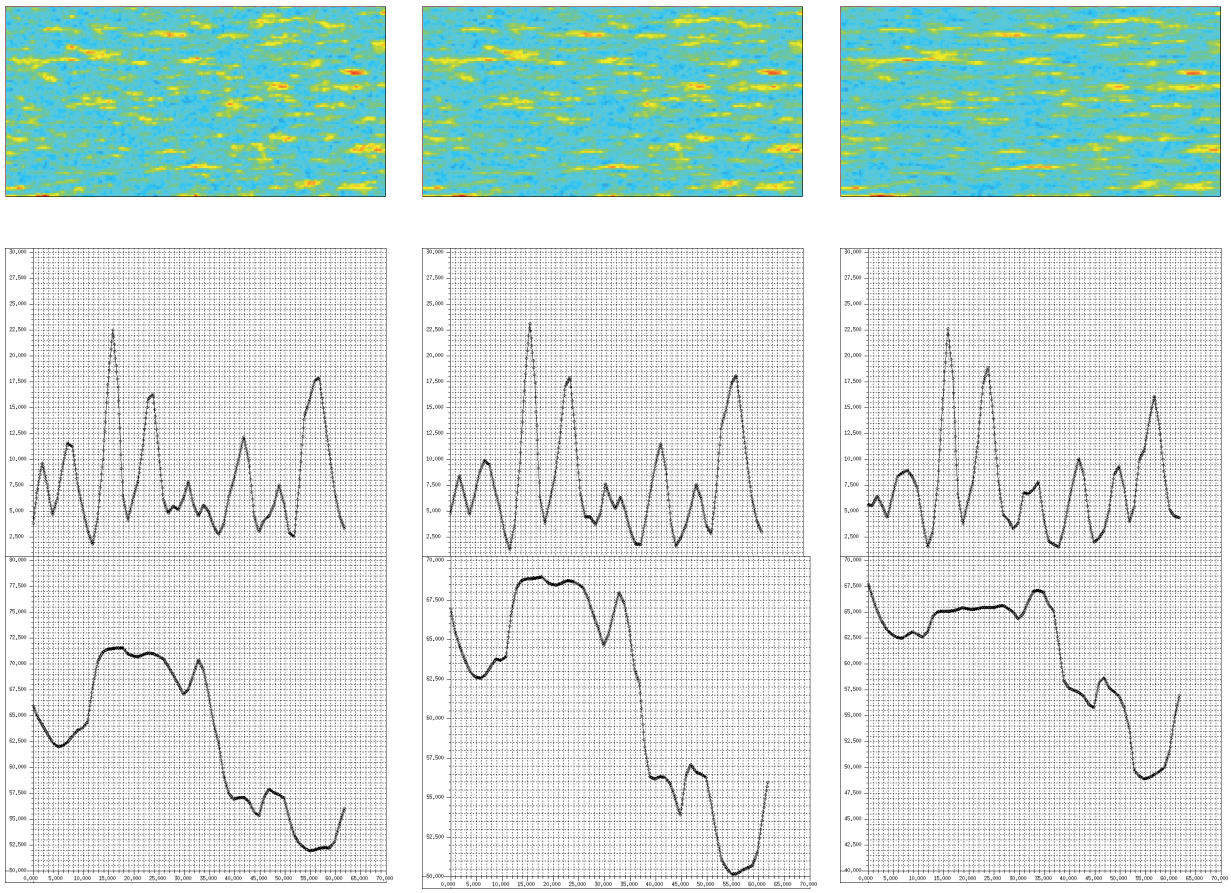

1A50 1A19 1A57

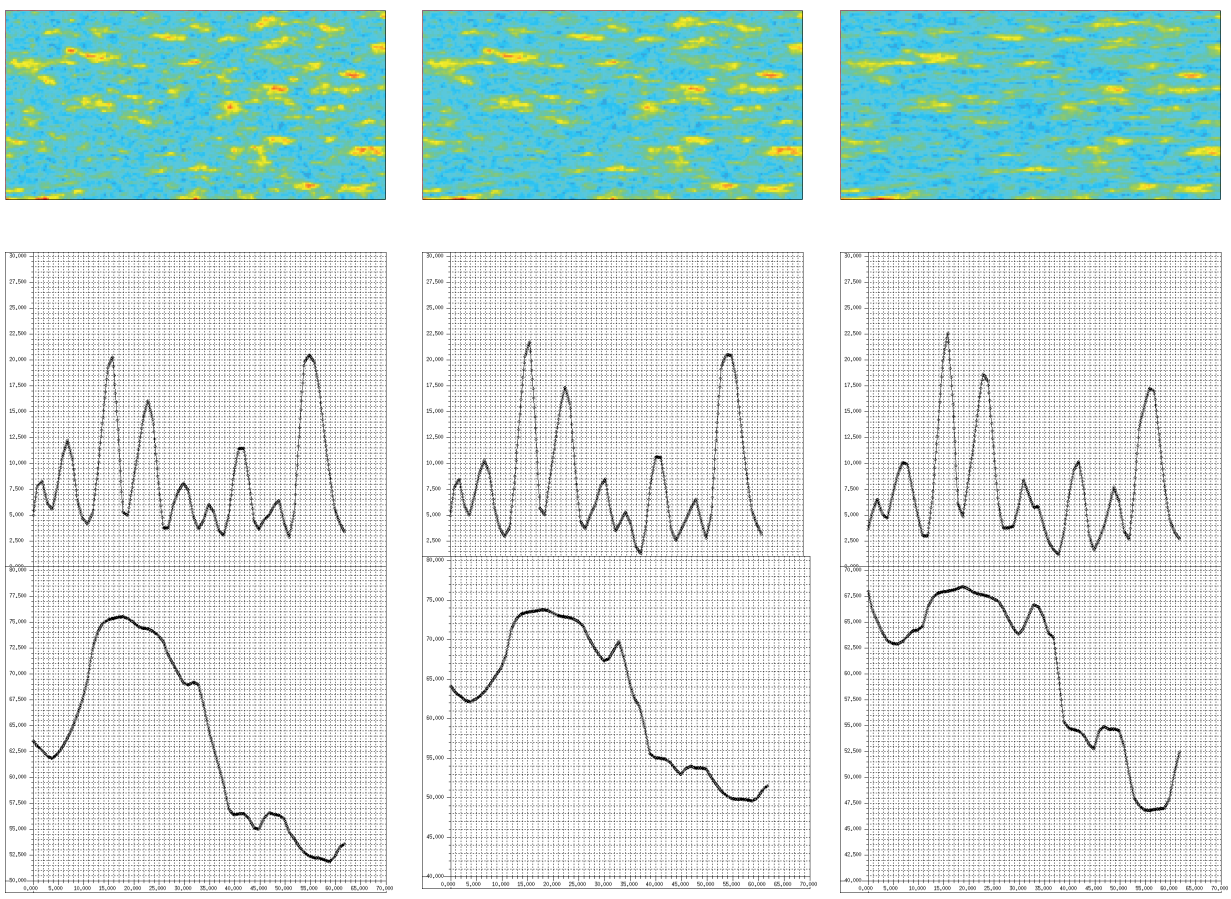

1A4 1A63 1A72

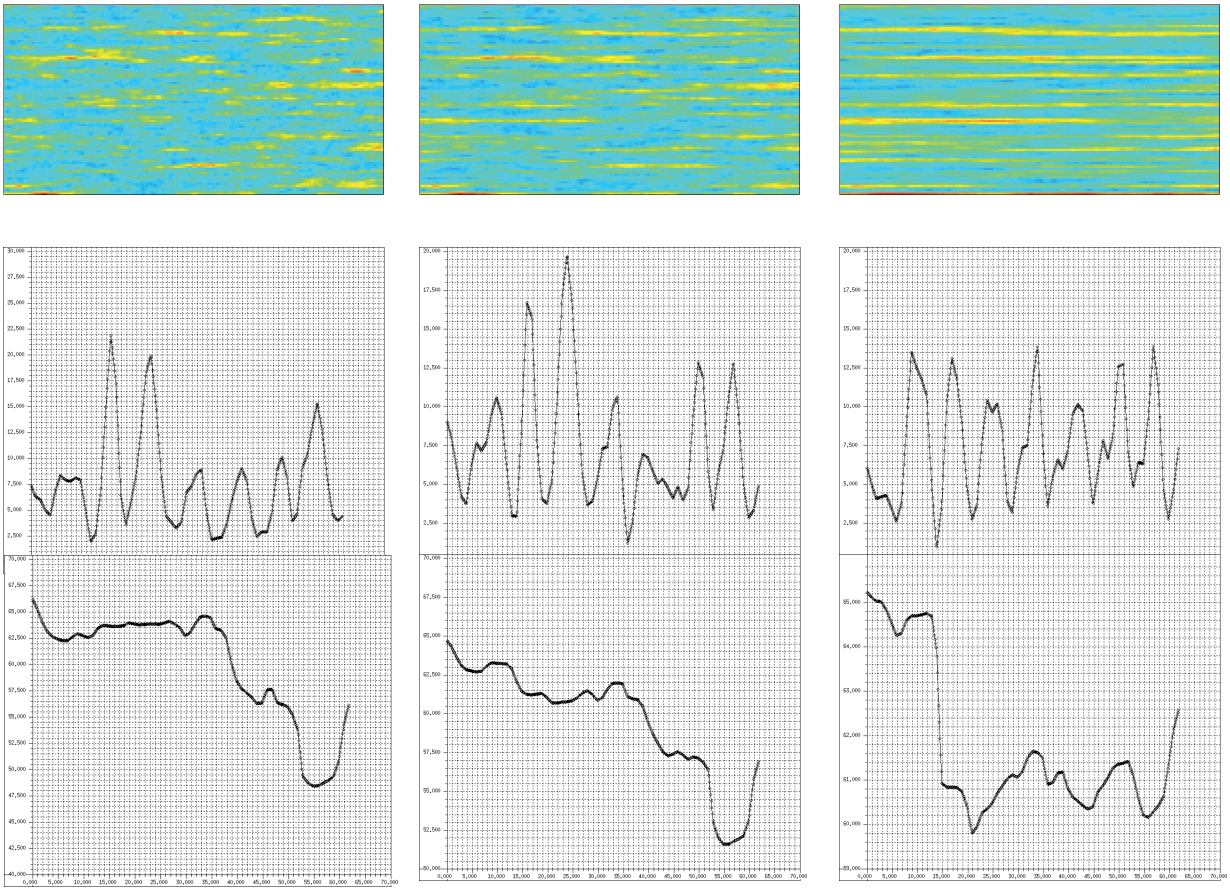

1A20 1A64 1A73

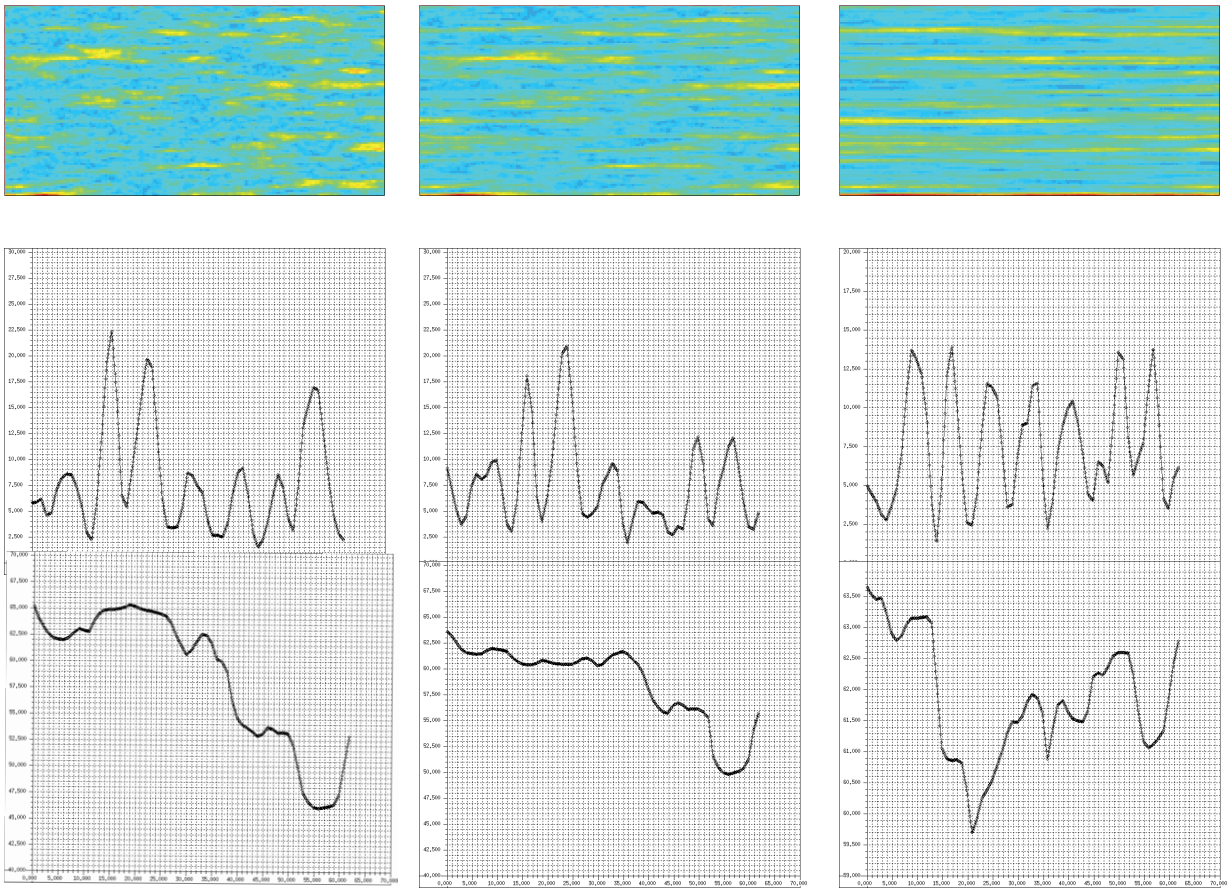

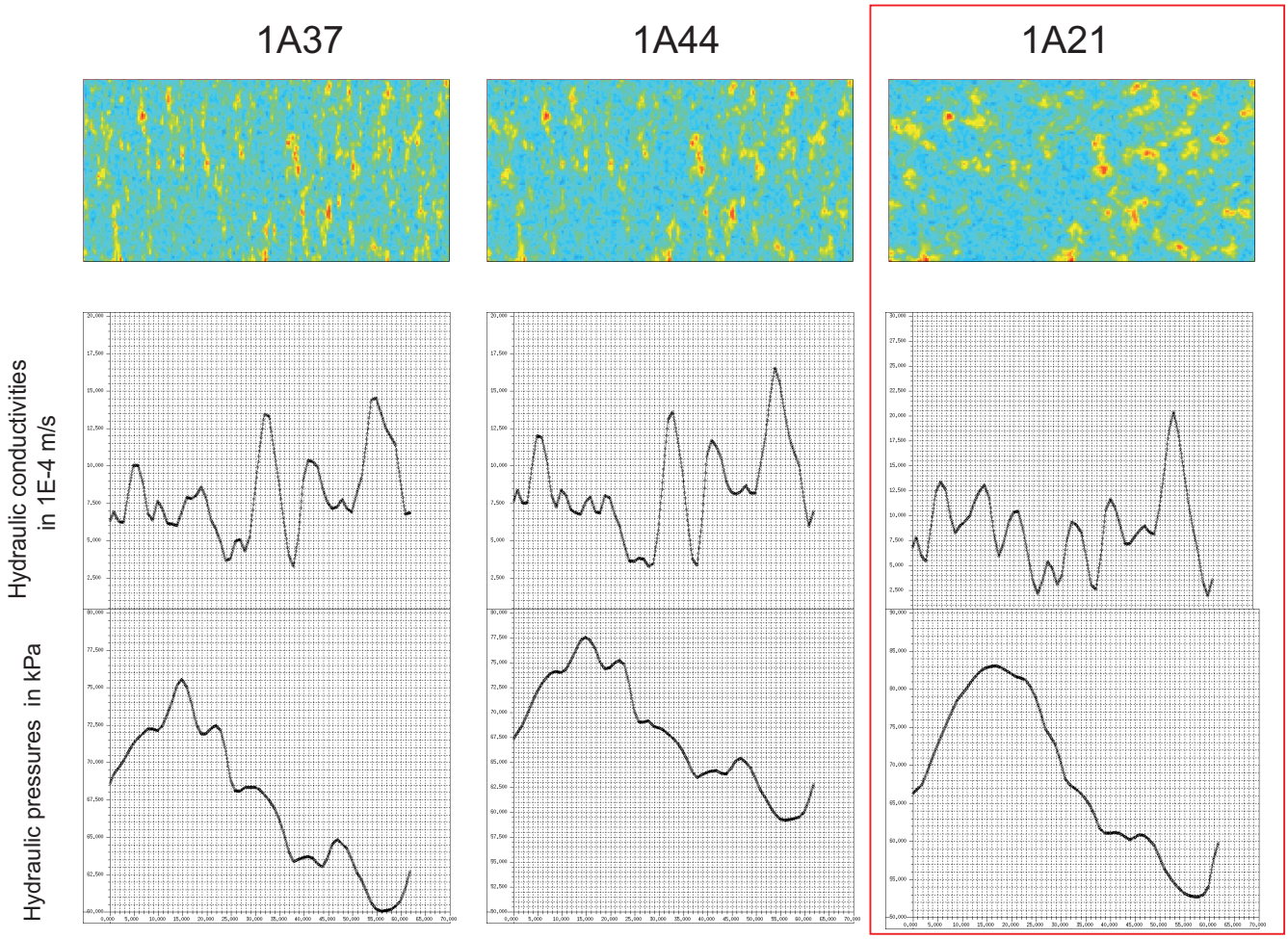
1A37
1A44
1A21
Hydraulic conductivities in 1E-4 m/s
Hydraulic pressures in kPa

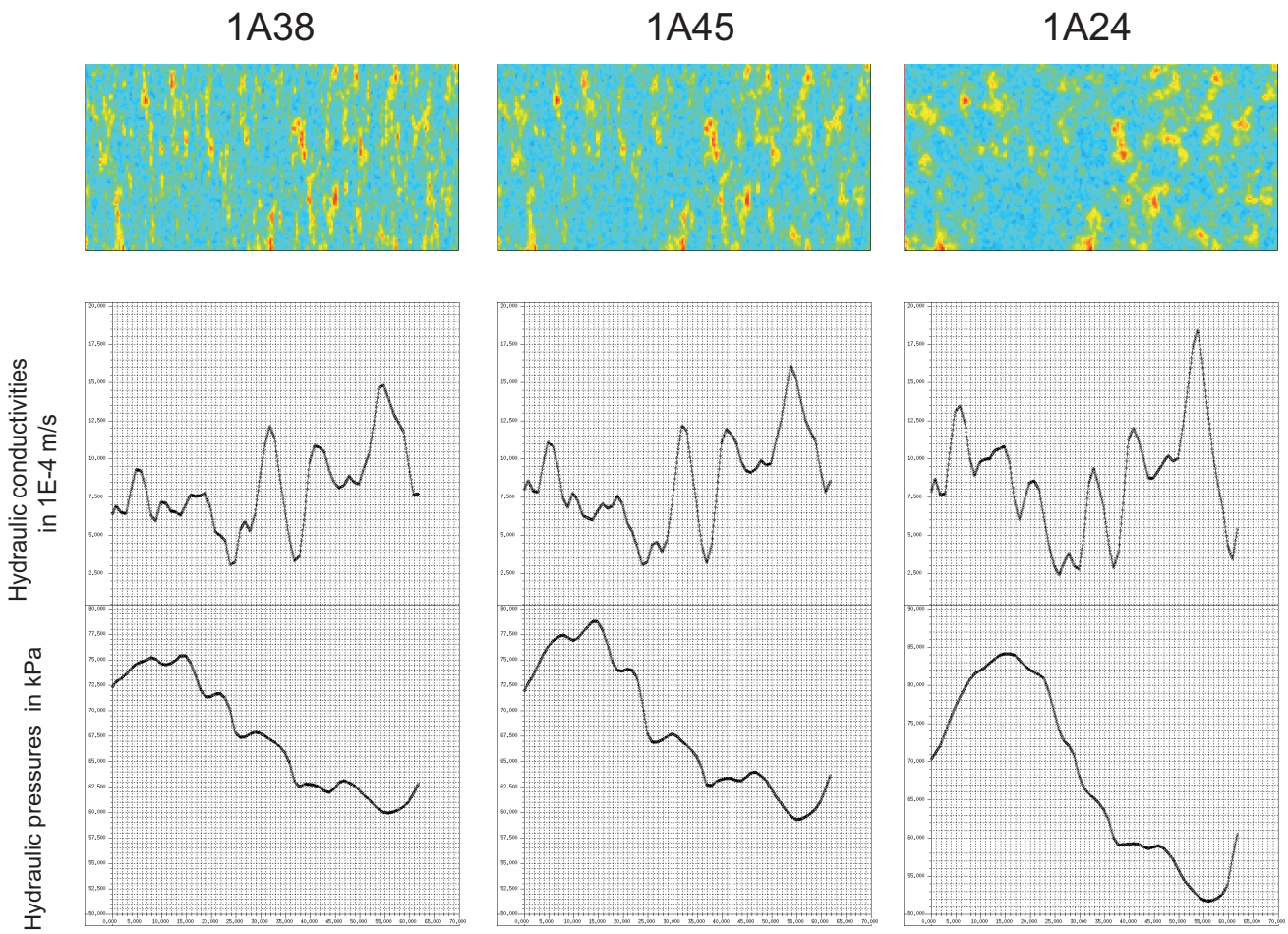
1A38
1A45
1A24
Hydraulic conductivities in 1E-4 m/s
Hydraulic pressures in kPa

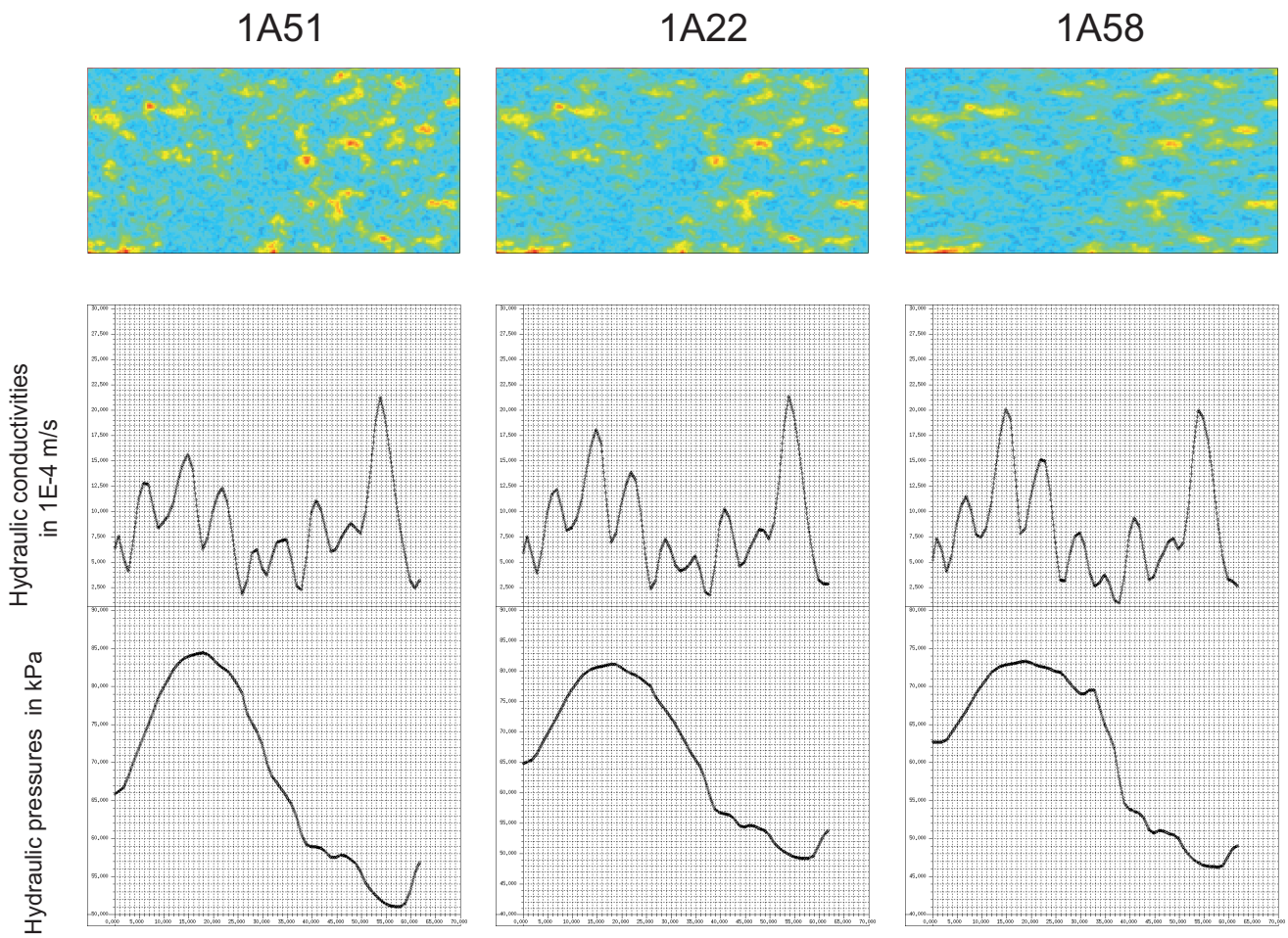
1A51
1A22
1A58
Hydraulic conductivities in 1E-4 m/s
Hydraulic pressures in kPa

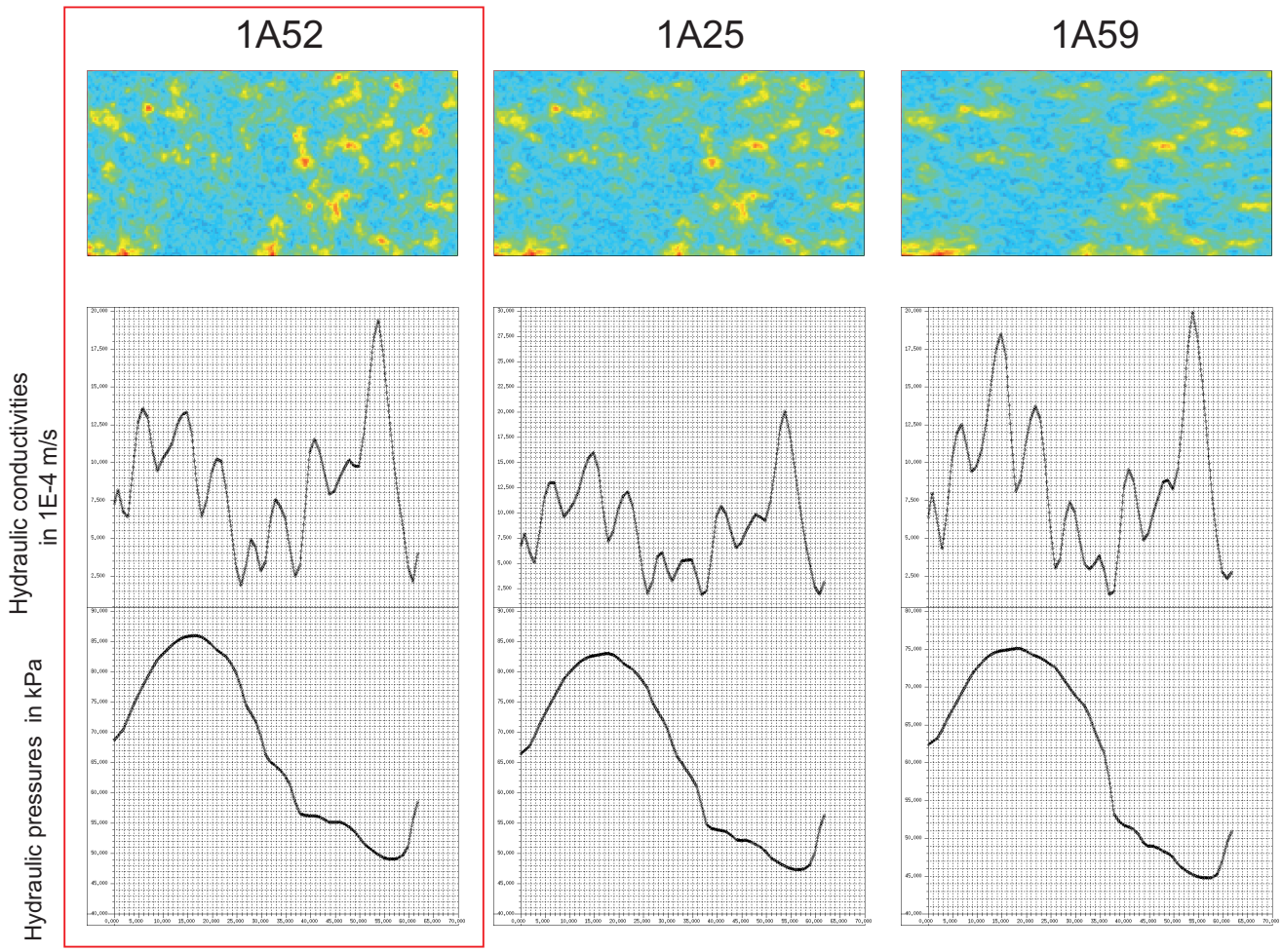
1A52
1A25
1A59
Hydraulic conductivities in 1E-4 m/s
Hydraulic pressures in kPa

1A23 1A65 1A74

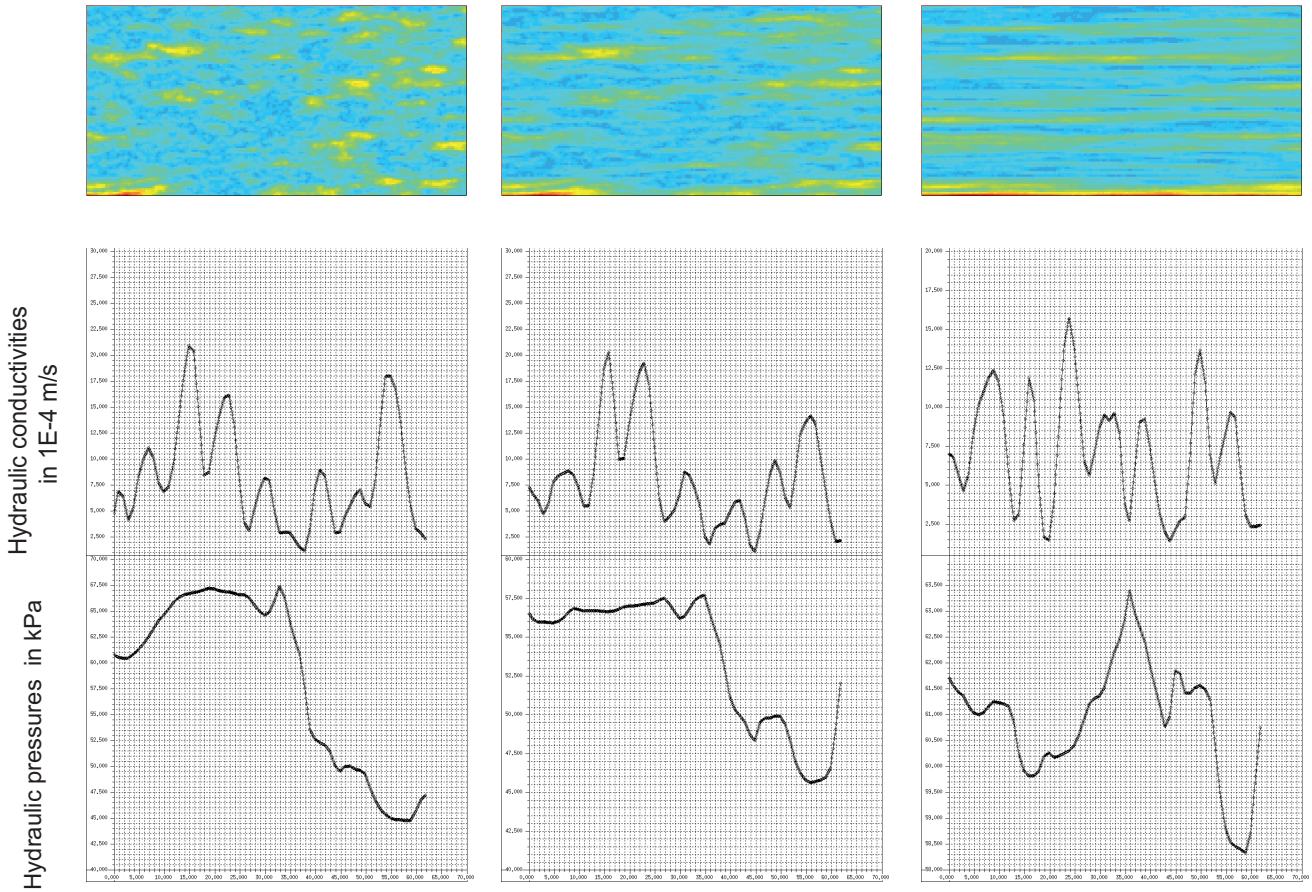

1A26 1A66 1A75

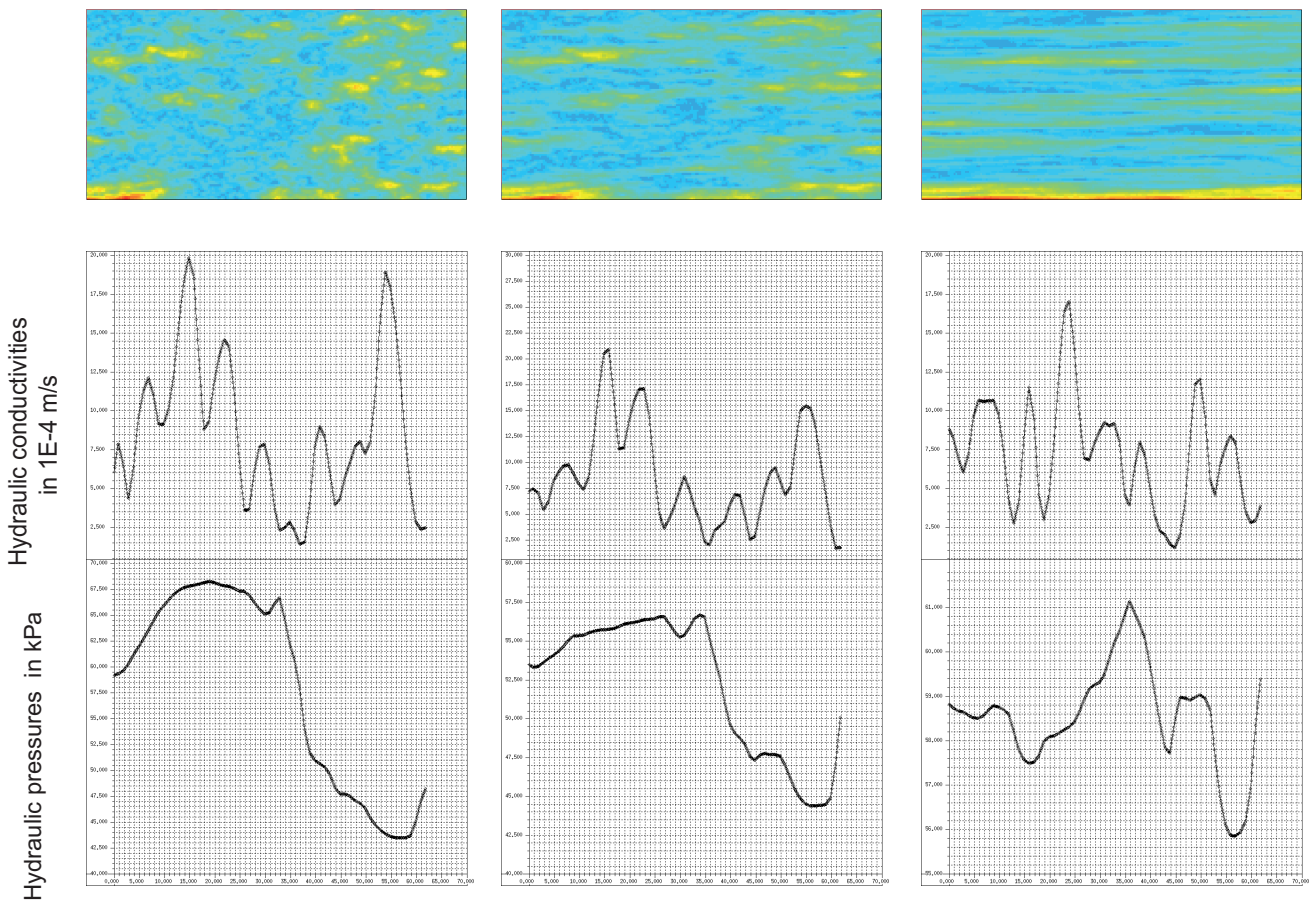

1A39 1A46 1A27

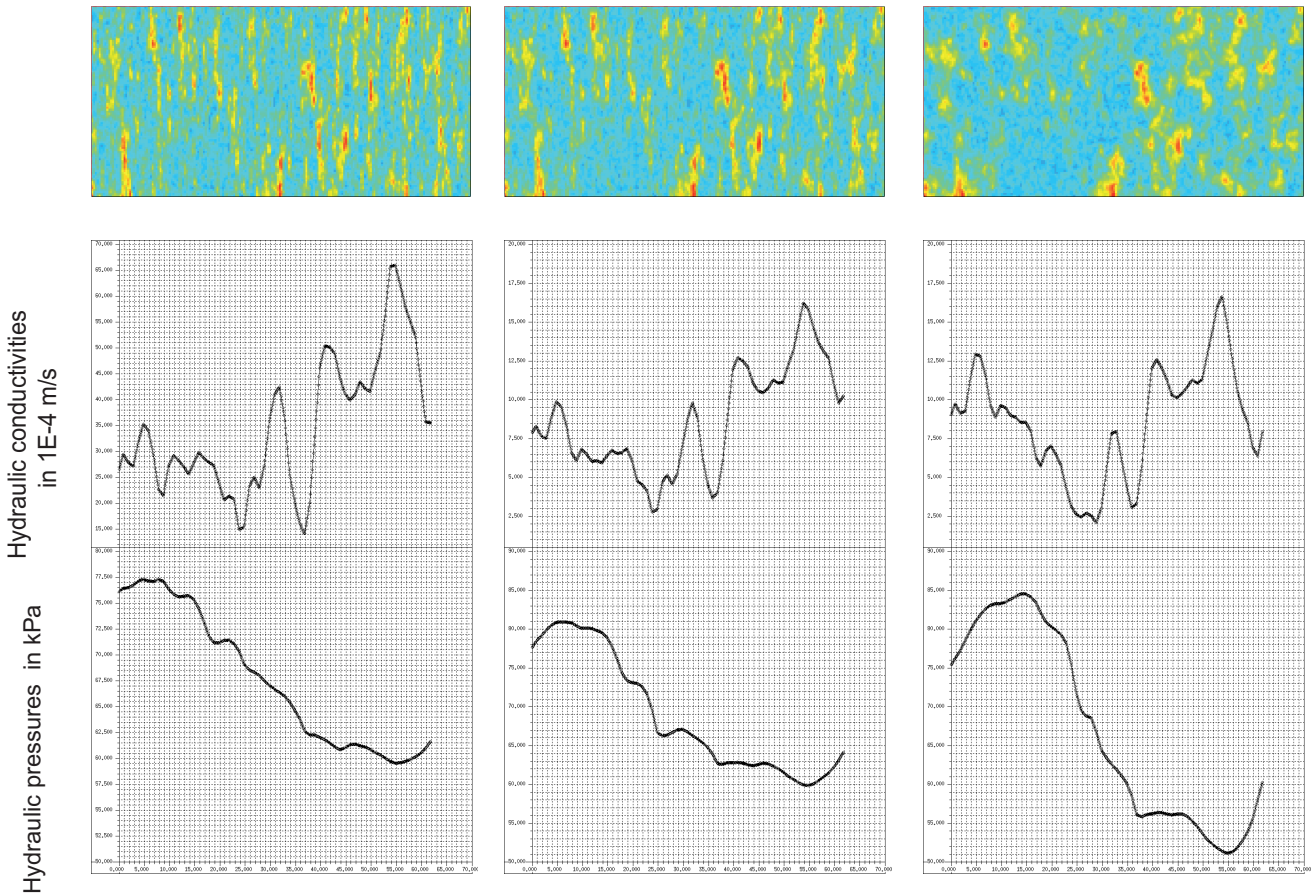

1A40 1A47 1A30

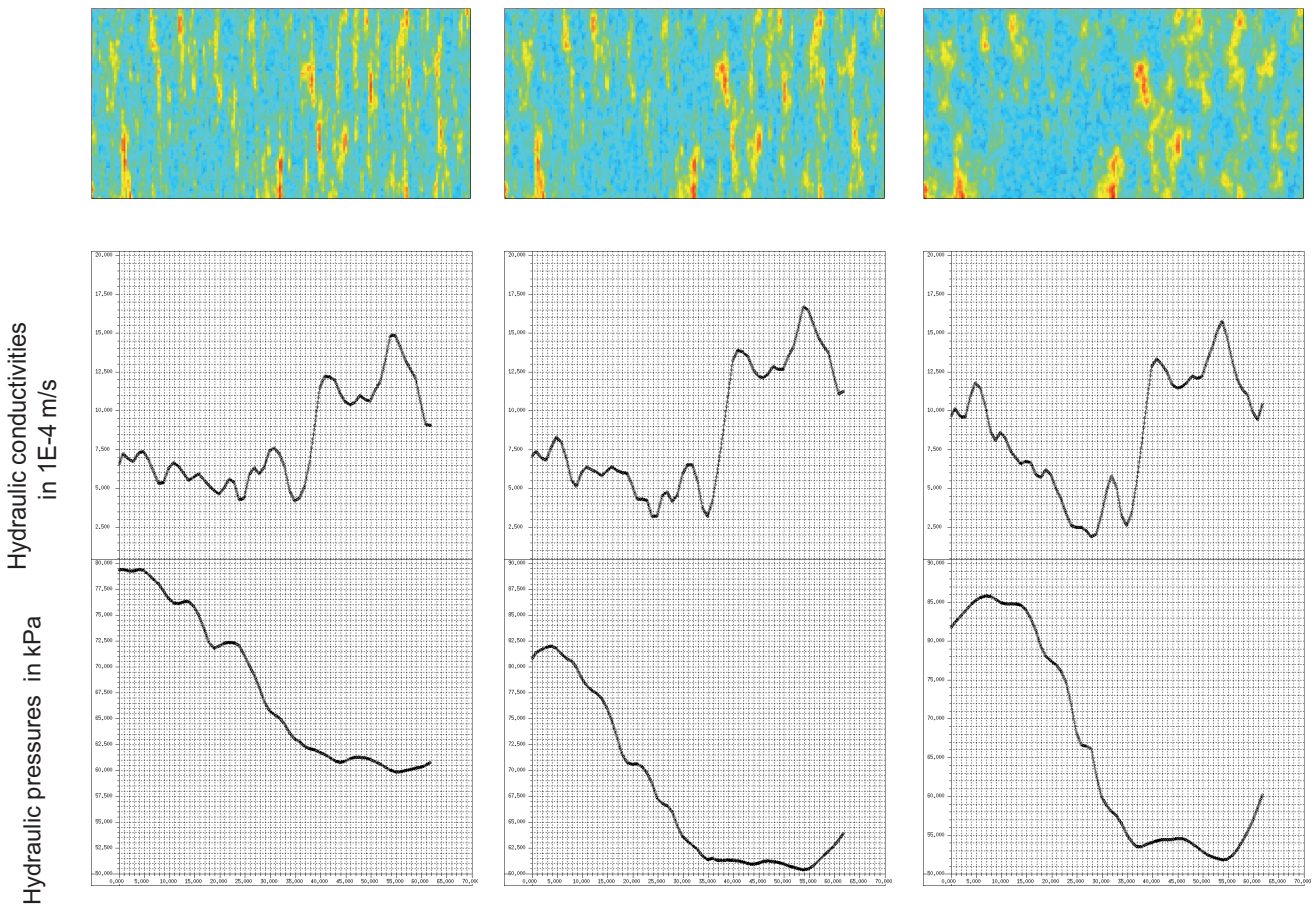

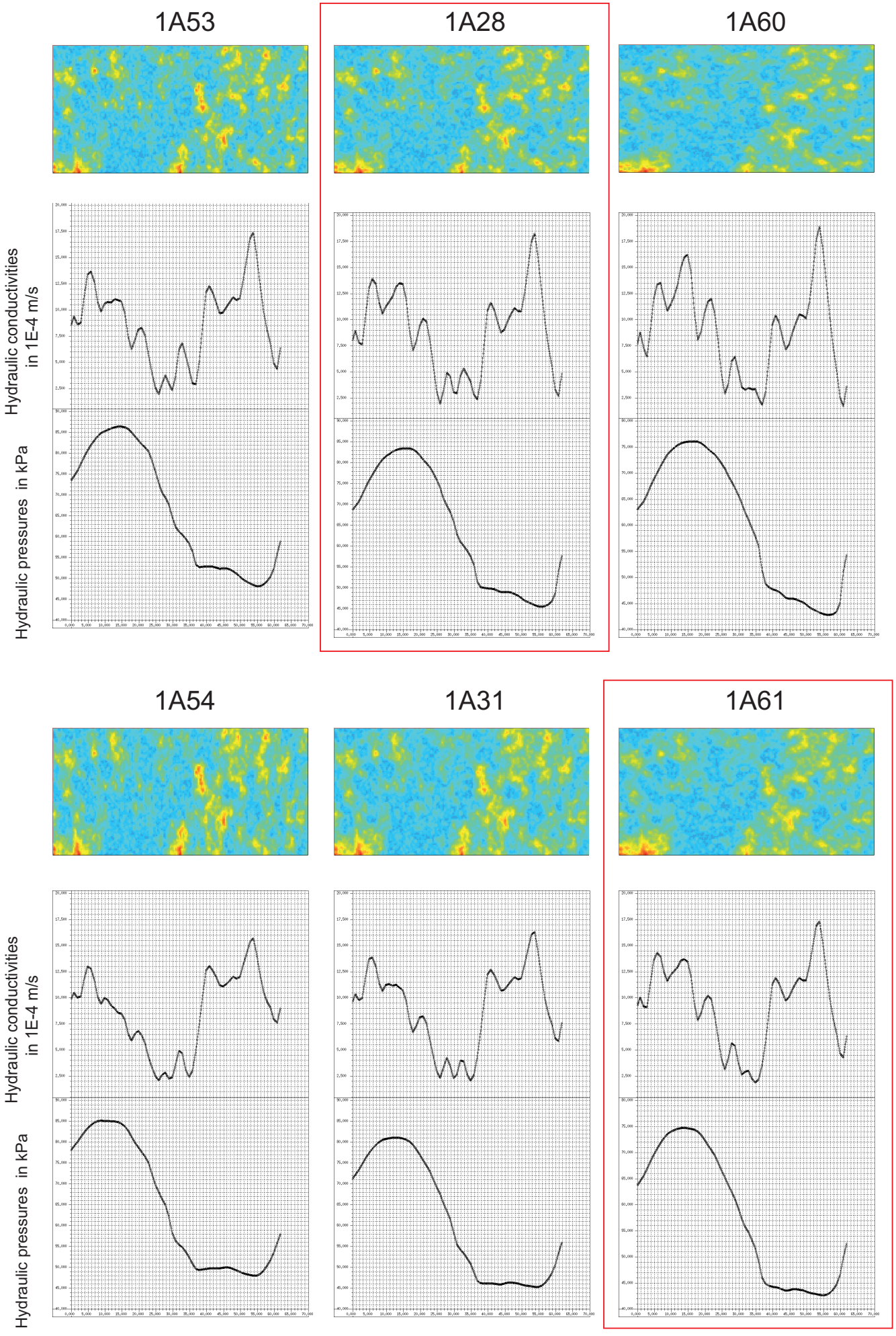
1A53
1A28
1A60
Hydraulic conductivities in 1E-4 m/s
Hydraulic pressures in kPa
1A54
1A31
1A61
Hydraulic conductivities in 1E-4 m/s
Hydraulic pressures in kPa

1A29 1A67 1A76

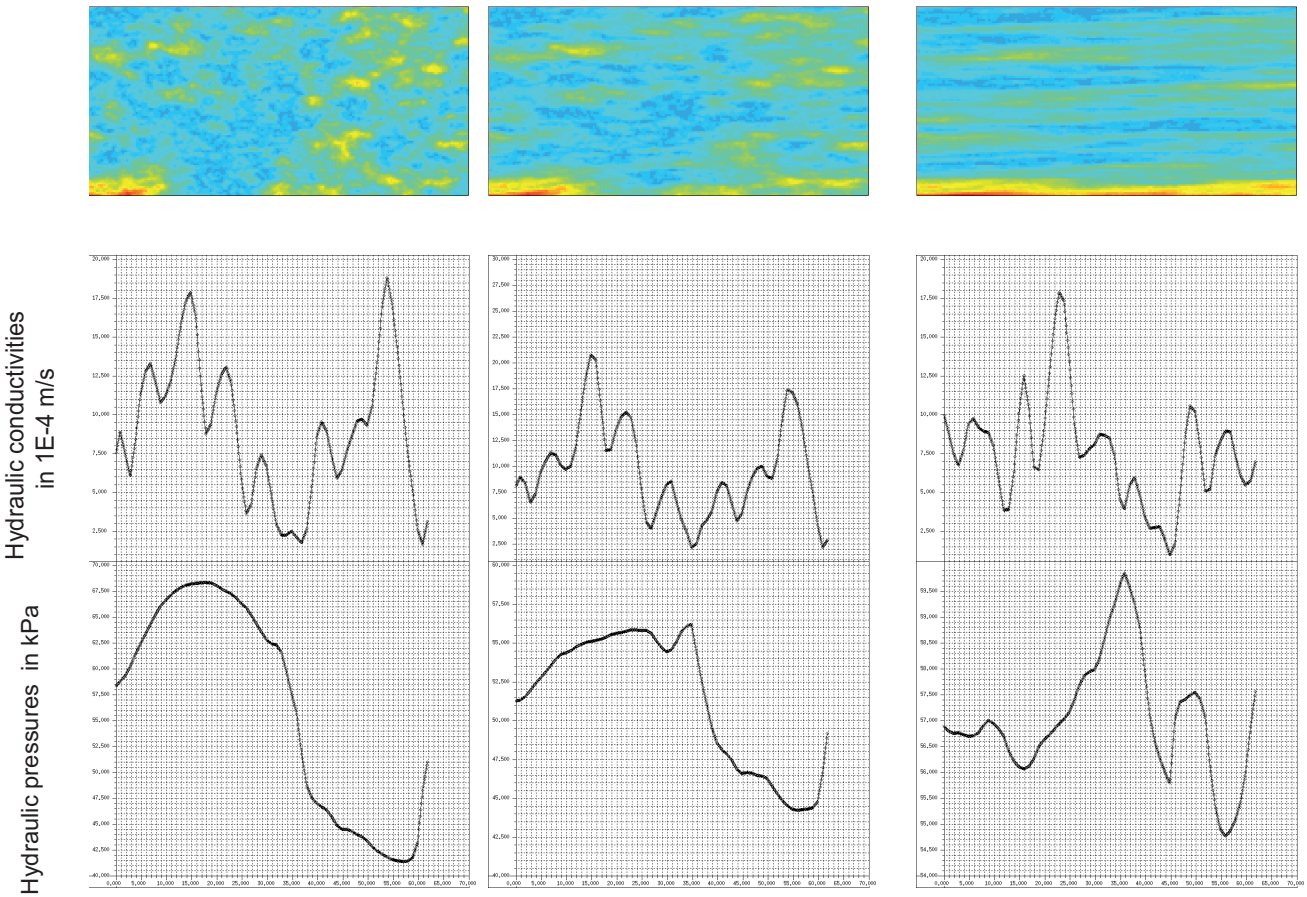

1A32 1A68 1A77

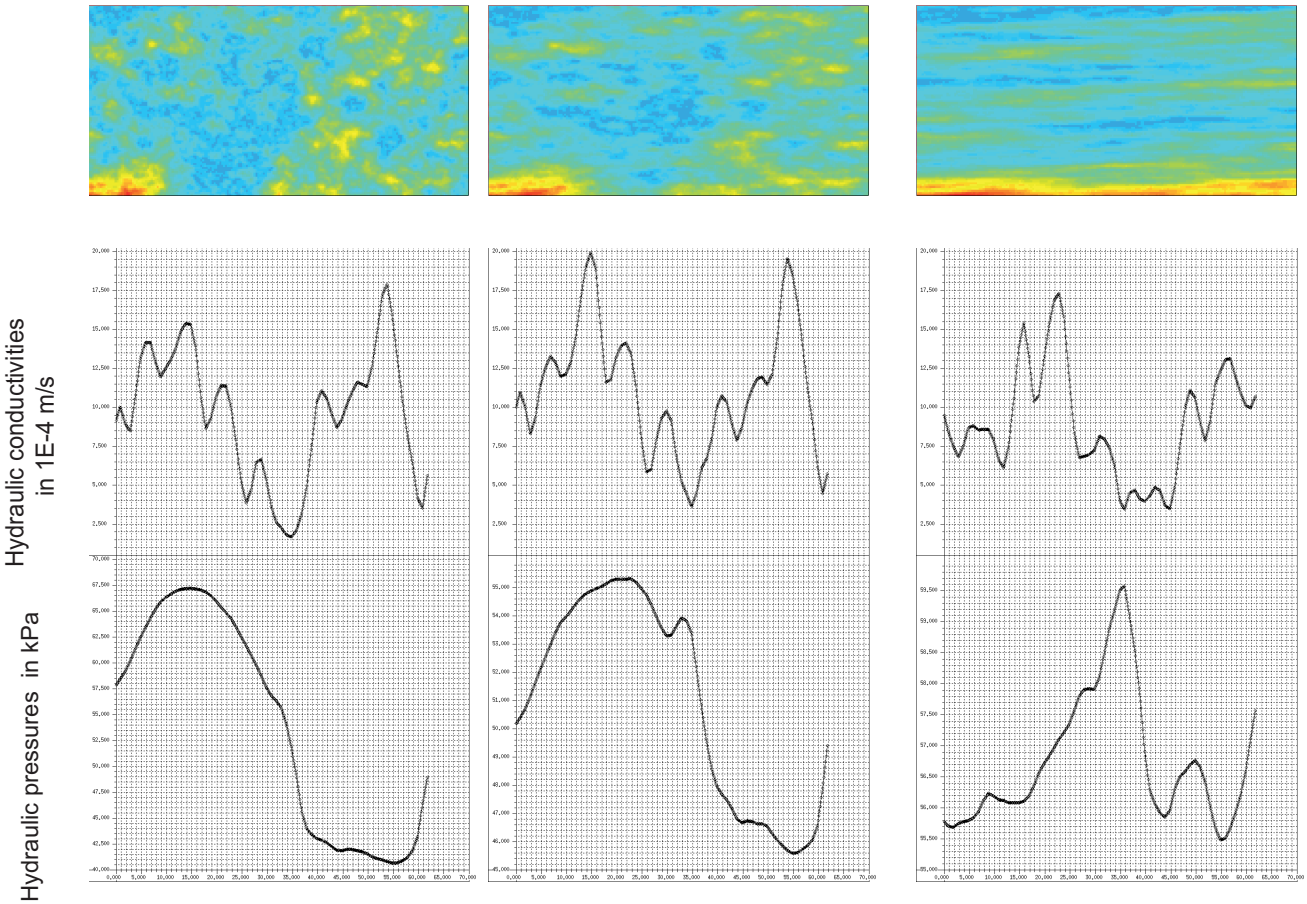

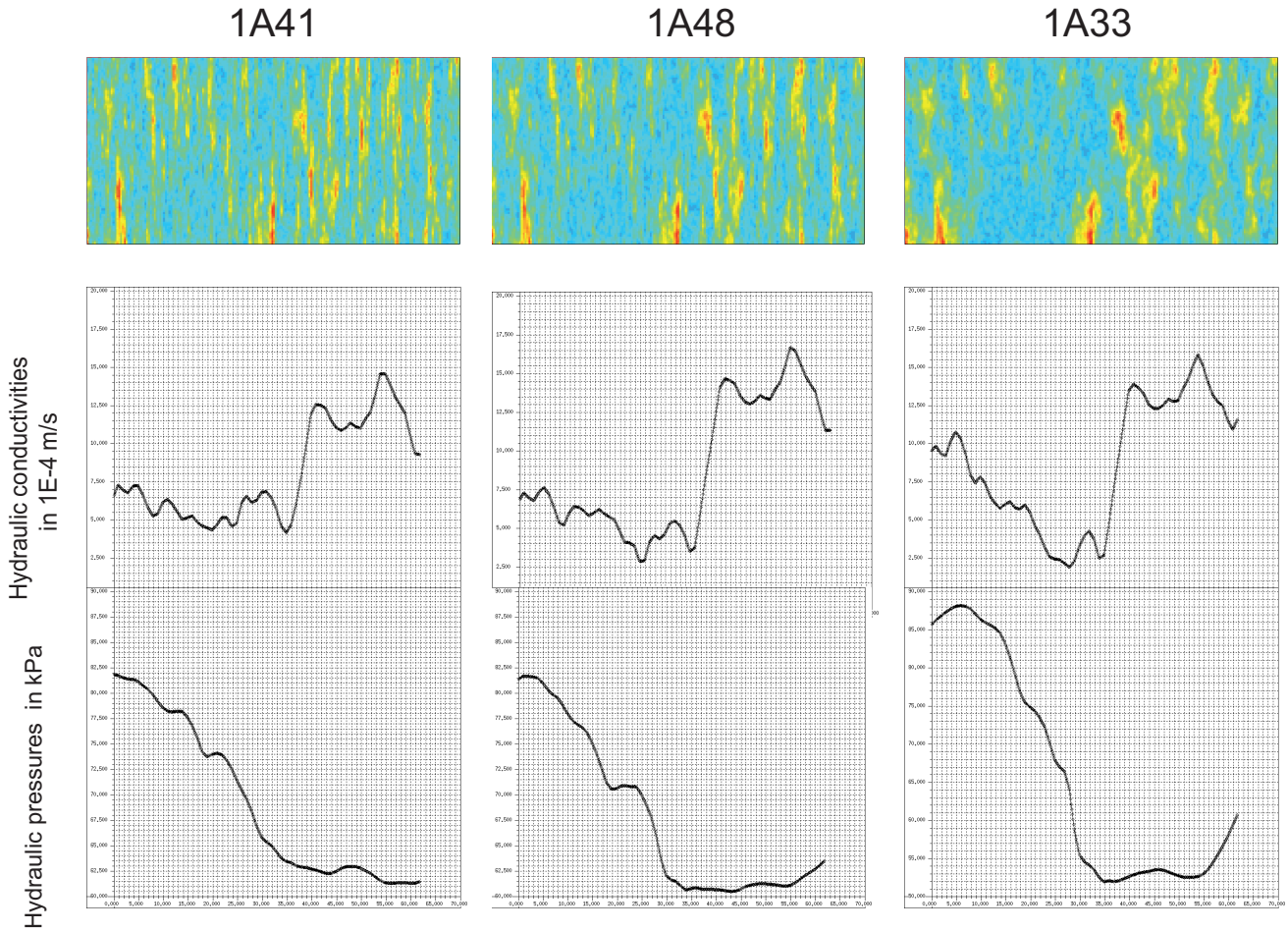
1A41
1A48
1A33
Hydraulic conductivities in 1E-4 m/s
Hydraulic pressures in kPa

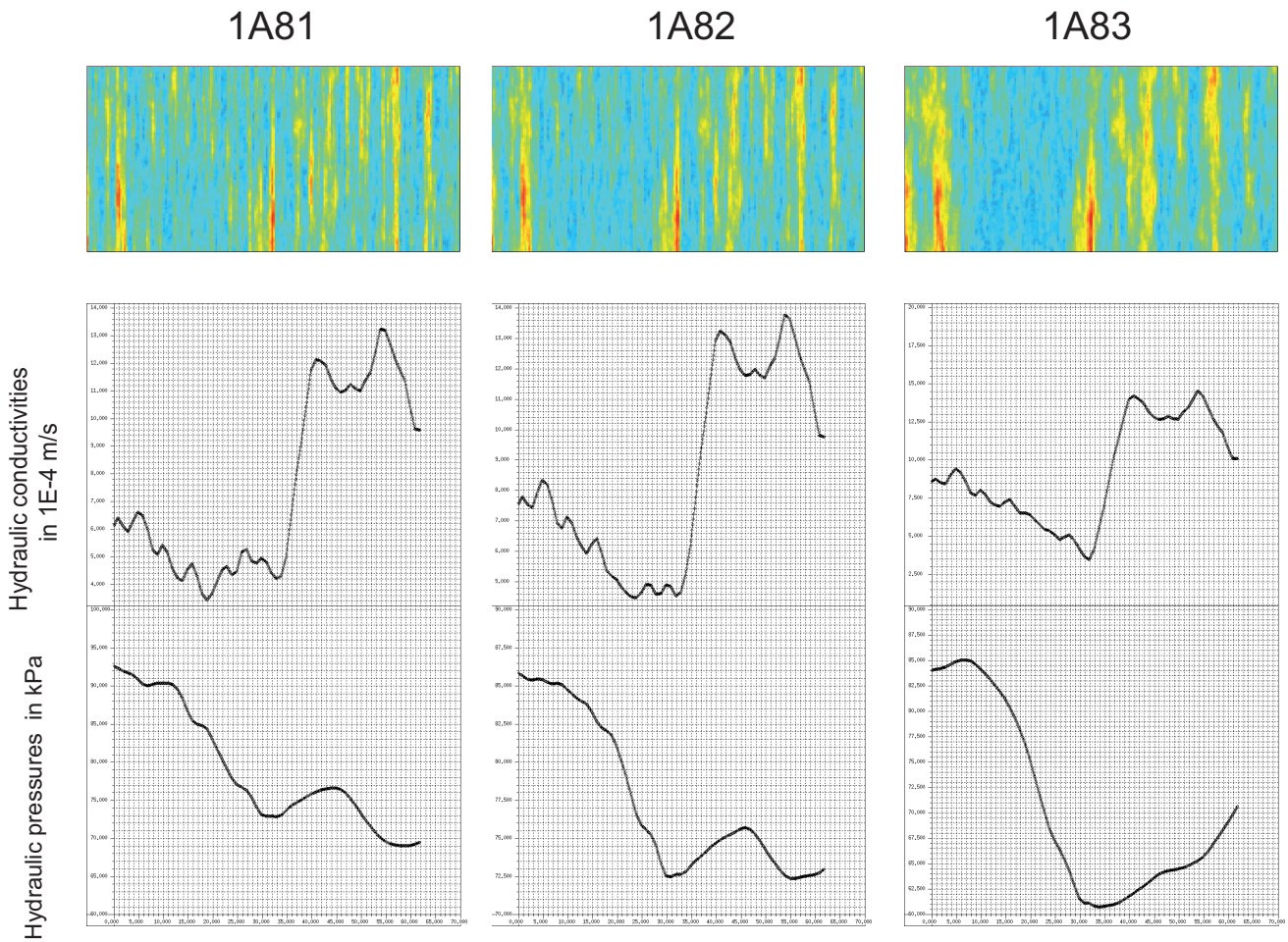
1A81
1A82
1A83
Hydraulic conductivities in 1E-4 m/s
Hydraulic pressures in kPa

1A55

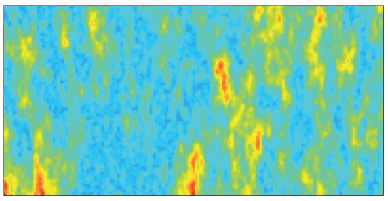

1A34

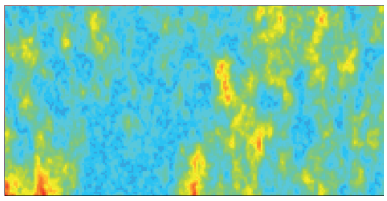

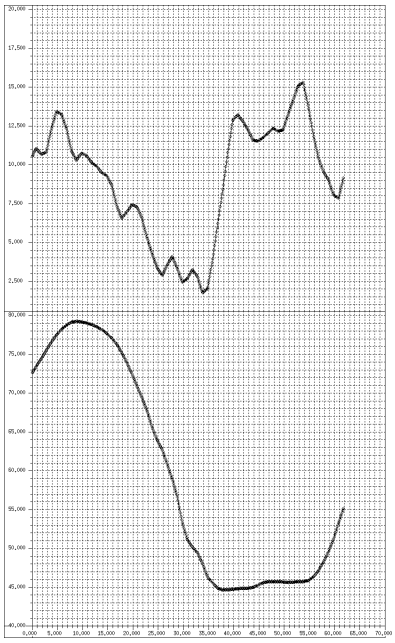

1A62

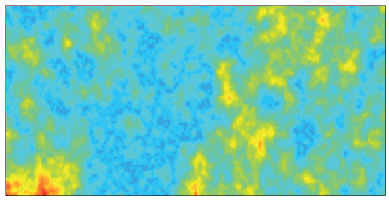

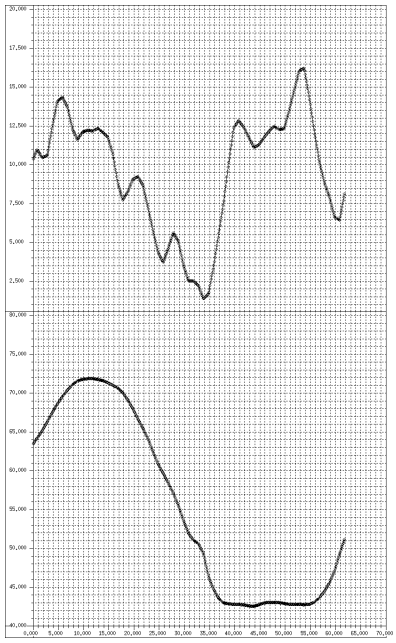

1A84

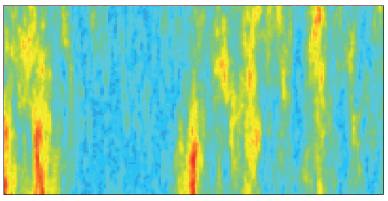

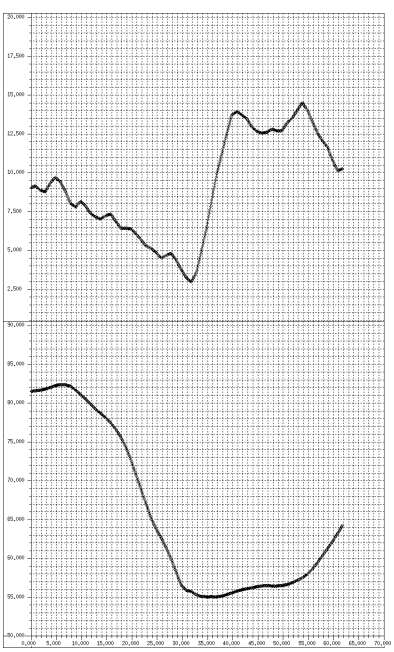

1A85

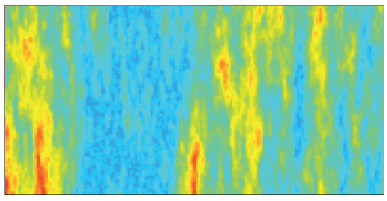

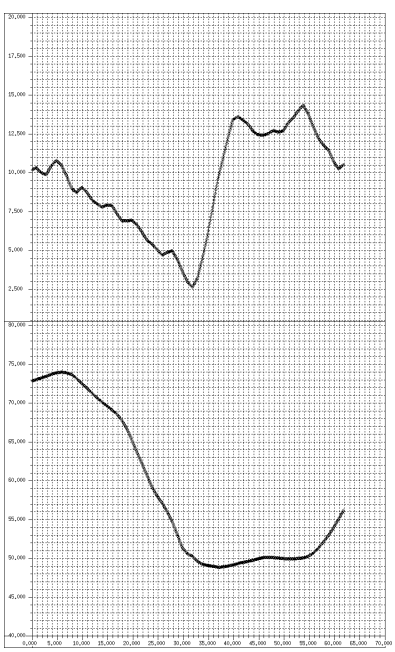

1A86

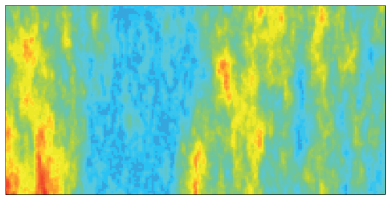

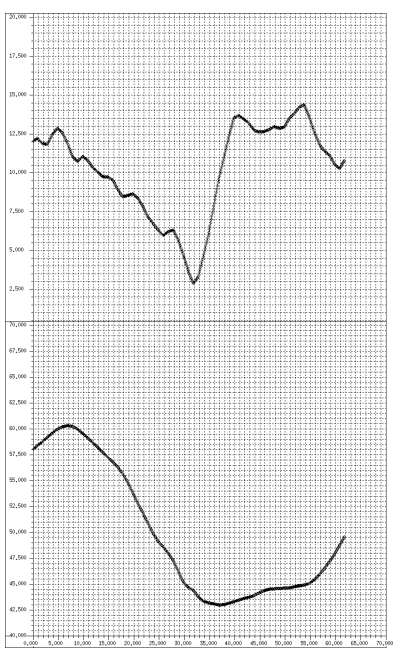

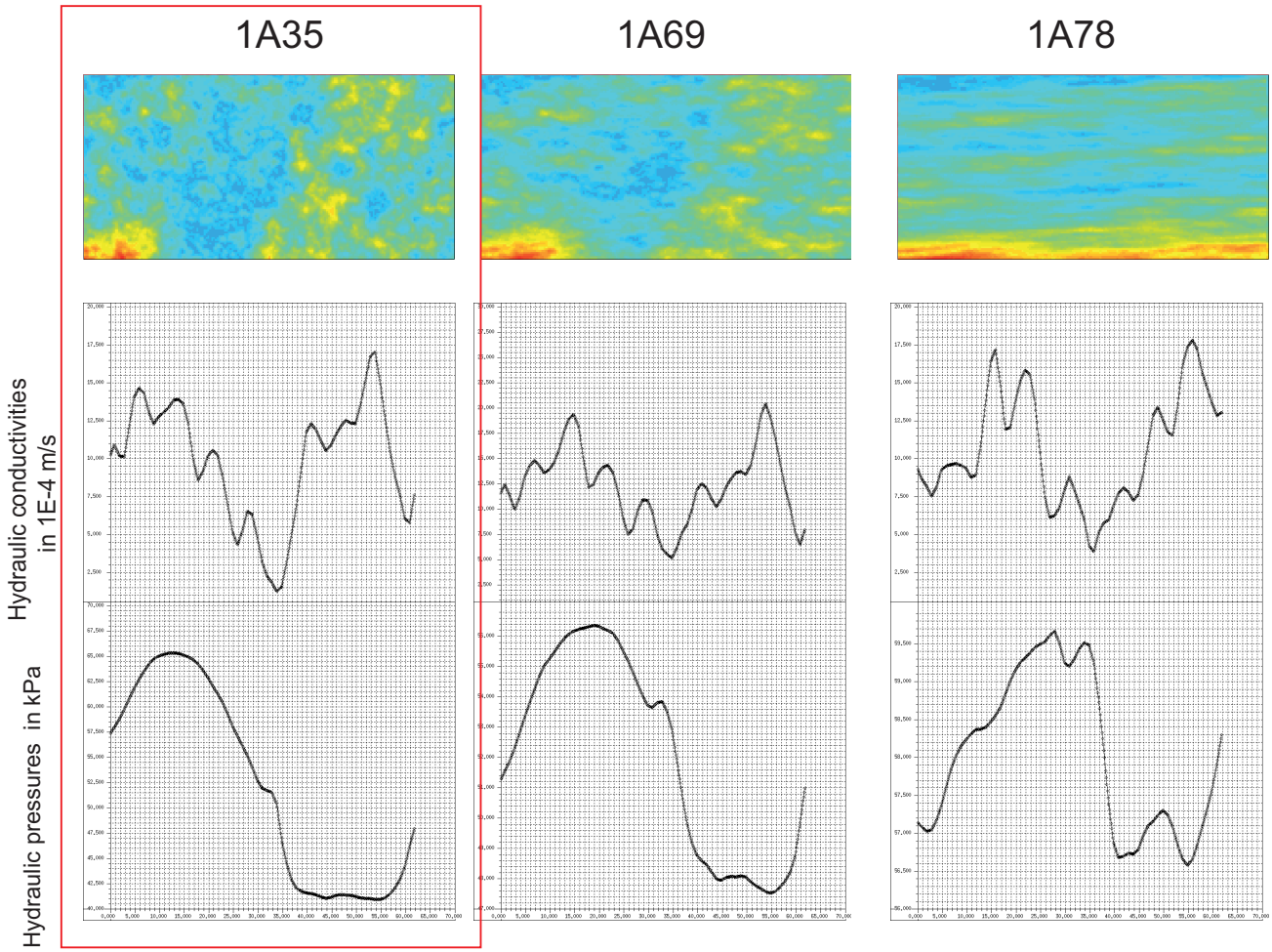
1A35
1A69
1A78
Hydraulic conductivities in 1E-4 m/s
Hydraulic pressures in kPa

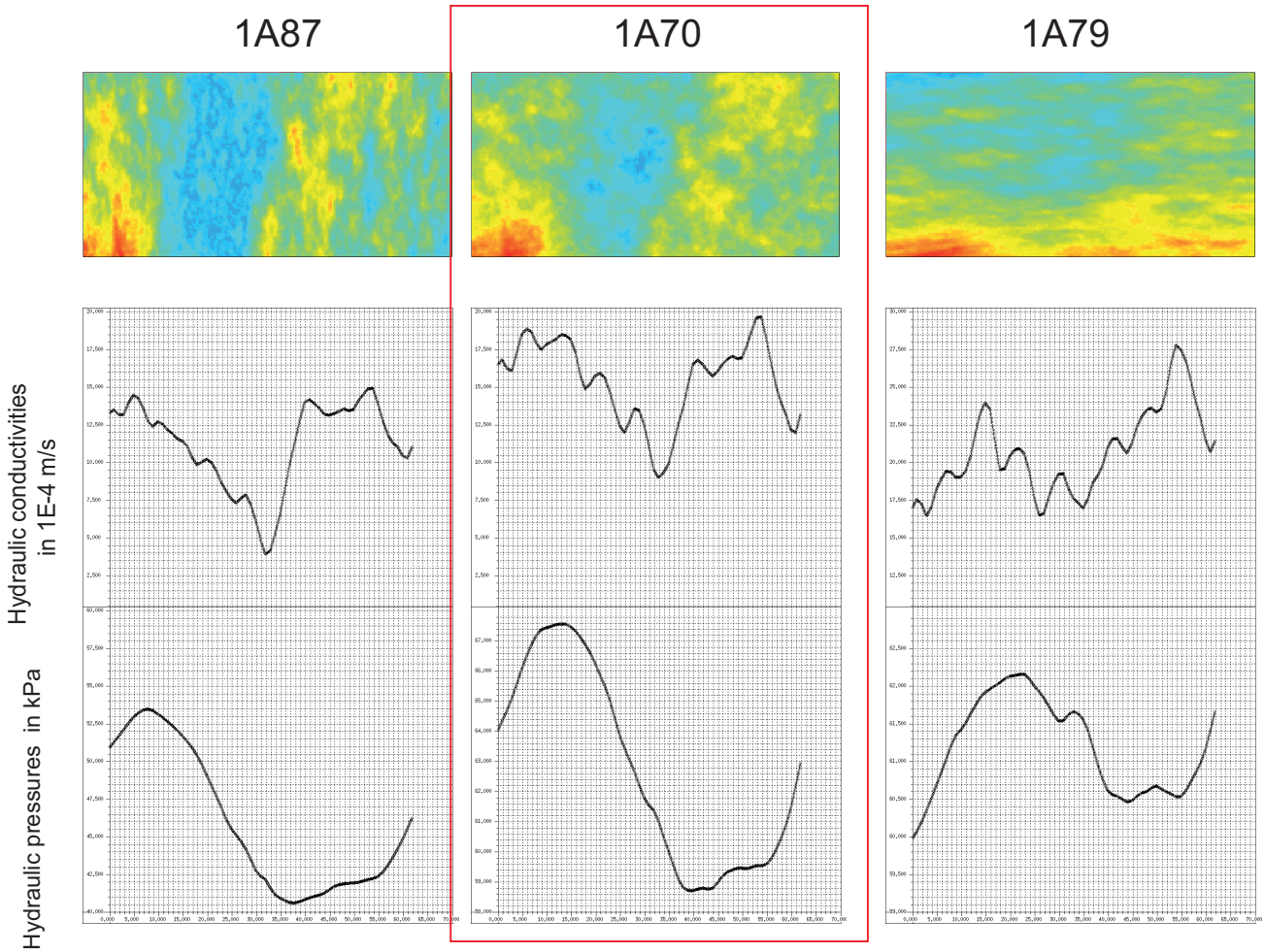
1A87
1A70
1A79
Hydraulic conductivities in 1E-4 m/s
Hydraulic pressures in kPa

1A88 1A89 1A90

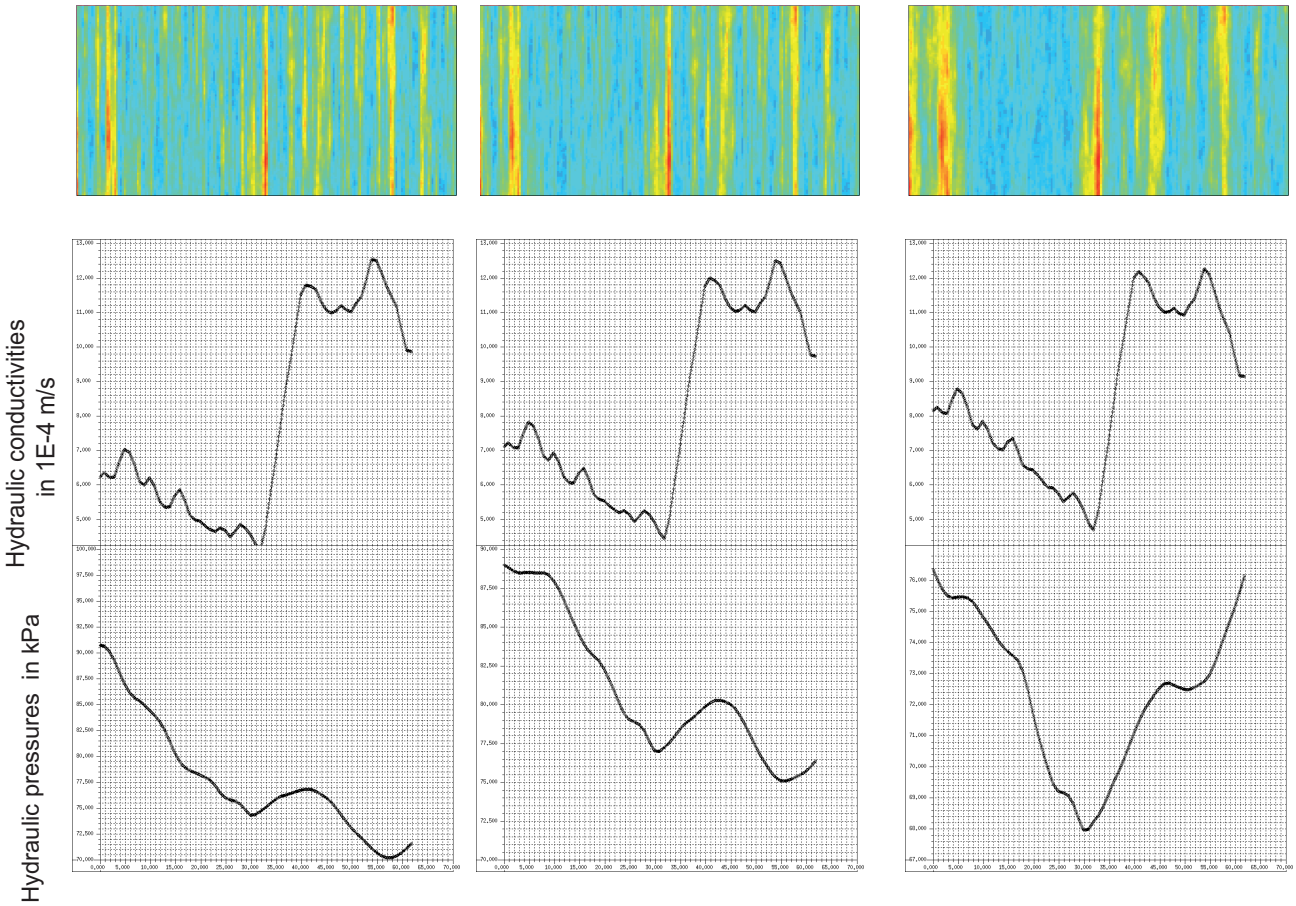

1A91 1A92 1A93

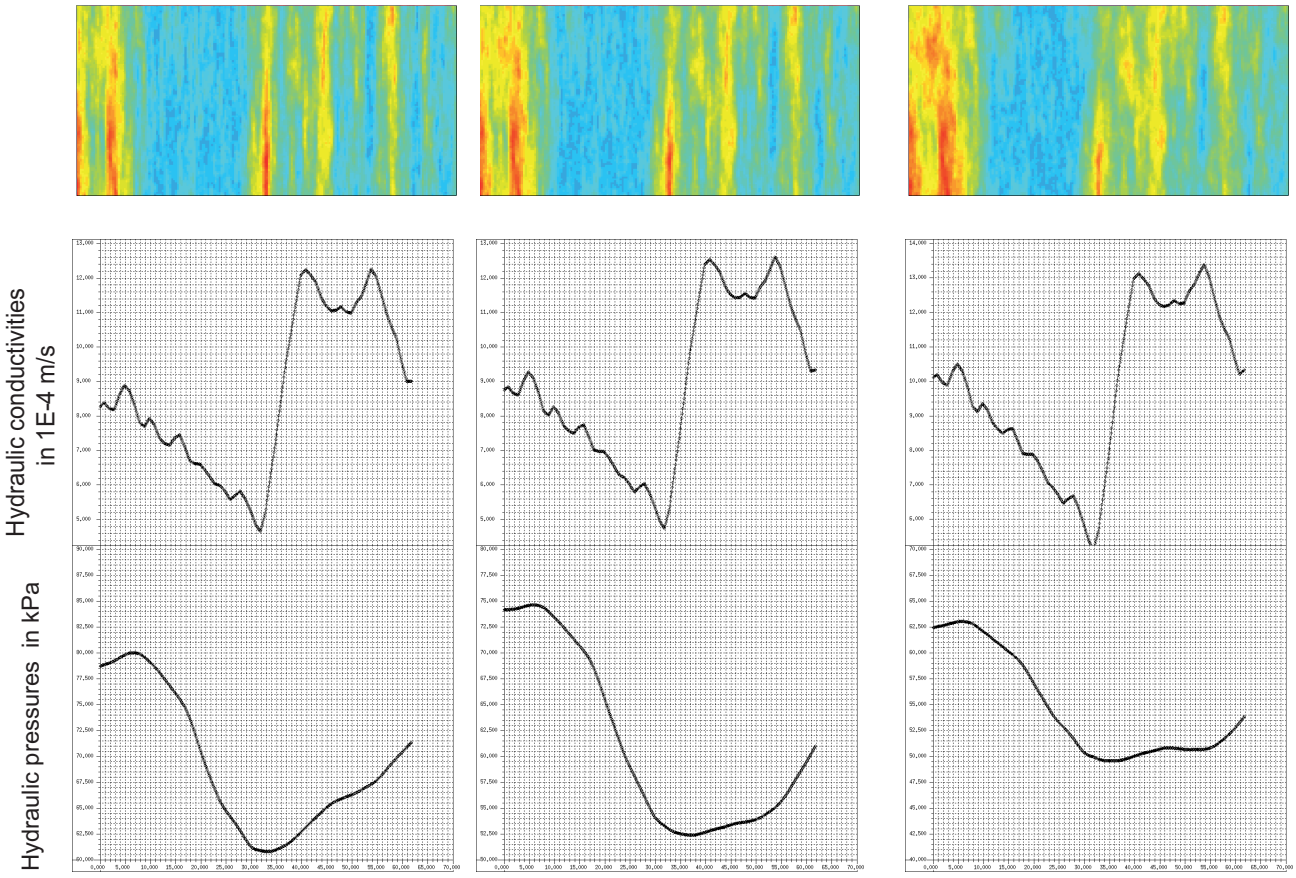

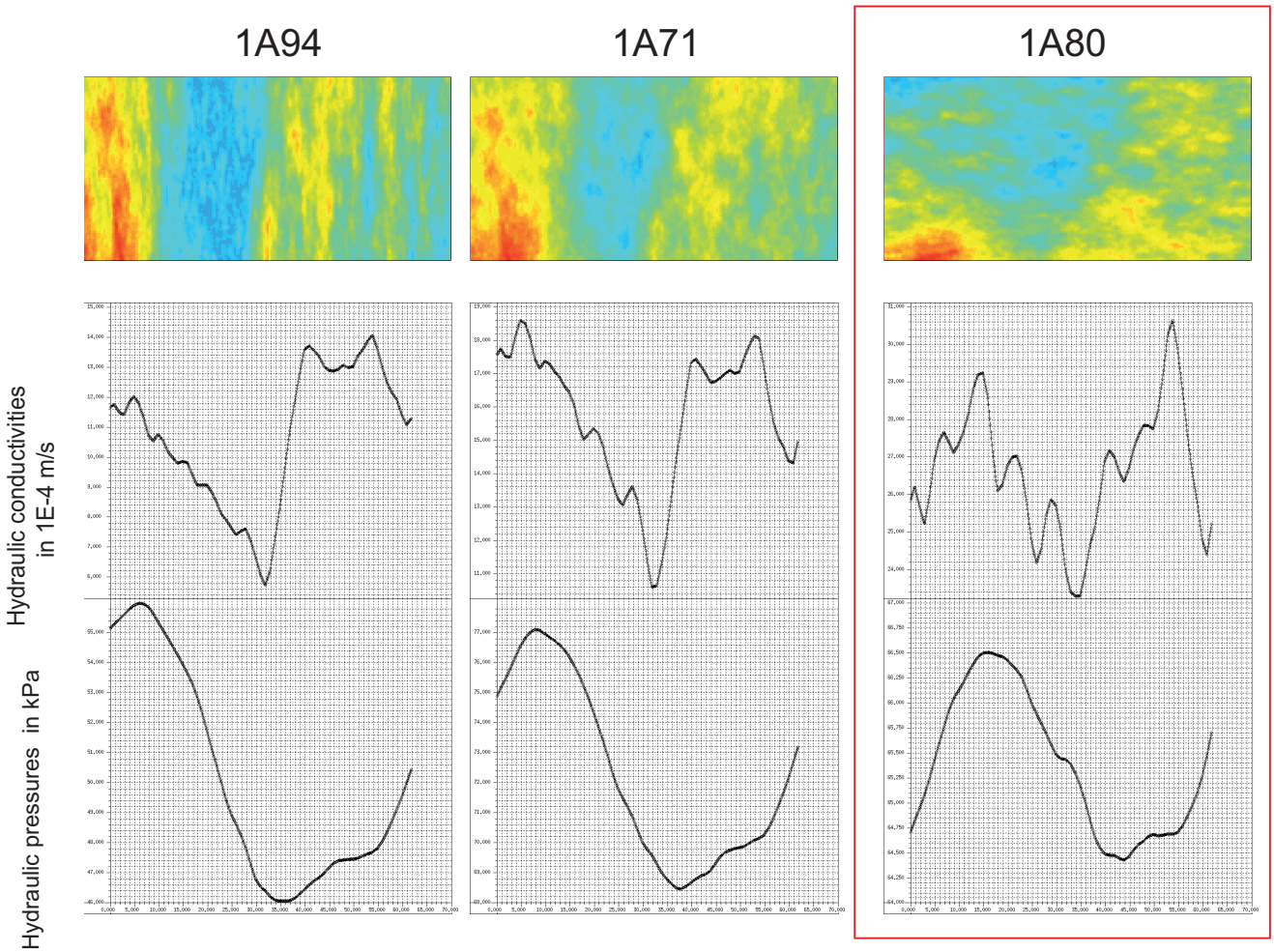
1A94
1A71
1A80
Hydraulic conductivities in 1E-4 m/s
Hydraulic pressures in kPa

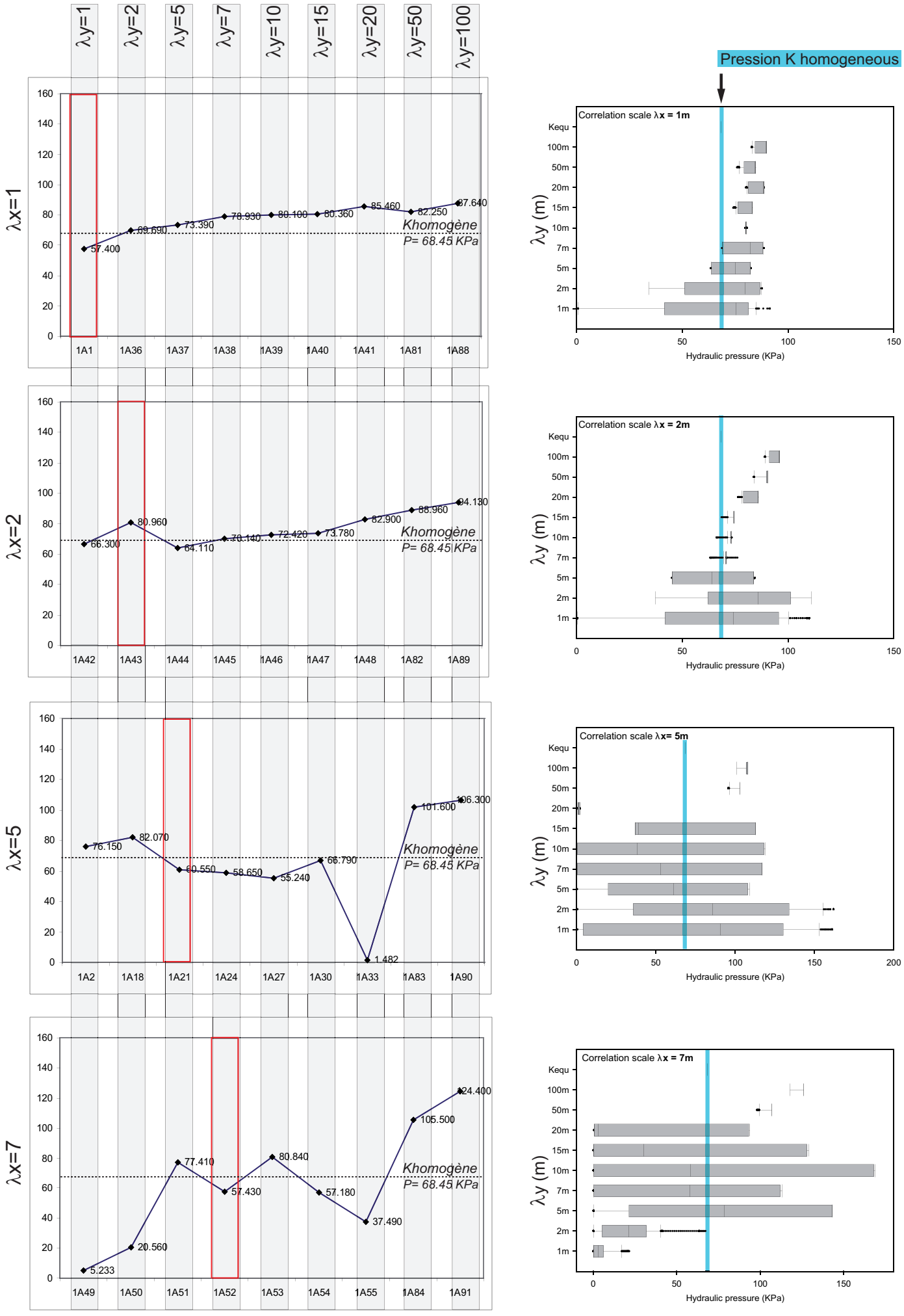
λy=1
λy=2
λy=5
λy=7
λy=10
λy=15
λy=20
λy=50
λy=100
λx=1
λx=2
λx=5
λx=7
Khomogène
P= 68.45 KPa
Pression K homogeneous
Correlation scale λx = 1m
Correlation scale λx = 2m
Correlation scale λx= 5m
Correlation scale λx = 7m
Kequ
100m
50m
20m
15m
10m
7m
5m
2m
1m
λy (m)
Hydraulic pressure (KPa)

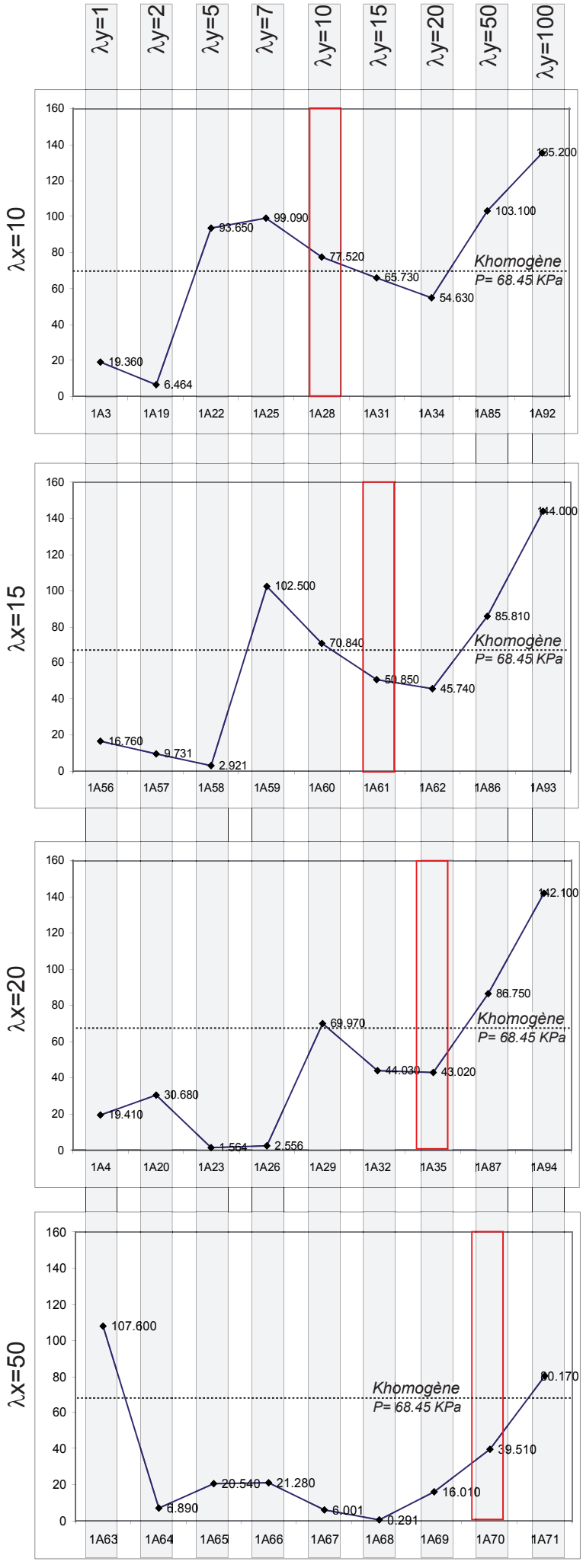
λy=1
λy=2
λy=5
λy=7
λy=10
λy=15
λy=20
λy=50
λy=100
λx=10
19.360
6.464
93.650
99.090
77.520
65.730
54.630
103.100
135.200
Khomogène
P= 68.45 KPa
1A3
1A19
1A22
1A25
1A28
1A31
1A34
1A85
1A92
λx=15
16.760
9.731
2.921
102.500
70.840
50.850
45.740
85.810
114.000
Khomogène
P= 68.45 KPa
1A56
1A57
1A58
1A59
1A60
1A61
1A62
1A86
1A93
λx=20
19.410
30.680
1.564
2.556
69.970
44.030
43.020
86.750
112.100
Khomogène
P= 68.45 KPa
1A4
1A20
1A23
1A26
1A29
1A32
1A35
1A87
1A94
λx=50
107.600
6.890
20.540
21.280
6.001
0.291
16.010
39.510
80.170
Khomogène
P= 68.45 KPa
1A63
1A64
1A65
1A66
1A67
1A68
1A69
1A70
1A71

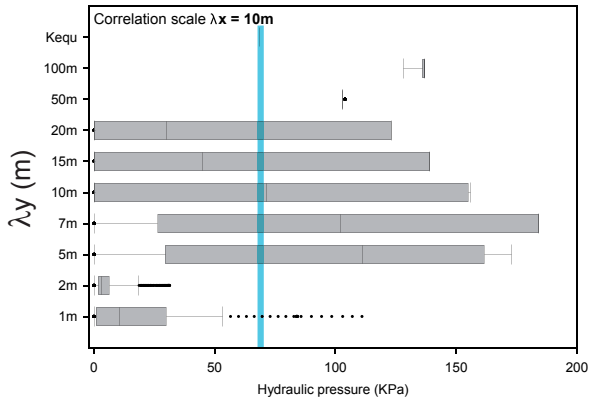
Correlation scale λx = 10m
Kequ
100m
50m
20m
15m
10m
7m
5m
2m
1m
λy (m)
Hydraulic pressure (KPa)

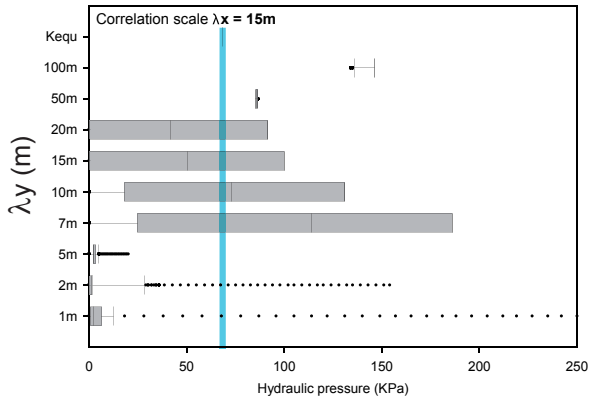
Correlation scale λx = 15m
Kequ
100m
50m
20m
15m
10m
7m
5m
2m
1m
λy (m)
Hydraulic pressure (KPa)

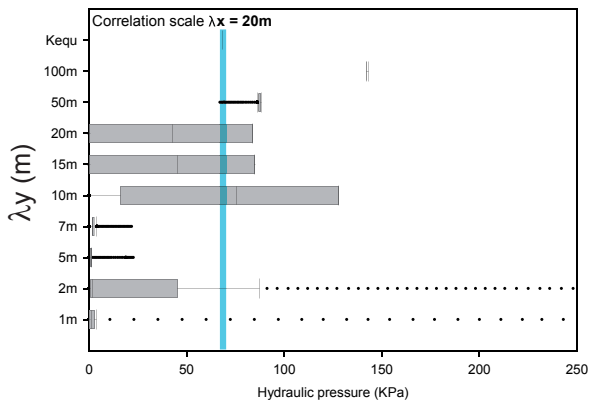
Correlation scale λx = 20m
Kequ
100m
50m
20m
15m
10m
7m
5m
2m
1m
λy (m)
Hydraulic pressure (KPa)

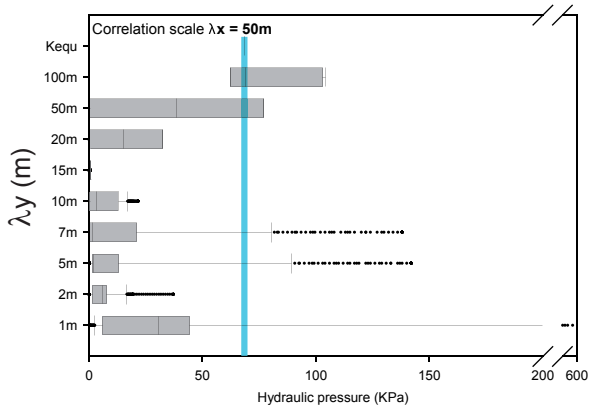
Correlation scale λx = 50m
Kequ
100m
50m
20m
15m
10m
7m
5m
2m
1m
λy (m)
Hydraulic pressure (KPa)

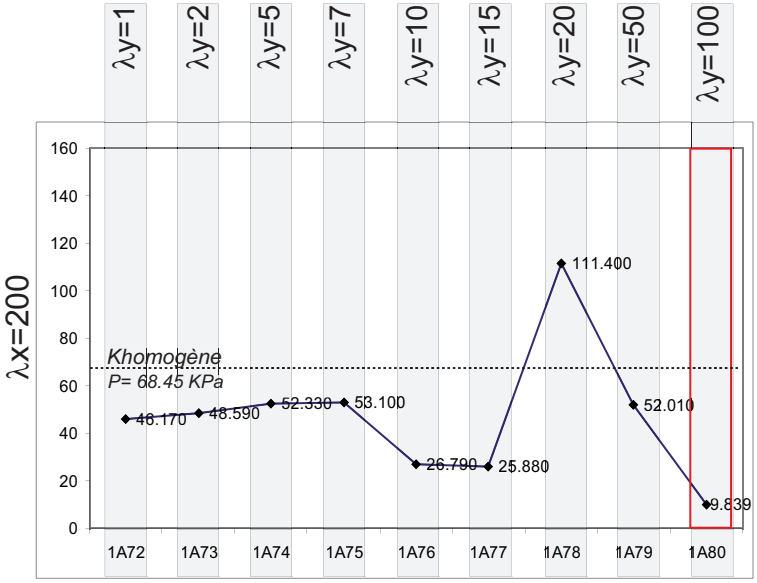
λy=1
λy=2
λy=5
λy=7
λy=10
λy=15
λy=20
λy=50
λy=100
λx=200
160
140
120
100
80
60
40
20
0
Khomogène
P= 68.45 KPa
46.170
48.590
52.330
53.100
26.790
25.880
111.400
52.010
9.839
1A72
1A73
1A74
1A75
1A76
1A77
1A78
1A79
1A80

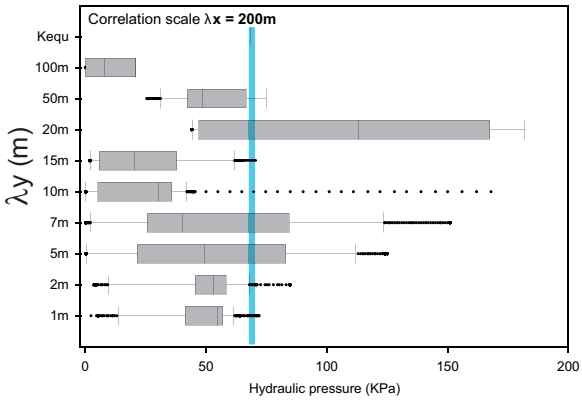
Correlation scale λx = 200m
Kequ
100m
50m
20m
15m
10m
7m
5m
2m
1m
λy (m)
0
50
100
150
200
Hydraulic pressure (KPa)

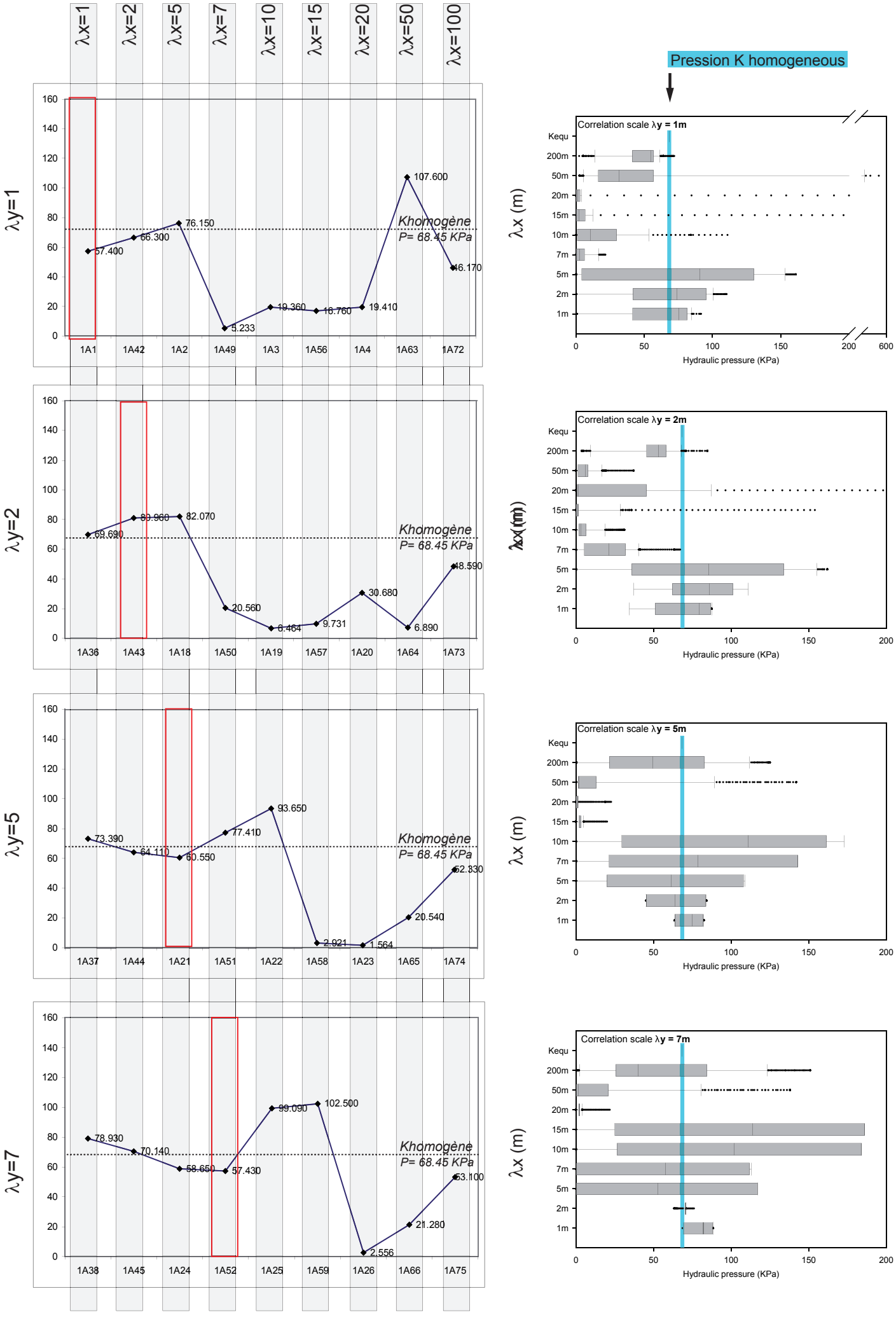
λx=1
λx=2
λx=5
λx=7
λx=10
λx=15
λx=20
λx=50
λx=100
λy=1
λy=2
λy=5
λy=7
Khomogène
P= 68.45 KPa
57.400
66.300
76.150
5.233
19.360
16.760
19.410
107.600
46.170
69.690
80.960
82.070
20.560
6.464
9.731
30.680
6.890
48.590
73.390
64.110
60.550
77.410
93.650
2.921
1.564
20.540
52.330
78.930
70.140
58.650
57.430
99.090
102.500
2.556
21.280
53.100
1A1
1A42
1A2
1A49
1A3
1A56
1A4
1A63
1A72
1A36
1A43
1A18
1A50
1A19
1A57
1A20
1A64
1A73
1A37
1A44
1A21
1A51
1A22
1A58
1A23
1A65
1A74
1A38
1A45
1A24
1A52
1A25
1A59
1A26
1A66
1A75
Pression K homogeneous
Correlation scale λy = 1m
Correlation scale λy = 2m
Correlation scale λy = 5m
Correlation scale λy = 7m
λx (m)
Hydraulic pressure (KPa)
Kequ
200m
50m
20m
15m
10m
7m
5m
2m
1m

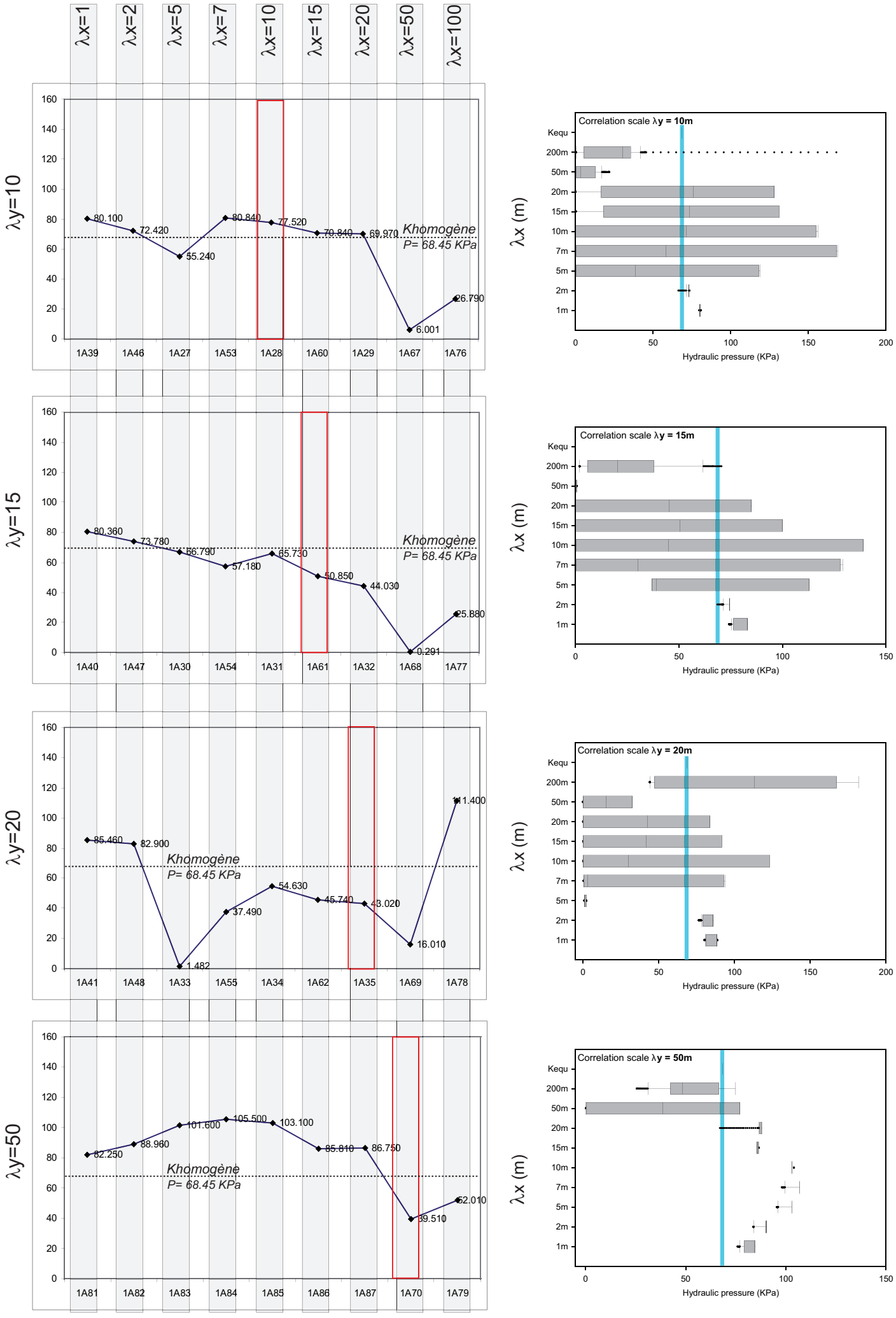
λx=1
λx=2
λx=5
λx=7
λx=10
λx=15
λx=20
λx=50
λx=100
λy=10
80.100
72.420
55.240
80.840
77.520
70.840
69.970
6.001
26.790
Khomogène
P= 68.45 KPa
1A39
1A46
1A27
1A53
1A28
1A60
1A29
1A67
1A76
Correlation scale λy = 10m
λy=15
80.360
73.780
66.790
57.180
65.730
50.850
44.030
0.291
25.880
1A40
1A47
1A30
1A54
1A31
1A61
1A32
1A68
1A77
Correlation scale λy = 15m
λy=20
85.460
82.900
1.482
37.490
54.630
45.740
43.020
15.010
111.400
1A41
1A48
1A33
1A55
1A34
1A62
1A35
1A69
1A78
Correlation scale λy = 20m
λy=50
82.250
88.960
101.600
105.500
103.100
85.810
86.750
39.510
62.010
1A81
1A82
1A83
1A84
1A85
1A86
1A87
1A70
1A79
Correlation scale λy = 50m
λx (m)
Kequ
200m
50m
20m
15m
10m
7m
5m
2m
1m
Hydraulic pressure (KPa)

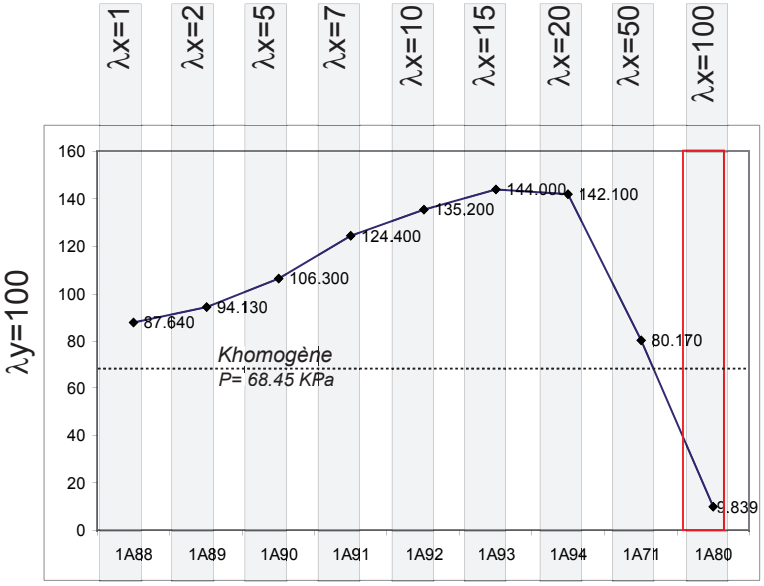
λx=1
λx=2
λx=5
λx=7
λx=10
λx=15
λx=20
λx=50
λx=100
λy=100
160
140
120
100
80
60
40
20
0
87.640
94.130
106.300
124.400
135.200
144.000
142.100
80.170
9.839
Khomogène
P= 68.45 KPa
1A88
1A89
1A90
1A91
1A92
1A93
1A94
1A71
1A80

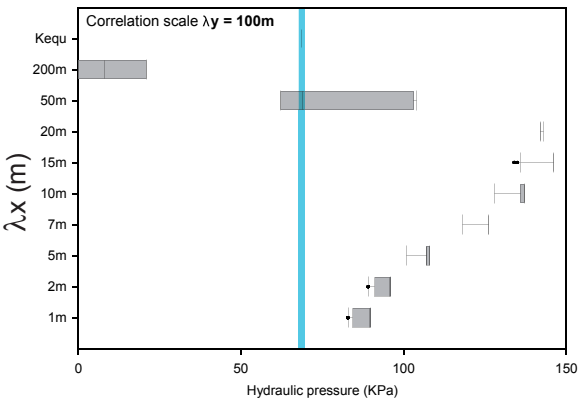
Correlation scale λy = 100m
Kequ
200m
50m
20m
15m
10m
7m
5m
2m
1m
λx (m)
0
50
100
150
Hydraulic pressure (KPa)

Fluid Flux Mass Balance (m3/jour)
Aquisynt_2K

Nx/Ny	Nx=1m	Nx=2m	Nx=5m	Nx=7m	Nx=10m	Nx=15m	Nx=20m	Nx=50m	Nx=200m
1	*1A1* 18.78	*1A42* 16.59	*1A2* 32.76	*1A49* 47.70	*1A3* 90.74	*1A56* 237.38	*1A4* 216.05	*1A63* 3764.59	*1A72* 10487.08
2	*1A36* 15.48	*1A43* 14.06	*1A18* 23.57	*1A50* 32.58	*1A19* 46.52	*1A57* 83.62	*1A20* 115.22	*1A64* 3313.40	*1A73* 11509.27
5	*1A37* 11.24	*1A44* 10.98	*1A21* 15.92	*1A51* 21.89	*1A22* 25.84	*1A58* 31.34	*1A23* 37.23	*1A65* 2645.28	*1A74* 13615.08
7	*1A38* 10.54	*1A45* 10.10	*1A24* 14.38	*1A52* 16.19	*1A25* 23.06	*1A59* 25.52	*1A26* 26.52	*1A66* 2860.61	*1A75* 16572.92
10	*1A39* 16.05	*1A46* 9.74	*1A27* 13.01	*1A53* 14.99	*1A28* 15.32	*1A60* 17.22	*1A29* 19.25	*1A67* 2802.37	*1A76* 11512.29
15	*1A40* 10.32	*1A47* 9.04	*1A30* 11.29	*1A54* 13.08	*1A31* 13.25	*1A61* 13.82	*1A32* 13.91	*1A68* 23.45	*1A77* 10134.84
20	*1A41* 10.33	*1A48* 8.65	*1A33* 11.75	*1A55* 12.73	*1A34* 12.83	*1A62* 12.56	*1A35* 12.45	*1A69* 15.85	*1A78* 9270.09
50	*1A81* 10.77	*1A82* 8.33	*1A83* 8.90	*1A84* 8.88	*1A85* 12.19	*1A86* 13.91	*1A87* 13.69	*1A70* 14.82	*1A79* 10647.49
100	*1A88* 9.36	*1A89* 8.15	*1A90* 8.62	*1A91* 10.08	*1A92* 10.93	*1A93* 12.17	*1A94* 14.00	*1A71* 16.08	*1A80* 17.35

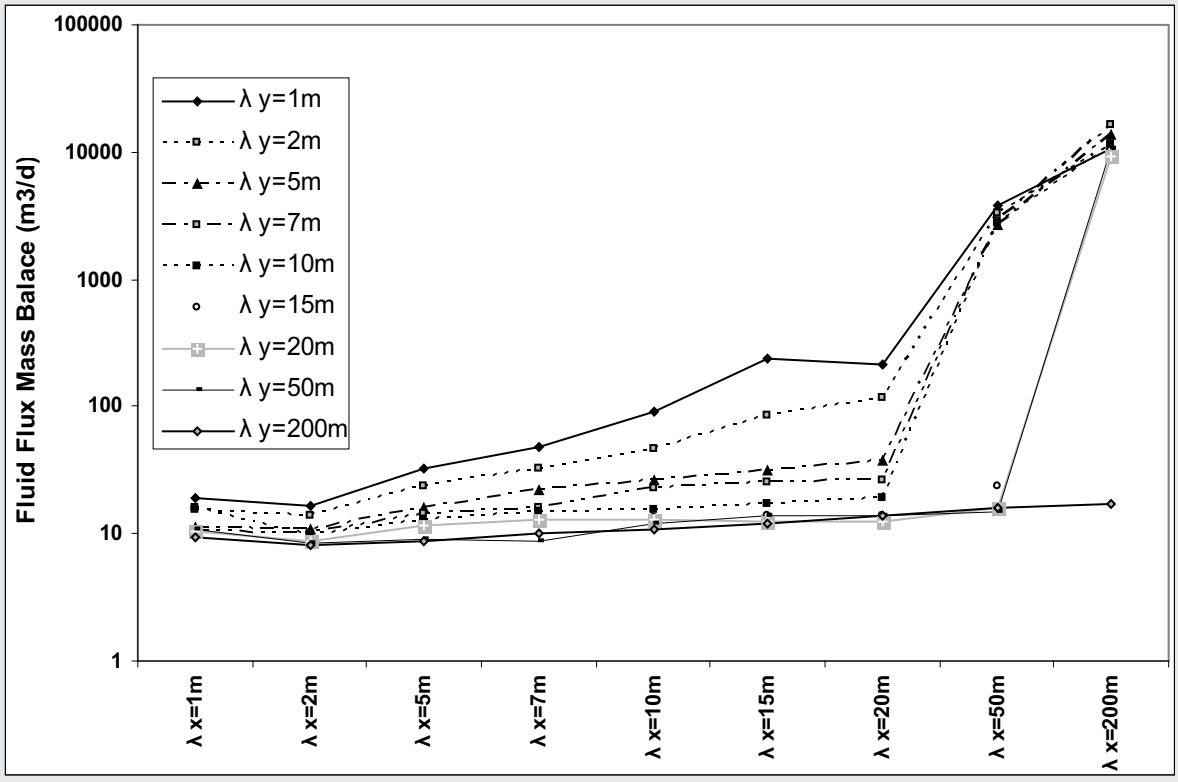

λx=λy

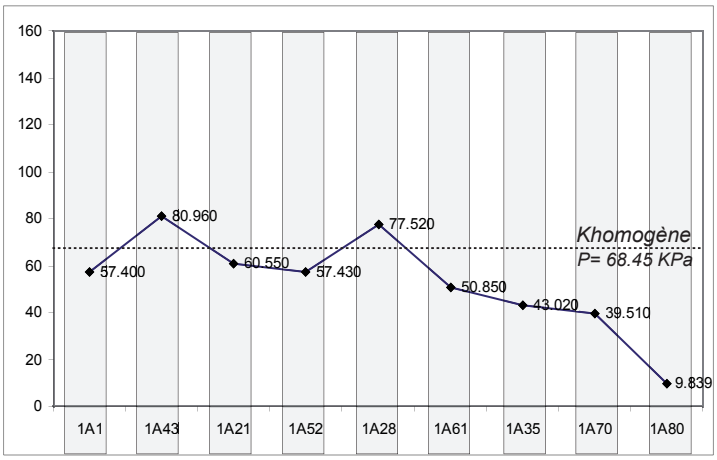

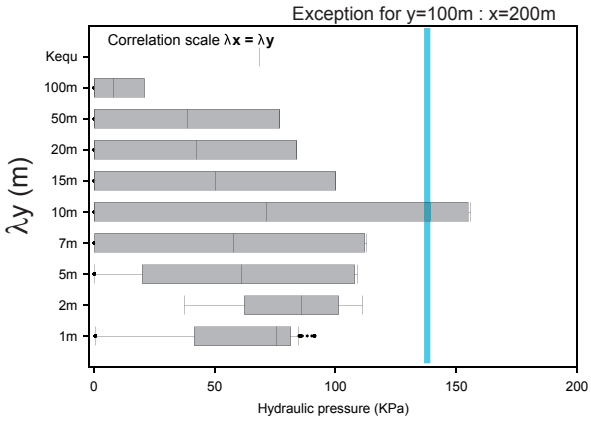

λx inv λy

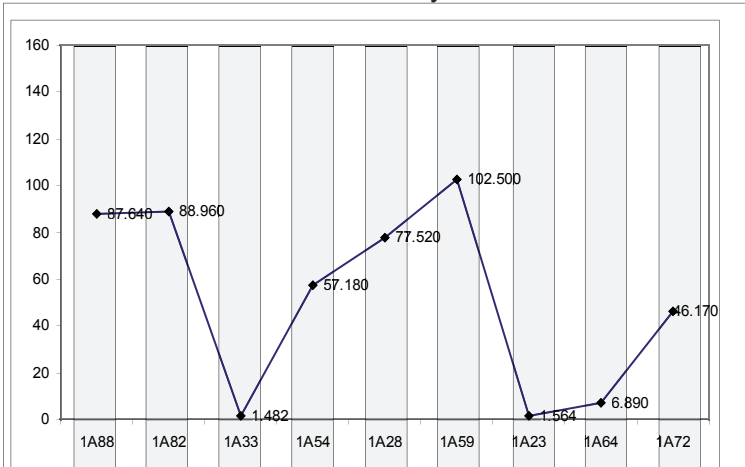

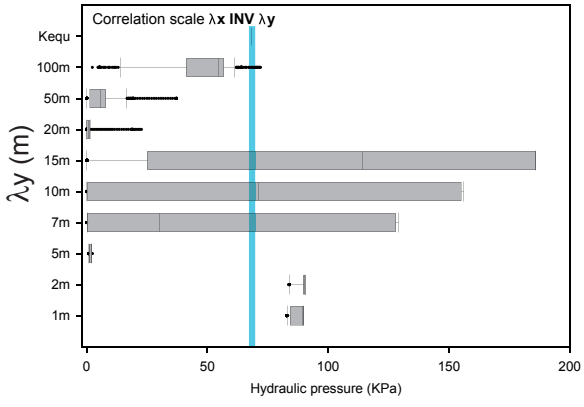

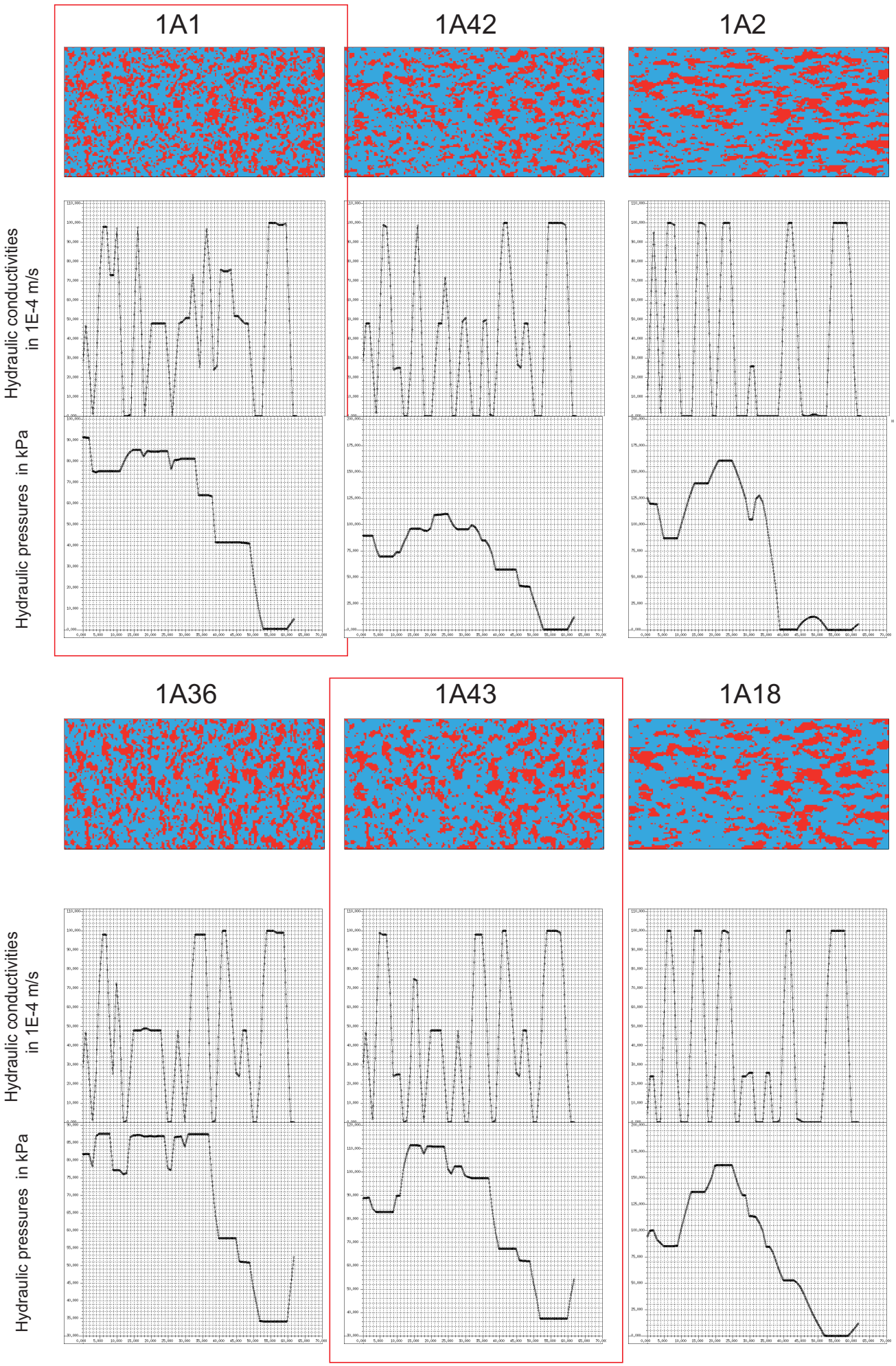
1A1
1A42
1A2
Hydraulic conductivities in 1E-4 m/s
Hydraulic pressures in kPa
1A36
1A43
1A18
Hydraulic conductivities in 1E-4 m/s
Hydraulic pressures in kPa

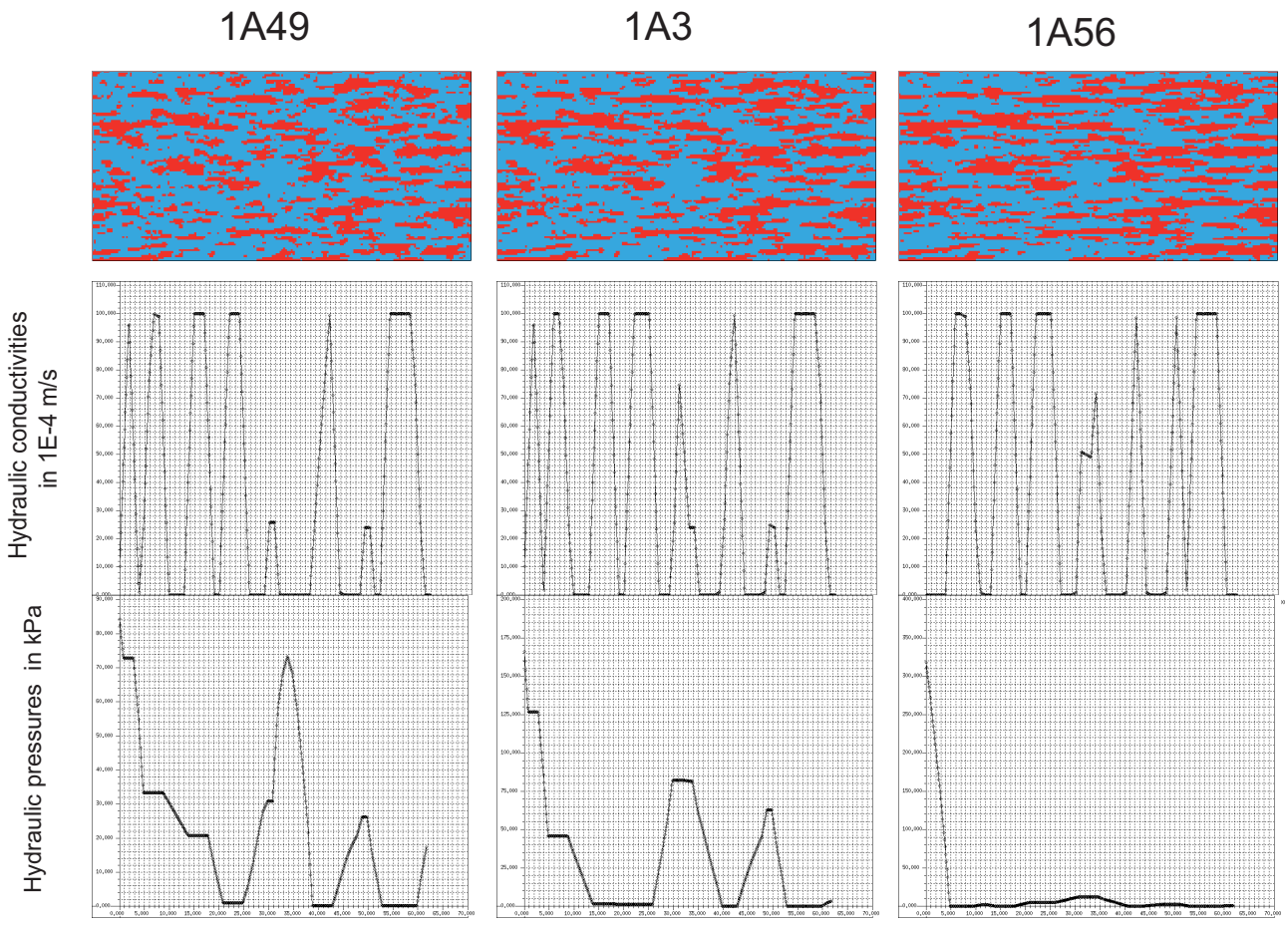
1A49
1A3
1A56
Hydraulic conductivities in 1E-4 m/s
Hydraulic pressures in kPa

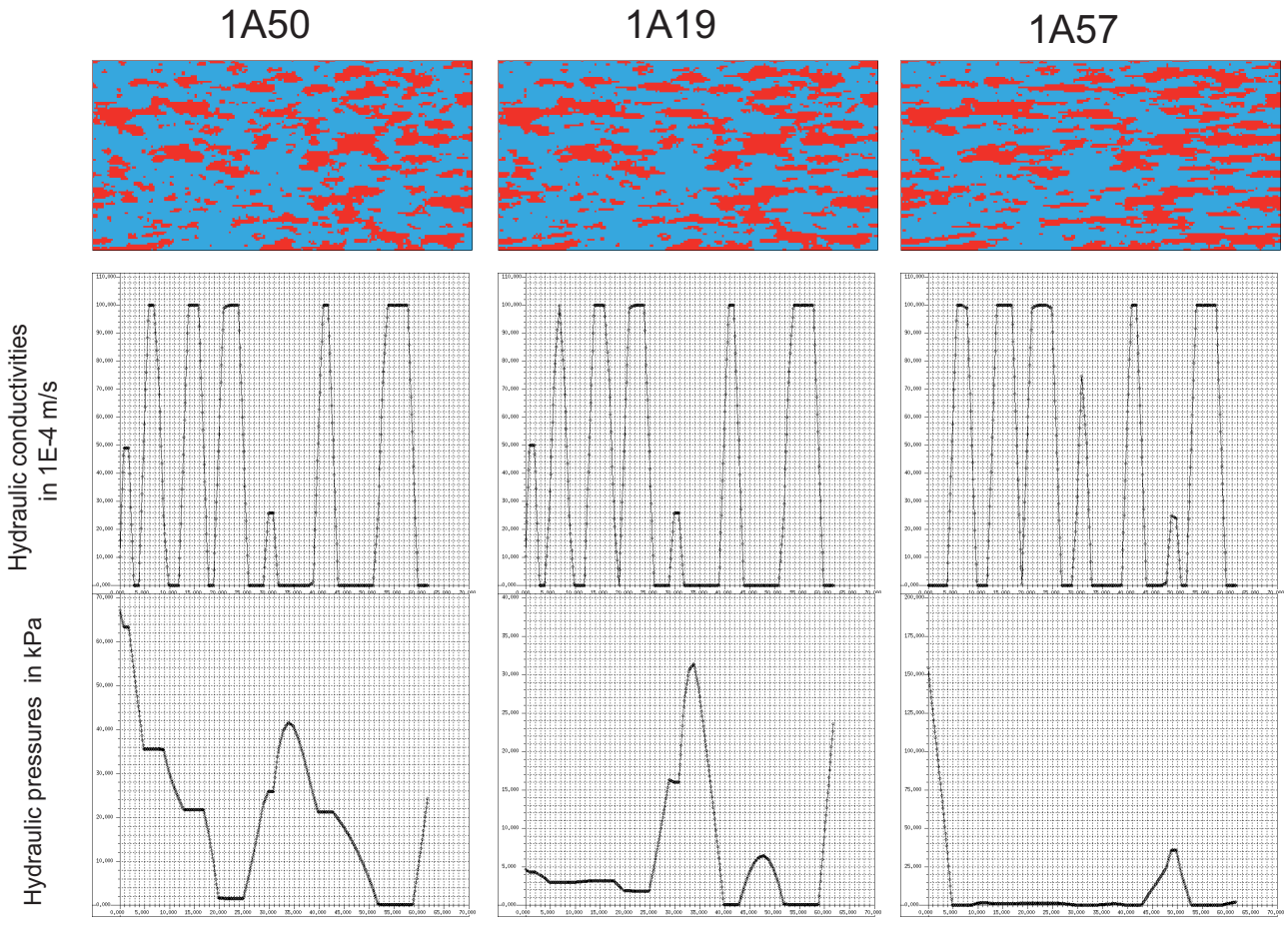
1A50
1A19
1A57
Hydraulic conductivities in 1E-4 m/s
Hydraulic pressures in kPa

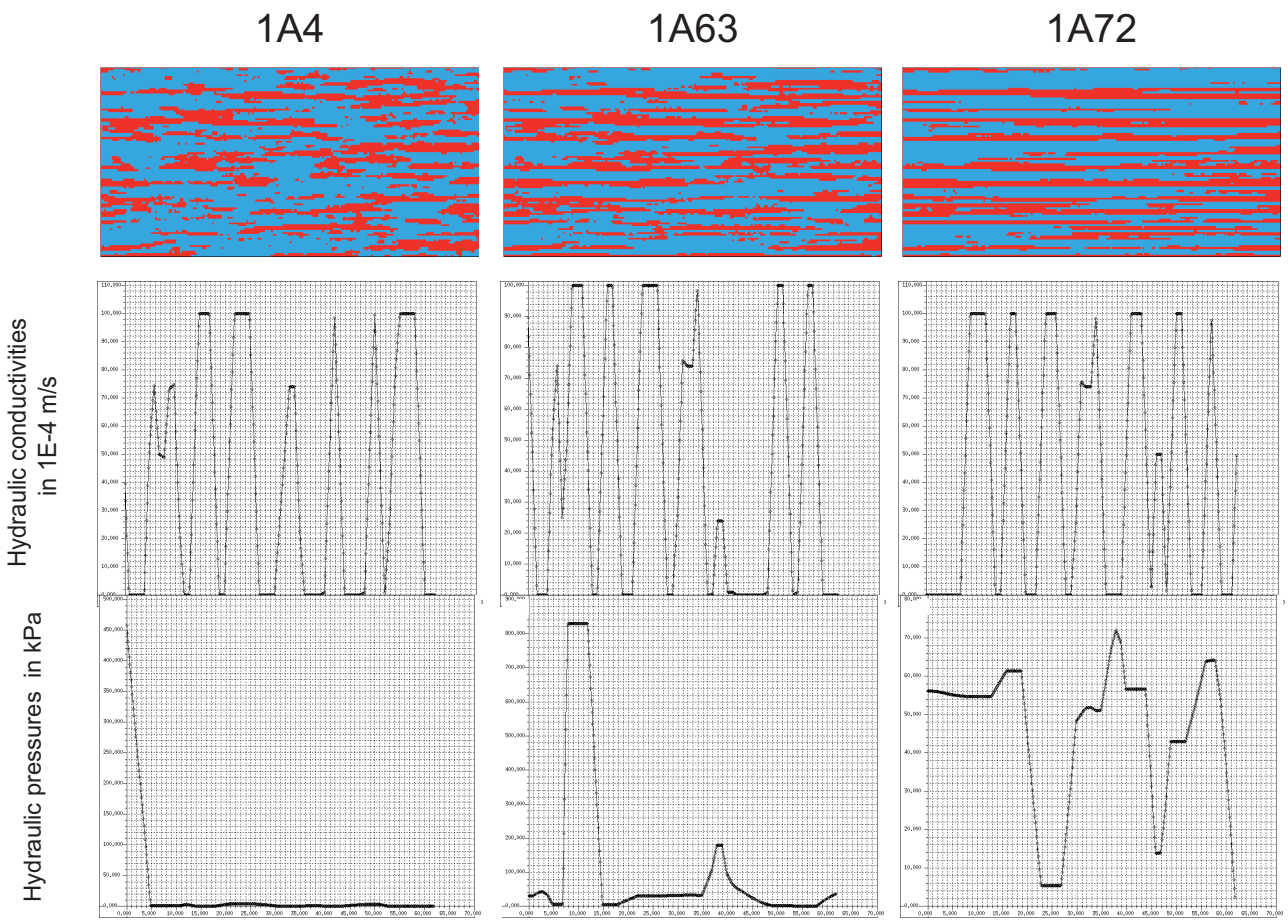
1A4
1A63
1A72
Hydraulic conductivities in 1E-4 m/s
Hydraulic pressures in kPa

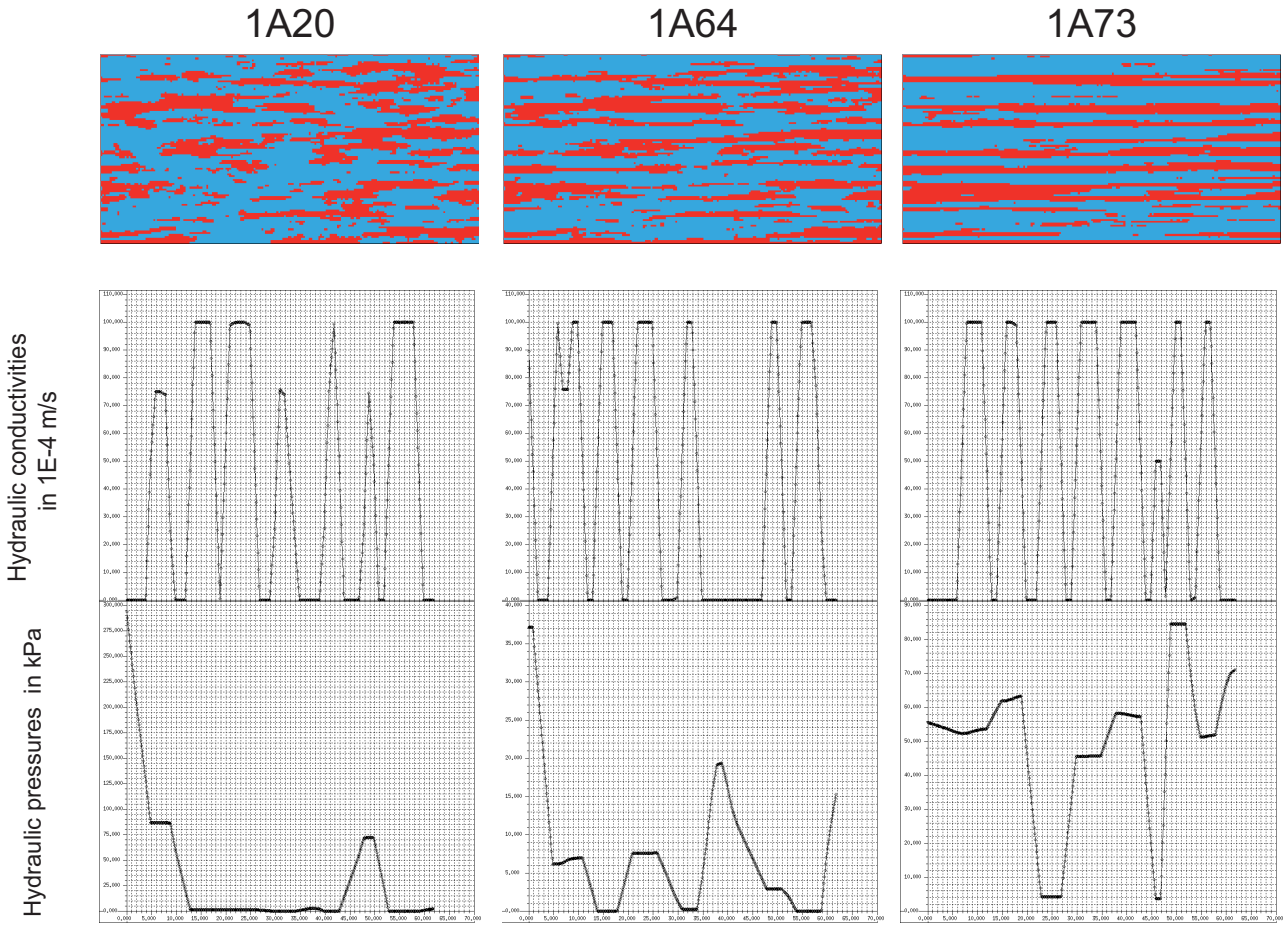
1A20
1A64
1A73
Hydraulic conductivities in 1E-4 m/s
Hydraulic pressures in kPa

1A37

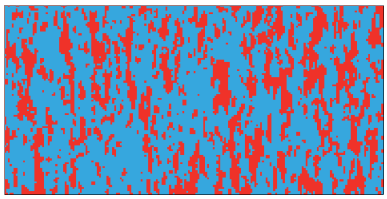

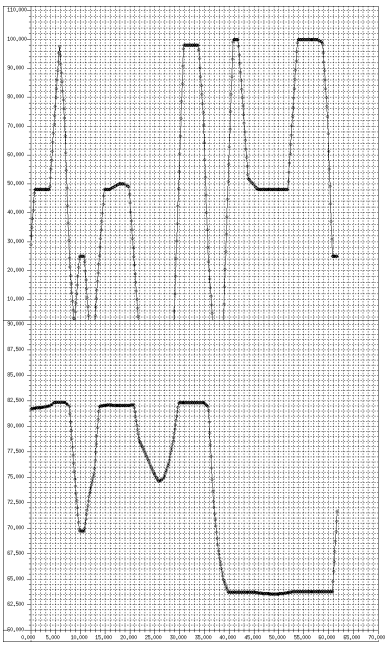

1A44

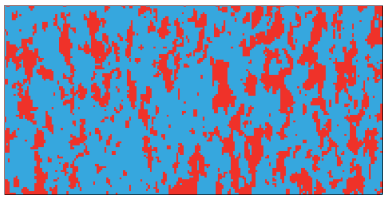

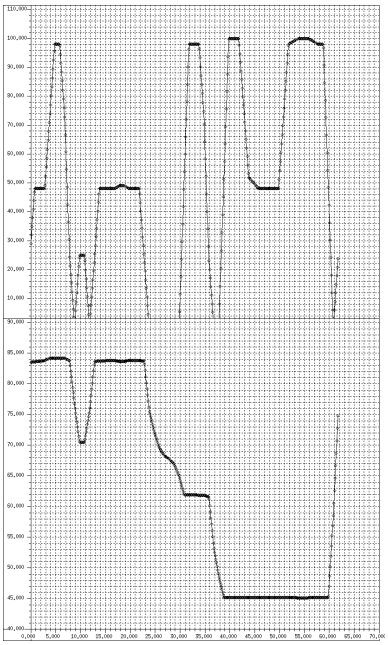

1A21

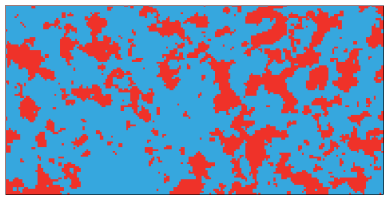

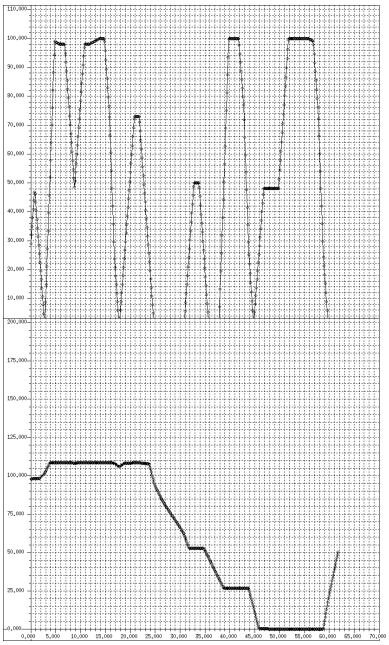

1A38

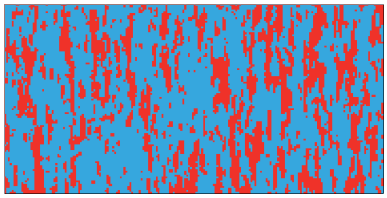

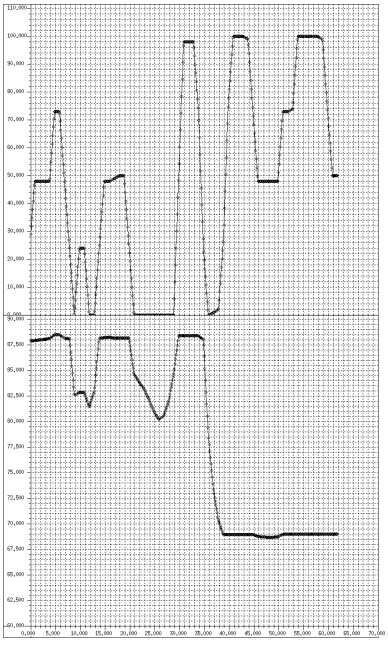

1A45

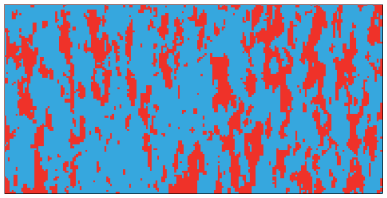

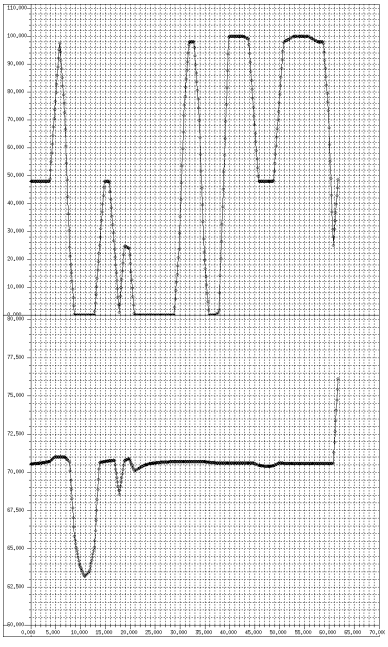

1A24

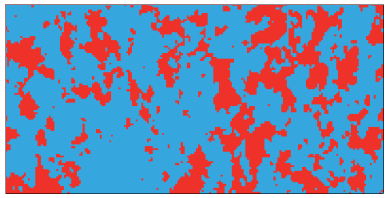

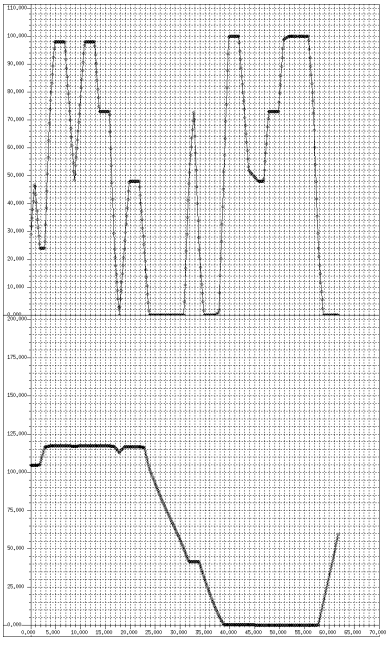

1A51 1A22 1A58

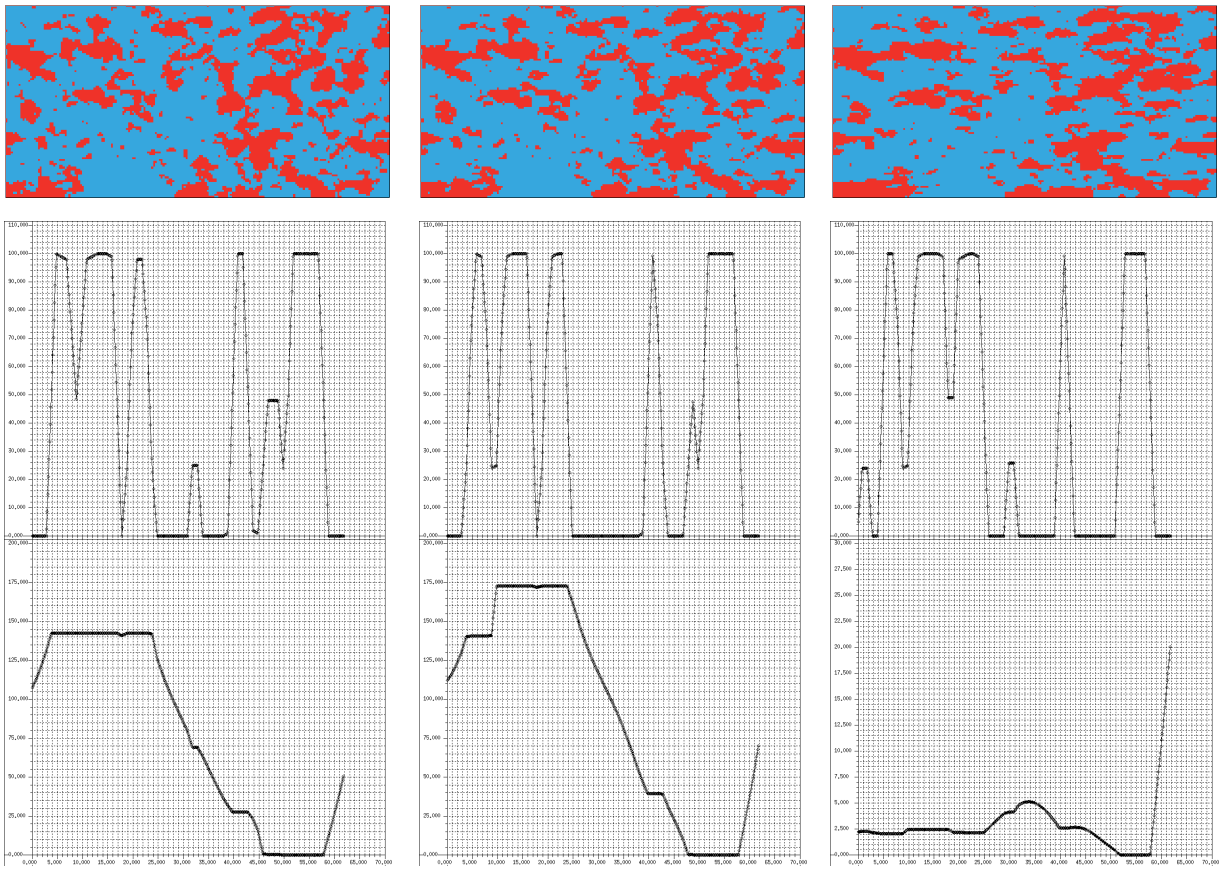

1A52 1A25 1A59

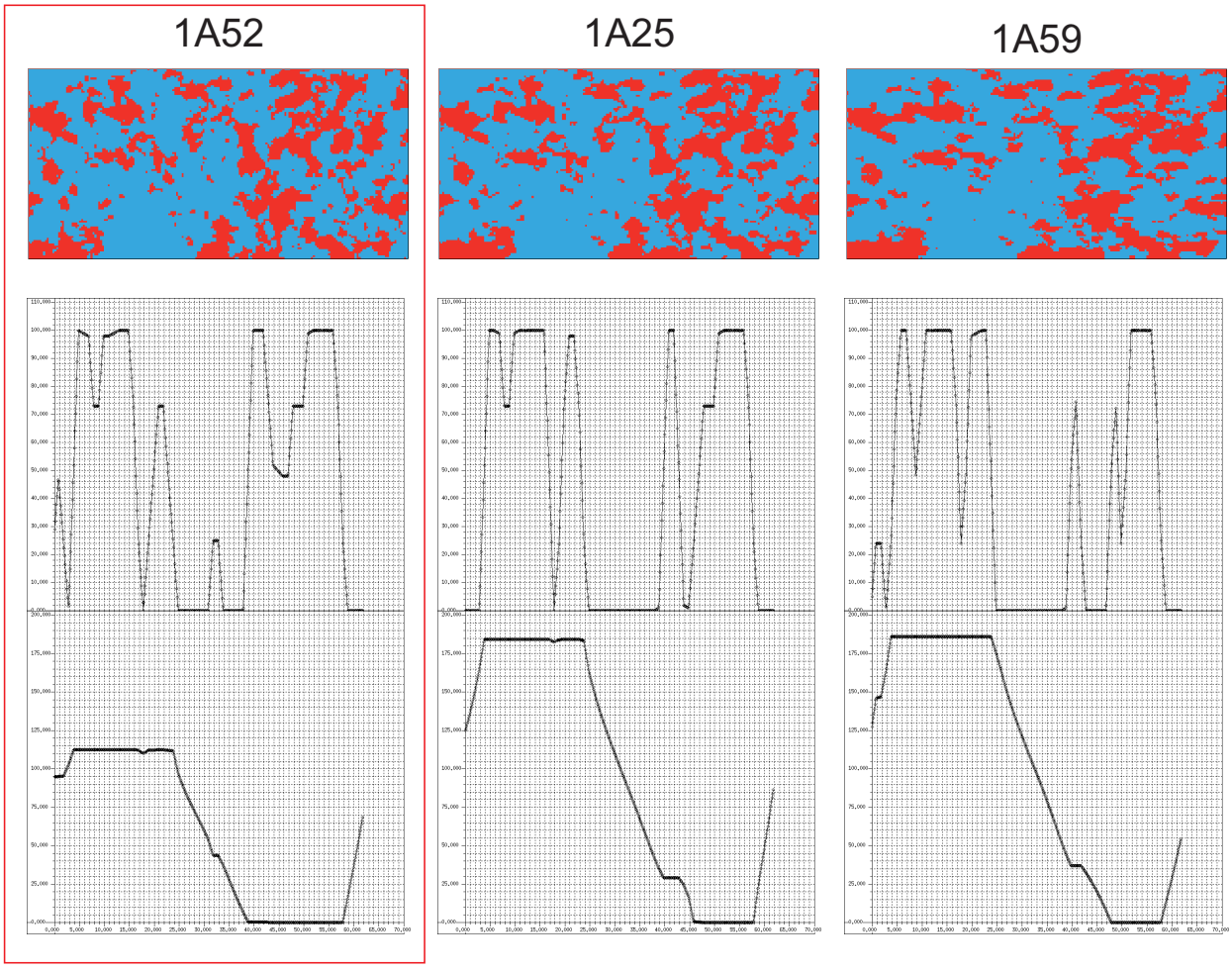

1A23 1A65 1A74

Hydraulic conductivities in 1E-4 m/s

Hydraulic pressures in kPa

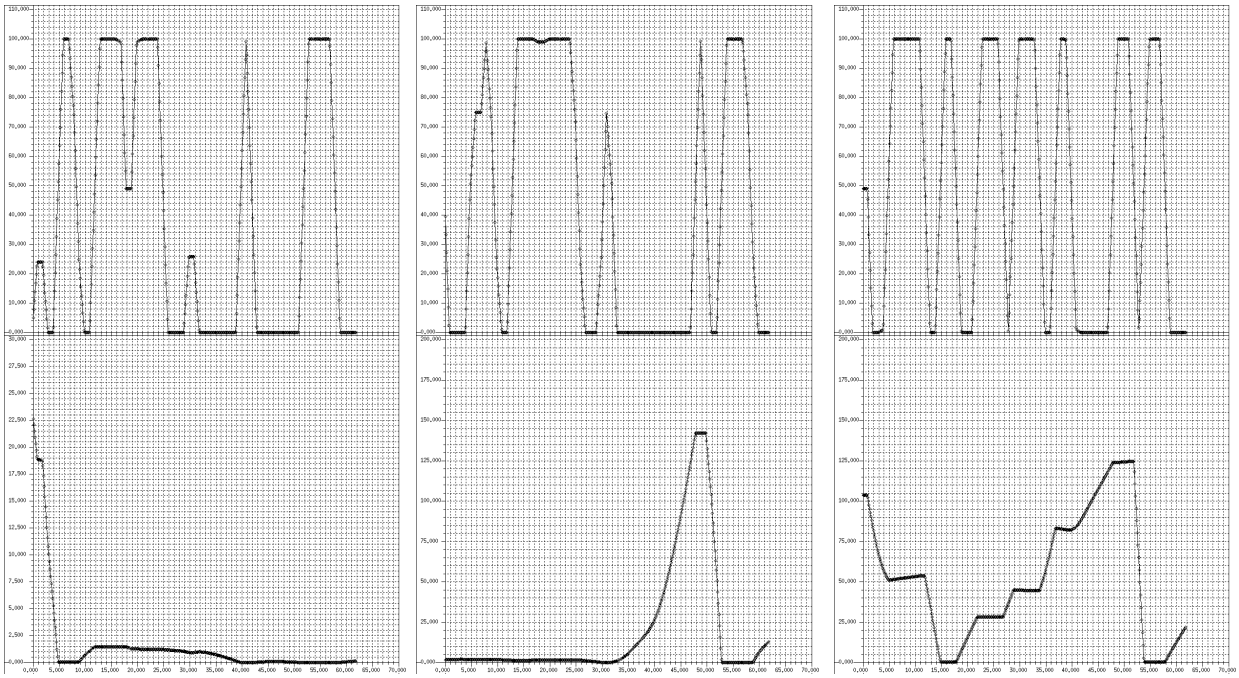

1A26 1A66 1A75

Hydraulic conductivities in 1E-4 m/s

Hydraulic pressures in kPa

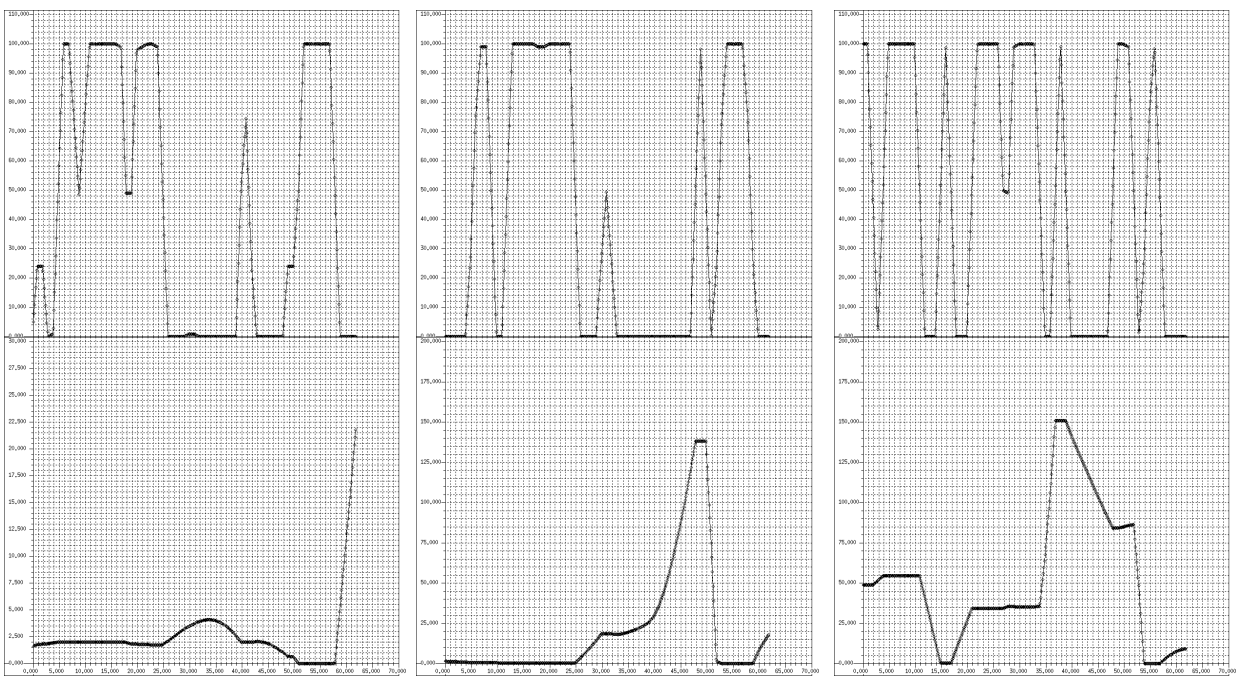

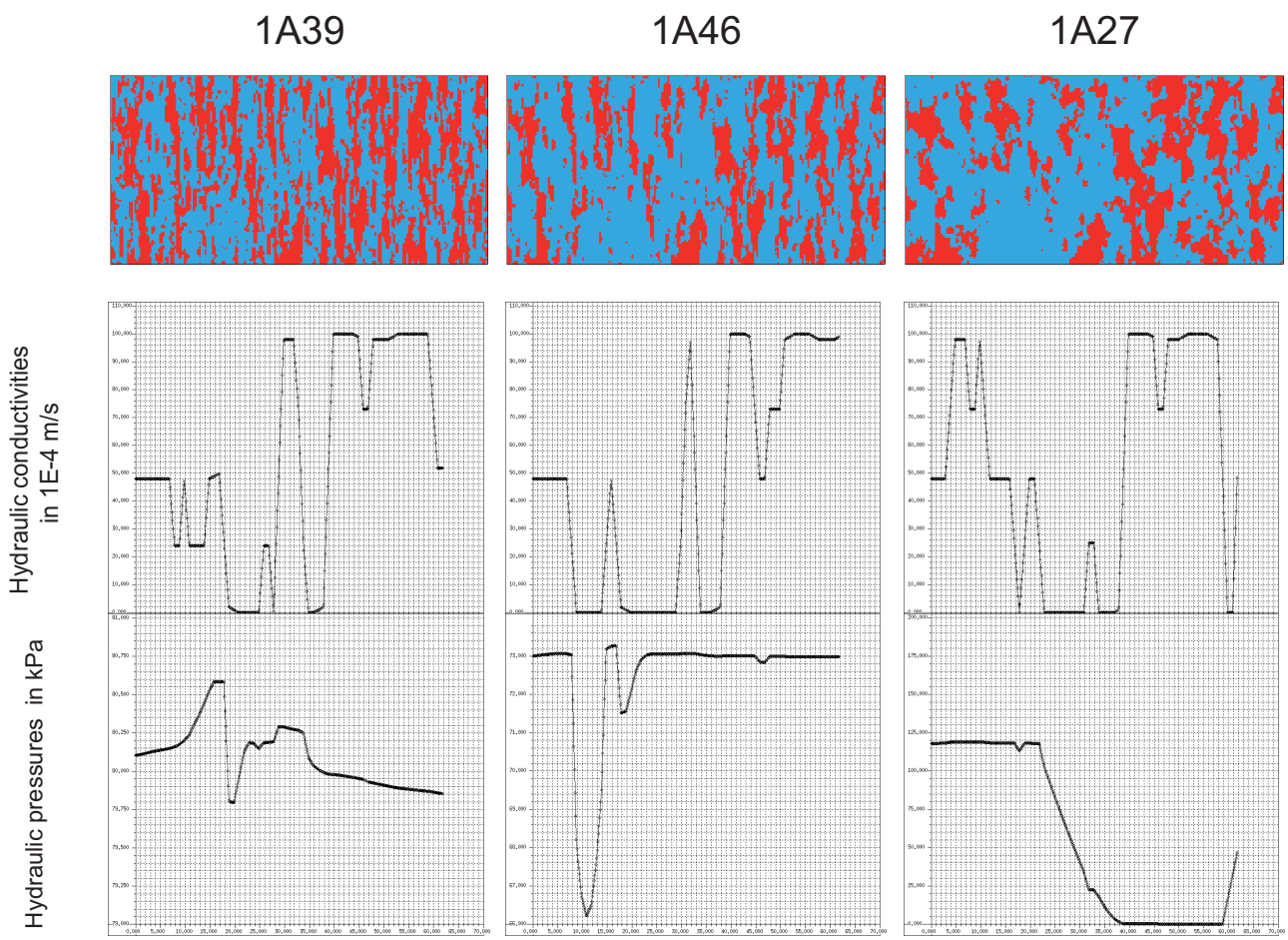
1A39
1A46
1A27
Hydraulic conductivities in 1E-4 m/s
Hydraulic pressures in kPa

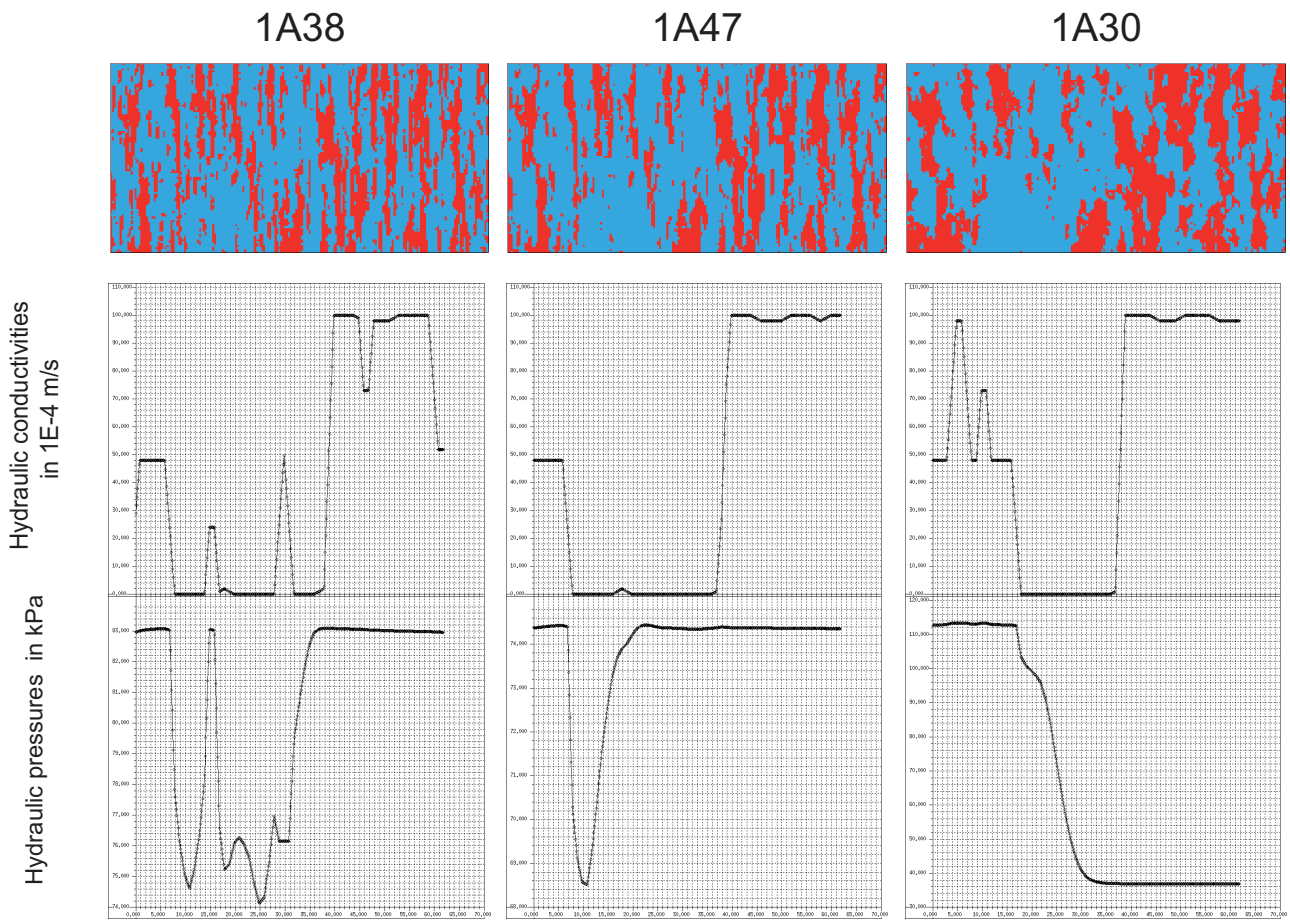
1A38
1A47
1A30
Hydraulic conductivities in 1E-4 m/s
Hydraulic pressures in kPa

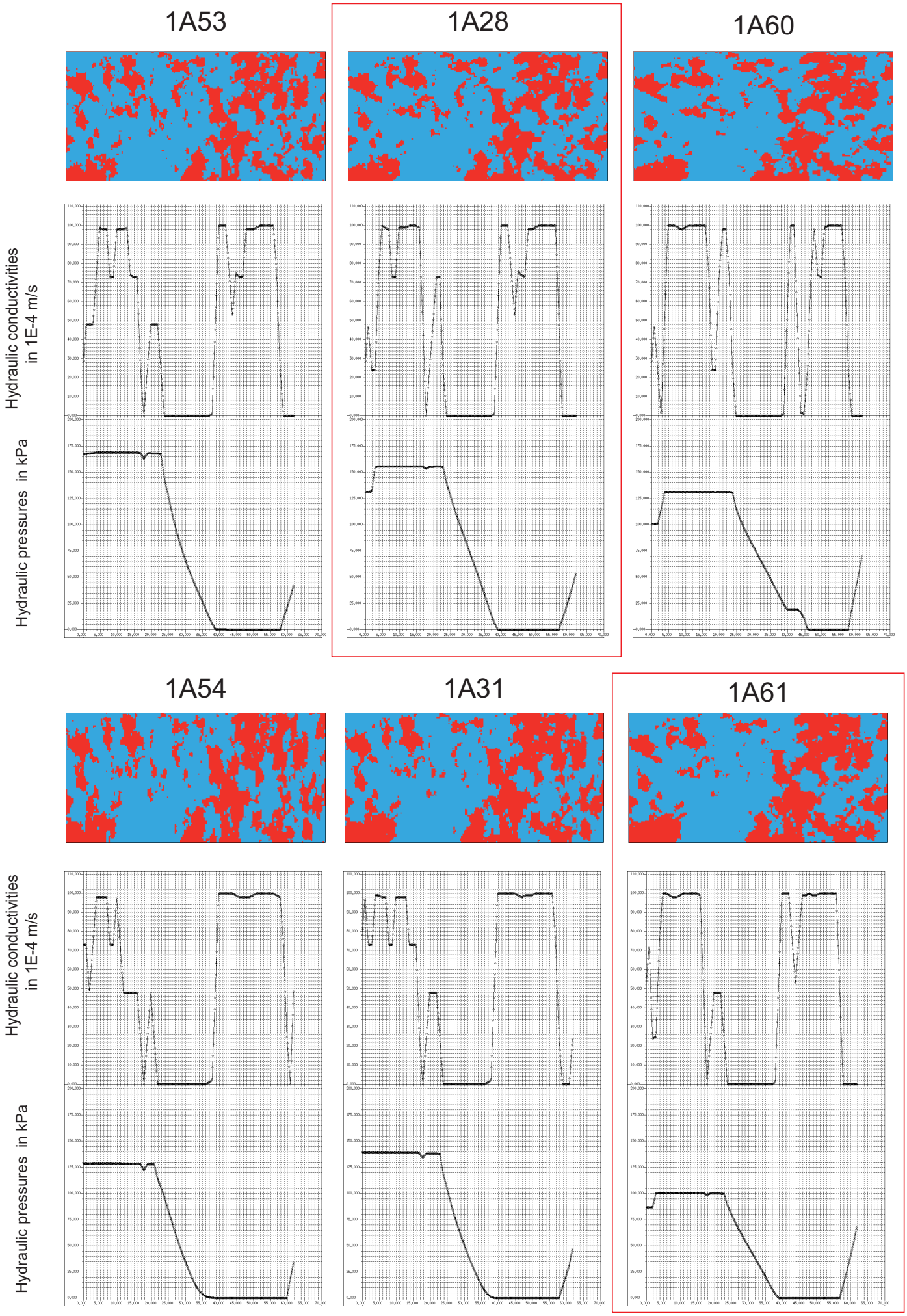
1A53
1A28
1A60
Hydraulic conductivities in 1E-4 m/s
Hydraulic pressures in kPa
1A54
1A31
1A61
Hydraulic conductivities in 1E-4 m/s
Hydraulic pressures in kPa

1A29 1A67 1A76

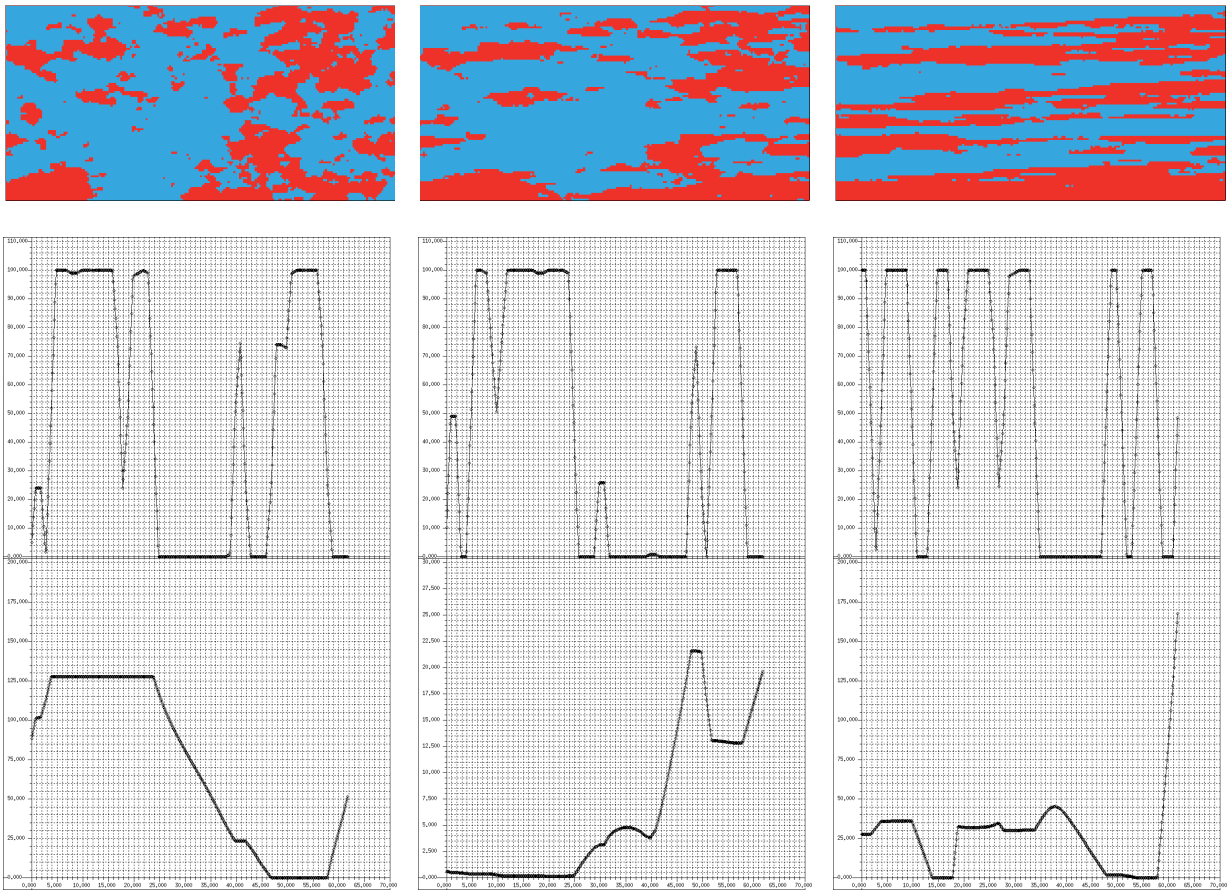

1A32 1A68 1A77

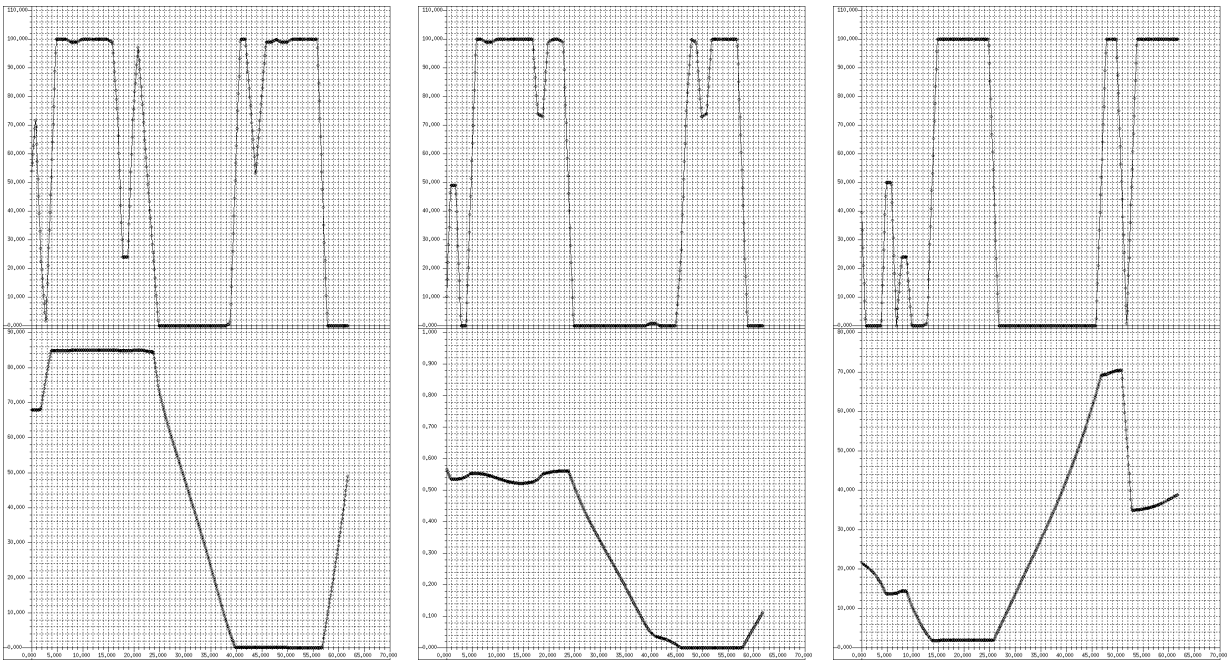

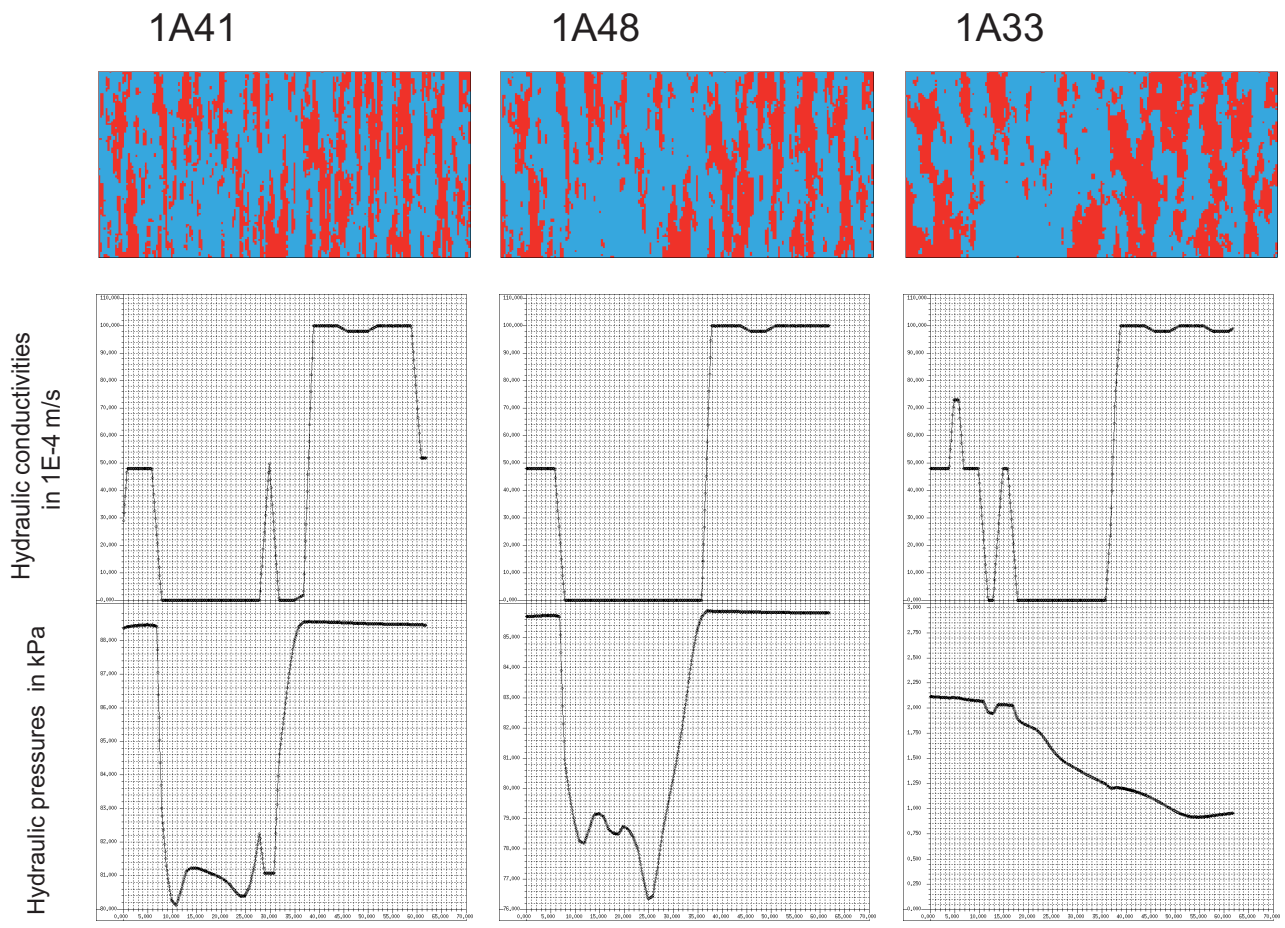
1A41
1A48
1A33
Hydraulic conductivities in 1E-4 m/s
Hydraulic pressures in kPa

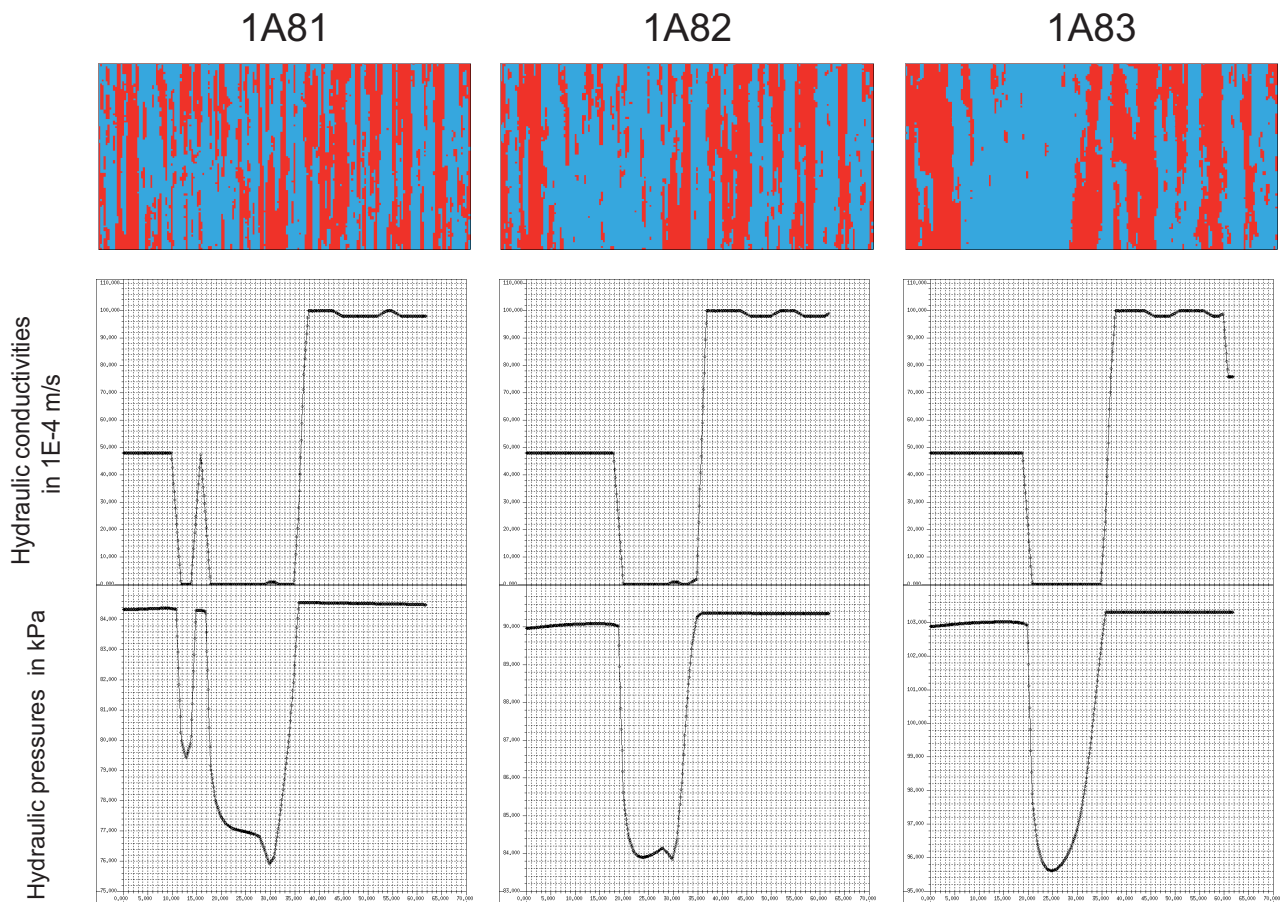
1A81
1A82
1A83
Hydraulic conductivities in 1E-4 m/s
Hydraulic pressures in kPa

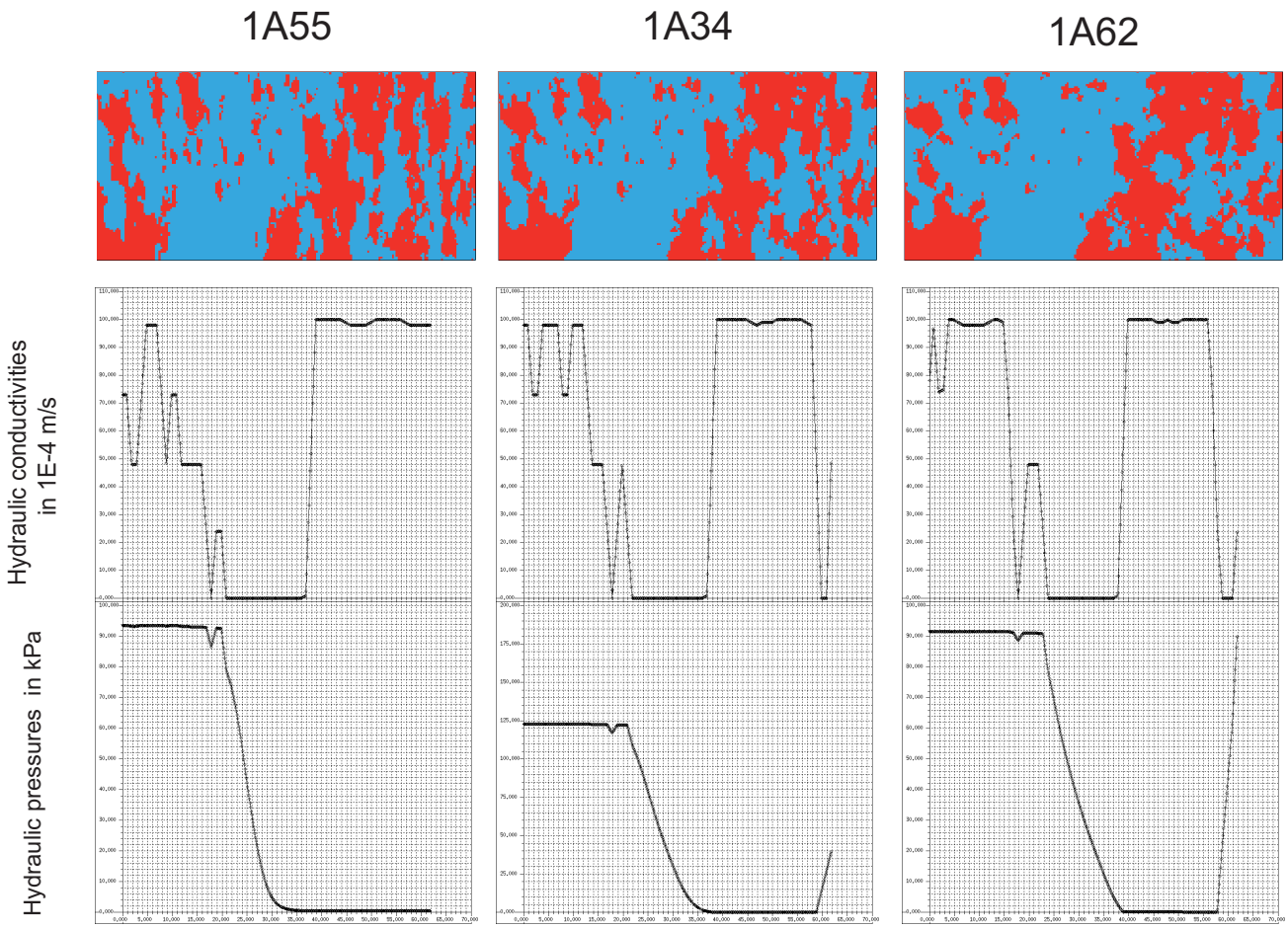
1A55
1A34
1A62
Hydraulic conductivities in 1E-4 m/s
Hydraulic pressures in kPa

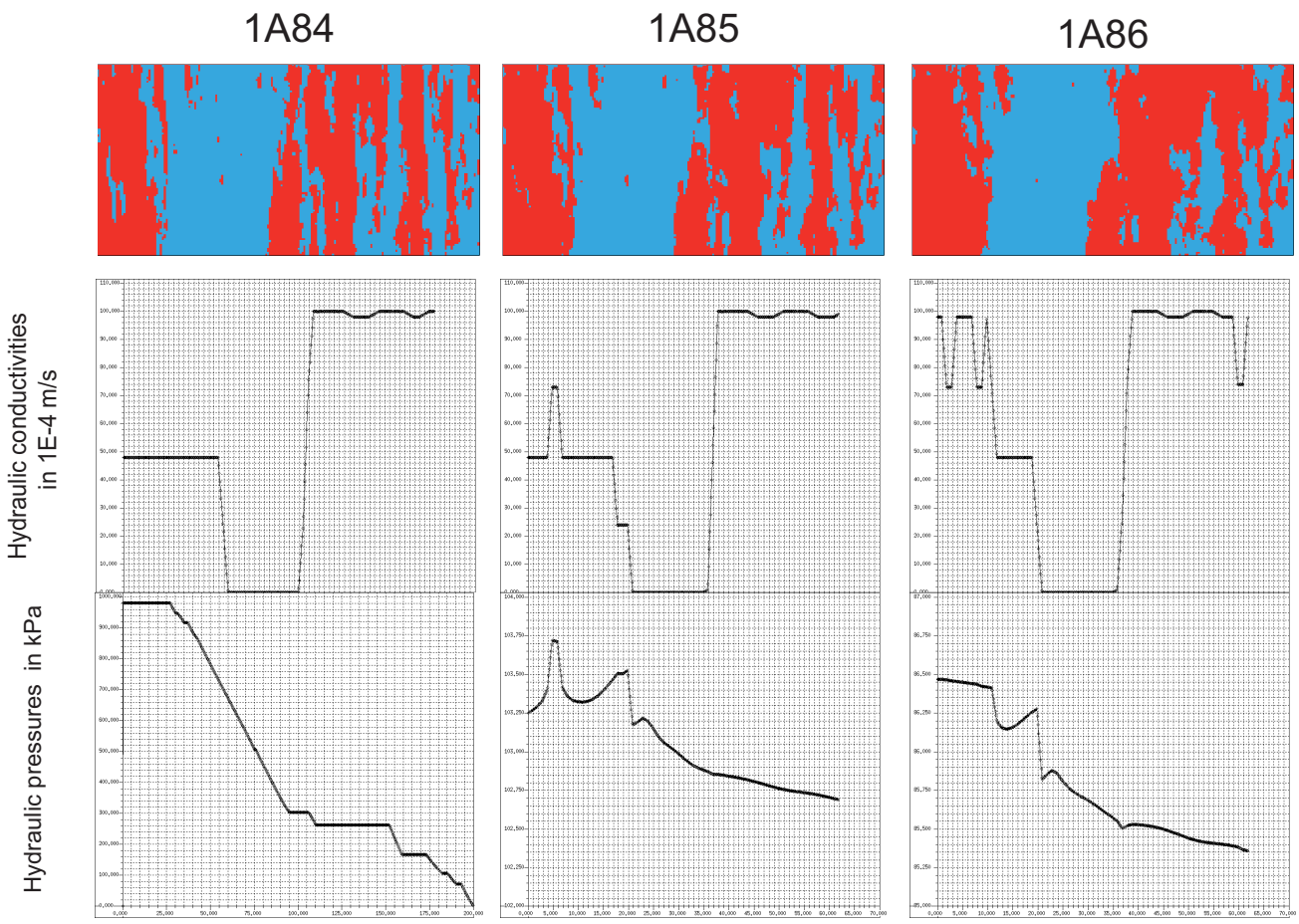
1A84
1A85
1A86
Hydraulic conductivities in 1E-4 m/s
Hydraulic pressures in kPa

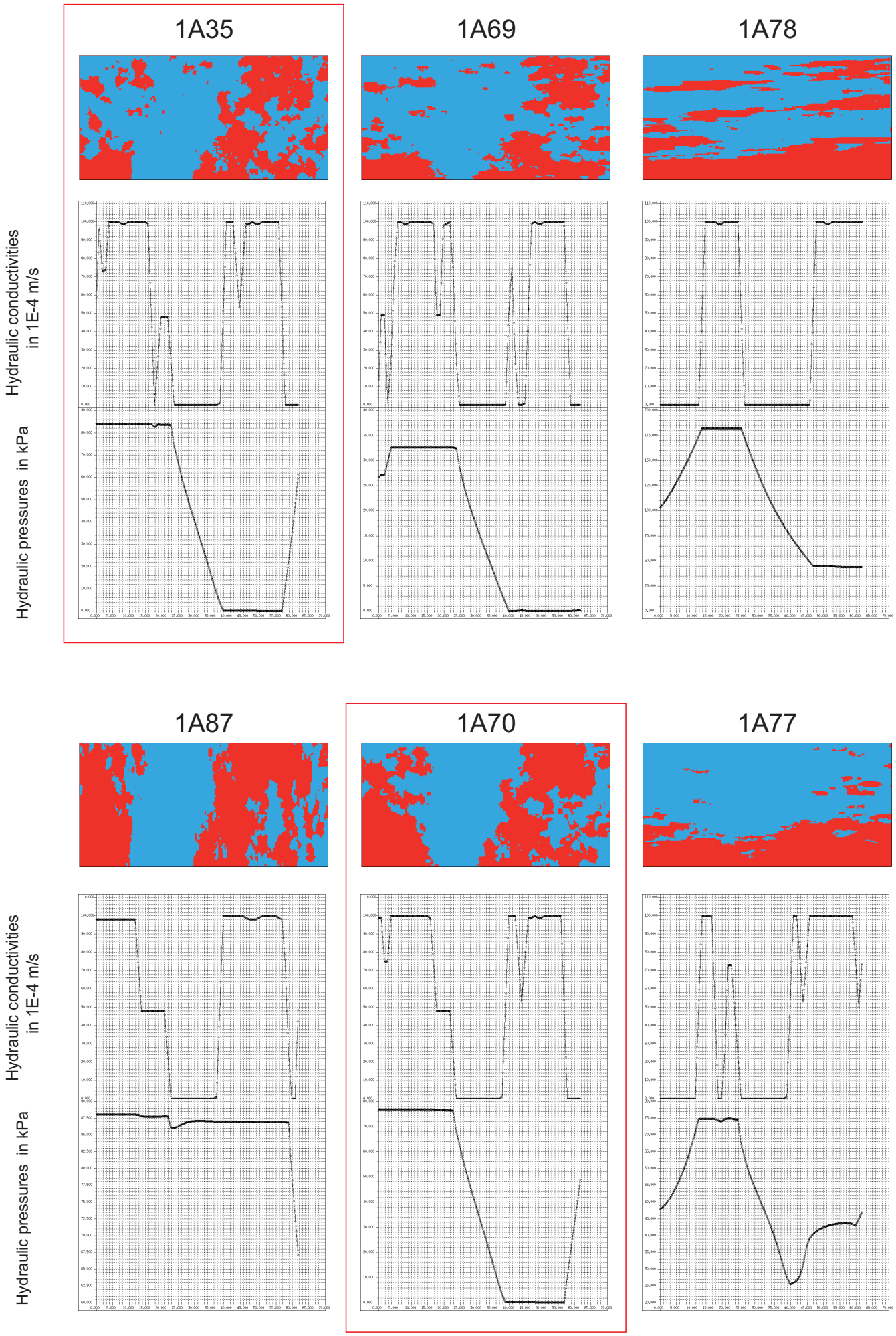
1A35
1A69
1A78
Hydraulic conductivities in 1E-4 m/s
Hydraulic pressures in kPa
1A87
1A70
1A77
Hydraulic conductivities in 1E-4 m/s
Hydraulic pressures in kPa

1A88 1A89 1A90

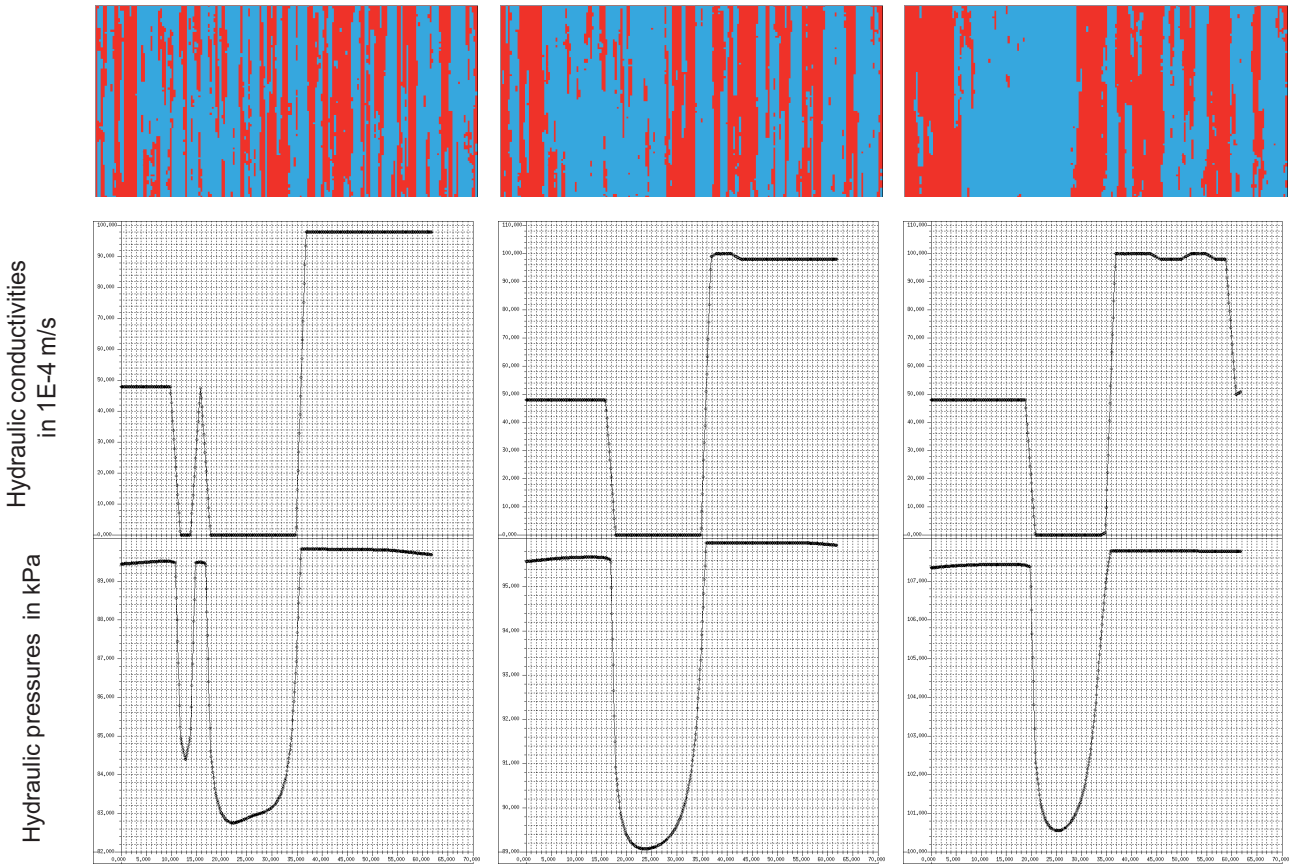

1A91 1A92 1A93

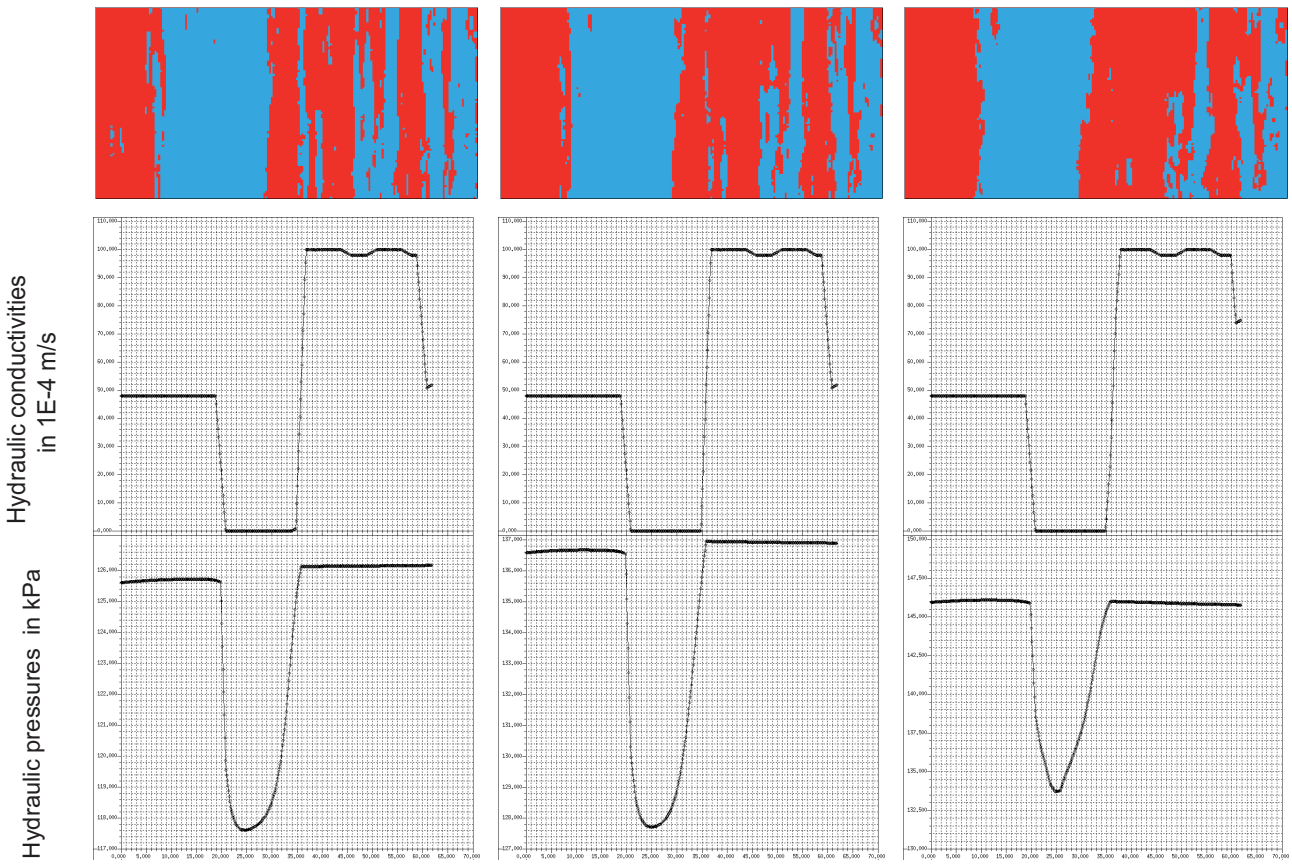

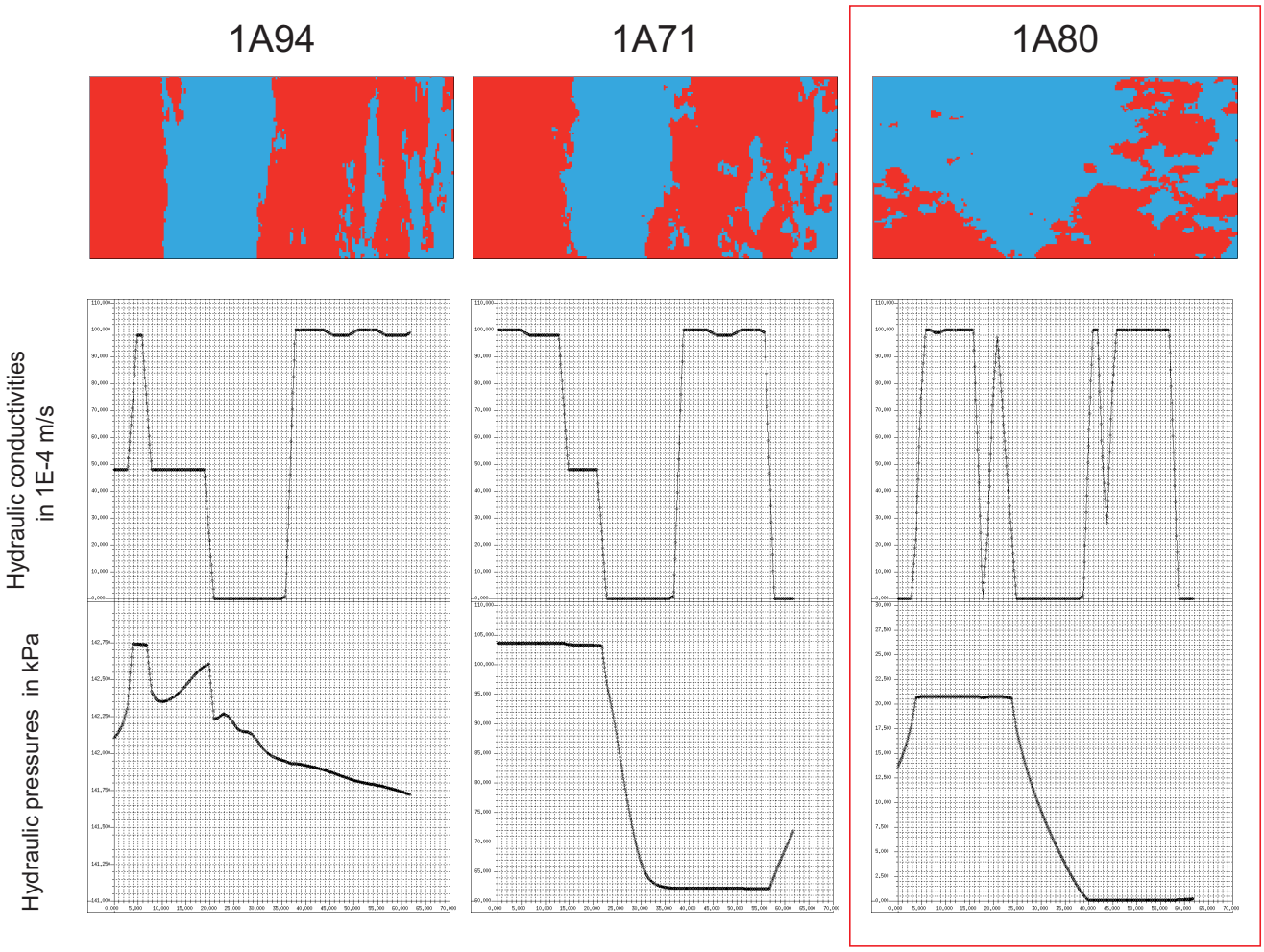
1A94
1A71
1A80
Hydraulic conductivities in 1E-4 m/s
Hydraulic pressures in kPa

K - Statistical characteristics

mean [ln]: -7.6
variance [ln]: 2.25

Correlation lengths

lx : 1m
ly : 1m
lz : 1m

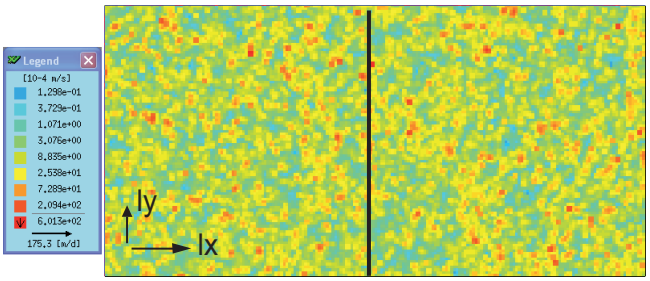

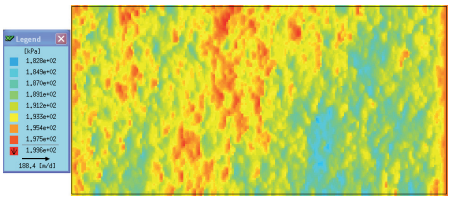

Hydraulic pressure distribution at sliding surface before drainage

	Configuration 1	Configuration 2	Configuration 3
2D Hydraulic pressures [KPa] sliding surface	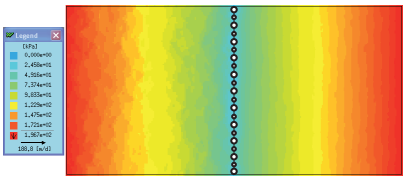 Drains spacing : 5m	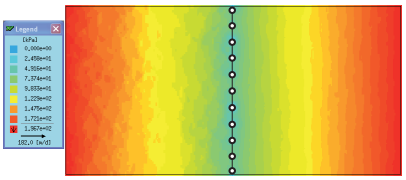 Drains spacing : 10m	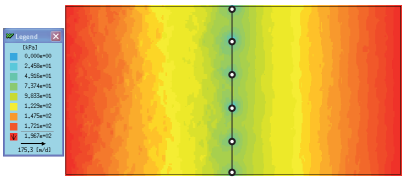 Drains spacing : 20m
2D Hydraulic pressures [KPa] through drainage galery section	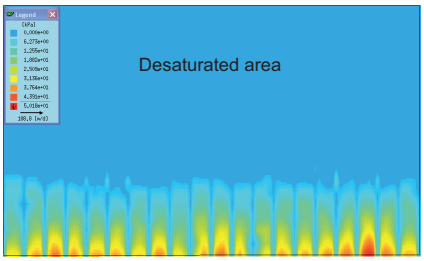 Desaturated area	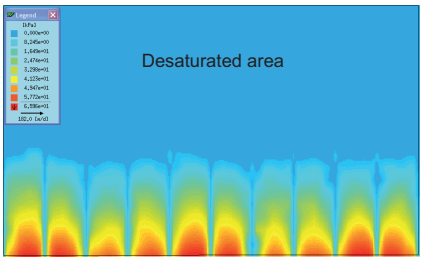 Desaturated area	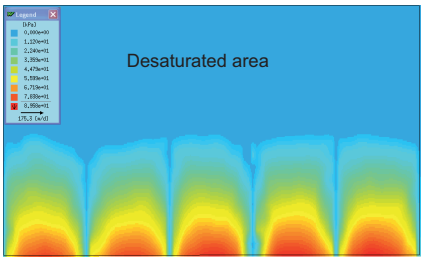 Desaturated area
2D Hydraulic heads [m] through drainage galery section	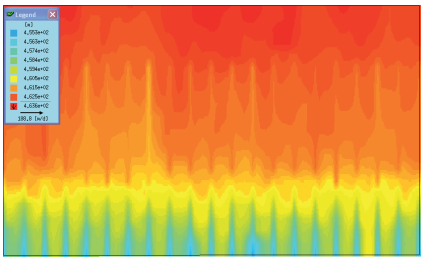	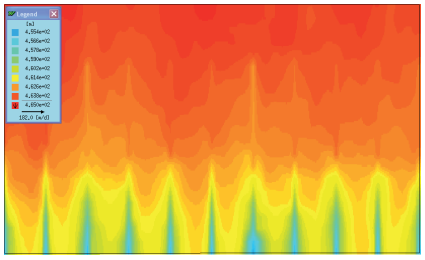	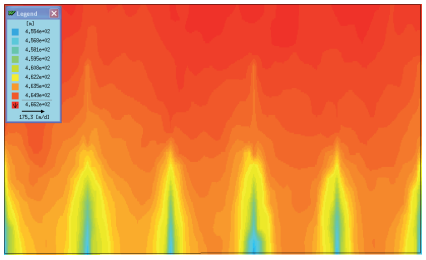
- FLOW OUT - DRAINAGE GALLERY CONTRIBUTION [%]	71.0 %	66.2 %	61.0 %

K - STATISTICAL CHARACTERISTICS

mean [ln]: -7.6
variance [ln]: 2.25

CORRELATION LENGTHS

lx : 20m
ly : 2m
lz : 1m

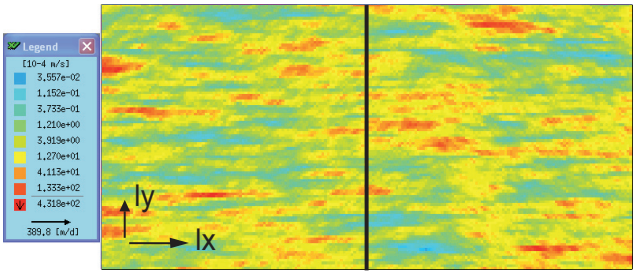

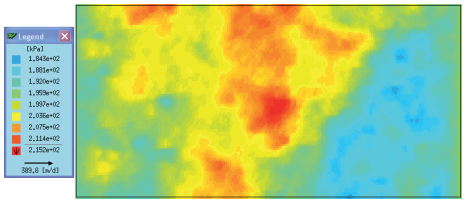

Hydraulic pressure distribution at sliding surface before drainage

	Configuration 1	Configuration 2	Configuration 3
2D Hydraulic pressures [KPa] sliding surface	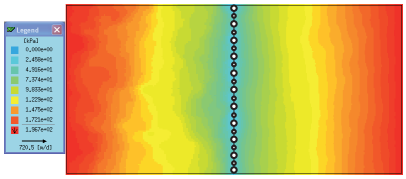 Drains spacing : 5m	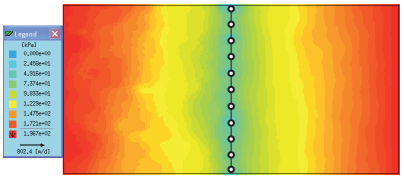 Drains spacing : 10m	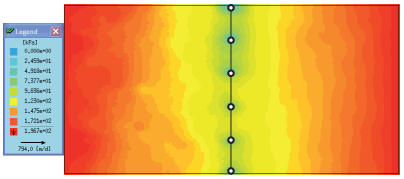 Drains spacing : 20m
2D Hydraulic pressures [KPa] through drainage galery section	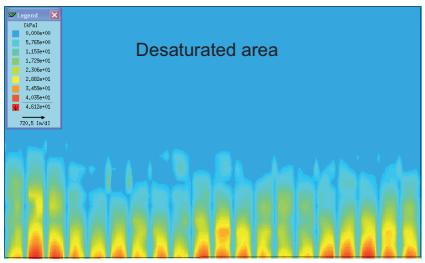	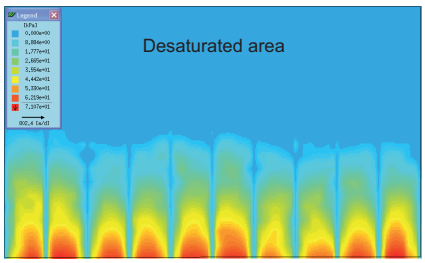	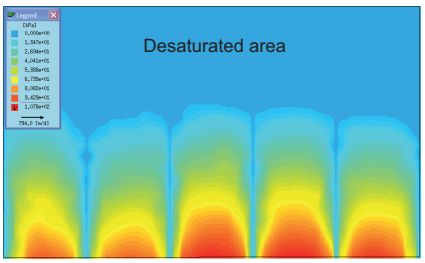
2D Hydraulic heads [m] through drainage galery section	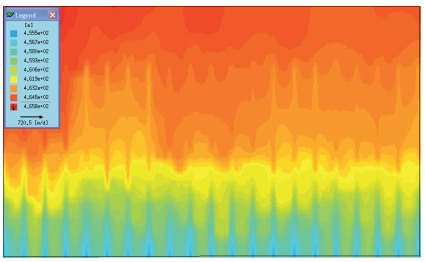	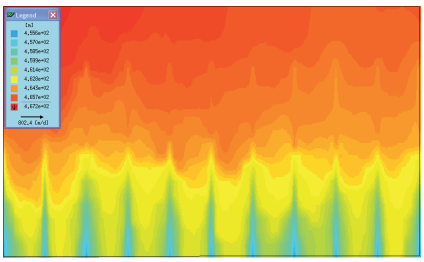	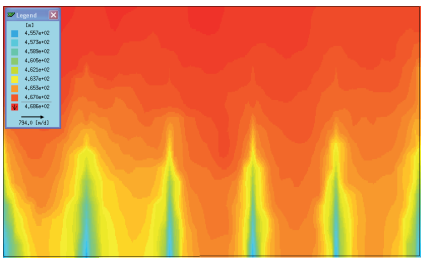

- FLOW OUT - DRAINAGE GALLERY CONTRIBUTION [%]	70.3 %	65.3 %	57.8 %

K - STATISTICAL CHARACTERISTICS

mean [ln]: -7.6
variance [ln]: 2.25

CORRELATION LENGTHS

lx : 20m
ly : 10m
lz : 1m

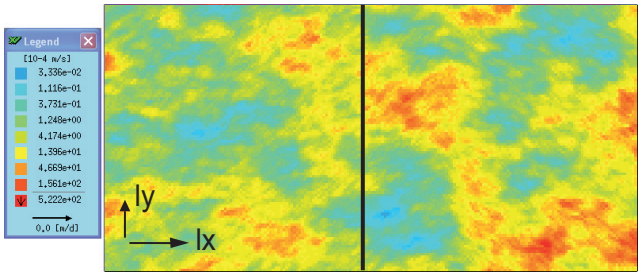

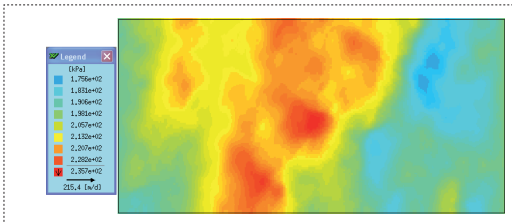

Hydraulic pressure distribution at sliding surface before drainage

	Configuration 1	Configuration 2	Configuration 3
2D Hydraulic pressures [KPa] sliding surface	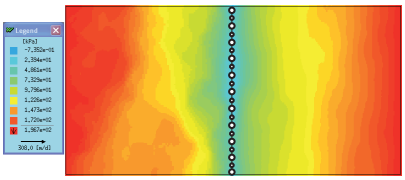 Drains spacing : 5m	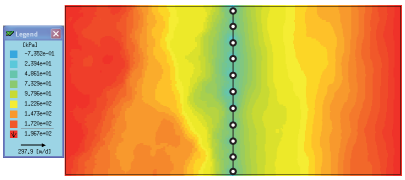 Drains spacing : 10m	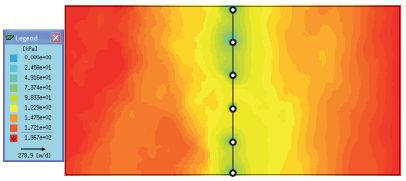 Drains spacing : 20m
2D Hydraulic pressures [KPa] through drainage galery section	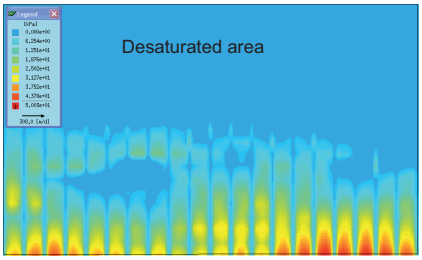	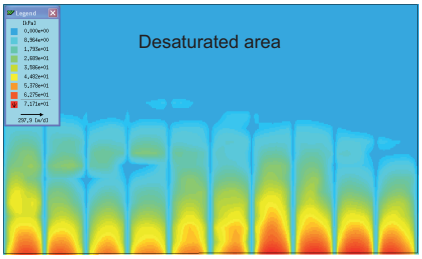	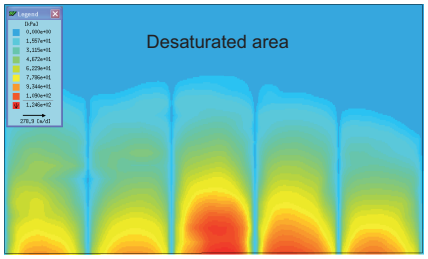
2D Hydraulic heads [m] through drainage galery section	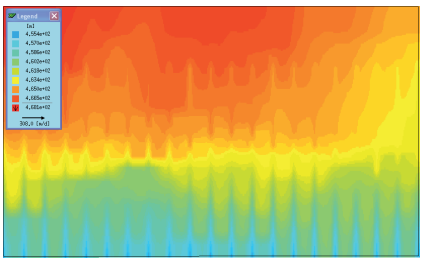	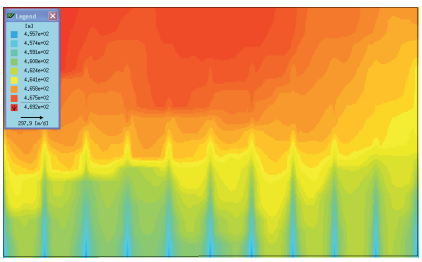	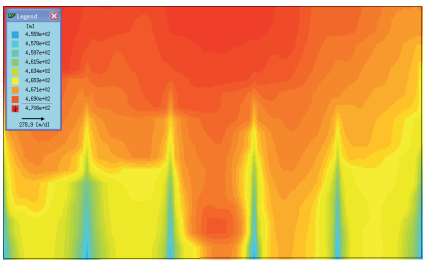

- FLOW OUT - DRAINAGE GALLERY CONTRIBUTION [%]	71.1 %	67.4 %	59.4 %

K - Statistical characteristics

mean [ln]: -7.6
variance [ln]: 2.25

Correlation lengths

lx : 50m
ly : 2m
lz : 1m

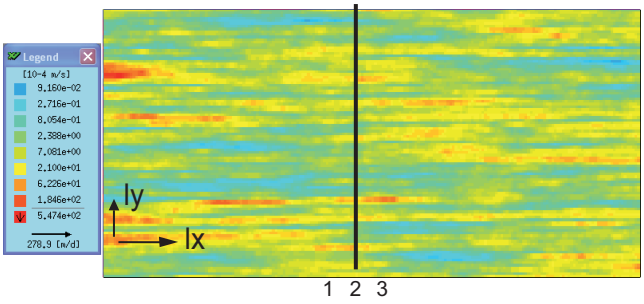

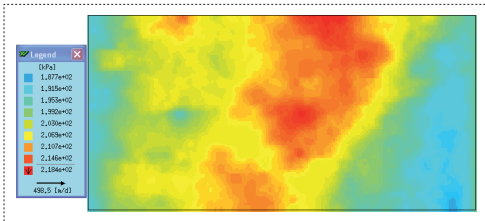

Hydraulic pressure distribution at sliding surface before drainage

	Configuration 1	Configuration 2	Configuration 3
2D Hydraulic pressures [KPa] sliding surface	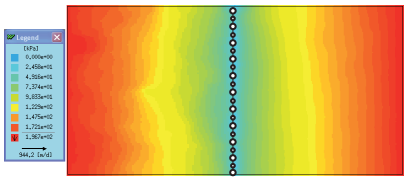 Drains spacing : 5m	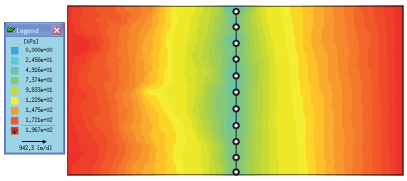 Drains spacing : 10m	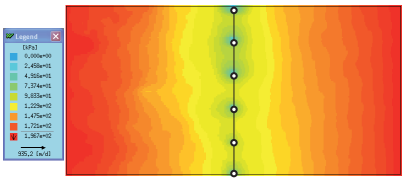 Drains spacing : 20m
2D Hydraulic pressures [KPa] through drainage galery section	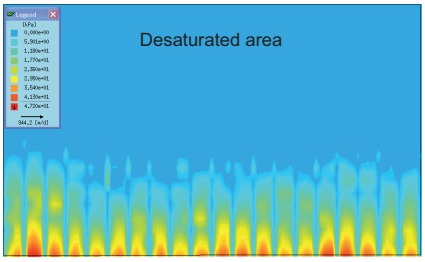	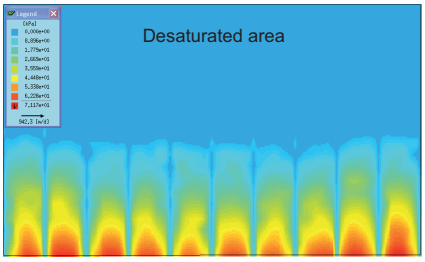	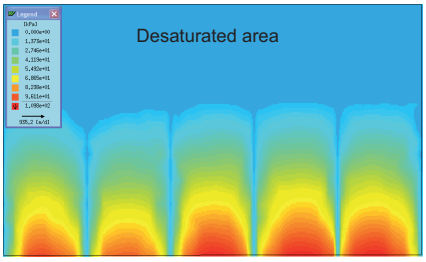
2D Hydraulic heads [m] through drainage galery section	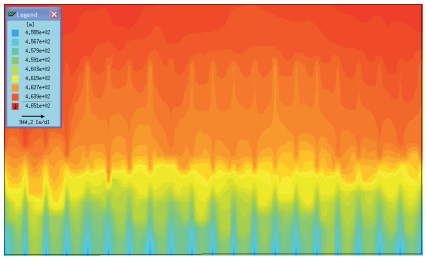	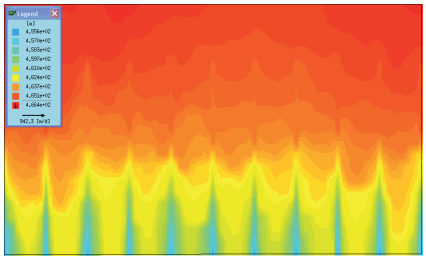	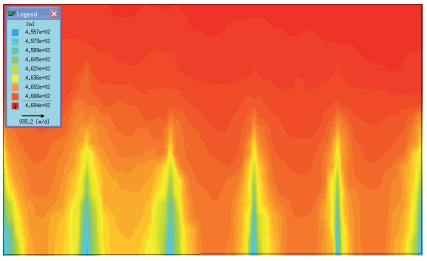
- FLOW OUT - DRAINAGE GALLERY CONTRIBUTION [%]	71.7 %	67.0 %	58.2 %

K - STATISTICAL CHARACTERISTICS

mean [ln]: -7.6
variance [ln]: 2.25

CORRELATION LENGTHS

lx : 50m
ly : 10m
lz : 1m

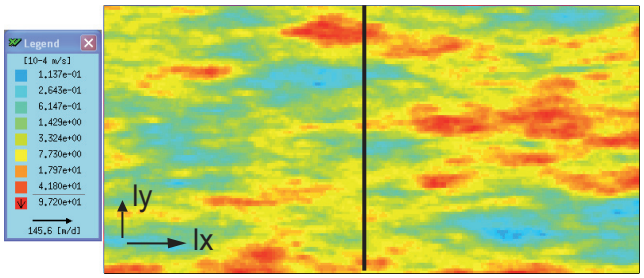

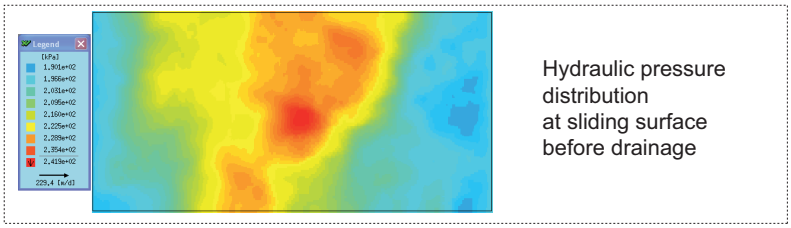

Hydraulic pressure distribution at sliding surface before drainage

	Configuration 1	Configuration 2	Configuration 3
2D Hydraulic pressures [KPa] sliding surface	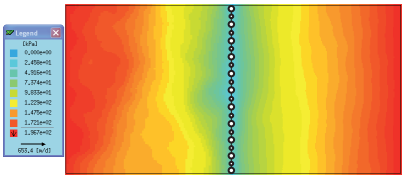 Drains spacing : 5m	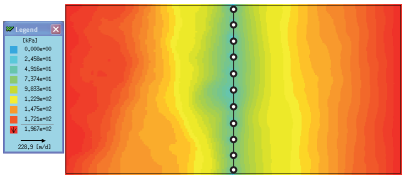 Drains spacing : 10m	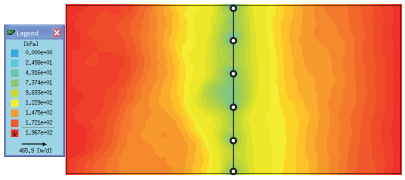 Drains spacing : 20m
2D Hydraulic pressures [KPa] through drainage galery section	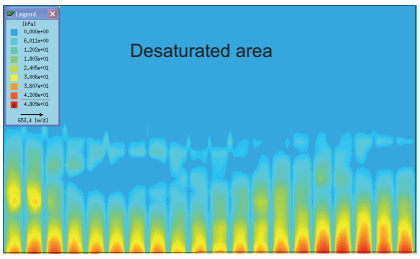	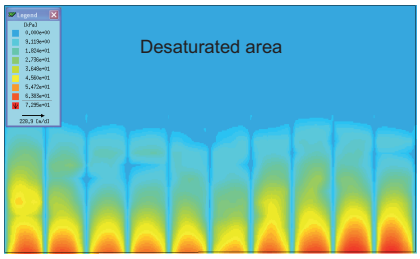	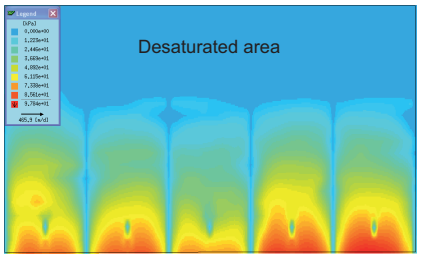
2D Hydraulic heads [m] through drainage galery section	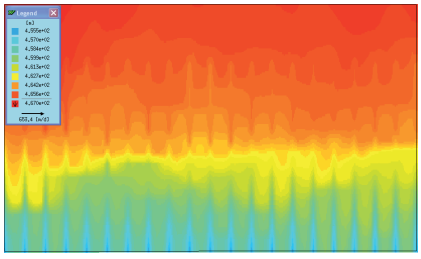	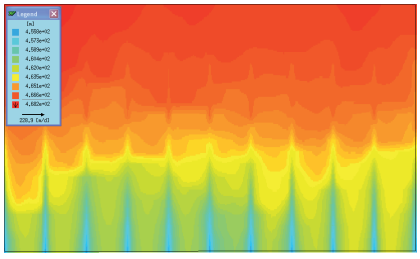	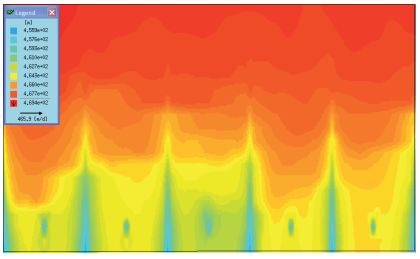

- FLOW OUT - DRAINAGE GALLERY CONTRIBUTION [%]	72.9 %	69.4 %	64.7 %

K - STATISTICAL CHARACTERISTICS

K_1 = 1E-2 m/s
K_2 = 1E-7 m/s

CORRELATION LENGTHS

lx : 20m
ly : 2m
lz : 1m

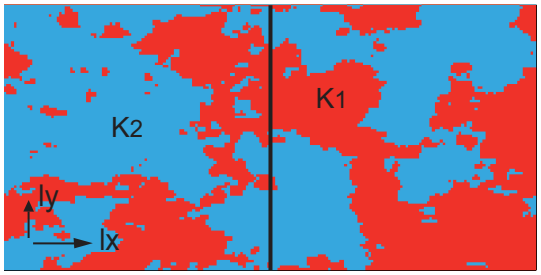

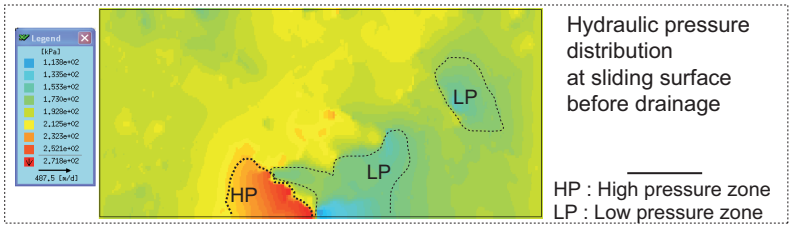

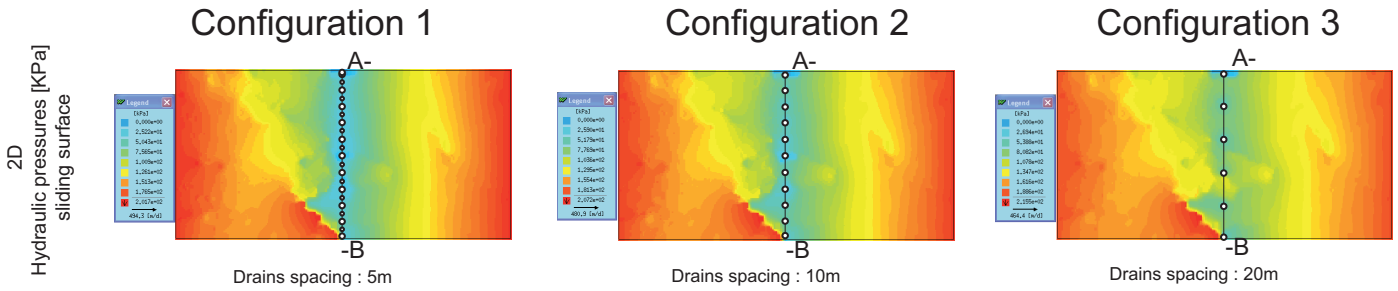

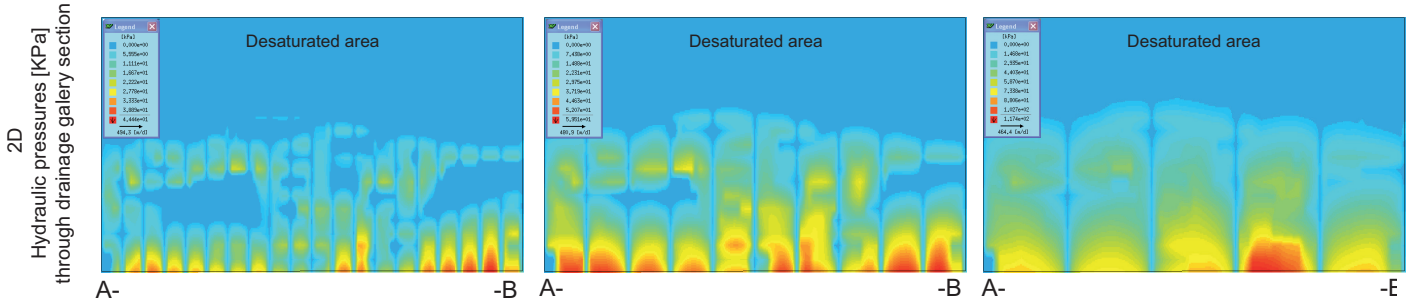

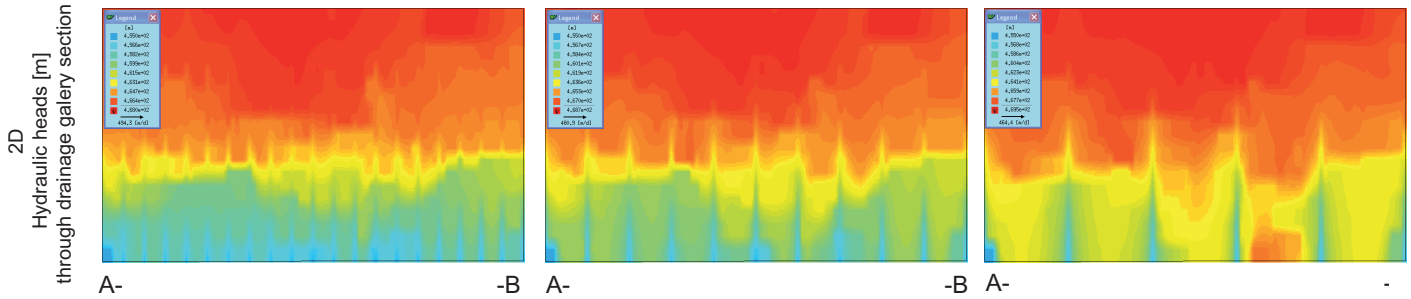

- FLOW OUT - DRAINAGE GALLERY CONTRIBUTION [%]	63.4 %	60.3 %	55.3 %

K - STATISTICAL CHARACTERISTICS

K1 = 1E-2 m/s
K2 = 1E-7 m/s

CORRELATION LENGTHS

lx : 50m
ly : 2m
lz : 1m

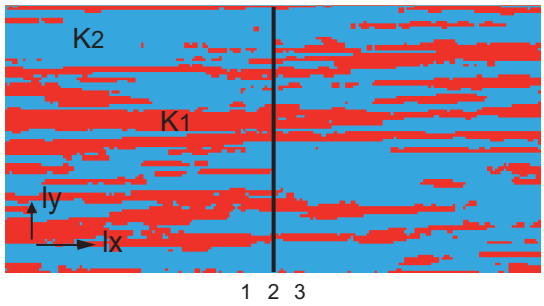

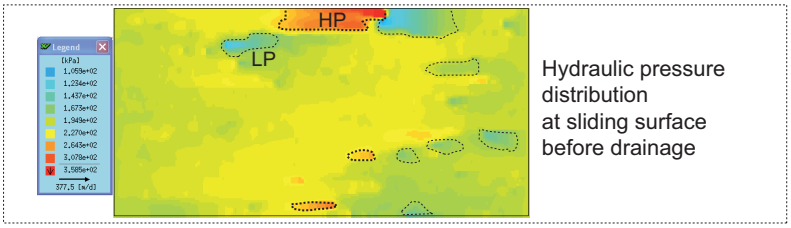

Hydraulic pressure distribution at sliding surface before drainage

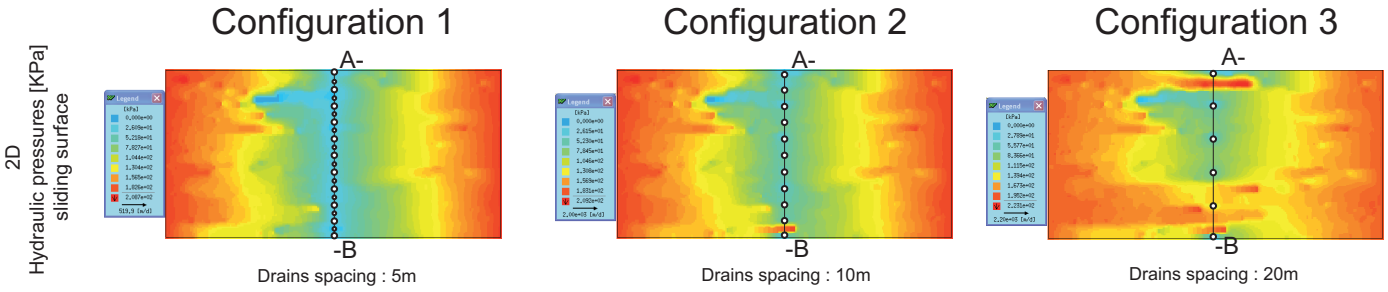

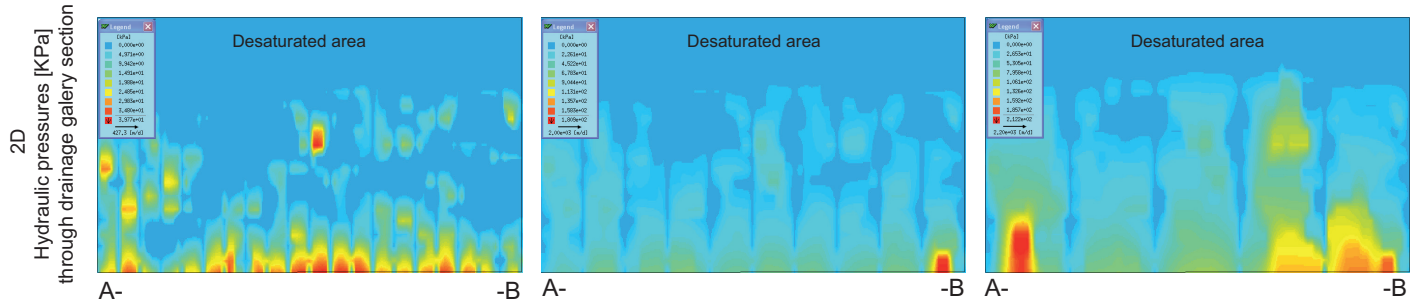

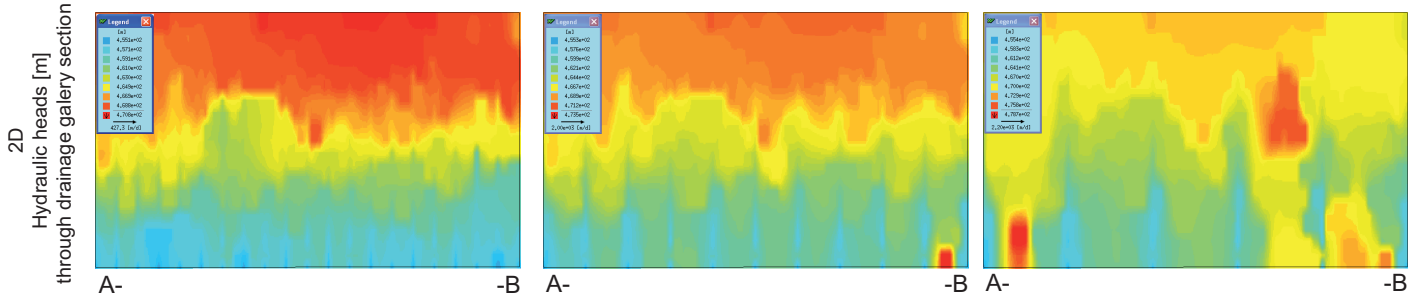

- FLOW OUT - DRAINAGE GALLERY CONTRIBUTION [%]	60.9 %	55.9 %	47.9 %

Computed hydraulic heads

A1 : Hydraulic heads (t=175 days)

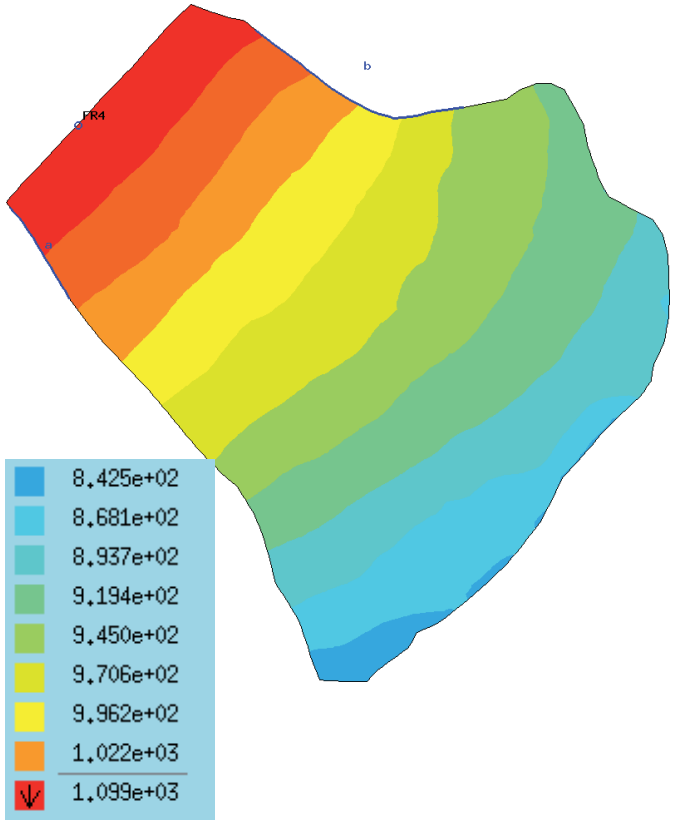

B1 : Hydraulic heads (t=400 days)

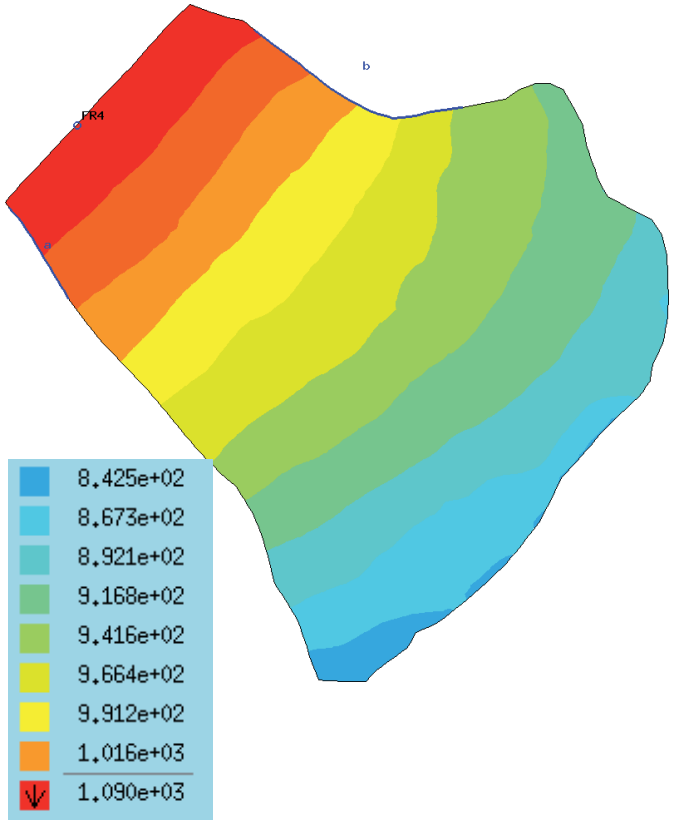

A2 : Differences between topography and hydraulic heads (t=175 days)

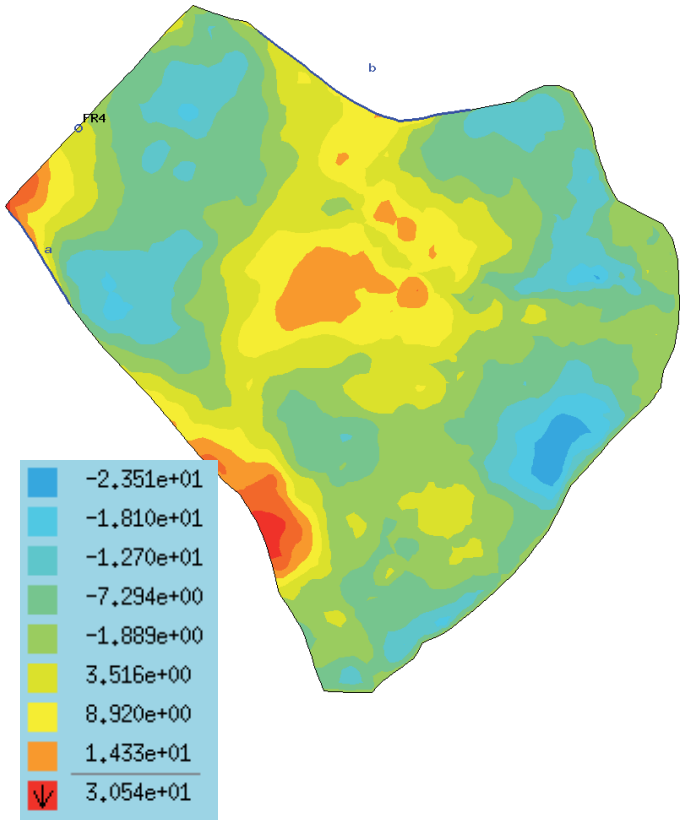

B2 : Differences between topography and hydraulic heads (t=400 days)

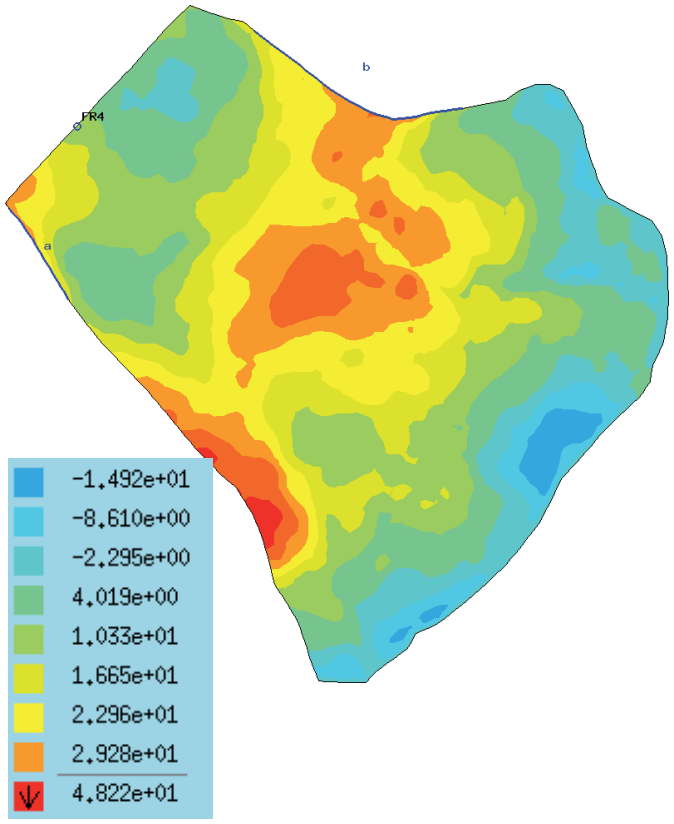

K V09D

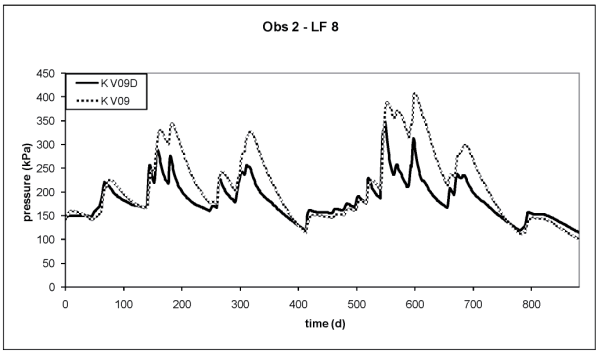
Obs 2 - LF 8
K V09D
K V09
pressure (kPa)
time (d)

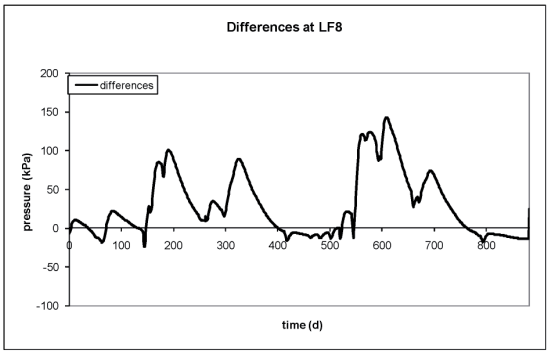
Differences at LF8
differences
pressure (kPa)
time (d)

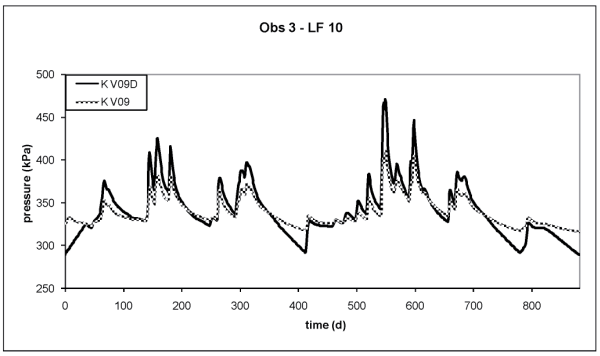
Obs 3 - LF 10
K V09D
K V09
pressure (kPa)
time (d)

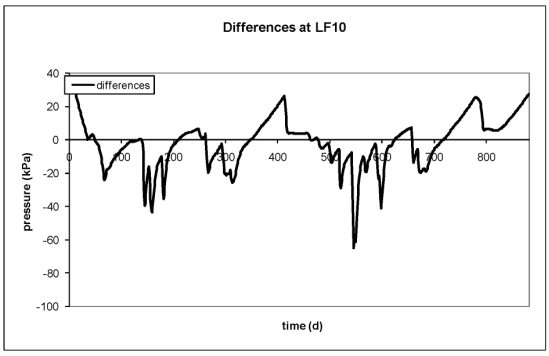
Differences at LF10
differences
pressure (kPa)
time (d)

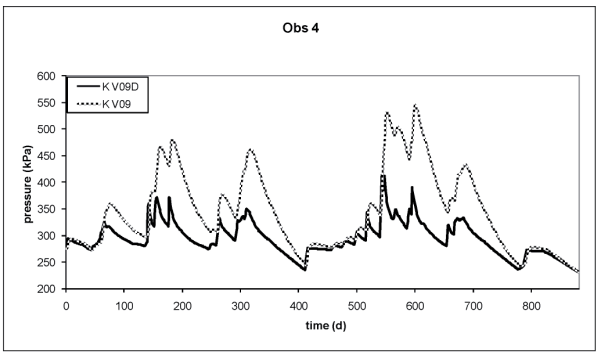
Obs 4
K V09D
K V09
pressure (kPa)
time (d)

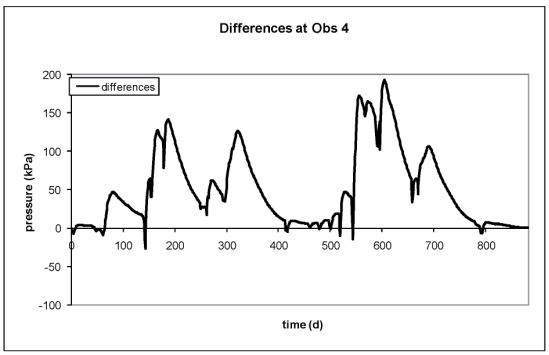
Differences at Obs 4
differences
pressure (kPa)
time (d)

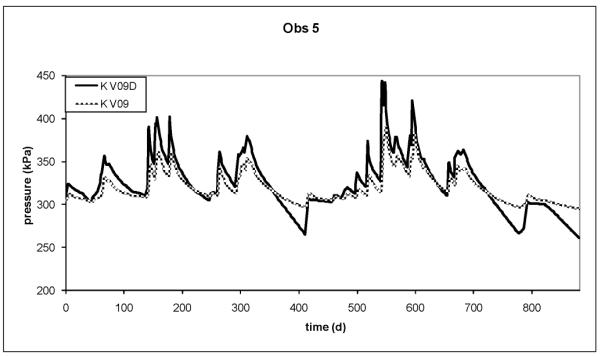
Obs 5
K V09D
K V09
pressure (kPa)
time (d)

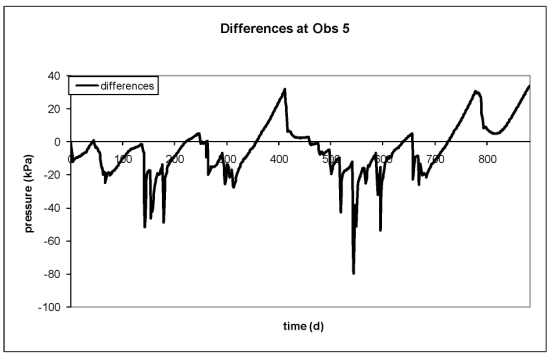
Differences at Obs 5
differences
pressure (kPa)
time (d)

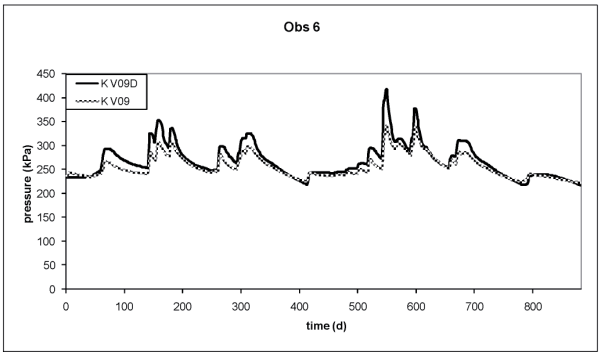
Obs 6
K V09D
K V09
pressure (kPa)
time (d)

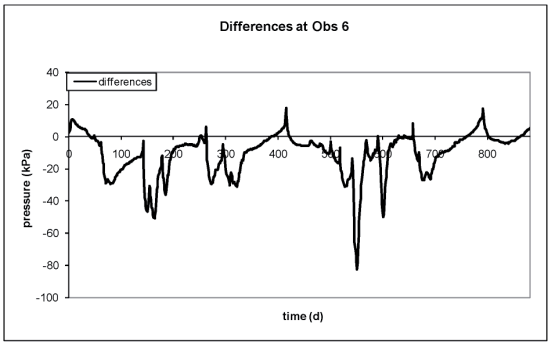
Differences at Obs 6
differences
pressure (kPa)
time (d)

K V09E

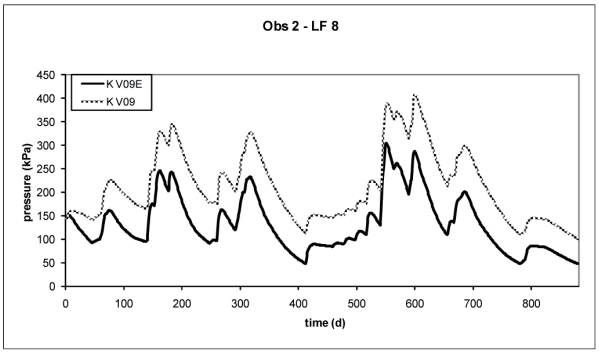
Obs 2 - LF 8
K V09E
K V09
pressure (kPa)
time (d)

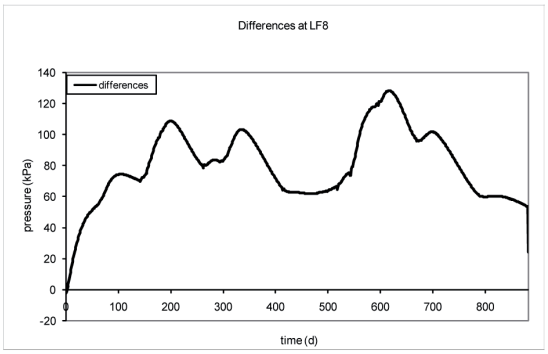
Differences at LF8
differences
pressure (kPa)
time (d)

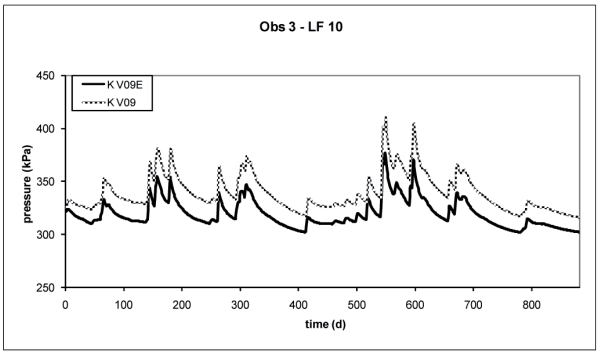
Obs 3 - LF 10
K V09E
K V09
pressure (kPa)
time (d)

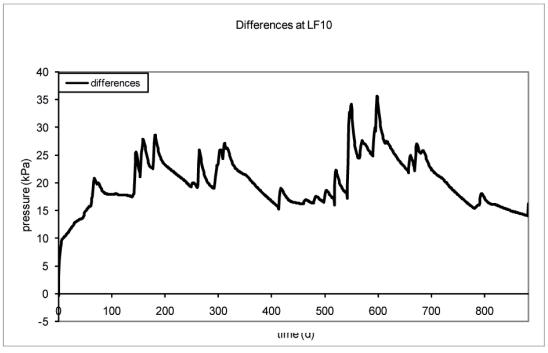
Differences at LF10
differences
pressure (kPa)

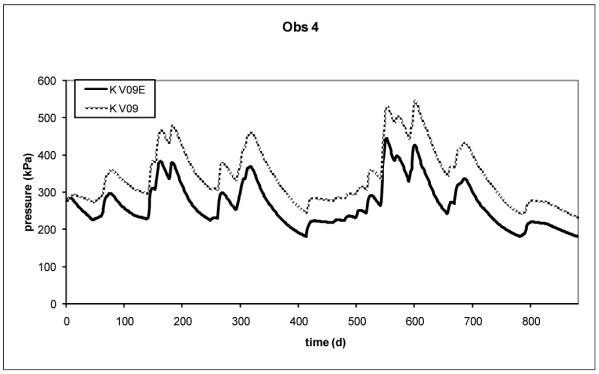
Obs 4
K V09E
K V09
pressure (kPa)
time (d)

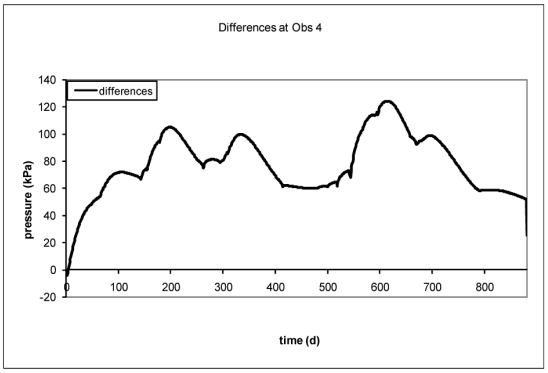
Differences at Obs 4
differences
pressure (kPa)
time (d)

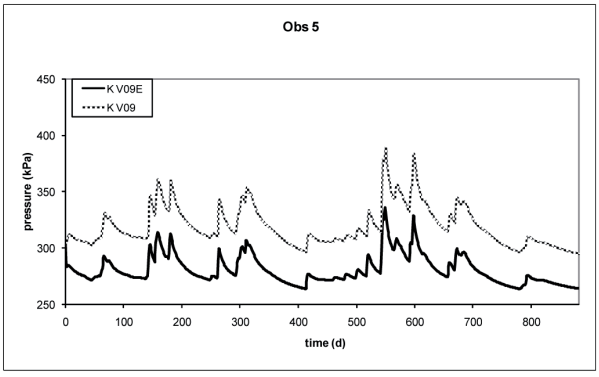
Obs 5
K V09E
K V09
pressure (kPa)
time (d)

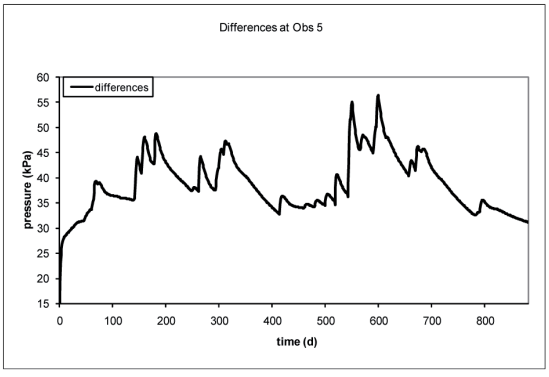
Differences at Obs 5
differences
pressure (kPa)
time (d)

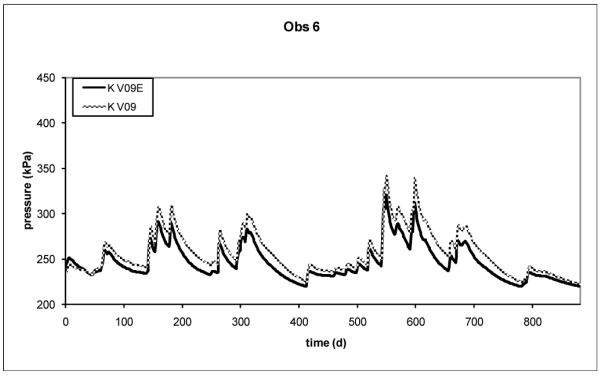
Obs 6
K V09E
K V09
pressure (kPa)
time (d)

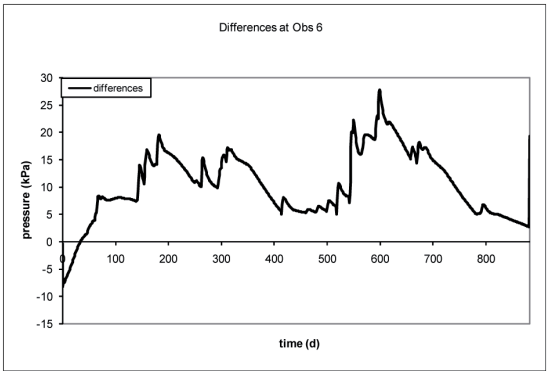
Differences at Obs 6
differences
pressure (kPa)
time (d)

K V09F

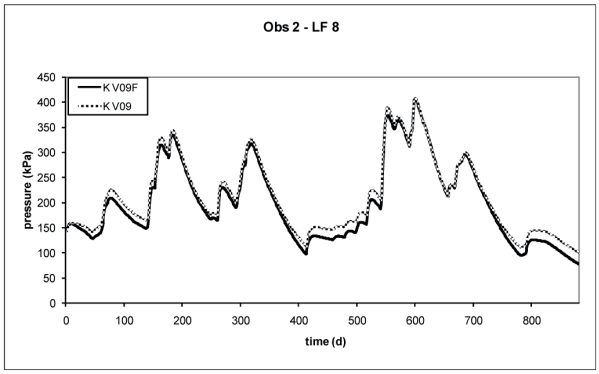
Obs 2 - LF 8
K V09F
K V09
pressure (kPa)
time (d)

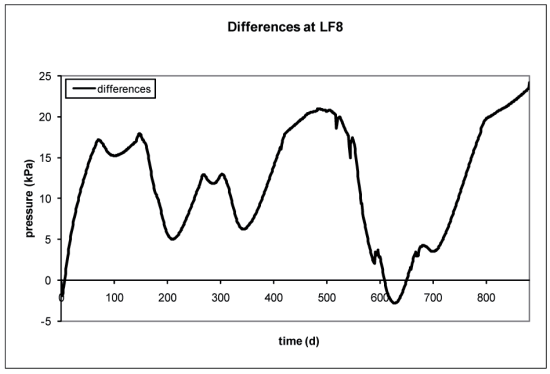
Differences at LF8
differences
pressure (kPa)
time (d)

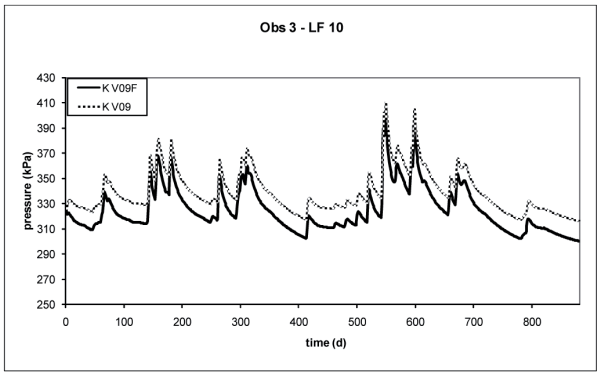
Obs 3 - LF 10
K V09F
K V09
pressure (kPa)
time (d)

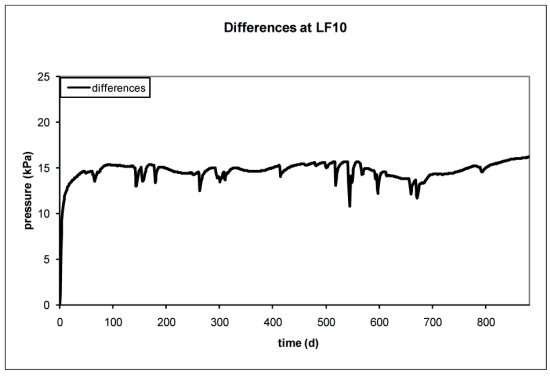
Differences at LF10
differences
pressure (kPa)
time (d)

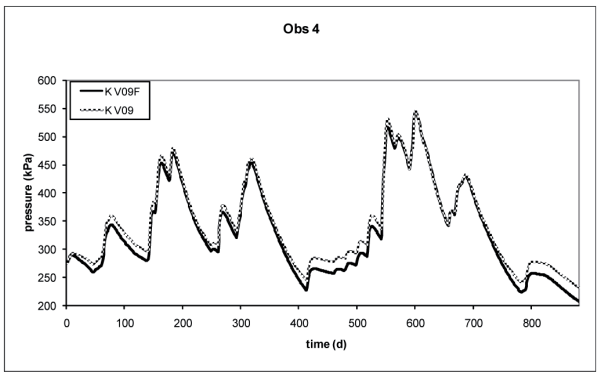
Obs 4
K V09F
K V09
pressure (kPa)
time (d)

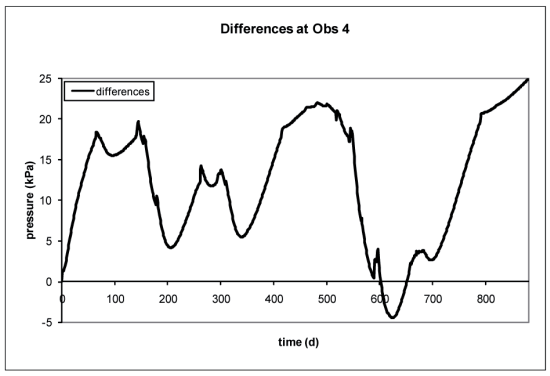
Differences at Obs 4
differences
pressure (kPa)
time (d)

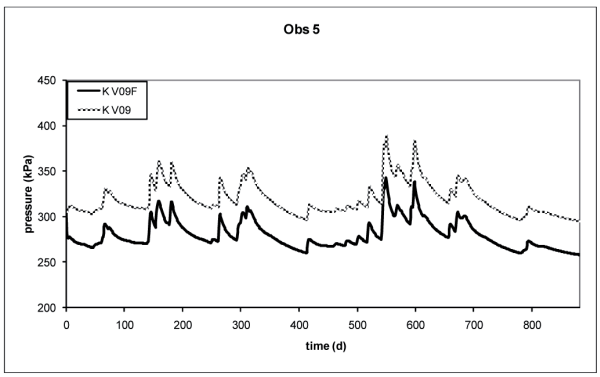
Obs 5
K V09F
K V09
pressure (kPa)
time (d)

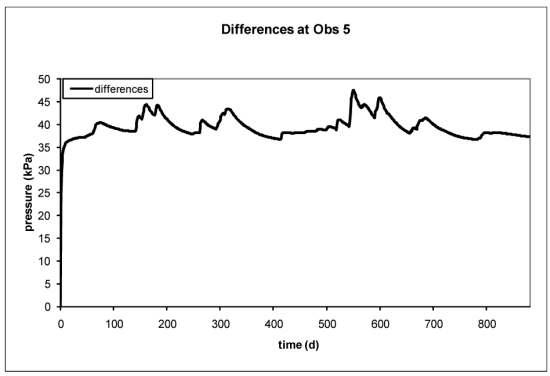
Differences at Obs 5
differences
pressure (kPa)
time (d)

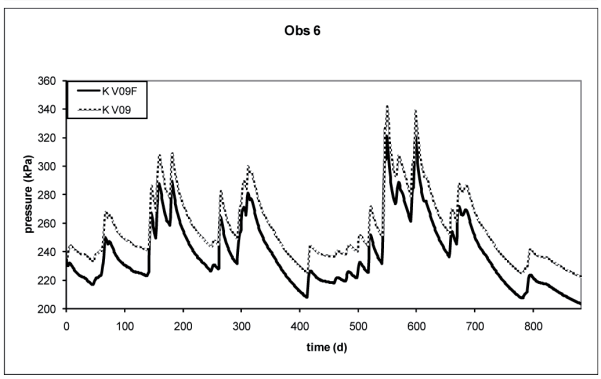
Obs 6
K V09F
K V09
pressure (kPa)
time (d)

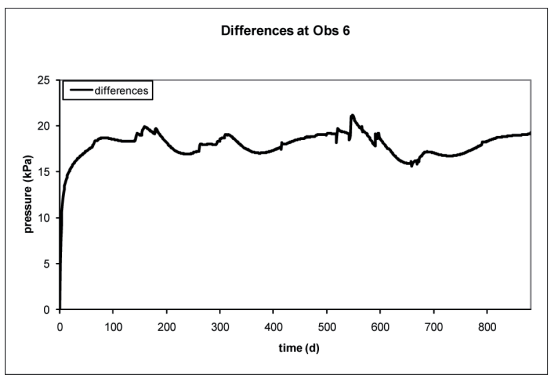
Differences at Obs 6
differences
pressure (kPa)
time (d)

K V09G

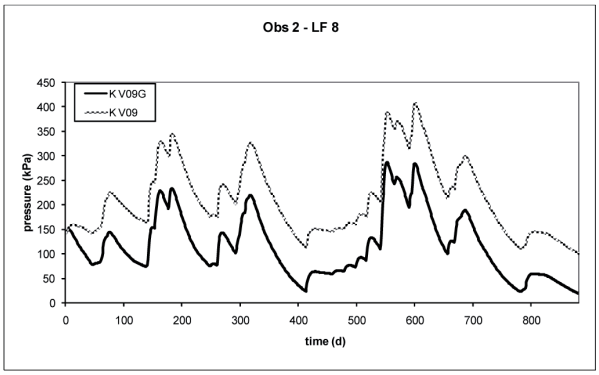
Obs 2 - LF 8
K V09G
K V09
pressure (kPa)
time (d)

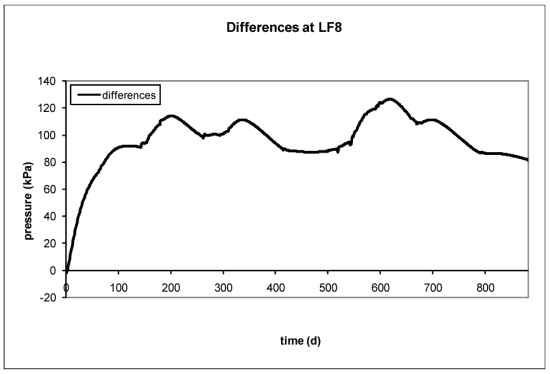
Differences at LF8
differences
pressure (kPa)
time (d)

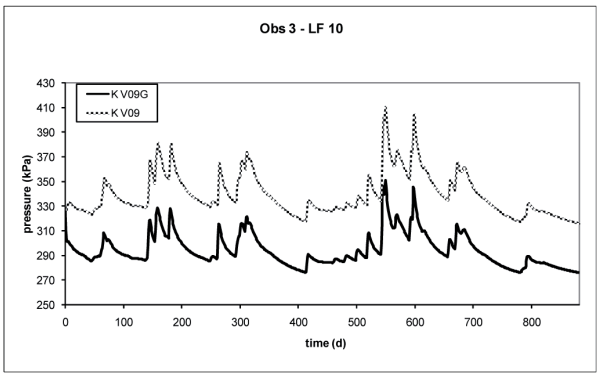
Obs 3 - LF 10
K V09G
K V09
pressure (kPa)
time (d)

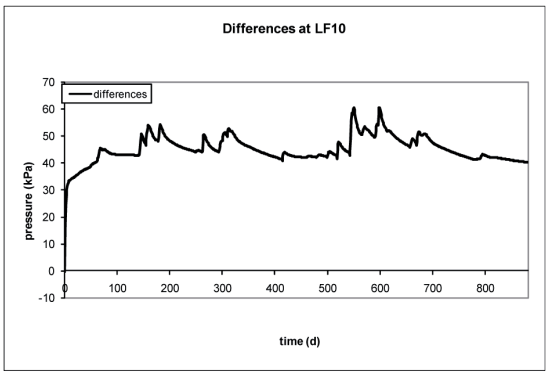
Differences at LF10
differences
pressure (kPa)
time (d)

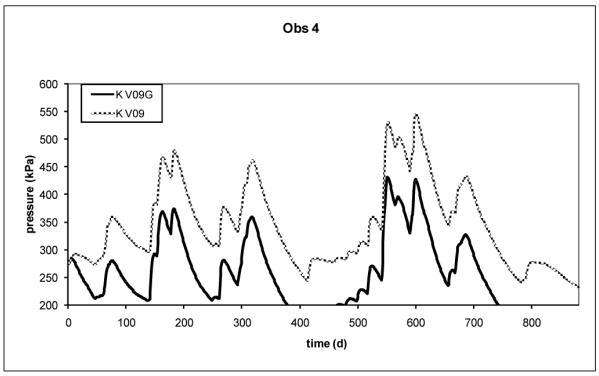
Obs 4
K V09G
K V09
pressure (kPa)
time (d)

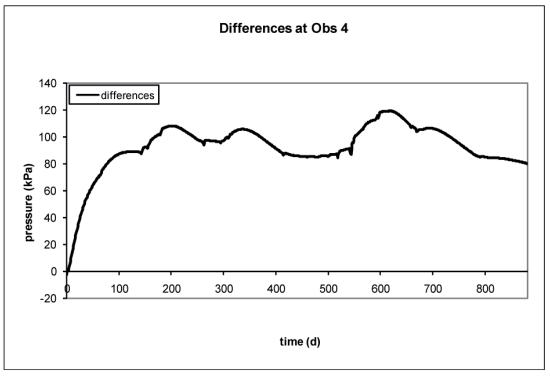
Differences at Obs 4
differences
pressure (kPa)
time (d)

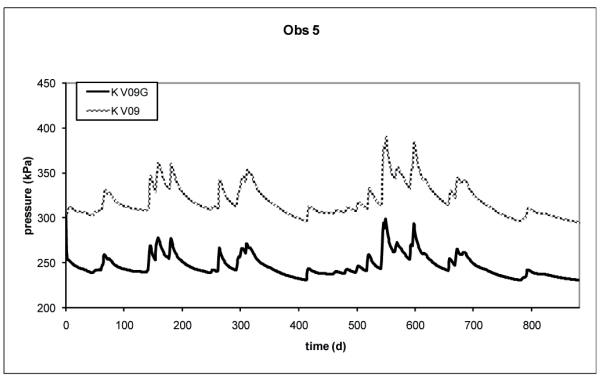
Obs 5
K V09G
K V09
pressure (kPa)
time (d)

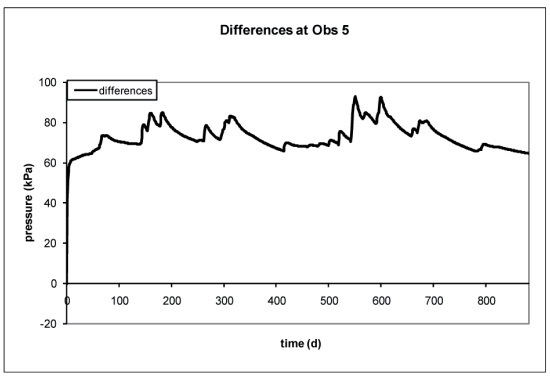
Differences at Obs 5
differences
pressure (kPa)
time (d)

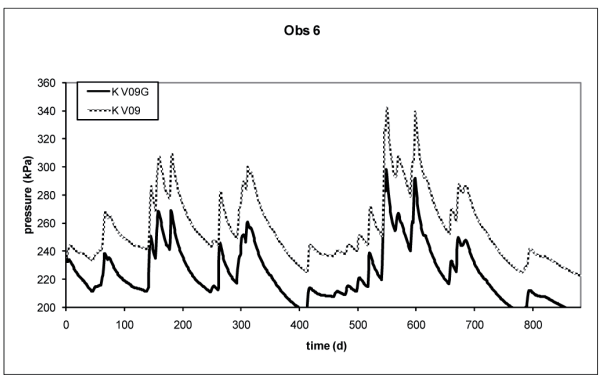
Obs 6
K V09G
K V09
pressure (kPa)
time (d)

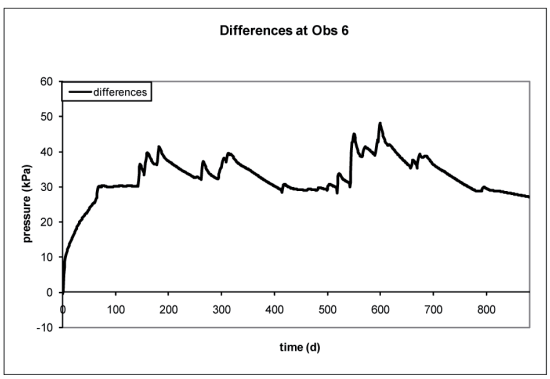
Differences at Obs 6
differences
pressure (kPa)
time (d)

K V09H

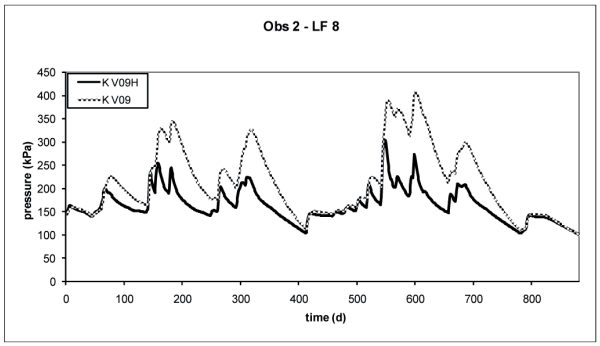
Obs 2 - LF 8
K V09H
K V09
pressure (kPa)
time (d)

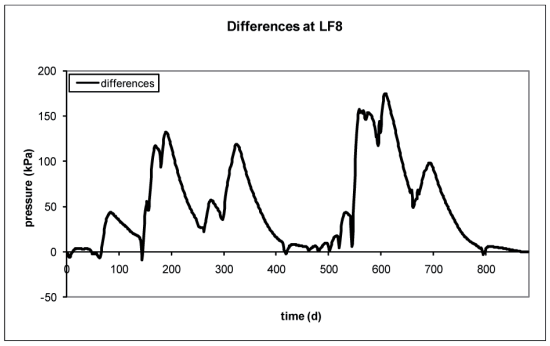
Differences at LF8
differences
pressure (kPa)
time (d)

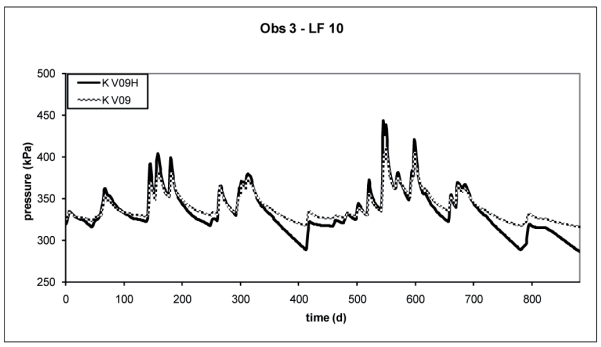
Obs 3 - LF 10
K V09H
K V09
pressure (kPa)
time (d)

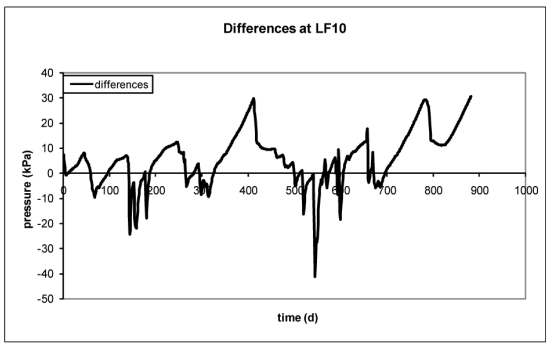
Differences at LF10
differences
pressure (kPa)
time (d)

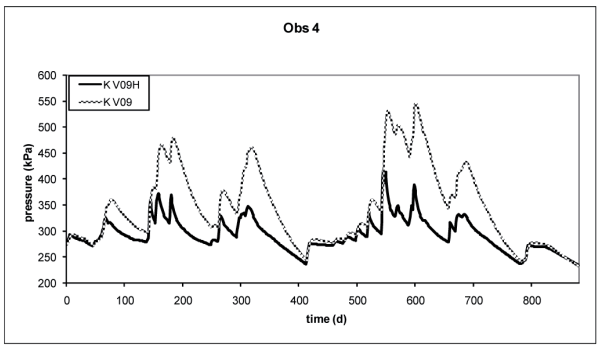
Obs 4
K V09H
K V09
pressure (kPa)
time (d)

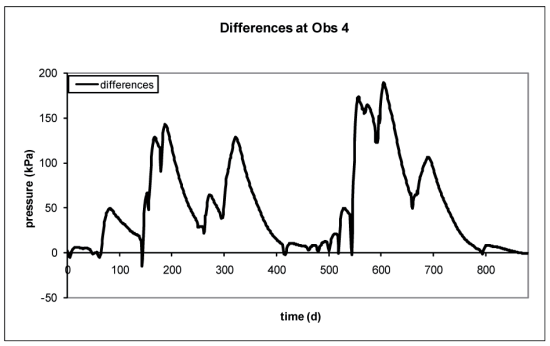
Differences at Obs 4
differences
pressure (kPa)
time (d)

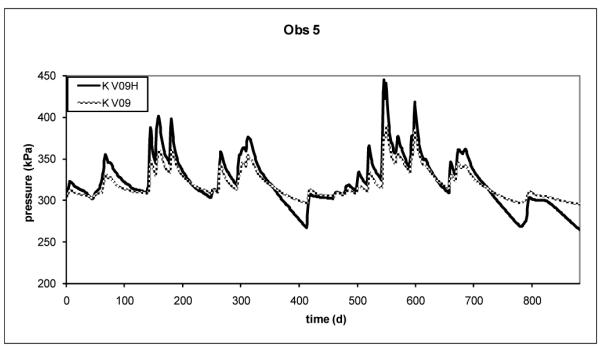
Obs 5
K V09H
K V09
pressure (kPa)
time (d)

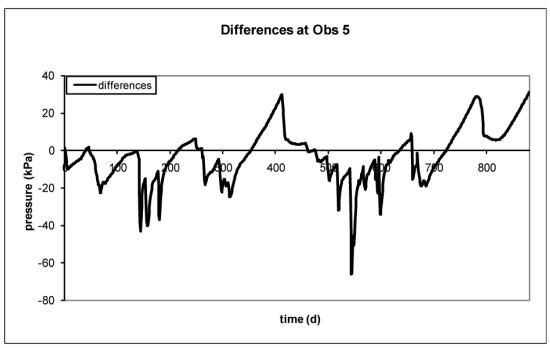
Differences at Obs 5
differences
pressure (kPa)
time (d)

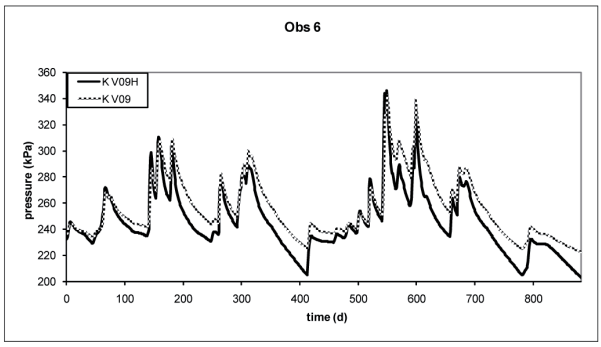
Obs 6
K V09H
K V09
pressure (kPa)
time (d)

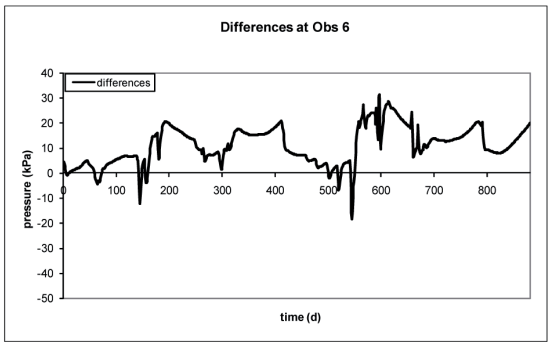
Differences at Obs 6
differences
pressure (kPa)
time (d)

K V09l

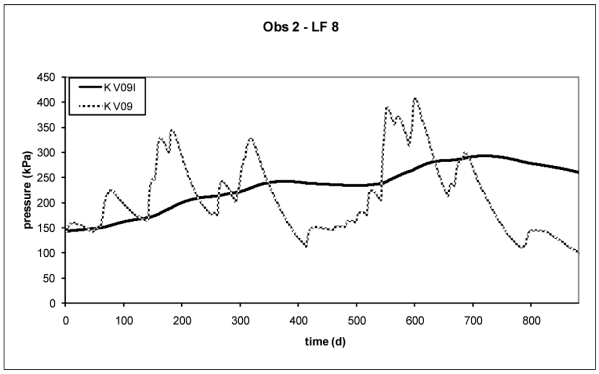
Obs 2 - LF 8
K V09l
K V09
pressure (kPa)
time (d)

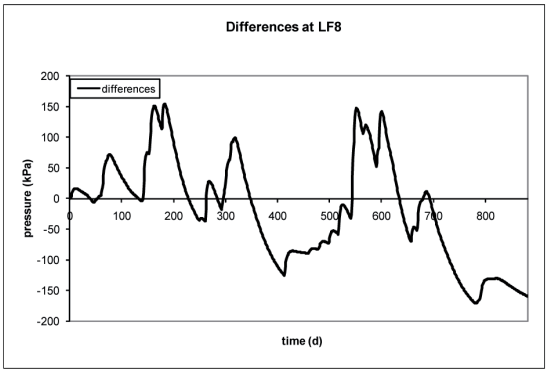
Differences at LF8
differences
pressure (kPa)
time (d)

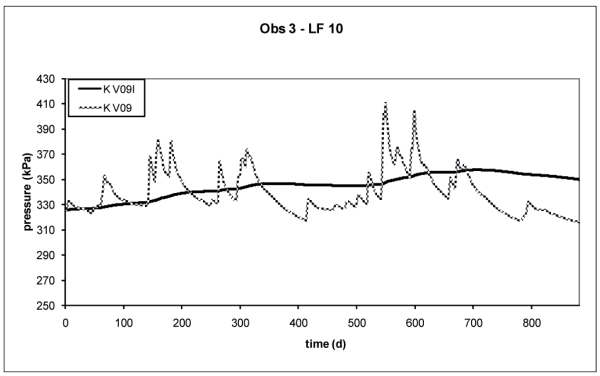
Obs 3 - LF 10
K V09l
K V09
pressure (kPa)
time (d)

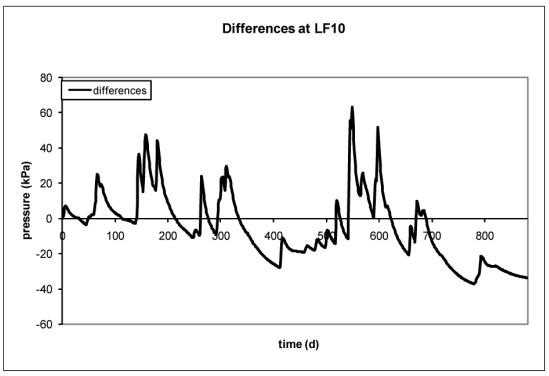
Differences at LF10
differences
pressure (kPa)
time (d)

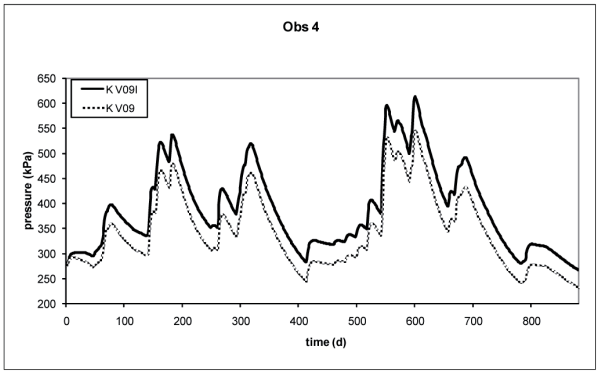
Obs 4
K V09l
K V09
pressure (kPa)
time (d)

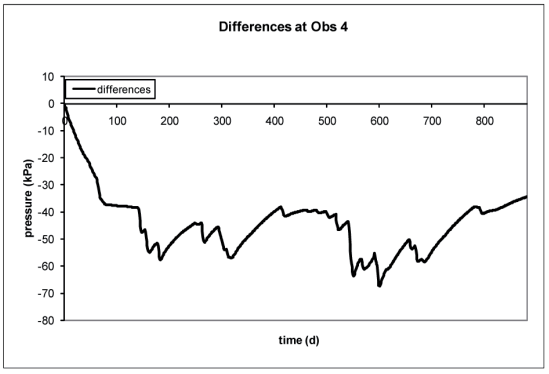
Differences at Obs 4
differences
pressure (kPa)
time (d)

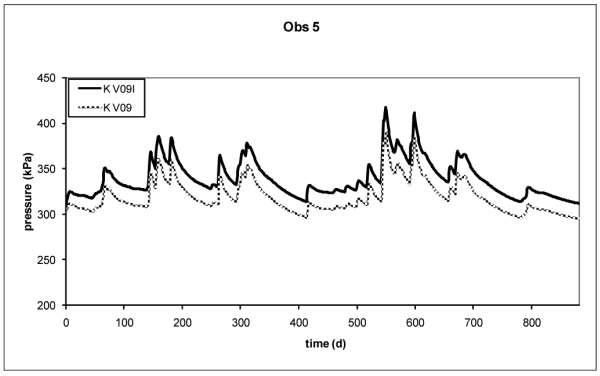
Obs 5
K V09l
K V09
pressure (kPa)
time (d)

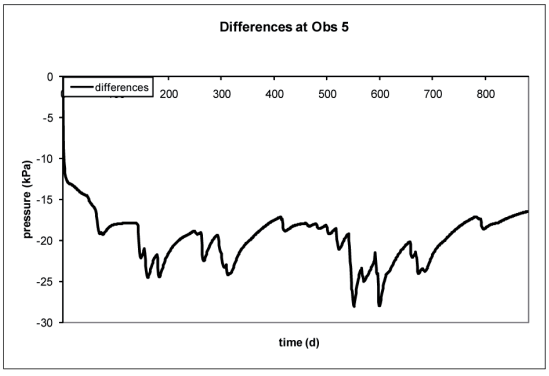
Differences at Obs 5
differences
pressure (kPa)
time (d)

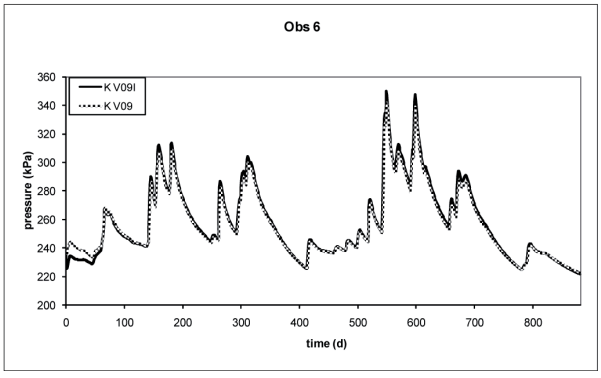
Obs 6
K V09l
K V09
pressure (kPa)
time (d)

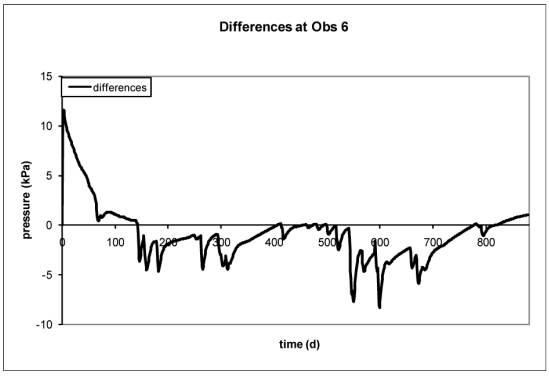
Differences at Obs 6
differences
pressure (kPa)
time (d)

K V09J

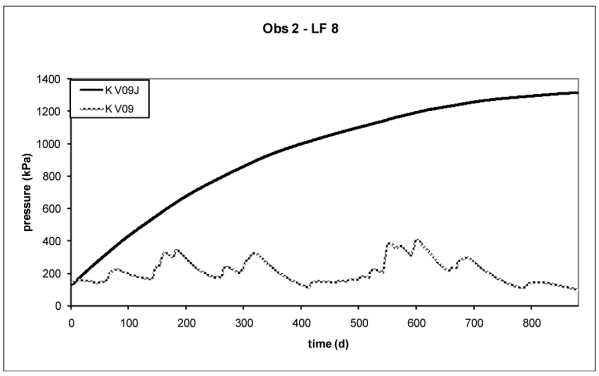
Obs 2 - LF 8
K V09J
K V09
pressure (kPa)
time (d)

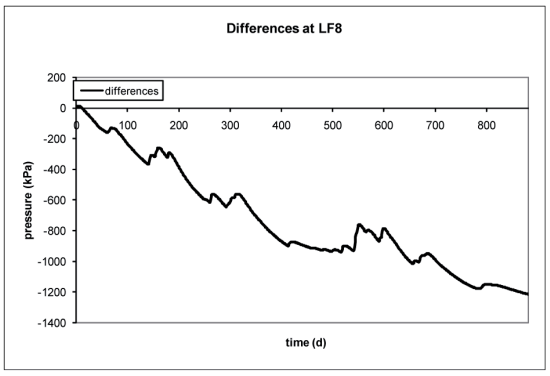
Differences at LF8
differences
pressure (kPa)
time (d)

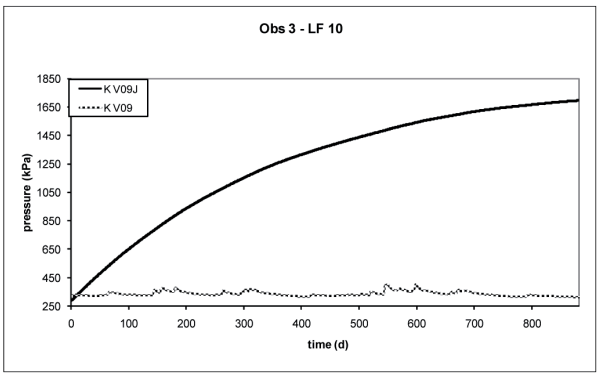
Obs 3 - LF 10
K V09J
K V09
pressure (kPa)
time (d)

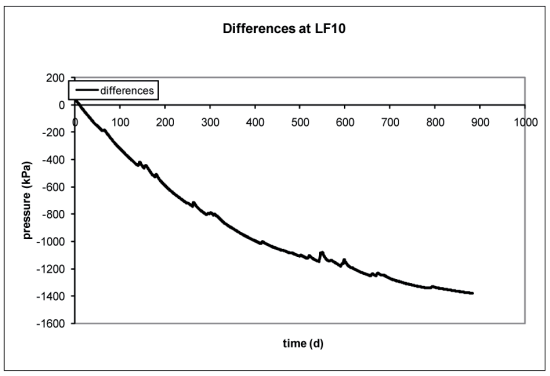
Differences at LF10
differences
pressure (kPa)
time (d)

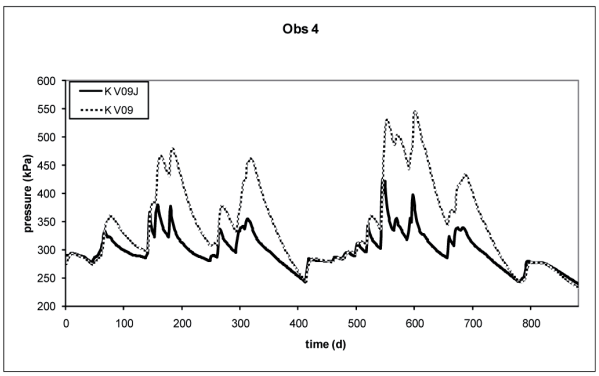
Obs 4
K V09J
K V09
pressure (kPa)
time (d)

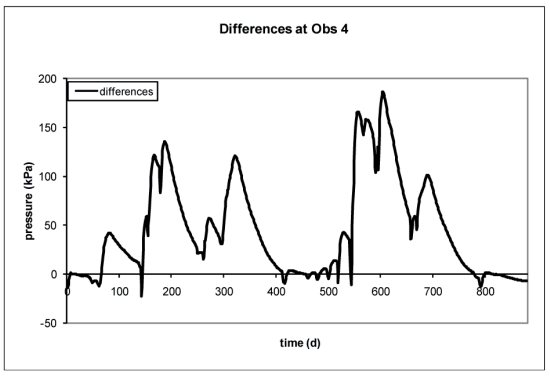
Differences at Obs 4
differences
pressure (kPa)
time (d)

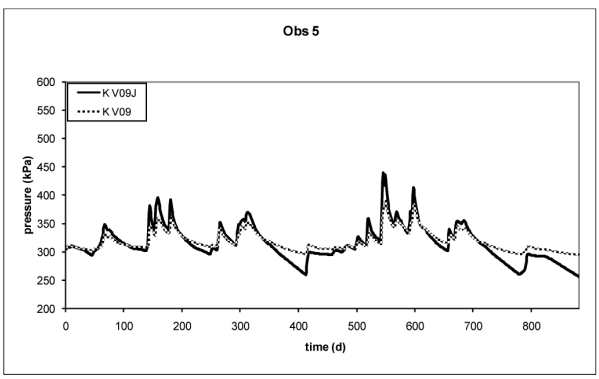
Obs 5
K V09J
K V09
pressure (kPa)
time (d)

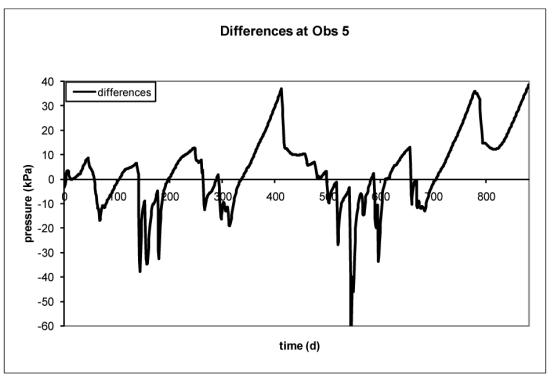
Differences at Obs 5
differences
pressure (kPa)
time (d)

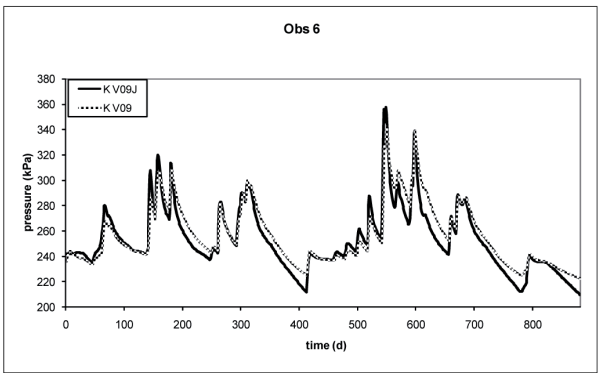
Obs 6
K V09J
K V09
pressure (kPa)
time (d)

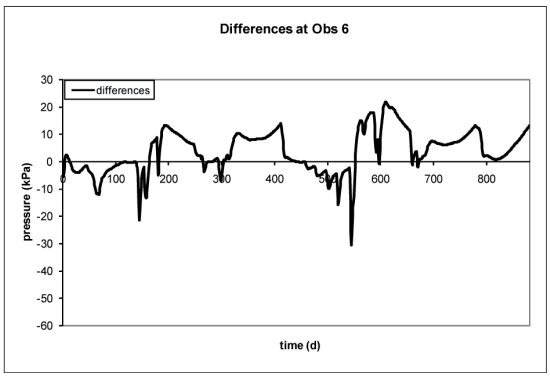
Differences at Obs 6
differences
pressure (kPa)
time (d)

K V09K

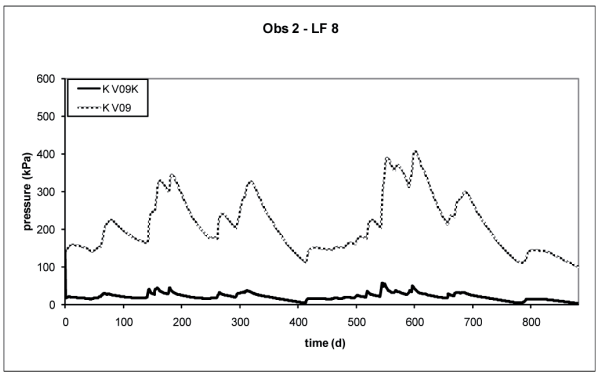
Obs 2 - LF 8
K V09K
K V09
pressure (kPa)
time (d)

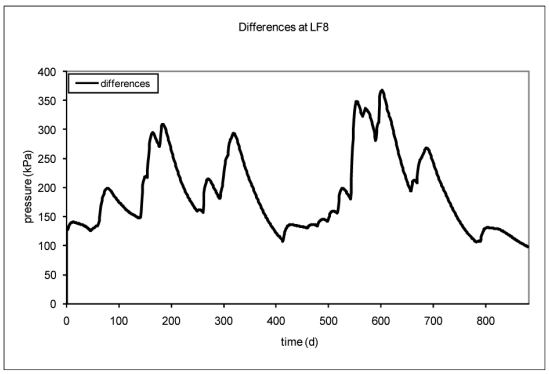
Differences at LF8
differences
pressure (kPa)
time (d)

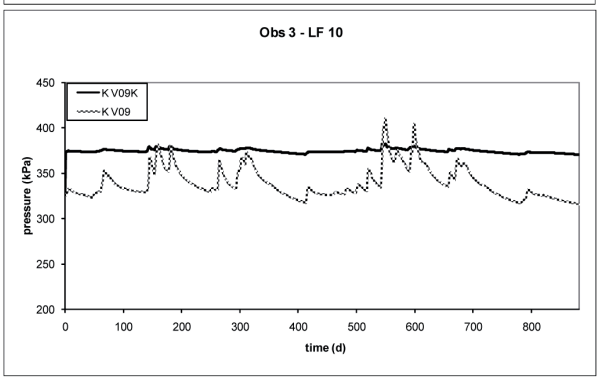
Obs 3 - LF 10
K V09K
K V09
pressure (kPa)
time (d)

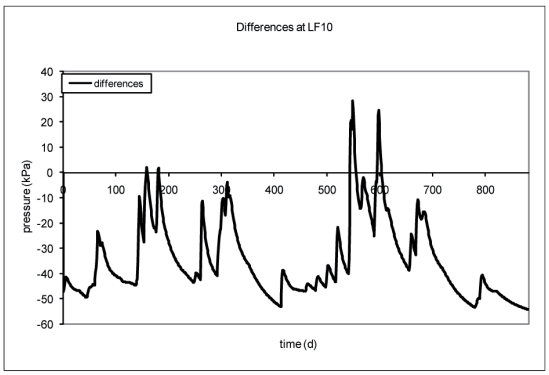
Differences at LF10
differences
pressure (kPa)
time (d)

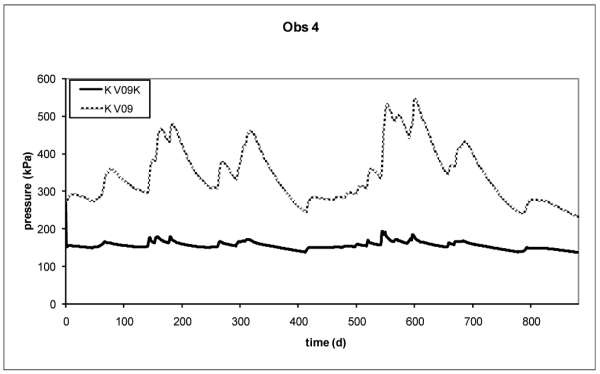
Obs 4
K V09K
K V09
pressure (kPa)
time (d)

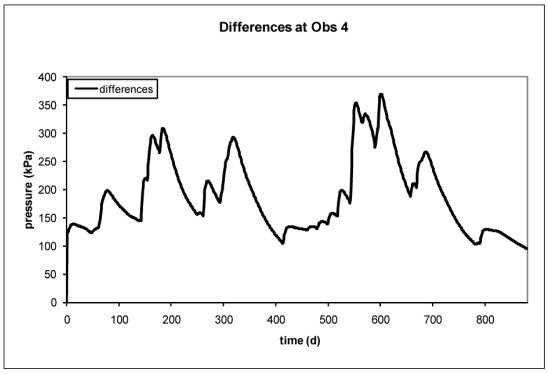
Differences at Obs 4
differences
pressure (kPa)
time (d)

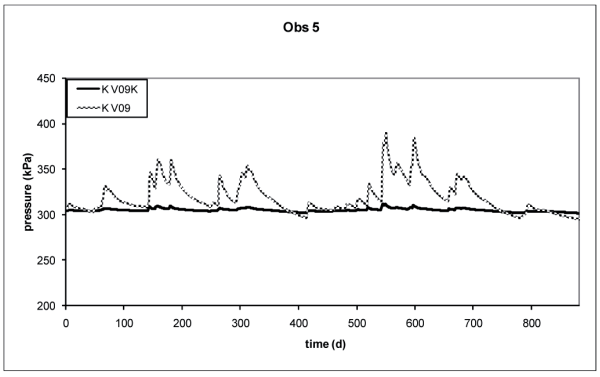
Obs 5
K V09K
K V09
pressure (kPa)
time (d)

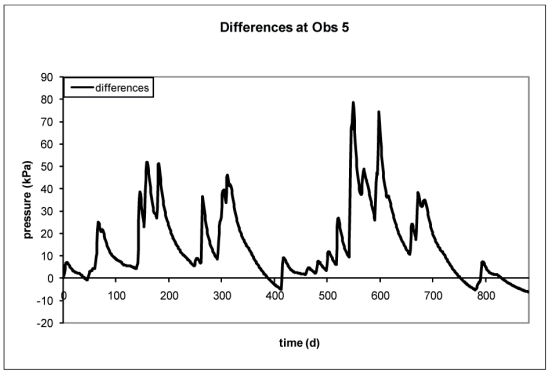
Differences at Obs 5
differences
pressure (kPa)
time (d)

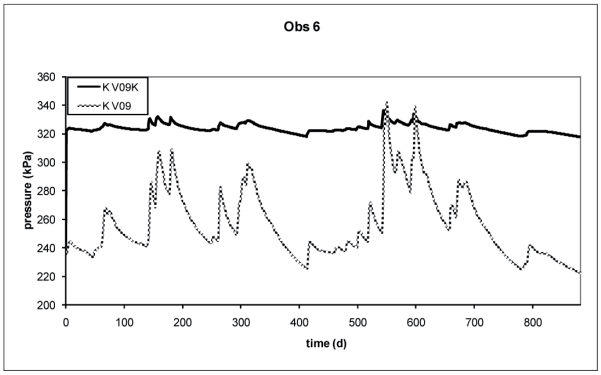
Obs 6
K V09K
K V09
pressure (kPa)
time (d)

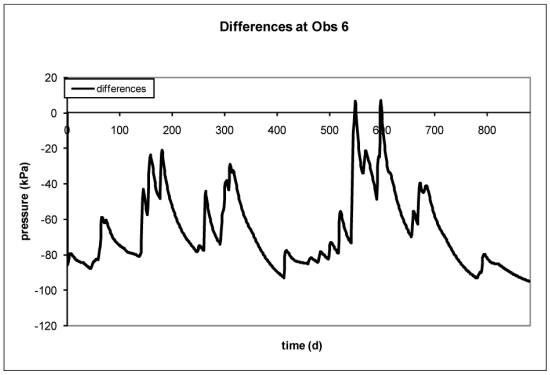
Differences at Obs 6
differences
pressure (kPa)
time (d)

K V09L

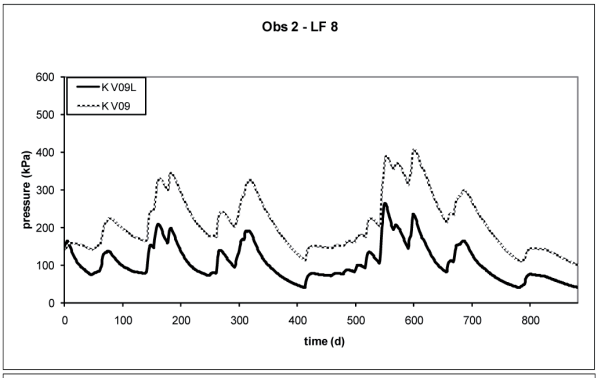
Obs 2 - LF 8
K V09L
K V09
pressure (kPa)
time (d)

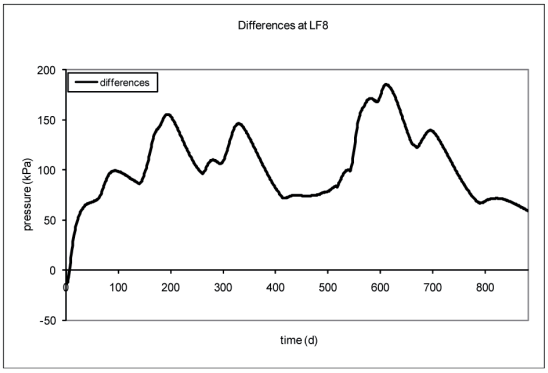
Differences at LF8
differences
pressure (kPa)
time (d)

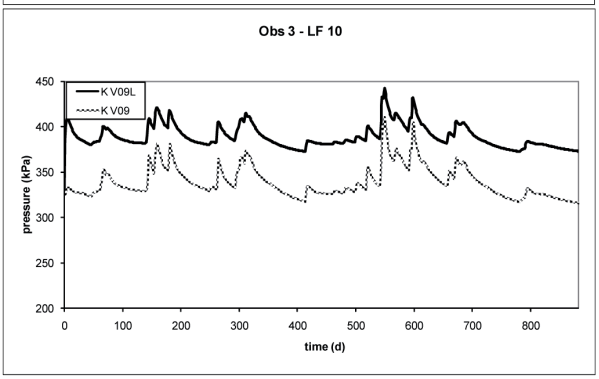
Obs 3 - LF 10
K V09L
K V09
pressure (kPa)
time (d)

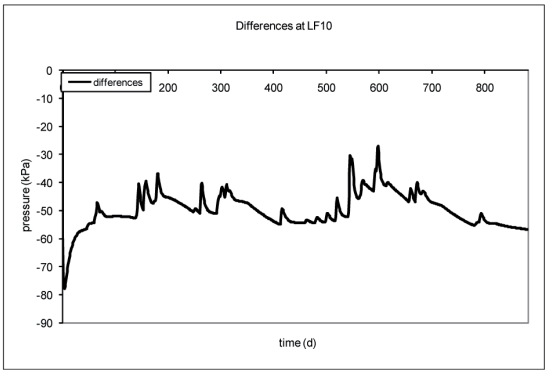
Differences at LF10
differences
pressure (kPa)
time (d)

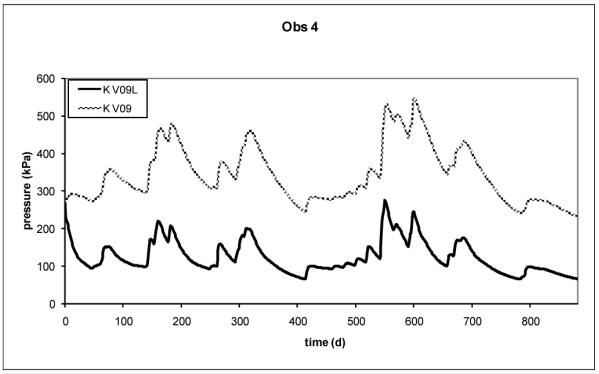
Obs 4
K V09L
K V09
pressure (kPa)
time (d)

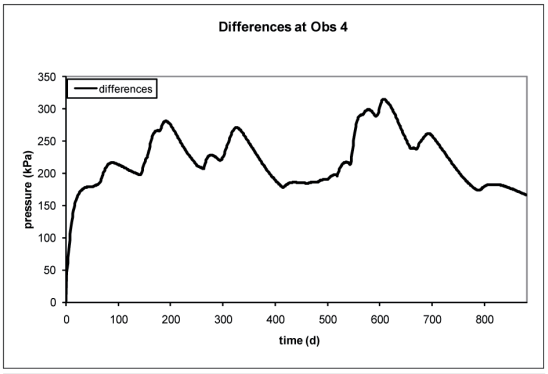
Differences at Obs 4
differences
pressure (kPa)
time (d)

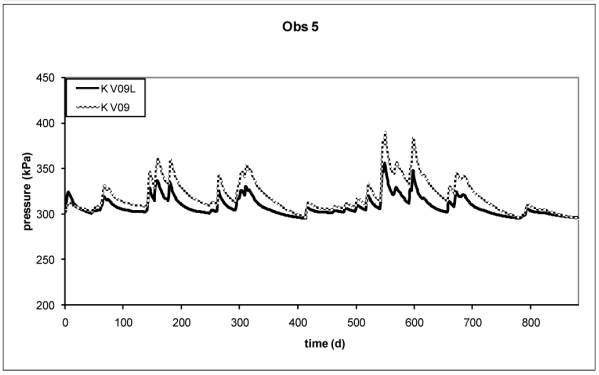
Obs 5
K V09L
K V09
pressure (kPa)
time (d)

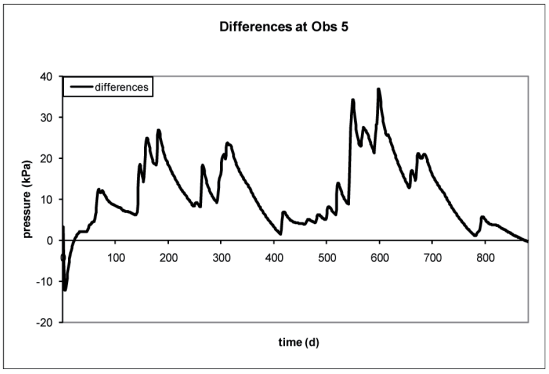
Differences at Obs 5
differences
pressure (kPa)
time (d)

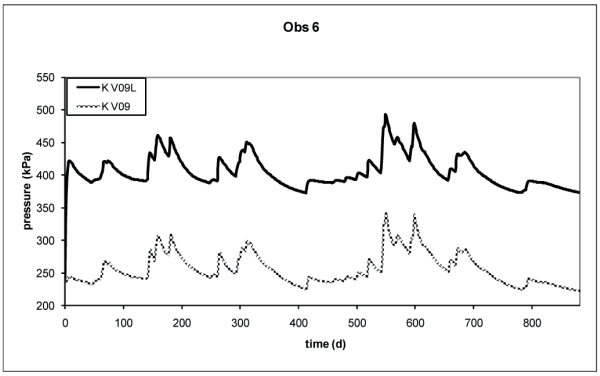
Obs 6
K V09L
K V09
pressure (kPa)
time (d)

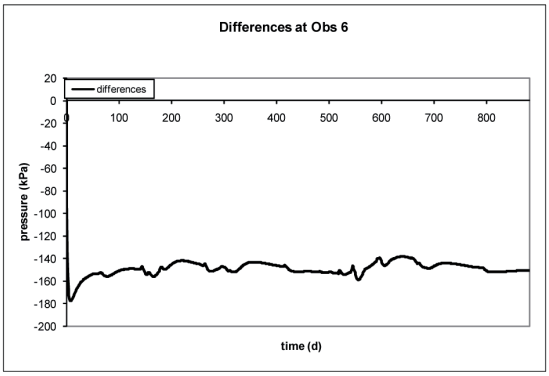
Differences at Obs 6
differences
pressure (kPa)
time (d)

K V09M

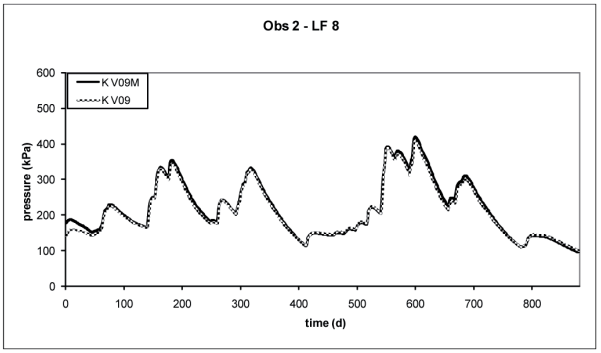
Obs 2 - LF 8
K V09M
K V09
pressure (kPa)
time (d)

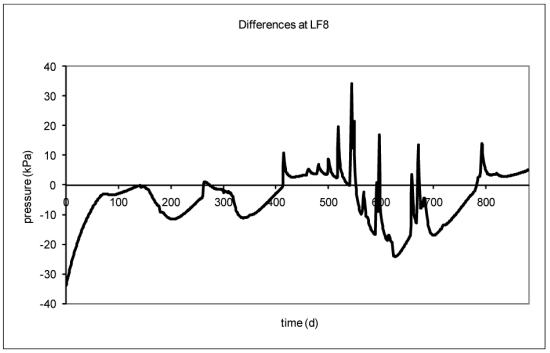
Differences at LF8
pressure (kPa)
time (d)

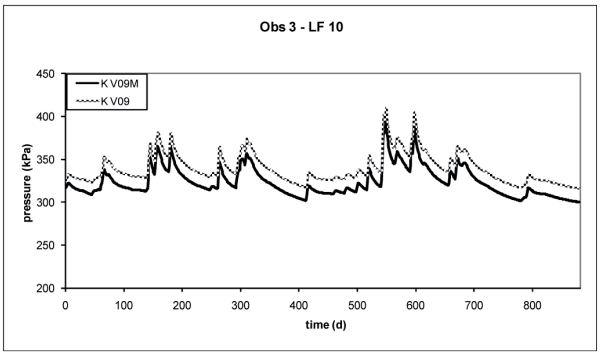
Obs 3 - LF 10
K V09M
K V09
pressure (kPa)
time (d)

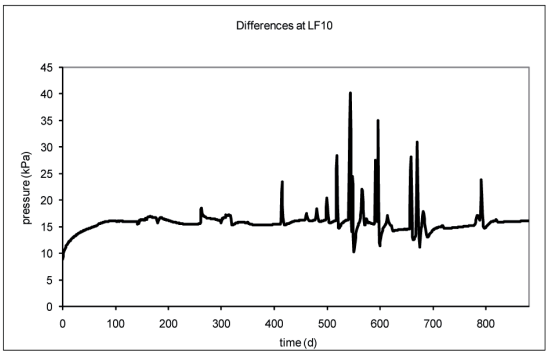
Differences at LF10
pressure (kPa)
time (d)

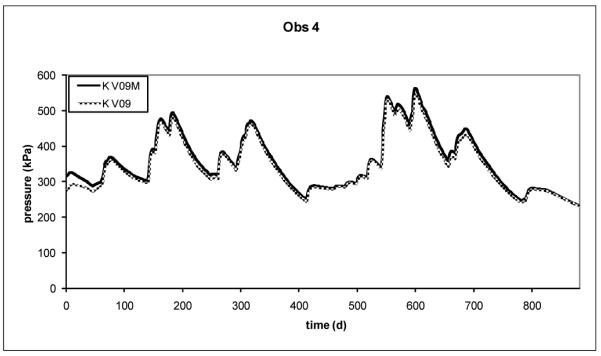
Obs 4
K V09M
K V09
pressure (kPa)
time (d)

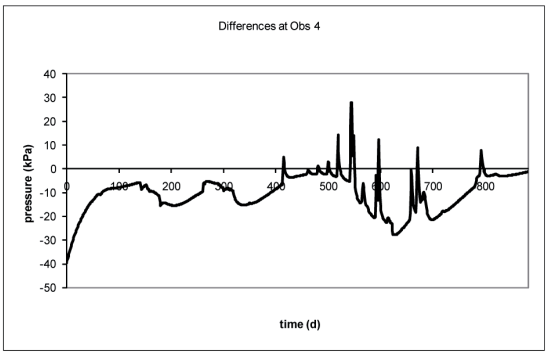
Differences at Obs 4
pressure (kPa)
time (d)

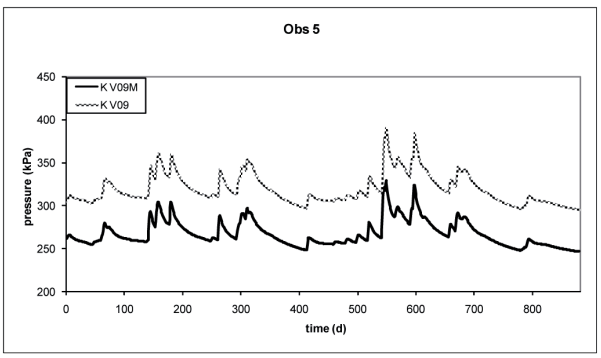
Obs 5
K V09M
K V09
pressure (kPa)
time (d)

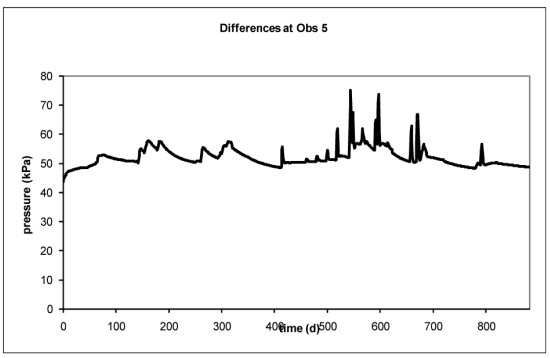
Differences at Obs 5
pressure (kPa)
time (d)

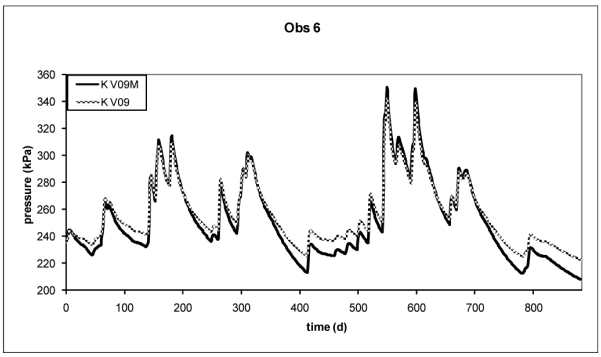
Obs 6
K V09M
K V09
pressure (kPa)
time (d)

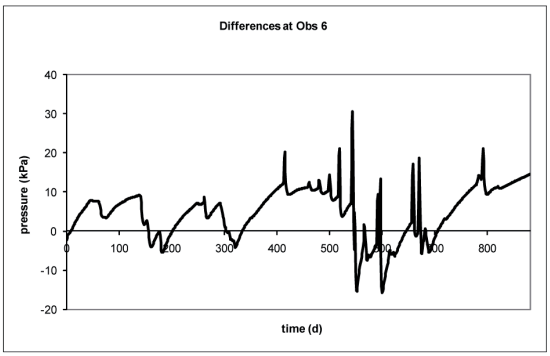
Differences at Obs 6
pressure (kPa)
time (d)

Curriculum vitae

Matti Boris
Born the 19th of September 1974, Saanen (Bern, Switzerland)
boris.matti@gmail.com

Education

2005-2008	PhD in Hydrogeology	*GEOLEP, EPFL, Switzerland*
2001-2002	Postgrade in Hydrogeology	*CHYN, Neuchâtel, Switzerland*
1996-2001	Master in Earth Sciences	*University of Lausanne, Switzerland*
1991-1995	Degree in Science type C	*Cessev, Burier, Switzerland*

Languages

French (mother tongue). Good knowledge in English, Italian, Spanish and German

Professional experiences

2005-2008	PhD thesis in hydrogeology at the GEOLEP (EPFL, Switzerland)
2004	A 4 months hydrogeological project at PRONAR - GTZ in Bolivia
2003	Midstream Data Analyst–Pipelines at IHS ENERGY in Geneva (www.ihsenergy.com)
2002	Traineeship and Master in hydrogeology at the GEOLEP (EPFL, Switzerland)
2001	Technical editor of a "Mémoires de Géologie: "*Geology of the western Swiss Alps, a guidebook*", edited by G.M Stampfli.
2000-2001	Assistant in field courses in France (Bassin des Causses): paleontology
1999-2001	Temporary works at the Museum of Geology in Lausanne.

Professional projects

Swiss projects
2008: Water Management *« Projet de nouveau captage, Délimitation de zones de protection, Commune de Savigny, 2007 »*
2007: Hydrogeological investigation for the elimination of wastewater « *Reconnaissances géologiques et hydrogéologiques en vue de l'élimination des eaux usées, Chalet de la Limasse, commune de Ste-Croix »*
2007: Hydrogeo-thermical numerical modelling *« Modélisation hydrogéologique de l'implantation d'un système de refroidissement eau-eau à l'hôpital de Sion (VS) »*
2007: Modelling the efficiency of a drainage gallery work in a large landslide *« Assainissement du glissement de la Frasse (VD, Switzerland): Modèles hydrogéologiques et géomécaniques. Etude sur l'efficacité d'une galerie de drainage »*
2006: Water Management *« Projet de nouveau captage, Etude hydrogéologique, Commune de Savigny »*
2002: Long-term simulations of thermal and hydraulic characteristics in a mountain massif: The Gothard massif, Master thesis CHYN (2002)
Foreign projects
2004: - Cat-Pronar (GTZ) projects, Hydrologic evaluation of the "Cuenca Misque" in Bolivia

Publications

Matti B. (2008): *Geological Heterogeneity in Landslides: Characterization and Flow Modelling. Unpublished PhD study, in progress since 2005, EPFL ENAC GEOLEP (Switzerland).*
Matti B., Tacher L. and Commend S. (2008): *Modelling the efficiency of a drainage gallery work in a large landslide with respect to hydrogeological and geomechanical parameter heterogeneity. Landslides. Submitted.*
Matti B. (2008): *Modelling the efficiency of a drainage gallery work in a large landslide with respect to hydrogeological and geomechanical parameter heterogeneity. Geophysical Research Abstracts,Vol. 10, EGU2008-A-00000, 2008. European Geosciences Union , EGU General Assembly 2008.*
Fischer Ch. and Matti B. (2004): *Estudio Hidrologico e Hidrogeologico de la Cuenca Salto Mayu con Modelos Matematicos. Publicación CAT-PRONAR (GTZ - 2004).*
Stampfli G. M., Vavassis I., De Bono A., Rosselet F., Matti B. and Bellini M. (2003): *Remnants of the Paleotethys oceanic suture-zone in the western Tethyan area. Bolletino della Società Geologica Italiana, Volume special.*
Matti B. (2002): - *Modélisation numérique de l'intéraction entre ouvrage du génie civil et les eaux souterraines : Le cas de la galerie de Polmengo (Alptransit). Bulletin d'Hydrogéologie No 20 (2002).*